UNIVERSIDAD NACIONAL AUTÓNOMA DE MÉXICO

DOCTORADO EN CIENCIAS BIOMÉDICAS
INSTITUTO DE FISIOLOGÍA CELULAR

ESTUDIO DE LAS INTERACCIONES QUE GUARDA LA SUBUNIDAD ASA1 EN EL BRAZO PERIFÉRICO DE LA ATP SINTASA DE *Polytomella* sp.

TESIS

QUE PARA OPTAR POR EL GRADO DE
DOCTORA EN CIENCIAS BIOMÉDICAS

PRESENTA:
MARTHA LILIA COLINA TENORIO

TUTOR PRINCIPAL
DR. DIEGO GONZÁLEZ HALPHEN
INSTITUTO DE FISIOLOGÍA CELULAR

MIEMBROS DEL COMITÉ TUTOR

DR. ÓSCAR FLORES HERRERA
FACULTAD DE MEDICINA

DR. SEBASTIÁN POGGIO GHILARDUCCI
INSTITUTO DE INVESTIGACIONES BIOMÉDICAS

CIUDAD UNIVERSITARIA, CIUDAD DE MÉXICO, AGOSTO DE 2018

Este trabajo se realizó en el laboratorio 342 Norte del Instituto de Fisiología Celular, bajo la dirección del Dr. Diego González Halphen

_____

Vo.Bo. Dr. Diego González Halphen

Índice

UNIVERSIDAD NACIONAL AUTÓNOMA DE MÉXICO

DOCTORADO EN CIENCIAS BIOMÉDICAS
INSTITUTO DE FISIOLOGÍA CELULAR

ESTUDIO DE LAS INTERACCIONES QUE GUARDA LA SUBUNIDAD ASA1 EN EL BRAZO PERIFÉRICO DE LA ATP SINTASA DE *Polytomella* sp.

TESIS

QUE PARA OPTAR POR EL GRADO DE
DOCTORA EN CIENCIAS BIOMÉDICAS

PRESENTA:

MARTHA LILIA COLINA TENORIO

TUTOR

DR. DIEGO GONZÁLEZ HALPHEN

MIEMBROS DEL COMITÉ TUTOR

DR. ÓSCAR FLORES HERRERA
DR. SEBASTIÁN POGGIO GHILARDUCCI

MÉXICO, D. F., 2018

Este trabajo se realizó en el laboratorio 342 Norte del Instituto de Fisiología Celular, bajo la dirección del Dr. Diego González Halphen

_____

Vo.Bo. Dr. Diego González Halphen

Índice

Resumen

La ATP sintasa mitocondrial del alga incolora *Polytomella* sp. tiene una estructura que difiere bastante de la de otros organismos. Dicha enzima está formada por un núcleo catalítico (subunidades α y β), un rotor (subunidades γ, δ, ε, y un anillo de diez subunidades *c*) y un estator o brazo periférico. Mientras las subunidades que componen tanto el núcleo catalítico como el rotor son canónicas y están conservadas, aquellas que componen el brazo periférico son nueve subunidades no conservadas cuyo origen evolutivo se desconoce. Estas subunidades se conocen como subunidades Asa (Asa1 a Asa9), algunas están encargadas de formar la estructura del brazo periférico y otras están involucradas en la dimerización de la enzima. Las subunidades Asa sólo se han encontrado en el linaje de las algas clorofíceas y no presentan homología con proteínas de linajes cercanos, como son las algas prasinofíceas, trebuxofíceas y ulvofíceas; ni con las subunidades que típicamente componen el brazo periférico de otras ATP sintasas rotatorias. Este trabajo se enfocó en el estudio de las interacciones que mantiene la subunidad Asa1, y se encontró que ésta se encuentra en contacto con las subunidades Asa2, Asa3, Asa7, Asa8 y OSCP. Se llevó a cabo la reconstitución de subcomplejos con todas estas subunidades con el propósito de confirmar las interacciones observadas. Se purificó la subunidad Asa3 y se encontró que adopta una estructura con repeticiones tipo armadillo. Finalmente, se reporta un método de replegamiento y purificación para la obtención de muestras de proteínas aptas para cristalización, con el que se obtuvieron y sembraron pruebas de cristalización de las subunidades Asa3 y Asa7. Con este trabajo se propone un modelo de la topología de las subunidades Asa y un método que abre la posibilidad de la obtención de cristales de estas subunidades.

Abstract

The mitochondrial ATP synthase of the colorless alga *Polytomella* sp. has a structure that is strikingly different from that of other organisms. This enzyme consists of a catalytic core (subunits α and β), a rotor (subunits γ, δ, ε, and *c*-ring) and a stator or peripheral stalk. While both of these sections are built with canonical and conserved subunits, those that make up the peripheral stalk are nine subunits that are not conserved and with an unknown evolutionary origin. These subunits are known as Asa subunits (Asa1 to Asa9), some of which build the structure of the peripheral stalk and some are involved in the dimerization of the enzyme. The Asa subunits have only been found in the chlorophycean lineage and they have no clear homology with proteins in closely related lineages (prasynophycean, trebuxophycean or ulvophycean) nor with any of the proteins that typically form the peripheral stalk in other rotary ATPases. This work focused on the interactions of subunit Asa1, which was found to maintain contacts with subunits Asa2, Asa3, Asa7, Asa8 and OSCP. The reconstitution of subcomplexes of all these subunits was carried out in order to confirm the observed interactions. Subunit Asa3 was purified and was found to adopt an armadillo-repeat structure. Finally, we report a refolding and purification method that results in samples suitable for crystallization. Based on this work, a topological model of the Asa subunits is proposed, as well as a method that opens the possibility of obtaining protein crystals of these subunits.

1. Introducción

1.1 El origen y la estructura de la mitocondria

Las mitocondrias son organelos muy dinámicos, semi-autónomos y esenciales por ser los encargados de producir energía, ya que dentro de ellos se sintetiza la mayoría del ATP celular en los organismos no fotosintéticos. La teoría sobre el origen de la mitocondria se dio a conocer en 1967 con la publicación de *On the Origin of Mitosing Cells* de Lynn Margulis, quien propuso y fundamentó que los organelos eucarióticos, incluyendo mitocondrias y cloroplastos, tienen un origen endosimbiótico (Sagan 1967). Actualmente se acepta que las mitocondrias derivaron de un organelo ancestral que nació de la unión de una α-proteobacteria con una célula hospedera. La hipótesis actual, basada en análisis filogenómicos, postula que la célula hospedera pertenece al grupo de arqueas llamado "Asgard" (Zaremba-Niedzwiedzka *et al*. 2017); la identidad precisa de la α-proteobacteria sigue en discusión, pero se propone que está relacionada con el grupo de las Rhodospirillales (Muñoz-Gómez *et al*. 2017). La transición de ser una bacteria a ser un organelo permanente, es decir, la integración del endosimbionte con la célula hospedera, estuvo acompañada de numerosos cambios y ajustes, entre ellos: la aparición de genes nuevos, de sistemas importadores de proteínas y transportadores de solutos, la reducción de genomas, la transferencia de genes y la relocalización de proteínas (Roger *et al*. 2017).

El origen de las mitocondrias implica la existencia de dos genomas, el genoma nuclear, el de la célula hospedera, y el eventual genoma mitocondrial, el de la α-proteobacteria. Durante la evolución, la mayoría de los genes bacterianos se perdieron o fueron transferidos al núcleo dejando sólo ciertos genes en el genoma mitocondrial. Notablemente, en todos los organismos estudiados existe una correlación entre la presencia de genoma mitocondrial y la existencia de mitocondrias con una cadena respiratoria funcional (Stewart y Larsson 2014). De esta forma, las proteínas que componen dicha cadena tienen un origen genético dual, es decir, algunas están codificadas en genes nucleares que se traducen por ribosomas citosólicos y se importan a la mitocondria; y otras, generalmente las más hidrofóbicas, están codificadas en genes

mitocondriales que son traducidos por ribosomas mitocondriales (Gustafsson *et al*. 2016). El ADN mitocondrial está compactado en estructuras supramoleculares llamadas nucleoides, que tienen un tamaño uniforme y se ha estimado que cada uno contiene una copia del genoma (Bogenhagen 2012).

Las mitocondrias están delimitadas por dos membranas altamente especializadas, la membrana externa y la membrana interna (Figura 1). La membrana externa mitocondrial, la línea de contacto entre la mitocondria y la citosol, es porosa y varios iones y solutos pueden difundir libremente a través de proteínas llamadas porinas (Kühlbrandt 2015); las tres más abundantes son el transportador de la membrana externa (TOM), el complejo SAM (*Sorting and Assembly Machinery*) y el canal VDAC (*Voltage Dependent Anion Channel*), que permite el paso de moléculas de hasta 5 kDa (Bayrhuber *et al*. 2008). Al contrario de la membrana externa, la membrana interna mitocondrial es muy impermeable y bastante más dinámica, tiene transportadores específicos para varias moléculas y toda la maquinaria generadora de energía se encuentra embebida en ella (Mannella 2008).

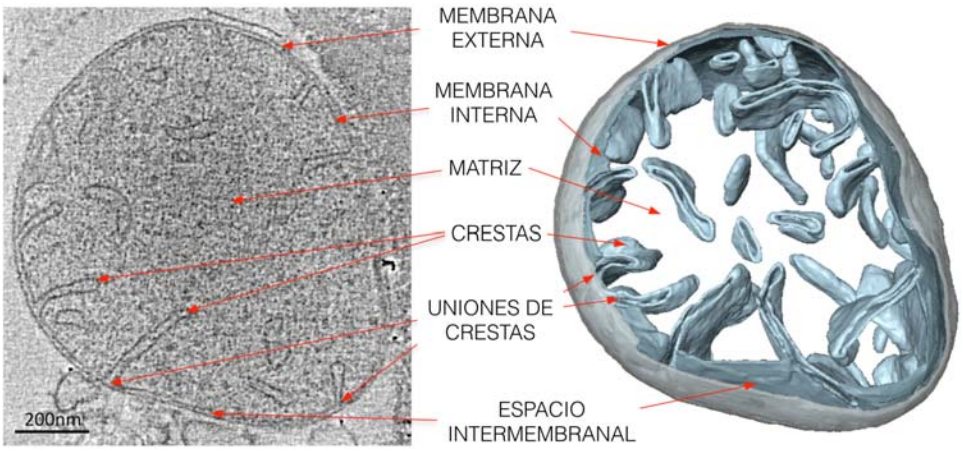

Figura 1. Morfología mitocondrial. A la izquierda se muestra el corte de una criotomografía electrónica de mitocondria de *Saccharomyces cerevisiae* y la derecha se muestra el volumen tridimensional generado para esa imagen. Se señalan las membranas mitocondriales, la matriz, las crestas, las uniones de las crestas y el espacio intermembranal. Figura modificada de Davies *et al*. 2014.

Las membranas mitocondriales generan tres compartimentos dentro de la mitocondria, cada uno con funciones diferentes y específicas (Mannella 2008) (Figura 1). La membrana interna encierra la matriz mitocondrial (el equivalente del citoplasma bacteriano), donde suceden la replicación y transcripción del ADN mitocondrial, así como la síntesis de proteínas y numerosas reacciones, entre ellas las del ciclo de Krebs. La matriz mitocondrial es entonces un compartimento muy rico en proteínas (se estima una concentración de 500 mg/mL, cercana a la concentración que se alcanza en un cristal de proteína) (Kühlbrandt 2015). El espacio entre las membranas (de aproximadamente 20 nm), el espacio intermembranal, es el equivalente del periplasma bacteriano y en él se encuentran altas cantidades de citocromo *c*, un acarreador proteico de electrones soluble (Kühlbrandt 2015).

La membrana interna se pliega para formar las llamadas crestas mitocondriales y dicho plegamiento genera el tercer compartimento, el lumen crestal, que tiene un impacto importante sobre la función bioenergética de la mitocondria (Mannella 2008). Las crestas mitocondriales se pueden encontrar en dos conformaciones, la lamelar y la tubular, que se pueden apreciar claramente en modelos tridimensionales obtenidos por tomografía electrónica (Frey y Mannella 2000). La conformación de las crestas, la cantidad y su arreglo en la matriz es variable según el tipo de célula, tejido, organismo y estado energético. Las crestas mitocondriales constituyen subcompartimentos esenciales para la función mitocondrial, ya que sirven para limitar la difusión de moléculas entre el lumen crestal y el espacio intermembranal, lo cual permite localizar el gradiente de protones, concentrar metabolitos y prevenir la salida de moléculas como el citocromo *c* (Muñoz-Gómez *et al.* 2017). Esta compartamentalización se consigue al conectar la membrana interna con las crestas mediante las llamadas uniones de cresta (*crista junctions*), que son estructuras tubulares pequeñas y cortas (Harner *et al*. 2011). La importancia de esta arquitectura mitocondrial radica en que permite que se genere un gradiente local de protones en el espacio generado por los pliegues de las crestas, lo cual evita su difusión y resulta en una síntesis eficiente de ATP (Davies *et al*. 2014).

1.2 La cadena respiratoria mitocondrial

El gradiente electroquímico a través de la membrana interna mitocondrial es generado por los complejos respiratorios: complejo I (NADH:ubiquinona oxidorreductasa), complejo III (complejo bc_1 o ubiquinol:citocromo *c* oxidorreductasa) y complejo IV (citocromo *c* oxidasa); el gradiente es luego utilizado por la ATP sintasa mitocondrial (complejo V) para llevar a cabo la síntesis de ATP. Estos complejos (I, III y IV), por medio de reacciones de óxido reducción, transfieren electrones de sustratos reductores hasta el oxígeno molecular, mientras simultáneamente bombean protones hacia el espacio intermembranal. Los equivalentes de reducción NADH y $FADH_2$, que se originan en diversas vías metabólicas (glucólisis, oxidación de ácidos grasos o ciclo de Krebs), entran a la cadena de transporte de electrones a través del complejo I y II, respectivamente. El complejo I transfiere electrones del NADH a una molécula de quinol y la energía liberada de esta reacción impulsa el bombeo de cuatro protones. El complejo III recibe los electrones de la molécula de quinol reducida (quinona) y los transfiere a un acarreador proteico soluble, el citocromo *c*, bombeando cuatro protones en el proceso. Finalmente, el complejo IV transfiere los electrones del citocromo *c* al oxígeno; la energía liberada de esta reacción impulsa el bombeo de cuatro protones. El complejo II (succinato:ubiquinona oxidorreductasa) tiene como sustrato al succinato, que transfiere electrones directamente a moléculas de quinol, por lo que este complejo participa en la transferencia de electrones pero no contribuye a la formación del gradiente electroquímico (Figura 2).

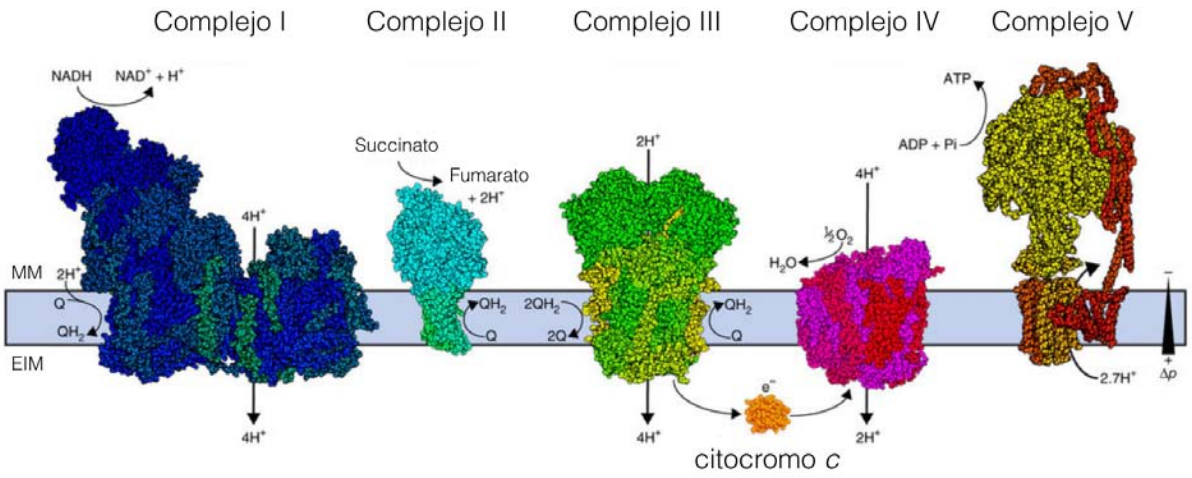

Figura 2. Cadena respiratoria mitocondrial. Se muestran los cuatro complejos respiratorios, el complejo V y sus reacciones correspondientes. Se indican ambos lados de la membrana interna: la matriz mitocondrial (MM) y el espacio intermembranal (EIM), y la fuerza protón motriz (Δ*p*). Figura modificada de Letts y Sazanov 2017.

La organización de los complejos respiratorios en la membrana interna mitocondrial ha sido materia de debate, pero actualmente se acepta un modelo de "plasticidad" en el que éstos complejos se pueden encontrar tanto aislados como asociados entre ellos formando supracomplejos, en un sistema de equilibrio dinámico (Enriquez 2016) (Figura 3A). Se han propuesto varias explicaciones con respecto a la relevancia funcional de esta asociación: la canalización de sustratos directamente de un complejo al siguiente, minimizando la producción de especies reactivas de oxígeno (Winge 2012); la estabilización estructural del complejo I (Schägger *et al*. 2004); evitar la agregación de los complejos respiratorios (Dudkina *et al*. 2010, Chaban *et al*. 2014) e influir en la regulación del metabolismo mitocondrial (Acin-Perez y Enriquez 2014). Por su parte, la ATP sintasa se asocia en dímeros que a su vez forman hileras oligoméricas, este arreglo se observó por primera vez en mitocondrias de mamíferos (Strauss *et al*. 2008), y hoy en día se considera una característica conservada y ubicua debido a que se ha encontrado en las mitocondrias de todas las especies estudiadas hasta la fecha (Davies *et al*. 2012).

La asociación de los complejos respiratorios en supracomplejos se ha reportado en mamíferos, levaduras (Schägger y Pfeiffer 2000) y recientemente en *Polytomella* sp. (Miranda-Astudillo *et al*. 2018); por su parte, las primeras estructuras tridimensionales completas de supracomplejos mitocondriales de mamíferos, I-III_2-IV y I-III_2, se obtuvieron por criomicroscopía electrónica a una resolución aproximada de 6 y 7.8 Å, respectivamente (Letts *et al*. 2016). En cuanto a su distribución espacial, los complejos respiratorios y la ATP sintasa se han encontrado localizados en puntos específicos de las crestas mitocondriales: los primeros se localizan, ya sea aislados o como supracomplejos, en las "caras" de las crestas mitocondriales, mientras que las hileras de dímeros de ATP sintasa se localizan a lo largo de los "cantos" de las crestas (Davies *et al*. 2011) (Figura 3B).

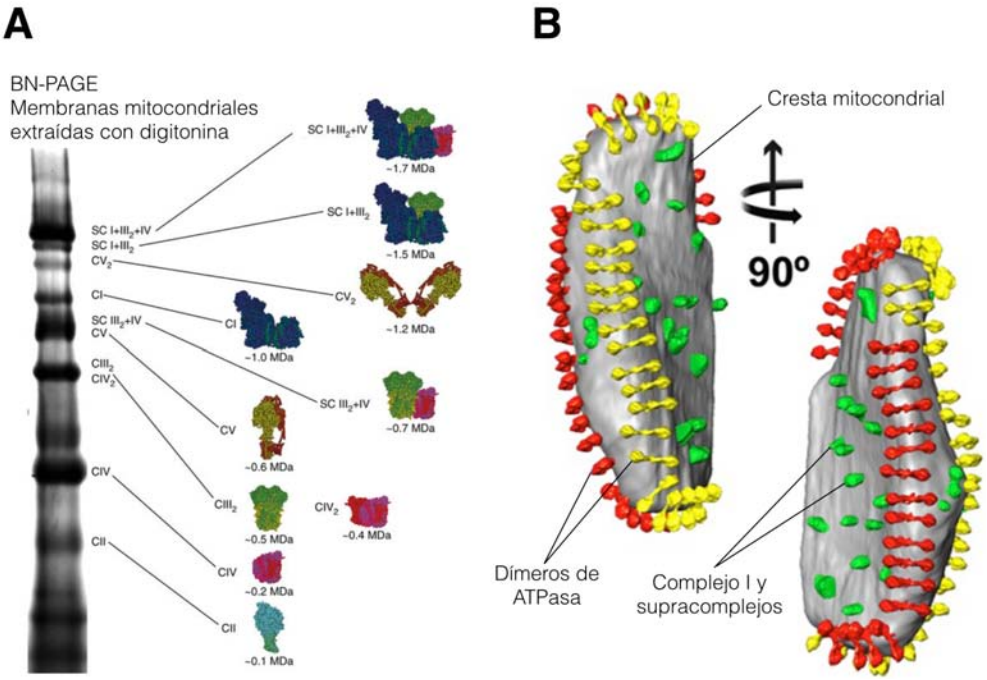

Figura 3. Supracomplejos mitocondriales y su distribución en la membrana interna mitocondrial. A. Se muestra un gel azul nativo (BN-PAGE) en el que se observa el patrón de migración de mitocondrias de corazón de ovino solubilizadas con digitonina. Se indica la identidad de cada banda y se ilustran las asociaciones de los complejos. Figura modificada de Letts y Sazanov 2017. **B.** Se muestra el modelo tridimensional de una cresta mitocondrial de *Podospora anserina*, generado por criotomografía electrónica, en el que se observan los dímeros de ATPasa a lo largo de los cantos de la cresta y el complejo I y asociaciones de complejos respiratorios en las caras. Figura modificada de Davies *et al*. 2014.

1.3 La estructura y función de la ATP sintasa mitocondrial

El ATP es la molécula energética por excelencia, es indispensable para que se lleven a cabo todas las funciones necesarias para vivir. La mayor parte de la síntesis de esta molécula está a cargo del complejo enzimático conocido como F_1F_O ATP sintasa o complejo V mitocondrial. Esta enzima se encuentra muy conservada y pertenece a la familia de las ATP sintasas rotatorias, en la que también se encuentran las ATPasas vacuolares y las ATPasas de arqueas. Las F-ATPasas se encuentran en las membranas transductoras de energía, es decir, en la membrana plasmática de bacterias, en la membrana interna mitocondrial y en la membrana tilacoidal de cloroplastos (Domínguez-Ramírez L. *et al.* 2005). Estas enzimas acoplan la síntesis de ATP con el potencial electroquímico de membrana generado por la cadena respiratoria mitocondrial, siguiendo el proceso conocido como acoplamiento quimiosmótico, propuesto por primera vez por Peter Mitchell en 1961 (Mitchell 1961).

La F_1F_O ATP sintasa se divide clásicamente en su parte soluble, llamada F_1, y su parte hidrofóbica, llamada F_O; y se pueden distinguir tres partes principales: el núcleo catalítico, formado por las subunidades alfa y beta (α_3/β_3); el rotor, que incluye el anillo oligomérico de subunidades *c* embebido en la membrana (su estequiometría varía según el organismo) y las subunidades gamma, delta y epsilon ($\gamma/\delta/\varepsilon$); y el estator o brazo periférico, que incluye la subunidad OSCP (del sector F_1) y la subunidad *a* (del sector F_O, también llamada ATP6), el resto de las subunidades que lo conforman varían de organismo a organismo (Figura 4). La unión del brazo periférico con las subunidades OSCP y *a* definen su función de estator, es decir, contrarrestar la tendencia de rotación del núcleo catalítico que sucede en respuesta al movimiento del rotor (Walker y Dickson 2006).

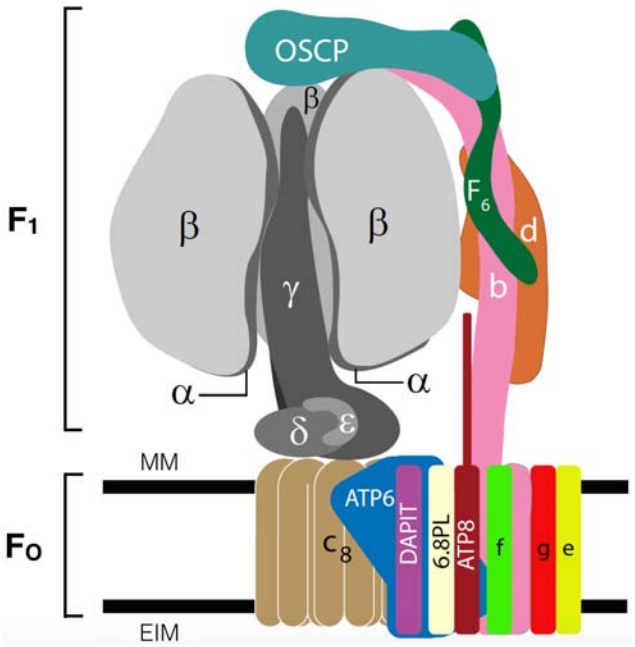

Figura 4. ATP sintasa mitocondrial. Representación de la F_1F_O ATP sintasa monomérica de humano en la que se indican la identidad y localización de sus subunidades. MM: matriz mitocondrial, EIM: espacio intermembranal. Figura modificada de He *et al*. 2018.

La síntesis del ATP sucede por medio de un mecanismo de catálisis rotatoria, propuesto por Paul Boyer en 1973 (Boyer P. *et al.* 1973), en el que los protones entran al complejo atravesando los canales formados por las subunidades *a* y *c*, fenómeno que provoca la rotación del anillo de subunidades *c* y, en consecuencia, de la subunidad γ, que se encuentra en contacto con éste y se extiende hacia adentro del núcleo catalítico. Tres movimientos de 120° de la subunidad γ inducen cambios conformacionales secuenciales en las tres subunidades catalíticas (β) que resultan en que dichas subunidades alternen sus afinidades por sustratos y productos, permitiendo así la unión de los sustratos (ADP y fosfato), la síntesis de ATP y su posterior liberación (Yasuda *et al*. 1998). De esta forma, funcionalmente la ATP sintasa es tripartita: i) un motor membranal que usa la energía del gradiente electroquímico para impulsar la rotación de subunidades, ii) un transmisor de energía, el rotor, que comunica el movimiento con las subunidades catalíticas (a una distancia de más de 100 Å) y iii) un catalizador que convierte la energía mecánica de la rotación a energía química de enlace (Senior *et al*. 2002).

La evidencia estructural de la traslocación de protones, una parte clave del funcionamiento de la enzima, se obtuvo recientemente a partir de estudios de criomicroscopía electrónica con la ATPasa de *Polytomella*. Éstos demostraron que la subunidad *a* tiene una topología particular en relación con la membrana y con el anillo de subunidades *c*, ya que presenta un conjunto de hélices integrales de membrana que forman dos horquillas, las cuales se acomodan paralelamente a la membrana (hélices casi horizontales) y parecen abrazar el anillo (Allegretti M. *et al*. 2015) (Figura 5A). En el modelo generado por Allegretti y colaboradores se observa que el arreglo de las subunidades *a* y *c* da lugar a dos medios canales con cavidades acuosas que definen el camino que siguen los protones al entrar al complejo (Figura 5B). La disposición de los medios canales, así como la conservación de los residuos clave de las subunidades *a* y *c*, se considera un atributo común a todas las ATPasas rotatorias, ya que se ha descrito en todas las estructuras generadas a la fecha (Zhou *et al*. 2015, Hahn *et al*. 2016, Schep *et al*. 2016, Sobti *et al*. 2016, Guo *et al*. 2017).

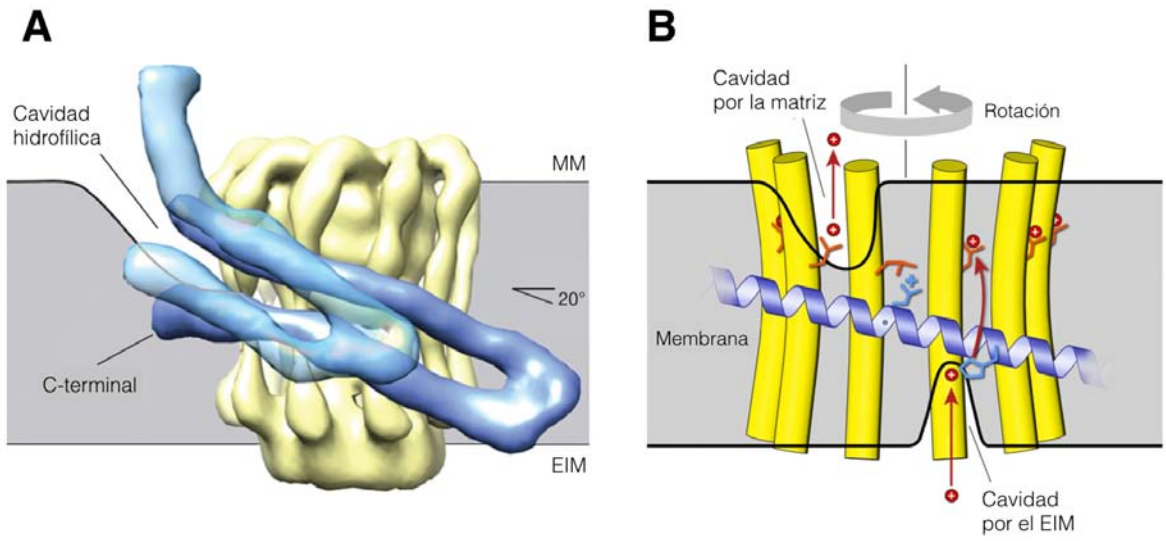

Figura 5. Traslocación de protones a través de las subunidades *a* y *c*. A. Mapa tridimensional de las subunidades *a* (azul) y el anillo de subunidades *c* (amarillo) de la ATPasa mitocondrial de *Polytomella*. MM: matriz mitocondrial, EIM: espacio intermembranal. Figura modificada de Allegretti *et al*. 2015. **B.** Modelo que explica el movimiento de los protones (en rojo): éstos llegan a un glutamato conservado en las subunidades *c*, a través de la cavidad hidrofílica del lado del espacio intermembranal, y compiten con una arginina altamente conservada en la subunidad *a* (en azul) para establecer la interacción H^+-cGlu. Cuando la subunidad *c* ha girado y se encuentra en la cavidad hidrofílica del lado de la matriz, se dice que el glutamato adopta una conformación abierta y el protón escapa hacia la matriz. Figura modificada de Kühlbrandt y Davies 2016.

Otra de las funciones de la ATPasa se refiere a la morfogénesis y el mantenimiento de las crestas mitocondriales. Como ya se mencionó la ATPasa se asocia en dímeros, la dimerización se da a través de las subunidades membranales del brazo periférico y está directamente relacionada con el plegamiento de la membrana interna que resulta en la formación de las crestas (Paumard *et al*. 2002, Dudkina *et al*. 2005, Fronzes *et al*. 2006, Davies *et al*. 2012, Mühleip *et al*. 2016). Estudios de simulaciones de dinámica molecular han demostrado que la conformación tubular de las crestas aumenta a medida que se incorporan dímeros de ATPasa (Davies *et al*. 2012, Mühleip *et al*. 2016), y que son éstos los que pliegan la membrana al asociarse en hileras (Davies *et al*. 2012) (Figura 6).

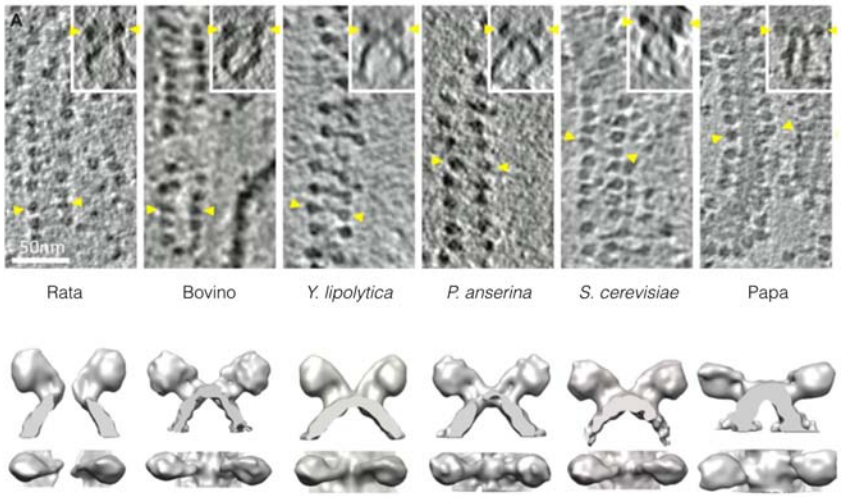

Figura 6. Hileras de dímeros de ATPasa en diferentes especies. En el panel de arriba se muestran cortes de tomografías de mitocondrias de distintas especies en los que se obervan claramente las hileras de dímeros de ATPasa; los triángulos amarillos señalan las cabezas F_1 de un dímero. En el panel de abajo se muestran las representaciones tridimensionales de los subtomogramas promediados. Figura modificada de Kühlbrandt 2015.

Recientemente, se ha propuesto que las subunidades membranales de los dímeros de ATPasa están implicadas en la formación del llamado poro de transición de la permeabilidad, relacionado con la generación de señales apoptóticas (Giorgio *et al*. 2013); sin embargo, esta área de estudio es controversial ya que desde un punto de vista estructural no es claro cómo el arreglo de la enzima permitiría la formación de dicho poro (Kühlbrandt 2015), además de que se ha demostrado que el poro persiste en ausencia de la subunidad *c* (He *et al*. 2017).

1.4 Las ATPasas rotatorias

Las ATPasas rotatorias son complejos enzimáticos oligoméricos presentes en las membranas celulares y organelares de organismos de los tres reinos de la vida, y funcionan como nanomotores para sintetizar o hidrolizar ATP (Müller y Grüber 2003) (Figura 7). Como se mencionó antes, la F-ATPasa mitocondrial pertenece a la familia de las ATPasas rotatorias y puede sintetizar o, en condiciones fisiológicas particulares, hidrolizar ATP (D'Alessandro y Melandri 2010). Las V-ATPasas, ATPasas vacuolares, reciben su nombre por haber sido purificadas de este organelo por primera vez, y funcionan como bombas de protones dependientes de la hidrólisis de ATP, por lo que también se les conoce como H^+-ATPasas. Se encuentran en membranas de vacuolas, endosomas, lisosomas y en las membranas plasmáticas de los eucariontes (Forgac 2007.). Las A-ATPasas, ATPasas de arqueas, pueden funcionar tanto para bombear protones como para sintetizar ATP. Una característica sobresaliente de las A-ATPasas es la variabilidad de tamaño del anillo de subunidades *c* y su capacidad de acoplar la unión de diferentes iones con la síntesis de ATP (Grüber *et al*. 2014).

Las V-ATPasas están relacionadas en cuanto a su estructura y mecanismo con las F-ATPasas, pero no son capaces de sintetizar ATP; y evolutivamente están más cercanas a las ATPasas de arqueas, que pueden funcionar tanto para bombear protones como para sintetizar ATP (Grüber *et al*. 2014). El común denominador de todas estas ATPasas es la capacidad de acoplar un dominio membranal translocador de protones con un dominio soluble que puede sintetizar o hidrolizar ATP; este acomplamiento y el correcto funcionamiento de la enzima es posible gracias a la presencia de la estructura que funciona como el estator de un motor, el llamado brazo periférico, cuya función principal es contrarrestar la tendencia de rotación del núcleo catalítico que sucede en respuesta al movimiento del rotor (Walker y Dickson 2006).

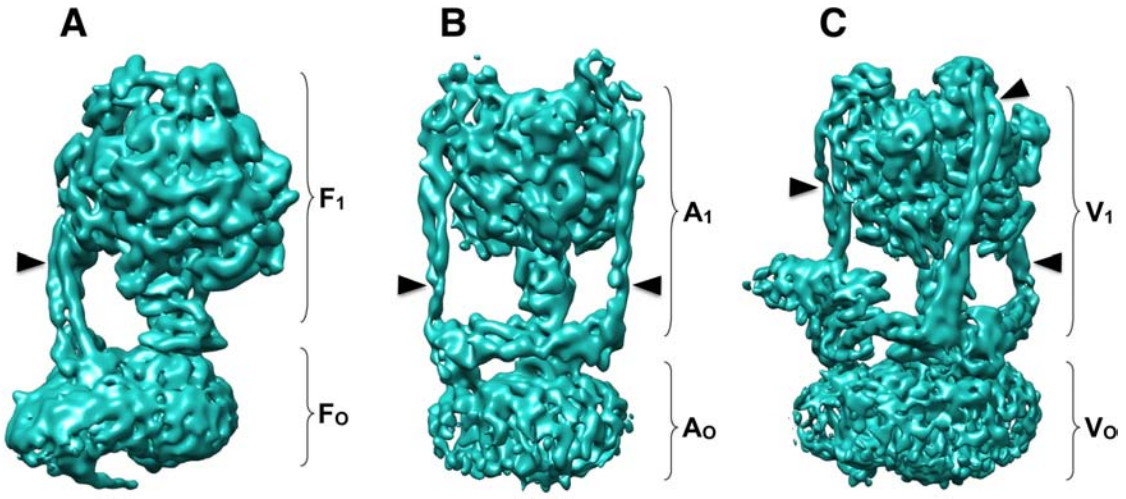

Figura 7. ATPasas rotatorias. A. Mapa tridimensional de la F-ATPasa de corazón de bovino generado a partir de imágenes de criomicroscopía electrónica (EMD 3164) (Zhou *et al*. 2015). **B.** Mapa tridimensional de la A-ATPasa de *Thermus thermophilus* generado a partir de imágenes de criomicroscopía electrónica (EMD 5335) (Schep *et al*. 2016). **C.** Mapa tridimensional de la V-ATPasa de *Saccharomyces cerevisiae* generado a partir de imágenes de criomicroscopía electrónica (EMD 6285) (Zhao *et al*. 2015). Los brazos periféricos están señalados con triángulos negros.

La hipótesis más aceptada acerca del origen de las ATPasas rotatorias postula que éstas evolucionaron de un ancestro común que después de cambios estructurales y funcionales dio lugar a las tres clases de enzimas. Inicialmente, se propuso que las ATPasas rotatorias han pasado por al menos dos transiciones en su historia evolutiva: la primera fue el paso de una bomba de protones progenitora a una ATP sintasa impulsada por protones; y la segunda fue el regreso a una bomba de protones (Cross *et al*. 1990). Posteriormente, se añadió una tercera transición de regreso a una ATP sintasa en la que, contrario a lo que se propone para las dos primeras, hubo una ganancia de función (Cross *et al*. 2004). Actualmente se considera que el último ancestro común universal (LUCA) era muy probablemente un organismo quimiosmótico con una ATP sintasa en su membrana (Mulkidjanian *et al*. 2007).

Las V-ATPasas están más relacionadas evolutivamente con las A-ATPasas, aunque las primeras no son capaces de sintetizar ATP en condiciones fisiológicas, por lo que se puede considerar que las A-ATPasas son más parecidas estructural y mecanísticamente a las F-ATPasas (Forgac 2007). Dado su origen común, las subunidades catalíticas y las del canal translocador de protones comparten un 50% de identidad, entre A y V ATPasas, y 25% entre A y F ATPasas (Müller y

Grüber 2003); por el contrario, las subunidades del brazo periférico están mucho menos conservadas, varían según el organismo, y no se ha encontrado identidad significativa entre ellas (Muench *et al*. 2011).

Estructuralmente, las tres clases de ATPasas están diseñadas de la misma manera: un dominio membranal (conocido clásicamente como F_O, V_O, A_O; R_O para referirse a este sector en general) que incluye al canal translocador de protones; y un dominio soluble (conocido clásicamente como F_1, V_1, A_1; R_1 para referirse a este sector en general) que incluye el núcleo catalítico donde sucede la síntesis o hidrólisis del ATP, el rotor central que comunica la actividad del canal translocador de protones con el núcleo catalítico; y uno o más brazos periféricos. El número de brazos periféricos se considera una característica de clasificación de las ATPasas rotatorias (Stewart *et al*. 2014), de las enzimas descritas hasta ahora: las F-ATPasas tienen uno (Figura 7A), las A-ATPasas tienen dos (Figura 7B) y las V-ATPasas tienen tres (Figura 7C); su función principal es la misma en los tres tipos de enzimas, sin embargo su composición y topología varían.

1.5 El brazo periférico

Las subunidades que componen tanto al núcleo catalítico como al rotor de las F-ATPasas se encuentran conservadas en todos los organismos; sin embargo, el brazo periférico tiene una composición polipeptídica y arreglo variables. La ATPasa bacteriana, la más sencilla, tiene un brazo periférico formado por un dímero de subunidades *b*, homólogas a la subunidad *b* de eucariontes, y la subunidad delta (δ), homóloga a la subunidad OSCP (Figura 8A). El brazo periférico de la ATPasa de *E. coli* se ha dividido en cuatro dominios: el dominio amino terminal, que atraviesa la membrana e interacciona con la subunidad *a* (Dmitriev *et al*. 1999, Stalz *et al*. 2003, Sobti *et al*. 2016); el dominio de unión entre ambas subunidades, el dominio de dimerización y el dominio carboxilo terminal, a través del que interacciona con la subunidad δ (OSCP en enzimas de organismos eucariontes), la última localizada en el ápice de la enzima en contacto con la subunidad α (Rubinstein *et al*. 2002, Carbajo *et al*. 2007, Sobti *et al*. 2016) (Figura 8B). En organismos eucariontes como bovino y levadura el brazo periférico está formado

por las subunidades *b*, *d*, F6, A6L, *e*, *f*, *g* y OSCP (ésta es la nomenclatura para las subunidades de la enzima de bovino, sus homólogos en levadura son Su4, *d*, *h*, Su8, *e*, *f*, *g*, OSCP). En todos los organismos en los que se ha descrito la subunidad *b* tiene un cruce transmembranal, por el cual contacta a la subunidad *a*, y un dominio de interacción con OSCP.

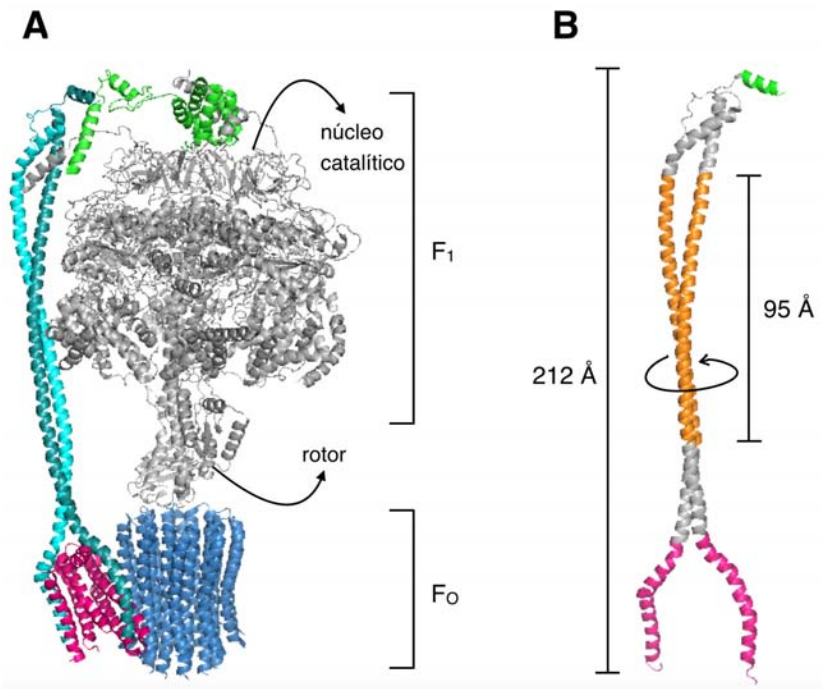

Figura 8. El brazo periférico de la F-ATPasa de *E. coli*. A. Se resaltan la subunidad δ (verde), el dímero b_2 (cian), la subunidad *a* (rosa) y el anillo de subunidades *c* (azul) en la F-ATPasa de *E. coli*. **B.** Se muestra el dímero b_2 y se resaltan sus dominios de interacción con las subunidades δ (verde) y *a* (rosa). Se indican el dominio de dimerización (naranja) y el enrollamiento dextrógiro de hélices entrecruzadas de las subunidades *b*. El modelo utilizado en A y B corresponde a los datos depositados con el PDB 5T4O (Sobti *et al.* 2016).

Actualmente existen estructuras de alta resolución de las tres clases de ATPasas rotatorias (Lau *et al*. 2011, Morales-Ríos *et al*. 2015, Zhao *et al*. 2015, Hahn *et al*. 2016) y de sus brazos periféricos (Dickson *et al*. 2006, Stewart *et al*. 2012, Oot *et al*. 2012), con las que se ha demostrado que, pese a la falta de homología de secuencia, la arquitectura general del brazo periférico es muy parecida en todas las enzimas (Figura 9). Éste se encuentra formado por proteínas alargadas en conformación de hélices alfa que interaccionan entre sí a través de hélices entrecruzadas (*coiled coils*) (Stewart *et al.* 2013). Las interacciones por hélices entrecruzadas resultan de la presencia motivos repetidos dentro de la secuencia de la proteína, cuando el enrollamiento es dextrógiro estos motivos se conocen como *hendecad repeats*, y son once residuos de composición

abcdefghijk, en donde *adeh* son residuos hidrofóbicos. El giro dextrógiro también puede darse por motivos *quindecad repeats*, 15 residuos *abcdefghijklmno*, en donde *adehl* son residuos hidrofóbicos (Lee *et al*. 2010). Los patrones *hendecad repeats* fueron descritos por primera vez en las subunidades del brazo periférico de la F-ATPasa de *Escherichia coli*, junto con la predicción de un giro dextrógiro de las hélices (Del Rizzo *et al*. 2002).

Las proteínas responsables de formar el brazo periférico de las ATPasas rotatorias deben recorrer una distancia de más de 100 Å, desde la membrana hasta el ápice de la enzima, lo cual se facilita al adoptar la conformación de hélices entrecruzadas alargadas, que es el caso de los brazos periféricos de todas las enzimas reportadas hasta la fecha (Stewart *et al*. 2013) (Figura 9); las interacciones que se han encontrado entre estas proteínas y el resto de las subunidades de la enzima confirman su papel como estructura de unión de los dos dominios, R_O y R_1.

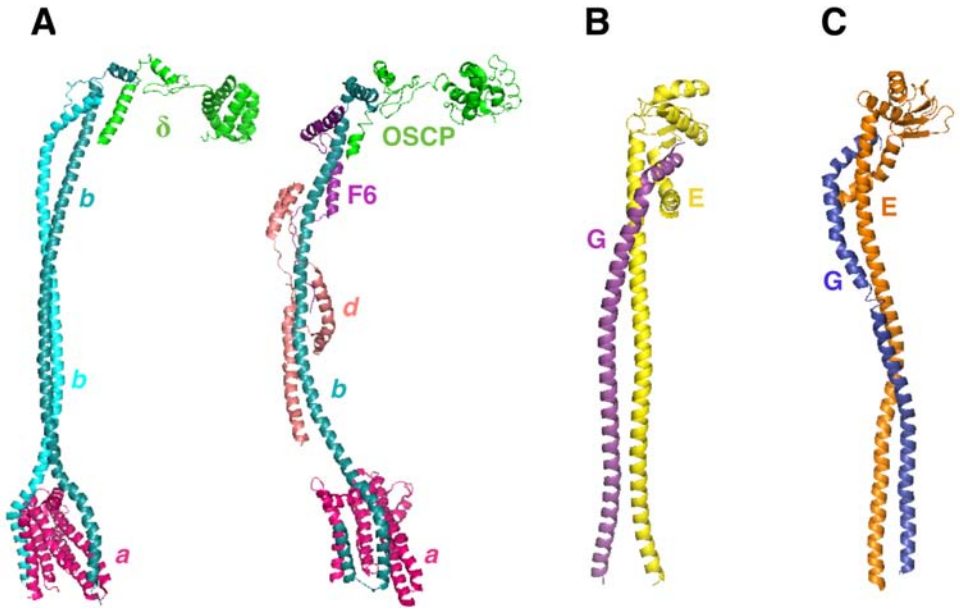

Figura 9. El brazo periférico de las ATPasas rotatorias. A. Modelos estructurales del brazo periférico de la F-ATPasa de *Escherichia coli* (izquierda), modelo generado a partir de los datos depositados con el PDB 54TO de Sobti et al. 2016; y *Bos taurus* (derecha), modelo generado a partir de los datos depositados con el PDB 5FIL de Zhou et al. 2015. **B.** Modelo estructural de uno de los brazos periféricos de la A-ATPasa de *Thermus thermophilus*, generado a partir de los datos depositados con el PDB 3V6I de Stewart et al. 2012. **C.** Modelo estructural de uno de los brazos periféricos de la V-ATPasa de *Saccharomyces cerevisiae*, generado a partir de los datos depositados con el PDB 3J9V de Zhao et al. 2015.

Mientras ese es el caso de todas las enzimas para las que se tienen estructuras tridimensionales, existen ATPasas para las cuales no hay estudios de alta resolución, pero la evidencia disponible indica que la estructura de sus brazos periféricos es notablemente distinta a la de aquéllos de las enzimas de mamíferos, levaduras y bacterias; y que las subunidades que lo componen no tienen homología con las de los organismos más estudiados. Recientemente se propuso una nueva clasificación de las F-ATPasas mitocondriales con la que los dímeros se han separado en dos grupos: dímeros tipo metazoarios, que incluyen la enzima de mamíferos, levaduras y bacterias; y dímeros tipo protozoarios, que incluyen la enzima de organismos como *Euglena gracilis* (Yadav *et al*. 2017), *Paramecium tetraurelia* (Mühleip *et al*. 2016), *Tetrahymena thermophila* (Balabaskaran-Nina *et al.* 2009), y parásitos como *Trypanosoma brucei* (Zíková *et al*. 2009). La principal diferencia entre estos dos tipos de dímeros es la diversidad estructural del brazo periférico y de la interfase de los monómeros (Mühleip *et al*. 2016) (Figura 10). Otro ejemplo de dímero tipo protozoario es la ATPasa de las algas clorofíceas, grupo al que pertenece *Polytomella* sp.

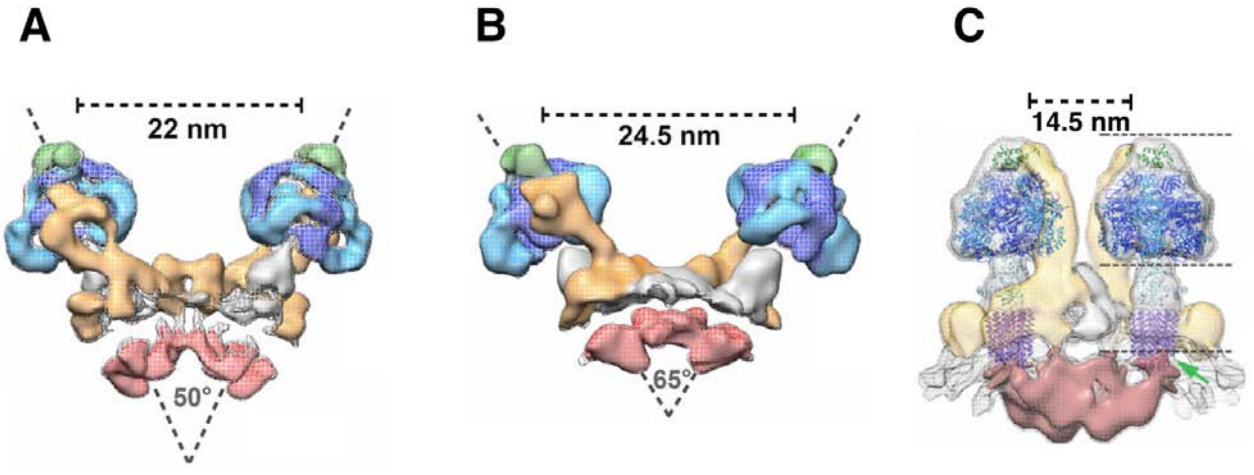

Figura 10. Dímeros de ATPasa tipo protozoario. Modelos tridimensionales generados por criotomografía electrónica *in situ* de membranas mitocondriales de **A.** *Euglena gracilis* **B.** *Trypanosoma brucei* y **C.** *Paramecium tetraurelia*, que muestran la disposición de los dímeros de ATPasa en la membrana. En A, B y C se indican las densidades correspondientes al núcleo catalítico en azules, a la subunidad OSCP en verde, al brazo periférico en naranja, al rotor en gris y a la región intracrestal en rojo. Figura modificada de Mühleip *et al*. 2017 (A y B); y de Mühleip *et al*. 2016 (C).

1.6 La ATP sintasa mitocondrial de *Polytomella* sp.

Polytomella sp. (Figura 11A) es un alga incolora flagelada, perteneciente al linaje Chlorophyta de algas verdes, y dentro de éste, al grupo de las algas clorofíceas. Es un organismo unicelular de vida libre que habita generalmente en ambientes acuáticos, puede utilizar ácidos orgánicos, alcoholes y polisacáridos como fuentes de carbono (De la Cruz y Gittleson 1981) y presenta un genoma mitocondrial muy reducido (Smith y Lee 2011). Existen varias algas incoloras que se consideran equivalentes no fotosintéticos de algas verdes debido a que comparten características morfológicas y reproductivas, este es el caso de *Polytomella* sp. y *Chlamydomonas reinhardtii*. La relación evolutiva entre las algas incoloras y las algas verdes se ha establecido por medio de análisis filogenéticos de secuencias ribosomales, del genoma mitocondrial o del genoma plastídico remanente (van Lis *et al*. 2005).

La caracterización bioquímica de la ATP sintasa mitocondrial de las algas clorofíceas se ha llevado a cabo utilizando como modelos de estudio a *C. reinhardtii*, alga verde modelo por excelencia, y a *Polytomella* sp., incluida en el linaje de algas verdes pero que perdió su maquinaria fotosintética (Vázquez-Acevedo *et al*. 2016). La ATP sintasa mitocondrial de *Polytomella* tiene varias características que la hacen diferente de la enzima de otros organismos, algunas de éstas se describen a continuación.

Las subunidades catalíticas de las enzimas de *C. reinhardtii* y *Polytomella* sp. presentan unas extensiones en su extremo carboxilo terminal (de 18 aminoácidos en la subunidad α y de 70 aminoácidos en la subunidad β) que no se encuentran en otros organismos (Atteia *et al*. 1997). Estas extensiones se han modelado sobre la estructura cristalográfica del sector F_1 de la enzima de bovino como una forma de analizar sus posibles funciones: las extensiones de la subunidad α podrían mantener interacción con algún componente del brazo periférico, y las de la subunidad β, dada su localización y por similitud de secuencia, podrían actuar como inhibidores de la F_1-ATPasa de *Polytomella* (Vázquez-Acevedo *et al*. 2016).

Por estudios previos en el laboratorio, se sabe que al solubilizar mitocondrias de *C. reinhardtii* o de *Polytomella* sp. con el detergente lauril maltósido, la migración del complejo V en un gel azul nativo corresponde a la de un dímero estable de 1600 kDa (Vázquez-Acevedo *et al.* 2006), y resistente a detergente, lo cual contrasta con el comportamiento de la enzima de *Bos taurus*, que en las mismas condiciones se disocia y migra como un monómero de aproximadamente 750 kDa (van Lis *et al.* 2003) (Figuras 11B y 11C); este fenómeno se reproduce en las enzimas de hongos y plantas superiores (van Lis *et al.* 2007).

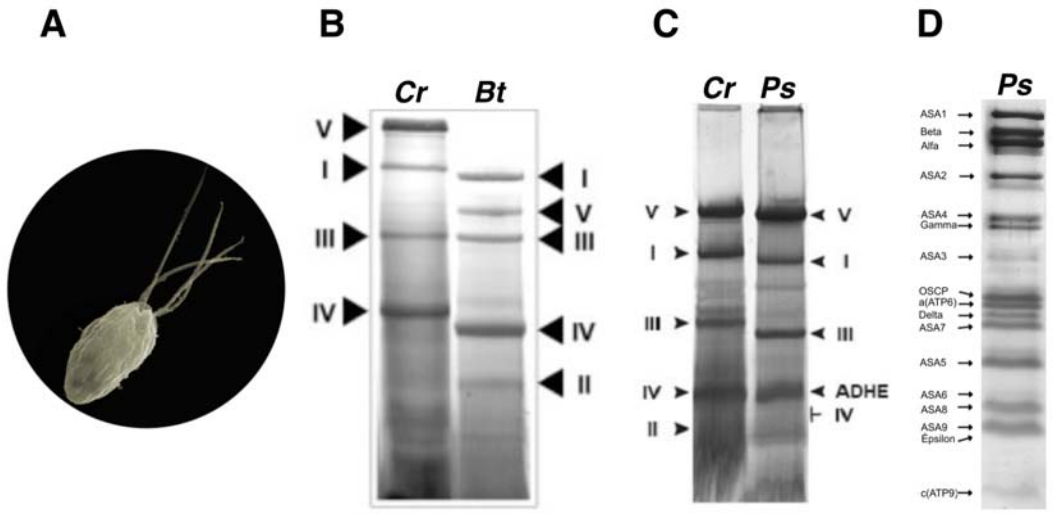

Figura 11. ATP sintasa mitocondrial de *Polytomella* sp. A. *Polytomella* sp. Imagen tomada de: http:// www.arrogantgenome.com/a-plastid-without-a-genome/ **B.** Gel nativo BN-PAGE en el que se muestra el patrón electroforético de mitocondrias de *C. reinhardtii* (Cr) y *Bos taurus* (Bt) solubilizadas con lauril maltósido. Se señalan los complejos respiratorios I, III, IV, y se observa la diferencia en la migración de la ATPasa (complejo V). Figura tomada de van Lis *et al*. 2003. **C.** Gel nativo BN-PAGE en el que se muestra el patrón electroforético de mitocondrias de *C. reinhardtii* (Cr) y *Polytomella* sp. (Ps) solubilizadas con lauril maltósido. Se señalan los complejos respiratorios I, III, IV, la aldehído deshidrogenasa (ADHE) y se muestra la migración del complejo V dimérico en ambas algas. Figura tomada de van Lis *et al*. 2005. **D.** Gel Tricina SDS-PAGE en el que se muestra el patrón electroforético de todas las subunidades que componen la ATPasa de *Polytomella* sp.

La asociación de dímeros de ATPasa en hileras a lo largo de las crestas mitocondriales es una característica presente y aumentada en las mitocondrias de *Polytomella*, como demuestran estudios de criotomografía electrónica con los que se observa que casi todas las crestas en las mitocondrias de esta alga tienen una conformación tubular y están densamente pobladas de dímeros de ATPasa (Dudkina *et al*. 2006 y 2010) (Figura 12). En relación con dicha evidencia, recientemente se encontró que la ATPasa de *Polytomella* se puede aislar en dos formas estables, dimérica y tetramérica, en presencia de lauril maltósido. (Miranda-Astudillo *et al*. 2018). Por el

contrario, las enzimas de levadura y mamífero sólo se mantienen en su forma dimérica en presencia del detergente suave digitonina y se disocian en monómeros al ser tratadas con lauril maltósido. Estas observaciones confirman la naturaleza de la ATPasa de *Polytomella* como un dímero altamente estable y resistente, lo cual, sumado a su tendencia a formar especies oligoméricas, se refleja en su morfología mitocondrial.

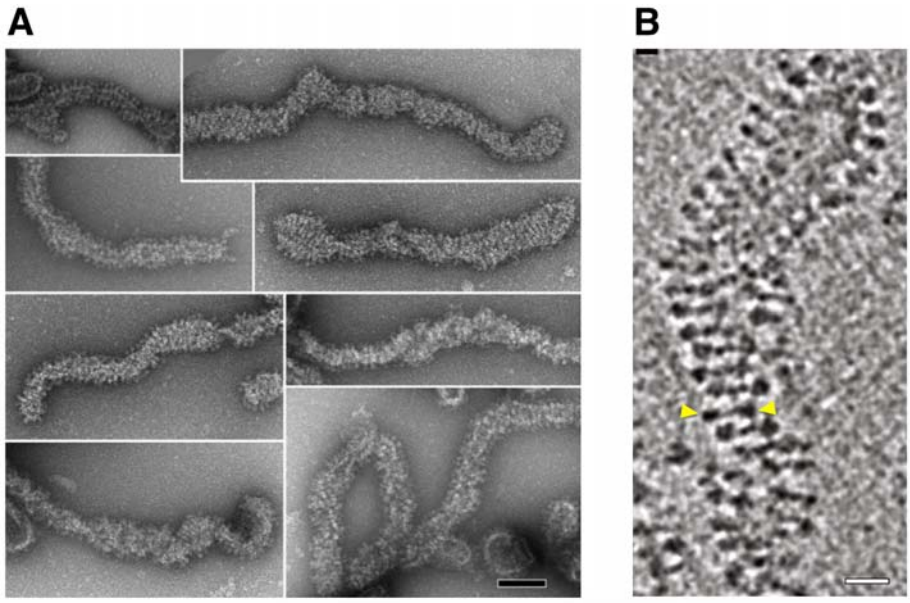

Figura 12. Hileras de dímeros de ATPasa en las crestas mitocondriales de *Polytomella* sp. A. Tinción negativa de fragmentos de crestas tubulares de *Polytomella*. Las densidades que protruyen corresponden a las cabezas F_1 de los dímeros de ATPasa. La barra representa 100 nm. Imagen tomada de Dudkina *et al*. 2006. **B.** Una cresta tubular completa en cuya parte inferior se observa claramente una hilera de dímeros de ATPasa, los triángulos amarillos señalan las cabezas F_1 de un dímero. La barra representa 20 nm. Imagen modificada de Dudkina *et al*. 2010.

El análisis de la composición polipeptídica de la ATP sintasa de *Polytomella* sp. reveló que conserva las subunidades catalíticas (α_3/β_3) y las del rotor ($\gamma/\delta/\varepsilon/c$), así como las subunidades *a* y OSCP; pero no contiene ninguna que tenga homología con las subunidades que forman el brazo periférico en mamíferos, levaduras o bacterias. En su lugar, presenta nueve subunidades llamadas subunidades Asa (del inglés, *ATP synthase associated*), Asa1 a Asa9 (Vázquez-Acevedo *et al.* 2006) (Figura 11D). Algunas de estas subunidades forman el brazo periférico y le confieren alta estabilidad a la enzima (Miranda-Astudillo *et al.* 2014) y otras están involucradas en su dimerización (Cano-Estrada *et al*. 2010, Sánchez-Vázquez *et al*. 2017). En la Tabla 1 se muestran algunas características de las subunidades Asa. De manera atípica, todas las subunidades de la

ATP sintasa de *Polytomella* están codificadas en el genoma nuclear, por lo que deben importarse a la mitocondria para ensamblar el complejo, y las subunidades Asa son exclusivas de las ATP sintasas de las algas clorofíceas, ya que no se encuentran en grupos filogenéticamente cercanos, como son las algas prasinofíceas, trebuxofíceas y ulvofíceas (Vázquez-Acevedo *et al*. 2006).

El modelo de la ATP sintasa de *Polytomella* sp. obtenido a partir de imágenes de criomicroscopía electrónica a una resolución promedio de 7.0 Å (Allegretti *et al.* 2015) (Figura 13A), demostró de manera indiscutible que su brazo periférico es una estructura mucho más robusta que la encontrada en mamíferos (Zhou *et al*. 2015), levaduras (Guo *et al*. 2017) y bacterias (Sobti *et al*. 2016), así como aquella encontrada en las ATPasas tipo A y V (Figura 13B y 13C).

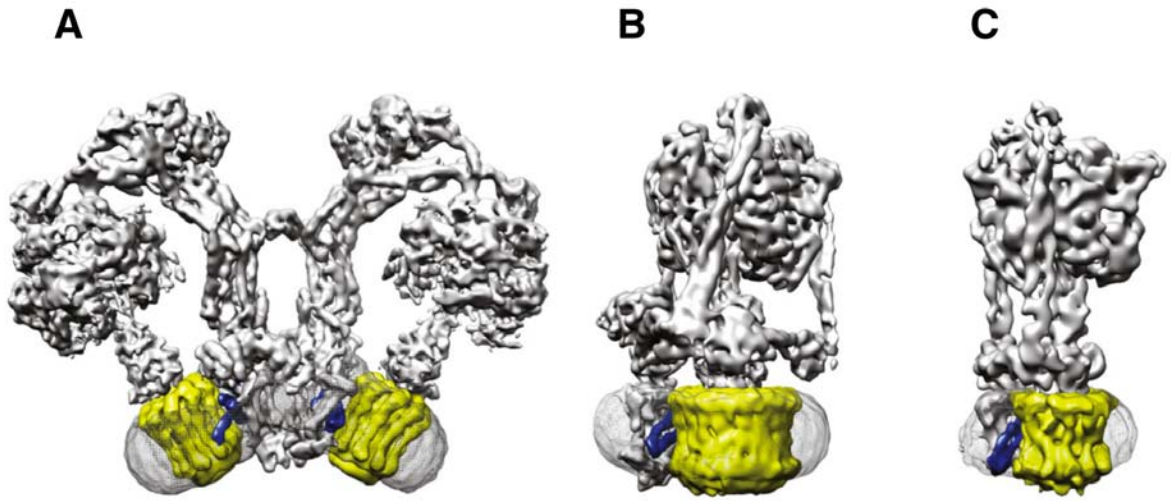

Figura 13. El brazo periférico de la ATPasa mitocondrial de *Polytomella* sp. Estructuras tridimensionales de ATPasas rotatorias, generadas a partir de imágenes de criomicroscopía electrónica, de **A.** *Polytomella* sp. (F-ATPasa), **B.** *Saccharomyces cerevisiae* (V-ATPasa) y **C.** *Thermus thermophilus* (A-ATPasa) con las que se observa claramente la diferencia en los brazos periféricos. En amarillo se muestra el anillo de subunidades *c* y en azul la subunidad *a*. Imagen tomada de Kühlbrandt y Davies 2016.

Nombre	Peso Molecular (kDa)	Cruces Transmembranales	Función
Asa1	66.1	-	Formación del brazo
Asa2	45.3	-	Formación del brazo
Asa3	32.9	-	¿?
Asa4	31.2	-	Formación del brazo
Asa5	13.9	-	¿?
Asa6	13.1	2	Dimerización
Asa7	19.0	-	Formación del brazo
Asa8	9.9	1	Dimerización
Asa9	11.0	1	Dimerización

Tabla 1. Las subunidades Asa de la ATPasa mitocondrial de *Polytomella* sp. Se indica el peso molecular, la presencia o ausencia de crucas transmembranales y la función de cada subunidad. Aquellas sin una función asignada se indican con signos de interrogación.

2. Antecedentes

El brazo periférico es una estructura común en la familia de las ATP sintasas rotatorias; sin embargo, es de las partes menos estudiadas de la enzima, ya que las subunidades que lo componen están poco conservadas. La mayoría de los datos que se tienen acerca de la estructura y la función del brazo periférico se ha obtenido de estudios sobre la enzima de corazón de bovino o de *E. coli* (Walker y Dickson 2006); sin embargo esta información no puede aplicarse a la enzima de las algas clorofíceas, por lo que es de nuestro interés dilucidar la topología de las subunidades Asa en la enzima de *Polytomella* sp.

En el laboratorio se han estudiado las interacciones de las subunidades Asa siguiendo diversas aproximaciones experimentales; una de ellas es el estudio de interacciones *in vitro* sobreexpresando y purificando las subunidades recombinantes. De esta forma hemos encontrado, por ejemplo, que las subunidades Asa4 y Asa7 interaccionan y que esta interacción está mediada por los extremos carboxilos de ambas proteínas; que a su vez, junto con Asa2, forman un subcomplejo estable (Miranda-Astudillo *et al.* 2014). Otra aproximación para el estudio de la topología de estas subunidades ha sido el análisis de proximidad con agentes entrecruzadores. Por medio de estos experimentos se han obtenido las interacciones típicas de una ATPasa mitocondrial, como son α + β, α + OSCP y γ + δ; y algunas de las interacciones que existen entre subunidades Asa extrínsecas a la membrana, como Asa2 + Asa4 y Asa2 + Asa7 (Cano-Estrada *et al.* 2010), y entre aquéllas de las que se predicen cruces transmembranales, Asa6 + Asa8 y Asa8 + Asa9 (Sánchez-Vázquez et al. 2017). La estequiometría de las subunidades Asa se ha estimado con el marcaje de residuos de cisteína con agentes fluorescentes, y los datos obtenidos indican una estequiometría 1:1:1 para las subunidades Asa3, Asa4 y Asa5 con respecto a la subunidad γ (Cano-Estrada *et al.* 2010). Por su parte, se determinó que el subcomplejo recombinante de las subunidades Asa2, Asa4 y Asa7 tiene igualmente una estequiometría 1:1:1 (Miranda-Astudillo *et al*. 2014).

La subunidad Asa1 es la más grande de las subunidades Asa (66.1 kDa) y análisis *in silico* predicen que alrededor del 60% de la proteína adopta una estructura helicoidal, lo que es consistente con la naturaleza de las proteínas que forman el brazo periférico en otras ATPasas. Su localización en la ATP sintasa de *Polytomella* ha sido controversial: por un lado, por medio de la disociación de la enzima con calor a diferentes tiempos, se encontró la formación de un subcomplejo transiente Asa1/Asa3/Asa5/Asa8/*a*/*c* (Vázquez-Acevedo *et al.* 2006), lo cual indicaría la presencia de Asa1 cerca de subunidades membranales (la subunidad *a* tiene 4-5 hélices embebidas en la membrana, la subunidad *c* tiene dos segmentos transmembranales y la subunidad Asa8 tiene un segmento transmembranal predicho) (Figura 14A). Por otro lado, se ha propuesto que la subunidad Asa1 se encuentra cerca del núcleo catalítico, ya que estudios de microscopía electrónica demuestran una región con densidad electrónica considerable en esa región de la enzima (van Lis *et al*. 2007) (Figura 14B).

Como parte de este trabajo obtuvimos evidencia que indica la interacción entre Asa1 y el extremo carboxilo de la subunidad OSCP (Colina-Tenorio *et al*. 2016) (Figura 15A), esta última es la subunidad encargada de unir el brazo periférico con el núcleo catalítico, ya que contacta directamente a la subunidad α, tanto en la enzima de *Polytomella* (Cano-Estrada *et al*. 2010), como en la de mamíferos (Carbajo *et al.* 2007), levaduras (Rubinstein *et al*. 2002) y bacterias (Weber *et al*. 2002). También se reprodujo el subcomplejo Asa1/Asa3/Asa5/Asa8/*a*/*c*, anteriormente generado por disociación con calor, al disociar la enzima con una concetración alta (3%) del detergente lauril maltósido (Colina-Tenorio *et al*. 2016) (Figura 15B).

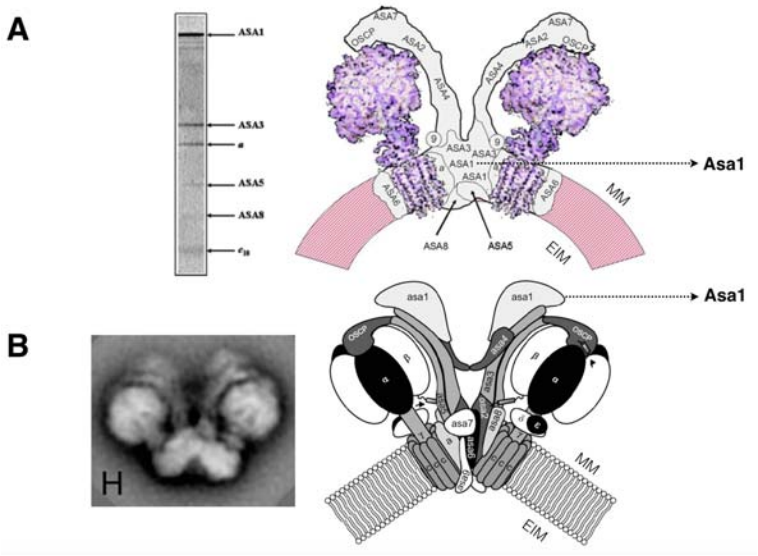

Figura 14. Ubicaciones propuestas de la subunidad Asa1 en la ATPasa mitocondrial de *Polytomella* sp. A. Gel Tricina SDS-PAGE teñido con azul de Coomassie en el que se resuelve el subcomplejo Asa1-Asa3-Asa5-Asa8-*a*-*c*; a la derecha se muestra el modelo propuesto con la subunidad Asa1 ubicada en la región membranal de la enzima. Figuras modificadas de Vázquez-Acevedo *et al*. 2006. **B.** Micrografía electrónica de la ATPasa dimérica de *Polytomella* sp. en la que se observa una densidad electrónica importante en el ápice de la enzima; a la derecha se muestra el modelo propuesto con la subunidad Asa1 ocupando ese lugar. Figuras modificadas de van Lis *et al*. 2007. MM: matriz mitocondrial, EIM: espacio intermembranal.

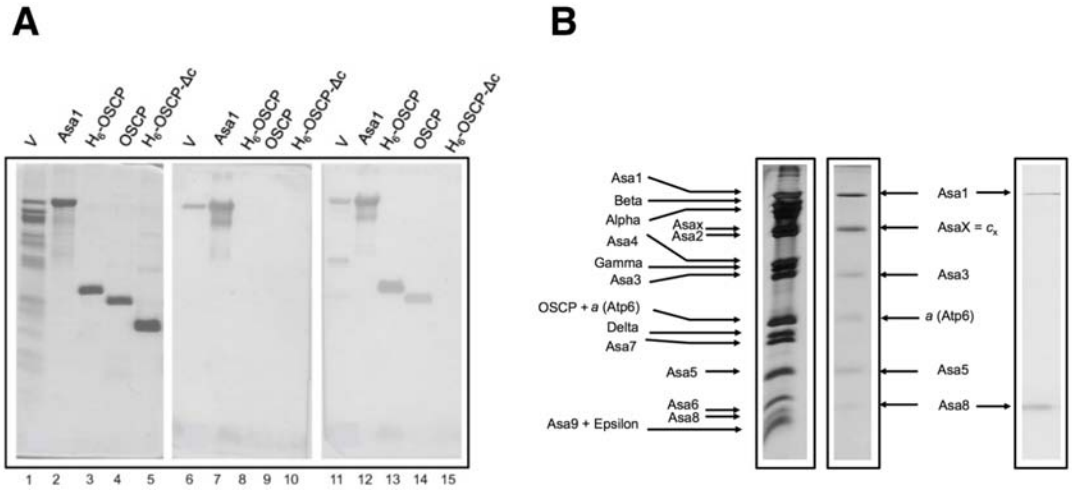

Figura 15. Interacción Asa1-OSCP y subcomplejo Asa1-Asa3-Asa5-Asa8-*a*-*c*. A. Interacción Asa1-OSCP observada por Far Western Blot: Gel Tricina SDS-PAGE teñido con azul de Coomassie en el que se muestran las subunidades utilizadas (1 a 5). Membrana revelada con anticuerpos específicos anti-Asa1 en la que se ve el reconocimiento de la subunidad Asa1 en la ATPasa purificada de *Polytomella* (V) y de la subunidad recombinante (6 a 10). Membrana incubada con la subunidad Asa1 y revelada con anticuerpos específicos anti-Asa1 en la que se ve señal correspondiente a las subunidades OSCP de la ATPasa (V), y las recombinantes con (H_6-OSCP) y sin etiqueta de histidinas (OSCP). No se observa señal en la subunidad OSCP trunca (H_6-OSCP-Δc) (11 a 15). **B.** Geles Tricina SDS-PAGE que muestran el subcomplejo obtenido por disociación de la enzima con detergente, y la inmunodetección de las subunidades Asa1 y Asa8. Figuras tomadas de Colina-Tenorio *et al*. 2016.

La interacción Asa1-OSCP apoya la idea de un modelo en el que parte de Asa1 se encuentra cerca del sector catalítico de la enzima, y el subcomplejo Asa1/Asa3/Asa5/Asa8/*a*/*c* sugiere que además podría mantener otras interacciones con una o más subunidades Asa. Dados los datos preliminares con los que contamos, es de nuestro interés explorar el resto de las interacciones que mantiene esta subunidad con las demás subunidades Asa del complejo, ya que la información obtenida hasta ahora sugiere un papel medular de Asa1 en la formación del brazo periférico de la ATP sintasa de *Polytomella*.

3. Objetivos

3.1 Objetivo general del trabajo

Establecer la topología de la subunidad Asa1 en relación con el resto de las subunidades del brazo periférico de la ATP sintasa mitocondrial de *Polytomella* sp.

3.2 Objetivos particulares

1. Clonar, sobreexpresar y purificar las subunidades recombinantes correspondientes a las subunidades: Asa1 sin etiqueta de histidinas, Asa1 en versiones truncas y Asa3^{6H}.
2. Definir la región de Asa1 (amino o carboxilo) que interacciona con OSCP.
3. Realizar ensayos de interacción de Asa1 con las demás subunidades Asa recombinantes.
4. Reconstituir una sección del brazo periférico de la ATPasa de *Polytomella* a partir de las subunidades recombinantes obtenidas.
5. Intentar obtener una estructura cristalográfica del brazo reconstituido.
6. Intentar obtener una estructura cristalográfica de la ATPasa íntegra de *Polytomella*.

4. Estrategia experimental

Los experimentos realizados en este trabajo se basaron en el uso de subunidades Asa recombinantes, para lo cual se amplificaron y clonaron los genes de interés en un vector de sobreexpresión, para posteriormente purificar las proteínas (algunas por primera vez en este trabajo, otras siguiendo los protocolos obtenidos anteriormente). Con las subunidades purificadas se llevaron a cabo ensayos de interacción (inmunorréplicas tipo Far Western Blot y ensayos de copurificación). También se trabajó con muestras de cuerpos de inclusión enriquecidos con las proteínas de interés durante los ensayos de reconstitución de subcomplejos. Finalmente se exploraron condiciones experimentales para la obtención de muestras que pudieran utilizarse para iniciar pruebas de cristalización. Los pasos seguidos en la realización de este trabajo se muestran en el siguiente esquema:

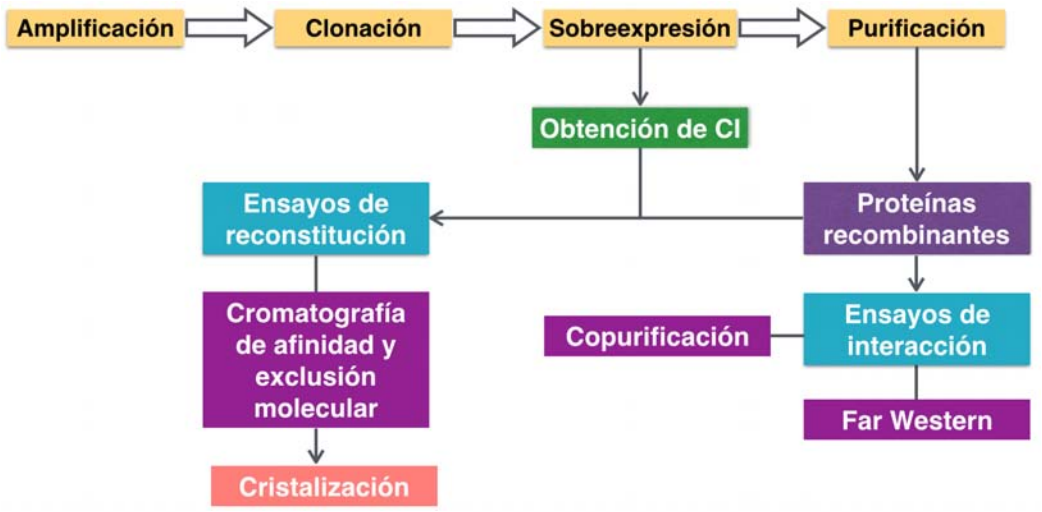

5. Metodologías

5.1 Amplificación de cDNAs y clonación en un vector de sobreexpresión

Los cDNAs correspondientes a la subunidad Asa1ΔC (residuos 23 a 389) y a la subunidad Asa3 se amplificaron a partir de una genoteca de cDNA de *Polytomella* utilizando oligonucleótidos específicos para obtener las subunidades maduras:

Para Asa1ΔC:

5’ GCGGCATGCGCTAGCTACCTTGCCCCCCTCCGCTCTGAT 3’

5’ GCGGCCGCTTAAGTGTACCTGTGCTCGGTAAT 3’

Para Asa3:

5’ CGC CATATG TCCTCTGGTCCTTCCCAGAACCTT 3’

5’ CGCGGATCCTTAATGACCATGGGCACCTTC 3’

El producto de amplificación de Asa1ΔC se clonó en el vector pET28a utilizando los sitios de restricción NheI y NotI; y el producto de amplificación de Asa3 se clonó en el mismo vector con los sitios de restricción NdeI y BamHI. Con el vector pET28a se puede añadir una etiqueta de histidinas (6His) en el extremo amino terminal de las proteínas, por medio de la cual se pueden purificar al usar una matriz de níquel. Los genes correspondientes a las subunidades Asa1, Asa2, Asa4, Asa7, Asa8 y OSCP fueron amplificados y clonados anteriormente, y las subunidades recombinantes correspondientes fueron purificadas como se describe en Cano-Estrada et al. 2010, Miranda-Astudillo et al. 2014 y Colina-Tenorio et al. 2016.

5.2 Sobreexpresión de las proteínas recombinantes en *Escherichia coli*

Las construcciones obtenidas (pET28a-Asa1ΔC y pET28a-Asa3) se transformaron por medio de choque térmico (42 °C por 2 min) en células competentes de *E. coli* de la cepa BL21 Codon Plus (DE3) RIL. Se seleccionaron colonias en medio LB adicionado con ampicilina (50 µg/mL) y las

pruebas de sobreexpresión de las proteínas se realizaron con cultivos de 30 mL de medio LB adicionados con ampicilina (50 µg/mL), crecidos a 37 °C con agitación e inducidos para llegar a una concentración final de 0.1 mM de IPTG (isopropil-β-D-1-tiogalactopiranósido) por 3 y 6 h.

5.3 Obtención, lavado y solubilización de cuerpos de inclusión enriquecidos con las proteínas de interés

Para todas las subunidades Asa utilizadas, partiendo de 1 L (proteínas sobreexpresadas a partir del vector pET28a, con etiqueta de histidinas) o 500 mL (proteínas sobreexpresadas a partir del vector pET3a, sin etiqueta de histidinas) de cultivo inducido, se obtuvo una pastilla celular que fue resuspendida en 30 mL de amortiguador de rompimiento (Anexo 2 inciso D) para llevar a cabo el rompimiento de las células por sonicación (en intervalos de 5 min a 5 Watts de potencia en pulsos de 50% por 30 minutos). La muestra obtenida se centrifugó a 12 000 rpm (en un rotor JA 25.50) por 10 min para obtener la pastilla de cuerpos de inclusión (CI). Esta pastilla fue tratada con lavados alternados con amortiguador de lavado de CI (Anexo 2 inciso D) y agua; las pastillas obtenidas después del último lavado con agua se consideran cuerpos de inclusión lavados. Para solubilizar los cuerpos de inclusión, las pastillas fueron resuspendidas en amortiguador de solubilización de CI (Anexo 2 inciso D) y dejadas en agitación por 12 h a 4 °C. Finalmente las muestras se centrifugaron a 12 000 rpm (en un rotor JA 25.50) por 10 min para eliminar el material no disuelto.

5.4 Purificación de las proteínas recombinantes: Asa1, Asa1ΔC^{6H}, Asa3^{6H} y Asa8^{6H}

La subunidad Asa1 sin etiqueta de histidinas se purificó por medio de cromatografía de intercambio iónico utilizando una columna Source 15Q 10/100 de 8 mL conectada a un equipo ÄKTA FPLC. La muestra centrifugada de cuerpos de inclusión solubilizados fue diluida 1:2 con un amortiguador con NaH_2PO_4 50 mM, NaCl 500 mM, urea 0.5 M, glicerol 2% y Tween 20 0.5% y fue dializada contra el mismo amortiguador por 12 h a 4 °C. Esta muestra se centrifugó a 12 000 rpm (en un rotor JA 25.50) para eliminar el material agregado y se dializó de nuevo contra el

mismo amortiguador pero con NaCl 200 mM. Se centrifugó igualmente y la muestra se cargó a la columna previamente equilibrada a un flujo de 1 mL/min. La proteína se eluyó al aplicar un gradiente de 200 a 500 mM de NaCl y se colectaron fracciones de 4 mL. Las fracciones obtenidas se analizaron en geles de poliacrilamida al 12% Tricina SDS-PAGE, aquellas enriquecidas con la proteína de interés se juntaron y la muestra resultante se concentró con un Amicon Ultra 10 000 MWCO.

La subunidades Asa1ΔC, Asa3 y Asa8, todas con etiqueta de histidinas, se purificaron en condiciones desnaturalizantes por medio de cromatografía de afinidad a níquel utilizando una columna HisTrap Sepharose FF de 5 mL conectada a un equipo ÄKTA FPLC. Para cada proteína, la muestra centrifugada de cuerpos de inclusión solubilizados fue diluida para tener concentraciones finales de 4.0 M de urea y 50 mM de imidazol; para la subunidad Asa8 se agregó Tween 20 para tener una concentración final de 0.1%. La muestra resultante se cargó a la columna previamente equilibrada con amortiguador de purificación (Anexo 2 inciso D), con un flujo de 0.5 mL/min. Las proteínas se eluyeron aplicando un gradiente de 0 a 500 mM de imidazol y se colectaron fracciones de 4 mL. Las fracciones obtenidas se analizaron en geles de poliacrilamida al 12% Tricina SDS-PAGE, aquellas enriquecidas con la proteína se juntaron y las muestras se concentraron con un Amicon Ultra 10 000 MWCO.

5.5 Obtención de mitocondrias de *Polytomella*

Se aislaron mitocondrias de *Polytomella* para posteriormente purificar la ATPasa mitocondrial. Para ese fin se cultivaron 35 L de células en medio de crecimiento de *Polytomella*, a temperatura ambiente. A partir de este punto todos los pasos se realizaron a 4 °C. La cosecha se realizó centrifugando a 7 500 x g por 10 min (5 000 rpm en un rotor JA 10). La pastilla celular se lavó con amortiguador de sacarosa y se recuperó centrifugando a 7 500 x g por 25 min (12 000 rpm en un rotor JA 25.50); de esta centrifugación se descartaron el sobrenadante y el botón de almidón. La pastilla resultante se resuspendió nuevamente en amortiguador de sacarosa (en 80 a 100 mL) y la muestra resultante se dividió en dos muestras iguales (50 mL) que se trataron por separado

como sigue: las células se rompieron pasándolas 6 veces por un vástago de teflón, se centrifugaron a 7 500 x g por 15 min y se guardó el sobrenadante (S1). El botón de células no rotas se resuspendió y se volvió a romper 6 veces con el vástago; se centrifugó nuevamente a 7 500 x g por 15 min y se guardó el sobrenadante (S2). Ambos sobrenadantes, S1 y S2, se juntaron y se centrifugaron a 17 500 x g por 20 min para obtener las mitocondrias en el botón. El botón de mitocondrias se resuspendió en la menor cantidad de amortiguador posible y se determinó la concentración de proteína (se obtuvieron entre 30 y 40 mg/mL finales de mitocondrias).

5.6 Purificación de la ATP sintasa mitocondrial de *Polytomella*

La muestra de mitocondrias obtenida se diluyó en amortiguador de solubilización para tener una concentración de 10 mg/mL (Anexo 2 inciso F). Se solubilizaron 250 mg de mitocondrias con lauril maltósido (2 mg de detergente por mg de proteína) a partir de una solución madre de 10 mg/mL. Esta muestra se dejó agitando levemente en hielo por 30 min, se centrifugó a 90 000 x g durante 20 min (30 000 rpm en un rotor Type 70Ti), se recuperó el sobrenadante y finalmente se diluyó 3 veces en amortiguador A (Anexo 2 inciso F). La muestra resultante se cargó a una columna Source 15Q 10/100 GL (VC 8 mL) a un flujo de 1 mL/min. Se lavó la columna primero con 20% de amortiguador B (50 mM NaCl, 2 VC) y después con 30% (75 mM NaCL, 2VC). Se eluyó con un gradiente de 30 a 100% de amortiguador B (20VC) (Anexo 2 inciso F) y se colectaron fracciones de 2 mL.

Las fracciones obtenidas se analizaron en geles nativos (BN-PAGE) y desnaturalizantes (SDS-PAGE) para identificar las fracciones correspondientes a ATPasa, mismas que se juntaron y se concentraron con un centricon 100 000 MWCO hasta tener 4 mL. A esta muestra se le añadió glicerol para tener una concentración final de 30% y ATP para tener una concentración final de 1 mM y se siguió concentrando hasta tener 400 uL, que se inyectaron a una columna Superose 6 10/300 GL (VC 24 mL) previamente equilibrada. La columna se corrió a un flujo de 0.25 mL/min y se colectaron fracciones de 500 µL. Las fracciones eluidas se analizaron en geles y se juntaron correspondientemente.

5.7 Inmunorréplicas tipo Far Western Blot

Esta técnica está basada en la descrita previamente (Hall 2004) con las modificaciones que se describen a continuación. Todas las soluciones y amortiguadores necesarios se describen en el Anexo 2 inciso C. En estos ensayos las proteínas se separaron en geles de poliacrilamida al 12% Tricina SDS-PAGE y fueron transferidas a una membrana de nitrocelulosa a 250 mA de corriente constante a 4 °C por 1 h en un sistema de transferencia húmeda. Para marcar las proteínas transferidas, las membranas se tiñeron con una solución de rojo de Ponceau y posteriormente se bloquearon toda la noche con un amortiguador TBS adicionado con 5% de leche. Para preparar las membranas para la incubación con las proteínas de interés, se lavaron dos veces por 5 min con el amortiguador específico de cada proteína (ver Anexo 2 inciso F) y finalmente se incubaron por 4 h con la proteína de interés en su amortiguador adicionado con 1% de leche. En todos los ensayos se utilizaron concentraciones de 0.05, 0.1, 0.5, 1, 2 y 5 nanomoles de proteína en la incubación y 3 µg de proteína en la membrana (la concentración de proteína fue estimada por el método de Lowry).

Al terminar la incubación con las proteínas las membranas fueron lavadas dos veces por 5 min en amortiguador TBS adicionado con 0.05% de Tween 20 (TBST) y posteriormente se incubaron por 3 h con los anticuerpos primarios correspondientes en amortiguador TBST adicionado con 1% de leche. Los anticuerpos primarios son producidos como se describe en el Anexo 1 inciso 11.1.4 y se utilizaron en las siguientes concentraciones: 1:100,000 para la subunidad Asa1, 1:100,000 para la subunidad Asa2, 1:50,000 para la subunidad Asa3, 1:100,000 para la subunidad Asa7, 1:1,000,000 para la subunidad Asa8 y 1:100,000 para la subunidad OSCP. Después de la incubación con el anticuerpo primario, las membranas se lavaron dos veces por 5 min con TBST y se incubaron con el anticuerpo secundario a una concentración de 1:8000 por 2 h. Finalmente, antes de revelar, las membranas se lavaron nuevamente dos veces por 5 min.

El anticuerpo secundario utilizado (Anti-Rabbit IgG, Sigma-Aldrich) está unido covalentemente a la enzima fosfatasa alcalina y para revelar las membranas se prepara al momento la solución

reveladora con una mezcla de sustratos: 5-bromo-4-cloro-3-indolil fostato + nitroazul de tetrazolio (BCIP + NBT) (Anexo 2 inciso C). Esta solución reacciona *in situ* y resulta en la formación de un precipitado en la membrana en el lugar de reconocimiento. Las membranas se incubaron con esta solución hasta la aparición de señal y la reacción se detuvo incubando en una solución de etanol al 20%.

5.8 Copurificación de subunidades recombinantes

5.8.1 Copurificación Asa1-Asa3^{6H}

Para este experimento se partió de muestras cuerpos de inclusión solubilizados de las dos subunidades. La muestra de Asa1 se diluyó para alcanzar una concentración 4.0 M de urea y se dializó contra un amortiguador con NaH_2PO_4 50 mM, NaCl 500 mM, urea 0.5 M, glicerol 2%, Tween 20 0.5%, pH 7.8 durante 8 h a 4 °C. Se centrifugó a 12 000 rpm (en un rotor JA 25.50) por 10 min para eliminar el material agregado y la muestra se dividió en dos partes: para unir a Asa3^{6H} y para el experimento control.

La muestra de Asa3^{6H} se diluyó para tener concentraciones finales de 4.0 M de urea y 50 mM de imidazol, se dividió en dos partes y cada una se cargó a una columna HisTrap Sepharose FF de 1 mL equilibrada y conectada a un equipo ÄKTA FPLC, a un flujo de 1 mL/min. Para ambas muestras se realizó un gradiente de replegado en la columna pasando de una concentración 4.0 M a 0.5 M de urea y hasta una concentración de 2% de glicerol. Finalizado el gradiente las columnas se lavaron con amortiguador de lavado con 30 mM de imidazol para eluir el exceso de proteína y lo que no se unió a la columna, y se procedió a agregar la muestra obtenida de la diálisis de Asa1; ésta se cargó a un flujo de 1 mL/min a las dos columnas (con Asa3^{6H} y sin Asa3^{6H} previamente unida). Se realizaron lavados para eliminar el exceso de proteína y finalmente se aplicó un gradiente de 0 a 500 mM de imidazol para eluir las proteínas. Las fracciones obtenidas se analizaron en geles de poliacrilamida al 12% Tricina SDS-PAGE.

5.8.2 Copurificación Asa1-OSCPΔC^{6H}

Para este experimento se partió de muestras de las dos subunidades purificadas. Las proteínas (2 mg de cada una) se dializaron juntas contra un amortiguador de diálisis (NaH_2PO_4 50 mM, NaCl 500 mM, urea 0.5 M, glicerol 2%, Tween 20 0.5%, pH 7.8) durante 8 h a 4 °C. El material agregado se eliminó por centrifugación a 12 000 rpm (en un rotor JA 25.50) por 10 min. A la muestra resultante se le añadieron 100 μL de resina equilibrada (Ni Sepharose 6 FF) e imidazol para tener una concentración de 30 mM. Esta muestra se incubó por 7 h y se recuperó el material no retenido centrifugando a 2 000 rpm por 5 min en una centrífuga de mesa Minispin Plus, Eppendorf. La resina se lavó diez veces con una concentración de 50 mM de imidazol y las proteínas se eluyeron con un gradiente de imidazol de 50 a 500 mM. El experimento control se realizó de la misma manera pero sin la subunidad Asa1. Las fracciones obtenidas se analizaron en geles de poliacrilamida al 12% Tricina SDS-PAGE.

5.9 Análisis de predicción *in silico* de las estructuras secundaria y terciaria de la subunidad Asa3

La secuencia de aminoácidos de la subunidad Asa3 se sometió a un análisis de predicción de presecuencia de localización mitocondrial en el servidor: http://mitf.cbrc.jp/MitoFates/cgi-bin/top.cgi para eliminar los aminoácidos correspondientes a la presecuencia de la proteína y hacer las predicciones de estructuras secundaria y terciaria a partir de la secuencia de la proteína madura. Se utilizó el servidor http://raptorx.uchicago.edu/StructurePrediction/predict/ para realizar tanto la predicción de estructura secundaria como para generar un modelo tridimensional de la probable estructura que adopta la subunidad Asa3. Este servidor se especializa en hacer predicciones para proteínas sin homólogos cercanos en el *Protein Data Bank* (Källberg et al. 2012).

5.10 Reconstitución de subcomplejos con las subunidades recombinantes: Asa1, Asa2, Asa3^{6H}, Asa4, Asa7 y OSCP

Para realizar estos experimentos primero se sobreexpresaron las subunidades correspondientes, se obtuvieron cuerpos de inclusión enriquecidos, que se lavaron y se solubilizaron con 8.0 M de urea como se explica en el punto 5.3 de la sección de materiales y métodos. Estas muestras fueron las utilizadas para llevar a cabo los experimentos que se describen en esta sección. Todos los pasos se llevaron a cabo a 4 °C. Todas las soluciones y los amortiguadores utilizados se describen en el Anexo 2 inciso G.

5.10.1 Subcomplejo Asa1-Asa2-Asa3^{6H}-Asa4-Asa7-OSCP

Partiendo de las muestras de cuerpos de inclusión solubilizados, se hizo una mezcla de las subunidades intentando tener aproximadamente la misma cantidad de cada proteína (una estimación de concentración de proteína sería poco útil debido a que se tienen las proteínas de interés mezcladas con proteínas de *E. coli*). Esta mezcla se diluyó 1:1 con amortiguador de diálisis y se le añadió: glicerol para tener una concentración de 10%, lauril maltósido para tener una concentración de 0.01%, DTT para tener una concentración 1 mM y dos mini tabletas de inhibidores de proteasas (cOmplete EDTA-free, Roche) para 15 mL de muestra. Para replegar las proteínas (de las concentraciones desnaturalizantes de 8 M de urea y 500 mM de NaCl), la muestra resultante se dializó en pasos contra amortiguadores de diálisis con concentración decreciente de urea (4.0 M a 2.0 M a 1.0 M a 0.5 M) y concentración constante de 150 mM NaCl. Se hicieron diálisis de tres horas para cada muestra a cada concentración, ultracentrifugando después de cada paso de diálisis a 20 000 rpm por 20 min, para eliminar el material agregado.

El sobrenadante de la muestra final se recuperó y se concentró hasta tener 500 µL usando un Amicon Ultra 100 000 MWCO con centrifugaciones de 15 min a 3 500 rpm. La muestra concentrada se inyectó a dos columnas de exclusión molecular equilibradas conectadas en serie (Superose 6 10/300 GL + Superdex 200 10/300 GL) a un equipo ÄKTA FPLC, a un flujo de 0.5

mL/min. Las fracciones eluidas se analizaron en geles Tricina SDS-PAGE y aquellas probablemente correspondientes a un subcomplejo Asa1-Asa2-Asa3^{6H}-Asa4-Asa7-OSCP se juntaron y se incubaron por 7 h con 1 mL de resina de níquel equilibrada (Ni NTA Agarose, QIAGEN) en presencia de 10 mM de imidazol, para realizar una purificación en *batch*, recuperando el subcomplejo por medio de la etiqueta de histidinas de la subunidad Asa3^{6H}.

Para recuperar el material no retenido por la resina, para lavarla y para eluir las fracciones del proceso de purificación, la resina se centrifugó a 2 000 rpm por 5 min. Se hicieron 20 lavados de la resina con un amortiguador adicionado con 25 mM de imidazol, después de los cuales se procedió a eluir las proteínas incubando la resina con amortiguadores con concentración creciente de imidazol en pasos de 50 en 50 (100, 150, 200, 250, 300, 350 mM). Las fracciones obtenidas de este proceso se analizaron en un gel de poliacrilamida al 12% Tricina SDS-PAGE.

5.10.2 Subcomplejo Asa1-Asa3^{6H}-OSCP

Partiendo nuevamente de las muestras de cuerpos de inclusión solubilizados, esta vez correspondientes a las subunidades Asa1, Asa3^{6H} y OSCP, se hizo una mezcla para tener aproximadamente la misma cantidad de cada proteína y se diluyó 1:1 con amortiguador de diálisis. A la muestra resultante se le añadió: glicerol para tener una concentración de 10%, lauril maltósido para tener una concentración de 0.01%, DTT para tener una concentración 1.0 mM y una mini tableta de inhibidores de proteasas (cOmplete EDTA-free, Roche) para 10 mL de muestra. El replegamiento se llevó a cabo con dilución lenta (por goteo) para pasar de la concentración inicial de 8.0 M de urea a 4.0 M; posteriormente se hicieron diálisis consecutivas como se explicó para el subcomplejo anterior, hasta alcanzar una concentración final de 0.5 M de urea y de 150 mM NaCl.

El sobrenadante de la muestra final se concentró hasta tener 500 µL usando un Amicon Ultra 30 000 MWCO con centrifugaciones de 15 min a 3 500 rpm. La muestra concentrada se inyectó a una columna de exclusión molecular Superdex 200 10/300 GL equilibrada y conectada a un

equipo ÄKTA FPLC, a un flujo de 0.5 mL/min. Las fracciones eluidas se analizaron en geles de poliacrilamida al 12% Tricina SDS-PAGE, se seleccionaron aquellas que podían corresponder a un subcomplejo Asa1-Asa3^{6H}-OSCP, se juntaron y se incubaron por 7 h con una resina de níquel equilibrada (Ni NTA Agarose, QIAGEN) en presencia de 20 mM de imidazol, y se procedió a realizar una purificación en *batch*.

La resina se centrifugó a 2 000 rpm por 5 min para recuperar lo no retenido, para lavarla y para eluir las proteínas. Nuevamente se hicieron 10 lavados y las proteínas se eluyeron incubando la resina con concentraciones crecientes de imidazol, desde 100 hasta 300 mM, de 50 en 50. Las fracciones obtenidas de este proceso se analizaron en un gel de poliacrilamida al 12% Tricina SDS-PAGE.

Este subcomplejo también se recuperó realizando los pasos de purificación invertidos. Se hizo la mezcla de subunidades y se le añadió: glicerol para tener una concentración de 10%, lauril maltósido para tener una concentración de 0.01%, DTT para tener una concentración 1 mM, NDSB-201 para tener una concentración de 500 mM y una mini tableta de inhibidores de proteasas (cOmplete EDTA-free, Roche) para 10 mL de muestra. El replegamiento se llevó a cabo con diálisis consecutivas hasta llegar a concentraciones finales de 0.5 M de urea y 150 mM de NaCl.

El primer paso fue realizar la purificación en *batch*, para lo cual la muestra recuperada de las diálisis se incubó con 1 mL de la resina de níquel equilibrada por 7 h. La resina se lavó 20 veces con un amortiguador con 35 mM de imidazol y las proteínas se eluyeron incubando la resina con concentraciones crecientes de imidazol, de 100 a 300 mM en pasos de 50. Las fracciones obtenidas de este proceso se analizaron en geles y se juntaron las correspondientes a la elución. La muestra resultante se concentró hasta tener 500 µL y se inyectó a una columna Superose 6 equilibrada conectada a un equipo ÄKTA FPLC, a un flujo de 0.5 mL/min. Las fracciones eluidas se analizaron en geles de poliacrilamida al 12% Tricina SDS-PAGE.

5.11 Replegamiento y purificación de las subunidades Asa para la obtención de muestras para cristalización

Para estos experimentos se partió igualmente de las muestras de cuerpos de inclusión solubilizados con 8.0 M de urea. Todos los amortiguadores utilizados se describen en el Anexo 2 inciso H.

5.11.1 Del subcomplejo Asa1-Asa3^{6H}-OSCP

Se hizo una mezcla para tener aproximadamente la misma cantidad de cada proteína, y el replegamiento se llevó a cabo diluyendo por goteo (10 veces el volumen inicial) en un amortiguador de replegado en presencia del osmolito TMAO (trimetilamina N-óxido) (ver Anexo 2 inciso H). La muestra se dejó agitando lentamente a temperatura ambiente por 8 h, después de lo cual se ultracentrifugó a 15 000 rpm por 20 min. Se recuperó el sobrenadante (aproximadamente 115 mL) y se incubó con 4.5 mL totales de resina de níquel equilibrada, por 7 h a 4 °C en presencia de 15 mM de imidazol.

Se centrifugó la resina como se describió arriba para recuperar el material no retenido, para lavarla y para hacer la elución. Se hicieron 20 lavados con un amortiguador con 25 mM de imidazol y las proteínas se eluyeron con concentraciones crecientes de imidazol, de 100 a 300 mM en pasos de 50 en 50. Las fracciones obtenidas se analizaron en un gel de poliacrilamida al 12% Tricina SDS-PAGE.

5.11.2 De la subunidad Asa3^{6H}

La muestra de cuerpos de inclusión solubilizados de la subunidad Asa3^{6H} se diluyó 10 veces en un amortiguador de replegado (con las modificaciones que se detallan en el Anexo 2 inciso G), lentamente por goteo. La muestra se dejó agitando lentamente a temperatura ambiente por 8 h. Posteriormente se ultracentrifugó a 15 000 rpm por 20 min y el sobrenadante recuperado

(aproximadamente 100 mL) se incubó con 4.5 mL totales de resina de níquel equilibrada por 7 h a 4 °C, en presencia de 15 mM de imidazol. Se procedió a realizar la purificación en *batch*, como ya se describió arriba, y se analizaron las fracciones en geles de poliacrilamida al 12% Tricina SDS-PAGE.

Se seleccionaron las fracciones más enriquecidas, se juntaron y se concentraron con un Amicon Ultra 10 000 MWCO hasta alcanzar una concentración de proteína de 4 mg/mL (estimada por el método de Lowry). Se tomó una alícuota de la muestra y el resto (900 µL) se dializó toda la noche a 4 °C contra 200 mL del amortiguador utilizado para purificación (Anexo 2 inciso H), para disminuir la concentración de TMAO. Se tomó una alícuota de la muestra recuperada de la diálisis y se siguió concentrando hasta tener una concentración de 6 mg/mL. Las muestras obtenidas en los tres estados descritos (sin dializar, dializada y concentrada hasta 6 mg/mL) se analizaron en un equipo DynaPro NanoStar (Wyatt) de dispersión dinámica de luz (DLS).

Se sembraron pruebas de cristalización de las tres muestras de la subunidad Asa3^{6H} con un robot de cristalización Honey Bee 961 (Cartesian) utilizando 6 kits especializados en la cristalización de proteínas de membrana o altamente hidrofóbicas: Nextal MbClass Suite, QIAGEN; Nextal MbClass Suite II, QIAGEN; Crystal Screen Cryo • Crystal Screen 2 Cryo Hampton Research; JBScreen Wizard 1 + 2, Jena Bioscience; PEGs Suite, QIAGEN; JBScreen Membranes, Jena Bioscience; más de 500 condiciones en total.

5.11.3 De la subunidad Asa7^{6H}

La muestra de cuerpos de inclusión solubilizados de la subunidad Asa7^{6H} se diluyó 10 veces en un amortiguador de replegado (con las modificaciones que se detallan en el Anexo 2 inciso H), lentamente por goteo. La muestra se dejó agitando lentamente a temperatura ambiente por 10 h, se ultracentrifugó a 15 000 rpm por 20 min, se recuperó el sobrenadante y se incubó con 2.7 mL totales de resina de níquel equilibrada por 10 h a 4 °C, en presencia de 50 mM de imidazol. Se

procedió a realizar la purificación en *batch*, como ya se describió arriba, y las fracciones se analizaron en geles de poliacrilamida al 12% Tricina SDS-PAGE.

Se seleccionaron las fracciones eluidas a 100 y 150 mM de imidazol y se concentraron por separado hasta alcanzar una concentración de aproximadamente 5 mg/mL. En ese punto se analizaron con un equipo DynaPro NanoStar (Wyatt) de dispersión dinámica de luz (DLS). Se sembraron pruebas de cristalización de ambas muestras con un robot de cristalización Honey Bee 961 (Cartesian) con los siguientes kits especializados en la cristalizción de proteínas de membrana o altamente hidrofóbicas: Crystal Screen, Hampton Research; Crystal Screen Cryo, Hampton Research; Nextal MbClass Suite, QIAGEN y Nextal Tubes Anions Suite, QIAGEN.

6. Resultados

6.1 Interacciones de la subunidad Asa1 con otras subunidades del brazo periférico de la ATPasa de *Polytomella*

Con el propósito de evaluar las interacciones que mantiene Asa1 con otras subunidades, se llevaron a cabo ensayos de inmunorréplicas tipo Far Western (ver punto 5.7 de la sección de materiales y métodos) utilizando las subunidades recombinantes purificadas (Asa1, Asa1ΔC, Asa2, Asa3, Asa4, Asa7, Asa8, OSCP y OSCPΔC) que se muestran en la figura 16. Esta técnica ha resultado ser útil para evaluar interacciones entre proteínas solubles a moderadamente hidrofóbicas (Edmonson y Rent 2001). Para tener un panorama general de las posibles interacciones de la subunidad Asa1 se hizo un experimento en el que se fijó una mezcla de subunidades recombinantes en la membrana (Asa2, Asa3, Asa4, Asa7, Asa8 y OSCP), se incubó con concentraciones crecientes de Asa1 y se reveló con un anticuerpo anti Asa1. Se observaron las señales correspondientes a las subunidades Asa3, OSCP, Asa7 y una ligera señal en las bandas correspondientes a Asa2 y Asa8 (Figura 17); este experimento sugiere que Asa1 mantiene interacciones con todas las subunidades probadas, excepto Asa4. Con estos resultados como antecedente, se procedió a evaluar cada interacción individualmente.

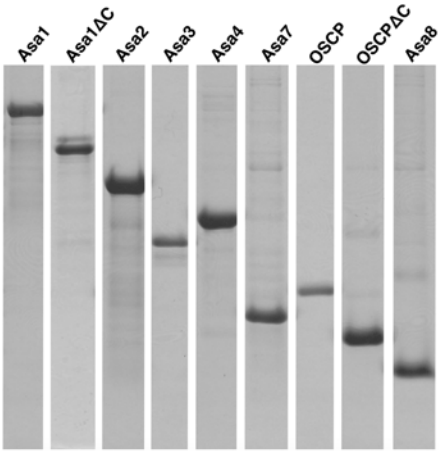

Figura 16: Subunidades purificadas utilizadas para los ensayos de interacción por Far Western Blot. Se muestran geles de Tricina SDS-PAGE al 12% teñidos con azul de Coomassie con las proteínas recombinantes purificadas utilizadas en los ensayos de Far Western Blot.

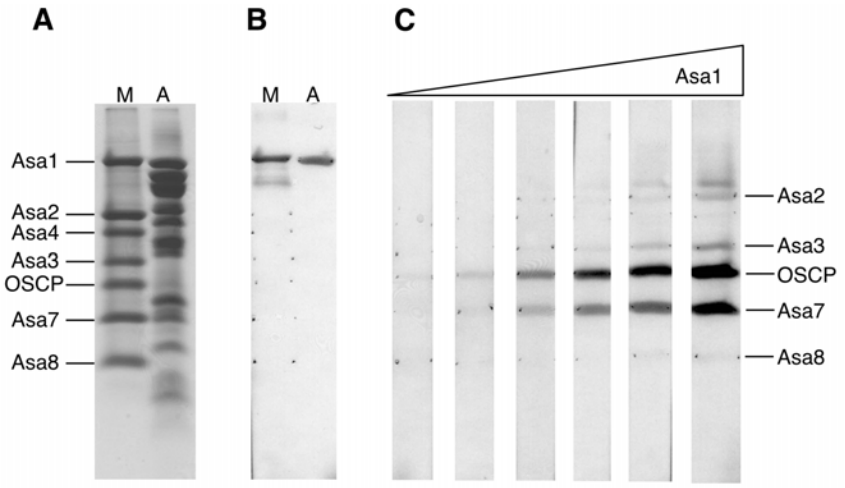

Figura 17: Interacciones de la subunidad Asa1 con otras subunidades del brazo periférico de la ATPasa evaluadas por Far Western Blot. A. Gel Tricina SDS-PAGE al 12% teñido con azul de Coomassie en el que se muestra la mezcla de proteínas recombinantes: Asa1, Asa2, Asa3, Asa4, Asa7, Asa8 y OSCP (M) y la ATPasa de *Polytomella* purificada (A). **B.** Western Blot revelado con anticuerpos anti Asa1 de una membrana con la mezcla de proteínas recombinantes y la ATPasa purificada, se observa el reconocimiento específico de la subunidad Asa1 recombinante (M) y la subunidad Asa1 nativa del complejo (A). **C.** Membranas con la mezcla de proteínas recombinantes incubadas con concentraciones crecientes de la subunidad Asa1 y reveladas con anticuerpos anti Asa1. Se observan señales crecientes correspondientes a las subunidades Asa2, Asa3, OSCP, Asa7 y Asa8.

Para el ensayo Asa1-Asa2 se fijó la subunidad Asa1 en la membrana, y se incubó con concentraciones crecientes de la subunidad Asa2, para después revelar con un anticuerpo anti Asa2 (Figura 18). Se hizo el experimento complementario, en el que se fijó la subunidad Asa2 en la membrana, se incubó con concentraciones crecientes de la subunidad Asa1 y se reveló con un anticuerpo anti Asa1 (Figura 18). En ambos experimentos se observó señal creciente, correspondiente con el aumento de concentración de proteína presente en el medio de incubación, lo cual es indicativo de una interacción Asa1-Asa2. Para el ensayo Asa1-Asa3 se realizaron experimentos similares, en uno se fijó la subunidad Asa1 en la membrana y se incubó con concentraciones crecientes de Asa3; al revelar con un anticuerpo anti Asa3 se observó la señal creciente de la banda correspondiente a Asa1 (Figura 19). Al realizar el experimento complementario, fijando la subunidad Asa3 en la membrana e incubando con la subunidad Asa1, igualmente se observó la señal creciente correspondiente con la interacción Asa1-Asa3 previamente observada (Figura 19).

Para evaluar la interacción entre Asa1 y Asa7 se llevaron a cabo los experimentos antes descritos, fijando una y otra en la membrana, y de ambas formas se observó una interacción (Figura 20). Para el caso de la interacción entre Asa1 y Asa8 el ensayo se realizó fijando la subunidad Asa1 en la membrana, incubando con concentraciones crecientes de la subunidad Asa8 y revelando con un anticuerpo anti Asa8; de esta forma se observa la señal indicativa de una interacción Asa1-Asa8 (Figura 21), sin embargo, al realizar el experimento complementario no se detectó una señal.

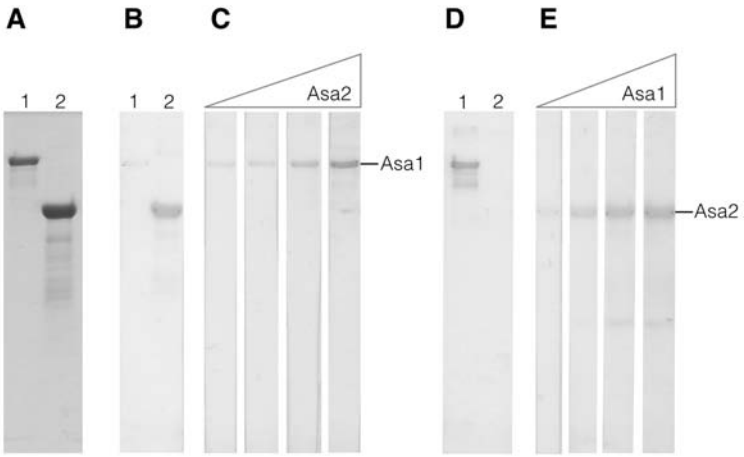

Figura 18: Interacción de la subunidad Asa1 con la subunidad Asa2 evaluada por Far Western Blot. A. Gel Tricina SDS-PAGE al 12% teñido con azul de Coomassie en el que se muestran las subunidades recombinantes purificadas: Asa1 (1) y Asa2 (2). **B.** Western Blot revelado con anticuerpos anti Asa2 de una membrana con las subunidades recombinantes Asa1 y Asa2, se observa el reconocimiento específico de la subunidad Asa2 recombinante. **C.** Membranas con la subunidad Asa1 incubadas con concentraciones crecientes de la subunidad Asa2 y reveladas con anticuerpos anti Asa2. Se observa la señal creciente correspondiente a la subunidad Asa1. **D.** Western Blot revelado con anticuerpos anti Asa1 de una membrana con las subunidades recombinantes Asa1 y Asa2, se observa el reconocimiento específico de la subunidad Asa1 recombinante. **E.** Membranas con la subunidad Asa2 incubadas con concentraciones crecientes de la subunidad Asa1 y reveladas con anticuerpos anti Asa1. Se observa la señal creciente correspondiente a la subunidad Asa2.

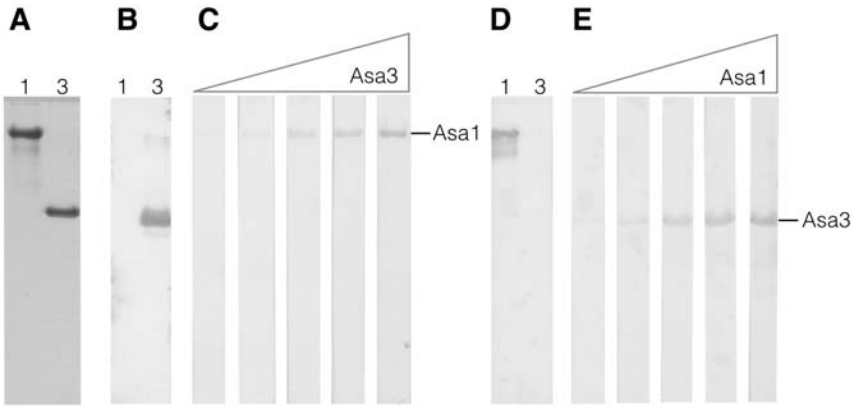

Figura 19: Interacción de la subunidad Asa1 con la subunidad Asa3 evaluada por Far Western Blot. A. Gel Tricina SDS-PAGE al 12% teñido con azul de Coomassie en el que se muestran las subunidades recombinantes purificadas: Asa1 (1) y Asa3 (3). **B.** Western Blot revelado con anticuerpos anti Asa3 de una membrana con las subunidades recombinantes Asa1 y Asa3, se observa el reconocimiento específico de la subunidad Asa3 recombinante. **C.** Membranas con la subunidad Asa1 incubadas con concentraciones crecientes de la subunidad Asa3 y reveladas con anticuerpos anti Asa3. Se observa la señal creciente correspondiente a la subunidad Asa1. **D.** Western Blot revelado con anticuerpos anti Asa1 de una membrana con las subunidades recombinantes Asa1 y Asa3, se observa el reconocimiento específico de la subunidad Asa1 recombinante. **E.** Membranas con la subunidad Asa3 incubadas con concentraciones crecientes de la subunidad Asa1 y reveladas con anticuerpos anti Asa1. Se observa la señal creciente correspondiente a la subunidad Asa3.

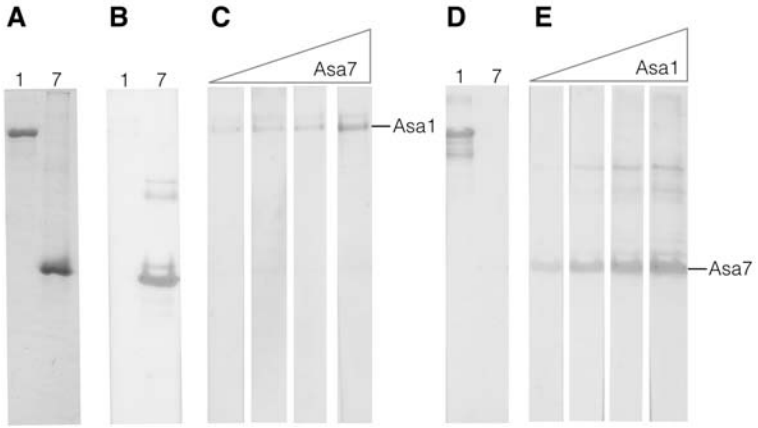

Figura 20: Interacción de la subunidad Asa1 con la subunidad Asa7 evaluada por Far Western Blot. A. Gel Tricina SDS-PAGE al 12% teñido con azul de Coomassie en el que se muestran las subunidades recombinantes purificadas: Asa1 (1) y Asa7 (7). **B.** Western Blot revelado con anticuerpos anti Asa7 de una membrana con las subunidades recombinantes Asa1 y Asa7, se observa el reconocimiento específico de la subunidad Asa7 recombinante. **C.** Membranas con la subunidad Asa1 incubadas con concentraciones crecientes de la subunidad Asa7 y reveladas con anticuerpos anti Asa7. Se observa la señal creciente correspondiente a la subunidad Asa1. **D.** Western Blot revelado con anticuerpos anti Asa1 de una membrana con las subunidades recombinantes Asa1 y Asa7, se observa el reconocimiento específico de la subunidad Asa1 recombinante. **E.** Membranas con la subunidad Asa7 incubadas con concentraciones crecientes de la subunidad Asa1 y reveladas con anticuerpos anti Asa1. Se observa la señal creciente correspondiente a la subunidad Asa7.

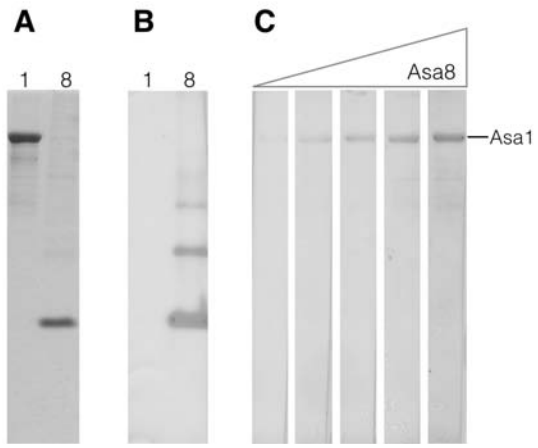

Figura 21: Interacción de la subunidad Asa1 con la subunidad Asa8 evaluada por Far Western Blot. A. Gel Tricina SDS-PAGE al 12% teñido con azul de Coomassie en el que se muestran las subunidades recombinantes purificadas: Asa1 (1) y Asa8 (8). **B.** Western Blot revelado con anticuerpos anti Asa8 de una membrana con las subunidades recombinantes Asa1 y Asa8, se observa el reconocimiento específico de la subunidad Asa8 recombinante y sus formas oligoméricas. **C.** Membranas con la subunidad Asa1 incubadas con concentraciones crecientes de la subunidad Asa8 y reveladas con anticuerpos anti Asa8. Se observa la señal creciente correspondiente a la subunidad Asa1.

Para evaluar la interacción de OSCP con la subunidad Asa1 que carece del extremo carboxilo terminal (Asa1ΔC) se realizaron los siguientes ensayos: primero se realizó un experimento fijando la subunidad OSCP en la membrana e incubando con Asa1, y al revelar con un anticuerpo anti Asa1 se observó la interacción Asa1-OSCP reportada. (Figura 22ABC). Se realizó el mismo experimento pero incubando con la subunidad Asa1ΔC y se observó señal disminuida (Figura 22DEF). Para confirmar la evidencia de que es el extremo carboxilo terminal de OSCP el que está involucrado en la interacción con Asa1 se realizó un experimento en el que se fijó OSCPΔC en la membrana y se incubó con Asa1ΔC, al revelar con un anticuerpo anti Asa1 no se observó señal (Figura 22GHI). Estos resultados confirman que es el extremo carboxilo terminal de OSCP el que une a Asa1 y sugieren que los residuos ausentes en la subunidad Asa1ΔC (390 a 618) están involucrados en la interacción de la subunidad Asa1 con la subunidad OSCP.

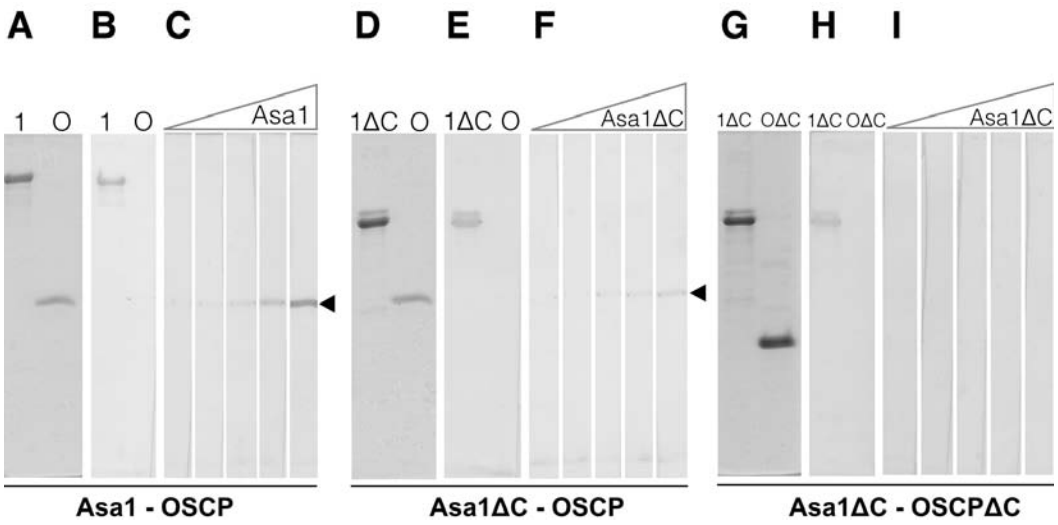

Figura 22: Interacción de la subunidad Asa1 con la subunidad OSCP evaluada por Far Western Blot. A. Gel Tricina SDS-PAGE al 12% teñido con azul de Coomassie en el que se muestran las subunidades recombinantes purificadas: Asa1 (1) y OSCP (O). **B.** Western Blot revelado con anticuerpos anti Asa1 de una membrana con las subunidades recombinantes Asa1 y OSCP, se observa el reconocimiento específico de la subunidad Asa1 recombinante. **C.** Membranas con la subunidad OSCP incubadas con concentraciones crecientes de la subunidad Asa1 y reveladas con anticuerpos anti Asa1. Se observa la señal creciente correspondiente a la subunidad OSCP. **D.** Gel Tricina SDS-PAGE al 12% teñido con azul de Coomassie en el que se muestran las subunidades recombinantes purificadas: Asa1ΔC (1ΔC) y OSCP (O). **E.** Western Blot revelado con anticuerpos anti Asa1 de una membrana con las subunidades recombinantes Asa1ΔC y OSCP, se observa el reconocimiento específico de la subunidad Asa1ΔC recombinante. **F.** Membranas con la subunidad OSCP incubadas con concentraciones crecientes de la subunidad Asa1ΔC y reveladas con anticuerpos anti Asa1. Se observa la señal disminuida correspondiente a la subunidad OSCP (comparada con el panel C). **G.** Gel Tricina SDS-PAGE al 12% teñido con azul de Coomassie en el que se muestran las subunidades recombinantes purificadas: Asa1ΔC (1ΔC) y OSCPΔC (OΔC). **H.** Western Blot revelado con anticuerpos anti Asa1 de una membrana con las subunidades recombinantes Asa1ΔC y OSCPΔC, se observa el reconocimiento específico de la subunidad Asa1ΔC recombinante. **I.** Membranas con la subunidad OSCPΔC incubadas con concentraciones crecientes de la subunidad Asa1ΔC y reveladas con anticuerpos anti Asa1. No se observa ninguna señal.

Para confirmar el papel del extremo carboxilo terminal de la subunidad OSCP en la interacción Asa1-OSCP, se realizó la copurificación de ambas subunidades con la subunidad Asa1 sin etiqueta de histidinas. El experimento se muestra en la figura 23, como era esperado, en ausencia del extremo carboxilo terminal, la interacción Asa1-OSCP se pierde y no se observa coelución.

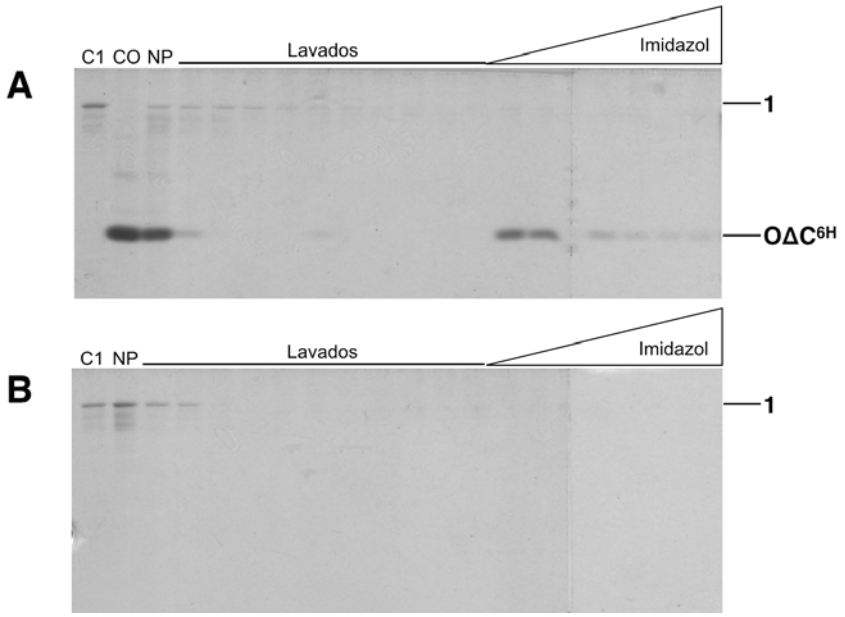

Figura 23: Copurificación de las subunidades recombinantes Asa1 y OSCPΔC^{6H} por cromatografía de afinidad a níquel. A. Gel Tricina SDS-PAGE al 12% teñido con azul de Coomassie en el que se muestran las fracciones correspondientes al experimento de copurificación de las subunidades Asa1 y OSCPΔC^{6H}. C1: carga de la muestra de la subunidad Asa1 purificada. CO: carga de la muestra de la subunidad OSCPΔC^{6H} purificada. NP: fracción correspondiente al material no retenido por la columna de níquel. El triángulo representa la serie de fracciones eluidas tras la aplicación de un gradiente de imidazol. Se señala la banda correspondiente a la subunidad OSCPΔC^{6H} en la elución (OΔC^{6H}). **B.** Gel Tricina SDS-PAGE al 12% teñido con azul de Coomassie en el que se muestran las fracciones correspondientes al experimento control. C1: carga de la muestra de la subunidad Asa1 purificada. NP: fracción correspondiente al material no retenido por la columna de níquel. El triángulo representa la elución con la aplicación de un gradiente de imidazol. No se observan la retención ni la elución de la subunidad Asa1.

Con estos experimentos se puede concluir que la subunidad Asa1 mantiene interacciones con las subunidades Asa2, Asa3, Asa7, Asa8 y OSCP, pero no con la subunidad Asa4, y que su interacción con OSCP requiere de los residuos ausentes en la subunidad Asa1ΔC. Estos resultados sugieren que la subunidad Asa1 recorre el brazo periférico de la ATPasa de *Polytomella* desde la parte membranal, dada su interacción con Asa8, hasta la parte más alejada de la membrana, dada su interacción con OSCP, y que en la parte media contacta a las subunidades Asa2 y Asa7.

6.2 Obtención de la subunidad Asa3 y estudio de sus interacciones con otras subunidades de la ATPasa de *Polytomella*

La subunidad Asa3 se encontró anteriormente en subcomplejos generados al disociar la ATPasa de *Polytomella* con calor (Vázquez-Acevedo et al. 2006) y con detergente (Colina-Tenorio et al. 2016), junto con Asa1, Asa5, Asa8 y las subunidades membranales *a* y *c*. Estos antecedentes sugerían una posible interacción de la subunidad Asa1 con la subunidad Asa3. Para evaluar esa posibilidad, y para ubicar a la subunidad Asa3 en un modelo topológico de la enzima (no existía la subunidad recombinante antes de este trabajo), se purificó la proteína recombinante y se realizaron ensayos de interacción. El proceso de clonación, sobreexpresión y purificación de la subunidad Asa3, así como la obtención de anticuerpos contra esta subunidad, se describen en el Anexo 1.

Como primera aproximación al estudio de las interacciones de la subunidad Asa3 con el resto de las subunidades de la enzima, se llevó a cabo un ensayo de Far Western Blot fijando en la membrana la ATP sintasa purificada de *Polytomella*, incubando con concentraciones crecientes de la subunidad Asa3 y revelando con los anticuerpos anti Asa3 generados. Este experimento se muestra en la figura 24, en la que se observan las señales correspondientes a las subunidades Asa1 y Asa3 y una banda que, por degradación de Edman y secuenciación del extremo amino terminal, se sabe que es una forma oligomérica de la subunidad *c* resistente a SDS (Colina-Tenorio et al. 2016) y que en este experimento se considera una unión inespecífica dado que no responde al aumento de concentración de proteína en la incubación.

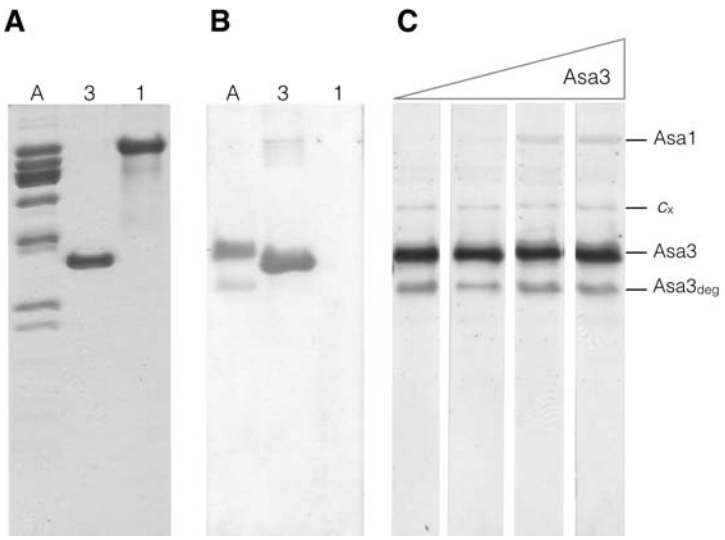

Figura 24: Interacciones de la subunidad Asa3 recombinante con otras subunidades de la ATPasa de *Polytomella* evaluadas por Far Western Blot. A. Gel Tricina SDS-PAGE al 12% teñido con azul de Coomassie en el que se muestran la ATPasa purificada (A) y las subunidades recombinantes purificadas Asa1 (1) y Asa3 (3). **B.** Western Blot revelado con anticuerpos anti Asa3 de una membrana con la ATPasa purificada y las subunidades recombinantes Asa1 y Asa3. Se observa el reconocimiento específico de la subunidad Asa3 nativa del complejo y una banda correspondiente a su degradación, y de la subunidad Asa3 recombinante. **C.** Membranas con la ATPasa purificada incubadas con concentraciones crecientes de la subunidad Asa3 y reveladas con anticuerpos anti Asa3. Se observa la señal creciente correspondiente a la subunidad Asa1, así como el reconocimiento de la subunidad Asa3 nativa y su producto de degradación. La banda indicada c_x corresponde a la unión inespecífica de Asa3 con una forma oligomérica de la subunidad *c*.

Para confirmar el resultado anterior se realizó otro ensayo de Far Western Blot, esta vez teniendo en la membrana a las subunidades recombinantes purificadas: Asa1, Asa2, Asa3, Asa4, Asa7 y OSCP e incubando nuevamente con la subunidad Asa3. Como se puede ver en la Figura 25, la única señal que se observa al revelar con anticuerpos anti Asa3 corresponde a la subunidad Asa1. Esta interacción se confirmó al copurificar las subunidades Asa1-$Asa3^{6H}$ por medio cromatografía de afinidad a níquel (Figura 26). El experimento de copurificación se explica en el punto 5.8 de la sección de materiales y métodos.

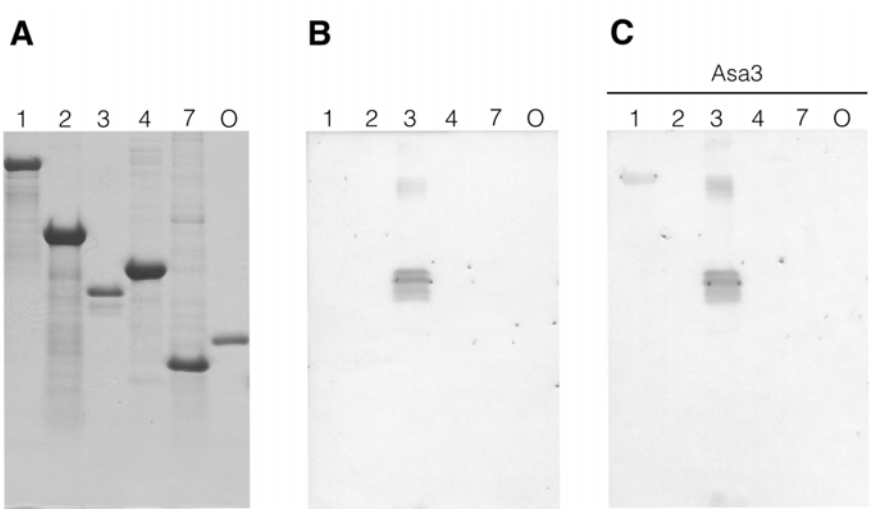

Figura 25: Interacción de la subunidad Asa3 con otras subunidades recombinantes evaluada por Far Western Blot. A. Gel Tricina SDS-PAGE al 12% teñido con azul de Coomassie en el que se muestran las subunidades recombinantes purificadas: Asa1 (1), Asa2 (2), Asa3 (3), Asa4 (4), Asa7 (7) y OSCP (O). **B.** Western Blot revelado con anticuerpos anti Asa3 de una membrana con las subunidades recombinantes purificadas: Asa1, Asa2, Asa3, Asa4, Asa7 y OSCP. Se observa el reconocimiento específico de la subunidad Asa3 y su degradación. **C.** Membrana con las subunidades recombinantes purificadas: Asa1, Asa2, Asa3, Asa4, Asa7 y OSCP, incubada con la subunidad Asa3 y revelada con anticuerpos anti Asa3. Sólo se observa la señal correspondiente a la subunidad Asa1.

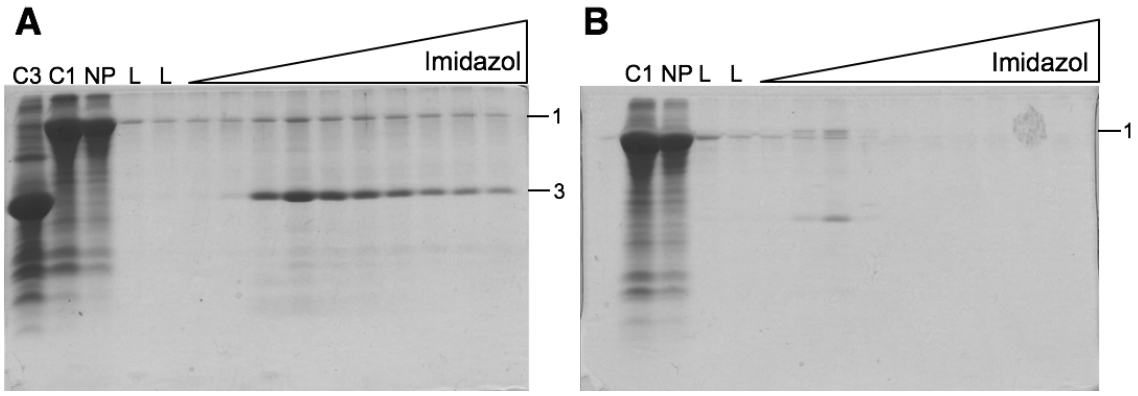

Figura 26: Copurificación de las subunidades recombinantes Asa1 y Asa3^{6H} por cromatografía de afinidad a níquel. A. Gel Tricina SDS-PAGE al 12% teñido con azul de Coomassie en el que se muestran las fracciones correspondientes al experimento de copurificación de las subunidades Asa1 y Asa3^{6H}. C3: carga de la muestra de los cuerpos de inclusión solubilizados de la subunidad Asa3^{6H}. C1: carga de la muestra de los cuerpos de inclusión solubilizados de la subunidad Asa1. NP: fracción correspondiente al material no retenido por la columna de níquel. L: fracciones correspondientes a dos lavados de la columna. El triángulo representa la serie de fracciones eluidas tras la aplicación de un gradiente de imidazol. Se señalan las bandas correspondientes a las subunidades Asa1 y Asa3^{6H}. **B.** Gel Tricina SDS-PAGE al 12% teñido con azul de Coomassie en el que se muestran las fracciones correspondientes al experimento control. C1: carga de la muestra de los cuerpos de inclusión solubilizados de la subunidad Asa1. NP: fracción correspondiente al material no retenido por la columna de níquel. L: fracciones correspondientes a dos lavados de la columna. El triángulo representa la elución con la aplicación de un gradiente de imidazol. No se observan la retención ni la elución de la subunidad Asa1.

El resultado de una única interacción de la subunidad Asa3 fue insuficiente para saber dónde ubicarla en la enzima de *Polytomella* o dónde ubicarla en relación con Asa1, por lo que se procedió a hacer análisis *in silico* buscando evidencia adicional. Al hacer un análisis de predicción de su estructura secundaria se encontró que es predominantemente helicoidal y con asas (Figura 27), la cual se observa claramente en el modelo que se obtuvo al hacer una predicción de la estructura terciaria de esta proteína (Figura 28A). En este modelo se puede ver que las hélices son cortas, unidas por asas y arregladas en motivos repetitivos; este tipo de motivos coinciden con las llamadas repeticiones armadillo (*armadillo repeats* o *ARM repeats*). Estas repeticiones se deben a la presencia de secciones de aproximadamente 42 aminoácidos que resultan en proteínas con una estructura repetitiva de tres alfa hélices cortas conectadas por asas, que a su vez se acomodan formando una superhélice dextrógira (Tewari et al. 2010). En el modelo tridimensional generado para la subunidad Asa3 se pueden identificar seis motivos repetitivos de este tipo, de 44 aminoácidos en promedio cada uno (Figura 28B).

En el mapa tridimensional construido para la ATPasa de *Polytomella* a partir de imágenes de criomicroscopía electrónica (Allegretti et al. 2015) se identificó un motivo estructural, cercano a la región membranal de la enzima, con la forma de una proteína con repeticiones armadillo que parece formar un puente entre los dos brazos periféricos (Figura 28C). Los datos generados aquí sugieren que Asa3 es la subunidad que puede adoptar ese tipo de estructura.

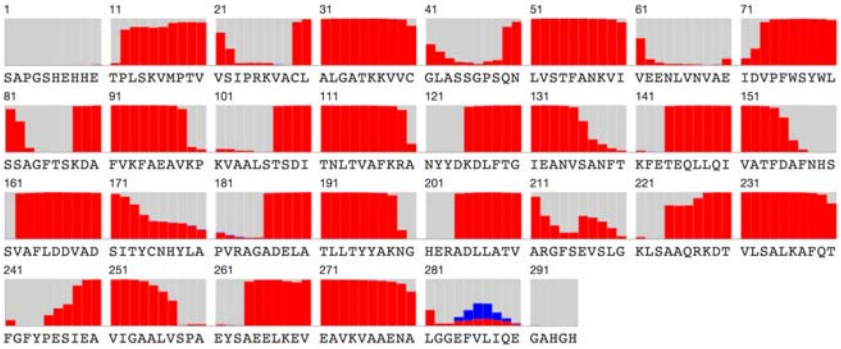

Figura 27: Análisis de predicción *in silico* de la estructura secundaria de la subunidad Asa3 de la ATPasa de *Polytomella*. Se muestra el resultado obtenido del análisis de la secuencia aminoacídica de la subunidad Asa3. Los residuos están numerados y su probabilidad de formación de cada tipo de estructura secundaria está representada con barras de colores: hélices alfa en rojo, láminas beta en azul y asas en gris.

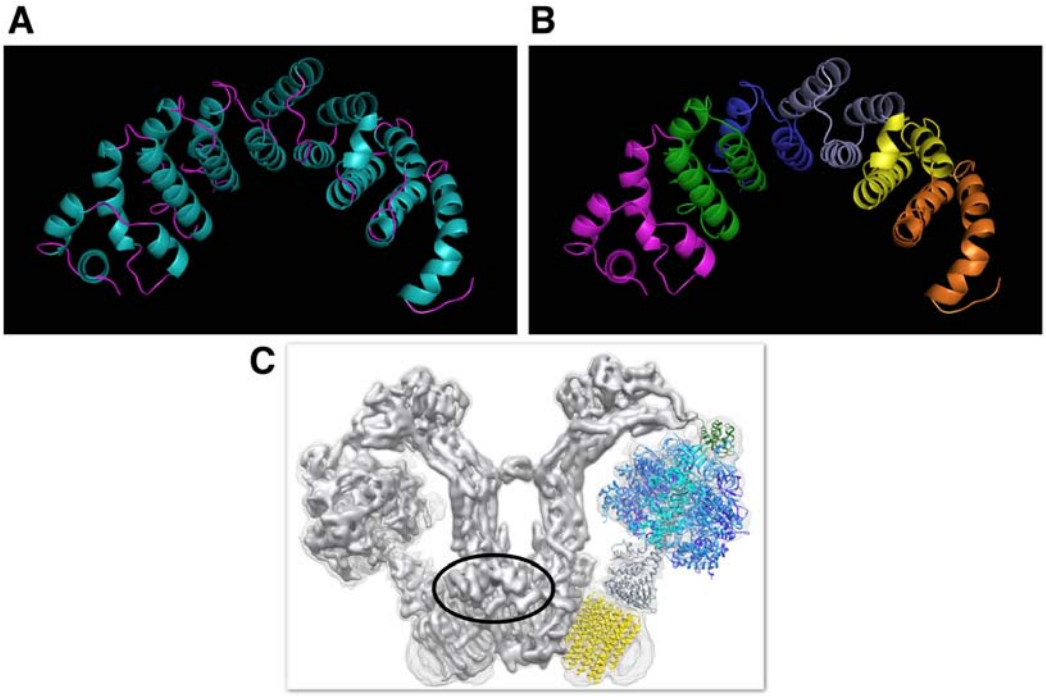

Figura 28: Análisis de predicción *in silico* de la estructura terciaria de la subunidad Asa3 y su localización en la ATPasa de *Polytomella*. A. Se muestra el modelo obtenido de la predicción de la estructura terciaria de la subunidad Asa3, con las alfa hélices en color cian y las asas en magenta. **B.** Se resaltan los seis motivos de repeticiones armadillo identificados en el modelo generado para la subunidad Asa3. **C.** Mapa tridimensional generado para la ATPasa de *Polytomella* en el que se señala la densidad correspondiente a una proteína con repeticiones armadillo. Los datos de difracción de rayos X ajustados en el mapa corresponden a los PDBs 2WSS (F_1) y 3U2Y (F_O). Imagen modificada de: Kühlbrandt 2015.

Resumiendo la evidencia obtenida de los ensayos de interacción y de los análisis de predicción *in silico*, podemos concluir que la subunidad Asa3 mantiene una interacción con la subunidad Asa1, con ninguna otra de las subunidades probadas (Asa2, Asa4, Asa7, OSCP) y que se localiza en una región cercana a la membrana ocupando el lugar de la densidad con la forma de repeticiones armadillo. Siendo así, la interacción Asa1-Asa3 es una evidencia más a favor de la presencia de una parte de Asa1 en la sección inferior del brazo periférico de la ATPasa de *Polytomella*, como se había sugerido anteriormente con base en la interacción Asa1-Asa8 (Figura 21).

6.3 Reconstitución de subcomplejos que involucran a la subunidad Asa1

6.3.1 Subcomplejo Asa1-Asa2-Asa3^{6H}-Asa4-Asa7-OSCP

Como continuación del estudio de las interacciones de la subunidad Asa1 con el resto de las subunidades Asa, y dadas las interacciones identificadas en este trabajo y en trabajos previos (Cano-Estrada et al. 2010, Miranda-Astudillo et al. 2014) se realizaron experimentos buscando reconstituir subcomplejos correspondientes a una parte del brazo periférico de la enzima con las subunidades recombinantes disponibles. Para este fin se sobreexpresaron y se obtuvieron cuerpos de inclusión independientes de las subunidades Asa1, Asa2, Asa3^{6H}, Asa4, Asa7 y OSCP, como se describe en los puntos 5.2 y 5.3 de la sección de materiales y métodos. Las pastillas de cuerpos de inclusión fueron tratadas como se explica en el punto 5.3 de la sección de materiales y métodos y se solubilizaron con urea 8.0 M. Todos los experimentos que se describen a continuación se realizaron a partir de las muestras de cuerpos de inclusión solubilizados de las subunidades Asa1, Asa2, Asa3^{6H}, Asa4, Asa7 y OSCP (Figura 29).

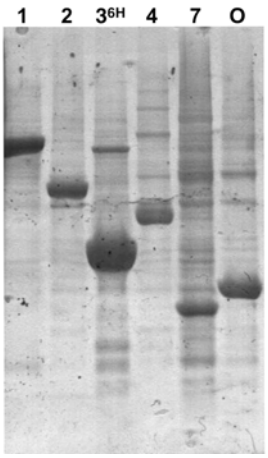

Figura 29: Cuerpos de inclusión solubilizados correspondientes a las subunidades recombinantes utilizadas en los ensayos de reconstitución de subcomplejos. Gel Tricina SDS-PAGE al 12% teñido con azul de Coomassie en el que se muestran las bandas enriquecidas de los cuerpos de inclusión lavados y solubilizados con urea 8 M. 1: Asa1, 2: Asa2, 3^{6H}: Asa3^{6H}, 4: Asa4, 7: Asa7, O: OSCP.

El primer paso del protocolo de reconstitución fue el replegamiento de las subunidades, para lo cual se hizo una diálisis escalonada de la mezcla de todas las proteínas, para disminuir gradualmente la concentración de urea de 8.0 M inicial a 0.5 M final y la concentración de NaCl de 500 mM inicial a 150 mM final. La muestra final se ultracentrifugó para eliminar el material agregado, en la figura 30 se observa que la mayor parte de las proteínas de interés se recuperaron en la fracción soluble de la muestra dializada. Este proceso se describe a detalle en el punto 5.10 de la sección de materiales y métodos.

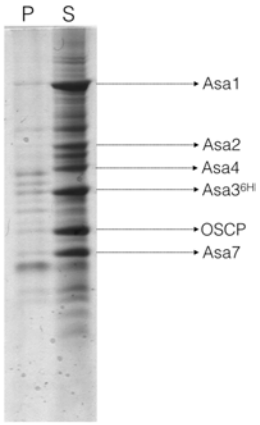

Figura 30: Muestra recuperada de la diálisis escalonada de la mezcla de subunidades Asa1-Asa2-Asa3^{6H}-Asa4-Asa7-OSCP. Gel Tricina SDS-PAGE al 12% teñido con azul de Coomassie en el que se observa la muestra dializada y centrifugada para separar las fracciones soluble e insoluble. Las proteínas de interés se recuperan en la fracción soluble. P: pastilla, S: sobrenadante.

El sobrenadante recuperado de la diálisis se concentró y se inyectó a dos columnas de exclusión molecular unidas en tándem, con el objetivo de aumentar la resolución y conseguir la mejor separación posible. El perfil de elución y las fracciones obtenidas de este paso de purificación se muestran en la figura 31. Las fracciones indicadas en el recuadro corresponden a un subcomplejo Asa1-Asa2-Asa3^{6H}-Asa4-Asa7-OSCP, y el resto del perfil corresponde a subunidades libres.

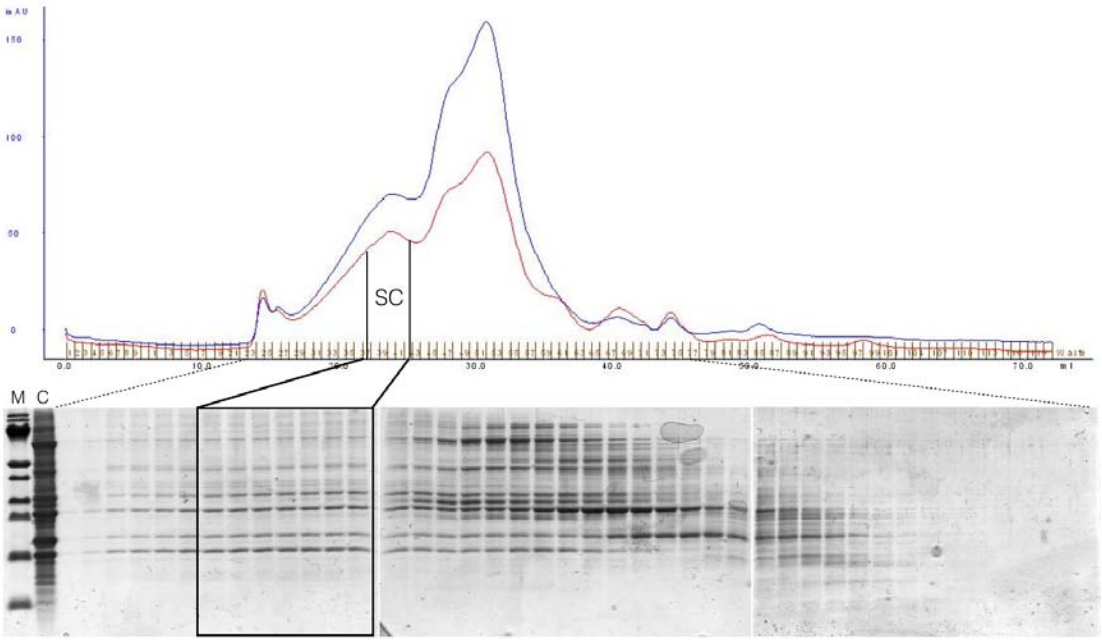

Figura 31: Subcomplejo Asa1-Asa2-Asa3^{6H}-Asa4-Asa7-OSCP reconstituido recuperado después de una purificación por cromatografía de exclusión molecular. En el panel superior se muestra el cromatograma obtenido de la purificación con las columnas Superose 6 10/300 GL + Superdex 200 10/300 GL. Se mide la absorbancia de la muestra (mAU) a dos longitudes de onda: 280 nm en azul y 214 nm en rojo. Se señala el pico correspondiente al subcomplejo (SC). En el panel inferior se muestran geles Tricina SDS-PAGE al 12% teñidos con azul de Coomassie en los que se observan las fracciones correspondientes al perfil de elución. M: marcador de peso molecular, C: muestra inyectada a las columnas.

Aprovechando la etiqueta de histidinas de la subunidad Asa3^{6H}, se buscó recuperar el subcomplejo después de un segundo paso de purificación, por medio de la retención de dicha subunidad en una matriz de níquel. Con este fin, las fracciones correspondientes al pico de elución del subcomplejo se juntaron y esa muestra se mezcló con resina de níquel equilibrada. Para asegurar la elución de un subcomplejo y disminuir la presencia de subunidades libres, la resina se lavó exhaustivamente con un amortiguador adicionado con 25 mM de imidazol. Posteriormente se procedió a incubar la resina con concentraciones crecientes de imidazol para

eluir las proteínas. Las fracciones obtenidas de los lavados y de la elución se muestran en la figura 32, en la que se observa que las seis proteínas coeluyen en un subcomplejo que se puede recuperar gracias a la etiqueta de histidinas que tiene la subunidad Asa3^{6H}.

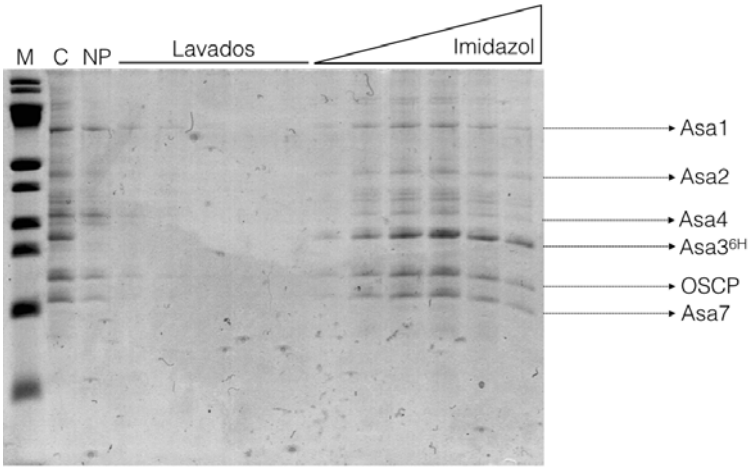

Figura 32: Subcomplejo Asa1-Asa2-Asa3^{6H}-Asa4-Asa7-OSCP reconstituido recuperado después de una cromatografía de afinidad. Gel Tricina SDS-PAGE teñido con azul de Coomassie en el que se muestran las fracciones obtenidas del proceso de purificación del subcomplejo proveniente de la purificación por exclusión molecular. Se indica la identidad de las proteínas eluidas al aplicar un gradiente de imidazol. M: marcador de peso molecular, C: muestra incubada con la resina de níquel, NP: muestra no retenida por la resina.

Las interacciones que explican el subcomplejo Asa1-Asa2-Asa3^{6H}-Asa4-Asa7-OSCP reconstituido se representan en el modelo de la figura 33, que se realizó rellenando las densidades de cada proteína, hasta donde lo permite la resolución, del mapa tridimensional de la ATPasa de *Polytomella* generado por Allegretti *et al.* 2015. Las subunidades Asa2, Asa3, Asa7 y OSCP mantienen interacciones con la subunidad Asa1 y la subunidad Asa4 se asocia con la subunidad Asa7.

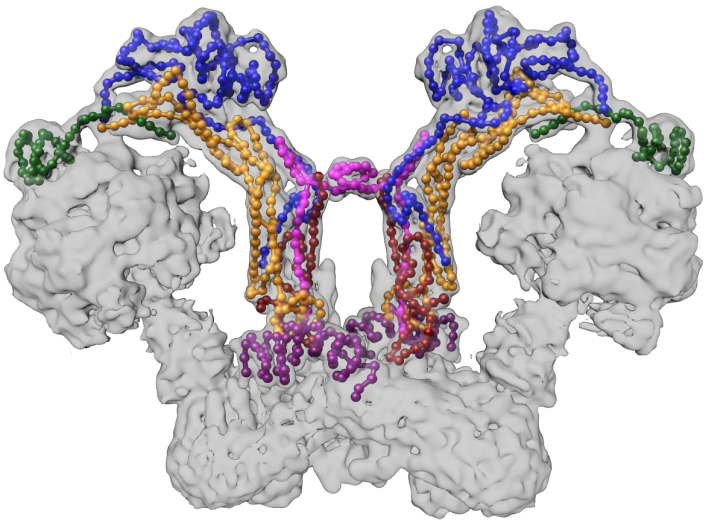

Figura 33: Modelo del subcomplejo Asa1-Asa2-Asa3^{6H}-Asa4-Asa7-OSCP. Mapa tridimensional de la ATPasa dimérica de *Polytomella* en el que se muestran las densidades correspondientes a las subunidades Asa1 (naranja), Asa2 (azul), Asa3 (morado), Asa4 (vino), Asa7 (rosa) y OSCP (verde oscuro). El mapa de densidad electrónica corresponde al generado por Allegretti *et al*. 2015 (EMD-2852).

6.3.2 Subcomplejo Asa1-Asa3^{6H}-OSCP

Con el objetivo de confirmar la hipótesis de que la subunidad Asa1 recorre el brazo periférico desde la parte cercana a la membrana (dadas las interacciones que mantiene con las subunidades Asa8 y Asa3) hasta la parte superior de la enzima (dada la interacción que mantiene con la subunidad OSCP), se planteó reconstituir un subcomplejo Asa1-Asa3^{6H}-OSCP. Como se hizo para el subcomplejo anterior, la mezcla de las tres proteínas se dializó en pasos disminuyendo la concentración de urea y de NaCl, y nuevamente se recuperaron las proteínas en la fracción soluble (Figura 34).

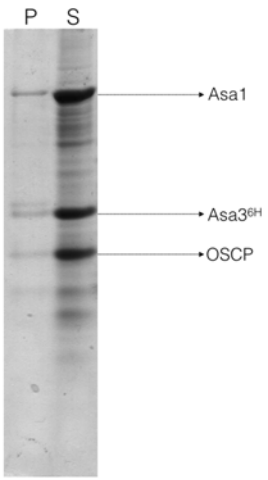

Figura 34: Muestra recuperada de la diálisis escalonada de la mezcla de subunidades Asa1-Asa3^{6H}-OSCP. Gel Tricina SDS-PAGE al 12% teñido con azul de Coomassie en el que se observa la muestra dializada y centrifugada para separar las fracciones soluble e insoluble. Las proteínas de interés se recuperan en la fracción soluble. P: pastilla, S: sobrenadante.

Siguiendo los pasos del protocolo de reconstitución establecidos para el subcomplejo anterior, se procedió a concentrar la muestra recuperada de la diálisis e inyectarla a una columna de exclusión molecular. El perfil de elución y las fracciones obtenidas se muestran en la figura 35, en la que se indica la parte de la elución que podría corresponder a un subcomplejo Asa1-Asa3^{6H}-OSCP. Esas fracciones se juntaron y se procedió a recuperar el subcomplejo después de un segundo paso de purificación por afinidad a una matriz de níquel (purificación en *batch*), por medio de la etiqueta de histidinas presente en la subunidad Asa3^{6H}. Las fracciones obtenidas de este proceso de purificación se muestran en la figura 36, en la que de nuevo se observa la coelución de las tres proteínas.

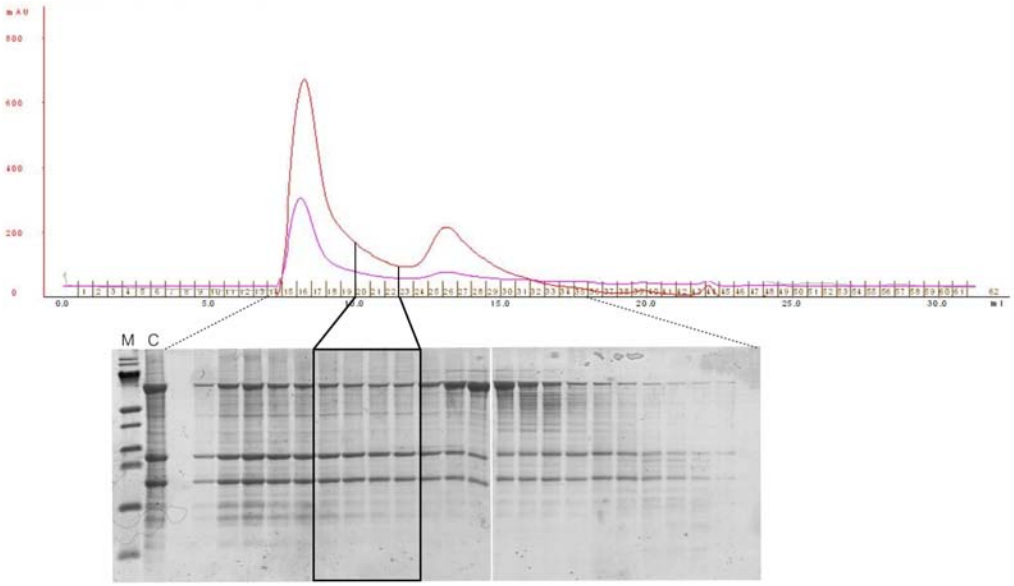

Figura 35: Subcomplejo Asa1-Asa3^{6H}-OSCP reconstituido recuperado después de una purificación por cromatografía de exclusión molecular. En el panel superior se muestra el cromatograma obtenido de la purificación con la columna Superdex 200 10/300 GL. Se mide la absorbancia de la muestra (mAU) a dos longitudes de onda: 280 nm en rojo y 214 nm en rosa. Se señala la parte correspondiente al subcomplejo Asa1-Asa3^{6H}-OSCP. En el panel inferior se muestran geles Tricina SDS-PAGE al 12% teñidos con azul de Coomassie en los que se observan las fracciones correspondientes al perfil de elución. M: marcador de peso molecular, C: muestra inyectada a las columnas.

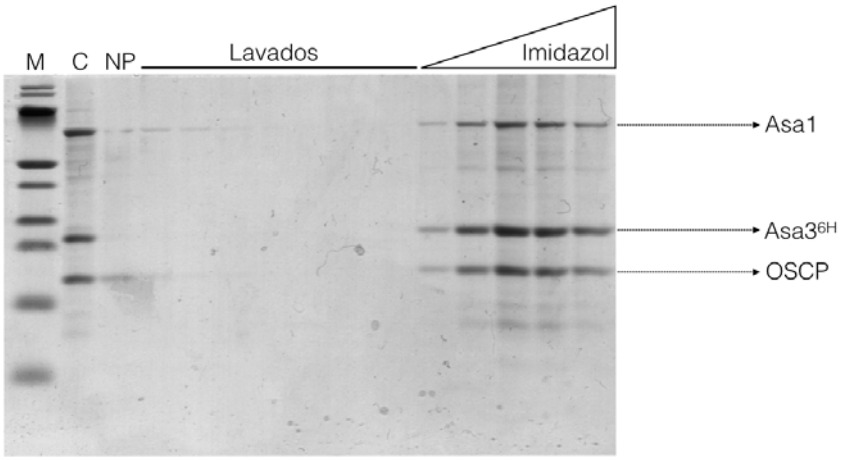

Figura 36: Subcomplejo Asa1-Asa3^{6H}-OSCP reconstituido recuperado después de una purificación por afinidad a níquel. Gel Tricina SDS-PAGE teñido con azul de Coomassie en el que se muestran las fracciones obtenidas del proceso de purificación del subcomplejo proveniente de la purificación por exclusión molecular. Se indica la identidad de las proteínas eluidas al aplicar un gradiente de imidazol. M: marcador de peso molecular, C: muestra incubada con la resina de níquel, NP: muestra no retenida por la resina.

El subcomplejo Asa1-Asa3^{6H}-OSCP también se pudo obtener al invertir los pasos de purificación: primero haciendo una purificación en *batch*, recuperándolo de la mezcla de proteínas proveniente de la diálisis, a través de la etiqueta de histidinas de la subunidad Asa3, y posteriormente concentrando e inyectando las fracciones eluidas a una columna de exclusión molecular. Como se puede ver en la figura 37, el subcomplejo Asa1-Asa3^{6H}-OSCP eluye con la presencia de muchos contaminantes después del paso de purificación por afinidad a níquel, mismos que disminuyen notoriamente después del paso de purificación por cromatografía de exclusión molecular; el subcomplejo Asa1-Asa3^{6H}-OSCP se recupera en el pico señalado en el cromatograma de la figura 38.

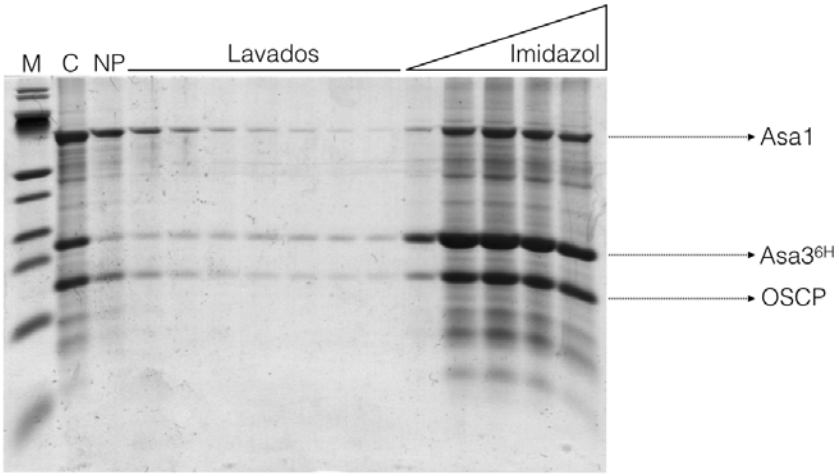

Figura 37: Subcomplejo Asa1-Asa3^{6H}-OSCP reconstituido recuperado después de una purificación por afinidad a níquel. Gel Tricina SDS-PAGE teñido con azul de Coomassie en el que se muestran las fracciones obtenidas del proceso de purificación del subcomplejo proveniente de la diálisis de replegado. Se indica la identidad de las proteínas eluidas al aplicar un gradiente de imidazol. M: marcador de peso molecular, C: muestra incubada con la resina de níquel, NP: muestra no retenida por la resina.

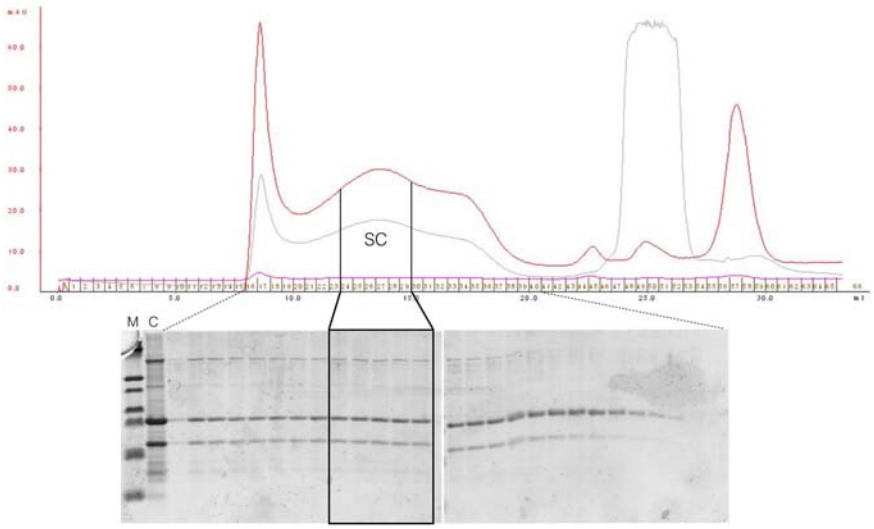

Figura 38: Subcomplejo Asa1-Asa3^{6H}-OSCP reconstituido recuperado después de una purificación por cromatografía de exclusión molecular. En el panel superior se muestra el cromatograma obtenido de la purificación del subcomplejo Asa1-Asa3^{6H}-OSCP, proveniente de la purificación por afinindad a níquel, con la columna Superose 6 10/300 GL. Se mide la absorbancia de la muestra (mAU) a tres longitudes de onda: 280 nm en rojo, 214 nm en gris y 254 nm en rosa. Se señala el pico correspondiente al subcomplejo Asa1-Asa3^{6H}-OSCP. En el panel inferior se muestran geles Tricina SDS-PAGE al 12% teñidos con azul de Coomassie en los que se observan las fracciones correspondientes a la sección indicada del perfil de elución. M: marcador de peso molecular, C: muestra inyectada a las columnas.

Las interacciones que explican el subcomplejo Asa1-Asa3^{6H}-OSCP reconstituido se representan en el modelo de la figura 39, en el cual se observa la posición que tiene cada subunidad en la enzima de *Polytomella* y la forma en la que la subunidad Asa1 puede unir a las subunidades Asa3 y OSCP.

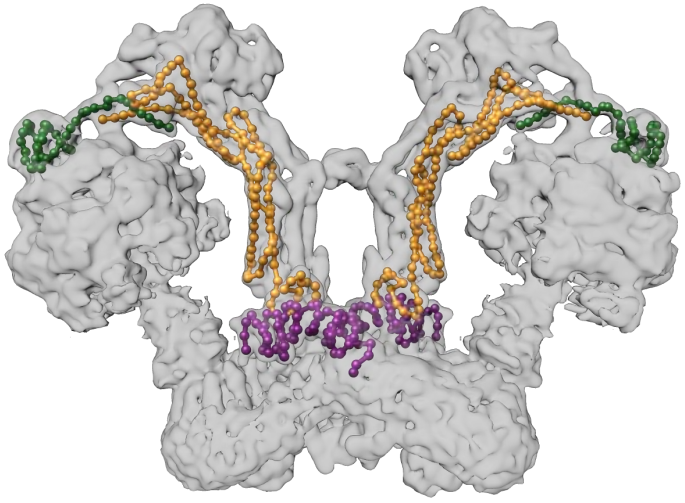

Figura 39: Modelo del subcomplejo Asa1-Asa3^{6H}-OSCP. Mapa tridimensional de la ATPasa dimérica de *Polytomella* en el que se muestran las densidades correspondientes a las subunidades Asa1 (naranja), Asa3 (morado) y OSCP (verde oscuro). El mapa de densidad electrónica corresponde al generado por Allegretti *et al*. 2015 (EMD-2852).

Con los resultados obtenidos en esta sección se puede concluir que las subunidades Asa utilizadas en los experimentos de reconstitución son capaces de interaccionar entre sí, pese a haber partido de un estado desnaturalizado, y formar subcomplejos estables Asa1-Asa2-Asa3^{6H}-Asa4-Asa7-OSCP y Asa1-Asa3^{6H}-OSCP. Sin embargo, es probable que durante el proceso de obtención de estos subcomplejos se formen agregados solubles que impiden una mejor separación, purificación (con menor presencia de contaminantes), y el enriquecimiento de las proteínas de interés. Estos resultados confirman el papel de Asa1 en el brazo periférico de la ATPasa de *Polytomella*, así como sus interacciones con las subunidades Asa3 y OSCP, ya que la coelución de las dos últimas subunidades, dadas las interacciones que mantiene cada una y sus posiciones en la enzima, sólo es posible gracias al puente que forma la subunidad Asa1 al conectar la parte inferior del brazo periférico (Asa1-Asa3) con la parte superior de la enzima (Asa1-OSCP) (Figura 39).

6.4 Nuevo método de replegamiento y exploración de las condiciones de cristalización de las subunidades Asa.

Experimentos realizados en colaboración con la Dra. Marie France Giraud del Institut de Biochimie et Génétique Cellulaires, en Burdeos, Francia.

Con el objetivo de intentar la cristalización de alguno de los subcomplejos formados, y para ese fin buscando favorecer el replegado correcto de las subunidades Asa y disminuir la formación de agregados, se decidió modificar la estrategia de replegamiento (el primer paso del protocolo de reconstitución). Se probaron numerosas y diversas estrategias y condiciones para obtener muestras puras y monodispersas que pudieran usarse para iniciar pruebas de cristalización. Finalmente se llegó a un protocolo de replegamiento y purificación, descrito a detalle en el punto 5.11 de la sección de materiales y métodos, con el que se obtuvieron los mejores resultados. Brevemente, la muestra de cuerpos de inclusión solubilizados con urea 8.0 M se diluye diez veces en un amortiguador de replegamiento en presencia de detergente y el osmolito TMAO. La muestra resultante se ultracentrifuga, el sobrenadante se incuba con una resina de níquel que se lava extensivamente y finalmente las proteínas se recuperan al hacer incubaciones con concentraciones crecientes de imidazol.

6.4.1 Recuperación del subcomplejo Asa1-Asa3^{6H}-OSCP con el nuevo método de replegamiento

El nuevo procedimiento de reconstitución se realizó para obtener el subcomplejo Asa1-Asa3^{6H}-OSCP. La mezcla de cuerpos de inclusión solubilizados de las tres proteínas se replegó por dilución como se describió arriba y el subcomplejo se recuperó por medio de purificación con una matriz de níquel. El patrón electroforético de las fracciones obtenidas se muestra en la figura 40. Una vez más se observó la coelución de las tres subunidades, aunque en muy baja cantidad, por lo que no fue posible utilizar estas muestras para sembrar pruebas de cristalización.

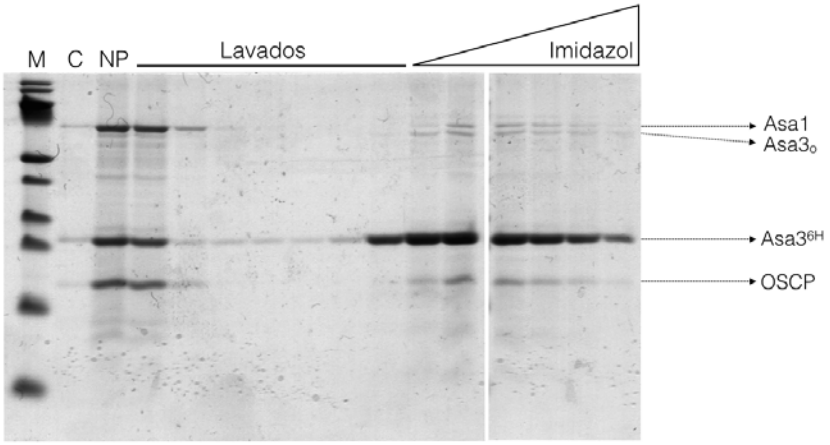

Figura 40: Purificación del subcomplejo Asa1-Asa3^{6H}-OSCP por afinidad a una matriz de níquel después de recuperarlo por medio del nuevo método de replegamiento. Geles Tricina SDS-PAGE al 12% teñidos con azul de Coomassie en los que se muestran las fracciones correspondientes al procedimiento de purificación del subcomplejo Asa1-Asa3^{6H}-OSCP que se recuperó del replegamiento por dilución. P y S: alícuotas de la pastilla (P) y la fracción soluble (S) obtenidas después de ultracentrifugar la muestra. NP: material no retenido por la resina. Se señalan las bandas correspondientes a la coelución de las subunidades Asa1, Asa3^{6H} y OSCP, y una banda que corresponde a una forma oligomérica de la subunidad Asa3 (Asa3$_o$).

6.4.2 Recuperación de las subunidades Asa con el nuevo método de replegamiento

Pensando en cristalizar las proteínas individualmente se planteó replegar y purificar las subunidades Asa que están marcadas con una etiqueta de histidinas, ya que éstas se pueden recuperar con relativa facilidad usando una matriz de níquel. Se llevó a cabo el protocolo de replegamiento y purificación descrito anteriormente con las subunidades Asa1^{6H}, Asa2^{6H}, Asa3^{6H}, Asa4^{6H} y Asa7^{6H}, pero las que se obtuvieron en las condiciones óptimas para sembrar pruebas de

cristalización fueron únicamente las subunidades Asa3^{6H} y Asa7^{6H} (con ligeras modificaciones del protocolo según las proteínas, ver punto 5.11 de materiales y métodos y Anexo 2 inciso H).

6.4.2.1 Subunidad Asa3^{6H}

El patrón polipeptídico de las fracciones que se obtuvieron de la purificación de la subunidad Asa3^{6H} se muestran en la Figura 41; se seleccionaron aquellas con la mayor cantidad de proteína y menor cantidad de contaminantes, se juntaron, se concentraron y posteriormente se analizaron mediante dispersión dinámica de luz (DLS) para evaluar su estado de agregación. La muestra de la subunidad Asa3^{6H} se concentró hasta alcanzar 4 mg/mL y se analizó con DLS (Figura 42A). Esta muestra se dejó dializando toda la noche, para evitar la formación de cristales de los componentes del amortiguador, y la muestra final se volvió a analizar con DLS (Figura 42B). Se tomó una alícuota de la muestra dializada que se siguió concentrando hasta alcanzar aproximadamente 6 mg/mL y se volvió a analizar (Figura 42C).

Las tres muestras (muestra con 4 mg/mL sin dializar, muestra dializada y muestra con 6 mg/mL) se obtuvieron con un porcentaje de polidispersión menor al 15%, que es el máximo porcentaje recomendable para sembrar pruebas de cristalización, por lo que se iniciaron pruebas de cristalización de las tres proteínas. Se obtuvieron dos cristales pequeños en una de las condiciones probadas para la subunidad Asa3 (acetato de sodio 1.4 M, MES 100 mM, pH 6.5), uno de ellos se sometió a una sesión de difracción en el sincrotrón del ESFR (*European Synchrotron Radiation Facility*) en Grenoble, Francia, pero no se obtuvieron patrones de difracción (Figura 43).

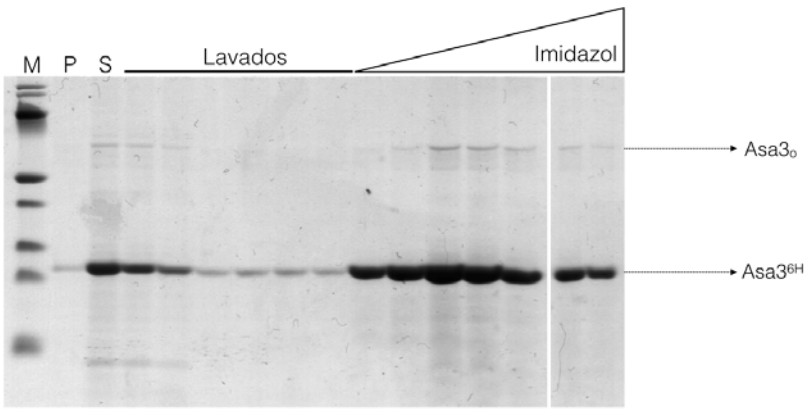

Figura 41: Obtención de la subunidad Asa3^{6H} por afinidad a una matriz de níquel después de recuperarla por medio del nuevo método de replegamiento. Geles Tricina SDS-PAGE al 12% teñidos con azul de Coomassie en los que se muestran las fracciones correspondientes al procedimiento de purificación de la subunidad Asa3^{6H} recuperada del replegamiento por dilución. P y S: alícuotas de la pastilla (P) y la fracción soluble (S) obtenidas después de ultracentrifugar la muestra. NP: material no retenido por la resina. Se señalan las bandas correspondientes a la subunidad Asa3^{6H} y a una forma oligomérica Asa3$_o$.

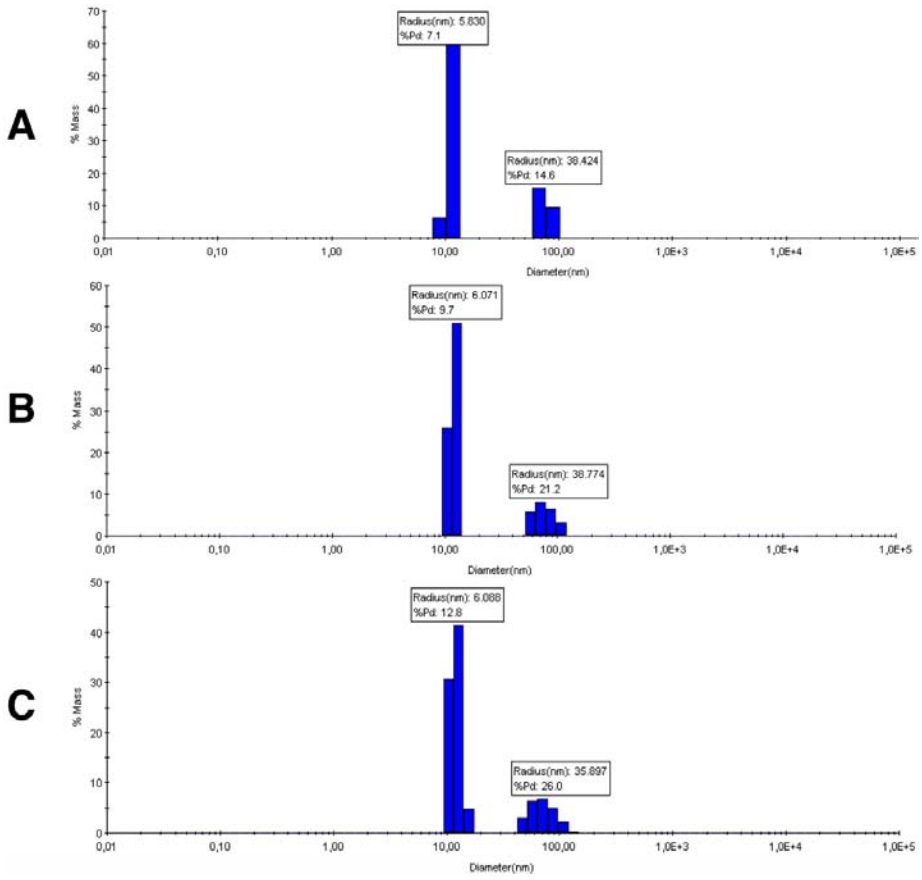

Figura 42: Análisis del estado de agregación de la subunidad Asa3^{6H} por medio de dispersión dinámica de luz. A. Estado de polidispersión de la muestra concentrada hasta 4mg/mL. **B.** Estado de polidispersión de la muestra después de una diálisis de 8 horas. **C.** Estado de polidispersión de la muestra dializada y concentrada hasta 6 mg/mL. En A, B y C las barras obtenidas en 10 nm corresponden a la banda principal de Asa3 y las barras obtenidas alrededor de 100 nm corresponden a la banda de la forma oligomérica observadas en los geles.

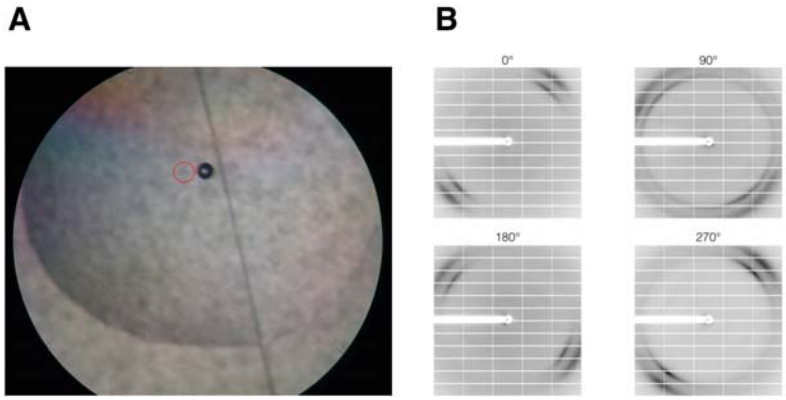

Figura 43: Cristal obtenido de la subunidad Asa3^{6H} y sus patrones de difracción. A. Fotografía del cristal que se utilizó para difractar. **B.** Patrones de difracción obtenidos a distintos ángulos de rotación.

6.4.2.2 Subunidad Asa7^{6H}

Las fracciones que se obtuvieron de la purificación de la subunidad Asa7^{6H} se muestran en la Figura 44; se seleccionaron aquellas con la menor cantidad de contaminantes, las eluidas con 100 y 150 mM de imidazol (Figura 43). Se concentraron por separado hasta alcanzar aproximadamente 5 mg/mL y se analizó su estado de polidispersión con DLS. Ambas se obtuvieron con un promedio de 10% de polidispersión (Figura 45) y ambas se utilizaron para sembrar pruebas de cristalización. Hasta la última revisión de las placas, se observan algunos objetos amorfos y algunos otros objetos que podrían ser cristales.

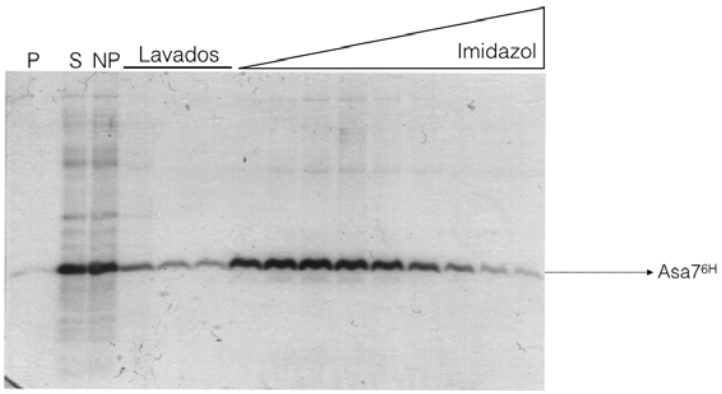

Figura 44: Obtención de la subunidad Asa7^{6H} por afinidad a una matriz de níquel después de recuperarla por medio del nuevo método de replegamiento. Gel Tricina SDS-PAGE al 12% teñido con azul de Coomassie en el que se muestran las fracciones correspondientes al procedimiento de purificación de la subunidad Asa7^{6H} que se recuperó del replegamiento por dilución. P y S: alícuotas de la pastilla (P) y la fracción soluble (S) obtenidas después de ultracentrifugar la muestra. NP: material no retenido por la resina. Se señala la banda correspondiente a la subunidad Asa7^{6H}.

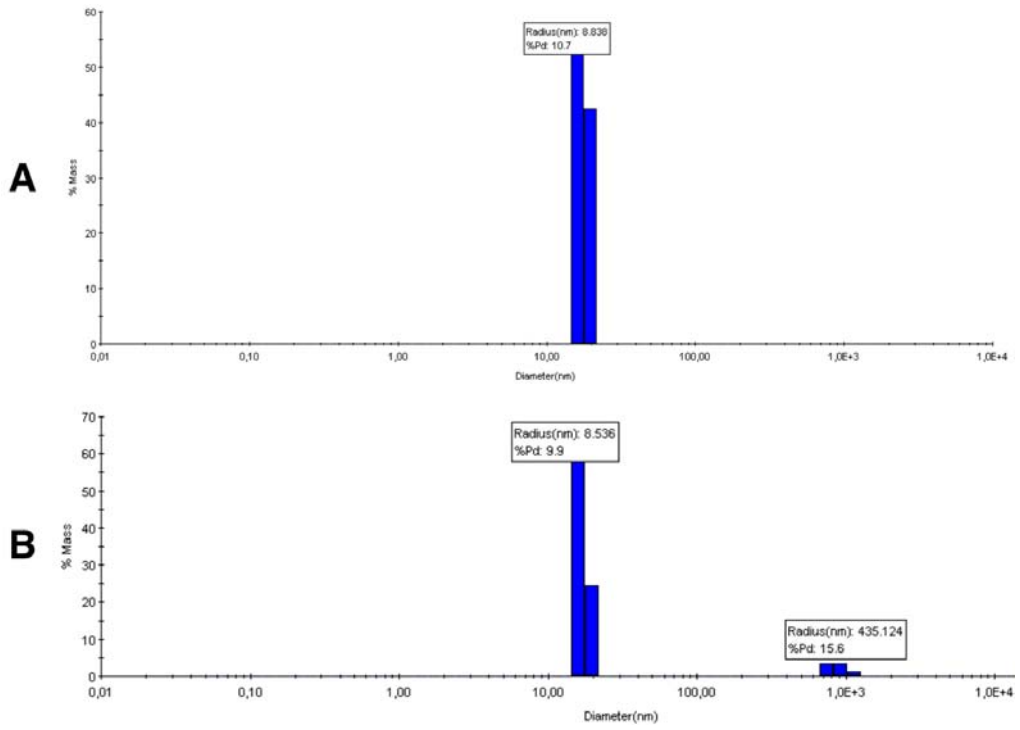

Figura 45: Análisis del estado de agregación de la subunidad Asa7^{6H} por medio de dispersión dinámica de luz. A. Estado de polidispersión de la muestra Asa7-100 concentrada hasta 5 mg/mL. **B.** Estado de polidispersión de la muestra Asa7-150 concentrada hasta 5 mg/mL.

Los resultados obtenidos en esta sección sugieren que el método de replegamiento seguido permite disminuir la formación de agregados de proteína, lo cual resulta en la obtención de muestras que pueden ser concentradas y aún así mantenerse en un estado de monodispersión que no se había logrado alcanzar antes, y que, en el caso de la subunidad Asa3, permitió su cristalización.

7. Resumen de los resultados obtenidos

Con este trabajo encontramos que la subunidad Asa1 mantiene interacciones con las subunidades Asa2, Asa3, Asa7, Asa8 y OSCP; y que la interacción Asa1-OSCP disminuye al usar una versión trunca de la subunidad Asa1 que no tiene el extremo carboxilo terminal. También exploramos la topología de la subunidad Asa3 y concluimos que mantiene una interacción con la subunidad Asa1 y con ninguna otra de las subunidades probadas. La predicción *in silico* de las estructuras secundaria y terciaria de Asa3 indica que adquiere una estructura de repeticiones tipo armadillo y esto es consistente con la presencia de un motivo estructural con esa forma en el mapa tridimensional de la ATPasa de *Polytomella*, lo cual permite ubicarla en ese sitio de la enzima y explica la ausencia de interacción con otras subunidades del brazo periférico que se encuentran extrínsecas a la membrana. Esta evidencia, además, confirma la presencia de Asa1 en la región cercana a la membrana de la ATPasa. Con la reconstitución de subcomplejos de subunidades Asa recombinantes se confirmaron las interacciones de Asa1 encontradas con las inmunorréplicas tipo Far Western, así como la hipótesis de que recorre todo el brazo periférico (Figura 46) y, además, podemos concluir que los métodos utilizados permiten recuperar las subunidades de cuerpos de inclusión y que éstas adopten la suficiente estructura para interaccionar y formar subcomplejos estables en solución. La obtención de cristales de la subunidad Asa3 indica que el protocolo de replegado y purificación diseñado permite la obtención de muestras en calidad y cantidad suficientes para que se lleve a cabo un proceso de cristalización.

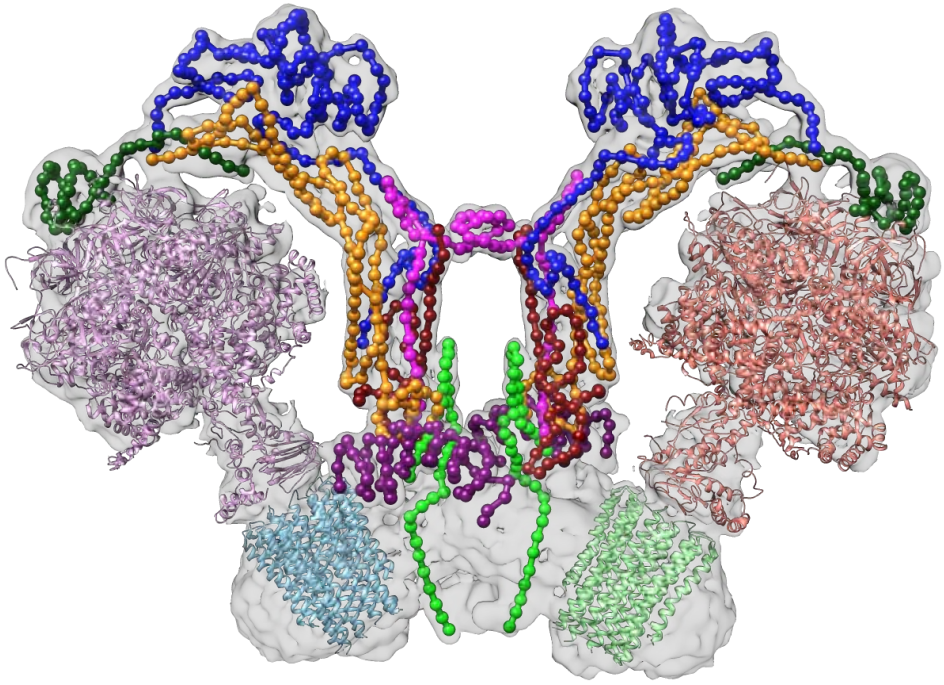

Figura 46: Modelo de las interacciones obtenidas en este trabajo. Mapa de densidad electrónica de la ATPasa dimérica de *Polytomella* en el que se muestran las densidades correspondientes a las subunidades Asa1 (naranja), Asa2 (azul), Asa3 (morado), Asa4 (vino), Asa7 (rosa), Asa8 (verde claro) y OSCP (verde oscuro). El mapa de densidad electrónica corresponde al generado por Allegretti *et al*. 2015 (EMD-2852). Los datos de difracción de rayos X ajustados en el mapa corresponden a la enzima de *S. cerevisiae* (PDB 2WPD, Dautant *et al*. 2010).

8. Discusión

La estructura general de las ATPasas rotatorias está conservada, todas son enzimas que funcionan como nanomotores que sintetizan y/o hidrolizan ATP y todas tienen tres partes distinguibles: un rotor, un estator o brazo periférico y un núcleo catalítico. Los brazos periféricos de las ATPasas tipo A y V están altamente conservados tanto estructural como funcionalmente, sin embargo, aquellos de las ATPasas tipo F tienen un estructura muy variable.

El brazo periférico más estudiado es el de la enzima de *E. coli*, que está formado por un homodímero de subunidades *b* que se asocia a través de una hélice entrecruzada con giro dextrógiro. Esta interacción se debe a la presencia de un patrón *hendecad repeat* conservado en las subunidades *b* de *E. coli* y otros procariontes, y que es característico del enrollamiento dextrógiro de hélices entrecruzadas (Del Rizzo *et al*. 2002) (Figura 8). Los brazos periféricos de las ATPasas de bovino y levadura están formados por más subunidades (*b*, *d*, F6, A6L, *e*, *f*, *g* y OSCP en bovino; Su4, *d*, *h*, Su8, *e*, *f*, *g*, OSCP en levadura) (Cano-Estrada *et al.* 2011). Las subunidades *b* son homólogas a las bacterianas y en todas estas enzimas se mantiene la interacción de un elemento del brazo periférico con uno del núcleo catalítico (δ/OSCP-α) y con uno del sector F_O (*b*-*a*), las interacciones a lo largo del brazo están mediadas por hélices entrecruzadas y su arquitectura general es la misma (Figura 9).

En contraste con lo anterior, las ATPasas de organismos como *Trypanosoma brucei* (Zíková et al. 2009), *Tetrahymena thermophila* (Balabaskaran Nina et al. 2010), *Paramecium tetraurelia* (Mühleip et al. 2016), *Euglena gracilis* (Yadav et al. 2017) y *Polytomella* sp. (Cano-Estrada et al. 2010), las llamadas dímeros tipo protozoario, son ejemplos de enzimas con características atípicas (diferentes de los dímeros tipo metazoario de bacterias, levaduras y mamíferos), principalmente con respecto a la estructura de sus brazos periféricos. La evidencia disponible sugiere que estos organismos perdieron las subunidades que normalmente forman el brazo periférico y adquirieron otras para formarlo; lo cual indica que el brazo periférico es una estructura específica de cada linaje de eucariontes estudiado a la fecha (Yadav et al. 2017).

Debido a que no existen estructuras de alta resolución de ninguna de estas enzimas, no se sabe si sus brazos periféricos mantienen la horma de aquellos de bacteria, levadura y bovino, es decir, si también están formados por hélices alargadas asociadas a través de hélices entrecruzadas, aunque considero probable que así sea. Cabe mencionar que el dímero de la enzima de *Polytomella* es el único, hasta ahora, que además de unirse por la parte membranal del brazo periférico se une también a la mitad del mismo (Allegretti et al. 2015), probablemente a través de la subunidad Asa7 (Vázquez-Acevedo et al. 2016) (Figura 46).

8.1 De la topología de la enzima

Una de las ATPasas atípicas más caracterizadas es la de *Polytomella* sp., de la que además existe una estructura tridimensional, aunque de baja resolución (7 Å). En este trabajo se estudiaron las interacciones que mantiene la subunidad Asa1 con otras subunidades del brazo periférico. Se encontró que la subunidad Asa1 interacciona con la subunidad OSCP y con las subunidades Asa2, Asa3, Asa7 y Asa8. Además, se encontró que la subunidad Asa3 adopta una estructura tipo armadillo, que coincide con la presencia de un motivo estructural con esa forma en el mapa tridimensional de la ATPasa de *Polytomella* (Allegretti et al. 2015), y que entonces permite ubicarla en una región de la enzima muy cercana a la membrana interna mitocondrial. Otra evidencia que apoya la presencia de la subunidad Asa3 en esa región es su interacción con la subunidad Asa8 (Cano-Estrada et al. 2010, Sánchez-Vásquez et al. 2017), ya que la última es una proteína pequeña (9.9 kDa) con un segmento transmembranal predicho (van Lis et al. 2007).

Las proteínas con estructura tipo armadillo no se caracterizan por tener alta identidad de secuencia, pero sí comparten un parecido estructural. Las repeticiones armadillo se dan por secuencias de 42 aminoácidos en promedio; se considera que estas secuencias tienen una naturaleza degenerada debido a que no hay una secuencia consenso definida, sin embargo, resultan en una estructura tridimensional conservada (Coates 2003). Las algas verdes unicelulares, como *C. reinhardtii*, tienen un contenido importante de proteínas tipo armadillo, comparadas con otros organismos con genomas de tamaño parecido (Tewari et al. 2010) y la

subunidad Asa3, presente tanto en *C. reinhardtii* como en *Polytomella*, podría ser un ejemplo. La falta de identidad de secuencia de Asa3 con otras proteínas de estructura semejante podría ser la razón por la que no se había detectado antes. Varias proteínas tipo armadillo se han identificado sólo hasta que se conoció su estructura cristalográfica (Tewari et al. 2010).

Las interacciones encontradas en este trabajo sugieren que la subunidad Asa1 recorre todo el brazo periférico, lo cual no es sorprendente dado el tamaño de esta proteína (618 residuos, 66.1 kDa), desde el sector F_O (Asa1-Asa8) hasta la parte más alta del sector F_1 (Asa1-OSCP) (Colina-Tenorio et al. 2016), y tiene superficie suficiente para mantener tres interacciones más (Asa1-Asa2, Asa1-Asa3 y Asa1-Asa7). Experimentos previos realizados con la enzima utilizando agentes entrecruzadores sugirieron una interacción Asa1-Asa4 (Cano-Estrada et al. 2010) que no fue detectada en este trabajo. Esto podría explicarse si las subunidades Asa1 y Asa4 no mantienen una interacción muy estrecha en el complejo, que si bien puede detectarse e interpretarse como proximidad entre ambas subunidades al utilizar agentes entrecruzadores, no se detecta al trabajar con las proteínas aisladas y evaluar su interacción por Far Western Blot. En otras palabras, es probable que las subunidades Asa1 y Asa4 no establezcan interacciones por hélices entrecruzadas. Por su parte, la interacción Asa1-Asa8 se ha encontrado utilizando agentes entrecruzadores (Sánchez-Vásquez et al. 2017) y aquí se detectó por Far Western Blot al tener en la membrana a la subunidad Asa1 pero no cuando Asa8 se fija a la membrana. Esto podría deberse a que la subunidad Asa8 estando en la membrana, dado su tamaño (9.9 kDa), no expone la suficiente superficie para que la subunidad Asa1 se una y pueda detectarse una señal.

Previamente se estableció que la subunidad OSCP está en contacto con la subunidad α (Cano-Estrada et al. 2010), que la subunidad Asa8 tiene una parte embebida en la membrana en contacto con la subunidad Asa6 (Sánchez-Vásquez et al. 2017), y que la subunidad Asa6 (membranal) está en contacto con la subunidad membranal *a* (Klusch et al. 2017). Siendo así, la interacción Asa1-OSCP es el contacto del brazo periférico con el sector F_1, y la interacción Asa1-Asa8 es el contacto del brazo periférico con el sector F_O (considerando que F_O en *Polytomella* incluye Asa8-Asa6-*a*-*c*). Entonces, se puede decir que en la enzima de *Polytomella* también se mantienen los

contactos del brazo periférico con el núcleo catalítico y con el sector F_O y que Asa1 es la subunidad responsable de establecer estos contactos; aunque en este caso no directamente como con la interacción *b*-*a*, sino a través de tres subunidades no conservadas (Asa1-Asa8-Asa6). Esta observación permite concluir que la interacción del brazo periférico con el núcleo catalítico y con el sector F_O, necesaria para cumplir con su papel de estator, es una característica conservada en todas las ATPasas rotatorias, sin importar qué tan divergentes, ya que también existe en las ATPasas tipo A (Schep et al. 2016) y V (Zhao et al. 2015).

Los experimentos de disociación de la enzima con distintos tratamientos representan evidencias relevantes para explicar las interacciones de las subunidades Asa en el brazo periférico de la ATPasa de *Polytomella*. Con éstos se ha observado que las subunidades Asa2-Asa4-Asa7 se comportan como una unidad independiente que se disocia fácilmente del complejo al calentar, lo cual deja un brazo periférico formado por Asa1-Asa5-Asa3-Asa8-F_O. Estos datos podrían explicar la ausencia de interacción de Asa1 con Asa4, y sugieren que el brazo periférico puede dividirse en dos secciones principales: Asa2-Asa4-Asa7 y Asa1-Asa3-Asa5-Asa8-F_O. Estos experimentos, además, han dejado ver que esta enzima tiene dos sitios de dimerización: uno en una parte completamente extrínseca a la membrana (dado por Asa7) y hasta ahora exclusivo de *Polytomella*, y otro embebido en la membrana (dado por Asa6/Asa8/Asa9).

Todas las interacciones entre subunidades Asa que se han encontrado hasta la fecha, con varios enfoques bioquímicos, se muestran en la Tabla 2. La única evidencia bioquímica que se tiene sobre la subunidad Asa5, la última subunidad que falta acomodar en el mapa topológico de la ATPasa de *Polytomella*, es su presencia en el subcomplejo Asa1-Asa3-Asa5-Asa8-*a*-*c* obtenido al disociar la enzima con calor y con detergente (Vázquez-Acevedo et al. 2006, Colina-Tenorio et al. 2016). Por predicciones *in silico* se sabe que esta subunidad tiene un bolsillo hidrofóbico (*hydrophobic pocket*), lo cual sugiere su presencia en una región de la enzima cercana a la membrana. Basados en su tamaño (13.9 kDa) y en los datos con que se cuenta, se puede proponer que una parte de Asa5 se localiza en la parte baja del complejo, probablemente en contacto con Asa1, razón por la cual se encuentra en el subcomplejo mencionado arriba. De ser así, las

interacciones en el subcomplejo pueden explicarse como: Asa3 + Asa8, ambas unidas a Asa1 y ésta unida a Asa5. La presencia de *a* y *c* no es tan clara, podría ser que la subunidad *a* mantenga una interacción con Asa8 que no se ha detectado. En el mapa tridimensional de la enzima de *Polytomella* obtenido recientemente (4.1 Å), se estableció la interacción de la subunidad Asa6 con la subunidad *a* (Klusch et al. 2017), pero hay más densidad correspondiente a cruces transmembranales, que no fue explicada y que podría deberse a la subunidad Asa8 y/o Asa9.

	Asa1	Asa2	Asa3	Asa4	Asa5	Asa6	Asa7	Asa8	Asa9	OSCP
Asa1		FW	FW CP	E			FW E	FW E		FW CP
Asa2	FW			E FW CP			E FW CP			E DC
Asa3	FW CP							E		
Asa4	E	E FW CP					FW CP SC			
Asa5								E		
Asa6						DH E CP			CP	
Asa7	FW E	E FW CP		FW CP RS						
Asa8	FW E		E		E			CP	DH FW E	
Asa9						CP		DH FW CP E		
OSCP	FW CP	E DC								

Tabla 2. Interacciones y proximidades entre las subunidades Asa de la ATPasa mitocondrial de *Polytomella* sp. Se muestran todas las interacciones que se han obtenido hasta la fecha. FW: Far Western, CP: copurificación de subunidades recombinantes, DC: disociación de la enzima con calor, E: experimentos con agentes entrecuzadores, RS: reconstitución de subcomplejos; DH: experimentos de doble híbrido Se incluyen lo datos obtenidos en este trabajo y los datos publicados por: Villavicencio-Queijeiro et al. 2009, Cano-Estrada et al. 2010, Miranda-Astudillo et al. 2014, Colina-Tenorio et al. 2016 y Sánchez-Vásquez et al. 2017.

8.2 Hacia la cristalización de la enzima

La recuperación de proteínas a partir de cuerpos de inclusión es una necesidad común en el trabajo con proteínas hidrofóbicas. El procedimiento consiste en solubilizar los cuerpos de inclusión, que contienen generalmente una buena cantidad de la proteína de interés, con agentes caotrópicos como urea o guanidina, y el paso crítico es posteriormente eliminar o disminuir la concentración del agente desnaturalizante para tener, idealmente, a la proteína de interés replegada. La eficiencia del método de replegado depende de muchos factores y es un juego de ensayo y error, pero en general se piensa que la recuperación de proteínas replegadas *in vitro* suele ser mayor cuando el replegado se hace por dilución que cuando se hace por diálisis (Yamaguchi y Miyazaki 2014). En este trabajo se probaron ambos métodos y se encontró que la diálisis permite recuperar cantidades mayores de proteína soluble, pero con la concomitante formación de agregados (solubles e insolubles) y/o intermediarios de plegamiento; y el replegado por dilución lleva a la recuperación de cantidades menores de proteína pero con menos agregados y una población mayormente plegada, tomando el bajo porcentaje de polidispersión observado como indicación de baja presencia de agregados.

La reconstitución de subcomplejos estables de subunidades Asa a partir de cuerpos de inclusión solubilizados con urea sugiere que al menos una fracción de las proteínas pueden replegarse y adoptar una estructura suficiente para que se den interacciones entre las proteínas. Sin embargo, con el procedimiento seguido inicialmente (replegamiento por diálisis escalonada), aún existe una fracción considerable de proteínas que se agregan e impiden una mejor separación durante el paso de exclusión molecular. Para juzgar estos resultados hay que considerar dos puntos importantes: i) la separación por cromatografía de exclusión molecular depende tanto del tamaño como de la forma de las proteínas, por lo que dos proteínas con pesos moleculares diferentes pueden eluir juntas o muy cerca una de la otra por su forma. Esto, aunado a la tendencia de agregación de las proteínas hidrofóbicas (y pensando que lo más probable es que las subunidades Asa adopten estructuras helicoidales alargadas), representa un obstáculo en la separación de las distintas poblaciones de proteína; y ii) con respecto al subcomplejo Asa1-Asa2-Asa3^{6H}-Asa4-

Asa7-OSCP, en este punto no podemos excluir la posibilidad de estar trabajando con un subcomplejo dimérico, dada la posibilidad de una dimerización mediada por la subunidad Asa7 (Vázquez-Acevedo et al. 2016) (Figura 45); esto implicaría que la elución de las columnas de exclusión molecular incluye las siguientes poblaciones: agregados solubles, complejos diméricos, complejos monoméricos, complejos pequeños y subunidades libres. Todos estos factores complican la separación y por lo tanto la obtención de muestras susceptibles de ser cristalizadas.

El método de replegamiento por dilución en presencia de TMAO mejoró considerablemente la calidad de las muestras, al punto de permitir sembrar pruebas de cristalización, si no para los subcomplejos, sí para las subunidades Asa3^{6H} y Asa7^{6H}. El TMAO es un osmolito que ocurre naturalmente en organismos con células en las que existe alta concentración de urea (peces cartilaginosos) y constituye un mecanismo de protección contra los efectos desnaturalizantes de la urea (Hamada et al. 2009), lo que lo hace particularmente útil para recuperar proteínas que fueron desnaturalizadas con urea (como las subunidades Asa en cuerpos de inclusión). El TMAO promueve el plegamiento a estados nativos funcionales, como demuestran estudios de recuperación de actividad enzimática después de distintos tratamientos desnaturalizantes (Yancey et al. 1982, Baskakov y Bolen 1998, Ishibashi et al. 2003). Asimismo, el TMAO induce el replegamiento de proteínas que fueron completamente desnaturalizadas, con urea y otros agentes, a juzgar por espectros de dicroísmo circular (Baskakov y Bolen 1998, Mello y Barrick 2003). Este osmolito, junto con otros agentes, fue utilizado en el replegamiento *in vitro* de una enzima de 69 kDa de *E. coli* con resultados exitosos (Paul et al. 2007). Todas estas evidencias apoyan la noción de que las subunidades Asa3^{6H} y Asa7^{6H} replegadas en presencia de TMAO muy probablemente recuperaron una estructura nativa y esto se reflejó en la obtención de muestras monodispersas aún con alta concentración de proteína. Se ha propuesto que el efecto del TMAO sobre el replegamiento de proteínas *in vitro* se debe a que su interacción con la cadena principal de la proteína es termodinámicamente desfavorable y desestabiliza los estados desnaturalizados, evitando así la formación de agregados, lo cual promueve el estado plegado (nativo) (Wang y Bolen 1997, Bolen y Rose 2008).

Una de las presiones selectivas más fuertes es el estrés relacionado con el agua, ya sea por exceso, por falta o por cambio de estado (Yancey et al. 1982). Los organismos que se enfrentan a alguna de estas situaciones deben tener mecanismos de control para contrarrestar los efectos adversos del ambiente sobre su fisiología. Estos mecanismos se conocen como sistemas de osmolitos, el TMAO entre ellos, y se han encontrado en todos los organismos que viven bajo estrés de agua. Estos sistemas son compatibles con la estructura y función de las macromoléculas y reducen la necesidad de modificar proteínas para que funcionen en condiciones de alta concentración (en ausencia de agua) (Yancey et al. 1982). *Polytomella* es un ejemplo de organismo bajo estrés de agua, ya que su hábitat pasa por temporadas de desecación durante las cuales el alga debe enquistarse y en cuanto las condiciones vuelven a ser favorables puede desenquistarse y ser funcional (De la Cruz y Gittleson 1981). A mi conocimiento, no hay reportes de la existencia de algún sistema de osmolitos en *Polytomella*, por lo que la presencia de un brazo periférico tan robusto y tan reforzado puede ser la forma que tiene esta alga de proteger, estabilizar y asegurar la función de su ATPasa, ya que de ésta depende en gran parte la función mitocondrial y de ésta, a su vez, la vida del alga.

Considero que en este trabajo se lograron dos contribuciones importantes. Por un lado se estableció el papel de la subunidad Asa1 como la columna vertebral del brazo periférico de la ATP sintasa mitocondrial de *Polytomella*, cumpliendo un papel análogo al de las subunidades *b* de otras F-ATPasas por medio de su interacción con otras subunidades conservadas, como OSCP, y no conservadas como Asa8. Por otro lado, se establecieron las condiciones experimentales que permitieron obtener preparaciones de proteínas recombinantes que eventualmente podrían proporcionar cristales, de obtenerse, éstos serían el primer paso hacia la determinación de la estructura tridimensional de alguna de las subunidades atípicas de la ATPasa de *Polytomella*.

9. Perspectivas

a) Continuar la exploración de condiciones de cristalización de las subunidades Asa3 y Asa7.

b) Realizar la reconstitución de subcomplejos a partir de proteínas purificadas.

c) Explorar el sistema de expresión fuera de célula (*cell-free*) para las subunidades Asa.

d) Continuar la exploración de condiciones de cristalización de la ATPasa completa.

10. Referencias

Acin-Perez, R., Enriquez, J.A., 2014. The function of the respiratory supercomplexes: The plasticity model. Biochim. Biophys. Acta - Bioenerg. 1837, 444–450. https://doi.org/10.1016/j.bbabio.2013.12.009

Allegretti, M., Klusch, N., Mills, D.J., Vonck, J., Kühlbrandt, W., Davies, K.M., 2015. Horizontal membrane-intrinsic α-helices in the stator a-subunit of an F-type ATP synthase. Nature 521, 237–240. https://doi.org/10.1038/nature14185

Atteia, A., Dreyfus, G., González-Halphen, D., 1997. Characterization of the α and β-subunits of the F0F1-ATPase from the alga Polytomella spp., a colorless relative of Chlamydomonas reinhardtii. Biochim. Biophys. Acta - Bioenerg. 1320, 275–284. https://doi.org/10.1016/S0005-2728(97)00031-5

Balabaskaran Nina, P., Dudkina, N. V., Kane, L.A., van Eyk, J.E., Boekema, E.J., Mather, M.W., Vaidya, A.B., 2010. Highly Divergent Mitochondrial ATP Synthase Complexes in Tetrahymena thermophila. PLoS Biol. 8, 3–6. https://doi.org/10.1371/journal.pbio.1000418

Baskakov, I., Bolen, D.W., 1998. Forcing thermodynamically unfolded proteins to fold. J. Biol. Chem. 273, 4831–4834. https://doi.org/10.1074/jbc.273.9.4831

Bayrhuber, M., Meins, T., Habeck, M., Becker, S., Giller, K., Villinger, S., Vonrhein, C., Griesinger, C., Zweckstetter, M., Zeth, K., 2008. Structure of the human voltage-dependent anion channel. Proc. Natl. Acad. Sci. 105, 15370–15375. https://doi.org/10.1073/pnas.0808115105

Bogenhagen, D.F., 2012. Mitochondrial DNA nucleoid structure. Biochim. Biophys. Acta - Gene Regul. Mech. 1819, 914–920. https://doi.org/10.1016/j.bbagrm.2011.11.005

Bolen, D.W., Rose, G.D., 2008. Structure and Energetics of the Hydrogen-Bonded Backbone in Protein Folding. Annu. Rev. Biochem. 77, 339–362. https://doi.org/10.1146/annurev.biochem.77.061306.131357

Boyer, P.D., Cross, R.L., William, M., 1973. A new concept for energy coupling in oxidative phosphorylation based on a molecular explanation of the oxygen exchange reactions. Proc. Natl. Acad. Sci. 70, 2837–2839. https://doi.org/10.1007/978-1-4471-2372-9_10

Cano-Estrada, A., Vázquez-Acevedo, M., Villavicencio-Queijeiro, A., Figueroa-Martínez, F., Miranda-Astudillo, H., Cordeiro, Y., Mignaco, J.A., Foguel, D., Cardol, P., Lapaille, M., Remacle, C., Wilkens, S., González-Halphen, D., 2010. Subunit-subunit interactions and overall topology of the dimeric mitochondrial ATP synthase of Polytomella sp. Biochim. Biophys. Acta - Bioenerg. 1797, 1439–1448. https://doi.org/10.1016/j.bbabio.2010.02.024

Carbajo, R.J., Kellas, F.A., Yang, J.C., Runswick, M.J., Montgomery, M.G., Walker, J.E., Neuhaus, D., 2007. How the N-terminal Domain of the OSCP Subunit of Bovine F1Fo-ATP Synthase Interacts with the N-terminal Region of an Alpha Subunit. J. Mol. Biol. 368, 310–318. https://doi.org/10.1016/j.jmb.2007.02.059

Chaban, Y., Boekema, E.J., Dudkina, N. V., 2014. Structures of mitochondrial oxidative phosphorylation supercomplexes and mechanisms for their stabilisation. Biochim. Biophys. Acta - Bioenerg. 1837, 418–426. https://doi.org/10.1016/j.bbabio.2013.10.004

Coates, J.C., 2003. Armadillo repeat proteins: Beyond the animal kingdom. Trends Cell Biol. 13, 463–471. https://doi.org/10.1016/S0962-8924(03)00167-3

Colina-Tenorio, L., Miranda-Astudillo, H., Cano-Estrada, A., Vázquez-Acevedo, M., Cardol, P., Remacle, C., González-Halphen, D., 2016. Subunit Asa1 spans all the peripheral stalk of the mitochondrial ATP synthase of the chlorophycean alga Polytomella sp. Biochim. Biophys. Acta - Bioenerg. 1857, 359–369. https://doi.org/10.1016/j.bbabio.2015.11.012

Cross, R.L., Müller, V., 2004. The evolution of A-, F-, and V-type ATP synthases and ATPases: Reversals in function and changes in the H+/ATP coupling ratio. FEBS Lett. 576, 1–4. https://doi.org/10.1016/j.febslet.2004.08.065

Cross, R.L., Taiz, L., 1990. Gene duplication as a means for altering H+/ATP ratios during the evolution of Fo F1 ATPases and synthases. FEBS Lett. 259, 227–229. https://doi.org/10.1016/0014-5793(90)80014-A

D'Alessandro, M., Melandri, B.A., 2010. ATP hydrolysis in ATP synthases can be differently coupled to proton transport and modulated by ADP and phosphate: A structure based model of the mechanism. Biochim. Biophys. Acta - Bioenerg. 1797, 755–762. https://doi.org/10.1016/j.bbabio.2010.03.007

Dautant, A., Velours, J., Giraud, M.F., 2010. Crystal structure of the Mg·ADP-inhibited state of the yeast F 1c10-ATP synthase. J. Biol. Chem. 285, 29502–29510. https://doi.org/10.1074/jbc.M110.124529

Davies, K.M., Anselmi, C., Wittig, I., Faraldo-Gomez, J.D., Kuhlbrandt, W., 2012. Structure of the yeast F1Fo-ATP synthase dimer and its role in shaping the mitochondrial cristae. Proc. Natl. Acad. Sci. 109, 13602–13607. https://doi.org/10.1073/pnas.1204593109

Davies, K.M., Daum, B., Gold, V.A.M., Mühleip, A.W., Brandt, T., Blum, T.B., Mills, D.J., Kühlbrandt, W., 2014. Visualization of ATP Synthase Dimers in Mitochondria by Electron Cryo-tomography. J. Vis. Exp. 1–9. https://doi.org/10.3791/51228

Davies, K.M., Strauss, M., Daum, B., Kief, J.H., Osiewacz, H.D., Rycovska, A., Zickermann, V., Kuhlbrandt, W., 2011. Macromolecular organization of ATP synthase and complex I in whole mitochondria. Proc. Natl. Acad. Sci. 108, 14121–14126. https://doi.org/10.1073/pnas.1103621108

de la Cruz, V.F., Gittleson, S.M., 1981. The genus Polytomella: A review of classification, morphology, life cycle, metabolism, and motility. Arch. fur Protistenkd. 124, 1–28. https://doi.org/10.1016/S0003-9365(81)80001-2

Del Rizzo, P.A., Bi, Y., Dunn, S.D., Shilton, B.H., 2002. The "second stalk" of Escherichia coli ATP synthase: Structure of the isolated dimerization domain. Biochemistry 41, 6875–6884. https://doi.org/10.1021/bi025736i

Dickson, V.K., Silvester, J.A., Fearnley, I.M., Leslie, A.G.W., Walker, J.E., 2006. On the structure of the stator of the mitochondrial ATP synthase. EMBO J. 25, 2911–2918. https://doi.org/10.1038/sj.emboj.7601177

Dmitriev, O., Jones, P.C., Jiang, W., Fillingame, R.H., 1999. Structure of the Membrane Domain of Subunit b of the Escherichia coli F 0 F 1 ATP Synthase. J. Biol. Chem. 274, 15598–15604.

Domínguez-Ramírez, L., Gómez-Puyou, M.T. De, 2005. Redalyc. La F1F0 ATP sintasa: un complejo proteico con gran versatilidad estructural y funcional 8, 18–27.

Dudkina, N. V., Heinemeyer, J., Keegstra, W., Boekema, E.J., Braun, H.P., 2005. Structure of dimeric ATP synthase from mitochondria: An angular association of monomers induces the strong curvature of the inner membrane. FEBS Lett. 579, 5769–5772. https://doi.org/10.1016/j.febslet.2005.09.065

Dudkina, N. V., Kouřil, R., Peters, K., Braun, H.P., Boekema, E.J., 2010. Structure and function of mitochondrial supercomplexes. Biochim. Biophys. Acta - Bioenerg. 1797, 664–670. https://doi.org/10.1016/j.bbabio.2009.12.013

Dudkina, N. V., Sunderhaus, S., Braun, H.P., Boekema, E.J., 2006. Characterization of dimeric ATP synthase and cristae membrane ultrastructure from Saccharomyces and Polytomella mitochondria. FEBS Lett. 580, 3427–3432. https://doi.org/10.1016/j.febslet.2006.04.097

Enríquez, J.A., 2016. Supramolecular Organization of Respiratory Complexes. Annu. Rev. Physiol. 78, 533–561. https://doi.org/10.1146/annurev-physiol-021115-105031

Forgac, M., 2007. Vacuolar ATPases: Rotary proton pumps in physiology and pathophysiology. Nat. Rev. Mol. Cell Biol. 8, 917–929. https://doi.org/10.1038/nrm2272

Frey, T.G., Mannella, C.A., 2000. Mannella - The Internal Structure of Mitochondria. Trends Biochem Sci 4, 1–6.

Fronzes, R., Weimann, T., Vaillier, J., Velours, J., Brèthes, D., 2006. The peripheral stalk participates in the yeast ATP synthase dimerization independently of e and g subunits. Biochemistry 45, 6715–6723. https://doi.org/10.1021/bi0601407

Giorgio, V., von Stockum, S., Antoniel, M., Fabbro, A., Fogolari, F., Forte, M., Glick, G.D., Petronilli, V., Zoratti, M., Szabo, I., Lippe, G., Bernardi, P., 2013. Dimers of mitochondrial ATP synthase form the permeability transition pore. Proc. Natl. Acad. Sci. 110, 5887–5892. https://doi.org/10.1073/pnas.1217823110

Grüber, G., Manimekalai, M.S.S., Mayer, F., Müller, V., 2014. ATP synthases from archaea: The beauty of a molecular motor. Biochim. Biophys. Acta - Bioenerg. 1837, 940–952. https://doi.org/10.1016/j.bbabio.2014.03.004

Guo, H., Bueler, S.A., Rubinstein, J.L., 2017. Atomic model for the dimeric FO region of mitochondrial ATP synthase. Science (80-.). 358, 936–940. https://doi.org/10.1126/science.aao4815

Gustafsson, C.M., Falkenberg, M., Larsson, N.-G., 2016. Maintenance and Expression of Mammalian Mitochondrial DNA. Annu. Rev. Biochem. 85, 133–160. https://doi.org/10.1146/annurev-biochem-060815-014402

Hahn, A., Parey, K., Bublitz, M., Mills, D.J., Zickermann, V., Vonck, J., Kühlbrandt, W., Meier, T., 2016. Structure of a Complete ATP Synthase Dimer Reveals the Molecular Basis of Inner Mitochondrial Membrane Morphology. Mol. Cell 63, 445–456. https://doi.org/10.1016/j.molcel.2016.05.037

Hall, R.A., 2004 Studying protein–protein interactions via blot overlay or FarWestern blot, Methods Mol. Biol. 261 (2004) 167–174.

Hamada, H., Arakawa, T., Shiraki, K., 2009. Effect of Additives on Protein Aggregation. Curr. Pharm. Biotechnol. 10, 400–407. https://doi.org/10.2174/138920109788488941

Harner, M., Körner, C., Walther, D., Mokranjac, D., Kaesmacher, J., Welsch, U., Griffith, J., Mann, M., Reggiori, F., Neupert, W., 2011. The mitochondrial contact site complex, a determinant of mitochondrial architecture. EMBO J. 30, 4356–4370. https://doi.org/10.1038/emboj.2011.379

He, J., Ford, H.C., Carroll, J., Ding, S., Fearnley, I.M., Walker, J.E., 2017. Persistence of the mitochondrial permeability transition in the absence of subunit c of human ATP synthase. Proc. Natl. Acad. Sci. 114, 3409–3414. https://doi.org/10.1073/pnas.1702357114

He, J., Ford, H.C., Carroll, J., Douglas, C., Gonzales, E., Ding, S., Fearnley, I.M., Walker, J.E., 2018. Assembly of the membrane domain of ATP synthase in human mitochondria. Proc. Natl. Acad. Sci. 201722086. https://doi.org/10.1073/pnas.1722086115

Ishibashi, M., Sakashita, K., Tokunaga, H., Arakawa, T., Tokunaga, M., 2003. Activation of halophilic nucleoside diphosphate kinase by a non-ionic osmolyte, trimethylamine N-oxide. J. Protein Chem. 22, 345–351. https://doi.org/10.1023/A:1025338106922

Källberg, M., Wang, H., Wang, S., Peng, J., Wang, Z., Lu, H., Xu, J., 2012. Template-based protein structure modeling using the RaptorX web server. Nat. Protoc. 7, 1511–1522. https://doi.org/10.1038/nprot.2012.085

Klusch, N., Murphy, B.J., Mills, D.J., Yildiz, Ö., Kühlbrandt, W., 2017. Structural basis of proton translocation and force generation in mitochondrial ATP synthase. Elife 6, 1–16. https://doi.org/10.7554/eLife.33274

Kühlbrandt, W., 2015. Structure and function of mitochondrial membrane protein complexes. BMC Biol. 13, 1–11. https://doi.org/10.1186/s12915-015-0201-x

Kühlbrandt, W., Davies, K.M., 2016. Rotary ATPases: A New Twist to an Ancient Machine. Trends Biochem. Sci. 41, 106–116. https://doi.org/10.1016/j.tibs.2015.10.006

Lau, W.C.Y., Rubinstein, J.L., 2012. Subnanometre-resolution structure of the intact Thermus thermophilus H +-driven ATP synthase. Nature 481, 214–219. https://doi.org/10.1038/nature10699

Lee, L.K., Stewart, A.G., Donohoe, M., Bernal, R.A., Stock, D., 2010. The structure of the peripheral stalk of Thermus thermophilus H +-ATPase/synthase. Nat. Struct. Mol. Biol. 17, 373–378. https://doi.org/10.1038/nsmb.1761

Letts, J.A., Fiedorczuk, K., Sazanov, L.A., 2016. The architecture of respiratory supercomplexes. Nature 537, 644–648. https://doi.org/10.1038/nature19774

Letts, J.A., Sazanov, L.A., 2017. Clarifying the supercomplex: The higher-order organization of the mitochondrial electron transport chain. Nat. Struct. Mol. Biol. 24, 800–808. https://doi.org/10.1038/nsmb.3460

Mannella, C.A., 2008. Structural diversity of mitochondria: Functional implications. Ann. N. Y. Acad. Sci. 1147, 171–179. https://doi.org/10.1196/annals.1427.020

Markwell, M.A.K., Haas, S.M., Bieber, L.L., Tolbert, N.E., 1978. Modification of Lowry Procedure To Simplify Protein Determination in Membrane and Lipoprotein Samples. Anal. Biochem. 87, 206–210. https://doi.org/10.1016/0003-2697(78)90586-9

Mello, C.C., Barrick, D., 2003. Measuring the stability of partly folded proteins using TMAO. Protein Sci. 12, 1522–1529. https://doi.org/10.1110/ps.0372903

Miranda-Astudillo, H., Cano-Estrada, A., Vázquez-Acevedo, M., Colina-Tenorio, L., Downie-Velasco, A., Cardol, P., Remacle, C., Domínguez-Ramírez, L., González-Halphen, D., 2014. Interactions of subunits Asa2, Asa4 and Asa7 in the peripheral stalk of the mitochondrial ATP synthase of the chlorophycean alga Polytomella sp. Biochim. Biophys. Acta - Bioenerg. 1837, 1–13. https://doi.org/10.1016/j.bbabio.2013.08.001

Miranda-Astudillo, H., Colina-Tenorio, L., Jiménez-Suárez, A., Vázquez-Acevedo, M., Salin, B., Giraud, M.-F., Remacle, C., Cardol, P., González-Halphen, D., 2018. Oxidative phosphorylation supercomplexes and respirasome reconstitution of the colorless alga Polytomella sp. Biochim. Biophys. Acta - Bioenerg. 1859, 434–444. https://doi.org/10.1016/j.bbabio.2018.03.004

Mitchell, P., 1961. Coupling of phosphorylation to electron and hydrogen transfer by a chemi-osmotic type of mechanism. Nature 191, 144–148.

Morales-Rios, E., Montgomery, M.G., Leslie, A.G.W., Walker, J.E., 2015. Structure of ATP synthase from *Paracoccus denitrificans* determined by X-ray crystallography at 4.0 Å resolution. Proc. Natl. Acad. Sci. 112, 13231–13236. https://doi.org/10.1073/pnas.1517542112

Muench, S.P., Trinick, J., Harrison, M.A., 2011. Structural divergence of the rotary ATPases, Quarterly Reviews of Biophysics. https://doi.org/10.1017/S0033583510000338

Mühleip, A.W., Dewar, C.E., Schnaufer, A., Kühlbrandt, W., Davies, K.M., 2017. In situ structure of trypanosomal ATP synthase dimer reveals a unique arrangement of catalytic subunits. Proc. Natl. Acad. Sci. 114, 992–997. https://doi.org/10.1073/pnas.1612386114

Mühleip, A.W., Joos, F., Wigge, C., Frangakis, A.S., Kühlbrandt, W., Davies, K.M., 2016. Helical arrays of U-shaped ATP synthase dimers form tubular cristae in ciliate mitochondria. Proc. Natl. Acad. Sci. 113, 8442–8447. https://doi.org/10.1073/pnas.1525430113

Mulkidjanian, A.Y., Makarova, K.S., Galperin, M.Y., Koonin, E. V, 2007. Inventing the dynamo machine : the evolution of the F − type and V − type ATPases. Nat. Rev. Microbiol. 11, 892–899. https://doi.org/10.1038/nrmicro1767

Müller, V., Grüber, G., 2003. ATP synthases: structure, function and evolution of unique energy converters. Cell. Mol. Life Sci. 60, 474–494. https://doi.org/10.1007/s00018-003-

Muñoz-Gómez, S.A., Wideman, J.G., Roger, A.J., Slamovits, C.H., Agashe, D., 2017. The origin of mitochondrial cristae from alphaproteobacteria. Mol. Biol. Evol. 34, 943–956. https://doi.org/10.1093/molbev/msw298

Oot, R.A., Huang, L.S., Berry, E.A., Wilkens, S., 2012. Crystal structure of the yeast vacuolar ATPase heterotrimeric EGC head peripheral stalk complex. Structure 20, 1881–1892. https://doi.org/10.1016/j.str.2012.08.020

Paul, S., Punam, S., Chaudhuri, T.K., 2007. Chaperone-assisted refolding of Escherichia coli maltodextrin glucosidase. FEBS J. 274, 6000–6010. https://doi.org/10.1111/j.1742-4658.2007.06122.x

Paumard, P., 2002. The ATP synthase is involved in generating mitochondrial cristae morphology. EMBO J. 21, 221–230. https://doi.org/10.1093/emboj/21.3.221

Roger, A.J., Muñoz-Gómez, S.A., Kamikawa, R., 2017. The Origin and Diversification of Mitochondria. Curr. Biol. 27, R1177–R1192. https://doi.org/10.1016/j.cub.2017.09.015

Rubinstein, J.L., Walker, J.E., 2002. ATP synthase from Saccharomyces cerevisiae: Location of the OSCP subunit in the peripheral stalk region. J. Mol. Biol. 321, 613–619. https://doi.org/10.1016/S0022-2836(02)00671-X

Sagan, L., 1967. On the origin of mitosing cells. J. Theor. Biol. 14, 225–IN6. https://doi.org/10.1016/0022-5193(67)90079-3

Sánchez-Vásquez, L., Vázquez-Acevedo, M., de la Mora, J., Vega-deLuna, F., Cardol, P., Remacle, C., Dreyfus, G., González-Halphen, D., 2017. Near-neighbor interactions of the membrane-embedded subunits of the mitochondrial ATP synthase of a chlorophycean alga. Biochim. Biophys. Acta - Bioenerg. 1858, 497–509. https://doi.org/10.1016/j.bbabio.2017.04.004

Schägger, H., De Coo, R., Bauer, M.F., Hofmann, S., Godino, C., Brandt, U., 2004. Significance of respirasomes for the assembly/stability of human respiratory chain complex I. J. Biol. Chem. 279, 36349–36353. https://doi.org/10.1074/jbc.M404033200

Schagger, H., Pfeiffer, K., 2000. Supercomplexes in the respiratory chains of yeast and mammalian mitochondria. EMBO J. 19, 1777–1783. https://doi.org/10.1093/emboj/19.8.1777

Schep, D.G., Zhao, J., Rubinstein, J.L., 2016. Models for the a subunits of the *Thermus thermophilus* V/A-ATPase and *Saccharomyces cerevisiae* V-ATPase enzymes by cryo-EM and evolutionary covariance. Proc. Natl. Acad. Sci. 113, 3245–3250. https://doi.org/10.1073/pnas.1521990113

Senior, A.E., Nadanaciva, S., Weber, J., 2002. The molecular mechanism of ATP synthesis by F1F 0 -ATP synthase. Current 1553, 188–211.

Smith, D.R., Lee, R.W., 2011. Nucleotide diversity of the colorless green alga polytomella parva (Chlorophyceae, Chlorophyta): High for the mitochondrial telomeres, surprisingly low everywhere else. J. Eukaryot. Microbiol. 58, 471–473. https://doi.org/10.1111/j.1550-7408.2011.00569.x

Sobti, M., Smits, C., Wong, A.S.W., Ishmukhametov, R., Stock, D., Sandin, S., Stewart, A.G., 2016. Cryo-EM structures of the autoinhibited E. coli ATP synthase in three rotational states. Elife 5, 1–18. https://doi.org/10.7554/eLife.21598

Stalz, W.D., Greie, J.C., Deckers-Hebestreit, G., Altendorf, K., 2003. Direct interaction of subunits a and b of the F0 complex of Escherichia coli ATP synthase by forming an ab2 subcomplex. J. Biol. Chem. 278, 27068–27071. https://doi.org/10.1074/jbc.M302027200

Stewart, A.G., Laming, E.M., Sobti, M., Stock, D., 2014. Rotary ATPases-dynamic molecular machines. Curr. Opin. Struct. Biol. 25, 40–48. https://doi.org/10.1016/j.sbi.2013.11.013

Stewart, A.G., Lee, L.K., Donohoe, M., Chaston, J.J., Stock, D., 2012. The dynamic stator stalk of rotary ATPases. Nat. Commun. 3, 687–688. https://doi.org/10.1038/ncomms1693

Stewart, J.B., Larsson, N.G., 2014. Keeping mtDNA in Shape between Generations. PLoS Genet. 10. https://doi.org/10.1371/journal.pgen.1004670

Strauss, M., Hofhaus, G., Schröder, R.R., Kühlbrandt, W., 2008. Dimer ribbons of ATP synthase shape the inner mitochondrial membrane. EMBO J. 27, 1154–1160. https://doi.org/10.1038/emboj.2008.35

Tewari, R., Bailes, E., Bunting, K.A., Coates, J.C., 2010. Armadillo-repeat protein functions: Questions for little creatures. Trends Cell Biol. 20, 470–481. https://doi.org/10.1016/j.tcb.2010.05.003

van Lis, R., Atteia, A., Mendoza-hernández, G., González-halphen, D., 2003. Identification of Novel Mitochondrial Protein Components of Chlamydomonas reinhardtii . A Proteomic Approach 1. Plant Physiol. 132, 318–330. https://doi.org/10.1104/pp.102.018325.proteins

van Lis, R., González-Halphen, D., Atteia, A., 2005. Divergence of the mitochondrial electron transport chains from the green alga Chlamydomonas reinhardtii and its colorless close relative Polytomella sp. Biochim. Biophys. Acta - Bioenerg. 1708, 23–34. https://doi.org/10.1016/j.bbabio.2004.12.010

van Lis, R., Mendoza-Hernandez, G., Groth, G., Atteia, A., 2007. New Insights into the Unique Structure of the F0F1-ATP Synthase from the Chlamydomonad Algae Polytomella sp. and Chlamydomonas reinhardtii. Plant Physiol. 144, 1190–1199. https://doi.org/10.1104/pp.106.094060

Vázquez-Acevedo, M., Cardol, P., Cano-Estrada, A., Lapaille, M., Remacle, C., González-Halphen, D., 2006. The mitochondrial ATP synthase of chlorophycean algae contains eight subunits of unknown origin involved in the formation of an atypical stator-stalk and in the dimerization of the complex. J. Bioenerg. Biomembr. 38, 271–282. https://doi.org/10.1007/s10863-006-9046-x

Vázquez-Acevedo, M., Vega-deLuna, F., Sánchez-Vásquez, L., Colina-Tenorio, L., Remacle, C., Cardol, P., Miranda-Astudillo, H., González-Halphen, D., 2016. Dissecting the peripheral stalk of the mitochondrial ATP synthase of chlorophycean algae. Biochim. Biophys. Acta - Bioenerg. 1857, 1183–1190. https://doi.org/10.1016/j.bbabio.2016.02.003

Villavicencio-Queijeiro, A., Vázquez-Acevedo, M., Cano-Estrada, A., Zarco-Zavala, M., Tuena De Gómez, M., Mignaco, J.A., Freire, M.M., Scofano, H.M., Foguel, D., Cardol, P., Remacle, C., González-Halphen, D., 2009. The fully-active and structurally-stable form of the mitochondrial ATP synthase of Polytomella sp. is dimeric. J. Bioenerg. Biomembr. 41, 1–13. https://doi.org/10.1007/s10863-009-9203-0

Walker, J.E., Dickson, V.K., 2006. The peripheral stalk of the mitochondrial ATP synthase. Biochim. Biophys. Acta - Bioenerg. 1757, 286–296. https://doi.org/10.1016/j.bbabio.2006.01.001

Wang, A., Bolen, D.W., 1997. A naturally occurring protective system in urea-rich cells: Mechanism of osmolyte protection of proteins against urea denaturation. Biochemistry 36, 9101–9108. https://doi.org/10.1021/bi970247h

Weber, J., Wilke-Mounts, S., Senior, A.E., 2002. Quantitative determination of binding affinity of δ-subunit in Escherichia coli F1-ATPase: Effects of mutation, Mg2+, and pH on Kd. J. Biol. Chem. 277, 18390–18396. https://doi.org/10.1074/jbc.M201047200

Winge, D.R., 2012. Sealing the Mitochondrial Respirasome. Mol. Cell. Biol. 32, 2647–2652. https://doi.org/10.1128/MCB.00573-12

Yadav, K.N.S., Miranda-Astudillo, H. V., Colina-Tenorio, L., Bouillenne, F., Degand, H., Morsomme, P., González-Halphen, D., Boekema, E.J., Cardol, P., 2017. Atypical composition and structure of the mitochondrial dimeric ATP synthase from Euglena gracilis. Biochim. Biophys. Acta - Bioenerg. 1858, 267–275. https://doi.org/10.1016/j.bbabio.2017.01.007

Yamaguchi, H., Miyazaki, M., 2014. Refolding techniques for recovering biologically active recombinant proteins from inclusion bodies. Biomolecules 4, 235–251. https://doi.org/10.3390/biom4010235

Yancey, P.H., Clark, M.E., Hand, S.C., Bowlus, R.D., Somero, G.N., 1982. Living with Water Stress : Evolution of Osmolyte Systems. Science (80). 217, 1214–1222.

Yasuda, R., Noji, H., Ishiwata, S., Yoshida, M., Kinosita Jr., K., 1998. F_1-ATPase Is a Highly Efficient Molecular Motor that Rotates with Discrete 120 Steps. Cell 93, 1117–1124.

Zaremba-Niedzwiedzka, K., Caceres, E.F., Saw, J.H., Bäckström, Di., Juzokaite, L., Vancaester, E., Seitz, K.W., Anantharaman, K., Starnawski, P., Kjeldsen, K.U., Stott, M.B., Nunoura, T., Banfield, J.F., Schramm, A., Baker, B.J., Spang, A., Ettema, T.J.G., 2017. Asgard archaea illuminate the origin of eukaryotic cellular complexity. Nature 541, 353–358. https://doi.org/10.1038/nature21031

Zhao, J., Benlekbir, S., Rubinstein, J.L., 2015. Electron cryomicroscopy observation of rotational states in a eukaryotic V-ATPase. Nature 521, 241–245. https://doi.org/10.1038/nature14365

Zhou, A., Rohou, A., Schep, D.G., Bason, J. V., Montgomery, M.G., Walker, J.E., Grigorieffniko, N., Rubinstein, J.L., 2015. Structure and conformational states of the bovine mitochondrial ATP synthase by cryo-EM. Elife 4, 1–15. https://doi.org/10.7554/eLife.10180

Zíková, A., Schnaufer, A., Dalley, R.A., Panigrahi, A.K., Stuart, K.D., 2009. The F0F1-ATP synthase complex contains novel subunits and is essential for procyclic Trypanosoma brucei. PLoS Pathog. 5. https://doi.org/10.1371/journal.ppat.1000436

11. Anexos

11.1 Anexo 1: Obtención de proteínas recombinantes

11.2 Anexo 2: Soluciones y amortiguadores

11.3 Anexo 3: Artículos publicados

11.4 Anexo 4: Artículo sometido a revisión

11.1 Anexo 1: Obtención de proteínas recombinantes

11.1.1 Subunidad AsaΔ1C^{6H}

Con el propósito de profundizar en el estudio de la interacción de las subunidades Asa1 y OSCP, y habiendo identificado la parte de OSCP responsable de la interacción (su extremo carboxilo), se planteó la obtención de dos construcciones de la subunidad Asa1, una en la que la proteína carezca del extremo carboxilo (Asa1ΔC) y otra en la que carezca del extremo amino (Asa1ΔN). Para obtener estas dos construcciones se diseñaron oligonucleótidos, se amplificaron los fragmentos correspondientes por PCR y se clonaron primero en el vector pGEM y posteriormente en el vector de expresión pET28a. Ambas construcciones se transformaron por choque térmico en células de *E. coli* de la cepa BL21 Codon Plus y se hicieron pruebas de sobreexpresión con IPTG en tres clonas. Ambas construcciones fueron secuenciadas y de ambas se obtuvo la secuencia correcta, sin embargo, pese a varios intentos, la subunidad Asa1ΔN no pudo ser sobreexpresada. El proceso de amplificación, clonación y sobreexpresión de la subunidad Asa1ΔC se muestra en la Figura A1.

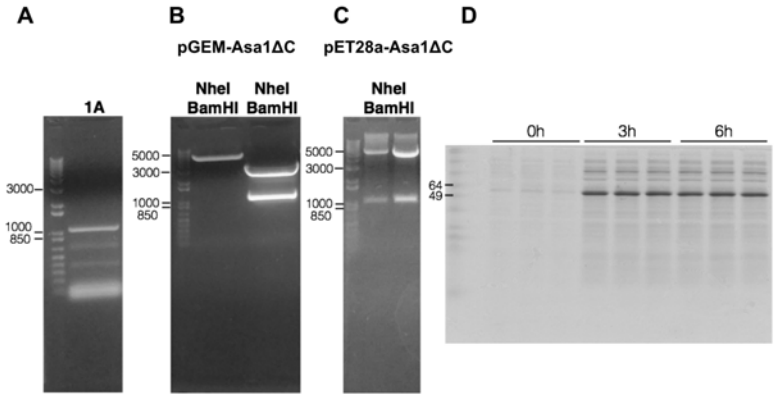

Figura A1. Proceso de amplificación, clonación y sobreexpresión de la subunidad Asa1ΔC. A. Gel de agarosa al 1% en el que se muestra el producto de amplificación por PCR del fragmento correspondiente a Asa1ΔC (1A) con un tamaño aproximado de 1100 pb. **B.** Gel de agarosa al 1% en el que se muestra la digestión del vector pGEM y de la construcción pGEM-Asa1ΔC con las enzimas de restricción NheI/ BamHI, de la que se libera el inserto correspondiente a 1100 pb. **C.** Gel de agarosa al 1% en el que se muestra la digestión de la construcción pET28a-Asa1A de dos clonas con las enzimas de restricción NheI/ BamHI; se observa la liberación del inserto correspondiente. **D.** Gel de Tricina SDS-PAGE al 12% teñido con azul de Coomassie en el que se muestran extractos totales de cultivos inducidos a una concentración final de 0.1 mM de IPTG por 0, 3 y 6 horas.

La subunidad Asa1ΔC^{6H} se purificó en condiciones desnaturalizantes por medio de cromatografía de afinidad a níquel utilizando una columna HisTrap Sepharose FF de 5 mL conectada a un equipo ÄKTA FPLC. La muestra centrifugada de cuerpos de inclusión solubilizados fue diluida para tener concentraciones finales de 4.0 M de urea y 50 mM de imidazol. Esta muestra se cargó a la columna previamente equilibrada con un amortiguador NaH_2PO_4 50 mM, NaCl 500 mM y urea 4.0 M, pH 7.8, con un flujo de 0.5 mL/min. La proteína se eluyó con un gradiente de 0 a 50 mM de imidazol y se colectaron fracciones de 4 mL. La muestra final obtenida y su inmunodetección con anticuerpos anti-Asa1 se muestra en la Figura A2.

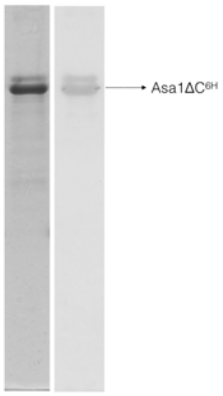

Figura A2. Subunidad Asa1ΔC^{6H} purificada. Gel de Tricina SDS PAGE al 12% teñido con azul de Coomassie y Western Blot anti Asa1 de la subunidad Asa1ΔC^{6H} después de juntar las fracciones y concentrar.

11.1.2 Subunidad Asa1

Para realizar la copurificación Asa1-OSCPΔC^{6H} era necesario purificar primero la subunidad Asa1 sin etiqueta de histidinas. Con ese objetivo, la construcción pET3a-Asa1 se sobreexpresó en *E. coli* y la proteína se purificó por intercambio iónico con una columna Source 15Q 10/100 de 8 mL conectada a un equipo ÄKTA FPLC. La muestra centrifugada de cuerpos de inclusión solubilizados fue diluida 1:2 con un amortiguador con NaH_2PO_4 50 mM, NaCl 500 mM, urea 0.5 M, glicerol 2% y Tween 20 0.5% y fue dializada contra el mismo amortiguador por 12 horas a 4 °C. Esta muestra se centrifugó a 12,000 rpm para eliminar el material agregado y se dializó de nuevo contra el mismo amortiguador pero con NaCl 200 mM. Se centrifugó igualmente y la muestra se cargó a la columna previamente equilibrada a un flujo de 1 mL/min.

La proteína se eluyó al aplicar un gradiente de 200 a 500 mM de NaCl y se colectaron fracciones de 4 mL. Las fracciones obtenidas se analizaron en geles de Tricina SDS-PAGE al 12%, aquellas enriquecidas con la proteína se juntaron y la muestra se concentró con un Amicon Ultra 10 000 MWCO. El perfil de elución se muestra en la Figura A3.

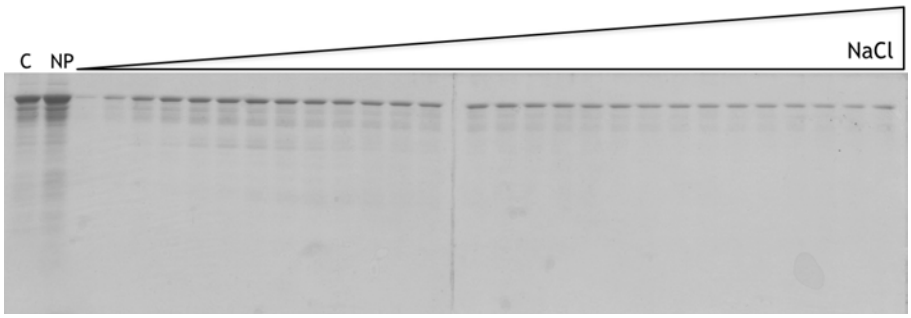

Figura A3. Subunidad Asa1^{6H} purificada por intercambio iónico. Gel de Tricina SDS PAGE al 12% teñido con azul de Coomassie en el que se muestra el perfil de elución de la subunidad Asa1. C: muestra cargada a la columna Source 15Q, NP: muestra no retenida por la columna. El triángulo indica la aplicación de un gradiente de NaCl.

11.1.3 Subunidad Asa3^{6H}

Para empezar a trabajar con la subunidad Asa3, se diseñaron oligonucléotidos específicos para amplificar el gen correspondiente a la proteína madura y el producto de amplificación se clonó en el vector de sobreexpresión pET28a. La construcción obtenida se transformó por choque térmico en células competentes de *E. coli* de la cepa BL21 Codon Plus y se realizaron pruebas de inducción de tres clonas con IPTG a diferentes tiempos. La construcción pET28a-Asa3 fue secuenciada y se obtuvo la secuencia esperada. El proceso de amplificación, clonación y sobreexpresión de la subunidad Asa3 se muestra en la Figura A4 con los geles correspondientes.

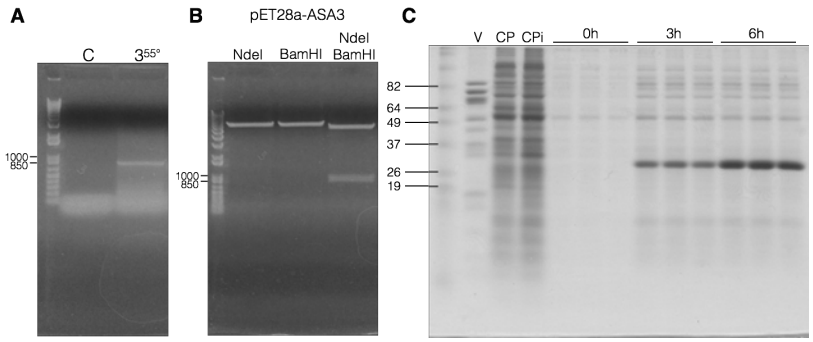

Figura A4. Proceso de amplificación, clonación y sobreexpresión de la subunidad Asa3. A. Gel de agarosa al 1% en el que se muestra el producto de amplificación por PCR del fragmento correspondiente a Asa3 obtenido a 55 °C ($3^{55°}$) con un tamaño aproximado de 850 pb y el control negativo de la reacción de amplificación (C) **B.** Gel de agarosa al 1% en el que se muestra la digestión de la construcción pET28a-Asa3 con las enzimas de restricción NdeI/BamHI; se muestran las digestiones sencillas y la digestión doble con la que se libera el fragmento correspondiente. **C.** Gel de Tricina SDS-PAGE al 12% teñido con azul de Coomassie en el que se muestra el complejo V purificado de Polytomella sp. seguido de muestras de extractos totales de células BL21 Codon Plus sin inducir (CP) e inducidas (CPi) y muestras de extractos totales de tres clonas inducidos a una concentración final de 0.1 mM de IPTG por 0, 3 y 6 horas.

La subunidad $Asa3^{6H}$ se purificó en condiciones desnaturalizantes por medio de cromatografía de afinidad a níquel utilizando una columna HisTrap Sepharose FF de 5 mL conectada a un equipo ÄKTA FPLC. La muestra centrifugada de cuerpos de inclusión solubilizados fue diluida para tener concentraciones finales de 4.0 M de urea y 50 mM de imidazol. Esta muestra se cargó a la columna previamente equilibrada con un amortiguador NaH_2PO_4 50 mM, NaCl 500 mM y urea 4.0 M, pH 7.8, con un flujo de 0.5 mL/min. La proteína se eluyó con un gradiente de 0 a 50 mM de imidazol y se colectaron fracciones de 4 mL. La muestra final obtenida y su inmunodetección con anticuerpos anti-Asa3 se muestra en la Figura A5.

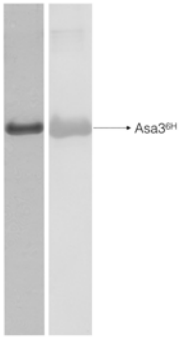

Figura A5. Subunidad $Asa3^{6H}$ purificada. Gel de Tricina SDS PAGE al 12% teñido con azul de Coomassie y Western Blot anti Asa3 de la subunidad $Asa3^{6H}$ después de juntar las fracciones y concentrar.

11.1.4 Obtención de anticuerpos contra la subunidad Asa3

Para generar anticuerpos específicos contra la subunidad Asa3 se corrió un gel SDS-PAGE con azul de Coomassie al 0.05% (SERVA Blue G) en el amortiguador del cátodo, cargando 30 ug de proteína purificada por carril. Posteriormente las bandas se cortaron y se molieron en un mortero con amortiguador TBS, la muestra se dividió en alícuotas que se guardaron a 4 °C hasta su uso. Se inoculó intramuscularmente a un conejo con una de las alícuotas mezclada con adyuvante completo de Freund (1:1). Después de tres semanas se tomó una muestra de sangre de la oreja del conejo para probar los anticuerpos y al ser positiva se sangró a blanco. Se separó el suero y las inmunoglobulinas se precipitaron con sulfato de amonio al 40% y se resuspendieron en 1/4 del volumen de suero inicial. La muestra final se dividió en alícuotas de 100 uL que se guardaron a -70 °C. Los anticuerpos funcionaron en el reconocimiento específico de la subunidad Asa3 (Figura A6).

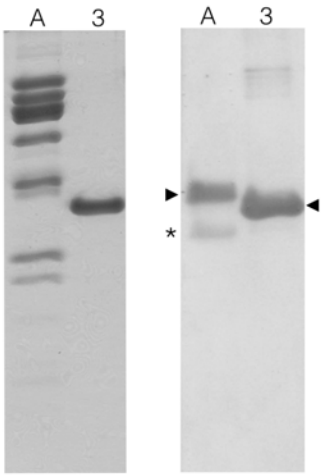

Figura A6. Prueba de los anticuerpos anti-Asa3 obtenidos. Gel de Tricina SDS PAGE al 12% teñido con azul de Coomassie con la ATPasa purificada de *Polytomella* (A) y la subunidad Asa3^{6H} recombinante (3), y Western Blot anti Asa3 en el que se observa el reconocimiento específico de la subunidad Asa3 en la ATPasa purificada y de la subunidad Asa3^{6H} recombinante. El asterisco señala la degradación de Asa3 en la preparación de ATPasa.

11.1.5 Subunidad Asa8^{6H}

La subunidad Asa8^{6H} se purificó en condiciones desnaturalizantes por medio de cromatografía de afinidad a níquel utilizando una columna HisTrap Sepharose FF de 5 mL conectada a un equipo ÄKTA FPLC. La muestra centrifugada de cuerpos de inclusión solubilizados fue diluida para tener concentraciones finales de 4 M de urea y 50 mM de imidazol. Esta muestra se cargó a la columna previamente equilibrada con un amortiguador NaH_2PO_4 50 mM, NaCl 500 mM y urea 4 M, pH 7.8, con un flujo de 0.5 mL/min. La proteína se eluyó con un gradiente de 0 a 50 mM de imidazol en un amortiguador con 0.1% de Tween, y se colectaron fracciones de 4 mL. La muestra final obtenida y su inmunodetección con anticuerpos anti-Asa8 se muestra en la Figura A7.

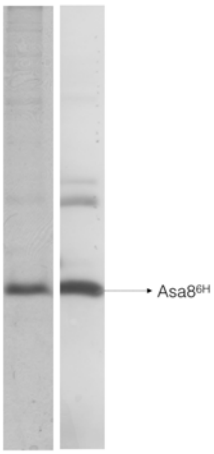

Figura A5. Subunidad Asa3^{6H} purificada. Gel de Tricina SDS PAGE al 12% teñido con azul de Coomassie y Western Blot anti Asa8 de la subunidad Asa8^{6H} después de juntar las fracciones y concentrar.

11.2 Anexo 2: Soluciones y amortiguadores

A. Biología molecular

Amortiguador TE

Tris	10 mM
EDTA	1 M
Ajustar a pH 8.5	

Amortiguador TENS

Amortiguador TE	1X
NaOH	0.1 N
SDS	0.5%

Amortiguador TAE (50X)	**1L**
Trizma Base	242 g
Ácido acético	57.1 mL
EDTA 0.5 M (pH 8.0)	100 mL

Medio LB (líquido)	**1 L**
Bactotriptona	10 g
Extracto de levadura	5 g
NaCl	10 g

Medio LB (sólido)	**1 L**
Bactotriptona	10 g
Extracto de levadura	5 g
NaCl	10 g
Agar	20 g

Antibióticos (stock)	**Concentración de uso**
Ampicilina 100 mg/mL en agua	100 ug/mL
Cloranfenicol 34 mg/mL en etanol	34 ug/mL
Kanamicina 50 mg/mL en agua	50 ug/mL

Amortiguador de carga en geles de agarosa

Azul de bromofenol	0.25%
Xilencianol FF	0.25%
Glicerol	30%

Gel de agarosa 1%

1 g de agarosa disuelta en 100 mL de amortiguador TAE 1X

Bromuro de etidio

100 mg de bromuro de etidio disueltos en 10 mL de agua

B. Electroforesis desnaturalizante de proteínas (SDS-PAGE)

	Gel separador 12%	Gel concentrador 3%
Acrilamida 30% Bisacrilamida 0.98%	3.0 mL	400 uL
Amortiguador electroforético	3.5 mL	800 uL
Glicerol 79.5%	1 mL	-
Agua	-	1.85 mL
Persulfato de amonio 10%	40 uL	40 uL
TEMED	5 uL	5 uL

Solución de acrilamida		**100 mL**
Acrilamida	30%	30 g
Bisacrilamida	0.98%	0.98 g

Amortiguador electroforético		**100 mL**
Tris	3 M	181.7 g
HCl	1 N	40.3 mL
SDS	0.3%	1.5 g

Amortiguador cátodo		**1 L**
Tris	0.1 M	12.1 g
Tricina	0.1 M	17.9 g
SDS	0.1%	1 g

Amortiguador ánodo		**1 L**
Tris-HCl	0.1 M	12.1 g
Ajustar a pH 8.9		

Solución de carga		**25 mL**
SDS	10%	2.5 g
Glicerol	30%	7.5 g
Tris	100 mM	1.25 g
Azul de Coomassie	0.3%	75 mg
Betamercaptoetanol	4%	1 mL
Ajustar a pH 6.8		

Solución teñidora		**1 L**
Etanol	50%	500 mL
Ácido acético	10%	100 mL
Coomassie Blue R-250	0.1%	1 g

Solución desteñidora
Ácido acético al 10% en agua

C. Western Blot y Far Western Blot

Amortiguador de transferencia		**1 L**
Tris	25 mM	3 g
Glicina	192 mM	14.4 g
Metanol	20%	200 mL
SDS	0.1 %	1g

Amortiguador TBS		**1 L**
Tris	20 mM	2.4 g
NaCl	0.5 M	29.2 g
Ajustar a pH 7.5		

Amortiguador TBST		**1 L**
Tris	20 mM	2.4 g
NaCl	0.5 M	29.2 g
Tween-20	0.05%	0.5 mL
Ajustar a pH 7.5		

Solución teñidora de rojo de Ponceau
0.1% de rojo de Ponceau en 5% de ácido acético

Solución reveladora

$NaHCO_3$	0.1 M
$MgCl_2$	1 mM

BCIP 15 mM
60 mg de BCIP en 2.8 mL de dimetilformamida y 1.2 mL de agua

NBT 15 mM
15 mg de NBT en 1 mL de agua

Para 10 mL de solución reveladora añadir al momento de revelar: 100 uL de BCIP y 100 uL de NBT

Amortiguadores de incubación en ensayos de Far Western Blot:

Amortiguador de Asa1		**100 mL**
NaH_2PO_4	50 mM	0.69 g
NaCl	150 mM	0.87 g
Glicerol	2 %	2 mL
Lauril maltósido	0.05%	0.05 g
Urea	0.5 M	3 g
Ajustar a pH 7.8		

Amortiguador de Asa2		**100 mL**
CAPS	50 mM	1.1 g
EDTA	0.5 mM	18.2 mg
DTT	1 mM	15.4 mg
Glicerol	2%	2 mL
Tween 20	0.05%	50 uL
Ajustar a pH 10		

Según: Miranda-Astudillo et al. 2014

Amortiguador de Asa3		**100 mL**
Tris	50 mM	0.6 g
NaCl	150 mM	0.87 g
Glicerol	2 %	2 mL
Lauril maltósido	0.05%	0.05 g
DTT	5 mM	75 mg
Urea	0.5 M	3 g
Ajustar a pH 8.4		

Amortiguador de Asa7
Amortiguador TTBS

Según: Miranda-Astudillo et al. 2014

Amortiguador de Asa8
Amortiguador TTBS

Amortiguador de OSCP		**100 mL**
MES	20 mM	0.43 g
EDTA	1 mM	36.4 mg
DTT	1 mM	15.4 mg
Glicerol	2%	2 mL
Tween 20	0.05%	50 uL

D. Para la purificación de proteínas recombinantes en condiciones desnaturalizantes

Amortiguador base		**100 mL**
NaH_2PO_4	50 mM	690 mg
NaCl	500 mM	2.9 g
Ajustar a pH 7.8		

Amortiguador de rompimiento		**100 mL**
NaH_2PO_4	50 mM	690 mg
NaCl	500 mM	2.9 g
Triton X-100	1%	1 mL
Ajustar a pH 7.8		

Amortiguador de lavado de CI		**100 mL**
NaH_2PO_4	50 mM	690 mg
NaCl	500 mM	2.9 g
Triton X-100	5%	5 mL
Ajustar a pH 7.8		

Amortiguador de solubilización de CI		**100 mL**
NaH_2PO_4	50 mM	690 mg
NaCl	500 mM	2.9 g
Urea	8 M	48.1 g
Ajustar a pH 7.8		

Amortiguador de purificación		**100 mL**
NaH_2PO_4	50 mM	690 mg
NaCl	500 mM	2.9 g
Urea	4 M	24 g
Ajustar a pH 7.8		

Diluir con el amortiguador base según la concentración de urea deseada

Amortiguador para elución		**100 mL**
NaH_2PO_4	50 mM	690 mg
NaCl	500 mM	2.9 g
Imidazol	1 M	6.8g
Ajustar a pH 7.8		

Diluir con el amortiguador base según la concentración de imidazol deseada

E. Para la obtención de mitocondrias de *Polytomella*

Medio *Polytomella*		**2L**
Acetato de sodio	29.4 mM	8 g
Bactotriptona	0.2%	4 g
Extracto de levadura	0.2%	4 g

Amortiguador de sacarosa		**500 mL**
Tris	20 mM	1.21 g
Sacarosa	0.37 M	63.3 g
EDTA-K	4 mM	0.74 g
Ajustar a pH 7.4		

Amortiguador de solubilización de mitocondrias		**50 mL**
Tris	50 mM	0.30 g
NaCl	100 mM	292 mg
$MgSO_4 \cdot 7H_2O$	1 mM	12.3 mg
Glicerol	10%	5 mL
PMSF	1 mM	8.71 mg
TLCK	50 ug/mL	2.5 mg
Ajustar a pH 8.4		

F. Para la purificación de la ATPasa mitocondrial de *Polytomella*

Amortiguador A (Source 15Q)		**100 mL**
Tris	50 mM	0.6 g
$MgSO_4 \cdot 7H_2O$	1 mM	25 mg
Ácido 6-aminocaproico	50 mM	0.65 g
Glicerol	10%	10 mL
PMSF	1 mM	17.4 mg
TLCK	50 ug/mL	5 mg
Lauril maltósido	0.01%	10 mg
Ajustar a pH 8.4		

Amortiguador B (Source 15Q)		**100 mL**
Tris	50 mM	0.6 g
NaCl	500 mM	2.92 g
$MgSO_4 \cdot 7H_2O$	1 mM	25 mg
Ácido 6-aminocaproico	50 mM	0.65 g
Glicerol	10%	10 mL
PMSF	1 mM	17.4 mg
TLCK	50 ug/mL	5 mg
Lauril maltósido	0.01%	10 mg
Ajustar a pH 8.4		

Amortiguador Superose 6		**100 mL**
Tris	50 mM	0.6 g
NaCl	150 mM	0.88 g
$MgSO_4 \cdot 7H_2O$	1 mM	25 mg
Glicerol	10%	10 mL
PMSF	1 mM	17.4 mg
TLCK	50 ug/mL	5 mg
Lauril maltósido	0.01%	10 mg
ATP	2 mM	110 mg
Ajustar a pH 8.4		

G. Para la reconstitución de subcomplejos

Amortiguador Asas D (diálisis)		**100 mL**
Tris	50 mM	0.6 g
NaCl	150 mM	0.87 g
Glicerol	10%	10 mL
Lauril maltósido	0.01%	0.01 g
Ajustar a pH 8.4		

Para las diálisis se preparan amortiguadores con 4, 2, 1 y 0.5 M de urea

Amortiguador Asas EM (exclusión molecular)		**100 mL**
Tris	50 mM	0.6 g
NaCl	150 mM	0.87 g
Glicerol	10%	10 mL
Lauril maltósido	0.01%	0.01 g
Urea	0.5 M	3 g
Ajustar a pH 8.4		

Amortiguador Asas N (afinidad a níquel)		**100 mL**
Tris	50 mM	0.6 g
NaCl	150 mM	0.87 g
Glicerol	10%	10 mL
Lauril maltósido	0.01%	0.01 g
Urea	0.5 M	3 g
Ajustar a pH 8.4		

Amortiguador Asas N (afinidad a níquel)		**100 mL**
Tris	50 mM	0.6 g
NaCl	150 mM	0.87 g
Glicerol	10%	10 mL
Lauril maltósido	0.01%	0.01 g
Urea	0.5 M	3 g
Imidazol	500 mM	3.4 g
Ajustar a pH 8.4		

Se diluyen los amortiguadores en 0 y 500 mM de imidazol para pegar, lavar y eluir

H. Para el replegado y purificación de proteínas para cristalización

Amortiguador de replegado subcomplejo Asa1-Asa3^{6H}-OSCP		**100 mL**
Tris	50 mM	0.6 g
NaCl	150 mM	0.87 g
Glicerol	10%	10 mL
DTT	10 mM	0.15 g
Urea	2 M	12 g
Lauril maltósido	0.1%	0.1 g
Polietilenglicol	0.1 g/L	0.1 g
TMAO	0.8 M	8.9 g
Ajustar a pH 8.4		

Amortiguador de replegado Asa3^{6H}		**100 mL**
Tris	50 mM	0.6 g
NaCl	150 mM	0.87 g
Glicerol	10%	10 mL
DTT	10 mM	0.15 g
Urea	2 M	12 g
Lauril maltósido	0.1%	0.1 g
Polietilenglicol	0.1 g/L	0.1 g
TMAO	0.6 M	6.7 g
Ajustar a pH 8.4		

Amortiguador de replegado Asa7^{6H}		**100 mL**
Tris	50 mM	0.6 g
NaCl	150 mM	0.87 g
Glicerol	10%	10 mL
DTT	5 mM	0.07 g
Urea	2 M	12 g
Lauril maltósido	0.1%	0.1 g
Polietilenglicol	0.1 g/L	0.1 g
TMAO	0.8 M	8.9 g
Ajustar a pH 8.4		

A todos los amortiguadores de replegado se les añade al momento la cantidad correspondiente de inhibidores de proteasas (cOmplete EDTA-free, Protease Inhibitor Cocktail, Roche)

Amortiguador de purificación (afinidad a níquel)		**100 mL**
Tris	50 mM	0.6 g
NaCl	150 mM	0.87 g
Glicerol	10%	10 mL
DTT	10 mM	0.15 g
Lauril maltósido	0.5%	0.5 g
Polietilenglicol	0.1 g/L	0.1 g
TMAO	0.1 M	1.1 g
Ajustar a pH 8.4		

Amortiguador de purificación (afinidad a níquel)		**100 mL**
Tris	50 mM	0.6 g
NaCl	150 mM	0.87 g
Glicerol	10%	10 mL
DTT	10 mM	0.15 g
Lauril maltósido	0.5%	0.5 g
Polietilenglicol	0.1 g/L	0.1 g
TMAO	0.1 M	1.1 g
Imidazol	500 mM	3. 4 g
Ajustar a pH 8.4		

Se diluyen los amortiguadores en 0 y 500 mM de imidazol para tener las concentraciones necesarias para pegar, lavar y eluir.

11.3 Anexo 3: Artículos publicados

Biochimica et Biophysica Acta 1857 (2016) 359–369

Contents lists available at ScienceDirect

Biochimica et Biophysica Acta

journal homepage: www.elsevier.com/locate/bbabio

Subunit Asa1 spans all the peripheral stalk of the mitochondrial ATP synthase of the chlorophycean alga *Polytomella* sp.

Lilia Colina-Tenorio [a], Héctor Miranda-Astudillo [a], Araceli Cano-Estrada [a], Miriam Vázquez-Acevedo [a], Pierre Cardol [b], Claire Remacle [b], Diego González-Halphen [a,*]

[a] Instituto de Fisiología Celular, Universidad Nacional Autónoma de México, México D.F., Mexico
[b] Genetics and Physiology of Microalgae, Department of Life Sciences, University of Liège, B-4000, Liège, Belgium

ARTICLE INFO

Article history:
Received 1 September 2015
Received in revised form 23 November 2015
Accepted 27 November 2015
Available online 30 November 2015

Keywords:
F_1F_O-ATP synthase peripheral stalk
Dimeric mitochondrial complex V
Chlorophycean algae
Chlamydomonas reinhardtii
Polytomella sp.
Asa subunits

ABSTRACT

Mitochondrial F_1F_O-ATP synthase of chlorophycean algae is dimeric. It contains eight orthodox subunits (alpha, beta, gamma, delta, epsilon, OSCP, *a* and *c*) and nine atypical subunits (Asa1 to 9). These subunits build the peripheral stalk of the enzyme and stabilize its dimeric structure. The location of the 66.1 kDa subunit Asa1 has been debated. On one hand, it was found in a transient subcomplex that contained membrane-bound subunits Asa1/Asa3/Asa5/Asa8/*a* (Atp6)/*c* (Atp9). On the other hand, Asa1 was proposed to form the bulky structure of the peripheral stalk that contacts the OSCP subunit in the F_1 sector. Here, we overexpressed and purified the recombinant proteins Asa1 and OSCP and explored their interactions *in vitro*, using immunochemical techniques and affinity chromatography. Asa1 and OSCP interact strongly, and the carboxy-terminal half of OSCP seems to be instrumental for this association. In addition, the algal ATP synthase was partially dissociated at relatively high detergent concentrations, and an Asa1/Asa3/Asa5/Asa8/a/c_{10} subcomplex was identified. Furthermore, Far-Western analysis suggests an Asa1–Asa8 interaction. Based on these results, a model is proposed in which Asa1 spans the whole peripheral arm of the enzyme, from a region close to the matrix-exposed side of the mitochondrial inner membrane to the F_1 region where OSCP is located. 3D models show elongated, helix-rich structures for chlorophycean Asa1 subunits. Asa1 subunit probably plays a scaffolding role in the peripheral stalk analogous to the one of subunit *b* in orthodox mitochondrial enzymes.

1. Introduction

Mitochondrial F_1F_O-ATP synthase (complex V) is an oligomeric membrane complex that works as a rotary motor driven by the electrochemical proton gradient generated by the respiratory chain. In fungi and animals, the enzyme comprises distinct multi-subunit domains: a soluble fraction (F_1) bearing the catalytic core [α_3/β_3] and a central rotor stalk [$\gamma/\delta/\varepsilon$], a membrane-bound sector F_O that translocates protons [$a/c_{8\text{-}14}$ ring], a peripheral stator stalk [OSCP/*b*/*d*/F6] and a dimerization module [A6L/*e*/*f*/*g*] [1].

Protons are translocated through subunit *a* and the *c*-ring, which in turn drives rotation of the central rotor stalk. The gamma subunit extends from the matrix-exposed side of the *c*-ring and inserts into the F_1 catalytic core, inducing conformational changes in the α_3/β_3 subunits that lead to ATP synthesis [2]. The main function of the peripheral stator stalk is to hold the F_1 sector against the movement of the rotor stalk [3]. In the inner mitochondrial membrane, the ATP synthase forms oligomeric structures [4], stabilized by the dimerization module A6L/*e*/*f*/*g*, that are responsible for the overall architecture of the mitochondrial cristae [5]. Subunits *b* (Atp4), *d*, F6, A6L, *e*, *f* and *g* are not common to all mitochondrial ATP synthases, since several enzymes exhibit different overall architecture and subunit composition. Such is the case of the ATP synthases from the ciliate *Tetrahymena thermophila* [6], the trypanosomatid *Trypanosoma brucei* [7], the euglenoid *Euglena gracilis* [8], and the chlorophycean algae like *Chlamydomonas reinhardtii* and *Polytomella* sp. [9].

The mitochondrial F_1F_O-ATP synthase of chlorophycean algae is isolated as a highly stable dimer of 1600 kDa after solubilization with detergents such as n-dodecyl-β-D-maltoside [10]. As in all known eukaryotes, the rotary and catalytic cores of the algal enzyme are formed by the eight conserved subunits α, β, γ, δ, ε, *a* (Atp6), *c* (Atp9), and OSCP [11]. Nevertheless, nine non-conventional subunits (Asa1 to Asa9), unique to the mitochondrial ATP synthases of chlorophycean algae, are also constituents of the enzyme. Some Asa subunits form the robust peripheral stalk observed in several electron microscopy analyses of the isolated enzyme [12–16] while others (Asa6, Asa8 and Asa9) may participate in the dimerization of the enzyme [17–20].

The neighboring interactions between Asa subunits in the ATP synthase of the colorless chlorophycean alga *Polytomella* sp. have been addressed in the past using several experimental approaches:

* Corresponding author at: Departamento de Genética Molecular, Instituto de Fisiología Celular, UNAM, Apartado Postal 70-600, Delegación Coyoacán, 04510, México D.F., Mexico.
E-mail address: dhalphen@ifc.unam.mx (D. González-Halphen).

http://dx.doi.org/10.1016/j.bbabio.2015.11.012
0005-2728/

characterizing enzyme subcomplexes generated by heat dissociation [9,17], defining near-neighbor relationships of subunits using cross-linking agents [14] and identifying protein–protein interactions *in vitro* employing recombinant subunits [20]. Thus, successive models for the topological disposition of the Asa polypeptides in the peripheral arm of the enzyme have been proposed [9,17,14,20]. An electron cryo-microscopy map at 7.0 Å overall resolution of the *Polytomella* dimeric ATP synthase revealed that the peripheral stalks consist of several entwined alpha-helices that give rise to a solid scaffold [16] that is strikingly more robust than the peripheral arm of enzymes from other biological sources, including bovine [21,22], yeast [23], spinach chloroplasts [24], and *Escherichia coli* [25]. Although many Asa subunits are thought to be localized in the peripheral stator stalk, the position of the Asa1 subunit remains controversial. On one hand, Asa1 was identified in a subcomplex that contained subunits Asa3/Asa5/Asa8/*a*/*c* and that appeared transiently during a time course of heat treatment of the enzyme before it further dissociated into its free components [9]. This result suggested that Asa1 may be interacting closely with subunits which are known to be membrane-bound, i.e. Asa8 (one transmembrane stretch or TMS), *a* (4–5 membrane-embedded helices), and *c* (two TMS). On the other hand, Asa1 was proposed to form a bulky structure near the catalytic region of the enzyme close to OSCP [17], based on electron microscopy studies [12] and on the fact that Asa1 behaved as an extrinsic membrane protein. Here, we studied the disposition of Asa1 in the peripheral stalk and suggest that Asa1 spans the whole peripheral stalk from the matrix-exposed side of the inner mitochondrial membrane to the F_1 region where OSCP resides. We propose that chlorophycean Asa1, although not anchored directly to the lipid bilayer, is the structural equivalent of subunit *b* (Atp4) found in the orthodox mitochondrial ATP synthases of yeasts, mammals and green plants.

2. Materials and methods

2.1. Algal strains and growth conditions

Polytomella spec. (Strain number 198.80, isolated by E.G. Pringsheim), identical to *Polytomella parva*, was originally obtained from the Culture Collection of Algae (University of Göttingen, Germany). Cells were grown for 48 h at room temperature in 2.5-l wide-bottom culture flasks without shaking, in a medium containing 4.0 g/l of sodium acetate, 2.0 g/l of Bacto™ Tryptone (Becton, Dickinson and Co.) and 2.0 g/l of Bacto™ Yeast Extract (Becton, Dickinson and Co.), supplemented with 10 μg/ml of vitamin B1 (thiamine) and 0.5 μg/ml of vitamin B12 (cobalamin).

2.2. Polytomella mitochondrial ATP synthase purification

Polytomella sp. cells were collected by centrifugation at 7500 *g* for 10 min and washed with sucrose buffer (20 mM Tris, 0.37 M sucrose, 4 M potassium EDTA, pH 7.4). The resulting pellet was suspended in the same buffer (80–100 ml). The cells were broken using a Potter homogenizer, centrifuged at 7500 *g* for 15 min and the supernatant was recovered. The unbroken cell pellet was treated again as described above; both supernatants were mixed and centrifuged at 17,500 *g* for 20 min to recover the mitochondria pellet, which was suspended in a small volume of sucrose buffer and stored at −70 °C until used. The mitochondria (250 mg of protein) were diluted to a final protein concentration of 10 mg/ml with solubilization buffer (50 mM Tris, 100 mM NaCl, 1 mM $MgSO_4 \cdot 7H_2O$, 10% glycerol, 1 mM PMSF, 50 μg/ml TLCK, pH 8.4) and were incubated with n-dodecyl β-D-maltoside (2 mg of detergent per mg of protein) under mild agitation for 30 min at 4 °C. The sample was centrifuged at 90,000 *g* for 20 min, the supernatant was recovered, diluted 3 times with loading buffer (50 mM Tris, 1 mM $MgSO_4 \cdot 7H_2O$, 10% glycerol, 1.0 mM PMSF, 50 μg/ml TLCK, 0.01% n-dodecyl β-D-maltoside pH 8.4) and loaded to a Source 15Q 10/100 GL column (CV 8 ml) (GE Healthcare) with a 1 ml/min flow. The column was washed with 75 mM NaCl and then eluted with a linear NaCl gradient (75–250 mM) in the same buffer. Two milliliter fractions were collected and analyzed by Tricine–SDS–PAGE. The fractions enriched with ATP synthase were pooled and concentrated to a volume of 4 ml using an Amicon Ultra 15 centrifugal filter 100,000 NMWL. Glycerol and ATP were added to final concentrations of 30% and 1.0 mM, respectively, and the sample was further concentrated to a final volume of 400 μl. This sample was injected to a Superose 6 10/300 GL (CV 24 ml) (GE Healthcare) previously equilibrated with Superose buffer (50 mM Tris, 150 mM NaCl, 1 mM $MgSO_4 \cdot 7H_2O$, 10% glycerol, 1 mM PMSF, 50 μg/ml TLCK, 0.01% n-dodecyl β-D-maltoside, 2 mM ATP, pH 8.4). The elution was carried out at a 0.25 ml/min flow. Fractions were collected (500 μl each) and analyzed by SDS–PAGE and BN-PAGE. The purified ATP synthase was aliquoted and stored at −70 °C until used.

2.3. Protein analysis

Denaturing gel electrophoresis was carried out in a Tricine–SDS–PAGE system [26], and when indicated, it was followed by 2D-Glycine–SDS–PAGE analysis [27]. Blue native polyacrylamide gel electrophoresis (BN-PAGE) was carried out as previously described [28]. When indicated, 1D-BN-PAGE was followed by 2D Tricine–SDS–PAGE [26]. Protein concentrations were determined as published [29]. Mass spectrometry and Edman degradation analyses were carried out at the "Unidad de Genómica, Proteómica y Metabolómica" at LaNSE, CINVESTAV del IPN, Mexico, and at the Protein Chemistry Laboratory at the Department of Biochemistry of Texas A&M University, USA, respectively.

2.4. Dissociation of the ATP synthase into subcomplexes

The purified algal ATP synthase (100 μg of protein) was incubated for 24 h at 4 °C under mild agitation in the presence of 3.0% lauryl maltoside and the solubilized sample subjected to BN-PAGE in 4–12% gradient acrylamide gels. The resulting lane of interest was excised and incubated in the presence of 1.0% SDS and 1.0% beta-mercaptoethanol for 15 min and then subjected to 2D Tricine–SDS–PAGE in 14% acrylamide gels.

2.5. Cloning of the cDNAs encoding subunits of the ATP synthase of Polytomella sp. in expression vectors

The cDNAs of *Asa1*, *Asa8*, *OSCP* and *OSCPΔC* were PCR-amplified from a *Polytomella* sp. cDNA library cloned in λ-ZapII phages [30] using specific oligonucleotide primers: for *Asa1*, forward 5′-GCGGCATGCGCTAG CTACCTTGCCCCCCTCCGCTCTGAT-3′ and reverse 5′-GCGCTGCAGGCG GCCGCTTAGTTACCGTTGACGAGATC-3′; for *Asa8* forward 5′-GCGGGA TCCGCTAGCATGGTCCTCGGTGAGGTCTAC-3′ and reverse 5′-GCGAAGCT TTAGTGACCACCAGCAGTGTAAG-3′; for *OSCP*, forward 5′-GCGGGATC CCATATGGCTGCCCAGGCTGAGCTCAAG-3′ and reverse 5′-GCGCTGCA GGTCGACAACGAACTAATTTAAATAGAAAGA-3′ and for *OSCPΔC*, forward 5′-GCGGGATCCCATATGGCTGCCCAGGCTGAGCTCAAG-3′ and reverse 5′-GCGCTGCAGGTCGACCTAAACCTCCTTCTTGTGAGCGAG-3′. The *Asa1* amplification product was cloned into a pET28a vector using the restriction sites *Nhe*I and *Bam*HI. This vector adds a hexa-histidine tag (6His-tag) to the N-terminus of the expressed protein (H_6-Asa1). To obtain the untagged version of Asa1 subunit, a new amplification was performed changing the restriction sites to *Nco*I. The amplicon was cloned into the pET28a vector upstream the hexa-histidine tag using the *Nco*I restriction site. The *Asa8* amplification product was cloned into a pQE30 vector using the restriction sites *Bam*HI and *Hind*III. The OSCP amplification product was cloned into a pET28a vector as well as into a pET3a vector using the restriction sites *Nhe*I and *Sal*I. The *OSCPΔC* product was obtained using the same forward primer as for OSCP and the reverse primer 5′-GCGCTGCAGGTCGACCTAAACCTCCTTCTTGTGA

GCGAG-3′. The *OSCPΔC* was cloned into pET28a using the restriction sites *Nhe*I and *Sal*I.

2.6. Overexpression of recombinant proteins

Competent *E. coli* BL21 Codon Plus (DE3) RIL cells (Agilent Technologies) were transformed with the construct of interest. Cells were grown in LB medium containing 64 μg/ml chloramphenicol and one of the following antibiotics: 50 μg/ml kanamycin for the pET28a vector or 100 μg/ml ampicillin for the pET3a vector. The overexpressed subunits were the complete Asa1 subunit (GenBank: AJ558193.2), the histidine-tagged H_6-Asa1, the complete histidine-tagged H_6-OSCP subunit (GenBank: GQ422707.1) and the tagged N-terminal region of OSCP (H_6-OSCP-ΔC, approximately 13.5 kDa, comprising residues 5 to 126 of OSCP). Asa8 recombinant subunit was overexpressed in *E. coli* XL1-Blue and cells grown in 100 μg/ml ampicillin and 40 μg/ml tetracycline.

2.7. Purification of proteins

Bacterial inclusion bodies (ICBs) retaining the overexpressed recombinant proteins were isolated, washed with detergent and stored as previously described [20]. The recombinant polypeptides Asa1, Asa8, H_6-Asa1, H_6-OSCP and H_6-OSCP-Δc were purified under denaturing conditions using affinity chromatography. The ICBs were solubilized in PBS buffer (50 mM NaH_2PO_4, 500 mM NaCl, pH 7.8) containing 8.0 M urea with mild agitation at 4 °C during 8 h. The insoluble material was removed by centrifugation at 17,500 *g* for 10 min. The sample was diluted with PBS buffer to a final concentration of 4.0 M urea; imidazole was added to a final concentration of 10 mM from a 1.0 M stock solution. Then the sample was loaded on a 5 ml HisTrap FF crude column (GE Healthcare Life Sciences) equilibrated with PBS buffer containing 4.0 M urea. The column was washed with 30 mM imidazole and the proteins were eluted with a 30–500 mM imidazole linear gradient in the same buffer. The fractions obtained from the elution were analyzed by Tricine–SDS–PAGE and those enriched with the recombinant protein of interest were pooled, concentrated, and stored at −70 °C until used. The ICBs containing untagged Asa1 were solubilized as described above. The resulting sample was dialyzed overnight against PBS buffer with 0.5 M urea, 500 mM NaCl, 2% glycerol and 0.1% Tween 20. The aggregated material was removed by centrifugation at 17,500 *g* for 10 min and the supernatant was dialyzed (4 h) against the same buffer containing 200 mM NaCl, centrifuged at 17,500 *g* for 10 min and loaded to a 8 ml Source 15Q 10/100 column (GE Healthcare Sciences) equilibrated with the same buffer. The protein was recovered after applying a 200–500 mM NaCl linear gradient with the same buffer; the enriched fractions were pooled, concentrated and stored at −70 °C until used. The solubilized untagged OSCP inclusion bodies were dialyzed overnight against a buffer containing 20 mM MES, 2.0% glycerol, 0.05% Tween 20, 1 mM EDTA, 1 mM DTT, pH 6.0. The recovered sample was centrifuged at 17,000 *g* for 10 min and the supernatant was loaded to a DEAE Sepharose FF column (24 ml) equilibrated with the same buffer. The protein was eluted with a 0–1.0 M NaCl linear gradient (10 column volumes) with the same buffer. The eluted fractions were analyzed by Tricine–SDS–PAGE and the enriched fractions were pooled, concentrated and stored at −70 °C until used.

2.8. Antibody production and immunoblotting

To generate antibodies against subunits Asa1 and OSCP, the polypeptides of the algal ATP synthase (50 μg of protein per lane) were resolved by Tricine–SDS–PAGE (14% acrylamide) in the presence of Serva Blue G as previously described [31]. The recombinant Asa8 subunit was purified and subjected to the same electrophoretic conditions. The subunits of interest were excised from the gels, grinded in a mortar in the presence of 20 mM Tris (pH 7.0), mixed with Freund's complete adjuvant and injected into rabbits. The presence of antibodies in the sera was ascertained by Western blot analysis carried out as previously described [32]. For Western blots, goat anti-rabbit IgG conjugated with alkaline phosphatase (1:3000 for 2 h) was used, and color developed with nitro-blue tetrazolium chloride and 5-bromo-4-chloro-3′-indolylphosphate p-toluidine salt. Western blot images were captured in an HP Scanjet G4050.

2.9. Protein–protein interaction assayed by Far-Western analysis

Far-Western analysis was carried out according as previously described [33] with modifications [20]. Purified *Polytomella* sp. ATP synthase was subjected to Tricine–SDS–PAGE and transferred to nitrocellulose membranes. The membranes containing the denatured enzyme were blocked with a 5.0% powdered milk suspension overnight and then incubated for 4 h in the presence of the externally added protein of interest in increasing concentrations in the corresponding buffer (for Asa1: PBS buffer with 0.5 M urea, 500 mM NaCl, 2.0% glycerol and 0.05% Tween 20, pH 7.8; and for Asa8 and OSCP: MES 20 mM, 500 mM NaCl, 2.0% glycerol, and 0.05% Tween 20, pH 6.0) supplemented with 1.0% powdered milk. Protein bands were visualized by Ponceau S red staining (0.1% in 5.0% acetic acid) for 10 min. The membranes were washed two times with the same buffer. The protein of interest was recognized using a specific antibody incubated in TTBS buffer (20 mM Tris–HCl pH 8.0, 500 mM NaCl and 0.05% Tween 20), followed by incubation with a secondary antibody in the same buffer. Finally, the membrane was immunochemically stained as described above for Western blot analyses [34].

2.10. Protein–protein interactions assayed by affinity chromatography

These experiments were carried out as described [20] with some modifications. The whole procedure is carried out at 4 °C unless otherwise stated. The corresponding purified recombinant proteins H_6-Asa1/OSCP and Asa1/H_6-OSCP-Δc (2 mg of each protein) were dialyzed together against PBS buffer containing 500 mM NaCl, 2.0% glycerol and 0.05% Tween 20, pH 7.8. The aggregated material was removed by centrifugation at 17,000 *g* for 10 min. Thirty microliters of equilibrated Ni Sepharose 6 FF resin (Amersham Biosciences) was added to the sample and imidazole was added to a final concentration of 30 mM from a 1 M stock solution. The sample was incubated with mild shaking for 5 h. The resin was recovered by centrifugation at 500 *g* for 5 min and then washed 10 times with PBS buffer containing 50 mM imidazole. The washed resin was poured into a column and the proteins were eluted with a step imidazole gradient from 50 mM to 500 mM. Fractions recovered from the column were analyzed by Tricine–SDS–PAGE.

2.11. Protein structure prediction

Sequences of 11 chlorophycean Asa1 subunits were retrieved from the data bases: *Dunaliella tertiolecta* (iMicrobe: CCMP1320), *Chlamydomonas chlamydogama* (iMicrobe: MMETSP1392), *Chlamydomonas Euryale* (iMicrobe: CAMPEP_0201452882); *Chlamydomonas leiostraca* (iMicrobe: MMETSP1391), *Chlamydomonas reinhardtii* (NCBI: XP_001692395), *Chlamydomonas* sp. (iMicrobe: MMETSP1180), *Polytomella* sp. (NCBI: CAD90158), *Polytomella parva* (iMicrobe: MMETSP0052_2–20,121,109); *Polytomella capuana* (iMicrobe: c26576_g1_i1); *Polytomella magna* (iMicrobe: c16202_g2_i1); *Polytomella pyriformis* (iMicrobe: c17010_g1_i1) and *Volvox carteri* (NCBI: XP_002951807). Sequences were aligned using ClustalW (https://npsa-prabi.ibcp.fr/cgi-bin/npsa_automat.pl?page=/NPSA/npsa_clustalw.html) [35]. 3D structure prediction of each individual sequence was carried out in the RaptorX server (http://raptorx.uchicago.edu/) [36].

3. Results

3.1. Overexpression and purification of recombinant Asa subunits

Our study focused on the interactions of subunits Asa1 and OSCP of the ATP synthase of *Polytomella* sp. using recombinant subunits. For this purpose, the proteins of interest were overexpressed and purified. Fig. 1 shows a Tricine–SDS–gel with the purified recombinant subunits Asa1, OSCP with and without a histidine tag (OSCP and H_6-OSCP respectively) and a histidine-tagged, recombinant fragment of OSCP comprising residues 5–126 of the mature protein and therefore lacking the final 71 residues of the carboxy-terminal region (hereby named H_6-OSCP-Δc).

3.2. On the interaction of Asa1 and OSCP

One strategy used to detect protein–protein interactions is Far-Western blotting. We assayed possible interactions of the purified, recombinant Asa1 subunit with the entire ATP synthase, searching for binding of the externally added, recombinant polypeptide to some of the subunits of the complex. The ATP synthase was resolved by SDS–PAGE and transferred to nitrocellulose membranes. The strips, containing the same concentration of enzyme, were incubated with increasing concentrations of the recombinant Asa1 subunit and afterwards decorated with an anti-Asa1 antibody and the appropriate secondary antibody (Fig 2A). The position of each of the ATP synthase subunits in the blots was identified beforehand by Ponceau S red staining.

In all lanes, as expected, the anti-Asa1 antibody recognized the Asa1 subunit of the ATP synthase, but at increasing concentrations of the externally added, recombinant Asa1, additional bands appeared on the blot, one of 31 kDa corresponding to either subunit Asa4 or gamma and one of 22 kDa corresponding to either OSCP or subunit *a* (Atp6) (Fig 2A, lanes 3 to 6). This indicated that the recombinant Asa1 subunit, incubated in a soluble form over the nitrocellulose membrane, interacted with some of the blotted polypeptides of the ATP synthase. Nevertheless, with this approach, it was impossible to distinguish if the 31 kDa band was Asa4 or gamma, since both polypeptides migrate together in the SDS–PAGE system used. The same happened with the 22 kDa band, which could correspond either to OSCP or to subunit *a* (Atp6), two polypeptides that exhibit the same mobility in the electrophoretic conditions used. At higher concentrations of the externally added, recombinant Asa1 subunit, additional faint bands were observed, that were interpreted to result from unspecific binding.

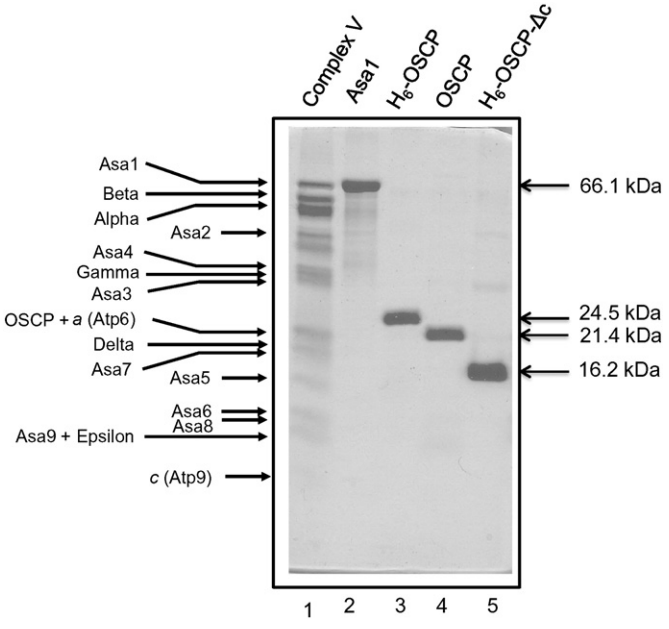

Fig. 1. *Polytomella* ATP synthase and some of the recombinant subunits used in this work. Tricine–SDS–polyacrylamide gel showing the identity of the 16 subunits of the *Polytomella* ATP synthase complex (25 μg of protein, lane 1). Three micrograms of each overexpressed and purified recombinant subunit were loaded in lanes 2 to 5. Molecular masses indicated by arrows were calculated using as molecular mass marker the well-characterized polypeptide composition of the algal ATP synthase (lane 1).

A variation of the above experiment was carried out in which the isolated, recombinant OSCP subunit was resolved by SDS–PAGE and transferred to nitrocellulose membranes. The strips, containing the same concentration of OSCP, were incubated with increasing concentrations of the recombinant Asa1 subunit and afterwards incubated with an anti-Asa1 antibody and the appropriate secondary antibody (Fig 2B). At increasing concentrations of the externally added recombinant Asa1, the anti-Asa1 antibody recognized the OSCP subunit bound to the nitrocellulose membrane (Fig 2B, lanes 3 to 6). This further suggested the interaction of Asa1 and OSCP.

We previously reported a combined gel electrophoresis system that allowed almost complete resolution of all the polypeptide components of the algal ATP synthase [14]. In this 2D system, subunit OSCP was resolved from subunit *a*, and subunit Asa4 was separated from the gamma subunit. The recombinant Asa1 polypeptide was incubated with nitrocellulose membranes in which all the subunits of the algal ATP synthase were resolved in a two dimensional array (Fig 3A). As in the 1D Far-Western blot experiments, the anti-Asa1 antibody recognized only the Asa1 subunit both in the 2D array and in the control lane in which the ATP synthase was loaded as a molecular mass standard (Fig 3B). In contrast, when the 2D array blot was pre-incubated with the isolated Asa1 recombinant protein, two additional main bands were observed that correspond to the gamma subunit and OSCP (Fig 3C). When a similar 2D-array (Fig 4A) was blotted and incubated with an anti-OSCP antibody, the OSCP subunit was clearly identified (Fig 4B). Finally, when this 2D array blot was pre-incubated with the isolated OSCP recombinant protein, three additional bands were observed, that were identified as Asa1, alpha subunit and the gamma subunit (Fig 4C). Thus, 2D-Far-Western analysis allowed us to resolve the ambiguities encountered in 1D-Far-Western and suggested the interactions Asa1-OSCP and Asa1-gamma. Smaller polypeptides with a molecular mass below 20 kDa were not observed in the 2D-Far-Western blot, probably because of their low concentration and more diffused spots.

An additional Far-Western assay was carried out in which three forms of OSCP were resolved and transferred to a nitrocellulose membrane: the recombinant protein (OSCP), the recombinant protein containing a hexa-histidine tag (H_6-OSCP), and the tagged amino-terminal fragment of the protein (H_6-OSCP-Δc). Complex V and the recombinant Asa1 protein were also transferred to the membrane (Fig 5A, lanes 1–5). As in previous Far-Western blot experiments, the anti-Asa1 antibody, in the absence of externally added Asa1 protein, recognized only the Asa1 subunit in complex V and the isolated Asa1 recombinant protein (Fig 5B, lanes 6–10). By contrast, when the membrane was incubated with the Asa1 protein before the addition of the anti-Asa1 antibody, additional bands appeared in the blot: gamma and OSCP in complex V (Fig 5C, lane 11), and the two forms of the intact OSCP protein (H_6-OSCP and OSCP, Fig 5C, lanes 13 and 14 respectively). No antibody was bound to the fragmented OSCP subunit (H_6-OSCP-Δc, lane 15 in Fig. 5C), suggesting that the carboxy-terminus of OSCP is instrumental for binding the externally added, recombinant Asa1 subunit. This experiment also suggested that the binding of Asa1 to OSCP is not spurious, since no binding of Asa1 to H_6-OSCP-Δc was observed, even when the latter was loaded at similar protein concentrations similar to OSCP.

To further explore the interaction of Asa1 and OSCP using a different experimental approach, the isolated, recombinant Asa1 protein containing a 6His-tag (H_6-Asa1), was bound to a Ni Sepharose resin. Then, the recombinant OSCP (lacking a 6His-tag) was added and the resin was washed with 30 mM imidazole. In order to discard the possibility of

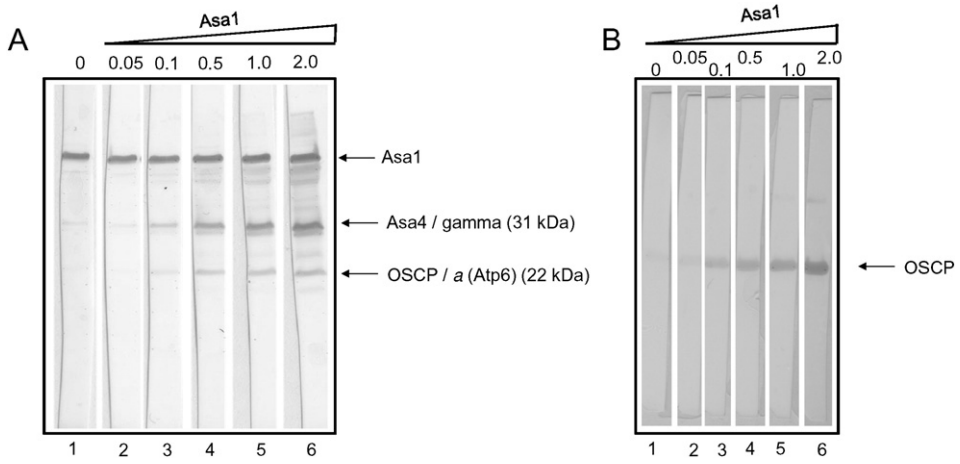

Fig. 2. Interaction of Asa1 with polypeptides of the algal ATP synthase and the OSCP subunit. Far-Western analysis of *Polytomella* ATP synthase (25 μg of protein per lane) (panel A) and of the purified, recombinant OSCP polypeptide (3 μg of protein per lane) (panel B) incubated for 4 h with increasing quantities of the isolated, recombinant Asa1 polypeptide as indicated (total nanomoles of Asa1 in a 5 ml final volume), and then decorated with an anti-Asa1 antibody. The identities of the main bands are indicated.

an adventitious binding of OSCP to the nickel matrix, a second experiment was performed in which no protein was bound to the resin, but a non-tagged OSCP recombinant protein was added in parallel. While OSCP eluted in the first fractions of the column lacking bound Asa1 (Fig 6A, upper panel), a fraction of OSCP was retained in the column that contained H_6-Asa1. When a 30 to 500 mM imidazole gradient was applied to the column, both OSCP and H_6-Asa1 were found to elute together in several fractions (Fig 6A, lower panel). This suggested that Asa1, when bound to the nickel column, is able to bind and retain OSCP. A complementary experiment was carried out. In this case, the isolated, recombinant H_6-OSCP-Δc fragment was bound to the nickel resin. Then, the recombinant Asa1 subunit (lacking a 6His-tag) was loaded on the column and washed with 30 mM imidazole. As a control, the same nickel matrix, with no bound protein to it, was also loaded with a non-tagged Asa1 recombinant subunit and run in parallel. Asa1 eluted in the first fractions, both from the resin that lacked (Fig 6B, upper panel) and the one that contained bound H_6-OSCP-Δc fragment (Fig 6B, lower panel). When the column was eluted with a 30 to 500 mM imidazole gradient, only the H_6-OSCP-Δc fragment was recovered (Fig 6, lower panel). These results confirmed that Asa1 does not bind to the H_6-OSCP-Δc fragment and that therefore the carboxy-terminus of OSCP is required for Asa1 binding.

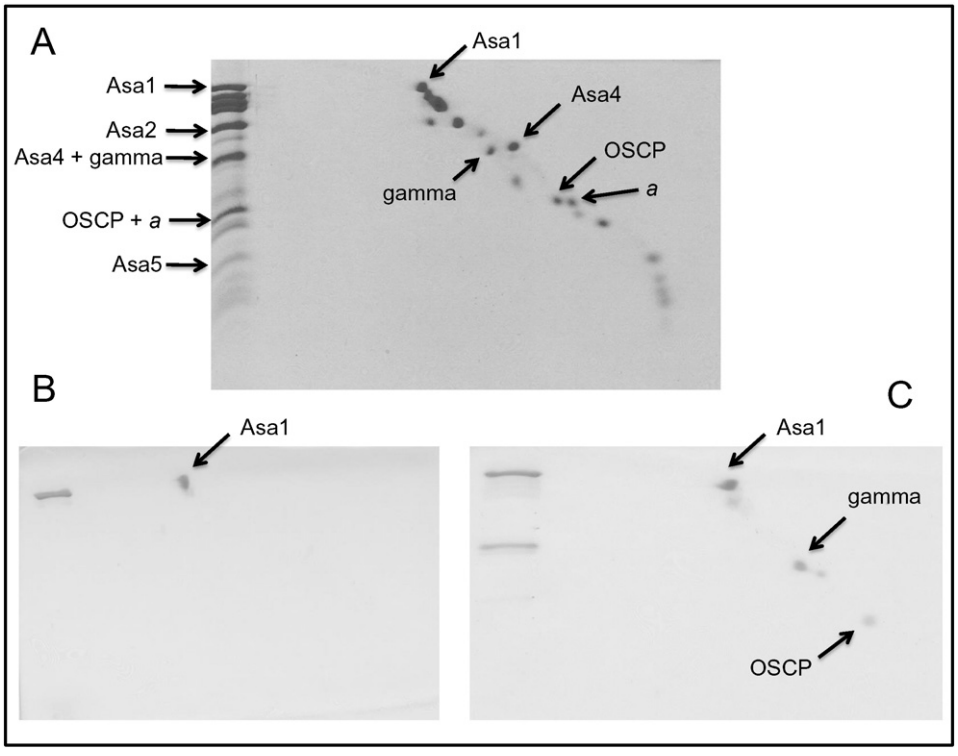

Fig. 3. Interaction of Asa1 with the gamma and OSCP subunits. A) 2D resolution of the polypeptides that constitute the mitochondrial *Polytomella* F_1Fo-ATP synthase. *Polytomella* ATP synthase (100 μg of protein) was resolved in a glycine–SDS–PAGE system (10% acrylamide). The 1D gel was then subjected to 2D Tricine–SDS–PAGE (14% acrylamide) and stained with Coomassie brilliant blue. A lane loaded with the enzyme (20 μg of protein) on the left-hand side of the 2D gel indicates the subunits of interest. B) Western blot analysis of the *Polytomella* ATP synthase resolved by 2D Tricine–SDS–PAGE. A gel equivalent to the one shown in panel A was transferred to a nitrocellulose membrane and decorated with an anti-Asa1 antibody. C) Far-Western blot analysis of the *Polytomella* ATP synthase resolved by 2D Tricine–SDS–PAGE. A gel equivalent to the one shown in panel A was transferred to a nitrocellulose membrane and incubated for 4 h with 2.0 nmol of the isolated, recombinant Asa1 protein, and then decorated with an anti-Asa1 antibody.

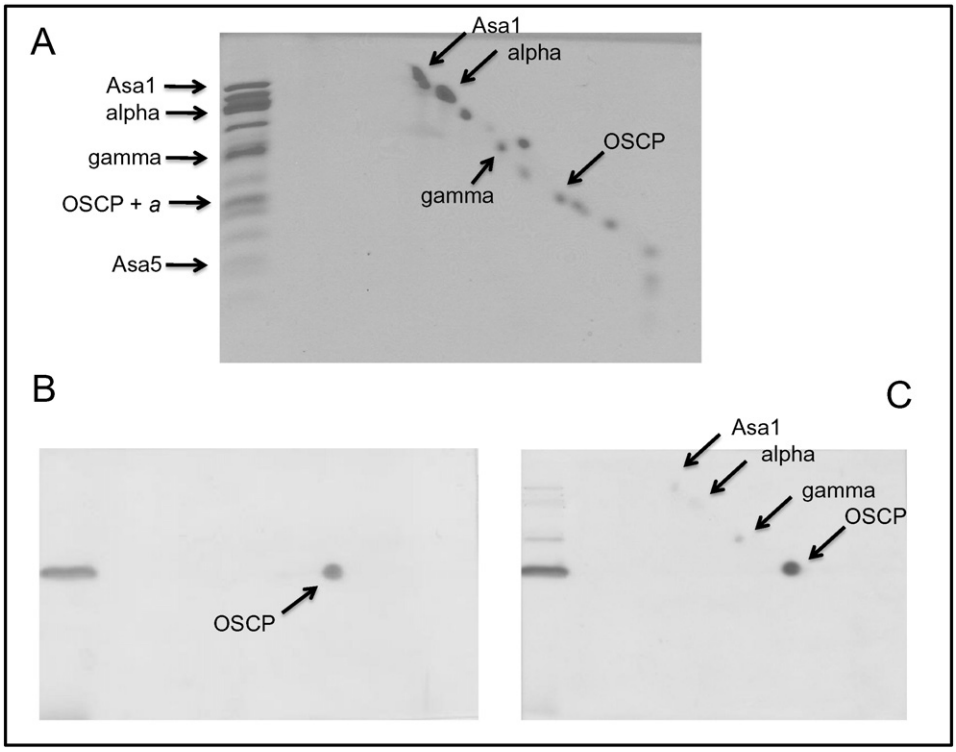

Fig. 4. Interaction of OSCP with subunits of the algal ATP synthase. A) 2D resolution of the algal F_1Fo-ATP synthase. *Polytomella* ATP synthase (100 μg of protein) was resolved in 1D in a glycine–SDS–PAGE system (10% acrylamide) and then in 2D in a Tricine–SDS–PAGE (14% acrylamide) and stained with Coomassie brilliant blue. The subunits of interest are indicated on the polypeptide pattern of the enzyme loaded on the left-hand side of the 2D gel. B) Western blot analysis of the *Polytomella* ATP synthase resolved by 2D Tricine–SDS–PAGE. A gel equivalent to the one shown in panel A was transferred to a nitrocellulose membrane and decorated with an anti-OSCP antibody. C) Far-Western blot analysis of the *Polytomella* ATP synthase resolved by 2D Tricine–SDS–PAGE. A gel equivalent to the one shown in panel A was transferred to a nitrocellulose membrane and incubated for 4 h with 2.0 nmol of the isolated, recombinant OSCP protein, and then decorated with an anti-OSCP antibody.

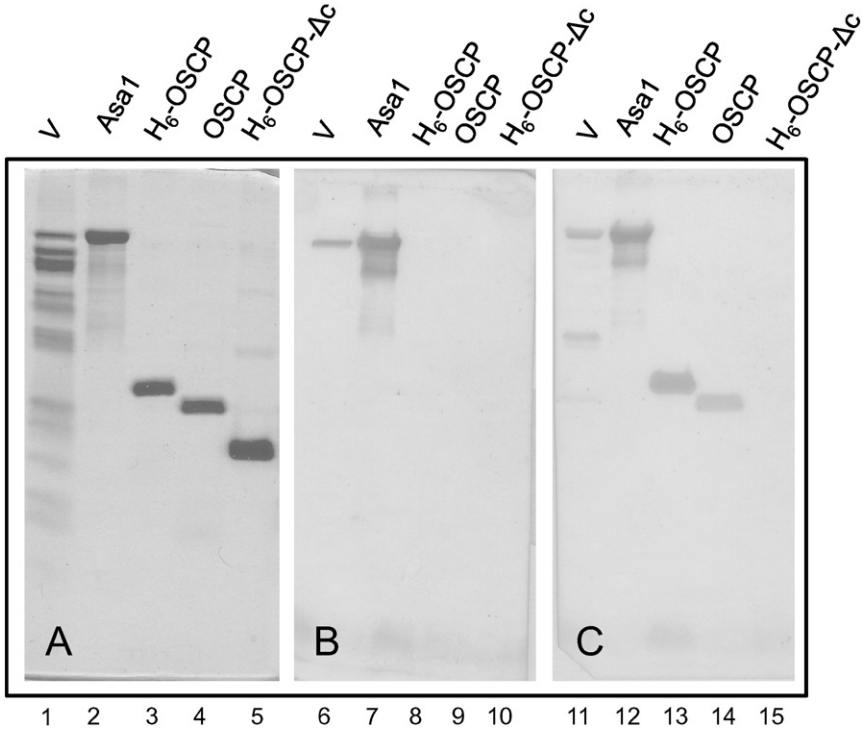

Fig. 5. The carboxy-terminus region of OSCP is instrumental for its interaction with Asa1. A) Coomassie blue-stained Tricine–SDS–polyacrylamide gel showing the *Polytomella* ATP synthase complex (25 μg of protein, lane 1) and 3 μg of each of the following overexpressed and purified recombinant proteins: Asa1 (lane 2); H_6-OSCP (lane 3); OSCP (lane 4) and H_6-OSCP-Δc (lane 5). [This gel is the same one shown in Fig. 1.] B) Western blot analysis of an equivalent gel as the one shown in panel A. After transfer to a nitrocellulose membrane, the blot was decorated with an anti-Asa1 antibody. C) Far-Western blot analysis of an equivalent gel as the one shown in panel A. After transfer to a nitrocellulose membrane, the blot was incubated for 4 h with 2.0 nmol of the isolated, recombinant Asa1 protein, and then decorated with an anti-Asa1 antibody.

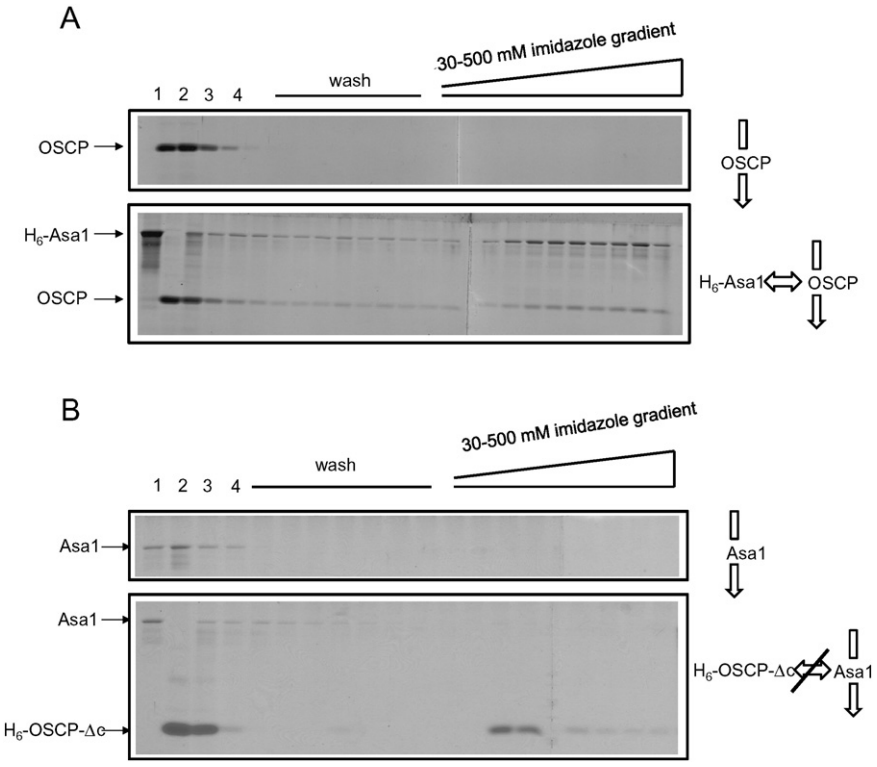

Fig. 6. The interaction of Asa1 with OSCP assayed by affinity chromatography. A) Interaction of Asa1 and OSCP assayed by affinity chromatography. The purified, recombinant OSCP subunit was bound to a Ni Sepharose resin containing no bound protein (upper panel) or to which H_6-Asa1 was bound (lower panel). Coomassie stained gels of the column fractions collected upon application of a 30–500 mM imidazole gradient. Lane 1, added sample; lane 2, protein excluded from the resin; lanes 3 and 4, proteins excluded after washing with 30 mM imidazole. B) Interaction of Asa1 and H_6-OSCP-Δc assayed by affinity chromatography. The experiment was carried out as described for panel A, except that the purified, recombinant H_6-OSCP-Δc fragment, lacking the carboxy-terminus of the OSCP subunit was used. The crossed arrow denotes no association between Asa1 and H_6-OSCP-Δc.

3.3. Subunit Asa1 is also found in a subcomplex containing membrane-embedded subunits

In previous work [9], the algal ATP synthase was dissociated at relatively high temperatures. When the enzyme was heated for 30–40 s at 60 °C a transient subcomplex of 200 kDa formed by subunits Asa1/Asa3/Asa5/Asa8/*a*/*c* was identified by first dimension blue native electrophoresis followed by 2D-SDS–PAGE; at longer time of heat treatment, this subcomplex further dissociated, giving rise to free individual subunits. Here, we looked for conditions in which a stable subcomplex containing Asa1 could be formed without heat treatment. For this purpose, the purified enzyme was incubated at 4 °C overnight with increasing concentrations of lauryl maltoside. As judged by blue native electrophoresis, in the presence of high detergent concentrations the dimeric complex (V_2) dissociated into its monomeric form (V) and released some free F_1 sector. A band, with a slightly faster migration than the F_1 sector was identified as a subcomplex (SC) (Fig 7A). A sample of the purified enzyme was incubated with 3.0% lauryl maltoside overnight and was further resolved in 2D-SDS–PAGE, where the polypeptides forming this subcomplex were separated (Fig 7B). Their identities were assigned by their apparent molecular masses as Asa1 (66.1 kDa), Asa3 (32.9 kDa), Asa5 (13.9 kDa) and Asa8 (9.9 kDa). Again, the band of 22 kDa could be either subunit *a* (Atp6) or OSCP. An additional band of around 45 kDa, exhibiting mobility slightly lower than Asa2, was named tentatively AsaX. The polypeptides Asa1 and Asa8 identities were assigned immunochemically by Western blot analysis using specific antibodies (Fig 7C). Mass spectrometry analysis unambiguously revealed that the 22 kDa was subunit *a* (Atp6, GenBank: CBK55668.1) since two polypeptides of this subunit were identified: TGSLPTNFLTGVYR and SQNPAEKPHPVNDRLLPAVVDASDKR. Mass spectrometry analysis did not reveal the nature of AsaX, since only minute amounts of human keratin, type II cytoskeletal keratin (NCBI Reference Sequence: NP_006112.3) were found in the sample. The band AsaX was therefore subjected to Edman degradation, revealing the N-terminal sequence S-V-L-A-A-S-K-M-V-G-A-G-X-A-T, which matches the N-terminus sequence (SVLAASKMVGAGCAT) of subunit *c* (Atp9) of *Polytomella* sp. (GenBank: ADE92942.1). Thus, AsaX seems to be an SDS-resistant oligomer of *c* subunits migrating with an apparent molecular mass of 46 kDa in SDS–PAGE. Most probably, subunit *c* escaped mass spectrometry detection due to its highly hydrophobic nature. The obtained subcomplex ASA1/ASA3/ASA5/ASA8/*a*/c_x seems to be identical to the one previously observed after heating for a short time the enzyme, except that subunit *c* is now found as an oligomer forming an SDS-resistant ring, probably a decamer of *c*-subunits, as deduced from the electron cryo-microscopy map of the algal ATP synthase [16]. Asa1 is therefore associated with the membrane-bound subunits *a* (Atp6), *c* (Atp9) and Asa8, and also with the extrinsic subunits Asa5 and Asa3. To further explore a possible interaction of Asa1 with membrane components, the isolated, recombinant Asa1 subunit was resolved by SDS–PAGE and transferred to nitrocellulose membranes. The strips, containing the same concentration of Asa1, were incubated with increasing concentrations of a recombinant Asa8 subunit and afterwards incubated with an anti-Asa8 antibody followed by the secondary antibody (Fig 7D). At increasing concentrations of the externally added recombinant Asa8, the anti-Asa8 antibody recognized the Asa1 subunit bound to the nitrocellulose membrane (Fig 7D, lanes 6 to 10). This further suggested the interaction Asa1–Asa8. Since Asa1 lacks any predictable transmembrane stretch, and therefore cannot be considered to be embedded in the lipid bilayer, the data strongly suggests that Asa1 may also contact membrane-embedded polypeptides like Asa8, and thus, may be the key component that bridges the region between the inner mitochondrial membrane and OSCP.

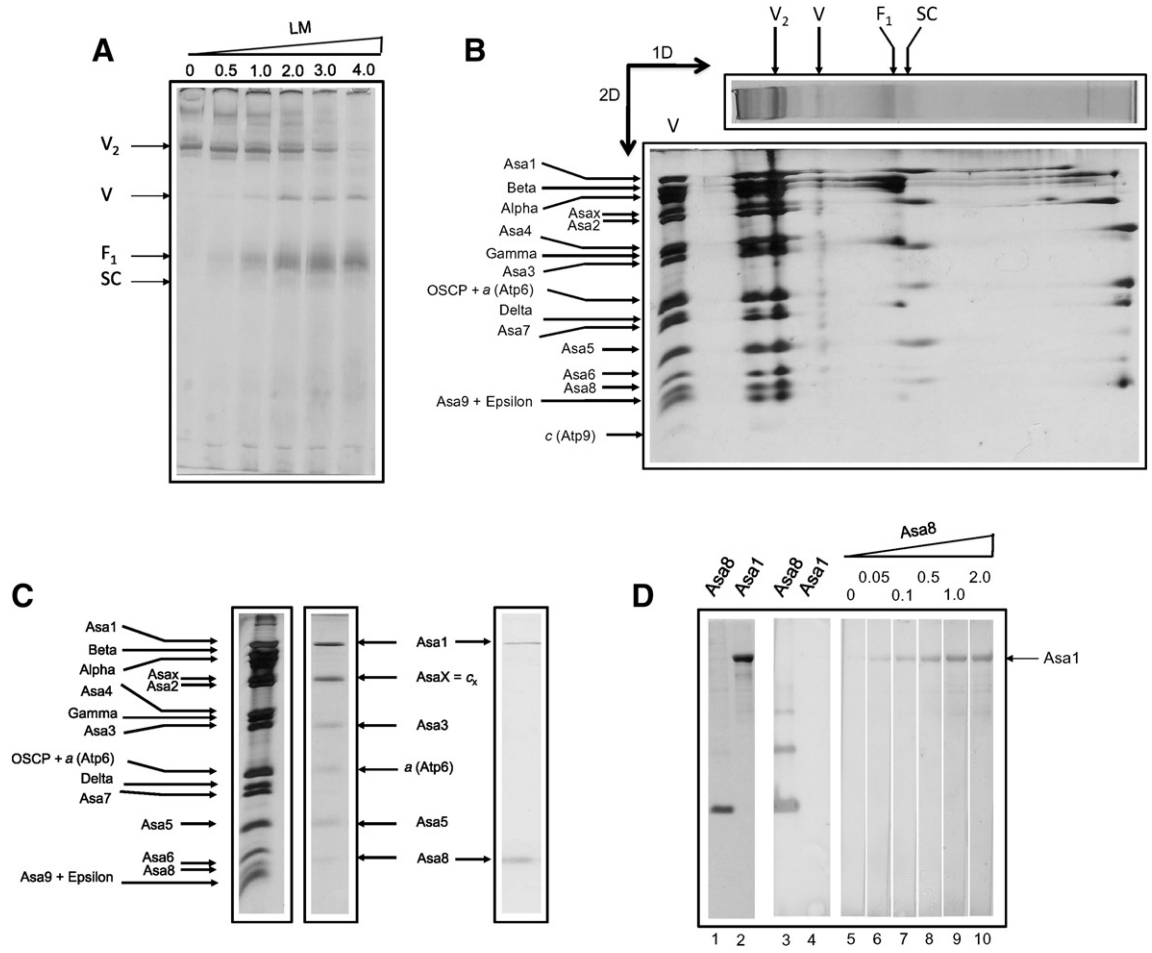

Fig. 7. Formation of an ASA1/ASA3/ASA5/ASA8/a/c subcomplex and detection of an Asa1–Asa8 association. A) BN-PAGE of purified ATP synthase samples incubated overnight at 4 °C under mild agitation in the presence of lauryl maltoside at the indicated increasing concentrations (% *w*/*v*). One hundred micrograms of protein was loaded in each lane. The control lane in the absence of the detergent is labeled 0. Dimer (V2), monomer (V); F_1 sector (F_1), and subcomplex (SC) are indicated. B) 2D gel of an ATP synthase sample incubated overnight in the presence of 3.0% lauryl maltoside. Six polypeptide bands were resolved for the subcomplex (SC) in the 2D SDS–Tricine gel. C) Immunochemical identification of subunits Asa1 and Asa8 as constituents of the subcomplex. D) Asa1–Asa8 interaction as revealed by Far-Western blots. Lanes 1 and 2: Coomassie blue-stained Tricine–SDS polyacrylamide gel showing the purified recombinant proteins Asa 8 (3 μg of protein) and Asa1 (3 μg of protein) respectively. Lanes 3 and 4: Western blot analysis of an equivalent gel. After transfer to a nitrocellulose membrane, the blot was decorated with an anti-Asa8 antibody. Recombinant Asa8 exhibits dimers and higher molecular mass oligomers in SDS–PAGE that are also detected by the antibody. Lanes 5–10: Far-Western blot analysis of an equivalent gel containing the recombinant Asa1 subunit. The blot was incubated for 4 h with the indicated amounts (nanomoles in 5 ml) of the isolated, recombinant Asa8 protein, and then decorated with an anti-Asa8 antibody.

4. Discussion

In ATP synthases, the peripheral stalks are the structures that counteract the torque generated by rotation of the central stalk during the function of the enzyme [37,38]. While the F-type ATPases contain only one peripheral stalk [39], A-type ATPases contain two [40] and eukaryotic V-type ATPases contain three [41]. Also, the subunit structures of the prokaryotic and eukaryotic peripheral stalks are very different. In bacteria like *Escherichia coli*, the peripheral stalk contains two identical *b* subunits, each one exhibiting one transmembrane stretch. Both subunits extend as coiled-coil structures to the top of F_1 where the δ subunit (the bacterial equivalent of OSCP) resides [42,43]. The A_1Ao-ATP synthases also exhibit coiled-coil structures formed by the heterodimeric subunits E and G [38]. The sequence of the *b* subunit of the eukaryotic peripheral stalk differs starkly from the bacterial one. The yeast and beef *b* subunits contain two transmembrane stretches near their N-terminal regions and extend towards the top of the F_1 sector associating with subunits *d* and F6 (*h*) and reaching OSCP [21,44]. In contrast with the above mentioned peripheral stalks, the ATP synthase of the colorless alga *Polytomella* sp. exhibits an extremely robust, electron-dense peripheral stalk as observed in electron microscope image reconstructions [16]. The Asa subunits, present only in mitochondrial ATP synthases of chlorophycean algae [19] have been pin-pointed as the main constituents of this peripheral stalk. We have previously studied the arrangement of Asa subunits and shown that Asa2, Asa4 and Asa7 bind together and that the interaction Asa4–Asa7 is mediated by the C-terminal halves of both proteins [20]. Also, subunits Asa2, Asa4 and Asa7 formed a subcomplex with a 1:1:1 stoichiometry that could be reconstituted *in vitro*. This subcomplex seems to establish contacts with Asa1 and with OSCP. Here, we addressed specifically the topology of Asa1, the larger polypeptide (66.1 kDa) of all Asa subunits. The location of the Asa1 subunit remained controversial since on one hand, it was proposed to represent the large bulk observed in the top region of the peripheral stalk in close contact with the F_1 sector [17] and on the other hand it was identified to constitute a subcomplex along with subunits Asa3, Asa5, Asa8, *a* and *c*, and therefore it was considered to be in close vicinity with the matrix-exposed surface of the inner mitochondrial membrane [9]. The data presented in this work suggest that Asa1 interacts strongly with the OSCP subunit. Asa1 seems to be one of the main components of the peripheral stalk of the algal enzyme forming a physical bridge between the extrinsic subunits (mainly OSCP) and other components of the enzyme either embedded or in close contact with the membrane (Asa3, Asa5, Asa8, *a* and c_{10}-ring) and in particular with the membrane-embedded Asa8 subunit, as judged by Far-Western blot analysis using the recombinant subunits. Thus, Asa1 seems to be the main support of the peripheral stalk, further reinforced by other

Asa subunits (Asa2, Asa4, Asa7 and maybe also Asa3 and Asa5), playing a structural role similar to the one of subunit *b* in orthodox enzymes. The model shown in Fig 8 integrates the results presented in this work. The model proposes Asa1 spanning the peripheral arm from a region in close proximity to the membrane (interacting with subunits Asa3, Asa5, Asa8, *a* and c_{10}), up to the F_1 region of the enzyme (where it interacts with OSCP).

The interaction Asa1 subunit-gamma subunit, as observed in the Far-Western blot experiments, is hard to explain, since in order for the ATP synthase to work as a nanomotor, the rotary components should not bind directly to stator components. A tight binding of Asa1 to the gamma subunit would obviously impede its rotation. We therefore consider that the binding of Asa1 to the gamma subunit, as judged by Far-Western blotting, to be unspecific and probably due to the propensity of both proteins to form coiled-coil structures. It is noted that chlorophycean gamma subunit sequences are very similar to the ones found in other algae and plants and exhibit no distinct features.

The electron cryo-microscopy map of the algal ATP synthase also shows that the *c*-ring is formed by 10 monomers [16]. In this work, we observed the presence of a high molecular mass *c*-ring in SDS–PAGE. This band was not observed before in other *Polytomella* ATP synthase preparations because it co-migrates with subunit Asa2 in SDS–PAGE with an apparent molecular mass of 45.3 kDa. The band, initially named AsaX, was identified as subunit *c* by Edman degradation N-terminal sequencing. Thus, the algal F_1Fo-ATP synthase exhibits an SDS-resistant *c*-ring similar to those previously observed in various isolated Na^+-dependent A_1Ao-ATP synthases, including the strictly anaerobic bacterium *Propionigenium modestum* [45], the fusobacterium *Ilyobacter tartaricus* [46], the acetogenic bacterium *Acetobacterium woodii* [47], and the hyperthermophilic archaea *Pyrococcus furiosus* [48] and *Thermococcus onnurineus* [49]. In eukaryotes, an H^+-dependent F_1Fo-ATP synthase exhibiting an SDS-resistant *c*-ring was reported in yeast [50].

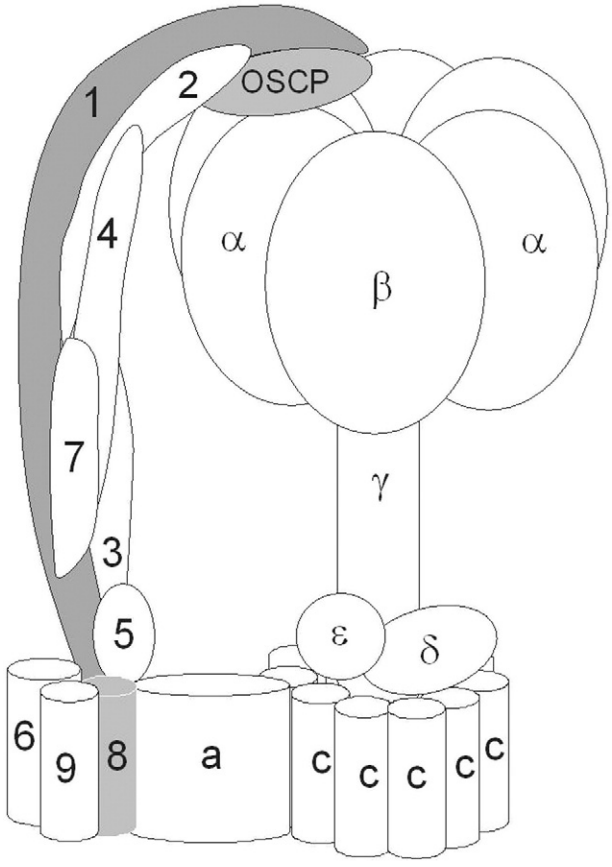

Fig. 8. Subunit arrangement of the algal mitochondrial ATP synthase. Only half of the dimer is shown. The disposition of Asa1, Asa8 and OSCP subunits is highlighted. The model is consistent with previous works reporting close vicinity of subunits as judged by cross-linking experiments [14] and the presence of an Asa4/Asa2/Asa7 subcomplex [20].

Analysis of the Asa subunit sequences indicated high propensity of Asa1, Asa2, Asa4 and Asa7 to form coiled-coil regions (30, 19, 35 and 32% respectively) [20]. These Asa subunits most probably interact through large contacts within alpha-helices that form the robust, intertwined peripheral arm observed in the electron cryo-microscopy map of the *Polytomella* ATP synthase dimer [16]. The size of the F_1 sector [$\alpha_3/\beta_3/\gamma/\delta/\varepsilon$] is around 150 Å, so one can estimate the length of the peripheral stalk of the *Polytomella* enzyme to be of 221 Å, taking into account the curvature observed in the electron cryo-microscopy map of the enzyme [16]. The mature Asa1 subunit has 596 residues, so if one considers the whole protein to be in an alpha-helical conformation, it should have a length of 894 Å, enough to transverse the peripheral stalk three to four times. In contrast, subunit *b* of the orthodox ATP synthases green algae, is around 190 residues (285 Å long), thus only one third of the Asa1 subunit. We carried out 3D modeling of several chlorophycean Asa1 subunits using the RaptorX homepage. Several models were obtained for each Asa1 sequence. Nevertheless only one template, PDB ID: 1HCI (the crystal structure of the rod domain of alpha-actinin), was consistently chosen by the program to model all the Asa1 sequences. The model for the *Polytomella parva* Asa1 subunit is shown in Suppl. Fig. 1. The prediction shows a protein 240 Å long with multiple alpha-helices forming coiled-coil structures and a highly conserved carboxy-terminus.

In this work, we provide evidence for the interaction of Asa1 subunit that seems to pertain solely to the chlorophycean algal lineage with one of the highly conserved subunits present in all mitochondrial ATP synthases known to date (the OSCP subunit). We suggest that Asa1 has taken the place of subunit *b* as the main constituent supporting the mitochondrial ATP synthase peripheral arm. Genes encoding orthodox *b* subunits are found in almost all land plants and green alga. The distribution of *b* subunits and Asa1 subunits in different photosynthetic organisms is shown in Suppl. Fig. 2. While land plants, Charophyte alga, Prasinophytes, and the class Trebouxiophyceae exhibit a gene encoding orthodox subunit *b*, this gene is absent and seems to be substituted by the gene encoding Asa1 in chlorophycean algae, both in the orders Chlamydomonadales and Sphaeropleales. The origin of Chlorophyceae occurred approximately 600 million years ago [51] and seems to be related to the drastic reduction of mitochondrial genome in size and in gene content, and to the appearance of nucleus-encoded atypical subunits of the enzyme (Asa subunits) [52,19].The phylogenetic distribution of orthodox *b* subunits and Asa1 subunits strongly suggests that the appearance during evolution of Asa subunits as constituents of the ATP synthase peripheral arm, only occurred in chlorophycean algae. One could predict that the OSCP subunit of chlorophycean algae must also differ from classical plant and algal OSCP subunits, in order to accommodate binding to the Asa1 subunit instead of the *b* subunit. Alignment of diverse OSCP sequences strongly suggests that this protein separates into two clearly distinct groups that exhibit conspicuously different amino acid sequences: one of Chlorophycean algae and another of all the other green algae and land plants (Suppl. Fig. 3).

It seems that Asa1 is neither a highly modified subunit *b* nor the result of a duplication of a gene encoding subunit *b*. Rather; it seems more likely that in the chlorophycean lineage, all the orthodox structural components of the peripheral arm were substituted by scaffold-forming proteins from a complete different origin, i.e., the Asa subunits.

Supplementary data to this article can be found online at http://dx.doi.org/10.1016/j.bbabio.2015.11.012.

Transparency document

The Transparency document associated with this article can be found, in online version.

Acknowledgments

We are grateful to Professor David R. Smith (Department of Biology, Western University, Canada) for providing us access to the Asa1 sequences of various *Polytomella* species. We thank Dr. Lawrence Dangott (Texas A&M University) for the Edman degradation analyses, and M.C. Emmanuel Ríos Castro (LaNSE, CINVESTAV del IPN) for the mass spectrometry data. Special thanks to Félix Vega de Luna (IFC, UNAM) for his help with the 3D modeling of the Asa1 subunits. We are also grateful to Laura Ongay Larios, Minerva Mora Cabrera and Guadalupe Códiz Huerta of the Molecular Biology Unit, IFC, UNAM for primer synthesis and sequencing. This research was supported by grant 245486 from the Consejo Nacional de Ciencia y Tecnología (CONACyT) and the Belgian Fonds de la Recherche Scientifique (F.R.S.-FNRS) (Mexico-Belgium). Additional support was received from grants 239219 (CONACyT, Mexico), IN203311-3 from the Dirección General de Asuntos del Personal Académico (DGAPA-UNAM, Mexico) and from the F.R.S.-FNRS(MIS F.4520, FRFC 2.4597). CONACyT also supported with fellowship 599282 the Ph.D. studies of L.C.-T. (Programa de Doctorado en Ciencias Biomédicas de la Universidad Nacional Autónoma de México).

References

[1] T. Xu, V. Pagadala, D.M. Mueller, Understanding structure, function, and mutations in the mitochondrial ATP synthase, Microb. Cell 2 (2015) 105–125.
[2] A. Wächter, Y. Bi, S.D. Dunn, B.D. Cain, H. Sielaff, F. Wintermann, S. Engelbrecht, W. Junge, Two rotary motors in F-ATP synthase are elastically coupled by a flexible rotor and a stiff stator stalk, Proc. Natl. Acad. Sci. U. S. A. 108 (2011) 3924–3929.
[3] J.E. Walker, V.K. Dickson, The peripheral stalk of the mitochondrial ATP synthase, Biochim. Biophys. Acta 1757 (2006) 286–296.
[4] H. Seelert, N.A. Dencher, ATP synthase superassemblies in animals and plants: two or more are better, Biochim. Biophys. Acta 1807 (2011) 1185–1197.
[5] P. Paumard, J. Vaillier, B. Coulary, J. Schaeffer, V. Soubannier, D.M. Mueller, D. Brèthes, J.P. di Rago, J. Velours, The ATP synthase is involved in generating mitochondrial cristae morphology, EMBO J. 21 (2002) 221–230.
[6] N.P. Balabaskaran, N.V. Dudkina, L.A. Kane, J.E. van Eyk, E.J. Boekema, M.W. Mather, A.B. Vaidya, Highly divergent mitochondrial ATP synthase complexes in *Tetrahymena thermophila*, PLoS Biol. 8 (2010), e1000418.
[7] A. Zikova, A. Schnaufer, R.A. Dalley, A.K. Panigrahi, K.D. Stuart, The F(0)F(1)-ATP synthase complex contains novel subunits and is essential for procyclic *Trypanosoma brucei*, PLoS Pathog. 5 (2009), e1000436.
[8] E. Perez, M. Lapaille, H. Degand, L. Cilibrasi, A. Villavicencio-Queijeiro, P. Morsomme, D. González-Halphen, M.C. Field, C. Remacle, D. Baurain, P. Cardol, The mitochondrial respiratory chain of the secondary green alga *Euglena gracilis* shares many additional subunits with parasitic Trypanosomatidae, Mitochondrion 19 (Pt B) (2014) 338–349.
[9] M. Vázquez-Acevedo, P. Cardol, A. Cano-Estrada, M. Lapaille, C. Remacle, D. González-Halphen, The mitochondrial ATP synthase of chlorophycean algae contains eight subunits of unknown origin involved in the formation of an atypical stator-stalk and in the dimerization of the complex, J. Bioenerg. Biomembr. 38 (2006) 271–282.
[10] R. van Lis, A. Atteia, G. Mendoza-Hernández, D. González-Halphen, Identification of novel mitochondrial protein components of *Chlamydomonas reinhardtii*. A proteomic approach, Plant Physiol. 132 (2003) 318–330.
[11] A. Atteia, G. Dreyfus, D. González-Halphen, Characterization of the alpha and beta-subunits of the F0F1-ATPase from the alga *Polytomella* spp., a colorless relative of *Chlamydomonas reinhardtii*, Biochim. Biophys. Acta 1320 (1997) 275–284.
[12] N.V. Dudkina, J. Heinemeyer, W. Keegstra, E.J. Boekema, H.P. Braun, Structure of dimeric ATP synthase from mitochondria: an angular association of monomers induces the strong curvature of the inner membrane, FEBS Lett. 579 (2005) 5769–5772.
[13] N.V. Dudkina, S. Sunderhaus, H.P. Braun, E.J. Boekema, Characterization of dimeric ATP synthase and cristae membrane ultrastructure from *Saccharomyces* and *Polytomella* mitochondria, FEBS Lett. 580 (2006) 3427–3432.
[14] A. Cano-Estrada, M. Vázquez-Acevedo, A. Villavicencio-Queijeiro, F. Figueroa-Martínez, H. Miranda-Astudillo, Y. Cordeiro, J.A. Mignaco, D. Foguel, P. Cardol, M. Lapaille, C. Remacle, S. Wilkens, D. González-Halphen, Subunit–subunit interactions and overall topology of the dimeric mitochondrial ATP synthase of *Polytomella* sp, Biochim. Biophys. Acta 1797 (2010) 1439–1448.
[15] N.V. Dudkina, G.T. Oostergetel, D. Lewejohann, H.P. Braun, E.J. Boekema, Row-like organization of ATP synthase in intact mitochondria determined by cryo-electron tomography, Biochim. Biophys. Acta 1797 (2010) 272–277.
[16] M. Allegretti, N. Klusch, D.J. Mills, J. Vonck, W. Kühlbrandt, K.M. Davies, Horizontal membrane-intrinsic α-helices in the stator a-subunit of an F-type ATP synthase, Nature 521 (2015) 237–240.
[17] R. van Lis, G. Mendoza-Hernández, G. Groth, A. Atteia, New insights into the unique structure of the F0F1-ATP synthase from the chlamydomonad algae *Polytomella* sp. and *Chlamydomonas reinhardtii*, Plant Physiol. 144 (2007) 1190–1199.
[18] A. Villavicencio-Queijeiro, M. Vázquez-Acevedo, A. Cano-Estrada, M. Zarco-Zavala, M. Tuena de Gómez, J.A. Mignaco, M.M. Freire, H.M. Scofano, D. Foguel, P. Cardol, C. Remacle, D. González-Halphen, The fully-active and structurally-stable form of the mitochondrial ATP synthase of *Polytomella* sp. is dimeric, J. Bioenerg. Biomembr. 41 (2009) 1–13.
[19] M. Lapaille, A. Escobar-Ramírez, H. Degand, D. Baurain, E. Rodríguez-Salinas, N. Coosemans, M. Boutry, D. Gonzalez-Halphen, C. Remacle, P. Cardol, Atypical subunit composition of the chlorophycean mitochondrial F1FO-ATP synthase and role of Asa7 protein in stability and oligomycin resistance of the enzyme, Mol. Biol. Evol. 27 (2010) 1630–1644.
[20] H. Miranda-Astudillo, A. Cano-Estrada, M. Vázquez-Acevedo, L. Colina-Tenorio, A. Downie-Velasco, P. Cardol, C. Remacle, L. Domínguez-Ramírez, D. González-Halphen, Interactions of subunits Asa2, Asa4 and Asa7 in the peripheral stalk of the mitochondrial ATP synthase of the chlorophycean alga *Polytomella* sp, Biochim. Biophys. Acta 1837 (2014) 1–13.
[21] V.K. Dickson, J.A. Silvester, I.M. Fearnley, A.G. Leslie, J.E. Walker, On the structure of the stator of the mitochondrial ATP synthase, EMBO J. 25 (2006) 2911–2918.
[22] L.A. Baker, I.N. Watt, M.J. Runswick, J.E. Walker, J.L. Rubinstein, Arrangement of subunits in intact mammalian mitochondrial ATP synthase determined by cryo-EM, Proc. Natl. Acad. Sci. U. S. A. 109 (2012) 11,675–11,680.
[23] W.C. Lau, L.A. Baker, J.L. Rubinstein, Cryo-EM structure of the yeast ATP synthase, J. Mol. Biol. 382 (2008) 1256–1264.
[24] C. Mellwig, B. Böttcher, A unique resting position of the ATP-synthase from chloroplasts, J. Biol. Chem. 278 (2003) 18,544–18,549.
[25] I. Ogilvie, S. Wilkens, A.J. Rodgers, R. Aggeler, R.A. Capaldi, The second stalk: the delta-b subunit connection in ECF1FO, Acta Physiol. Scand. Suppl. 643 (1998) 169–175.
[26] H. Schägger, Denaturing electrophoretic techniques, in: G. von Jagow, H. Schägger (Eds.), A Practical Guide to Membrane Protein Purification, Academic Press, San Diego 1994, pp. 59–79.
[27] U.K. Laemmli, Cleavage of structural proteins during the assembly of the head of bacteriophage T4, Nature 227 (1970) 680–685.
[28] H. Schägger, Native gel electrophoresis, in: G. von Jagow, H. Schägger (Eds.), A Practical Guide to Membrane Protein Purification, Academic Press, San Diego 1994, pp. 81–104.
[29] M.A.K. Markwell, S.M. Hass, L.L. Biber, N.E. Tolbert, A modification of the Lowry procedure to simplify protein determination in membrane and lipoprotein samples, Anal. Biochem. 87 (1978) 206–210.
[30] A. Atteia, R. van Lis, S.I. Beale, Enzymes of the heme biosynthetic pathway in the nonphotosynthetic alga *Polytomella* sp, Eukaryot. Cell 4 (2005) 2087–2097.
[31] H. Schägger, H. Aquila, G. Von Jagow, Coomassie blue–sodium dodecyl sulfate–polyacrylamide gel electrophoresis for direct visualization of polypeptides during electrophoresis, Anal. Biochem. 173 (1988) 201–205.
[32] D. González-Halphen, M.A. Lindorfer, R.A. Capaldi, Subunit arrangement in beef heart complex III, Biochemistry 27 (1988) 7021–7031.
[33] R.A. Hall, Studying protein–protein interactions via blot overlay or Far Western blot, Methods Mol. Biol. 261 (2004) 167–174.
[34] H. Towbin, T. Staehelin, J. Gordon, Electrophoretic transfer of proteins from polyacrylamide gels to nitrocellulose sheets: procedure and some applications, Proc. Natl. Acad. Sci. U. S. A. 76 (1979) 4350–4354.
[35] J.D. Thompson, D.G. Higgins, T.J. Gibson, CLUSTAL W: improving the sensitivity of progressive multiple sequence alignment through sequence weighting, position-specific gap penalties and weight matrix choice, Nucleic Acids Res. 22 (1994) 4673–4680.
[36] M. Källberg, H. Wang, S. Wang, J. Peng, Z. Wang, H. Lu, J. Xu, Template-based protein structure modeling using the RaptorX web server, Nat. Protoc. 7 (2012) 1511–1522.
[37] W. Junge, H. Sielaff, S. Engelbrecht, Torque generation and elastic power transmission in the rotary F(O)F(1)-ATPase, Nature 459 (2009) 364–370.
[38] A.G. Stewart, L.K. Lee, M. Donohoe, J.J. Chaston, D. Stock, The dynamic stator stalk of rotary ATPases, Nat. Commun. 3 (2012) 687.
[39] S. Wilkens, R.A. Capaldi, ATP synthase's second stalk comes into focus, Nature 393 (1998) 29.
[40] J. Vonck, K.Y. Pisa, N. Morgner, B. Brutschy, V. Muller, Three-dimensional structure of A_1A_0 ATP synthase from the hyperthermophilic archaeon *Pyrococcus furiosus* by electron microscopy, J. Biol. Chem. 284 (2009) 10,110–10,119.
[41] Z. Zhang, Y. Zheng, H. Mazon, E. Milgrom, N. Kitagawa, E. Kish-Trier, A.J. Heck, P.M. Kane, S. Wilkens, Structure of the yeast vacuolar ATPase, J. Biol. Chem. 283 (2008) 35,983–35,995.
[42] K.S. Wood, S.D. Dunn, Role of the asymmetry of the homodimeric b_2 stator stalk in the interaction with the F1 sector of *Escherichia coli* ATP synthase, J. Biol. Chem. 282 (2007) 31,920–31,927.
[43] K. Brandt, S. Maiwald, B. Herkenhoff-Hesselmann, K. Gnirß, J.C. Greie, S.D. Dunn, G. Deckers-Hebestreit, Individual interactions of the b subunits within the stator of the *Escherichia coli* ATP synthase, J. Biol. Chem. 288 (2013) 24,465–24,479.
[44] M.F. Paul, B. Guerin, J. Velours, The C-terminal region of subunit 4 (subunit b) is essential for assembly of the F0 portion of yeast mitochondrial ATP synthase, Eur. J. Biochem. 205 (1992) 163–172.
[45] W. Laubinger, P. Dimroth, Characterization of the ATP synthase of *Propionigenium modestum* as a primary sodium pump, Biochemistry 27 (1988) 7531–7537.
[46] H. Stahlberg, D.J. Müller, K. Suda, D. Fotiadis, A. Engel, T. Meier, U. Matthey, P. Dimroth, Bacterial Na(+)-ATP synthase has an undecameric rotor, EMBO Rep. 2 (2001) 229–233.
[47] M. Fritz, V. Müller, An intermediate step in the evolution of ATPases—the F1FO-ATPase from *Acetobacterium woodii* contains F-type and V-type rotor subunits and is capable of ATP synthesis, FEBS J. 274 (2007) 3421–3428.

[48] K.Y. Pisa, H. Huber, M. Thomm, V. Müller, A sodium ion-dependent A_1AO ATP synthase from the hyperthermophilic archaeon *Pyrococcus furiosus*, FEBS J. 274 (2007) 3928–3938.
[49] F. Mayer, J.K. Lim, J.D. Langer, S.G. Kang, V. Müller, Na+ transport by the A1AO-ATP synthase purified from *Thermococcus onnurineus* and reconstituted into liposomes, J. Biol. Chem. 290 (2015) 6994–7002.
[50] J. Velours, G. Arselin, The *Saccharomyces cerevisiae* ATP synthase, J. Bioenerg. Biomembr. 32 (2000) 383–390.
[51] M.D. Herron, J.D. Hackett, F.O. Aylward, R.E. Michod, Triassic origin and early radiation of multicellular volvocine algae, Proc. Natl. Acad. Sci. U. S. A. 106 (2009) 3254–3258.
[52] P. Cardol, D. González-Halphen, A. Reyes-Prieto, D. Baurain, R.F. Matagne, C. Remacle, The mitochondrial oxidative phosphorylation proteome of *Chlamydomonas reinhardtii* deduced from the Genome Sequencing Project, Plant Physiol. 137 (2005) 447–459.
[53] L.A. Lewis, R.M. McCourt, Green algae and the origin of land plants, Am. J. Bot. 91 (2004) 1535–1556.
[54] F. Leliaert, D.R. Smith, H. Moreau, M.D. Herron, H. Verbruggen, C.F. Delwiche, O. De Clerck, Phylogeny and molecular evolution of the green algae, Crit. Rev. Plant Sci. 31 (2012) 1–46.

Biochimica et Biophysica Acta 1857 (2016) 1183–1190

Contents lists available at ScienceDirect

Biochimica et Biophysica Acta

journal homepage: www.elsevier.com/locate/bbabio

Review

Dissecting the peripheral stalk of the mitochondrial ATP synthase of chlorophycean algae☆,☆☆

Miriam Vázquez-Acevedo [a], Félix Vega-deLuna [a], Lorenzo Sánchez-Vásquez [a], Lilia Colina-Tenorio [a], Claire Remacle [b], Pierre Cardol [b], Héctor Miranda-Astudillo [b], Diego González-Halphen [a,*]

[a] Instituto de Fisiología Celular, Universidad Nacional Autónoma de México, México D.F., Mexico
[b] Genetics and Physiology of Microalgae, Department of Life Sciences, University of Liège, B-4000 Liège, Belgium

ARTICLE INFO

Article history:
Received 10 December 2015
Received in revised form 25 January 2016
Accepted 5 February 2016
Available online 10 February 2016

Keywords:
F_1F_O-ATP synthase peripheral-stalk
Dimeric mitochondrial complex V
Amphipol A8-35
Chlamydomonas reinhardtii
Polytomella sp.
Asa subunits

ABSTRACT

The algae *Chlamydomonas reinhardtii* and *Polytomella* sp., a green and a colorless member of the chlorophycean lineage respectively, exhibit a highly-stable dimeric mitochondrial F_1Fo-ATP synthase (complex V), with a molecular mass of 1600 kDa. *Polytomella*, lacking both chloroplasts and a cell wall, has greatly facilitated the purification of the algal ATP-synthase. Each monomer of the enzyme has 17 polypeptides, eight of which are the conserved, main functional components, and nine polypeptides (Asa1 to Asa9) unique to chlorophycean algae. These atypical subunits form the two robust peripheral stalks observed in the highly-stable dimer of the algal ATP synthase in several electron-microscopy studies. The topological disposition of the components of the enzyme has been addressed with cross-linking experiments in the isolated complex; generation of subcomplexes by limited dissociation of complex V; detection of subunit–subunit interactions using recombinant subunits; *in vitro* reconstitution of subcomplexes; silencing of the expression of Asa subunits; and modeling of the overall structural features of the complex by EM image reconstruction. Here, we report that the amphipathic polymer Amphipol A8-35 partially dissociates the enzyme, giving rise to two discrete dimeric subcomplexes, whose compositions were characterized. An updated model for the topological disposition of the 17 polypeptides that constitute the algal enzyme is suggested. This article is part of a Special Issue entitled 'EBEC 2016: 19th European Bioenergetics Conference, Riva del Garda, Italy, July 2-6, 2016', edited by Prof. Paolo Bernardi.

1. The mitochondrial ATP synthase

Mitochondrial F_1Fo-ATP synthase (complex V) is a key participant of oxidative phosphorylation (OXPHOS) and the main ATP producing enzyme in non-photosynthetic eukaryotes. Classic dissociation experiments characterized two oligomeric domains in the enzyme, an extrinsic moiety (F_1 factor) and the membrane bound sector Fo [1]. F_1Fo-ATP synthase is also a molecular motor [2] in which a central rotor-stalk [γ/δ/ε/c-ring] rotates around an axis perpendicular to the plane of the membrane, while the fixed elements (stator components) are subunit *a*, the catalytic core (α_3/β_3), the peripheral stalk (OSCP/b/d/F6), and the dimerization module (A6L/*e*/*f*/*g*) [3,4]. Proton-flux through the two hemi-channels of subunit *a*, formed by membrane-embedded α-helices, causes the rotary movement of a *c*-subunit ring with a species-dependent variable stoichiometry (c_{8-14}) and concomitantly, the rotation of the central-stalk (γ/δ/ε) [5]. Three sequential 120° movements of subunit γ induce conformational changes in the three catalytic β subunits leading to successive substrate binding (ADP + Pi), ATP synthesis, and ATP release [6]. Other subunits play a regulatory role, such as the inhibitory protein IF_1 [7] that prevents futile ATP hydrolysis. The peripheral stator-stalk counteracts the torque generated by the rotation of the central stalk during the function of the enzyme [8]. In the yeast and beef enzymes, the main axis of the peripheral stalk is formed by subunit *b*, that contains two transmembrane stretches near its N-terminal region and extends towards OSCP at the top of the F_1 sector associating also with subunits *d* and F6 (*h* in yeast) [9].

In the inner mitochondrial membrane, the ATP synthase forms oligomeric associations [10–12] that are responsible for the overall architecture of the mitochondrial cristae [13]. In yeast, dimerization is mediated by the small subunits *e*, *g*, *h* and *i* [14,15]. Subunits *b* (Atp4), *d*, F6, A6L, *e*, *f* and *g*, present in the bovine enzyme, are not common to all mitochondrial ATP synthases; atypical subunit compositions have been identified in trypanosomatids [16], euglenoids [17], chlorophycean algae [18] and ciliates [19]. Also, electron microscopy studies have shown stark structural differences in the enzymes of ciliates [19] and algae [18] as compared to the orthodox enzymes isolated from beef and yeast [11,20].

☆ This article is part of a Special Issue entitled 'EBEC 2016: 19th European Bioenergetics Conference, Riva del Garda, Italy, July 2-6, 2016', edited by Prof. Paolo Bernardi.
☆☆ Peripheral stalk of algal ATP synthases

* Corresponding author at: Departamento de Genética Molecular, Instituto de Fisiología Celular, UNAM, Apartado Postal 70-600, Delegación Coyoacán, 04510 México D.F., Mexico.
E-mail address: dhalphen@ifc.unam.mx (D. González-Halphen).

http://dx.doi.org/10.1016/j.bbabio.2016.02.003
0005-2728/

2. The mitochondrial ATP synthase of chlorophycean algae

2.1. Subunit composition

Chlorophycean algae originated approximately 600 million years ago [21]. Some characteristics of this lineage are the drastic reduction of its mitochondrial genomes in size and in gene content [22], the fragmentation of the mitochondrial *cox2* gene and its migration to the nucleus [23], and the appearance of nucleus-encoded atypical subunits of ATP synthase (Asa subunits) [24,25]. Genes encoding homologs of Asa subunits were identified in several other chlorophycean algae including *Volvox carteri*, *Scenedesmus obliquus* and *Chloroccocum ellipsoideum* [25]. The list can be updated to include the green unicellular algae *Chlamydomonas chlamydogama*, *Chlamydomonas leiostraca*, *Chlamydomonas* sp. and *Dunaliella tertiolecta* and the colorless algae *Polytomella capuana*, *Polytomella magna*, *Polytomella piriformis* and *Polytomella parva* [26].

The biochemical characterization of the mitochondrial ATP synthase of chlorophycean algae has been carried out mainly with two organisms, the unicellular green alga *Chlamydomonas reinhardtii* and its colorless close relative *Polytomella* sp. Early works identified immunochemically the β-subunit of mitochondrial ATP synthase in preparations of thylakoid and mitochondria membranes of *C. reinhardtii* [27]. A fraction enriched in the green algal complex V was obtained after sucrose gradient centrifugation in the presence of Triton X-100 [28]. The cDNA of the β-subunit of *C. reinhardtii* mitochondrial ATP synthase was sequenced and the corresponding protein was found to contain a unique C-terminal extension of 70 residues not present in the β-subunits of plant enzymes [29]. A pure and active mitochondrial ATP synthase preparation from the green alga was obtained by extraction with lauryl maltoside followed by ion exchange and gel permeation chromatography and found to be composed of at least 14 polypeptides [30]. Also, the cDNA encoding the α-subunit of the enzyme was sequenced and the mature subunit was found to exhibit an 18-residues extension not present in other organisms.

Subsequently, a mitochondrial F_1Fo-ATP synthase was isolated by gel permeation chromatography from *Polytomella* sp., that lacks both chloroplasts and cell wall, and thus facilitates the isolation of mitochondria and purification of the OXPHOS complexes without the interference of thylakoid components [31]. The enzyme from this colorless alga exhibited at least 10 polypeptides with apparent molecular masses that ranged from 6 to 63 kDa [32] and its α and β subunits exhibited high sequence similarities with the ones of *Chlamydomonas* [see also Ref. 33]. Here, the *Polytomella* α and β subunits were modeled on the crystallographic structure of the bovine enzyme to visualize the location of these extensions in the F_1 sector. Fig. 1 shows two of the possible conformations for each of the algal extensions. The α subunit extensions could have a role in stabilizing contacts with the peripheral stalk, while the β subunit extensions were proposed to act as the IF_1 ATPase inhibitor based on sequence similarities [32]. When the extension of the β subunit was overexpressed, partially purified, and added to the algal ATPase at relatively high concentrations, the hydrolytic activity of the enzyme diminished less than 20% [Villavicencio-Queijeiro and González-Halphen, unpublished results]. Although this result suggests a null or very limited inhibitory effect of the C-terminal extension of the beta subunit, it would be necessary to delete this extremity using site-directed mutagenesis to ascertain its role.

In order to assess if subunit *a* (Atp6) was present in the mitochondrial ATP synthase of *C. reinhardtii*, isolated mitochondria from the green alga were subjected to blue native electrophoresis (BN–PAGE), a technique that uses the charge shift generated by the binding of Coomassie Blue to detergent-solubilized membrane complexes to separate them under native conditions [34]. The first dimensional BN–PAGE gel was then subjected to 2D-denaturing SDS–PAGE to identify the polypeptide composition of complex V [35]. At least 13 different polypeptides were found to be associated to the complex, five of which were unambiguously identified as subunits α, β, γ, δ and *a*. Nevertheless, eight polypeptides of the ATP synthase showed no evident similarity with other ATPase subunits nor with other proteins in the databases, so their identities remained obscure at that time. These results prompted a detailed analysis of mitochondrial protein components of *C. reinhardtii* by BN–PAGE, followed by 2D-SDS–PAGE and Edman degradation of selected bands [36]. Complex V was found to migrate exclusively as a dimer that resolved into at least 13 polypeptides in 2D-SDS–PAGE. In addition, a novel 60-kDa protein with no known counterpart in any other organism, named MASAP for mitochondrial ATP synthase-associated protein and later on renamed Asa1, was described and its corresponding cDNA sequence was obtained [36]. It was put forth that this novel polypeptide was extrinsic to the membrane, probably not a chaperone and that it could play a structural role in stabilizing the chlorophycean ATP synthase dimer.

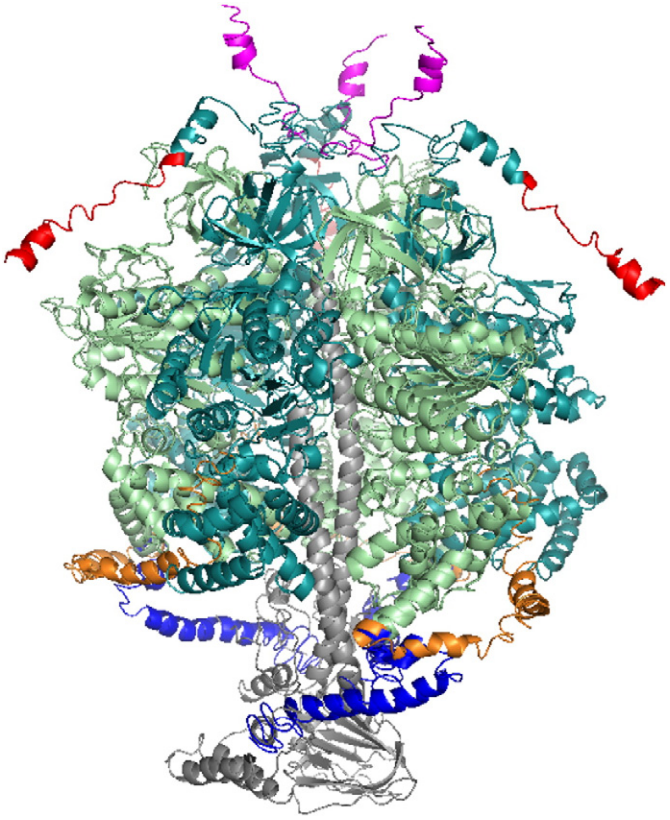

Fig. 1. Model of the *Polytomella* sp. ATP synthase subunits α and β and their corresponding extensions. The *Polytomella* sp. sequences of the mature α subunit with its C-terminal extension of 67 residues, and the β subunit with its N-terminal extension of 21 residues were modeled *in silico* using the I-TASSER server [71]. Two of the obtained models that showed no steric hindrances were selected for each subunit. The algal F_1 sector was modeled on the bovine crystallographic structure (PDB Id: 2WSS) [72]. Subunits in the complex are colored: α subunits (dark green), β subunits (light green), γ subunit (gray), algal α subunit extensions (one possible conformation in red, the other in magenta), algal β subunit extensions (one possible conformation in orange, the other in dark blue).

Mitochondrial F_1Fo-ATP synthases of *C. reinhardtii* and *Polytomella* sp. migrated in BN–PAGE in the presence of lauryl-maltoside as stable dimers of 1600 kDa [36,37] while the monomeric F_1Fo or free F_1 moieties could not be detected. This suggested the presence of a highly stable, detergent-resistant dimeric enzyme and contrasted starkly with the behavior of other complex V from different sources, including mammals, fungi and land plants that usually migrate in BN–PAGE in the presence of lauryl-maltoside as monomers of 550–600 kDa [14,20,38,39]. Also, conventional enzymes tend to partially dissociate during electrophoresis, releasing the F_1 sector [38]. In order to obtain dimers from these latter biological sources, milder solubilization conditions, usually with digitonin, are required [20].

The completion of the *C. reinhardtii* genome [40] allowed the identification of the ATP synthase subunits whose N-terminal sequences had been obtained previously [35]. Thus, the mitochondrial ATP synthase from *C. reinhardtii* was now found to contain 14 subunits of 7 to 60 kDa [41]. Seven polypeptides were identified as the classical subunits α, β, γ, δ, *a* (ATP6), *c* (ATP9), and OSCP. Besides Asa1, several other polypeptides with no counterparts in the databases were identified and named Asa2 to Asa7 (this last one previously known as Nuop6) in accordance with the *C. reinhardtii* genome project nomenclature. In addition, no homologs of the ε, *b*, *d*, *e*, *f*, *g*, IF_1, A6L, and F6 subunits were found encoded in the algal genome. This reinforced the idea that unique proteins were associated with chlorophycean mitochondrial ATP synthases [24] and pin-pointed the Asa subunits as the main constituents of the peripheral stalk of the enzyme. The mitochondrial ATP synthase of *Polytomella* sp. was isolated; its polypeptide composition was characterized and found to be similar to that of the *C. reinhardtii* enzyme [18,33]. Furthermore, small-angle X-ray scattering analysis estimated a molecular mass of the complex of 1696 kDa [42]. In addition, the presence of two additional low molecular mass subunits, Asa8 and Asa9, was described. Asa subunits were found associated to the algal ATP synthase even when the complex was isolated following different purification procedures; thus, the possibility that they were only contaminants of the preparations was discarded [18]. It seems that in the chlorophycean lineage, all the orthodox structural components of the peripheral arm were substituted by polypeptides from a completely different origin, probably proteins that already had a structural role in some other cell compartment.

2.2. Hydrolytic activity of the purified algal enzyme

When isolated, the *Polytomella* sp. enzyme exhibits a very low ATPase activity that increases either with heat treatment (due to the release of the F_1 sector) or when being unmasked by the presence of non-ionic detergents in an activity assay [43]. The biochemical state of the enzyme in the absence of externally added detergent is however not known; it could be partially aggregated and therefore inactive, or it could be fully restrained by an inhibitor that is released upon detergent addition. The algal dimer hydrolyzes ATP on a wide range of pH's and temperatures and shows sensitivity to the classical inhibitors oligomycin and DCCD [44], the dimeric ATPase exhibited and apparent Km for Mg-ATP of 0.19 mM and a V_{max} of 0.065 U/mg in the absence of detergent. The V_{max} increased 60-fold in the presence of detergent (Km of 0.24 mM and a V_{max} of 3.8 U/mg). Independent measurements of the hydrolytic activity of the *Polytomella* mitochondrial ATPase have reported activities up to 8.0 U/mg, full DCCD sensitivity, and more than 90% inhibition by oligomycin [45]. These specific activity values are comparable to those of purified ATPases from the green alga *C. reinhardtii* (2.9 U/mg) [30] or from the fungi *Yarrowia lipolytica* (8.4 U/mg) and *Pichia pastoris* (9.3 U/mg), but considerably lower than the enzymes from *Pichia angusta* (21.8 U/mg) and *Saccharomyces cerevisiae* (35.8 U/mg) [46]. Overall, the enzyme does not exhibit strong differences in its hydrolytic activity as compared with the enzymes obtained from many other sources. Oligomycin seems to bind loosely to the algal enzyme, probably due to structural differences in its subunit *c* [44] that may affect the antibiotic binding site [47]. It is therefore necessary both to pre-incubate the enzyme in the presence of the inhibitor and to add an equal concentration of oligomycin in the assay medium. Incidentally, growth, respiration, and ATP levels in Chlorophycean algae were also barely affected by oligomycin concentrations that affect representatives of the other classes of Chlorophytes [25].

2.3. Three dimensional structure of the enzyme

The stable dimeric nature of the algal ATP synthase prompted a series of electron-microscopy studies. The *Polytomella* enzyme, obtained by digitonin solubilization of mitochondria and sucrose gradient centrifugation, was subjected to electron microscopy and single particle analysis. Projection maps with a resolution of about 17 Å showed a dimeric enzyme stabilized by interactions between the membrane-bound Fo sectors that formed an angle of 70° [37]. This implied that the enzyme could induce a strong local bending of the inner mitochondrial membrane [13]. Also, the peripheral stalks of the algal dimeric enzyme were noted to be much more robust than their counterparts in other F-type ATPases, including the ones from bovine [48], yeast [49], spinach chloroplasts [50], and *Escherichia coli* [51].

Polytomella sp. mitochondria were subjected to ultrathin sectioning, and cristae membranes were found to fold into lamellae and tubuli. The ATP synthase oligomers seem to make helical arrangements along these tubular membranes, confirming the role of complex V in determining the shape of the inner mitochondrial membrane [52]. This has been further substantiated by RNA interference silencing of the *Atp2* gene encoding subunit β of the *C. reinhardtii* ATP synthase: ATP synthesis was fully impaired, the enzyme failed to assemble, and the algal mitochondria were deprived of cristae [53].

Dual-axis cryo-electron tomography confirmed a supramolecular organization of dimeric ATP synthase in the cristae membranes of *Polytomella* sp. mitochondria that exhibited rows of dimers at 12 nm intervals [54]. In addition, averaged 3D subvolumes of the algal oligomeric enzyme were obtained at 5.7 nm resolution. These 3D tomography data were the first indicators that contacts existed between the peripheral stalks of the monomers [54] suggesting their very rigid architecture. An additional EM analysis of the *Polytomella* sp. mitochondrial ATP synthase complex supported the dimeric nature of the enzyme and presence of robust peripheral stalks [42].

More recently, an electron cryo-microscopy map at 6.2 Å resolution of the *Polytomella* sp. dimeric ATP synthase was obtained [45]. Fig. 2A shows the electron density map of the dimer and the principal domains that constitute the oligomeric complex. The model has several salient features: i) subunit *a* exhibits horizontally membrane-embedded α-helices that seem to embrace the *c*-ring and that form the two proton-translocating hemi-channels; the presence of these horizontal helices has been subsequently observed in the bacterial [55] and in the beef heart mitochondrial enzymes [56], ii) the robust peripheral stalks are constituted by several entwined α-helices that form a very solid scaffold as compared to the one from other enzymes (Fig. 2B); this is in accordance with the high propensity of several Asa subunits (Asa1, Asa2, Asa4 and Asa7) to form coiled-coils [57], iii) local resolution estimates indicated that the peripheral stalk is more ordered than the catalytic F_1 sector; furthermore, these peripheral stalks are united in their middle region by protein–protein contacts; the Asa subunit responsible for forming this extra-membranous bridge between the monomers is unknown, but could be either Asa4 as suggested previously [33] or Asa7 (see below), iv) the peripheral stalk, besides its substantial mass, seems to make several contacts with the F_1 sector; these contacts may be, among others, the interactions Asa2-α [57] and Asa1-OSCP [26], and v) the *c*-ring is formed by 10 monomers and seems to be SDS-resistant [26], as those observed in yeast [58], in Na^+-dependent ATP synthases of bacteria [59] and in the A_1Ao-ATP synthases of archaea [60].

3. Addressing the topology of the components of the peripheral arm of algal mitochondrial ATP synthase

The neighboring interactions of Asa subunits in the ATP synthase of the colorless chlorophycean alga *Polytomella* sp. have been addressed using a variety of experimental approaches: defining near-neighbor relationships of subunits after treating the whole enzyme with cross-linking agents; characterizing protein–protein interactions *in vitro* with recombinant subunits; and dissociating the enzyme into subcomplexes by heat or high detergent concentrations. Thus, models for the topological disposition of the Asa polypeptides in the peripheral arm of the enzyme have been successively refined [18,26,33,42,57].

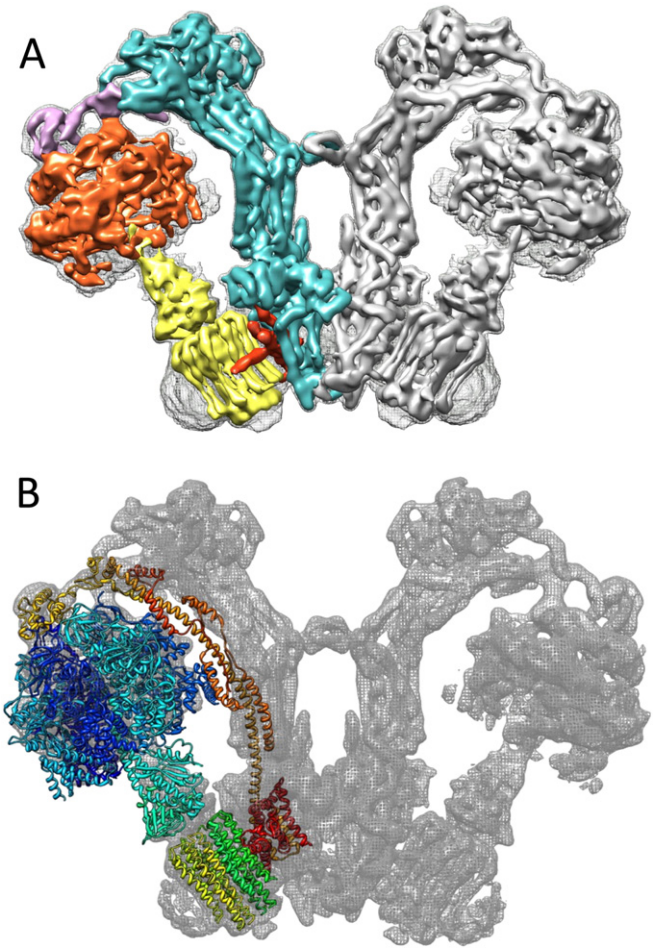

Fig. 2. Electron cryo-microscopy map of the algal *Polytomella* sp. ATP synthase. A) The model shown corresponds to EMDB accession number EMD-2852 [45]. The main domains of the complex were visualized and colored with the UCSF Chimera package [73]: rotor in yellow (subunits γ/δ/ε/*c*-ring), subunit *a* in red, the catalytic domain (α_3/β_3) in orange, OSCP in violet, and the peripheral stalk (Asa1 to 5 and Asa7) plus the membrane dimerization domain (Asa6, Asa8 and Asa9) in cyan. B) The model of the algal dimeric enzyme (EMD-2852 [45]) and the model of the bovine enzyme obtained by single particle electron cryomicroscopy (PDB Id: 5ARA) [74] were superimposed. The sturdiness of the peripheral stalk of the algal dimer as compared to the one of the bovine enzyme is evident.

3.1. Neighboring interactions between Asa subunits as revealed by cross-linking agents

To assess neighboring interactions between subunits in the algal ATP synthase subunits, cross-linking experiments with several water-soluble and water-insoluble homo-bifunctional and hetero-bifunctional reagents were carried out. Besides some expected cross-link products between the orthodox subunits (*i.e.*, α-β or α-OSCP), the cross-link products that were reproducibly obtained with the atypical subunits were (Asa1–Asa4), (Asa1–Asa7), (Asa2–Asa4), (Asa2–Asa7), (Asa3–Asa8), (Asa6–Asa6) and the triple cross-link product (Asa2–Asa4–Asa7) [42]. The inferred close vicinities between polypeptides were used to predict an overall topology of the algal ATP synthase.

3.2. Silencing and overexpression of subunits

The Asa7 subunit of the green algae *C. reinhardtii* was knocked-down using RNA interference. The absence of this polypeptide neither affected growth nor the OXPHOS of the alga [25]. Nevertheless, attempts to purify the ATP synthase from the Asa7-silenced mutant invariably failed, because lauryl maltoside solubilization dissociated the complex and released its F_1 sector. Subunit Asa7 is known to bind to at least three other subunits (Asa1, Asa2 and Asa4); it therefore must play a pivotal role in stabilizing the overall architecture of the peripheral stalk.

In order to gain more insights on how Asa proteins interact, recombinant subunits were over-expressed and purified and their interactions *in vitro* explored. It was shown that Asa2, Asa4 and Asa7 interact, and furthermore, that the interaction Asa4–Asa7 is mediated by the C-terminal halves of both proteins [57]. Asa2 can bind Asa7 and the C-terminal half of Asa4. An interaction Asa2-α was also observed, suggesting the proximity of Asa2 with the catalytic head of the enzyme. In addition, subunits Asa2, Asa4 and Asa7 formed a subcomplex with a 1:1:1 stoichiometry that could be reconstituted *in vitro*. This subcomplex was proposed to establish additional contacts with Asa1 and with OSCP.

Subunit Asa1 was shown to be a membrane-extrinsic subunit using sodium carbonate treatment on mitochondrial membranes. It was proposed to represent the bulky structure observed near the F_1 sector in EM studies, and therefore to interact with OSCP [33]. Indeed, subunit Asa1 seems to be one of the main components of the peripheral stalk of the algal enzyme, probably forming the main column that unites the extrinsic subunit OSCP with other components of the enzyme in close contact with the membrane (Asa3, Asa5, Asa8, *a* and c_{10}-ring). Thus, Asa1 may be the main support of the peripheral stalk and may have a scaffolding role similar to the one of subunit *b* in orthodox enzymes [26]. Sequence alignment analysis shows that OSCP subunits can be separated into two clearly distinct groups based on their amino acid sequences: one pertaining to the Chlorophycean algae (where OSCP binds an Asa1 subunit), and another that belongs to land plants and other green algae like Prasinophyceae, Ulvophyceae, and Trebouxiophyceae (where OSCP binds an orthodox *b* subunit) [26].

3.3. Dissociation of the enzyme into subcomplexes

Work carried out with the *Polytomella* ATP synthase established other subunit–subunit interactions, mainly through the identification of subcomplexes formed by heat dissociation [18,43]. Upon heat treatment, the ATPase is dissociated into its monomers and immediately afterwards it releases its F_1 sector and disassembles [18,33]. Subunits Asa2, Asa4 and Asa7 and OSCP seem to dissociate concomitantly with the liberation of the F_1 sector. In addition, a subcomplex that contained subunits Asa1/Asa3/Asa5/Asa8/*a*/*c* appeared transiently [18]. A stable Asa1/Asa3/Asa5/Asa8/*a*/c_{10} subcomplex could be obtained by treating the enzyme with relatively high lauryl maltoside concentrations [26]. Furthermore, heat denaturation or taurodeoxycholate treatment of the dimeric enzyme leads to a monomeric form with substoichiometric amounts of Asa6 and Asa9 subunits [43]; thus these two proteins seem to promote enzyme dimerization. In addition, the monomeric form of the complex is less active than the dimer, exhibits diminished oligomycin sensitivity, and is more labile to heat treatment, high hydrostatic pressures, and protease digestion [43].

Amphipols, the short amphipathic polymers that can substitute detergents, help the folding and stability of several integral membrane proteins [61]. To find whether Amphipol A8-35 would also help stabilize the algal ATP synthase, the purified enzyme was incubated with the polymer. As judged by BN–PAGE, in the presence of increasing concentrations of Amphipol A8-35 the dimeric enzyme (V_2) partially dissociated into free F_1 sector, comprising at least α, β, γ, and δ subunits, and a subcomplex named SC1 that is composed of Fo and the peripheral stalk (Fig. 3A). Another sample of the purified enzyme was incubated with 3.5% Amphipol A8-35 for 40 min (Fig. 3B, lane 1) and subjected to 2D-SDS–PAGE, where the polypeptides of subcomplex SC1 were resolved (Fig. 3C). Subunit OSCP was found to readily dissociate, migrating towards the front of the BN–PAGE gel. In parallel, a second sample of the purified enzyme was incubated with 3.5% Amphipol A8-35 for 24 h (Fig. 3B, lane 2) and then resolved in 2D-SDS–PAGE. In these conditions, a second subcomplex (SC2), with higher mobility in BN–PAGE than SC1,

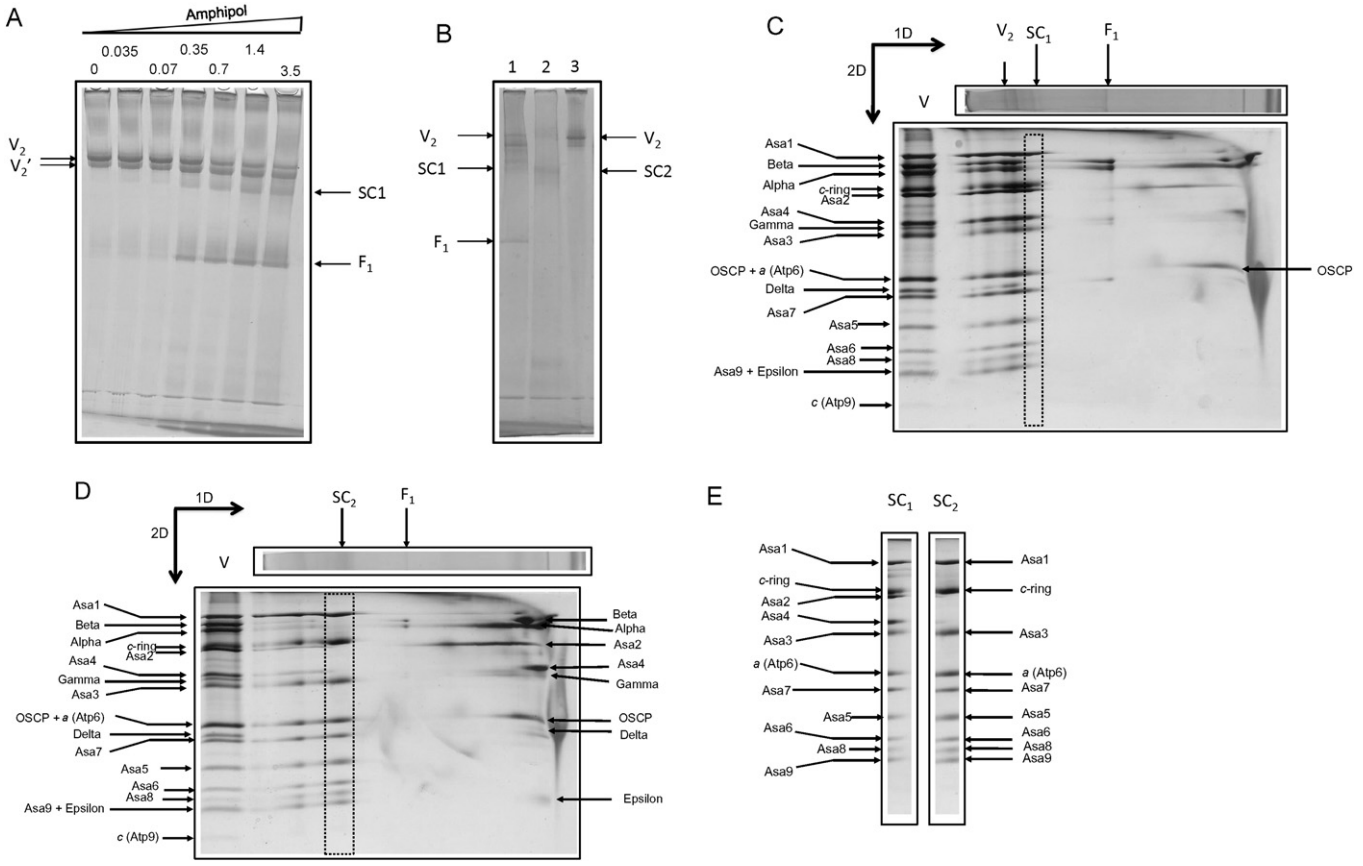

Fig. 3. Amphipol A8-35 dissociates the dimeric algal ATP synthase into discrete subcomplexes. A) BN–PAGE of purified ATP synthase samples [18] incubated for 40 min at 4 °C under mild agitation in the presence of Amphipol A8-35 (Anatrace) at the indicated increasing concentrations (% *w*/*v*). One hundred micrograms of protein was loaded in each lane. The control lane in the absence of the detergent is labeled 0. Dimer (V_2), F_1 sector (F_1), and subcomplex (SC1) are indicated. V_2' denotes an isoform of the algal ATP synthase with a different electrophoretic migration, whose subunit composition is identical to the one of V_2. B) BN–PAGE of purified ATP synthase samples (50 μg of protein in each lane) incubated with or without Amphipol A8-35. Lane 1: sample incubated in the presence of 3.5% Amphipol A8-35 for 40 min; lane 2: sample incubated in the presence of 3.5% Amphipol A8-35 for 24 h; lane 3: control ATP synthase without treatment. Dimer (V_2), F_1 sector (F_1), and subcomplexes SC1 and SC2 are indicated. C) Silver-stained 2D gel of an ATP synthase sample incubated for 40 min in the presence of 3.5% Amphipol A8-35. D) Silver-stained 2D gel of an ATP synthase sample incubated for 24 h in the presence of 3.5% Amphipol A8-35. E) Identity of the subunits that form the SC1 and SC2 subcomplexes. Gels were taken from the 2D polypeptide patterns shown in panels C and D.

was formed (Fig. 3D). The population of free F_1 was much smaller, and the dissociated subunits α, β, γ, δ, ε, Asa2, Asa4 and OSCP were found to migrate towards the front of the BN–PAGE polypeptide pattern. The subunit composition of the two Amphipol A8-35-generated subcomplexes SC1 and SC2 is shown in Fig. 3E. Their identities were assigned by their apparent molecular masses as Asa1 (66.1 kDa), *c*-ring (45.5 kDa), Asa2 (45.3 kDa), Asa3 (32.9 kDa), subunit *a* (25.1 kDa), Asa7 (19.0 kDa), Asa5 (13.9 kDa), Asa6 (13.1 kDa), Asa8 (9.9 kDa) and Asa9 (11.0 kDa). The apparent molecular masses of the SC1 and SC2 subcomplexes are of 681 and 528 kDa respectively, suggesting that these subcomplexes are dimeric. Upon Amphipol A8-35 treatment, the dimeric enzyme liberates OSCP and its F_1 sectors to

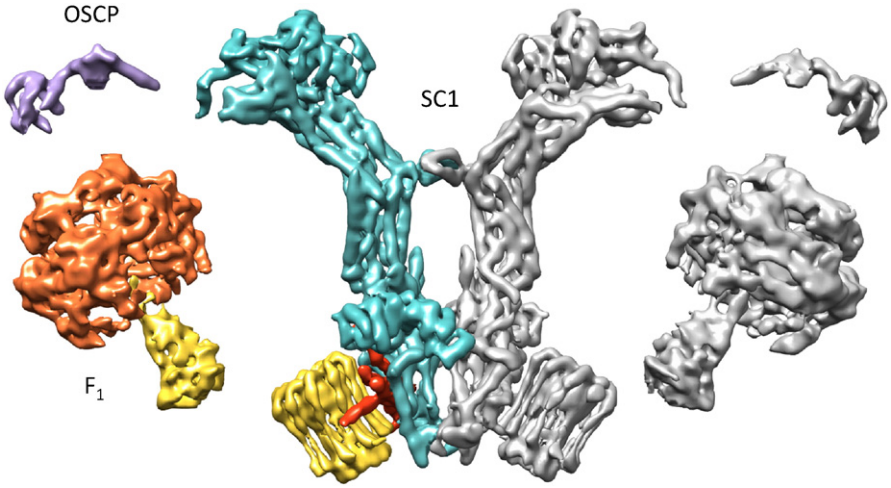

Fig. 4. Model showing the dissociation of the ATP synthase induced by Amphipol A8-35. The model illustrates the dissociation of the algal ATP synthase by Amphipol A8-35 (40 min incubation) to form the dimeric SC1 subcomplex after the dissociation of the F_1 sector and subunit OSCP.

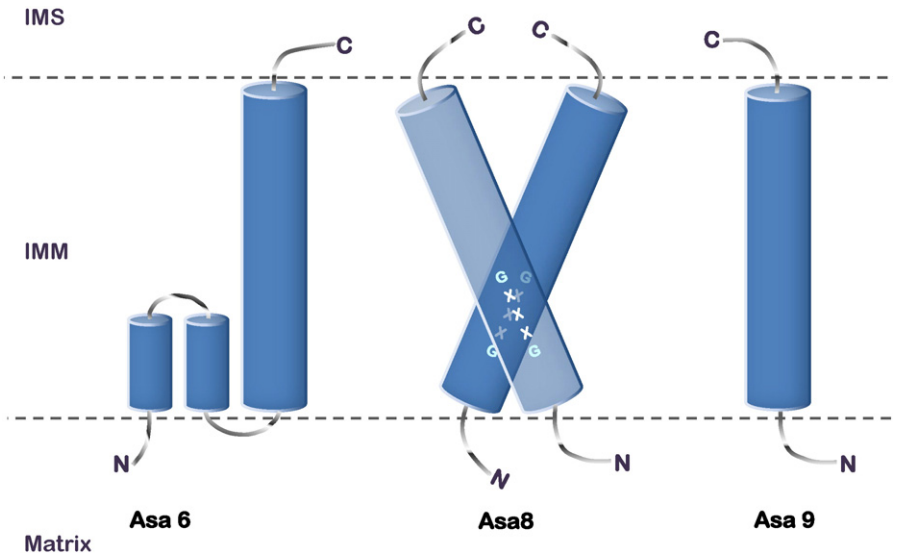

Fig. 5. Hydrophobicity-based models of the individual subunits involved in the membrane-embedded dimerization domain. Several algorithms predict the Asa8 and Asa9 subunits with a single TMS. The GxxxG motif in the Asa8 subunit could prompt its dimerization. The predicted models for Asa6 vary with the different programs used: one TMS, two TMS, or one TMS with a reentrant helix (depicted).

form the SC1 subcomplex (illustrated in Fig. 4), while longer polymer treatment additionally releases the Asa2 and Asa4 subunits and forms the SC2 subcomplex (not shown). Thus, it seems that Amphipol A8-35 does not destabilize the membrane-embedded subunits of complex V, but destabilizes other extrinsic components, mainly OSCP, Asa2 and Asa4. It is notable that subunit Asa7 remains bound to the dimeric SC2 subcomplex even after the dissociation of the Asa2 and Asa4 subunits, most probably attaching to Asa1. It is therefore tempting to speculate that Asa7 is the extrinsic protein bridge that unites the peripheral stalks of the algal model observed in the 3-D model of the *Polytomella* sp. ATP synthase [45].

3.4. The dimerization domain of the algal mitochondrial ATP synthase

Only small-molecular mass polypeptides of the algal ATP synthase seem to be embedded in the membrane: subunits Asa6, Asa8 and Asa9 are predicted to have transmembrane stretches (TMS), two, one and one, respectively [33].

The stoichiometry of all the Asa subunits in the algal ATP synthase has not been established yet. An estimated stoichiometry based on cysteine-labeling fluorescent probes revealed a 1:1:1 stoichiometry for subunits Asa3:Asa4:Asa5 per monomer [42], although this assessment was limited to those subunits that contain at least one cysteine residue.

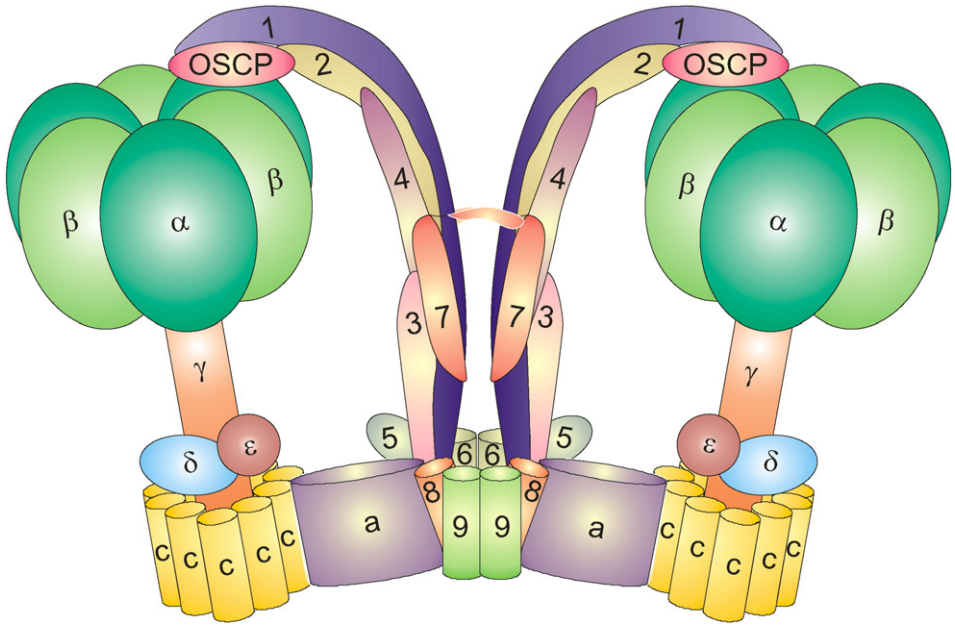

Fig. 6. Arrangement of subunits in the algal mitochondrial ATP synthase. The model is consistent with the data summarized in this article and illustrates the dimeric enzyme with a colored subunit composition. Letters denote the conserved ATP synthase subunits, while numbers refer to Asa subunits (Asa1-Asa9). Subunits Asa6, 8 and 9 form the dimerization module, while the rest of them are constituents of the peripheral stalks.

Cross-sections through the membrane domains of the electron cryomicroscopy map of the algal enzyme show the four horizontal-embedded helices of subunit *a*, the c_{10}-ring and six additional transmembrane helices per monomer [45]. These six TMS could be ascribed, in principle, to the fifth vertical α-helix of subunit *a* [56], the two reentrant helices and one TMS of subunit Asa6, one TMS of Asa8, and one TMS of Asa9 (Fig. 5). Asa8 may be instrumental for the dimerization of the enzyme, since it contains a GxxxG domain, which is a weak predictor of membrane protein dimerization [62]. The presence of GxxxG domains in subunits *e* and *g* is known to play an important role in dimerizing the yeast ATP synthase [63–65].

All the above mentioned data can be summarized in an updated model for the topological disposition of the 17 polypeptides that constitute the algal enzyme (Fig. 6).

4. Perspectives

A regulatory protein that may control the ATPase activity of the algal enzyme has not been characterized yet. Nevertheless, one of its subunits is expected to have a regulatory role similar to subunit IF_1 in mitochondrial enzymes [66], to the γ-proteobacterial ε subunit [67] or to the α-proteobacterial ζ subunit [68].

Many biochemical data have been obtained on the Asa subunits arrangement in the peripheral stalk, but to elaborate a more precise model of organization and to validate or invalidate the model in Fig. 6, high resolution structural data is needed. In the model available to date [45], it is still not possible to pin-point unambiguously the individual Asa subunits.

All the subunits of the chlorophycean mitochondrial ATP synthases are nucleus-encoded, since no gene encoding any complex V polypeptide has been found in the mitochondrial genomes of these algae [69,70]. It is of interest to learn how all the nucleus-encoded subunits, especially the Asa subunits, are imported into mitochondria and how they assemble to form the very large, 1600 kDa algal complex V.

Transparency document

The Transparency document associated with this article can be found, in online version.

Acknowledgments

This paper is dedicated to our Emeritus Professor Marietta Tuena-Sangri (IFC, UNAM), for always providing us unfading encouragement and support. Research in our group is being supported by the grant 245486 from the Consejo Nacional de Ciencia y Tecnología (CONACyT) and the Belgian Fonds de la Recherche Scientifique (F.R.S.–FNRS) (Mexico-Belgium). Additional support was received from grants 239219 and 239487 (CONACyT, Mexico), IN203311-3 from the Dirección General de Asuntos del Personal Académico (DGAPA–UNAM, Mexico) and from the Belgian F.R.S.–FNRS (MIS F.4520, FRFC 2.4597, CDR J.0032). CONACyT also supports the Ph.D. studies of L.C.-T. and L.S.-V. (fellowships 599282 and 290733 respectively, Programa de Doctorado en Ciencias Biomédicas, UNAM) and the Masters studies of F.V.D. (fellowship 660082, Programa de Maestría y Doctorado en Ciencias Bioquímicas, UNAM).

References

[1] M. Alfonzo, M.A. Kandrach, E. Racker, Isolation, characterization, and reconstitution of a solubilized fraction containing the hydrophobic sector of the mitochondrial proton pump, J. Bioenerg. Biomembr. 13 (1981) 375–391.
[2] G. Oster, H. Wang, Rotary protein motors, Trends Cell Biol. 13 (2003) 114–121.
[3] G. Arselin, J. Vaillier, B. Salin, J. Schaeffer, M.F. Giraud, A. Dautant, D. Brèthes, J. Velours, The modulation in subunits e and g amounts of yeast ATP synthase modifies mitochondrial cristae morphology, J. Biol. Chem. 279 (2004) 40392–40399.
[4] J.E. Walker, V.K. Dickson, The peripheral stalk of the mitochondrial ATP synthase, Biochim. Biophys. Acta 1757 (2006) 286–296.
[5] A. Wächter, Y. Bi, S.D. Dunn, B.D. Cain, H. Sielaff, F. Wintermann, S. Engelbrecht, W. Junge, Two rotary motors in F-ATP synthase are elastically coupled by a flexible rotor and a stiff stator stalk, Proc. Natl. Acad. Sci. U. S. A. 108 (2011) 3924–3929.
[6] R. Yasuda, H. Noji, K. Kinosita Jr., M. Yoshida, F1-ATPase is a highly efficient molecular motor that rotates with discrete 120 degree steps, Cell 93 (1998) 1117–1124.
[7] J.R. Gledhill, J.E. Walker, Inhibition sites in F1-ATPase from bovine heart mitochondria, Biochem. J. 386 (2005) 591–598.
[8] A.G. Stewart, L.K. Lee, M. Donohoe, J.J. Chaston, D. Stock, The dynamic stator stalk of rotary ATPases, Nat. Commun. 3 (2012) 687.
[9] V.K. Dickson, J.A. Silvester, I.M. Fearnley, A.G. Leslie, J.E. Walker, On the structure of the stator of the mitochondrial ATP synthase, EMBO J. 25 (2006) 2911–2918.
[10] H. Seelert, N.A. Dencher, ATP synthase superassemblies in animals and plants: two or more are better, Biochim. Biophys. Acta 1807 (2011) 1185–1197.
[11] D. Thomas, P. Bron, T. Weimann, A. Dautant, M.F. Giraud, P. Paumard, B. Salin, A. Cavalier, J. Velours, D. Brèthes, Supramolecular organization of the yeast F1Fo-ATP synthase, Biol. Cell. 100 (2008) 591–601.
[12] M. Strauss, G. Hofhaus, R.R. Schröder, W. Kühlbrandt, Dimer ribbons of ATP synthase shape the inner mitochondrial membrane, EMBO J. 27 (2008) 1154–1160.
[13] P. Paumard, J. Vaillier, B. Coulary, J. Schaeffer, V. Soubannier, D.M. Mueller, D. Brèthes, J.P. di Rago, J. Velours, The ATP synthase is involved in generating mitochondrial cristae morphology, EMBO J. 21 (2002) 221–230.
[14] I. Arnold, K. Pfeiffer, W. Neupert, R.A. Stuart, H. Schägger, Yeast mitochondrial F1F0-ATP synthase exists as a dimer: identification of three dimer-specific subunits, EMBO J. 17 (1998) 7170–7178.
[15] R. Fronzes, T. Weimann, J. Vaillier, J. Velours, D. Brèthes, The peripheral stalk participates in the yeast ATP synthase dimerization independently of e and g subunits, Biochemistry 45 (2006) 6715–6723.
[16] A. Zikova, A. Schnaufer, R.A. Dalley, A.K. Panigrahi, K.D. Stuart, The F(0)F(1)-ATP synthase complex contains novel subunits and is essential for procyclic *Trypanosoma brucei*, PLoS Pathog. 5 (2009) e1000436.
[17] E. Perez, M. Lapaille, H. Degand, L. Cilibrasi, A. Villavicencio-Queijeiro, P. Morsomme, D. González-Halphen, M.C. Field, C. Remacle, D. Baurain, P. Cardol, The mitochondrial respiratory chain of the secondary green alga *Euglena gracilis* shares many additional subunits with parasitic Trypanosomatidae, Mitochondrion 19 (Pt B) (2014) 338–349.
[18] M. Vázquez-Acevedo, P. Cardol, A. Cano-Estrada, M. Lapaille, C. Remacle, D. González-Halphen, The mitochondrial ATP synthase of chlorophycean algae contains eight subunits of unknown origin involved in the formation of an atypical stator-stalk and in the dimerization of the complex, J. Bioenerg. Biomembr. 38 (2006) 271–282.
[19] N.P. Balabaskaran, N.V. Dudkina, L.A. Kane, J.E. van Eyk, E.J. Boekema, M.W. Mather, A.B. Vaidya, Highly divergent mitochondrial ATP synthase complexes in *Tetrahymena thermophila*. PLoS Biol. 8 (2010) e1000418.
[20] S.J. Couoh-Cardel, S. Uribe-Carvajal, S. Wilkens, J.J. García-Trejo, Structure of dimeric F1F0-ATP synthase, J. Biol. Chem. 285 (2010) 36447–36455.
[21] M.D. Herron, J.D. Hackett, F.O. Aylward, R.E. Michod, Triassic origin and early radiation of multicellular volvocine algae, Proc. Natl. Acad. Sci. U. S. A. 106 (2009) 3254–3258.
[22] E. Rodríguez-Salinas, C. Remacle, D. González-Halphen, Green Algae Genomics: A Mitochondrial Perspective, in: L. Maréchal-Drouard (Ed.), Mitochondrial Genome Evolution, Advances in Botanical Research, Volume 63, Elsevier Inc., San Diego 2012, pp. 187–214.
[23] E. Rodríguez-Salinas, H. Riveros-Rosas, Z. Li, K. Fucíková, J.J. Brand, L.A. Lewis, D. González-Halphen, Lineage-specific fragmentation and nuclear relocation of the mitochondrial cox2 gene in chlorophycean green algae (Chlorophyta), Mol. Phylogenet. Evol. 64 (2012) 166–176.
[24] P. Cardol, D. González-Halphen, A. Reyes-Prieto, D. Baurain, R.F. Matagne, C. Remacle, The mitochondrial oxidative phosphorylation proteome of *Chlamydomonas reinhardtii* deduced from the Genome Sequencing Project, Plant Physiol. 137 (2005) 447–459.
[25] M. Lapaille, A. Escobar-Ramírez, H. Degand, D. Baurain, E. Rodríguez-Salinas, N. Coosemans, M. Boutry, D. Gonzalez-Halphen, C. Remacle, P. Cardol, Atypical subunit composition of the chlorophycean mitochondrial F1FO-ATP synthase and role of Asa7 protein in stability and oligomycin resistance of the enzyme, Mol. Biol. Evol. 27 (2010) 1630–1644.
[26] L. Colina-Tenorio, H. Miranda-Astudillo, A. Cano-Estrada, M. Vázquez-Acevedo, P. Cardol, C. Remacle, D. González-Halphen, Subunit Asa1 spans all the peripheral stalk of the mitochondrial ATP synthase of the chlorophycean alga *Polytomella* sp, Biochim. Biophys. Acta (2015 Nov 30), http://dx.doi.org/10.1016/j.bbabio.2015.11.012 [pii: S0005-2728(15)00244-3, Epub ahead of print].
[27] A. Atteia, C. de Vitry, Y. Pierre, J.L. Popot, Identification of mitochondrial proteins in membrane preparations from *Chlamydomonas reinhardtii*, J. Biol. Chem. 267 (1992) 226–234.
[28] A. Atteia, Identification of mitochondrial respiratory proteins from the green alga *Chlamydomonas reinhardtii*, C. R. Acad. Sci. III. 317 (1994) 11–19.
[29] L.G. Franzén, G. Falk, Nucleotide sequence of cDNA clones encoding the beta subunit of mitochondrial ATP synthase from the green alga *Chlamydomonas reinhardtii*: the precursor protein encoded by the cDNA contains both an N-terminal presequence and a C-terminal extension, Plant Mol. Biol. 19 (1992) 771–780.
[30] G. Nurani, L.-G. Franzén, Isolation and characterization of the mitochondrial ATP synthase from *Chlamydomonas reinhardtii*. cDNA sequence and deduced protein sequence of the alpha subunit, Plant Mol. Biol. 31 (1996) 1105–1116.
[31] E.B. Gutiérrez-Cirlos, A. Antaramian, M. Vázquez-Acevedo, R. Coria, D. González-Halphen, A highly active ubiquinol-cytochrome c reductase (bc1 complex) from the

colorless alga *Polytomella* spp., a close relative of *Chlamydomonas*. Characterization of the heme binding site of cytochrome c_1, J. Biol. Chem. 269 (1994) 9147–9154.
[32] A. Atteia, G. Dreyfus, D. González-Halphen, Characterization of the alpha and beta-subunits of the F0F1-ATPase from the alga *Polytomella* spp., a colorless relative of *Chlamydomonas reinhardtii*, Biochim. Biophys. Acta 1320 (1997) 275–284.
[33] R. van Lis, G. Mendoza-Hernández, G. Groth, A. Atteia, New insights into the unique structure of the F0F1-ATP synthase from the chlamydomonad algae *Polytomella* sp. and *Chlamydomonas reinhardtii*, Plant Physiol. 144 (2007) 1190–1199.
[34] H. Schägger, Native Gel Electrophoresis, in: G. von Jagow, H. Schägger (Eds.), A Practical Guide to Membrane Protein Purification, Academic Press, San Diego 1994, pp. 81–104.
[35] S. Funes, E. Davidson, M.G. Claros, R. van Lis, X. Pérez-Martínez, M. Vázquez-Acevedo, M.P. King, D. González-Halphen, The typically mitochondrial DNA-encoded ATP6 subunit of the F1F0-ATPase is encoded by a nuclear gene in, *Chlamydomonas reinhardtii*, J. Biol. Chem. 277 (2002) 6051–6058.
[36] R. van Lis, A. Atteia, G. Mendoza-Hernández, D. González-Halphen, Identification of novel mitochondrial protein components of *Chlamydomonas reinhardtii*. A proteomic approach, Plant Physiol. 132 (2003) 318–330.
[37] N.V. Dudkina, J. Heinemeyer, W. Keegstra, E.J. Boekema, H.P. Braun, Structure of dimeric ATP synthase from mitochondria: an angular association of monomers induces the strong curvature of the inner membrane, FEBS Lett. 579 (2005) 5769–5772.
[38] L. Jänsch, V. Kruft, U.K. Schmitz, H.P. Braun, New insights into the composition, molecular mass and stoichiometry of the protein complexes of plant mitochondria, Plant J. 9 (1996) 357–368.
[39] S. Guerrero-Castillo, M. Vázquez-Acevedo, D. González-Halphen, S. Uribe-Carvajal, In *Yarrowia lipolytica* mitochondria, the alternative NADH dehydrogenase interacts specifically with the cytochrome complexes of the classic respiratory pathway, Biochim. Biophys. Acta 1787 (2009) 75–85.
[40] S.S. Merchant, S.E. Prochnik, O. Vallon, E.H. Harris, S.J. Karpowicz, G.B. Witman, A. Terry, A. Salamov, L.K. Fritz-Laylin, L. Maréchal-Drouard, W.F. Marshall, L.H. Qu, D.R. Nelson, A.A. Sanderfoot, M.H. Spalding, V.V. Kapitonov, Q. Ren, P. Ferris, E. Lindquist, H. Shapiro, S.M. Lucas, J. Grimwood, J. Schmutz, P. Cardol, H. Cerutti, G. Chanfreau, C.L. Chen, V. Cognat, M.T. Croft, R. Dent, S. Dutcher, E. Fernández, H. Fukuzawa, D. González-Ballester, D. González-Halphen, A. Hallmann, M. Hanikenne, M. Hippler, W. Inwood, K. Jabbari, M. Kalanon, R. Kuras, P.A. Lefebvre, S.D. Lemaire, A.V. Lobanov, M. Lohr, A. Manuell, I. Meier, L. Mets, M. Mittag, T. Mittelmeier, J.V. Moroney, J. Moseley, C. Napoli, A.M. Nedelcu, K. Niyogi, S.V. Novoselov, I.T. Paulsen, G. Pazour, S. Purton, J.P. Ral, D.M. Riaño-Pachón, W. Riekhof, L. Rymarquis, M. Schroda, D. Stern, J. Umen, R. Willows, N. Wilson, S.L. Zimmer, J. Allmer, J. Balk, K. Bisova, C.J. Chen, M. Elias, K. Gendler, C. Hauser, M.R. Lamb, H. Ledford, J.C. Long, J. Minagawa, M.D. Page, J. Pan, W. Pootakham, S. Roje, A. Rose, E. Stahlberg, A.M. Terauchi, P. Yang, S. Ball, C. Bowler, C.L. Dieckmann, V.N. Gladyshev, P. Green, R. Jorgensen, S. Mayfield, B. Mueller-Roeber, S. Rajamani, R.T. Sayre, P. Brokstein, I. Dubchak, D. Goodstein, L. Hornick, Y.W. Huang, J. Jhaveri, Y. Luo, D. Martínez, W.C. Ngau, B. Otillar, A. Poliakov, A. Porter, L. Szajkowski, G. Werner, K. Zhou, I.V. Grigoriev, D.S.Rokhsar, A.R. Grossman, The *Chlamydomonas* genome reveals the evolution of key animal and plant functions, Science 318 (2007) 245–250.
[41] P. Cardol, F. Figueroa, C. Remacle, L.-G. Franzén, D. González-Halphen, Oxidative phosphorylation: building blocks and related components, in: David B. Stern (Ed.) The Chlamydomonas Sourcebook, Organellar and Metabolic Processes, Volume 2, Elsevier Inc., San Diego 2009, pp. 469–502.
[42] A. Cano-Estrada, M. Vázquez-Acevedo, A. Villavicencio-Queijeiro, F. Figueroa-Martínez, H. Miranda-Astudillo, Y. Cordeiro, J.A. Mignaco, D. Foguel, P. Cardol, M. Lapaille, C. Remacle, S. Wilkens, D. González-Halphen, Subunit–subunit interactions and overall topology of the dimeric mitochondrial ATP synthase of *Polytomella* sp, Biochim. Biophys. Acta 1797 (2010) 1439–1448.
[43] A. Villavicencio-Queijeiro, M. Vázquez-Acevedo, A. Cano-Estrada, M. Zarco-Zavala, M. Tuena de Gómez, J.A. Mignaco, M.M. Freire, H.M. Scofano, D. Foguel, P. Cardol, C. Remacle, D. González-Halphen, The fully-active and structurally-stable form of the mitochondrial ATP synthase of *Polytomella* sp. is dimeric. J. Bioenerg. Biomembr. 41 (2009) 1–13.
[44] A. Villavicencio-Queijeiro, J.P. Pardo, D. González-Halphen, Kinetic and hysteretic behavior of ATP hydrolysis of the highly stable dimeric ATP synthase of *Polytomella* sp, Arch. Biochem. Biophys. 575 (2015) 30–37.
[45] M. Allegretti, N. Klusch, D.J. Mills, J. Vonck, W. Kühlbrandt, K.M. Davies, Horizontal membrane-intrinsic α-helices in the stator a-subunit of an F-type ATP synthase, Nature 521 (2015) 237–240.
[46] S. Liu, T.J. Charlesworth, J.V. Bason, M.G. Montgomery, M.E. Harbour, I.M. Fearnley, J.E. Walker, The purification and characterization of ATP synthase complexes from the mitochondria of four fungal species, Biochem. J. 468 (2015) 167–175.
[47] J. Symersky, D. Osowski, D.E. Walters, D.M. Mueller, Oligomycin frames a common drug-binding site in the ATP synthase, Proc. Natl. Acad. Sci. U. S. A. 109 (2012) 13961–13965.
[48] L.A. Baker, I.N. Watt, M.J. Runswick, J.E. Walker, J.L. Rubinstein, Arrangement of subunits in intact mammalian mitochondrial ATP synthase determined by cryo-EM, Proc. Natl. Acad. Sci. U. S. A. 109 (2012) 11675–11680.
[49] W.C. Lau, L.A. Baker, J.L. Rubinstein, Cryo-EM structure of the yeast ATP synthase, J. Mol. Biol. 382 (2008) 1256–1264.
[50] C. Mellwig, B. Böttcher, A unique resting position of the ATP-synthase from chloroplasts, J. Biol. Chem. 278 (2003) 18544–18549.
[51] I. Ogilvie, S. Wilkens, A.J. Rodgers, R. Aggeler, R.A. Capaldi, The second stalk: the delta-b subunit connection in ECF1F0, Acta Physiol. Scand. Suppl. 643 (1988) 169–175.
[52] N.V. Dudkina, S. Sunderhaus, H.P. Braun, E.J. Boekema, Characterization of dimeric ATP synthase and cristae membrane ultrastructure from *Saccharomyces* and *Polytomella* mitochondria, FEBS Lett. 580 (2006) 3427–3432.
[53] M. Lapaille, M. Thiry, E. Perez, D. González-Halphen, C. Remacle, P. Cardol, Loss of mitochondrial ATP synthase subunit beta (Atp2) alters mitochondrial and chloroplastic function and morphology in Chlamydomonas, Biochim. Biophys. Acta 1797 (2010) 1533–1539.
[54] N.V. Dudkina, G.T. Oostergetel, D. Lewejohann, H.P. Braun, E.J. Boekema, Row-like organization of ATP synthase in intact mitochondria determined by cryo-electron tomography, Biochim. Biophys. Acta 1797 (2010) 272–277.
[55] E. Morales-Rios, M.G. Montgomery, A.G. Leslie, J.E. Walker, Structure of ATP synthase from *Paracoccus denitrificans* determined by X-ray crystallography at 4.0 Å resolution, Proc. Natl. Acad. Sci. U. S. A. 112 (2015) 13231–13236.
[56] A. Zhou, A. Rohou, D.G. Schep, J.V. Bason, M.G. Montgomery, J.E. Walker, N. Grigorieff, J.L. Rubinstein, Structure and conformational states of the bovine mitochondrial ATP synthase by cryo-EM, Elife (2015), http://dx.doi.org/10.7554/eLife.10180.
[57] H. Miranda-Astudillo, A. Cano-Estrada, M. Vázquez-Acevedo, L. Colina-Tenorio, L,.A. Downie-Velasco, P. Cardol, C. Remacle, L. Domínguez-Ramírez, D. González-Halphen, Interactions of subunits Asa2, Asa4 and Asa7 in the peripheral stalk of the mitochondrial ATP synthase of the chlorophycean alga *Polytomella* sp, Biochim. Biophys. Acta 1837 (2014) 1–13.
[58] J. Velours, G. Arselin, The *Saccharomyces cerevisiae* ATP synthase, J. Bioenerg. Biomembr. 32 (2000) 383–390.
[59] M. Fritz, V. Müller, An intermediate step in the evolution of ATPases–the F1F0-ATPase from *Acetobacterium woodii* contains F-type and V-type rotor subunits and is capable of ATP synthesis, FEBS J. 274 (2007) 3421–3428.
[60] F. Mayer, J.K. Lim, J.D. Langer, S.G. Kang, V. Müller, Na + transport by the A1AO-ATP synthase purified from *Thermococcus onnurineus* and reconstituted into liposomes, J. Biol. Chem. 290 (2015) 6994–7002.
[61] J.L. Popot, Amphipols, nanodiscs, and fluorinated surfactants: three nonconventional approaches to studying membrane proteins in aqueous solutions, Annu. Rev. Biochem. 79 (2010) 737–775.
[62] M.G. Teese, D. Langosch, Role of GxxxG motifs in transmembrane domain interactions, Biochemistry 54 (2015) 5125–5135.
[63] G. Arselin, M.F. Giraud, A. Dautant, J. Vaillier, D. Brèthes, B. Coulary-Salin, J. Schaeffer, J. Velours, The GxxxG motif of the transmembrane domain of subunit e is involved in the dimerization/oligomerization of the yeast ATP synthase complex in the mitochondrial membrane, Eur. J. Biochem. 270 (2003) 1875–1884.
[64] D.M. Bustos, J. Velours, The modification of the conserved GXXXG motif of the membrane-spanning segment of subunit g destabilizes the supramolecular species of yeast ATP synthase, J. Biol. Chem. 280 (2005) 29004–29010.
[65] S. Saddar, R.A. Stuart, The yeast F(1)F(0)-ATP synthase: analysis of the molecular organization of subunit g and the importance of a conserved GXXXG motif, J. Biol. Chem. 280 (2005) 24435–24442.
[66] M.J. Van Raaij, G.L. Orriss, M.G. Montgomery, M.J. Runswick, I.M. Fearnley, J.M. Skehel, J.E. Walker, The ATPase inhibitor protein from bovine heart mitochondria: the minimal inhibitory sequence, Biochemistry 35 (1996) 15618–15625.
[67] R. Iino, R. Hasegawa, K.V. Tabata, H. Noji, Mechanism of inhibition by C-terminal alpha-helices of the epsilon subunit of *Escherichia coli* FoF1-ATP synthase, J. Biol. Chem. 284 (2009) 17457–17464.
[68] M. Zarco-Zavala, E. Morales-Ríos, G. Mendoza-Hernández, L. Ramírez-Silva, G. Pérez-Hernández, J.J. García-Trejo, The ζ subunit of the F1FO-ATP synthase of α-proteobacteria controls rotation of the nanomotor with a different structure, FASEB J. 28 (2014) 2146–2157.
[69] C. Vahrenholz, G. Riemen, E. Pratje, B. Dujon, G. Michaelis, Mitochondrial DNA of *Chlamydomonas reinhardtii*: the structure of the ends of the linear 15.8-kb genome suggests mechanisms for DNA replication, Curr. Genet. 24 (1993) 241–247.
[70] D.R. Smith, J. Hua, R.W. Lee, Evolution of linear mitochondrial DNA in three known lineages of *Polytomella*, Curr. Genet. 56 (2010) 427–438.
[71] J. Yang, R. Yan, A. Roy, D. Xu, J. Poisson, Y. Zhang, The I-TASSER suite: protein structure and function prediction, Nat. Methods 12 (2015) 7–8.
[72] D.M. Rees, A.G.W. Leslie, J.E. Walker, The structure of the membrane extrinsic region of bovine ATP Synthase, Proc. Natl. Acad. Sci. U. S. A. 106 (2009) 21597–21601.
[73] E.F. Pettersen, T.D. Goddard, C.C. Huang, G.S. Couch, D.M. Greenblatt, E.C. Meng, T.E. Ferrin, UCSF chimera–a visualization system for exploratory research and analysis, J. Comput. Chem. 25 (2004) 1605–1612.
[74] A. Zhou, A. Rohou, D.G. Schep, J.V. Bason, M.G. Montgomery, J.E. Walker, N. Grigorieff, J.L. Rubinstein, Structure and conformational states of the bovine mitochondrial ATP synthase by cryo-EM, Elife 4 (2015), http://dx.doi.org/10.7554/eLife.10180 (pii: e10180).

Biochimica et Biophysica Acta 1858 (2017) 267–275

Contents lists available at ScienceDirect

Biochimica et Biophysica Acta

journal homepage: www.elsevier.com/locate/bbabio

Atypical composition and structure of the mitochondrial dimeric ATP synthase from *Euglena gracilis*

K.N. Sathish Yadav [a,1], Héctor V. Miranda-Astudillo [b,1], Lilia Colina-Tenorio [c], Fabrice Bouillenne [d], Hervé Degand [e], Pierre Morsomme [e], Diego González-Halphen [c], Egbert J. Boekema [a,*], Pierre Cardol [b,**]

[a] Department of Electron Microscopy, Groningen Biological Sciences and Biotechnology Institute, University of Groningen, Groningen, The Netherlands
[b] Genetics and Physiology of Microalgae, InBioS/Phytosystems, University of Liège, Belgium
[c] Departamento de Genética Molecular, Instituto de Fisiología Celular, Universidad Nacional Autónoma de México, Mexico
[d] InBioS/Centre for Protein Engineering, University of Liège, Belgium
[e] Institut des Sciences de la Vie, Université Catholique de Louvain, Louvain-la-Neuve, Belgium

ARTICLE INFO

Article history:
Received 10 October 2016
Received in revised form 22 December 2016
Accepted 10 January 2017
Available online 12 January 2017

Keywords:
Euglenozoa
Trypanosomatidae
Dimeric mitochondrial complex V
F_1F_O ATP synthase
Electron microscopy
ATP synthasome

ABSTRACT

Mitochondrial respiratory-chain complexes from Euglenozoa comprise classical subunits described in other eukaryotes (*i.e.* mammals and fungi) and subunits that are restricted to Euglenozoa (*e.g. Euglena gracilis* and *Trypanosoma brucei*). Here we studied the mitochondrial F_1F_O-ATP synthase (or Complex V) from the photosynthetic eukaryote *E. gracilis* in detail. The enzyme was purified by a two-step chromatographic procedure and its subunit composition was resolved by a three-dimensional gel electrophoresis (BN/SDS/SDS). Twenty-two different subunits were identified by mass-spectrometry analyses among which the canonical α, β, γ, δ, ε, and OSCP subunits, and at least seven subunits previously found in *Trypanosoma*. The ADP/ATP carrier was also associated to the ATP synthase into a dimeric ATP synthasome. Single-particle analysis by transmission electron microscopy of the dimeric ATP synthase indicated that the structures of both the catalytic and central rotor parts are conserved while other structural features are original. These new features include a large membrane-spanning region joining the monomers, an external peripheral stalk and a structure that goes through the membrane and reaches the inter membrane space below the *c*-ring, the latter having not been reported for any mitochondrial F-ATPase.

1. Introduction

Within living cells, adenosine-5′-triphosphate (ATP) is mainly produced by membrane-embedded F_1F_O-, C_1C_O-, and A_1A_O-ATP synthases. These complexes found in bacteria, mitochondria and chloroplasts work like rotary motors. The activity of photosynthetic and respiratory complexes generates a proton gradient (proton motive force or pmf) across specialized membranes (bacterial plasma membrane, inner mitochondrial membrane, thylakoid membrane). The back flow of protons through the ATP synthase F_O membrane sector (a/c-ring) promotes the rotation of the central stalk (γ/δ/ε; bovine nomenclature) in the F_1 sector, and the interactions of the γ subunit with the catalytic core (α_3/β_3) induce conformational changes to synthesize and release ATP [1,8,42,52]. In well described enzymes (*e.g.* ATPase from mammals and yeasts), additional polypeptides constitute (i) a peripheral stator-stalk (OSCP/b/d/F6) that link F_O and F_1 parts and prevent the rotation of F_1 sector [33], and (ii) a dimerization module (A6L/e/f/g) that link the two monomers into large dimeric supercomplexes and rows of supercomplexes [25,30]. Complex V oligomerization is proposed to be responsible of the curvature of the inner membrane to form the mitochondrial cristae [54].

Given that rotary ATPases share a common ancestor [14,40], it was expected of the F-type ATP synthase complexes to be highly conserved. In this respect, very similar overall structures of ATP synthase monomers or dimers have been described in non-related organisms like the prokaryotic model organism *Paracoccus denitrificans* [38], the yeast *Y. lipolytica* [31], and mammalian species such as *Bos taurus* [64]. Chlorophycean algae, including the green algal model *Chlamydomonas reinhardtii* and its colorless relative *Polytomella* sp., were the first organisms in which an atypical ATP synthase subunit composition and structure were described [24,59]. The classical stator made mainly of b subunit(s) in bacteria, yeasts, and mammals is absent and a more robust stator structure, composed of at least 4 subunits, connects the two monomers by some large hydrophobic and hydrophilic subunits [2,12]. Similarly, the dimeric ATP synthase complex from the ciliate *Tetrahymena thermophila* also includes atypical subunits, unrelated to those

* Corresponding author.
** Correspondence to: P. Cardol, Chemin de la vallée, 4, B22, Institut de Botanique, Dept of Life Sciences, University of Liège, 4000 Liège, Belgium.
E-mail addresses: e.j.boekema@rug.nl (E.J. Boekema), Pierre.cardol@ulg.ac.be (P. Cardol).
[1] The authors contributed equally to the work.

http://dx.doi.org/10.1016/j.bbabio.2017.01.007
0005-2728/

described in *Polytomella* sp., that shape novel domains flanking the c subunit ring, and an unusually large domain in the intermembrane space [3]. In sharp contrast, the yeast dimer-specific subunits are smaller and do not contribute much to the water-soluble moiety of the dimeric supercomplex [31,58]. Given the large structural differences among the peripheral stator and dimerization modules of mitochondrial F_1F_O, it is of relevance to study a wider number of species to gain insight into the structural diversity of ATP synthases. In this respect, it was recently shown that mitochondrial ATP synthase from parasite species (*e.g. Trypanosoma brucei*) and photosynthetic species (*e.g. Euglena gracilis*) belonging to the lineage of Euglenozoa (phylum of Excavates) share a similar subunit composition [46,65], including a set of subunits that are specific to Euglenozoa. In this study, we thus further analyzed the subunit composition of purified mitochondrial ATP synthase from the photosynthetic Euglenozoa *Euglena gracilis* and characterized its dimeric structure by single particle electron microscopy.

2. Methods

2.1. Isolation of mitochondria from Euglena gracilis

Euglena gracilis (SAG 1224-5/25) was obtained from the University of Göttingen (Sammlung von Algenkulturen, Germany) and was grown at 25 °C in the dark with orbital agitation in liquid mineral Tris-minimum-phosphate medium (TMP) at pH 7.0 supplemented with a mix of vitamins (Biotin 10^{-7}% (w/v), B_{12} vitamin 10^{-7}% and B_1 vitamin 2×10^{-5}%) and with 1% ethanol as carbon source. The cells were harvested at the middle of the logarithmic phase by centrifugation (7000 ×*g*/10 min) and stored at −70 °C until used.

Mitochondria were obtained following the described procedure [39] with slight modifications. All steps were performed at 4 °C. The cells were thawed and suspended to a final concentration of 2×10^8 cells/mL in SHE buffer (sucrose 250 mM, Hepes 10 mM, EDTA 1 mM, pH 7.3) supplemented with 0.4% of bovine serum albumin (BSA). The cell suspension was sonicated in ice with a microprobe of 3 mm tip diameter for 20 s two times, with a 20 s resting period, at 40% of maximal output in a Vibracell Sonifier (Sonics & Material, Connecticut, USA). The sonicated sample was diluted 3 times in SHE buffer and centrifuged 600 ×*g*, 10 min. The supernatant was centrifuged at 8500 ×*g*, 10 min to recover the mitochondrial fraction. Mitochondria were suspended in 5 mL of sucrose buffer (0.3 M sucrose, 4 mM EDTA, and 20 mMTris, pH 7.2) and stored at −70 °C until used. Protein concentration was determined as previously described [9].

2.2. Purification of mitochondrial ATP synthase complex

All steps were performed at 4 °C. Seventy five milligrams of mitochondrial proteins were solubilized with n-dodecyl-β-D-maltoside (DDM, 4 g detergent per g protein) in A buffer containing Tris 50 mM, amino caproic acid 50 mM, $MgSO_4$ 1 mM, NaCl 50 mM, glycerol 10%, phenylmethylsulfonyl fluoride (PMSF) 1 mM, tosyl-lysyl-chloromethylketone (TLCK) 50 μg/mL. The mixture was incubated with gentle stirring for 30 min, and centrifuged at 38,000 ×*g* for 30 min. The supernatant was diluted three times in A buffer without NaCl and supplemented with DDM 0.01%. After a filtration step (0.22 μm) the sample was loaded on an anion exchange column (Mono Q HR 5/5, 1 mL) connected to an ÄKTA explorer 100 (GE Healthcare Life Sciences) equilibrated with the same buffer and washed until a base line was obtained. The column was washed with 50 mM NaCl in the A buffer plus DDM 0.01% (10 VC) and eluted with a 50–500 mM NaCl linear gradient (40 VC). Two milliliter fractions were collected and visualized by BN-PAGE.

The fractions from the anion exchange column enriched with ATP synthase were pooled and concentrated with an Amicon Ultra-15 Centrifugal Filter (EMD Millipore) to a final volume of 500 μL and injected to a Superose 6 10/300 (GE Healthcare Life Sciences) previously equilibrated with A buffer containing NaCl 200 mM and DDM 0.01%. The elution was carried out at 0.3 mL/min, 0.5 mL fractions were collected and visualized by BN-PAGE. The samples enriched with mitochondrial ATP synthase were pooled and stored at −70 °C until used.

2.3. Non-denaturating and denaturating protein electrophoresis

All steps were performed at 4 °C. Mitochondrial respiratory complexes were resolved in a 1D BN-PAGE using a 3%–10% acrylamide gradient gel. *In-gel* ATPase activity was carried out as in [62] with the addition of 30 mMtaurodeoxycholate (TDOC) as in [55]. *In-gel* NADH/NBT oxido-reductase activity was performed as described previously [29]. Two-dimensional SDS/SDS PAGE experiments were conducted as described [12]. Briefly, the subunits of ATPase from the BN-PAGE were separated in a Glycine-SDS-PAGE (12% acrylamide) and then the 2D lane was excised and separated again into a Tricine-SDS-PAGE (14% acrylamide), after the migration, the 3D gel was stained with Coomassie Brilliant Blue. An aliquot of the sample used for the microscopy analysis was also subjected to the same 3D BN/SDS-glycine/SDS-tricine PAGE to search for degradation or loss of subunits after the freezing and thawing steps.

Stained proteins associated with spots were manually excised and analyzed by mass spectrometry (MS) as described [46]. For direct protein identification with MASCOT, protein scores >60 were considered as significant ($P < 0.05$). To determine the molecular mass of individual subunits, the purified ATPase complex was resolved in a Tricine-SDS-PAGE and PageRuler plus prestained protein ladder (Thermo Scientific) was used as a size molecular marker. The logarithm of the distance migrated from each peptide was interpolated into a Log(distance migrated) *versus* size (kDa) regression of the molecular marker ($R^2 = 0.989$).

2.4. In silico analysis of ATPase subunits

To further characterize the sequences identified by MS, each protein sequence was submitted to a tBLASTn analysis against the expressed sequence tags (EST) database from *Euglena gracilis* (taxid: 3039) available in the NCBI server. The obtained translated nucleotide sequences were manually assembled to generate the longest possible polypeptide. The resulting polypeptides were submitted to similarity searches by BLASTp against the non-redundant protein sequences database (NRPS) (http://blast.ncbi.nlm.nih.gov/Blast.cgi), and against the Kinetoplastid genomic resource database (TriTrypDB) (http://www.tritrypdb.org/tritrypdb/). The first methionine codon of each sequence was arbitrarily chosen as the putative start codon, except when alignments with homologs from other organisms allowed us to choose another codon. The theoretical isoelectric point, molecular mass and grand average of hydropathicity (GRAVY) were determined using the algorithm ProtParam (http://web.expasy.org/protparam/), transmembrane helixes (TMH) were predicted using Phobius server (http://phobius.sbc.su.se/) and TMHMM Server v. 2.0 (http://www.cbs.dtu.dk/services/TMHMM-2.0/), local conserved domains (CD) were searched using the NRPS Blastp, DELTA-Blast and Conserved Domain Blast (http://www.ncbi.nlm.nih.gov/Structure/cdd/wrpsb.cgi), Coiled coil regions (CC) where predicted using the Marcoil 1.0 server (http://bcf.isb-sib.ch/webmarcoil/webmarcoilC1.html) when a TMH, CD or CC was found the topological localization inside the peptide was annotated. ClustalW version 2 (http://www.ebi.ac.uk/Tools/msa/clustalw2/) was used for direct alignments of protein sequences. The N-terminus and C-terminus parts of the alpha subunit were modelled using as template the crystal structure of the F_1-ATPase from the thermoalkaliphilic bacterium *Bacillus sp*. ta2.a1 [53] using Swiss-Model in the ExPASy web server (https://swissmodel.expasy.org/) and visualized using Chimera 1.6.2. (http://www.cgl.ucsf.edu/chimera).

2.5. Electron microscopy and analysis

A drop of ATP synthase solution was absorbed onto glow discharged carbon coated grids and subsequently stained with 2% uranyl acetate for contrast. Imaging was performed on a Philips CM120 equipped with a LaB6 tip operating at 120 kV. The "GRACE" system for semi-automated specimen selection and data acquisition [44] was used to record 2048 × 2048 pixel images at 80,000 × magnifications using a Gatan 4000 SP 4 K slow-scan CCD camera with a pixel size of 0.224 nm. Single particles were analyzed with the Groningen Image Processing (GRIP) software (including multi-reference and non-reference alignments, multivariate statistical analysis and classification, as in [7] and RELION software [49].

3. Results

3.1. Purification of the DDM stable ATP synthase from E. gracilis mitochondria

In agreement with previous work [46], mitochondrial ATP synthase (complex V) from *E. gracilis* migrates as a ~2.2 MDa band above the identified NADH:ubiquinone oxidoreductase (complex I, ~1.5 MDa) in a Blue-Native (BN) gel experiment conducted with n-dodecyl-maltoside treated mitochondria (Fig. 1a and c). This complex, probably a dimer, is capable to hydrolyze ATP (Fig. 1b). It was previously resolved in 18 protein spots by 2D BN-SDS PAGE analysis, among which six ATP synthase canonical subunits (α, β, γ, δ, ε and OSCP) and four Euglenozoa-specific subunits (p18, ATPTB1, ATPTB4, and ATPTB12) were identified [46]. In order to prove the *bona-fide* association of these atypical subunits to the *Euglena* mitochondrial ATP synthase, and to identify new subunits that may have escaped detection due to the comigration with other proteins, it was first purified by a two-step chromatographic procedure (see Methods section for further details). After the chromatographic purification, a fraction enriched with complex V was obtained, in which only a very small amount of complex I can be observed (Fig. 1d).

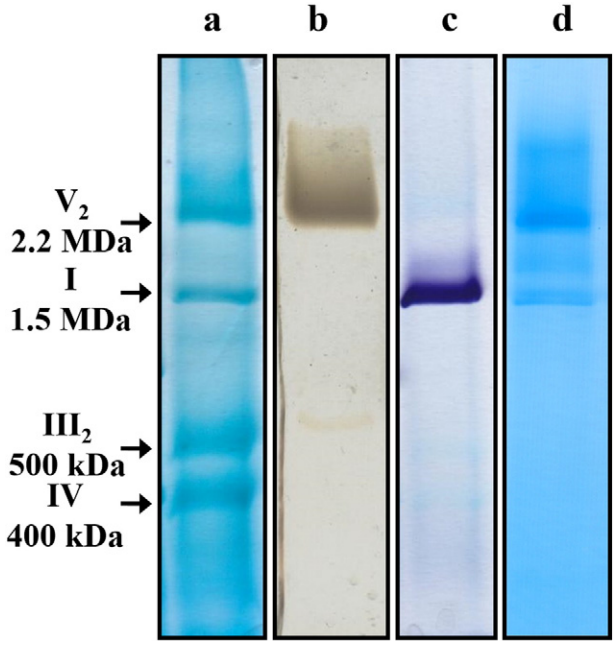

Fig. 1. Electrophoretic patterns of purified dimeric ATP synthase from *Euglena gracilis*. (a) Total mitochondrial protein from *Euglena gracilis* was solubilized in presence of β-dodecyl-n-maltoside and subjected to a BN-PAGE. Estimated molecular masses and identities of Coomassie brilliant blue-stained protein complexes are indicated. *In-gel* activity stains for ATP hydrolysis (b) and NADH:Nitro Blue tetrazolium (NBT) oxidoreductase (c). Enriched fraction of dimeric ATP synthase from the two-step chromatographic purification, remaining complex I could be observed (Coomassie brilliant blue staining) (d).

3.2. Further determination of atypical subunit composition of Euglena mitochondrial ATP synthase

The protein spot corresponding to mitochondrial ATP synthase from the enriched fraction was then excised from BN-gel and its polypeptides were resolved by two-dimensional SDS-glycine/SDS-tricine PAGE (Fig. 2). A total of 21 spots were numbered, excised out of the gel and analyzed by tandem mass spectrometry (MS/MS). Fifteen of the 21 analyzed spots matched to a single protein in our database. Interestingly, the alpha subunit was found as two different polypeptides, one with a mass of 47.4 kDa and the other with a mass of 13.3 kDa, corresponding to the N-terminal and C-terminal part, respectively. Together they would form a 60 kDa protein, which is the molecular mass predicted for this subunit. In three spots (2, 16, and 17), two different polypeptides were identified by MS analysis probably because a comigration of these proteins during the electrophoresis steps. At last, three spots remained unidentified (3, 20, and 21). Based on this analysis, the complex V from *E. gracilis* comprises at least 24 polypeptides with molecular masses ranging from 5.5 to 51.6 kDa. The same protein spot profile was obtained after freezing/thawing the purified complex (Supplemental Fig. 1), which reinforces the idea that these subunits are *bona*-fide components of ATP synthase. All the obtained sequences (Supplemental File 1) were analyzed *in silico* to search for possible homologs and conserved domains (CD) in protein databases (NRPS, TriTrypDB) (Table 1). Seven protein spots correspond to the canonical subunits α (present in two independent spots in the gel polypeptide pattern), β, γ, δ, ε and OSCP. Conversely, seven polypeptides are Euglenozoa-specific proteins first described as components of ATP synthase subunits from *Trypanosoma* species (ATPTB1, ATPTB2, ATPTB3, ATPTB4, ATPTB6, ATPTB12 and p18). Six other polypeptides do not have any homolog and remain as unnamed proteins (UP), and three spots were not identified (NI). Two additional subunits (ATPTB7, ATPTB10) described in *Trypanosoma* ATP synthase [65] and previously identified at genomic level in *Euglena* [46] were not identified here. Among the largest subunits found in this complex are the trypanosomatid specific proteins ATPTB1 and ATPTB2 with predicted molecular masses of 55.9 kDa and 53.9 kDa respectively, in the same range of subunits α and β from the catalytic

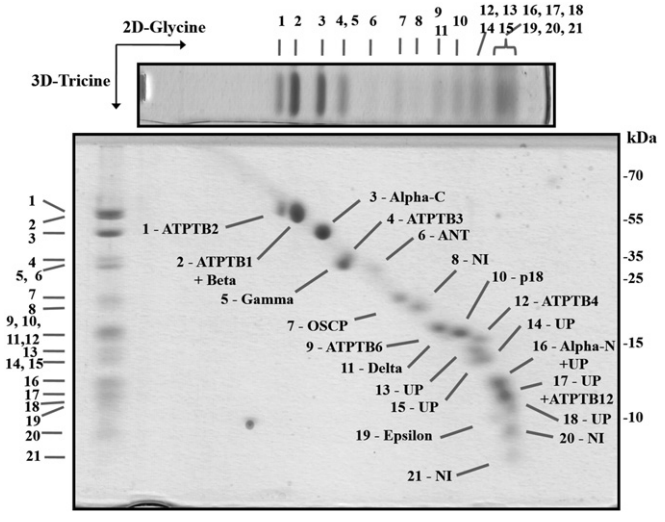

Fig. 2. 3D resolution of the polypeptides that constitute the *Euglena* mitochondrial F_1F_O ATP synthase. Dimeric *Euglena* ATP synthase was resolved by BN-PAGE. The band of interest was excised and resolved in a glycine-SDS-PAGE (12% acrylamide). The 2D gel was then subjected to 3D tricine-SDS-PAGE (14% acrylamide) and stained with Coomassie brilliant blue. The identified subunits and molecular mass markers are indicated. NI, not identified; UP, unnamed protein with no homolog in other species.

Table 1
Subunit composition of *Euglena gracilis* mitochondrial ATP synthase.

Subunit	Name	Accession number	MW	MW (calc)	IP	TMH (putative)	GRAVY	Conserved domain[3]	Blast Hits[3]	Mascot score	Coverage %	Signal peptide*	Coiled coil¥
1	ATPTB2	comp59678_c0_seq2_c	51.6	53.9	4.9	0	−0.329	–[1,2]	–[a,c]; EJS84964.1[b]	868	42	–[α] 29[β] (0.9829)	83.7% 53 to 104
2	ATPTB1	comp62248_c0_seq5_c	50.6	55.9	6.0	1 (N)	−0.481	–[1,2]	–[a,b,c]	690	47	–[α, β]	21.6% 227 to 252
3	beta	comp59738_c0_seq2_m F1-ATPase_beta(A)[1,2]	50.6	53.2	5.0	0	0.074	EPY14967.1[a]; WP_006997680.1[b]; Tgr.527.1020[c]	1180	64	–[α, β]	100.0% 467 to 529	
4	Alpha-C	comp63233_c0_seq1_m	43.3	47.4	9.2	0	−0.157	F_0F_1 ATP synthase subunit alpha(A)[1,2]	EPY14967.1[a]; WP_006997680.1[b]; Tgr.527.1020[c]	1120	55	–[α, β]	0.0%
5	ATPTB3	comp60477_c0_seq4_c	35.7	31.3	5.4	0	−0.013	–[1,2]	WP_045088137.1[a]; WP_027960470.1[b]; –[c]	337	28	–[α] 27[β] (0.8534)	0.0%
6	gamma	comp52980_c0_seq1_m	34.0	31.7	6.5	0	−0.375	F1-ATPase_gamma super family (A)[1,2]	XP_822278.1[a]; EHX84368.1[b]; Tb927.10.180[c]	240	51	–[α] 19[β] (0.5827)	49.4% 205 to 252
7	ANT	comp62013_c0_seq2	33.2	25.9	9.6	3 (C) 4 (C)[#]	−0.078	Mitochondrial carrier protein (N) Mitochondrial carrier protein (C)[1,2]	ABV25601.1[a]; ABV25601.1[b]; TRSC58_06358[c]	70	38	–[α, β]	0.0%
8	OSCP	comp56779_c0_seq1_m	27.2	25.9	4.9	0	−0.250	ATP synthase delta (OSCP) subunit (M)[1,2]	XP_823037.1[a]; WP_008075436.1[b]; Tb927.10.8030[c]	678	78	–[α, β]	30.4% 87 to 113 36.4% 124 to 140
9	a*	–	24.3	–	–	–	–	–	–	NI	–	–	–
10	ATPTB6	comp48437_c0_seq2_c	21.3	21.7	9.6	2 (N,C)	−0.297	–[1,2]	CCW71114.1[a]; CCW71114.1[b]; Tgr.480.1070[c]	236	31	–[α, β]	0.0%
11	p18	comp56597_c0_seq3	20.8	21.0	8.4	0	0.205	–[1,2]	EPY41275.1[a]; CDX69249.1[b]; TcCLB.510821.60[c]	780	73	–[α] 16[β] (0.9847)	0.0%
12	delta	comp55732_c0_seq1_c	20.3	19.5	4.6	0	−0.280	F1-ATPase_delta (M,C)[1,2]	EPY33170.1[a]; EHX56372.1[b]; TcCLB.506945.240[c]	197	77	18[α] (0.4384) 18[β] (0.9514)	18.8% 135 to 151
13	ATPTB4	comp38662_c0_seq1_c	19.2	18.8	8.7	0	−0.476	–[1,2]	EPY25620.1[a]; ESL07652.1[b]; TRSC58_04655[c]	258	29	–[α,β]	17.9% 115 to 145
14	UP14	comp51661_c0_seq2	17.7	19.7	5.8	1 (M)	−0.209	–[1,2]	–[a,c]; WP_010879713.1[b]	306	39	–[α] 25[β] (0.9162)	100.0% 128 to 171
15	UP15	comp46683_c0_seq1_c	17.0	16.2	9.3	1 (M)	−0.717	–[1,2]	–[a,b,c]	565	73	–[α,β]	0.0%
16	UP16	comp48845_c0_seq1_c	16.2	13.4	9.1	0	−0.355	–[1,2]	–[a,b,c]	170	71	–[α,β]	0.0%
17	Alpha-N	comp63233_c0_seq1_m	13.3	12.9	8.2	0	0.332	ATPase alpha subunit(A)[1,2]	XP_803362.1[a]; CCW61345.1[b]; TvY486_0707020[c]	332	39	–[α,β]	0.0%
18	UP18	gi|109777597_c	13.3	13.8	8.8	0	−0.661	–[1,2]	–[a,b,c]	62	21	–[α,β]	0.0%
19	UP19	comp35985_c0_seq2	11.2	12.5	9.7	1(N)	0.419	–[1,2]	–[a,b,c]	136	57	–[α] 22[β] (0.9604)	0.0%
20	ATPTB12	comp45696_c0_seq1_c	11.2	11.3	9.4	0	−0.784	–[1,2]	–[a,b]; TRSC58_04996[c]	64	55	–[α,β]	0.0%
21	UP21	gi|125988729_c	10.6	12.7	9.7	1 (C)	−0.183	–[1,2]	–[a,b,c]	172	27	–[α,β]	0.0%
22	Epsilon	comp44213_c0_seq1_c	9.7	8.7	7.9	0	−0.418	F1-ATPase_epsilon super family (N)[1,2]	–[a]; ERN7205.1[b]; TcCLB.508661.34[c]	192	68	–[α] 22[β] (0.7313)	0.0%
23	C*	–	8.8	–	–	–	–	–	–	NI	–	–	–
24	NI	–	5.5	–	–	–	–	–	–	–	–	–	–

ND not determined.
_m proposed mature sequence.
_c start from the first Methionine.
(N) Amino terminus, (C) Carboxi terminus, (M) Middle region, (A) Almost all sequence.
[α] Phobius; Cleavage site (Probability of the peptide signal).
[β] MitoProt; Cleavage site (Probability of export to mitochondria).
[a] Blastp.
[b] DELTA-BLAST.
[c] BlAST TriTrypDB.
[1] CCD.
[2] DELTA-BLAST.
[3] The e-value threshold for the blast results was 10^{-5}.
¥ % Probability (Region).
[#] According to the reported AAC from other organisms.
* Putative subunit (see Discussion).

core. No CD could be confidently identified for ATPTB and UP proteins and it is important to note that none of these identified polypeptides share any similarity with the canonical hydrophobic subunits present in the proton translocation channel sector (a/c-ring which have not been identified here) of the known F-Type ATP synthases. Incidentally, subunits a and c have probably escaped identification in this analysis but corresponding transcripts have been identified [46]. Finally, one polypeptide matched to the ADP/ATP transporter of adenylate translocase superfamily (ANT). The ANT sequence is incomplete in our database (Supplemental File 2), so the predicted molecular mass (25.9 kDa) of this polypeptide is smaller than the value of ~33 kDa determined in Fig. 2, a molecular mass which is similar to the mass of ANT in other species [11].

The Table 1 also summarizes predicted physico-chemical properties for each individual subunit, such as hydrophobicity (GRAVY) and isoelectric point (IP), and predicted structural features like transmembrane helices (TMH) and coiled-coil domains (CC). Seven of the identified subunits (ATPTB1, ATPTB6, UP14, UP15, UP19, UP21, and ANT) contain at least one putative TMH with a total of eleven TMH. In agreement with the partial sequence of ANT in our database, only three of the four classical TMH that are usually predicted in the carboxyl terminus of ANT have been found. A CC region is predicted for the subunits ATPTB2 and ATPTB4. In addition to a putative TMH in the amino terminal part, ATPTB1 and UP14 also present a CC region, which suggests that these subunits might contribute to an original peripheral stator (see Discussion).

3.3. Atypical structures of ATP synthase visualized by electron microscopy

In our previous study, we suggested that the ~2 MDa Complex corresponds to a dimeric ATP synthase [46]. In order to confirm this hypothesis and to determine if the identified polypeptides might be associated to an atypical stator structure, electron microscopy in combination with single particle analysis was performed. About 2000 images were recorded, and a total of 30,000 particle projections were collected and analyzed. The particles projections grouped into 14 classes (an average of 2000 particles per class) among which 12 are shown in Fig. 3. Negatively stained ATP synthase complexes are present in mainly three positions on the carbon support film. These projections confirm first that the complex is a dimer. The dimer is in an almost non-tilted situation from a side (Fig. 3F) as suggested by the homogeneous negative staining around the particle. Like most other mitochondrial ATP synthases, the two monomers are not parallel, but make an angle of about 45° (marked by red lines, Fig. 3F). This indicates a local curvature of the membrane. In three classes (panels A-C), the dimer is slightly tilted so the apparent angle between the two monomers is decreased (~30°). In these views, the shape of the F_1 headpiece, connected to the membrane-bound F_O part via the stalk region, is well outlined. A novel feature is the large density below the F_O part, which is lacking in mammalian ATPase (orange arrowheads; Fig. 3A). In several other maps of tilted dimers (Fig. 3D-E, G-H), the left monomer is in a position that allows an outer peripheral density between the F_O and F_1 parts to be optimally visible (green arrowhead). In contrast, blue arrowheads (Fig. 3B,

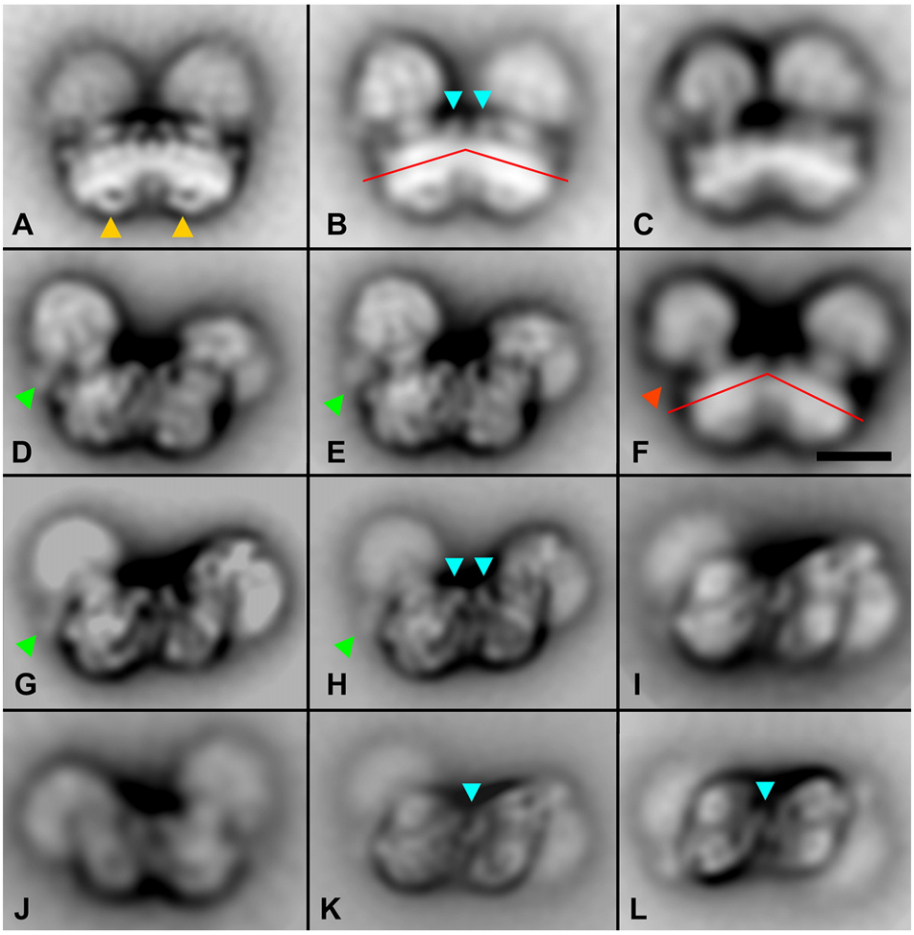

Fig. 3. 2D Projection maps of purified dimeric ATP synthase complexes from *E. gracilis* obtained by single particle averaging. The dimeric complex V was purified by two-step chromatographic procedure in presence of β-dodecyl-n-maltoside and analyzed by EM. In side view projections (A-C), an unusual density can be observed below de F_O part (orange arrows). The two monomers make an angle of about 30° (red lines) while in almost non-tilted view (F) the angle is about 45°. In side view from tilted dimers (D, E, G, H), peripheral density between the F_O and F_1 parts is marked with green arrows. Top view projections (I, K, L) show that the two monomers are related by a two-fold rotational symmetry. Blue arrowheads indicate densities not connected to F_1 (B, H, K, L) but connecting the two monomers.

H) indicate densities at the interface between monomers that do not connect F_O to F_1. This suggests that the peripheral stator, necessary to prevent futile rotation between the F_O and F_1, is at the outer periphery rather than in the interface between the two monomers. Other maps (Fig. 3I-K, L) show the dimer in a position closer to the plane of the membrane. In this position the F_O parts are attached to the carbon support film and the F_1 headpieces appear blurred, due to an insufficient embedding in the negative stain layer. One view (Fig. 3L) clearly shows that the two monomers are related by a two-fold rotational symmetry. Interestingly, the outer peripheral density visible in the slightly-tilted projections (green arrowheads on panels D-E,G-H) appears to be part of a structure connecting F_O and F_1. These views also suggest that the central densities (blue arrowheads on panels K-L) are part of a structure connecting the two monomers in the membrane region.

4. Discussion

In a previous work, we identified 10 polypeptides by mass spectrometry in the *Euglena gracilis* mitochondrial F_1F_O-ATP synthase purified by BN-PAGE: six canonical subunits (α, β, γ, δ, ε, OSCP) and four subunits typical of *Trypanosoma* ATP synthase (ATPTB1, ATPTB4, ATPTB12 and p18) [46]. In the present work, by further purifying the ATP synthase complex by a two-step chromatography approach, we confirmed the presence of these 10 subunits and identified 12 additional subunits, among which three *Trypanosoma* ATP synthase subunits (ATPTB2, ATPTB3, and ATPTB6) and the ATP/ADP translocase (ANT).

Although we cannot fully exclude the possibility that the association of ANT, as well as for other ATPTB and UP proteins, is an artifact of purification, the fact that these subunits remain associated to the mitochondrial ATP synthase after two chromatographic steps, one step of freezing/thawing and one step of gel electrophoresis, strongly suggest that they are true components of the supercomplex. In mammals, the ATP/ADP carrier (ANT) has been found in association with the inorganic phosphate carrier (PiC) and the mitochondrial ATP synthase, in a supercomplex called ATP synthasome [11,34,43]. Similarly the ANT was found in association with ATP synthase in trypanosomatids after purification by sucrose gradient centrifugation [19]. We thus suggest that the supercomplex isolated here is the first biochemical and structural evidence for an ATP synthasome under dimeric form. A PiC homolog is present in *Euglena gracilis* (EST, EC682656.1) but due to its highly hydrophobic nature, it might have escaped identification [48]. Similarly, the highly hydrophobic membrane conserved subunits (a/c-ring), involved in the proton translocation and rotation of the central stalk, probably also escaped identification. These two F_O subunits are proposed to be present in the mitochondrial F-ATP synthase from *Trypanosoma brucei* (subunit *c*, Tb10.70.6340; subunit *a*, AAA97428), based on a detailed analysis of amino acid sequences and hydropathic profiles [6,50,65]. In our analysis the spot 8 (24.3 kDa, Fig. 2) might correspond to subunit *a*. This would be in good agreement with the observation that the trypanosmatid subunit *a* (28.7 kDa) has a very high hydrophobic nature (Gravy 1.959). Similarly, the value of 8.8 kDa determined for spot 20 (Fig. 2) is similar to 8.7 kDa for the mature c subunit in *Trypanosoma brucei* after cleavage of its the mitochondrial targeting sequence (~40 residues with a 0.9766 probability), suggesting that this spot might correspond to subunit *c* previously identified in *E. gracilis* using bioinformatic approaches [46]. The number of subunit *c* copies present in the *Euglena* complex remains unknown. In other mitochondrial and α-proteobacterial ATP synthases, the number of polypeptides that build the *c*-ring varies: eight in the bovine complex [64,66], ten in yeast [27,31], *E. coli* [4] and chlorophycean algae [2], and twelve in the bacterium *P. denitrificans* [38]. Taking into account the presence of subunits not yet identified at the protein level (*a* and *c*), and assuming a c_{10} subunit ring stoichiometry, the monomeric form of *E. gracilis* F_oF_1-ATP synthase complex might have a molecular mass around 860 kDa, a value which is in good agreement with the ~2 MDa apparent molecular mass determined for the dimeric complex by BN-PAGE. The dimeric nature of ATP synthase is no longer a matter of debate, since it is acknowledged that in many other organisms the oligomeric form of the enzyme is responsible for shaping the mitochondrial cristae [16,41]. Another notable feature of the polypeptides associated to the purified enzyme is the presence of a fragmented alpha subunit into two polypeptides of 47.4 kDa (C-terminal region) and 13.3 kDa (N-terminal region). A single transcript encoding the whole 60 kDa protein has been however identified. Because protease inhibitors were used during the purification procedure, and because no trace of the whole alpha subunit has been detected, these fragments most probably arose by a proteolytic cleavage *in vivo*, so the generated fragments remain attached to the F_1 domain, and become separated only upon denaturing gel electrophoresis. When modelling the two polypeptides on a F_1 crystallographic structure, an exposed loop region was revealed, that may be readily cleaved by an unknown protease (Supplemental Fig. S2).

The subunit composition determined here shows two striking features. Firstly, it shares seven components with the ATP synthase of *Trypanosoma brucei*. This reinforces the conclusion that the enzyme is quite well conserved among Euglenozoa [46]. Secondly, in *E. gracilis*, the canonical subunits involved in the F_1 catalytic core (α,β), the rotor and central axis (δ, ε, γ and *c*-ring) and the subunits OSCP and *a* that may bind the peripheral stalk have been identified. However the subunits involved in building the peripheral stator (b/ATP4, d, e, f, g, etc.) are missing and have been replaced by a new set of subunits without counterparts in other lineages. The first organisms where an unusual structure and subunit composition of the mitochondrial ATP synthase was found were the green alga *C. reinhardtii* and its colorless relative *Polytomella* sp. [25,59]. More recently, an unusual subunit composition for the ATP synthase was also reported in the ciliate (alveolates) *T. thermophila* [3], and in *T. brucei* [65]. Altogether, these observations indicate that the peripheral stator is quite specific to each main lineage of eukaryotes investigated to date (mammals & yeasts belonging to Opisthokonts, ciliates to Alveolata, Euglena to Excavates, and *Polytomella* to Archaeplastida). The reason behind this structural diversity was proposed ten years ago [35,59]: it might be related to the unsuccessful trials to transfer the ATP4 gene, coding for b subunit, from the mitochondrial genome to the nuclear genome, and the concomitant recruitment of structural subunits to build a very robust peripheral stator.

The predicted properties of Euglena atypical subunits provide some clues on their topological disposition. The most noteworthy observation is the presence of a total of eleven predicted transmembrane helices (TMH) in these atypical subunits. In comparison, all the membrane-bound yeast subunits i, f, 8, and b make up a total of 5 TMH [31]. Overall, the numerous TMH could explain the high electron density observed in the membrane region of Euglena ATP synthase (Fig. 3). Another interesting feature is the putative presence of CC regions in at least four of the subunits (ATPTB1, ATPTB2, ATPTB4 and UP14). CC regions are indeed known to be involved in the formation of the peripheral stalks of various rotary ATPases: between the *b* subunits in *E. coli* [17,18]; between subunits *b*, *F6* and *d* in bovine complex [20,47]; putatively between Asa1, Asa2, Asa4 and Asa7 [37] inside the robust peripheral stalk of chlorophycean algae [2], and between subunits E and G in both the archaeal A_1/A_o ATP synthase [36,51], and in the vacuolar V_1/V_o ATPase [63]. We thus suggest that some CC regions of atypical subunits (ATPTB1, ATPTB2, ATPTB4 and UP14) might be involved in the formation of the peripheral stalk from Euglenozoa mitochondrial ATP synthase. Some low-resolution features observed by single particle electron microscopy are quite unique to the mitochondrial ATP synthase of *Euglena gracilis*. In comparison to the best studied dimer from the colorless alga *Polytomella* [2,24], two differences are noteworthy: (i) The stators of the *Polytomella* ATPase are at the dimer interface, whereas those of *Euglena* are suggested to be located at the periphery (green arrowheads, Fig. 3), and (ii) the dimer-specific subunits in *Euglena* are smaller, because the F_1 headpieces are closer together. However, the latter difference is in part depending on the overall angle between the

monomers. In maps of *Euglena* dimers this angle is around 30°, but in *Polytomella* and in yeast the kink is substantially larger [24,25]. The *Euglena* stator appears thicker because a protein density of roughly 20 Å appears to be part of it (Fig. 3, green arrowheads). This density is unique, although it may have escaped detection in other organisms, due to overlap in projection maps. In *E. coli* ATP synthase the stator is quite thin and composed of two long coiled α-helices [17,18]. In the ciliate *T. thermophila* there is possibly a peripheral stator [3,10], but the extra mass was not resolved. Finally, the mass connected to the F_o part of *Euglena* ATP synthase, right under the c-subunit ring, could indicate that it is part of the rotor inside the enzyme. Usually, the ATP synthase dimers have no extra mass connected to the c-subunit ring at the other side of the membrane, although some V-type ATPases show a ~35 Å protrusion from the bottom of Vo (exposed to the lumen of the endomembrane compartment, or extracellular).This feature, for example was observed in the bovine clathrin-coated vesicles [60,61] but not in those from the yeast vacuolar membrane [21,22,63] or the enzyme of plant tonoplasts [23]. This density has been assigned to the glycosylated accessory subunit Ac45 [56,61], a polypeptide that associates with other Vo subunits in osteoclasts and appears to be involved in maintaining proton pumping activity [26], although this hypothesis is still a matter of controversy [32,56].

Gathering all the information presented in this study, we can propose a model of how these novel subunits are present in the atypical mitochondrial enzyme of *Euglena* (Fig. 4). Our interpretation shows a dimer with a slight angle in which the stator of each monomer is located in the outer periphery and binds OSCP in the top of the enzyme. The location of the non-conserved subunits remains largely unknown, since the resolution of the structure does not allow us to pinpoint individual components. We have assigned locations for the small hydrophobic subunits both in the dimer interface and in the outer part of each monomer. ANT is also tentatively proposed near to the subunit a, according to the EM studies of the ATP synthasome from rat liver mitochondria [11]. In our model, there are a total of 23 TMH per monomer: seven putative

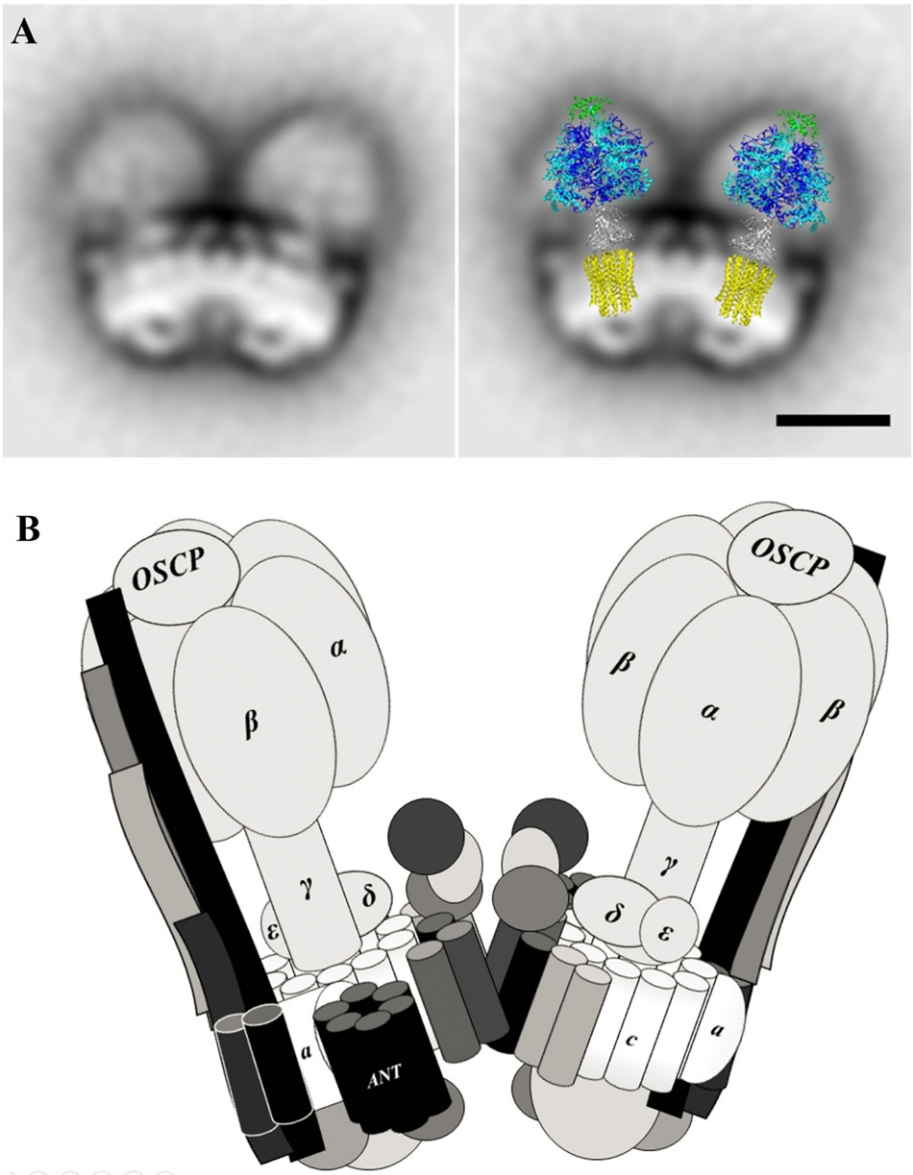

Fig. 4. Proposed topological model of the dimeric ATP synthase from *Euglena gracilis*. (A) Side view projection map from dimeric ATP synthase complex from *E. gracilis* obtained with EM (left panel). Overlap of the F_1/c-ring/OSCP structures from bovine mitochondrial enzyme (PDB ID: 2WSS and 3U2Y; [47,57]) inside the EM projection (right panel). The bar is 10 nm. (B) Proposed model of the arrangement of the subunits in the dimeric complex. Even though the position of each atypical subunit (dark grey) remains largely unknown, subunits containing coil-coiled structures (ATPTB1, ATPTB2, ATPTB4 and UP14) are proposed to be part of the peripheral stalks and subunits with putative TMH surround both monomers (see Discussion for details). Conserved subunits of the F-ATPase (light grey) are labeled.

TMH for UP and ATPTB proteins according to the *in silico* analysis (Table 1), 10 TMH in the proposed c_{10}-ring and six TMH for ANT according to crystallographic data (pdb 1OKC [45]). We suggest the position of the peripheral stalk at the outer periphery of the dimeric structure, mainly because (i) a stronger electron density is observed in this region and because (ii) there was no evidence from side projections of a peripheral stator at the interface between the two monomers like the one described in mitochondrial ATP synthase dimers from *Saccharomyces cerevisiae* [15], *Yarrowia lipolytica* [31], *Polytomella* sp. [2], and *Bos taurus* [13]. Therefore, the presence of more than one peripheral arm per each monomer of the *Euglena* enzyme is very unlikely, although this kind of architecture with multiple peripheral stators has been observed in the archaeal [28] and vacuolar [5] enzymes.

Supplementary data to this article can be found online at http://dx.doi.org/10.1016/j.bbabio.2017.01.007.

Transparency document

The Transparency document associated with this article can be found, in the online version.

Acknowledgments

We thank E. Perez for her help in the identification of *Euglena* genomic data. P.C acknowledges financial support from the Belgian Fonds de la Recherche Scientifique F.R.S.-F.N.R.S. (FRFC 2.4597, CDR J.0032, CDR J.0079 and Incentive Grant for Scientific Research F.4520), FRS-FNRS/CONACyT B330/123/11 (Belgium-Mexico) and European Research Council (H2020-EU BEAL project 682580). P.C is a Senior Research Associate from F.R.S.-FNRS. Support from grants 239219 (Fondo SEP-CONACYT), 245486 (FNRS-CONACyT), and IN20311423 (DGAPA-UNAM) is also acknowledged.

References

[1] J.P. Abrahams, A.G.W. Leslie, R. Lutter, J.E. Walker, Structure at 2.8 (angstrom) resolution of F(1)-ATPase from bovine heart mitochondria, Nature 370 (1994) 621–628.
[2] M. Allegretti, N. Klusch, D.J. Mills, J. Vonck, W. Kühlbrandt, K.M. Davies, Horizontal membrane-intrinsic α-helices in the stator a-subunit of an F-type ATP synthase, Nature 521 (2015) 237–240, http://dx.doi.org/10.1038/nature14185.
[3] P. Balabaskaran Nina, N.V. Dudkina, L.A. Kane, J.E. van Eyk, E.J. Boekema, M.W. Mather, A.B. Vaidya, Highly divergent mitochondrial ATP synthase complexes in tetrahymena thermophila, PLoS Biol. 8 (2010) 3–6, http://dx.doi.org/10.1371/journal.pbio.1000418.
[4] B. Ballhausen, K. Altendorf, D.H. Gabriele, Constant c10 ring stoichiometry in the *Escherichia coli* ATP synthase analyzed by cross-linking, J. Bacteriol. 191 (2009) 2400–2404, http://dx.doi.org/10.1128/JB.01390-08.
[5] S. Benlekbir, S.A. Bueler, J.L. Rubinstein, Structure of the vacuolar-type ATPase from *Saccharomyces cerevisiae* at 11-Å resolution, Nat. Struct. Mol. Biol. 19 (2012) 1356–1362, http://dx.doi.org/10.1038/nsmb.2422.
[6] G.J. Bhat, D.J. Koslowsky, J.E. Feagin, B.L. Smiley, K. Stuart, An extensively edited mitochondrial transcript in kinetoplastids encodes a protein homologous to ATPase subunit 6, Cell 61 (1990) 885–894.
[7] E. Boekema, H. van Roon, J. van Breemen, J.P. Dekker, Supramolecular organization of photosystem II and its light-harvesting antenna in partially solubilized photosystem II membranes, Eur. J. Biochem. 266 (1999) 444–452, http://dx.doi.org/10.1046/j.1432-1327.1999.00876.x.
[8] P.D. Boyer, The ATP synthase–a splendid molecular machine, Annu. Rev. Biochem. 66 (1997) 717–749, http://dx.doi.org/10.1146/annurev.biochem.66.1.717.
[9] M.M. Bradford, A rapid and sensitive method for the quantitation of microgram quantities of protein utilizing the principle of protein-dye binding, Anal. Biochem. 72 (1976) 248–254, http://dx.doi.org/10.1016/0003-2697(76)90527-3.
[10] Y. Chaban, E.J. Boekema, N.V. Dudkina, Structures of mitochondrial oxidative phosphorylation supercomplexes and mechanisms for their stabilisation, Biochim. Biophys. Acta Bioenerg. 1837 (2014) 418–426, http://dx.doi.org/10.1016/j.bbabio.2013.10.004.
[11] C. Chen, Y. Ko, M. Delannoy, S.J. Ludtke, W. Chiu, P.L. Pedersen, Mitochondrial ATP synthasome: three-dimensional structure by electron microscopy of the ATP synthase in complex formation with carriers for Pi and ADP/ATP, J. Biol. Chem. 279 (2004) 31761–31768, http://dx.doi.org/10.1074/jbc.M401353200.
[12] L. Colina-Tenorio, H. Miranda-Astudillo, A. Cano-Estrada, M. Vázquez-Acevedo, P. Cardol, C. Remacle, D. González-Halphen, Subunit Asa1 spans all the peripheral stalk of the mitochondrial ATP synthase of the chlorophycean alga Polytomella sp, Biochim. Biophys. Acta Bioenerg. 1857 (2016) 359–369, http://dx.doi.org/10.1016/j.bbabio.2015.11.012.
[13] S.J. Couoh-Cardel, S. Uribe-Carvajal, S. Wilkens, J.J. García-Trejo, Structure of dimeric F1F0-ATP synthase, J. Biol. Chem. 285 (2010) 36447–36455, http://dx.doi.org/10.1074/jbc.M110.144907.
[14] R.L. Cross, L. Taiz, Gene duplication as a means for altering H+/ATP ratios during the evolution of Fo F1 ATPases and synthases, FEBS Lett. 259 (1990) 227–229, http://dx.doi.org/10.1016/0014-5793(90)80014-A.
[15] K.M. Davies, C. Anselmi, I. Wittig, J.D. Faraldo-Gomez, W. Kuhlbrandt, Structure of the yeast F1Fo-ATP synthase dimer and its role in shaping the mitochondrial cristae, Proc. Natl. Acad. Sci. 109 (2012) 13602–13607, http://dx.doi.org/10.1073/pnas.1204593109.
[16] K.M. Davies, M. Strauss, B. Daum, J.H. Kief, H.D. Osiewacz, A. Rycovska, V. Zickermann, W. Kuhlbrandt, Macromolecular organization of ATP synthase and complex I in whole mitochondria, Proc. Natl. Acad. Sci. 108 (2011) 14121–14126, http://dx.doi.org/10.1073/pnas.1103621108.
[17] P.A. Del Rizzo, Y. Bi, S.D. Dunn, ATP synthase b subunit dimerization domain: a right-handed coiled coil with offset helices, J. Mol. Biol. 364 (2006) 735–746, http://dx.doi.org/10.1016/j.jmb.2006.09.028.
[18] P.A. Del Rizzo, Y. Bi, S.D. Dunn, B.H. Shilton, The "second stalk" of *Escherichia coli* ATP synthase: structure of the isolated dimerization domain, Biochemistry 41 (2002) 6875–6884, http://dx.doi.org/10.1021/bi025736i.
[19] S. Detke, R. Elsabrouty, Identification of a mitochondrial ATP synthase-adenine nucleotide translocator complex in Leishmania, Acta Trop. 105 (2008) 16–20, http://dx.doi.org/10.1016/j.actatropica.2007.08.008.
[20] V.K. Dickson, J.A. Silvester, I.M. Fearnley, A.G.W. Leslie, J.E. Walker, On the structure of the stator of the mitochondrial ATP synthase, EMBO J. 25 (2006) 2911–2918, http://dx.doi.org/10.1038/sj.emboj.7601177.
[21] M. Diepholz, M. Börsch, B. Böttcher, Structural organization of the V-ATPase and its implications for regulatory assembly and disassembly, Biochem. Soc. Trans. 36 (2008) 1027–1031, http://dx.doi.org/10.1042/BST0361027.
[22] M. Diepholz, D. Venzke, S. Prinz, C. Batisse, B. Flörchinger, M. Rössle, D.I. Svergun, B. Böttcher, J. Féthière, A different conformation for EGC stator subcomplex in solution and in the assembled yeast V-ATPase: possible implications for regulatory disassembly, Structure 16 (2008) 1789–1798, http://dx.doi.org/10.1016/j.str.2008.09.010.
[23] I. Domgall, D. Venzke, U. Lüttge, R. Ratajczak, B. Böttcher, Three-dimensional map of a plant V-ATPase based on electron microscopy, J. Biol. Chem. 277 (2002) 13115–13121, http://dx.doi.org/10.1074/jbc.M112011200.
[24] N.V. Dudkina, J. Heinemeyer, W. Keegstra, E.J. Boekema, H.P. Braun, Structure of dimeric ATP synthase from mitochondria: an angular association of monomers induces the strong curvature of the inner membrane, FEBS Lett. 579 (2005) 5769–5772, http://dx.doi.org/10.1016/j.febslet.2005.09.065.
[25] N.V. Dudkina, S. Sunderhaus, H.P. Braun, E.J. Boekema, Characterization of dimeric ATP synthase and cristae membrane ultrastructure from Saccharomyces and Polytomella mitochondria, FEBS Lett. 580 (2006) 3427–3432, http://dx.doi.org/10.1016/j.febslet.2006.04.097.
[26] H. Feng, T. Cheng, N.J. Pavlos, K.H.M. Yip, A. Carrello, R. Seeber, K. Eidne, M.H. Zheng, J. Xu, Cytoplasmic terminus of vacuolar type proton pump accessory subunit Ac45 is required for proper interaction with V0 domain subunits and efficient osteoclastic bone resorption, J. Biol. Chem. 283 (2008) 13194–13204, http://dx.doi.org/10.1074/jbc.M709712200.
[27] D. Stock, A.G. Leslie, J.E. Walker, Molecular architecture of the rotary motor in ATP synthase, Science 5445 (1999) 1700–1705.
[28] G. Grüber, M.S.S. Manimekalai, F. Mayer, V. Müller, ATP synthases from archaea: the beauty of a molecular motor, Biochim. Biophys. Acta Bioenerg. 1837 (2014) 940–952, http://dx.doi.org/10.1016/j.bbabio.2014.03.004.
[29] S. Guerrero-Castillo, M. Vázquez-Acevedo, D. González-Halphen, S. Uribe-Carvajal, In Yarrowia lipolytica mitochondria, the alternative NADH dehydrogenase interacts specifically with the cytochrome complexes of the classic respiratory pathway, Biochim. Biophys. Acta Bioenerg. 1787 (2009) 75–85, http://dx.doi.org/10.1016/j.bbabio.2008.10.008.
[30] J. Habersetzer, W. Ziani, I. Larrieu, C. Stines-Chaumeil, M.F. Giraud, D. Brèthes, A. Dautant, P. Paumard, ATP synthase oligomerization: from the enzyme models to the mitochondrial morphology, Int. J. Biochem. Cell Biol. 45 (2013) 99–105, http://dx.doi.org/10.1016/j.biocel.2012.05.017.
[31] A. Hahn, K. Parey, M. Bublitz, D.J. Mills, V. Zickermann, J. Vonck, W. Kühlbrandt, T. Meier, Structure of a complete ATP synthase dimer reveals the molecular basis of inner mitochondrial membrane morphology, Mol. Cell 63 (2016) 445–456, http://dx.doi.org/10.1016/j.molcel.2016.05.037.
[32] M. Huss, H. Wieczorek, Influence of ATP and ADP on dissociation of the V-ATPase into its V1 and VO complexes, FEBS Lett. 581 (2007) 5566–5572, http://dx.doi.org/10.1016/j.febslet.2007.11.004.
[33] W. Junge, H. Lill, S. Engelbrecht, ATP synthase: an electrochemical transducer with rotary mechanics, Trends Biochem. Sci. 22 (1997) 420–423, http://dx.doi.org/10.1016/S0968-0004(97)01129-8.
[34] Y.H. Ko, M. Delannoy, J. Hullihen, W. Chiu, P.L. Pedersen, Mitochondrial ATP synthasome: cristae-enriched membranes and a multiwell detergent screening assay yield dispersed single complexes containing the ATP synthase and carriers for Pi and ADP/ATP, J. Biol. Chem. 278 (2003) 12305–12309, http://dx.doi.org/10.1074/jbc.C200703200.
[35] M. Lapaille, A. Escobar-Ramírez, H. Degand, D. Baurain, E. Rodríguez-Salinas, N. Coosemans, M. Boutry, D. Gonzalez-Halphen, C. Remacle, P. Cardol, Atypical subunit composition of the chlorophycean mitochondrial F 1FO-ATP synthase and role of asa7 protein in stability and oligomycin resistance of the enzyme, Mol. Biol. Evol. 27 (2010) 1630–1644, http://dx.doi.org/10.1093/molbev/msq049.
[36] L.K. Lee, A.G. Stewart, M. Donohoe, R.A. Bernal, D. Stock, The structure of the peripheral stalk of Thermus thermophilus H+-ATPase/synthase, Nat. Struct. Mol. Biol. 17 (2010) 373–378, http://dx.doi.org/10.1038/nsmb.1761.

[37] H. Miranda-Astudillo, A. Cano-Estrada, M. Vázquez-Acevedo, L. Colina-Tenorio, A. Downie-Velasco, P. Cardol, C. Remacle, L. Domínguez-Ramírez, D. González-Halphen, Interactions of subunits Asa2, Asa4 and Asa7 in the peripheral stalk of the mitochondrial ATP synthase of the chlorophycean alga Polytomella sp, Biochim. Biophys. Acta Bioenerg. 1837 (2014) 1–13, http://dx.doi.org/10.1016/j.bbabio.2013.08.001.

[38] E. Morales-Rios, M.G. Montgomery, A.G.W. Leslie, J.E. Walker, Structure of ATP synthase from Paracoccus denitrificans determined by X-ray crystallography at 4.0 Å resolution, Proc. Natl. Acad. Sci. U. S. A. 112 (2015) 13231–13236, http://dx.doi.org/10.1073/pnas.1517542112.

[39] R. Moreno-Sánchez, R. Covián, R. Jasso-Chávez, S. Rodríguez-Enríquez, F. Pacheco-Moisés, M.E. Torres-Márquez, Oxidative phosphorylation supported by an alternative respiratory pathway in mitochondria from Euglena, Biochim. Biophys. Acta Bioenerg. 1457 (2000) 200–210, http://dx.doi.org/10.1016/S0005-2728(00)00102-X.

[40] S.P. Muench, J. Trinick, M.A. Harrison, Structural divergence of the rotary ATPases, Q. Rev. Biophys. (2011), http://dx.doi.org/10.1017/S0033583510000338.

[41] A.W. Mühleip, F. Joos, C. Wigge, A.S. Frangakis, W. Kühlbrandt, K.M. Davies, Helical arrays of U-shaped ATP synthase dimers form tubular cristae in ciliate mitochondria, Proc. Natl. Acad. Sci. U. S. A. 113 (2016) 8442–8447, http://dx.doi.org/10.1073/pnas.1525430113.

[42] H. Noji, M. Yoshida, The rotary machine in the cell, ATP synthase, J. Biol. Chem. 276 (2001) 1665–1668, http://dx.doi.org/10.1074/jbc.R000021200.

[43] H. Núsková, T. Mráček, T. Mikulová, M. Vrbacký, N. Kovářová, J. Kovalčíková, P. Pecina, J. Houštěk, Mitochondrial ATP synthasome: expression and structural interaction of its components, Biochem. Biophys. Res. Commun. 464 (2015) 787–793, http://dx.doi.org/10.1016/j.bbrc.2015.07.034.

[44] G.T. Oostergetel, W. Keegstra, A. Brisson, Automation of specimen selection and data acquisition for protein electron crystallography, Ultramicroscopy 74 (1998) 47–59, http://dx.doi.org/10.1016/S0304-3991(98)00022-9.

[45] E. Pebay-Peyroula, C. Dahout-Gonzalez, R. Kahn, V. Trézéguet, G.J.-M. Lauquin, G. Brandolin, Structure of mitochondrial ADP/ATP carrier in complex with carboxyatractyloside, Nature 426 (2003) 39–44, http://dx.doi.org/10.1038/nature02056.

[46] E. Perez, M. Lapaille, H. Degand, L. Cilibrasi, A. Villavicencio-Queijeiro, P. Morsomme, D. González-Halphen, M.C. Field, C. Remacle, D. Baurain, P. Cardol, The mitochondrial respiratory chain of the secondary green alga *Euglena gracilis* shares many additional subunits with parasitic Trypanosomatidae, Mitochondrion 19 (2014) 338–349, http://dx.doi.org/10.1016/j.mito.2014.02.001.

[47] D.M. Rees, A.G.W. Leslie, J.E. Walker, The structure of the membrane extrinsic region of bovine ATP synthase, Proc. Natl. Acad. Sci. U. S. A. 106 (2009) 21597–21601, http://dx.doi.org/10.1073/pnas.0910365106.

[48] J. Schaller, B.C. Pellascio, U.P. Schlunegger, Analysis of hydrophobic proteins and peptides by electrospray ionization mass spectrometry, Rapid Commun. Mass Spectrom. 11 (1997) 418–426, http://dx.doi.org/10.1006/abio.1993.1418.

[49] S.H.W. Scheres, RELION: Implementation of a Bayesian approach to cryo-EM structure determination, J. Struct. Biol. 180 (2012) 519–530, http://dx.doi.org/10.1016/j.jsb.2012.09.006.

[50] D. Speijer, C.K.D. Breek, A.O. Muijsers, A.F. Hartog, J.A. Berden, S.P.J. Albracht, B. Samyn, J. Van Beeumen, R. Benne, Characterization of the respiratory chain from cultured Crithidia fasciculata, Mol. Biochem. Parasitol. 85 (1997) 171–186, http://dx.doi.org/10.1016/S0166-6851(96)02823-X.

[51] A.G. Stewart, L.K. Lee, M. Donohoe, J.J. Chaston, D. Stock, The dynamic stator stalk of rotary ATPases, Nat. Commun. 3 (2012) 687, http://dx.doi.org/10.1038/ncomms1693.

[52] D. Stock, C. Gibbons, I. Arechaga, A.G.W. Leslie, J.E. Walker, The rotary mechanism of ATP-synthase, Curr. Opin. Struct. Biol. 10 (2000) 672–679, http://dx.doi.org/10.1016/j.abb.2008.05.004.

[53] A. Stocker, S. Keis, J. Vonck, G.M. Cook, P. Dimroth, The Structural basis for unidirectional rotation of thermoalkaliphilic F1-ATPase, Structure 15 (2007) 904–914, http://dx.doi.org/10.1016/j.str.2007.06.009.

[54] M. Strauss, G. Hofhaus, R.R. Schröder, W. Kühlbrandt, Dimer ribbons of ATP synthase shape the inner mitochondrial membrane, EMBO J. 27 (2008) 1154–1160, http://dx.doi.org/10.1038/emboj.2008.35.

[55] T. Suhai, N.G. Heidrich, N.A. Dencher, H. Seelert, Highly sensitive detection of ATPase activity in native gels, Electrophoresis 30 (2009) 3622–3625, http://dx.doi.org/10.1002/elps.200900114.

[56] F. Supek, L. Supekova, S. Mandiyan, Y.C.E. Pan, H. Nelson, N. Nelson, A novel accessory subunit for vacuolar H+-ATPase from chromaffin granules, J. Biol. Chem. 269 (1994) 24102–24106.

[57] J. Symersky, V. Pagadala, D. Osowski, A. Krah, T. Meier, J.D. Faraldo-Gómez, D.M. Mueller, Structure of the c10 ring of the yeast mitochondrial ATP synthase in the open conformation, Nat. Struct. Mol. Biol. 19 (2012) 485–491, http://dx.doi.org/10.1038/nsmb.2284.

[58] D. Thomas, P. Bron, T. Weimann, A. Dautant, M.-F. Giraud, P. Paumard, B. Salin, A. Cavalier, J. Velours, D. Brèthes, Supramolecular organization of the yeast F1Fo-ATP synthase, Biol. Cell. 100 (2008) 591–601, http://dx.doi.org/10.1042/BC20080022.

[59] M. Vázquez-Acevedo, P. Cardol, A. Cano-Estrada, M. Lapaille, C. Remacle, D. González-Halphen, The mitochondrial ATP synthase of chlorophycean algae contains eight subunits of unknown origin involved in the formation of an atypical stator-stalk and in the dimerization of the complex, J. Bioenerg. Biomembr. 38 (2006) 271–282, http://dx.doi.org/10.1007/s10863-006-9046-x.

[60] S. Wilkens, M. Forgac, Three-dimensional structure of the vacuolar ATPase proton channel by electron microscopy, J. Biol. Chem. 276 (2001) 44064–44068, http://dx.doi.org/10.1074/jbc.M106579200.

[61] S. Wilkens, E. Vasilyeva, M. Forgac, Structure of the vacuolar ATPase by electron microscopy, J. Biol. Chem. 274 (1999) 31804–31810, http://dx.doi.org/10.1074/jbc.274.45.31804.

[62] I. Wittig, H. Schägger, Advantages and limitations of clear-native PAGE, Proteomics 5 (2005) 4338–4346, http://dx.doi.org/10.1002/pmic.200500081.

[63] Z. Zhang, Y. Zheng, H. Mazon, E. Milgrom, N. Kitagawa, E. Kish-Trier, A.J.R. Heck, P.M. Kane, S. Wilkens, Structure of the yeast vacuolar ATPase, J. Biol. Chem. 283 (2008) 35983–35995, http://dx.doi.org/10.1074/jbc.M805345200.

[64] A. Zhou, A. Rohou, D.G. Schep, J.V. Bason, M.G. Montgomery, J.E. Walker, N. Grigorieff, J.L. Rubinstein, Structure and conformational states of the bovine mitochondrial ATP synthase by cryo-EM, Elife 4 (2015) 1–15, http://dx.doi.org/10.7554/eLife.10180.

[65] A. Zíková, A. Schnaufer, R.A. Dalley, A.K. Panigrahi, K.D. Stuart, The F0F1-ATP synthase complex contains novel subunits and is essential for procyclic Trypanosoma brucei, PLoS Pathog. 5 (2009), http://dx.doi.org/10.1371/journal.ppat.1000436.

[66] I.N. Watt, M.G. Montgomery, M.J. Runswick, A.G. Leslie, J.E. Walker, Bioenergetic cost of making an adenosine triphosphate molecule in animal mitochondria, Proc. Natl. Acad. Sci. U. S. A. 107 (2010) 16823–16827.

BBA - Bioenergetics 1859 (2018) 434–444

Contents lists available at ScienceDirect

BBA - Bioenergetics

journal homepage: www.elsevier.com/locate/bbabio

Oxidative phosphorylation supercomplexes and respirasome reconstitution of the colorless alga *Polytomella* sp.

Héctor Miranda-Astudillo[a,d,*], Lilia Colina-Tenorio[a], Alejandra Jiménez-Suárez[a], Miriam Vázquez-Acevedo[a], Bénédicte Salin[b,c], Marie-France Giraud[b,c], Claire Remacle[d], Pierre Cardol[d], Diego González-Halphen[a]

[a] *Departamento de Genética Molecular, Instituto de Fisiología Celular, Universidad Nacional Autónoma de México, Mexico*
[b] *CNRS, UMR5095, IBGC, 1 rue Camille Saint-Saëns, 33077 Bordeaux, France*
[c] *Université de Bordeaux, Campus Carreire, 146 Rue Léo Saignat, 33077 Bordeaux, France*
[d] *Genetics and Physiology of microalgae, InBioS/Phytosystems, University of Liège, Belgium*

ARTICLE INFO

Keywords:
Chlorophycean algae
Oxidative phosphorylation
F_1F_O ATP synthase
Oligomeric complex V
Mitochondrial supercomplexes
Respirasome

ABSTRACT

The proposal that the respiratory complexes can associate with each other in larger structures named supercomplexes (SC) is generally accepted. In the last decades most of the data about this association came from studies in yeasts, mammals and plants, and information is scarce in other lineages. Here we studied the supramolecular association of the F_1F_O-ATP synthase (complex V) and the respiratory complexes I, III and IV of the colorless alga *Polytomella* sp. with an approach that involves solubilization using mild detergents, n-dodecyl-β-D-maltoside (DDM) or digitonin, followed by separation of native protein complexes by electrophoresis (BN-PAGE), after which we identified oligomeric forms of complex V (mainly V_2 and V_4) and different respiratory supercomplexes (I/IV_6, I/III_4, I/IV). In addition, purification/reconstitution of the supercomplexes by anion exchange chromatography was also performed. The data show that these complexes have the ability to strongly associate with each other and form DDM-stable macromolecular structures. The stable V_4 ATPase oligomer was observed by electron-microscopy and the association of the respiratory complexes in the so-called "respirasome" was able to perform *in-vitro* oxygen consumption.

1. Introduction

Mitochondria are thought to be the product of an ancient endosymbiosis of an α-proteobacterium [1], which already contained an oxidative enzymatic system [2] and an ancestral archaeon host [3–7]. Mitochondria play a key role in eukaryotic energetic metabolism by generating ATP primarily through oxidative phosphorylation (OXPHOS). Part of this process involves the respiratory chain which transfers electrons from reduced NADH or succinate to oxygen by a set of protein-bound redox cofactors. Classically, the respiratory chain comprises two mobile electron carriers, ubiquinone and cytochrome *c*, which are located in the inner membrane and in the intermembrane space, respectively, and four multi-protein complexes: complex I (CI or NADH:ubiquinone oxidoreductase, EC 1.5.6.3), complex II (CII or succinate:ubiquinone oxidoreductase, EC 1.3.5.1), complex III (CIII or ubiquinol:cytochrome *c* oxidoreductase, EC 1.10.2.2) and complex IV (CIV or cytochrome *c* oxidase, EC 1.9.3.1). Three of these complexes (CI, CIII and CIV) use the energy from the electron flow to drive the active transport of protons across the membrane, generating the electrochemical gradient that is then utilized by the F_1F_o-ATP synthase (EC 3.6.3.14) to generate ATP [8].

The F_1F_o-ATPases belong to a family of rotary membrane complexes that includes the vacuolar H^+-translocating V_1V_o-ATPase (V-ATPase) and A_1A_o-ATPase (A-ATPase) and that probably originated from a common evolutionary ancestor [9–11]. The most conserved regions of these enzymes correspond to the catalytic core and the rotor domains. For decades, most of the structural studies of the F-type ATP synthases were carried out in the classical models of the bacterium *E. coli*, or in yeast, rat liver or bovine heart mitochondria [12–18]. Pioneering experiments using cleavable cross-linkers [19], polarized photobleaching and recovery techniques [20,21], video-micrography [22,23] and x-ray diffraction studies of ATPase crystals [24–28] allowed the elucidation of the structure and the catalytic mechanism of the F_1/c_{ring} domain.

The subunit composition and the shape of the peripheral stalk vary among the mitochondrial ATP synthases described so far, from the classical yeast and mammalian enzymes [29–32] that resemble the

* Corresponding author.
E-mail address: hvmirandaastudillo@uliege.be (H. Miranda-Astudillo).

https://doi.org/10.1016/j.bbabio.2018.03.004
Received 31 October 2017; Received in revised form 5 March 2018; Accepted 10 March 2018
Available online 11 March 2018
0005-2728/

bacterial one [33], to the atypical stators present in other sources like *Polytomella* sp. [34], *Tetrahymena thermophila* [35], *Trypanosoma brucei* [36] and *Euglena gracilis* [37,38]. The dimeric nature of the mitochondrial ATP synthase is no longer a matter of debate since they are clearly observed in the structures of the purified complexes from *Polytomella* sp. [39] and *Yarrowia lipolytica* [40] obtained by high resolution cryo-electron microscopy. The dimeric shape is also found in the low resolution images of the enzymes isolated from *S. cerevisiae* [41], *E. gracilis* [38] and *T. thermophila* [35]. Electron cryotomography from the membrane-embedded complex of *Paramecium tetraurelia* [42], *S. cerevisiae* [43], *Polytomella* sp. [44], the trypanosomatid enzyme [45] and other sources like *B. taurus, Y. lipolytica*, *P. anserina* and *S. tuberosum* [46] also support this dimeric disposition. In addition, an association of dimers is observed in the membrane which may form two main contact sites: a dimerization interface and an oligomerization interface [46–48]. This oligomerization of the ATP synthase has been proposed to be involved in the generation and maintenance of the mitochondrial cristae [42,43,49–52].

In earlier studies, OXPHOS complexes were proposed to be associated in one functional unit according to the "solid state" theory [53,54]. This idea was later confronted by a "fluid model". In the latter, all membrane proteins and redox components involved in electron transport and ATP synthesis are in constant and independent diffusional motion [55]. More recently, the proposal that the OXPHOS complexes can associate with each other in larger structures named supercomplexes (SC) [56,57] is generally accepted. This association can allow a more efficient transport of electrons to minimize the generation of reactive oxygen species (ROS) during electron transfer reactions [58], and can also be involved in the regulation of the mitochondrial metabolism in response to different stimuli, carbon sources, or stress conditions in a "plasticity model" [59,60]. In this study we present an extensive characterization of the supramolecular association of the OXPHOS complexes of the colorless alga *Polytomella* sp. using mild detergent extraction followed by BN-PAGE. The data show that some of these complexes could re-associate from detergent solubilized species to form stable entities that can be recovered by liquid chromatography.

2. Materials and methods

2.1. Algal strain, growth conditions and mitochondria isolation

Polytomella sp. (strain number 198.80, isolated by *E.G.* Pringsheim) was obtained from the Culture Collection of Algae at the University of Göttingen (SAG) and was grown aerobically without agitation at room temperature in 2-L flasks containing 1 L of culture medium. The culture medium contained sodium acetate 30 mM, bactotryptone 0.2%, yeast extract 0.2% and a mix of trace elements as previously described [61]. Cells were collected in the middle of the logarithmic phase by centrifugation 7000 × *g* for 20 min. The cellular pellet was stored at −80 °C until use. Cells were broken and mitochondria were obtained by differential centrifugation following the described procedure [62].

2.2. Blue Native (BN) and denaturing (SDS) electrophoresis

Mitochondrial proteins were solubilized with 2.0 g n-dodecyl-β-D-maltoside (laurylmaltoside, DDM)/g protein (1.6%), or 4.0 g digitonin/g protein (3.2%) in solubilization buffer (SB) containing 50 mM Tris-HCl, 1.5 mM $MgSO_4$, 100 mM NaCl, 10%glycerol, 1 mM phenylmethylsulfonyl fluoride (PMSF), and 50 μg/mL tosyl-lysyl-chloromethylketone (TLCK) (pH 8.4). The mixture was incubated at 4 °C with gentle stirring for 30 min, and centrifuged at 30,000 × *g* for 30 min. The supernatants were subjected to BN-PAGE [63]. BN-PAGE was carried out in 3%–10% acrylamide gradient gels, 0.05% digitonin was added in the acrylamide gradient when the same detergent was used for solubilization [64]. Denaturing SDS Tricine-PAGE was carried out in 12% polyacrylamide gels as reported [65]. Three dimensional BN/SDS-glycine/SDS-tricine gels were carried out as previously described [38].

2.3. In-gel enzymatic activities

In-gel NADH/NBT oxido-reductase activity was assayed as described previously [66]. *In-gel* cytochrome *c* oxidase activity was determined using diaminobenzidine as described in [67]. *In-gel* ATPase activity was performed as in [64].

2.4. Immunoassays

From BN-PAGE, proteins were electrotransferred onto a nitrocellulose membrane for immunodetection. Membranes were washed, blocked and incubated with antibodies generated in rabbits against the complete NADH:ubiquinone oxidoreductase from *Polytomella* sp. (complex I), subunit 2 from ubiquinol:cytochrome *c* oxidoreductase from *Polytomella* sp. (complex III), and the COX2B subunit from cytochrome *c* oxidase from *Polytomella* sp. (complex IV). Colorimetric detection was carried out using a goat anti-rabbit IgG conjugated with alkaline phosphatase in the presence of nitro blue tetrazolium chloride and 5-bromo-4-chloro-3′-indolyphosphate p-toluidine salt. The images of the polypeptide bands decorated with the insoluble black-purple precipitates were captured in a HP Scanjet G4050.

2.5. ATPase oligomers purification and supercomplex reconstitution by ion exchange chromatography

All steps were performed at 4 °C unless otherwise stated. Two hundred milligrams of mitochondria were solubilized with n-dodecyl-β-D-maltoside as described above. The mixture was incubated with gentle stirring for 30 min, and centrifuged at 90,000 × *g* for 30 min. The supernatant was diluted in 3 volumes of SB supplemented with 0.01% DDM. The sample was loaded onto an anion exchange column (Source 15Q 10/100, 8 mL) connected to an ÄKTA monitor UPC-900 Workstation (GE Healthcare Life Sciences) equilibrated with the same buffer and washed until a constant base line was obtained. The proteins were eluted with a three-step NaCl gradient in SB supplemented with 0.01% DDM using the following program: 10 column volumes (CV) wash with 75 mM NaCl; 20 CV of 75–250 mM NaCl; 10 CV step with 250 mM NaCl; 20 CV linear gradient 250–500 mM NaCl; and a final 5 CV wash with 500 mM NaCl. Three milliliter fractions were collected and visualized by BN-PAGE.

The fractions corresponding to the ATP synthase were pooled (sample A) and the re-associated respiratory supercomplexes (SC) were selected and separated in two different batches depending on the main presence of either complex I or III, named samples B and C, respectively. The samples enriched with re-associated respiratory supercomplexes (samples B and C) were concentrated separately with an Amicon Ultra-15 Centrifugal Filter 100 kDa (EMD Millipore) to a final volume of 3 mL, from which 500 μL aliquots were made and stored at −80 °C until use. An aliquot of each sample was loaded into three lanes of a BN-PAGE gel. After migration, complexes I and IV were detected by specific *in-gel* activity stain, and the last lane was subjected to a 2D-SDS-PAGE in order to identify the subunit profile of each complex.

2.6. ATPase oligomers separation by size exclusion chromatography and density gradients

Sample A (enriched with ATP synthase) was concentrated with an Amicon Ultra-15 Centrifugal Filter 100kDa (EMD Millipore) to a final volume of 1000 μL and used for two independent treatments: size

exclusion chromatography and discontinuous glycerol gradient. 500 μL were injected to a size exclusion Superose 6 10/300 column (GE Healthcare Life Sciences) previously equilibrated with buffer containing Tris-HCl 50 mM, NaCl 150 mM, $MgSO_4$ 1 mM, glycerol 10%, PMSF 1 mM, TLCK 50 μg/ml, and n-dodecyl-β-D-maltoside 0.01% pH 8.4. The elution was carried out at 0.25 mL/min. Fractions of 0.5 mL were collected and visualized with BN-PAGE. A similar sample (500 μL) was loaded onto seven-ml tubes containing a 10 to 50% discontinued glycerol gradient in the same buffer. The gradients were centrifuged at 40000 × *g* for 17 h in a SW41Ti swing out rotor (Beckman Coulter). Fractions of 0.5 mL were collected and visualized on BN-PAGE.

2.7. Preliminary electron microscopy of the ATPase oligomers

The algal oligomeric ATP synthase obtained from the size exclusion chromatography was diluted to a final concentration of 12.5 μg/mL with 20 mM Tris-HCl (pH 8.4) buffer. Samples of 6 μL were applied to glow discharged carbon-coated copper grids for negative staining. Grids were washed twice with water and stained with 1% uranyl acetate for 1 min, dried and examined with a HITACHI H7650 transmission electron microscope (Hitachi High-Technologies Corporation) operating at 120 kV. Images (3284 × 2600 pixels) were recorded on a SC1000 ORIUS 11 Mpx (GATAN).

2.8. Oxygen consumption of the reconstituted respirasome

Oxygen consumption was assessed in a YSI model 5300 oxygraph equipped with a Clark-Type electrode. The reaction vessel was a 200 μL water-jacketed chamber maintained at 30 °C. The activity buffer contained MOPS 50 mM, NaCl 100 mM, DDM 0.01% (pH 7.2). NADH 5 mM was used as electron donor, 2,3-dimethoxy-5-methyl-p-benzoquinone and horse cytochrome *c* were used to complete the electron transfer chain at 5 mM and 50 mM concentrations, respectively. The reaction was initiated with the addition of 160 μg of the reconstituted respirasome (sample B, sample C or a 1:1 mix B + C). Rotenone 500 μM, antimycin A 100 μM and potassium cyanide 50 μM were used as inhibitors of complex I, III and IV, respectively. To observe the inhibitory effect from rotenone or antimycin A the samples were preincubated 30 min in the presence of each inhibitor before starting the measurements.

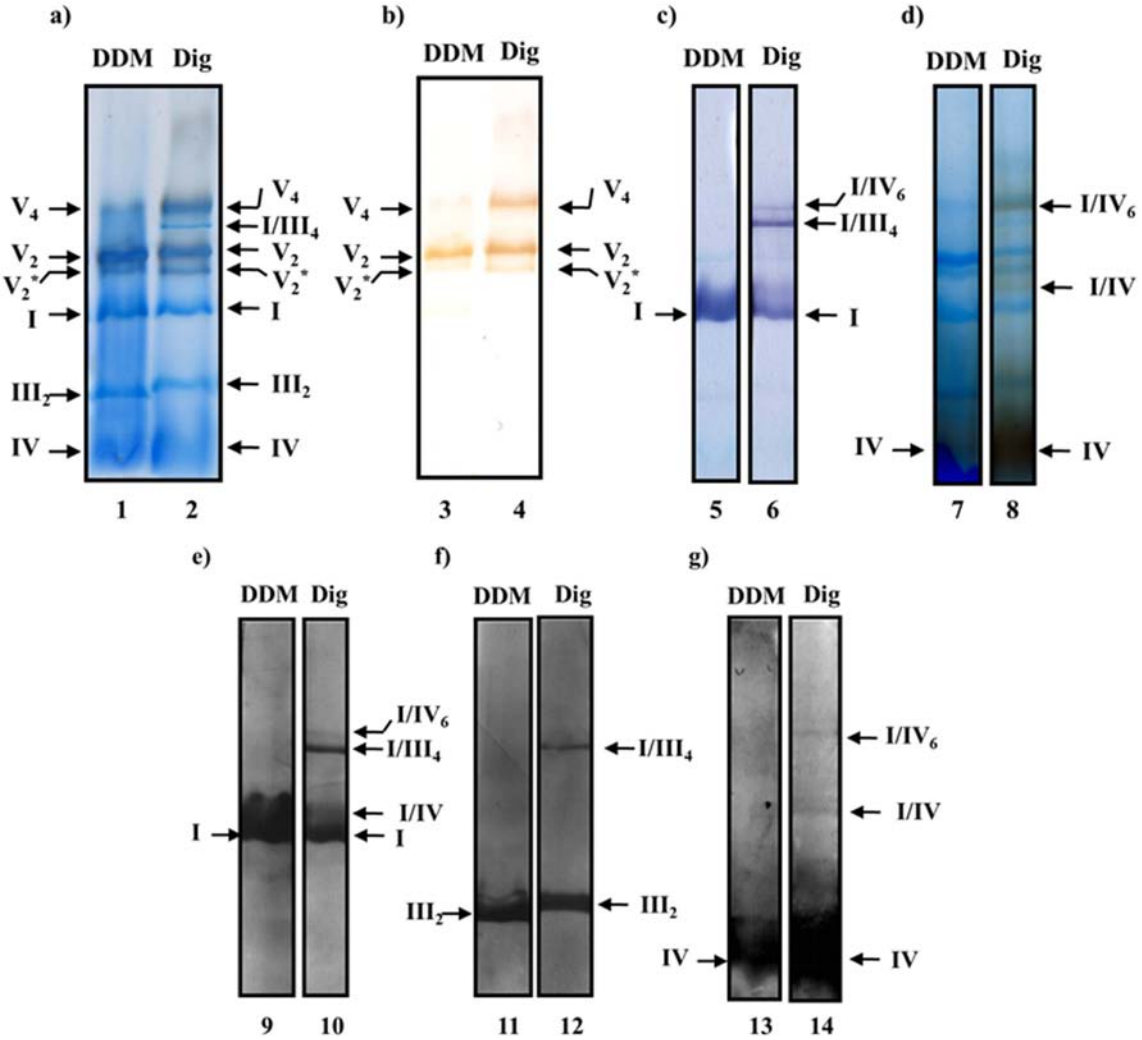

Fig. 1. ATPase oligomers and respiratory supercomplexes in *Polytomella* sp. Isolated mitochondria were solubilized with the indicated detergent: n-dodecyl-β-D-maltoside (DDM) at 2.0 g/g protein or digitonin (Dig) at 4.0 g/g protein. (a) soluble fractions resolved by BN-PAGE in a 3–10% polyacrylamide gradient gel. (b) BN-gel and detection of *in-gel* ATPase activity. The gel was incubated with ATP, $MgSO_4$ and $Pb(NO_3)_2$ (c) *in-gel* NADH-dehydrogenase activity; the BN-gel was incubated in the presence of NADH and Nitro blue tetrazolium chloride (NBT). (d) cytochrome *c* oxidase (COX) *in-gel* activity. The BN-gel was incubated with diaminobenzidine and horse-heart cytochrome *c*. Western blot was performed using antibodies against: (e) the complete NADH:ubiquinone oxidoreductase from *Polytomella* sp.; (f) subunit 2 from ubiquinol:cytochrome *c* oxidoreductase from *Polytomella* sp. and (g) the COX2B subunit from cytochrome *c* oxidase from *Polytomella* sp. Nomenclature used for *Polytomella* sp. mitochondria: I, III and IV for the corresponding mitochondrial complexes, V_2 for the dimeric ATP synthase. Supercomplexes were: I–IV, I–IV_6 and I–III_4 and their stoichiometries are indicated as subindexes. $V_2{}^*$ corresponds to the dimeric complex V with a slight proteolysis in subunits alpha, beta and Asa3 (See Supplemental Fig. S1 for details).

3. Results

3.1. ATPase oligomers and respiratory supercomplexes in Polytomella sp.

Mitochondria from *Polytomella* sp. were solubilized with either DDM (1.6%) or digitonin (3.2%). After removing the insoluble fraction, each sample was subjected to BN-PAGE. When proteins are solubilized with DDM, the 3–10% acrylamide gradient gels stained with Coomasie blue allowed the resolution of the four prominent classical bands corresponding to dimeric complex V (V_2), complex I (I), dimeric complex III (III_2), and complex IV (IV) (Fig. 1 lane 1). Additional bands corresponding to supramolecular complexes could be visualized when other lanes were used to perform immuno-detection (Fig. 1, lanes 9–14) and *in-gel* activity staining (Fig. 1, lanes 3–8) of respiratory complexes I, IV, and V. This linear regression obtained with a relatively high confidence value for the log (molecular mass) *vs* distance migrated ($R^2 = 0.997$) was used to calculate the molecular masses and stoichiometries of these supramolecular associations as described [66] (Fig. S2). The ATP synthase corresponds to two main bands exhibiting ATP hydrolysis activity (Fig. 1 lanes 1–4), both of them migrating above complex I (Fig. 1 lanes 1–2). In addition to the lower band (V_2) corresponds to the previously described dimeric complex V from chlorophycean alga (~1.6 MDa) [68], the upper band (V_4) would correspond to a tetrameric complex V according to its calculated molecular mass (~3.2 MDa). This multimeric complex became more evident when digitonin was used for the solubilization (Fig. 1 lanes 2 and 4). A third fainter band can be observed below the dimeric complex (V_2*) and corresponds to the dimeric complex V exhibiting partial proteolysis of the alpha, beta and Asa3 subunits (Supplemental Fig. S1).

The respiratory complexes I, III_2 and IV migrated as single bands when DDM was used to extract the membranes as revealed with specific antibodies (Fig. 1 lanes 9, 11 and 13). In contrast, when digitonin was used, supramolecular associations of the respiratory complexes could be detected (Fig. 1 lanes 2, 6, 8, 10, 12 and 14). The association of complex III is mainly with complex I giving rise to the I/III_4 SC (Fig. 1 lanes 6, 10 and 12) that has no detectable complex IV, the latter being mainly associated with complex I, forming two I:IV SCs with different stoichiometries (Fig. 1 lanes 6, 8, 10 and 14). No complex III could be detected in these SCs (Fig. 1 lane 12).

3.2. ATPase purification and supercomplex reconstitution by ion exchange chromatography

To further characterize the OXPHOS complexes with a different experimental approach, mitochondria were solubilized with DDM and loaded into an anion exchange column. After washing out the unbound material, the complexes were eluted with a three-step NaCl gradient; Fig. 2A shows a representative elution profile. Each fraction was then submitted to native gel analysis followed by *in-gel* activity staining for complexes I and IV (Fig. 2B). The gradient allowed the separation of the oligomeric complex V (V_2, V_2* and V_4), which eluted earlier than the respiratory complexes and could be recovered in the first peak (sample A). The respiratory complexes I, III and IV were distributed in the two following peaks. All of these three respiratory complexes were found in a mixture of the individual and oligomeric associations in the eluted fractions (Fig. 2B). Complex I eluted mainly in the second peak (sample B) forming a SC with a molecular mass similar to the dimeric ATP synthase (~1.6 MDa). Complex III eluted mainly in the third peak (sample C) together with some SCs containing complexes I and IV (Fig. 2B).

3.3. Separation and characterization of ATPase oligomers

In order to further characterize the nature of the observed oligomeric states of the ATP synthase (Fig. 2B), two additional separation techniques were performed: size exclusion chromatography and glycerol density gradient centrifugation. Fig. 3A shows the fractions eluted from the Superose 6 10/300 GL column (Optimal resolution range: 5–5000 kDa), where a separation of the putative V_4 and V_2 oligomers was observed (Fig. 3A). A faint band could be observed above the V_4. This band showed ATPase activity and was prominent when lower digitonin concentrations were used to solubilize the complexes (Fig. S3A and S3B). This indicates the formation of a higher molecular association (e.g. V_6) after the concentration step. Separation of the main Complex V oligomeric forms was also achieved by density gradient centrifugation (Fig. 3B).

To further validate the presence of the different complex V oligomeric states, electron microscopy images were taken from samples enriched in V_2 and in the putative V_4 oligomers from the size exclusion column (Fig. 3A). The observation of tetramers associated through the membrane domain of the enzyme (Fig. 4) supports our previous suggestion of the presence of a V_4 oligomeric form. To discard possible unspecific, hydrophobic-driven associations due to an insufficient detergent/protein ratio, a mixture of V_4 and V_2 oligomers was incubated with increasing concentration of DDM. Fig. 5A shows that these oligomeric states are able to resist relative high concentrations of DDM, even though some small molecular bands can be observed in the last lanes (> 1%) that could reflect partial dissociation of the complexes. Nevertheless, the two oligomers (V_4 and V_2) remain clearly distinct even at high DDM concentrations. Similarly, increasing concentrations of the zwitterionic surfactant CHAPS had no visible effect on the stability of the V_4/V_2 oligomeric forms (Fig. 5B). Taken together, these results indicate that the supramolecular association of ATP synthase in *Polytomella* sp. gives rise to stable V_2 and V_4 oligomeric states.

To explore if specific subunits are implicated in the formation of the ATP synthase tetrameric complex, fractions enriched with V_2 and V_4 were also analyzed by SDS-PAGE (Fig. 6A). A similar subunit composition and stoichiometry was found for both oligomers (Fig. 6B). Although protease inhibitors were used during the purification procedure, a slight Asa3 subunit degradation (Asa3*) was observed in both the V_2 and V_4 fractions (Fig. 6A). This subunit profile was corroborated when a 2D BN/SDS-PAGE was performed (Fig. S4). As in the extracted complexes (Fig. 1a and b), the purified ATPase oligomers exhibited ATP hydrolysis activity (Fig. S4). Together, these results suggest that the ATPase dimer contains all the subunits required to form higher oligomeric associations.

3.4. Characterization of the reconstituted respirasome

To characterize the composition of the reconstituted respiratory SCs, 2D-BN/SDS-PAGE was performed from enriched fractions obtained from anion exchange chromatography (Fig. 2B). Two lanes from the native first dimension were analyzed by *in-gel* activity stain for complexes I and IV, and the identification of complex III was assessed by its well characterized polypeptide profile [69]. As described above, sample B was enriched with complexes I and IV (Fig. 2B). Complex IV mainly migrated as a free complex, while complex I was distributed into two species, the isolated complex and the so-called "respirasome" ($I/III_2/IV_2$ SC) (Fig. 7A). A higher molecular mass band could be observed; this band does not present cytochrome *c* oxidase activity and possess characteristic polypeptide patterns from complex I and complex III. In accordance with its calculated molecular mass (~3.4 MDa) it could correspond to a I_2/III_4 SC. On the other hand, sample C was enriched with Complex III which mainly migrated independently from the rest of the complexes (Fig. 7B). In contrast with sample B, small quantities of the I/III_2 SC could also be recovered. As in sample B, the three complexes migrated independently; however, small quantities of the reconstituted respirasome ($I/III_2/IV_2$) were observed (Fig. 7B).

To assess the activity of the reconstituted respirasomes *in-vitro*, oxygen consumption was measured upon addition of an electron donor (NADH) and the electron carriers quinone and soluble cytochrome *c*. In both samples B and C, a cyanide-sensitive NADH-dependant oxygen

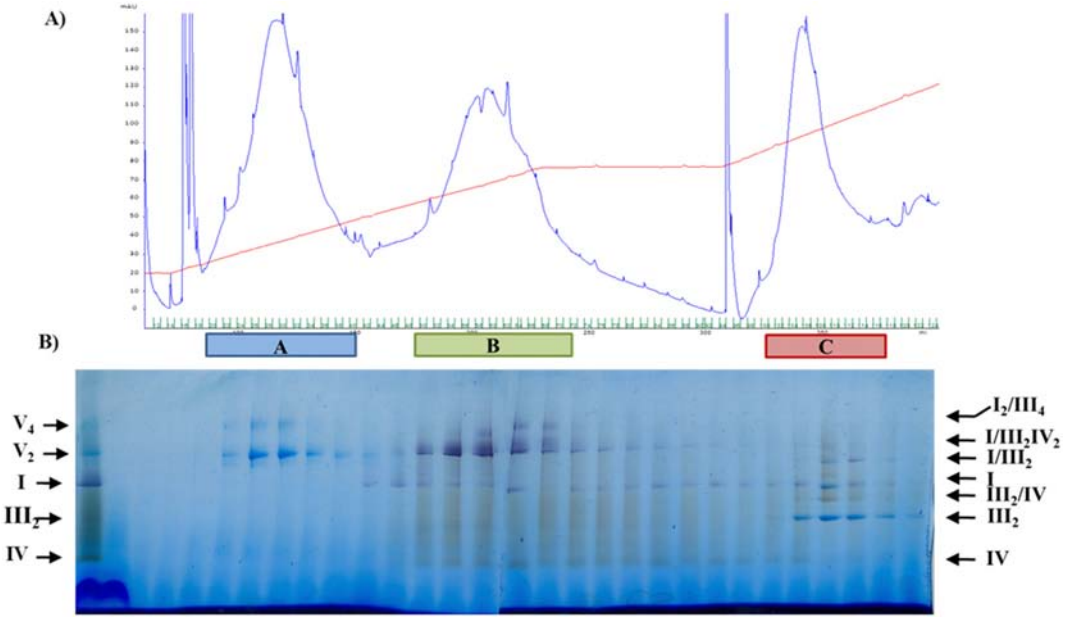

Fig. 2. ATPase oligomers purification and supercomplexes reconstitution by ion exchange chromatography. Two hundred milligrams of mitochondria were solubilized with n-dodecyl-β-D-maltoside and loaded into an anion exchange column, then eluted with a three-step NaCl gradient (see Material and Methods for details). A) Elution profile the blue line is the absorbance at 280 nm, the red line represents the NaCl gradient, the green marks below represent the elution fractions. Three main peaks (samples A, B and C) could be separated. B) BN-PAGE from the fractions corresponding to the samples A, B and C. Sample A corresponds to the ATP synthase oligomers, while sample C and B contain the respiratory supercomplexes. The first lane shows the free complexes obtained after lauryl-maltoside solubilization of the algal mitochondria.

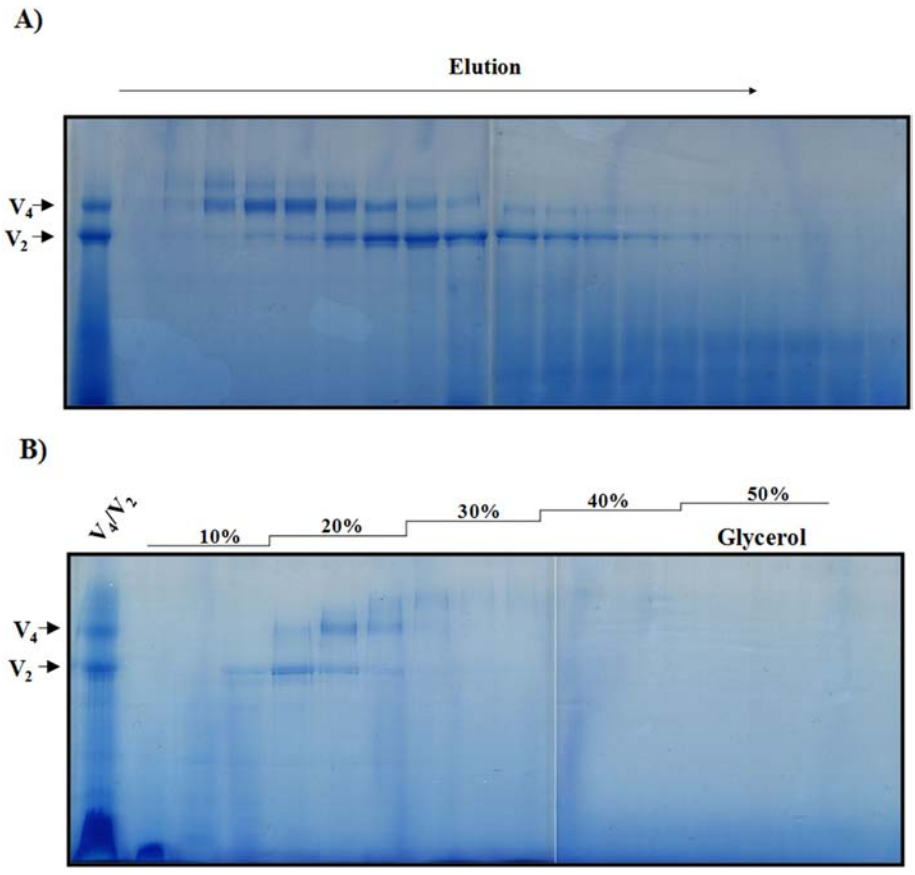

Fig. 3. ATPase oligomers separation by size exclusion chromatography and density gradients. Oligomers of ATP synthase from the anion exchange chromatography (sample A) were separated by two different separation techniques. (A) BN-PAGE of the fractions obtained from the size exclusion chromatography in a Superose 6 10/300 GL column. (B) BN-PAGE of the fractions obtained from a glycerol discontinuous density gradient (10–50%). The first lane in both images represents the loaded sample.

consumption could be measured (Fig. 8). The relative amplitude of observed activities roughly corresponds to the relative amounts of the reconstituted respirasome present in each sample (Figs. 2B, 7A and B). The effects of the specific complex I and III inhibitors, rotenone and antimycin A respectively, were also evaluated. A full inactivation of the reconstituted respirasome was observed only after 30 min incubation at 4 °C in the presence of the inhibitors (Fig. 8 dotted line). Taken together, these results show that the reconstituted respirasome is stable in presence of DDM and exhibits *in vitro* electron transport activity.

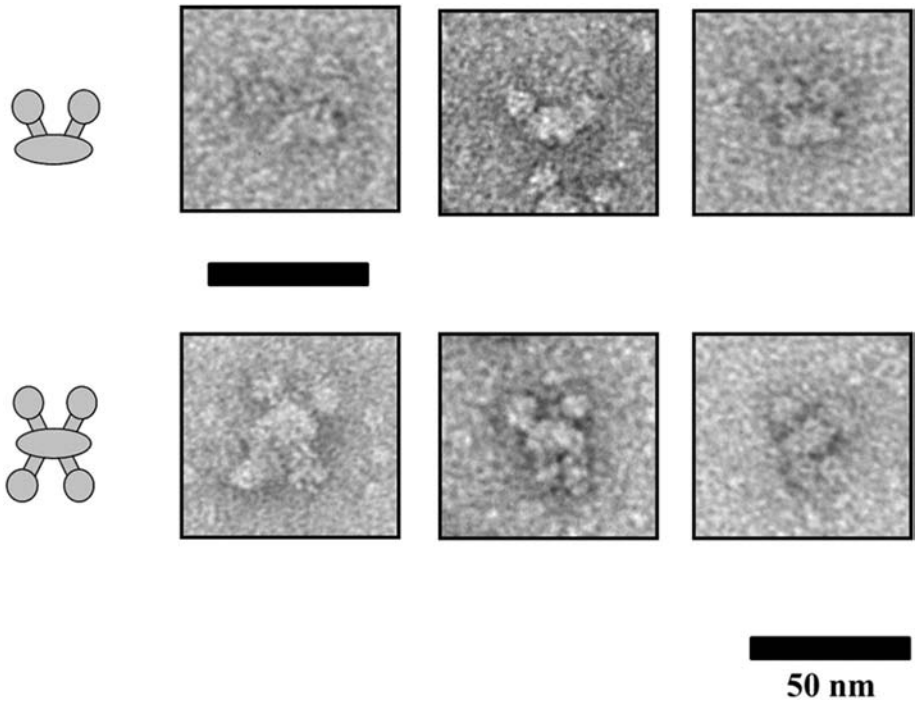

Fig. 4. Electron microscopy images of the ATPase oligomers. Enriched fractions of the dimeric and tetrameric ATP synthase oligomers were analyzed by electron microscopy. Single particles from the EM micrographs. The black line represents 50 nm.

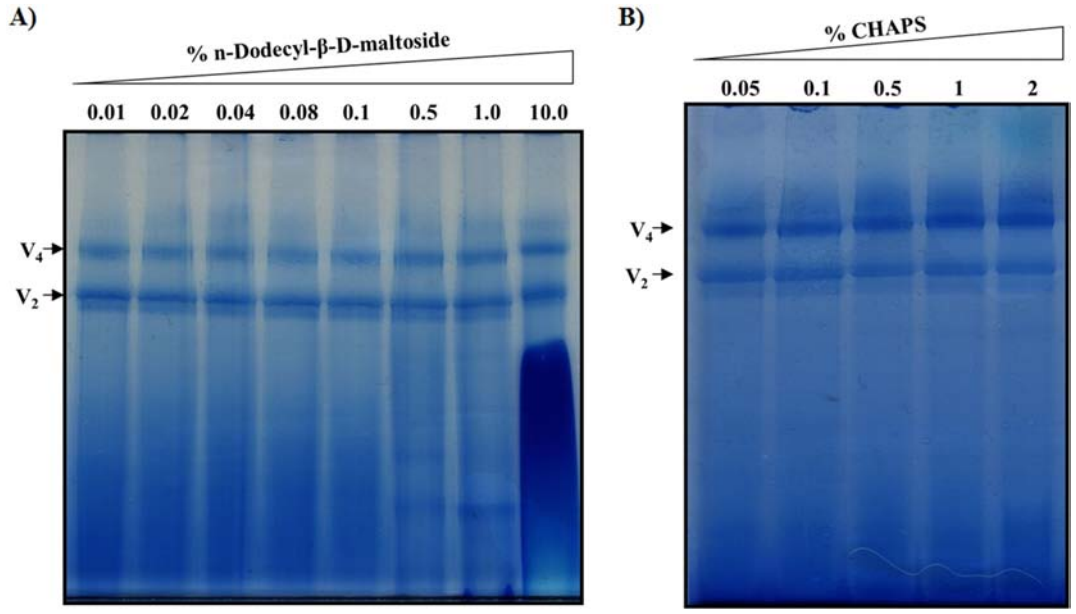

Fig. 5. Stability of the ATP synthase oligomers at increasing concentrations of detergents, the non-ionic DDM and the zwitterionic CHAPS. One hundred microgram of enriched V_2 and V_4 oligomers were incubated 30 min at 4 °C with increasing concentrations of DDM (A) and CHAPS (B). Numbers represent the % concentration of each detergent.

4. Discussion

The *Polytomella* mitochondrial ATP synthase is found forming mainly dimeric and tetrameric complexes, the former being the most prominent form after solubilization with DDM and the latter being more stable in the presence of the milder detergent digitonin. This high stability of the dimeric F_1F_o-ATP synthase is a common feature of chlorophycean algae [70,71]. In contrast, stable dimeric forms in yeast, bovine and rat mitochondria has been previously described only when digitonin was used to solubilize the membranes [51,64,72]. In the presence of DDM, the ATP synthase from these organisms readily dissociates into monomers in BN-PAGE [71,73,74], explaining why this enzyme is usually purified in its monomeric form [27,75,76]. In contrast, in the case of chlorophycean algae, the dissociation of the dimer gives rise to unstable monomers [68,77].

The ATP synthase from *Polytomella* contains atypical polypeptides named Asa subunits [62] that seem to be unique to the chlorophycean lineage [77,78]. It has been proposed that these subunits form the robust peripheral stalk observed in the algal complex [34] and their interactions have been extensively characterized [77,79–82]. Recently, two other ATP synthases were shown to have stable dimers in BN-PAGE when extracted with DDM: the enzymes from *T. brucei* [36] and *E. gracilis* [37,38]. In both cases the subunit composition of the peripheral stalk differs from the yeast/bovine enzyme, but is not related to the

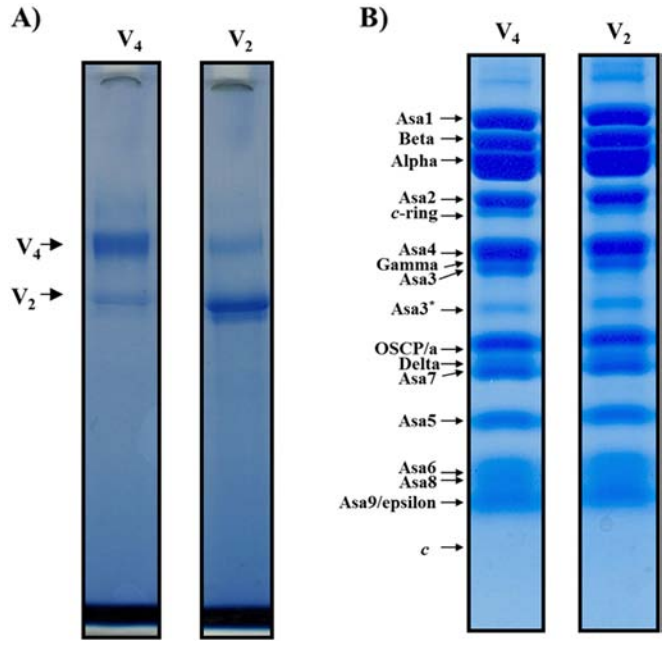

Fig. 6. Subunit composition of the V_2 and V_4 oligomers of the ATP synthase from *Polytomella* sp. BN-PAGE 3–10% acrylamide gradient (A) and SDS-PAGE 12% acrylamide concentration (B) of enriched fractions with V_2 and V_4 oligomers.

chlorophycean one.

All dimeric ATP synthases studied so far have the dimerization interface in the membrane domain. In the yeast ATP synthase the association between monomers occurs mostly inside the membrane, where five supernumerary subunits (e, f, g, i and k) are found associated in the dimeric form of the enzyme [29,40,50,83,84]. A topological model based on crosslink interactions has been proposed for the yeast enzyme [48]. In this model, all the subunits involved in the oligomerization are present in the dimeric complex, similarly, both oligomeric forms of the ATPase from *Polytomella* (V_2 and V_4) seem to have the same subunit composition. Moreover, the fact that the tetrameric or higher oligomerization forms can be enriched and recovered after removing the excess of detergent during chromatographic/concentration steps indicates that all the subunits involved in the oligomerization of the enzyme are present in the dimeric complex. Finally, the electron microscopy images reveal that the interface between both dimers in the V_4 oligomer must be present in the membrane domain. Although the arrangement of the V_4 complex over the carbon grid is not optimal, the four F_1 headpieces are evident and the contact between the dimers is observed across the membrane domain, although in a different plane of the negative staining.

In addition to the protein-protein interactions established by the membrane-embedded subunits, two other interactions between the monomers in the upper region of the peripheral arms have been observed in the *Polytomella* complex. The so-called "Armadillo repeat"-like density links the two monomers in a region just above the membrane, and a "helix–turn–helix" motif halfway through the peripheral stalks seem to reinforce the associations of the two monomers [39]. Fig. 5A and B show the stability of the purified V_2 and V_4 when they are incubated 30 min in presence of high concentrations of DDM or CHAPS. In contrast, when the purified V_2 is incubated overnight with high concentrations of DDM or the amphipathic polymer Amphipol A8–35 the enzyme readily dissociates. First, the F_1 domain separates from the V_2 complex followed by the dissociation of the OSCP, Asa2 and Asa4 subunits. The rest of the V_2 complex, comprising two peripheral stalks with their corresponding membrane domain (a/*c*-ring), migrates as a subcomplex in BN-PAGE [34,80]. This dimeric peripheral stalk complex has been observed by electron microscopy in *Chlamydomonas*

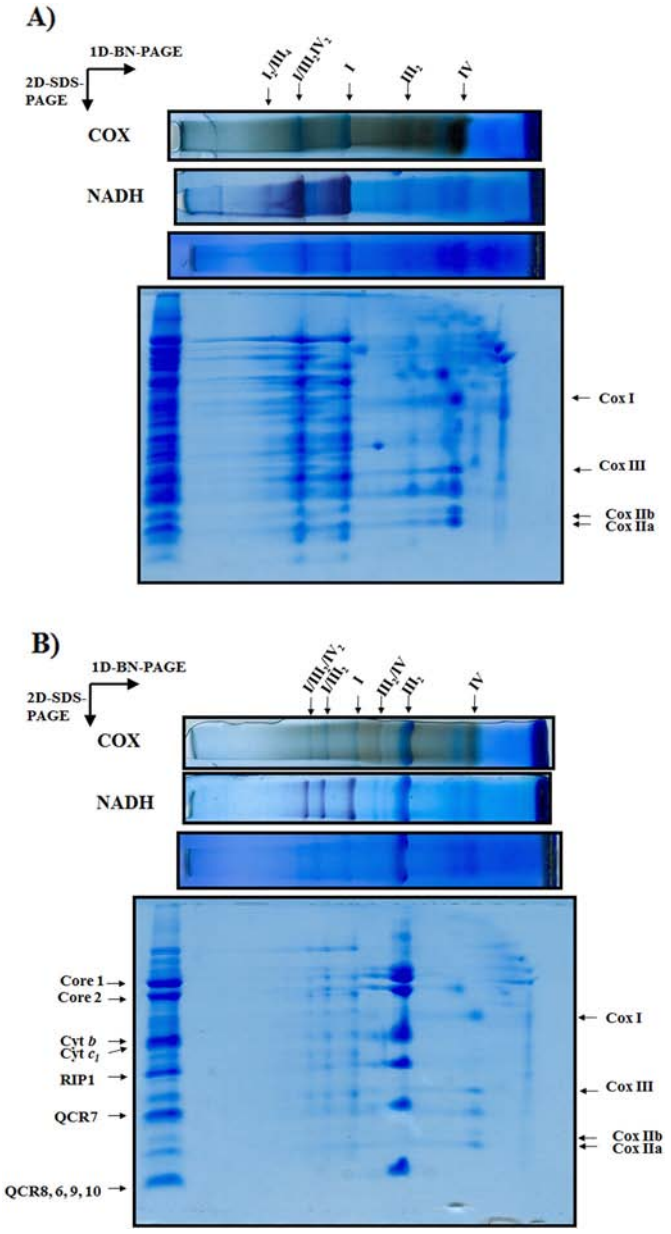

Fig. 7. Characterization of the reconstituted supercomplexes and the respirasome. Samples from the two enriched fractions from the ion exchange column (samples B and C) were subjected to a BN-PAGE and *in-gel* activity stain for complexes I (NADH) and IV (COX). A) Sample B, highly enriched in complex I and in the respirasome; B) sample C, highly enriched in complex III. The subunit composition was analyzed by 2D SDS-PAGE. The main subunits of complexes III and IV are indicated.

reindhardtii partially dissociated preparations (Prof. Egbert Boekema *personal communication*). These partial dissociations could explain the appearance of low molecular mass bands when the enzyme is incubated with increasing concentrations of DDM. We can hypothesize that the two unusual linker domains in the peripheral stalks described above play a major role in the stability of the complex. Subunit Asa7 has been proposed to be the "helix–turn–helix" motif that links both arms in the extrinsic region of the enzyme [34], while the subunit with the "armadillo" motif remains unidentified. All of these observations suggest that the dimeric form (V_2) is the "structural unit" of ATP synthase in chlorophycean algae, and that free monomers most probably do not exist *in vivo*.

The inner mitochondrial membrane folds into structures known as cristae. A 3D model of their shape inside native mitochondria was obtained by EM tomography [85,86]. This model shows two major regions

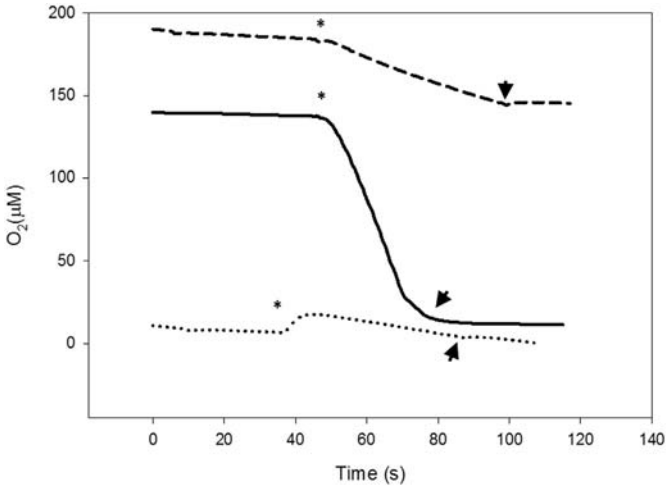

Fig. 8. Oxygen consumption of the reconstituted respirasome. The reconstituted SCs and respirasome were incubated in the presence of 2,3-Dimethoxy-5-methyl-p-benzoquinone and horse cytochrome *c*. NADH was used as electron donor. Oxygen consumption of the sample B (continuous line) and sample C (segmented line). The asterisks indicate the addition the protein sample and the arrow heads indicate the addition of KCN. Evaluation of the inhibitory effect of specific complex III inhibitor antimycin A over sample B is shown (dotted line). The lines were moved along the y axis for clarity.

across the cristae: the lamellar and the tubular. Both regions can be explained in biophysical terms as a way of minimizing the free energy of the system [87], and several studies have linked these structures with complex V dimerization [51,52]. Molecular dynamics simulations showed that the tubular shape of the cristae increases as more ATPase dimers incorporate into rows [42,43]. A highly packed tubular cristae has been described in *Polytomella* mitochondria by electron microscopy and cryo-electron tomography [44,47,88,89]. In these condensed cristae, the membrane domains of each V_2 are in direct contact with the surrounding dimers, but no contact in the extrinsic region can be observed [44].

The electron cryotomography of mitochondria from various organisms revealed the segregation between the respiratory complexes and the row of ATPase dimers [46]. Diverse associations of the respiratory complexes in stoichiometric SCs have been described in various organisms [90]. The respiratory SCs are increasingly accepted as structural entities, although their functional relevance remains unclear. Some explanations include: the structural stabilization of complex I [91], the substrate channeling directly from one electron transfer complex to the next, avoiding the production of reactive oxygen species, the metabolic regulation of all the electron transport chain, or impeding aggregation of the complexes [56,58–60,89,92–96]. Interestingly, when *Polytomella* mitochondria are solubilized with digitonin, no SC containing CI, CIII and CIV was observed; instead three SCs with I and III or I with IV were found (Fig. 1 lanes 6, 8, 10, 12 and 14), suggesting that the *Polytomella* complex I interacts strongly with either complex III or complex IV in an independent manner.

Most studies of the SCs and the respirasome involve the use of the very mild detergent digitonin or amphipol molecules [97–99]. With these detergents high resolution models of respirasomes from bovine (9 Å), ovine (5.8 Å) and porcine (5.4 and 4 Å) were obtained [100–103]. In contrast, when high concentration of DDM (1.6%) are used, all the complex-complex interactions are lost and the SCs dissociate and migrate into individual respiratory complexes (I, III_2 and IV) on BN-PAGE (this study, [62,70,73]). Here we show that DDM-solubilized complexes I, III and IV from *Polytomella* associate into several SCs when excess of detergent is removed (Fig. 2). This reconstitution into the so-called respirasome is however not complete, as free complexes elute separately in the NaCl gradient, probably because of competition between the complex-complex and the complex-matrix interactions. We

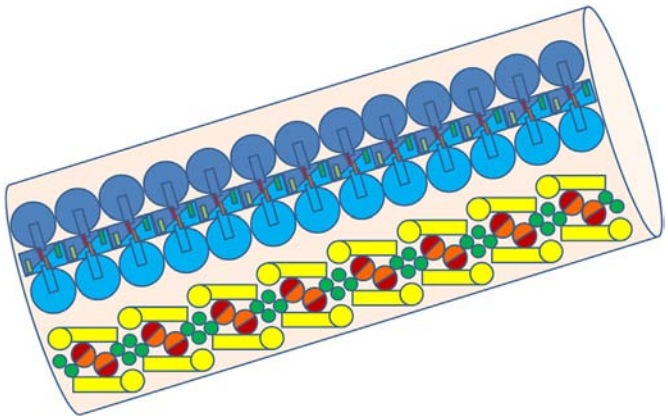

Fig. 9. Model of the association of OXPHOS complexes in *Polytomella* sp. cristae. The ATP synthase dimers are represented with dark blue and monomers with light blue. The association between dimers is by the membrane domain, the two interactions between the monomers in the upper region of the peripheral arms are "Armadillo repeat"-like density (dark and light green) and "helix–turn–helix" motif (red and orange) (see discussion for details). The respiratory complexes are represented in yellow (monomeric complex I), red and orange (dimeric complex III), green (monomeric complex IV).

hypothesize that the CIII-matrix interaction (sample C) is stronger than the CI-matrix interaction (Sample B), albeit some $I/III_2/IV_2$ respirasomes can be recovered in sample B. Meanwhile, CIV shows no significant affinity for the matrix, and seems to be bound to CI or CIII along the gradient. The reconstituted respirasome migrates with a molecular mass similar to the V_2 complex (~1.6 MDa). SCs showed oxygen consumption in presence of NADH after the addition of an excess of external electron carriers (2,3-dimethoxy-5-methyl-p-benzoquinone and horse cytochrome *c*). This result strongly suggests that CoQ and cyt *c* were lost during the solubilization/chromatographic steps. Although functional respirasomes have been already isolated from digitonin-solubilized mitochondria [104], this is, to our knowledge, the first successful reconstitution of a complete DDM-stable and functional respirasome from isolated respiratory complexes.

The data obtained in this work show that the OXPHOS complexes of *Polytomella* have the ability to strongly associate with each other and form two stable macromolecular structures: (i) ATP synthase oligomers formed by the association of dimers, which allow the purification of the V_4 oligomer and (ii) the respirasome, which can be reconstituted *in column* when the excess of DDM is removed. It is likely that the highly condensed and tubular cristae observed in *Polytomella* arise from an extraordinary capacity to maintain a tight association of its OXPHOS complexes (Fig. 9).

Supplementary data to this article can be found online at https://doi.org/10.1016/j.bbabio.2018.03.004.

Transparency document

The Transparency document associated with this article can be found, in online version.

Acknowledgments

We thank Alfredo Octaviano García (IFC, UNAM) for his auxiliary support. P.C. acknowledges financial support from the Belgian Fonds de la Recherche Scientifique F.R.S.-F.N.R.S. (FRFC 2.4597, CDR J.0079) and European Research Council (H2020-EU BEAL project 682580). P.C. is a Senior Research Associate from F.R.S.-FNRS. D.G.H. acknowledges financial support from 279125 Grant ECOS Nord-ANUIES-CONACyT, support from grants 239219 (Fondo SEP-CONACYT) CONACyT and IN208917 (PAPIIT-DGAPA-UNAM) are also acknowledged.

References

[1] Z. Wang, M. Wu, An integrated phylogenomic approach toward pinpointing the origin of mitochondria, Sci. Rep. 5 (2015) 7949, , http://dx.doi.org/10.1038/srep07949.

[2] C.G. Kurland, S.G.E. Andersson, Origin and evolution of the mitochondrial proteome, Microbiol. Mol. Biol. Rev. 64 (2000) 786–820, http://dx.doi.org/10.1128/MMBR.64.4.786-820.2000.

[3] M.W. Gray, B.F. Lang, G. Burger, Mitochondria of protists, Annu. Rev. Genet. 38 (2004) 477–524, http://dx.doi.org/10.1146/annurev.genet.37.110801.142526.

[4] E.V. Koonin, The origin and early evolution of eukaryotes in the light of phylogenomics, Genome Biol. 11 (2010) 209, http://dx.doi.org/10.1186/gb-2010-11-5-209.

[5] W. Martin, M. Müller, The hydrogen hypothesis for the first eukaryote, Nature 392 (1998) 37–41, http://dx.doi.org/10.1038/32096.

[6] A. Spang, J.H. Saw, S.L. Jørgensen, K. Zaremba-Niedzwiedzka, J. Martijn, A.E. Lind, R. van Eijk, C. Schleper, L. Guy, T.J.G. Ettema, Complex archaea that bridge the gap between prokaryotes and eukaryotes, Nature 521 (2015) 173–179, http://dx.doi.org/10.1038/nature14447.

[7] K. Zaremba-Niedzwiedzka, E.F. Caceres, J.H. Saw, D. Bäckström, L. Juzokaite, E. Vancaester, K.W. Seitz, K. Anantharaman, P. Starnawski, K.U. Kjeldsen, M.B. Stott, T. Nunoura, J.F. Banfield, A. Schramm, B.J. Baker, A. Spang, T.J.G. Ettema, Asgard archaea illuminate the origin of eukaryotic cellular complexity, Nature 541 (2017) 353–358, http://dx.doi.org/10.1038/nature21031.

[8] M. Saraste, Oxidative phosphorylation at the fin de siècle, Science 283 (1999) 1488–1494.

[9] R.L. Cross, V. Müller, The evolution of A-, F-, and V-type ATP synthases and ATPases: reversals in function and changes in the H+/ATP coupling ratio, FEBS Lett. 576 (2004) 1–4, http://dx.doi.org/10.1016/j.febslet.2004.08.065.

[10] R.L. Cross, L. Taiz, Gene duplication as a means for altering H+/ATP ratios during the evolution of Fo F1 ATPases and synthases, FEBS Lett. 259 (1990) 227–229, http://dx.doi.org/10.1016/0014-5793(90)80014-A.

[11] S.P. Muench, J. Trinick, M.A. Harrison, Structural Divergence of the Rotary ATPases. (2011), http://dx.doi.org/10.1017/S0033583510000338.

[12] P.D. Boyer, The ATP synthase–a splendid molecular machine, Annu. Rev. Biochem. 66 (1997) 717–749, http://dx.doi.org/10.1146/annurev.biochem.66.1.717.

[13] W. Junge, Protons, proteins and ATP, Photosynth. Res. 80 (2004) 197–221, http://dx.doi.org/10.1023/B:PRES.0000030677.98474.74.

[14] P.L. Pedersen, The machine that makes ATP, Curr. Biol. 4 (1994) 1138–1141.

[15] A.E. Senior, Two ATPases, J. Biol. Chem. 287 (2012) 30049–30062, http://dx.doi.org/10.1074/jbc.X112.402313.

[16] J.E. Walker, The ATP synthase: the understood, the uncertain and the unknown, Biochim. Biophys. Acta Bioenerg. 1817 (2012) S1, http://dx.doi.org/10.1016/j.bbabio.2012.06.013.

[17] J.E. Walker, I.R. Collinson, The role of the stalk in the coupling mechanism of F1F0-ATPases, FEBS Lett. 346 (1994) 39–43, http://dx.doi.org/10.1016/0014-5793(94)00368-8.

[18] M. Yoshida, E. Muneyuki, T. Hisabori, ATP synthase–a marvellous rotary engine of the cell, Nat. Rev. Mol. Cell Biol. 2 (2001) 669–677, http://dx.doi.org/10.1038/35089509.

[19] T.M. Duncan, V.V. Bulygin, Y. Zhou, M.L. Hutcheon, R.L. Cross, Rotation of subunits during catalysis by Escherichia coli F1-ATPase, Proc. Natl. Acad. Sci. U. S. A. 92 (1995) 10964–10968, http://dx.doi.org/10.1073/pnas.92.24.10964.

[20] D. Sabbert, S. Engelbrecht, W. Junge, Functional and idling rotatory motion within F1-ATPase, Proc. Natl. Acad. Sci. U. S. A. 94 (1997) 4401–4405, http://dx.doi.org/10.1073/pnas.94.9.4401.

[21] D. Sabbert, S. Engelbrecht, W. Junge, Intersubunit rotation in active F-ATPase, Nature 381 (1996) 623–625, http://dx.doi.org/10.1038/381623a0.

[22] H. Noji, R. Yasuda, M. Yoshida, K. Kinosita, Direct observation of the rotation of F1-ATPase, Nature 386 (1997) 299–302, http://dx.doi.org/10.1038/386299a0.

[23] H. Noji, M. Yoshida, The rotary machine in the cell, ATP synthase, J. Biol. Chem. 276 (2001) 1665–1668, http://dx.doi.org/10.1074/jbc.R000021200.

[24] J.P. Abrahams, A.G.W. Leslie, R. Lutter, J.E. Walker, Structure at 2.8 (angstrom) resolution of F(1)-ATPase from bovine heart mitochondria, Nature 370 (1994) 621–628.

[25] A. Dautant, J. Velours, M.F. Giraud, Crystal structure of the Mg.ADP-inhibited state of the yeast F 1c10-ATP synthase, J. Biol. Chem. 285 (2010) 29502–29510, http://dx.doi.org/10.1074/jbc.M110.124529.

[26] C. Gibbons, M.G. Montgomery, A.G. Leslie, J.E. Walker, The structure of the central stalk in bovine F(1)-ATPase at 2.4 A resolution, Nat. Struct. Biol. 7 (2000) 1055–1061, http://dx.doi.org/10.1038/80981.

[27] D. Stock, A.G. Leslie, J.E. Walker, Molecular architecture of the rotary motor in ATP synthase, Science 286 (1999) 1700–1705, http://dx.doi.org/10.1126/science.286.5445.1700.

[28] I.N. Watt, M.G. Montgomery, M.J. Runswick, A.G.W. Leslie, J.E. Walker, Bioenergetic cost of making an adenosine triphosphate molecule in animal mitochondria, Proc. Natl. Acad. Sci. U. S. A. 107 (2010) 16823–16827, http://dx.doi.org/10.1073/pnas.1011099107.

[29] I. Arnold, K. Pfeiffer, W. Neupert, R.A. Stuart, H. Schägger, Yeast mitochondrial F1F0-ATP synthase exists as a dimer: identification of three dimer-specific subunits, EMBO J. 17 (1998) 7170–7178, http://dx.doi.org/10.1093/emboj/17.24.7170.

[30] R.J. Devenish, M. Prescott, A.J.W. Rodgers, The structure and function of mitochondrial F1F0-ATP synthases, Int. Rev. Cell Mol. Biol. 267 (2008) 1–58, http://dx.doi.org/10.1016/S1937-6448(08)00601-1.

[31] J. Velours, G. Arselin, The Saccharomyces cerevisiae ATP synthase, J. Bioenerg. Biomembr. 32 (2000) 383–390 http://www.ncbi.nlm.nih.gov/pubmed/11768300.

[32] J.E. Walker, V.K. Dickson, The peripheral stalk of the mitochondrial ATP synthase, Biochim. Biophys. Acta Bioenerg. 1757 (2006) 286–296, http://dx.doi.org/10.1016/j.bbabio.2006.01.001.

[33] J. Weber, ATP synthase: subunit-subunit interactions in the stator stalk, Biochim. Biophys. Acta Bioenerg. 1757 (2006) 1162–1170, http://dx.doi.org/10.1016/j.bbabio.2006.04.007.

[34] M. Vázquez-Acevedo, F. Vega-deLuna, L. Sánchez-Vásquez, L. Colina-Tenorio, C. Remacle, P. Cardol, H. Miranda-Astudillo, D. González-Halphen, Dissecting the peripheral stalk of the mitochondrial ATP synthase of chlorophycean algae, Biochim. Biophys. Acta Bioenerg. 1857 (2015) 1183–1190, http://dx.doi.org/10.1016/j.bbabio.2016.02.003.

[35] P. Balabaskaran Nina, N.V. Dudkina, L.A. Kane, J.E. van Eyk, E.J. Boekema, M.W. Mather, A.B. Vaidya, Highly divergent mitochondrial ATP synthase complexes in *Tetrahymena thermophila*, PLoS Biol. 8 (2010) 3–6, http://dx.doi.org/10.1371/journal.pbio.1000418.

[36] A. Zíková, A. Schnaufer, R.A. Dalley, A.K. Panigrahi, K.D. Stuart, The F0F1-ATP synthase complex contains novel subunits and is essential for procyclic *Trypanosoma brucei*, PLoS Pathog. 5 (2009) e1000436, , http://dx.doi.org/10.1371/journal.ppat.1000436.

[37] E. Perez, M. Lapaille, H. Degand, L. Cilibrasi, A. Villavicencio-Queijeiro, P. Morsomme, D. González-Halphen, M.C. Field, C. Remacle, D. Baurain, P. Cardol, The mitochondrial respiratory chain of the secondary green alga Euglena gracilis shares many additional subunits with parasitic Trypanosomatidae, Mitochondrion 19 ((2014) 338–349, http://dx.doi.org/10.1016/j.mito.2014.02.001.

[38] K.N. Sathish Yadav, H.V. Miranda-Astudillo, L. Colina-Tenorio, F. Bouillenne, H. Degand, P. Morsomme, D. González-Halphen, E.J. Boekema, P. Cardol, Atypical composition and structure of the mitochondrial dimeric ATP synthase from Euglena gracilis, Biochim. Biophys. Acta Bioenerg. 1858 (2017) 267–275, http://dx.doi.org/10.1016/j.bbabio.2017.01.007.

[39] M. Allegretti, N. Klusch, D.J. Mills, J. Vonck, W. Kühlbrandt, K.M. Davies, Horizontal membrane-intrinsic α-helices in the stator a-subunit of an F-type ATP synthase, Nature 521 (2015) 237–240, http://dx.doi.org/10.1038/nature14185.

[40] A. Hahn, K. Parey, M. Bublitz, D.J. Mills, V. Zickermann, J. Vonck, W. Kühlbrandt, T. Meier, Structure of a complete ATP synthase dimer reveals the molecular basis of inner mitochondrial membrane morphology, Mol. Cell 63 (2016) 445–456, http://dx.doi.org/10.1016/j.molcel.2016.05.037.

[41] S.J. Couoh-Cardel, S. Uribe-Carvajal, S. Wilkens, J.J. García-Trejo, Structure of dimeric F1F0-ATP synthase, J. Biol. Chem. 285 (2010) 36447–36455, http://dx.doi.org/10.1074/jbc.M110.144907.

[42] A.W. Mühleip, F. Joos, C. Wigge, A.S. Frangakis, W. Kühlbrandt, K.M. Davies, Helical arrays of U-shaped ATP synthase dimers form tubular cristae in ciliate mitochondria, Proc. Natl. Acad. Sci. U. S. A. 113 (2016) 8442–8447, http://dx.doi.org/10.1073/pnas.1525430113.

[43] K.M. Davies, C. Anselmi, I. Wittig, J.D. Faraldo-Gomez, W. Kuhlbrandt, Structure of the yeast F1Fo-ATP synthase dimer and its role in shaping the mitochondrial cristae, Proc. Natl. Acad. Sci. 109 (2012) 13602–13607, http://dx.doi.org/10.1073/pnas.1204593109.

[44] N.V. Dudkina, G.T. Oostergetel, D. Lewejohann, H.P. Braun, E.J. Boekema, Row-like organization of ATP synthase in intact mitochondria determined by cryo-electron tomography, Biochim. Biophys. Acta Bioenerg. 1797 (2010) 272–277, http://dx.doi.org/10.1016/j.bbabio.2009.11.004.

[45] A.W. Mühleip, C.E. Dewar, A. Schnaufer, W. Kühlbrandt, K.M. Davies, In-Situ Structure of Trypanosomal ATP Synthase Dimer Reveals Unique Arrangement of Catalytic Subunits, PNAS, (2017), http://dx.doi.org/10.1073/pnas.1612386114.

[46] K.M. Davies, M. Strauss, B. Daum, J.H. Kief, H.D. Osiewacz, A. Rycovska, V. Zickermann, W. Kuhlbrandt, Macromolecular organization of ATP synthase and complex I in whole mitochondria, Proc. Natl. Acad. Sci. 108 (2011) 14121–14126, http://dx.doi.org/10.1073/pnas.1103621108.

[47] N.V. Dudkina, S. Sunderhaus, H.P. Braun, E.J. Boekema, Characterization of dimeric ATP synthase and cristae membrane ultrastructure from Saccharomyces and Polytomella mitochondria, FEBS Lett. 580 (2006) 3427–3432, http://dx.doi.org/10.1016/j.febslet.2006.04.097.

[48] J. Habersetzer, W. Ziani, I. Larrieu, C. Stines-Chaumeil, M.F. Giraud, D. Brèthes, A. Dautant, P. Paumard, ATP synthase oligomerization: from the enzyme models to the mitochondrial morphology, Int. J. Biochem. Cell Biol. 45 (2013) 99–105, http://dx.doi.org/10.1016/j.biocel.2012.05.017.

[49] M.F. Giraud, P. Paumard, V. Soubannier, J. Vaillier, G. Arselin, B. Salin, J. Schaeffer, D. Brèthes, J.P. Di Rago, J. Velours, Is there a relationship between the supramolecular organization of the mitochondrial ATP synthase and the formation of cristae? Biochim. Biophys. Acta Bioenerg. 1555 (2002) 174–180, http://dx.doi.org/10.1016/S0005-2728(02)00274-8.

[50] P. Paumard, G. Arselin, J. Vaillier, S. Chaignepain, K. Bathany, J.M. Schmitter, D. Brèthes, J. Velours, Two ATP synthases can be linked through subunits i in the inner mitochondrial membrane of Saccharomyces cerevisiae, Biochemistry 41 (2002) 10390–10396, http://dx.doi.org/10.1021/bi025923g.

[51] M. Strauss, G. Hofhaus, R.R. Schröder, W. Kühlbrandt, Dimer ribbons of ATP synthase shape the inner mitochondrial membrane, EMBO J. 27 (2008) 1154–1160, http://dx.doi.org/10.1038/emboj.2008.35.

[52] D. Thomas, P. Bron, T. Weimann, A. Dautant, M.-F. Giraud, P. Paumard, B. Salin, A. Cavalier, J. Velours, D. Brèthes, Supramolecular organization of the yeast F1Fo-ATP synthase, Biol. Cell. 100 (2008) 591–601, http://dx.doi.org/10.1042/

BC20080022.
[53] D. Keilin, E.F. Hartree, Activity of the cytochrome system in heart muscle preparations, Biochem. J. 41 (1947) 500–502, http://dx.doi.org/10.1042/bj0410500.
[54] E.C. Slater, Keilin, cytochrome, and the respiratory chain, J. Biol. Chem. 278 (2003) 16455–16461, http://dx.doi.org/10.1074/jbc.X200011200.
[55] C.R. Hackenbrock, B. Chazotte, S.S. Gupte, The random collision model and a critical assessment of diffusion and collision in mitochondrial electron transport, J. Bioenerg. Biomembr. 18 (1986) 331–368, http://dx.doi.org/10.1007/BF00743010.
[56] Y. Chaban, E.J. Boekema, N.V. Dudkina, Structures of mitochondrial oxidative phosphorylation supercomplexes and mechanisms for their stabilisation, Biochim. Biophys. Acta Bioenerg. 1837 (2014) 418–426, http://dx.doi.org/10.1016/j.bbabio.2013.10.004.
[57] I. Wittig, H. Schägger, Supramolecular organization of ATP synthase and respiratory chain in mitochondrial membranes, Biochim. Biophys. Acta 1787 (2009) 672–680, http://dx.doi.org/10.1016/j.bbabio.2008.12.016.
[58] D.R. Winge, Sealing the mitochondrial Respirasome, Mol. Cell. Biol. 32 (2012) 2647–2652, http://dx.doi.org/10.1128/MCB.00573-12.
[59] R. Acin-Perez, J.A. Enriquez, The function of the respiratory supercomplexes: the plasticity model, Biochim. Biophys. Acta Bioenerg. 1837 (2014) 444–450, http://dx.doi.org/10.1016/j.bbabio.2013.12.009.
[60] M.L. Genova, G. Lenaz, Functional role of mitochondrial respiratory supercomplexes, Biochim. Biophys. Acta 1837 (2014) 427–443, http://dx.doi.org/10.1016/j.bbabio.2013.11.002.
[61] A. Atteia, R. Van Lis, J. Ramírez, D. González-Halphen, Polytomella spp. growth on ethananol. Extracellular pH affects the accumulation of mitochondrial cytochrome c550, Eur. J. Biochem. 267 (2000) 2850–2858, http://dx.doi.org/10.1046/j.1432-1327.2000.01288.x.
[62] M. Vázquez-Acevedo, P. Cardol, A. Cano-Estrada, M. Lapaille, C. Remacle, D. González-Halphen, The mitochondrial ATP synthase of chlorophycean algae contains eight subunits of unknown origin involved in the formation of an atypical stator-stalk and in the dimerization of the complex, J. Bioenerg. Biomembr. 38 (2006) 271–282, http://dx.doi.org/10.1007/s10863-006-9046-x.
[63] H. Schägger, Native Gel Electrophoresis, in: G. von Jagow, H. Schägger (Eds.), A Pract. Guid. To Membr. Protein Purif, Academic Press, 1994, pp. 81–104.
[64] I. Wittig, H. Schägger, Advantages and limitations of clear-native PAGE, Proteomics 5 (2005) 4338–4346, http://dx.doi.org/10.1002/pmic.200500081.
[65] H. Schägger, Denaturing Electrophoretic Techniques, in: G. von Jagow, H. Schägger (Eds.), A Pract. Guid. to Membr. Protein Purif, Academic Press, 1994, pp. 59–79.
[66] S. Guerrero-Castillo, M. Vázquez-Acevedo, D. González-Halphen, S. Uribe-Carvajal, In *Yarrowia lipolytica* mitochondria, the alternative NADH dehydrogenase interacts specifically with the cytochrome complexes of the classic respiratory pathway, Biochim. Biophys. Acta Bioenerg. 1787 (2009) 75–85, http://dx.doi.org/10.1016/j.bbabio.2008.10.008.
[67] I. Wittig, M. Karas, H. Schägger, High resolution clear native electrophoresis for in-gel functional assays and fluorescence studies of membrane protein complexes, Mol. Cell. Proteomics 6 (2007) 1215–1225, http://dx.doi.org/10.1074/mcp.M700076-MCP200.
[68] A. Villavicencio-Queijeiro, M. Vázquez-Acevedo, A. Cano-Estrada, M. Zarco-Zavala, M. Tuena De Gómez, J.A. Mignaco, M.M. Freire, H.M. Scofano, D. Foguel, P. Cardol, C. Remacle, D. González-Halphen, The fully-active and structurally-stable form of the mitochondrial ATP synthase of Polytomella sp. is dimeric, J. Bioenerg. Biomembr. 41 (2009) 1–13, http://dx.doi.org/10.1007/s10863-009-9203-0.
[69] P. Cardol, F. Figueroa, C. Remacle, L.-G. Franzén, D. González-Halphen, Chapter 13 – Oxidative Phosphorylation: Building Blocks and Related Components, Chlamydomonas Sourceb, 2009, pp. 469–502, , http://dx.doi.org/10.1016/B978-0-12-370873-1.00021-6.
[70] R. van Lis, D. González-Halphen, A. Atteia, Divergence of the mitochondrial electron transport chains from the green alga *Chlamydomonas reinhardtii* and its colorless close relative Polytomella sp, Biochim. Biophys. Acta Bioenerg. 1708 (2005) 23–34, http://dx.doi.org/10.1016/j.bbabio.2004.12.010.
[71] R. van Lis, A. Atteia, G. Mendoza-hernández, D. González-halphen, Identification of novel mitochondrial protein components of Chlamydomonas reinhardtii. A proteomic approach, Plant Physiol. 132 (2003) 318–330, http://dx.doi.org/10.1104/pp.102.018325.proteins.
[72] P. Paumard, J. Vaillier, B. Coulary, J. Schaeffer, V. Soubannier, D.M. Mueller, D. Brèthes, J.P. Di Rago, J. Velours, The ATP synthase is involved in generating mitochondrial cristae morphology, EMBO J. 21 (2002) 221–230, http://dx.doi.org/10.1093/emboj/21.3.221.
[73] R. van Lis, G. Mendoza-Hernández, G. Groth, A. Atteia, New insights into the unique structure of the F0F1-ATP synthase from the chlamydomonad algae Polytomella sp. and *Chlamydomonas reinhardtii*, Plant Physiol. 144 (2007) 1190–1199, http://dx.doi.org/10.1104/pp.106.094060.
[74] I. Wittig, H.-P. Braun, H. Schägger, Blue native PAGE, Nat. Protoc. 1 (2006) 418–428, http://dx.doi.org/10.1038/nprot.2006.62.
[75] J.L. Rubinstein, V.K. Dickson, M.J. Runswick, J.E. Walker, ATP synthase from Saccharomyces cerevisiae: location of subunit h in the peripheral stalk region, J. Mol. Biol. 345 (2005) 513–520, http://dx.doi.org/10.1016/j.jmb.2004.10.060.
[76] J.L. Rubinstein, J.E. Walker, R. Henderson, Structure of the mitochondrial ATP synthase by electron cryomicroscopy, EMBO J. 22 (2003) 6182–6192, http://dx.doi.org/10.1093/emboj/cdg608.
[77] M. Lapaille, A. Escobar-Ramírez, H. Degand, D. Baurain, E. Rodríguez-Salinas, N. Coosemans, M. Boutry, D. Gonzalez-Halphen, C. Remacle, P. Cardol, Atypical subunit composition of the chlorophycean mitochondrial F 1FO-ATP synthase and role of asa7 protein in stability and oligomycin resistance of the enzyme, Mol. Biol. Evol. 27 (2010) 1630–1644, http://dx.doi.org/10.1093/molbev/msq049.
[78] P. Cardol, D. González-Halphen, A. Reyes-Prieto, D. Baurain, R.F. Matagne, C. Remacle, The mitochondrial oxidative phosphorylation proteome of Chlamydomonas reinhardtii deduced from the genome sequencing project, Plant Physiol. 137 (2005) 447–459, http://dx.doi.org/10.1104/pp.104.054148.
[79] A. Cano-Estrada, M. Vázquez-Acevedo, A. Villavicencio-Queijeiro, F. Figueroa-Martínez, H. Miranda-Astudillo, Y. Cordeiro, J.A. Mignaco, D. Foguel, P. Cardol, M. Lapaille, C. Remacle, S. Wilkens, D. González-Halphen, Subunit-subunit interactions and overall topology of the dimeric mitochondrial ATP synthase of Polytomella sp, Biochim. Biophys. Acta Bioenerg. 2010 (1797), http://dx.doi.org/10.1016/j.bbabio.2010.02.024.
[80] L. Colina-Tenorio, H. Miranda-Astudillo, A. Cano-Estrada, M. Vázquez-Acevedo, P. Cardol, C. Remacle, D. González-Halphen, Subunit Asa1 spans all the peripheral stalk of the mitochondrial ATP synthase of the chlorophycean alga Polytomella sp, Biochim. Biophys. Acta Bioenerg. 1857 (2016) 359–369, http://dx.doi.org/10.1016/j.bbabio.2015.11.012.
[81] H. Miranda-Astudillo, A. Cano-Estrada, M. Vázquez-Acevedo, L. Colina-Tenorio, A. Downie-Velasco, P. Cardol, C. Remacle, L. Domínguez-Ramírez, D. González-Halphen, Interactions of subunits Asa2, Asa4 and Asa7 in the peripheral stalk of the mitochondrial ATP synthase of the chlorophycean alga Polytomella sp, Biochim. Biophys. Acta Bioenerg. 1837 (2014) 1–13, http://dx.doi.org/10.1016/j.bbabio.2013.08.001.
[82] L. Sánchez-Vásquez, M. Vázquez-Acevedo, J. de la Mora, F. Vega-deLuna, P. Cardol, C. Remacle, G. Dreyfus, D. González-Halphen, Near-neighbor interactions of the membrane-embedded subunits of the mitochondrial ATP synthase of a chlorophycean alga, Biochim. Biophys. Acta Bioenerg. 1858 (2017) 497–509, http://dx.doi.org/10.1016/j.bbabio.2017.04.004.
[83] S. Brunner, V. Everard-Gigot, R.A. Stuart, Su e of the yeast F1F0-ATP synthase forms homodimers, J. Biol. Chem. 277 (2002) 48484–48489, http://dx.doi.org/10.1074/jbc.M209382200.
[84] V. Everard-gigot, C.D. Dunn, B.M. Dolan, S. Brunner, R.E. Jensen, A. Rosemary, R.A. Stuart, Functional Analysis of Subunit e of the F 1 F o -ATP Synthase of the Yeast Saccharomyces cerevisiae: Importance of the N-Terminal Membrane Anchor Region, Eukaryot. Cell 4 (2005) 346–355, http://dx.doi.org/10.1128/EC.4.2.346.
[85] T.G. Frey, C.A. Mannella, The internal structure of mitochondria, Trends Biochem. Sci. 4 (2000) 1–6, http://dx.doi.org/10.1016/S0968-0004(00)01609-1.
[86] C.A. Mannella, Introduction: our changing views of mitochondria, J. Bioenerg. Biomembr. 32 (2000) 1–4, http://dx.doi.org/10.1023/A:1005562109678.
[87] M. Ghochani, J.D. Nulton, P. Salamon, T.G. Frey, A. Rabinovitch, A.R.C. Baljon, Tensile forces and shape entropy explain observed crista structure in mitochondria, Biophys. J. 99 (2010) 3244–3254, http://dx.doi.org/10.1016/j.bpj.2010.09.038.
[88] N.V. Dudkina, R. Kouřil, J.B. Bultema, E.J. Boekema, Imaging of organelles by electron microscopy reveals protein-protein interactions in mitochondria and chloroplasts, FEBS Lett. 584 (2010) 2510–2515, http://dx.doi.org/10.1016/j.febslet.2010.03.027.
[89] N.V. Dudkina, R. Kouril, K. Peters, H.P. Braun, E.J. Boekema, Structure and function of mitochondrial supercomplexes, Biochim. Biophys. Acta Bioenerg. 1797 (2010) 664–670, http://dx.doi.org/10.1016/j.bbabio.2009.12.013.
[90] H. Schägger, K. Pfeiffer, Supercomplexes in the respiratory chains of yeast and mammalian mitochondria, EMBO J. 19 (2000) 1777–1783, http://dx.doi.org/10.1093/emboj/19.8.1777.
[91] H. Schägger, R. De Coo, M.F. Bauer, S. Hofmann, C. Godino, U. Brandt, Significance of respirasomes for the assembly/stability of human respiratory chain complex I, J. Biol. Chem. 279 (2004) 36349–36353, http://dx.doi.org/10.1074/jbc.M404033200.
[92] J.N. Blaza, R. Serreli, A.J.Y. Jones, K. Mohammed, J. Hirst, Kinetic evidence against partitioning of the ubiquinone pool and the catalytic relevance of respiratory-chain supercomplexes, Proc. Natl. Acad. Sci. 111 (2014) 15735–15740, http://dx.doi.org/10.1073/pnas.1413855111.
[93] N.V. Dudkina, J. Heinemeyer, S. Sunderhaus, E.J. Boekema, H.P. Braun, Respiratory chain supercomplexes in the plant mitochondrial membrane, Trends Plant Sci. 11 (2006) 232–240, http://dx.doi.org/10.1016/j.tplants.2006.03.007.
[94] J.A. Enríquez, Supramolecular organization of respiratory complexes, Annu. Rev. Physiol. 78 (2016) 533–561, http://dx.doi.org/10.1146/annurev-physiol-021115-105031.
[95] H. Schägger, Respiratory chain supercomplexes of mitochondria and bacteria, Biochim. Biophys. Acta Bioenerg. 1555 (2002) 154–159, http://dx.doi.org/10.1016/S0005-2728(02)00271-2.
[96] I. Wittig, R. Carrozzo, F.M. Santorelli, H. Schägger, Supercomplexes and subcomplexes of mitochondrial oxidative phosphorylation, Biochim. Biophys. Acta Bioenerg. 1757 (2006) 1066–1072, http://dx.doi.org/10.1016/j.bbabio.2006.05.006.
[97] T. Althoff, D.J. Mills, J.-L. Popot, W. Kühlbrandt, Arrangement of electron transport chain components in bovine mitochondrial supercomplex I $_1$ III $_2$ IV $_1$, EMBO J. 30 (2011) 4652–4664, http://dx.doi.org/10.1038/emboj.2011.324.
[98] N.V. Dudkina, M. Kudryashev, H. Stahlberg, E.J. Boekema, Interaction of complexes I, III, and IV within the bovine respirasome by single particle cryoelectron tomography, Proc. Natl. Acad. Sci. U. S. A. 108 (2011) 15196–15200, http://dx.doi.org/10.1073/pnas.1107819108.
[99] E. Schäfer, H. Seelert, N.H. Reifschneider, F. Krause, N.A. Dencher, J. Vonck, Architecture of active mammalian respiratory chain supercomplexes, J. Biol. Chem. 281 (2006) 15370–15375, http://dx.doi.org/10.1074/jbc.M513525200.
[100] J. Gu, M. Wu, R. Guo, K. Yan, J. Lei, N. Gao, M. Yang, The architecture of the

mammalian respirasome, Nature 537 (2016) 1–16, http://dx.doi.org/10.1038/nature19359.
[101] J.A. Letts, K. Fiedorczuk, L.A. Sazanov, The architecture of respiratory supercomplexes, Nature 537 (2016) 644–648, http://dx.doi.org/10.1038/nature19774.
[102] J.S. Sousa, D.J. Mills, J. Vonck, W. Kühlbrandt, Functional asymmetry and electron flow in the bovine respirasome, elife 5 (2016) 1–17, http://dx.doi.org/10.7554/eLife.21290.
[103] M. Wu, J. Gu, R. Guo, Y. Huang, M. Yang, Structure of mammalian respiratory supercomplex I1III2IV1, Cell 167 (2016) 1598–1609 e10 https://doi.org/10.1016/j.cell.2016.11.012.
[104] E. Lapuente-Brun, R. Moreno-Loshuertos, R. Acin-Perez, A. Latorre-Pellicer, C. Colas, E. Balsa, E. Perales-Clemente, P.M. Quiros, E. Calvo, M.A. Rodriguez-Hernandez, P. Navas, R. Cruz, A. Carracedo, C. Lopez-Otin, A. Perez-Martos, P. Fernandez-Silva, E. Fernandez-Vizarra, J.A. Enriquez, Supercomplex assembly determines electron flux in the mitochondrial electron transport chain, Science 340 (2013) 1567–1570 (80-.), https://doi.org/10.1126/science.1230381.
[105] A. Atteia, R. Van Lis, G. Mendoza-Hernández, K. Henze, W. Martin, H. Riveros-Rosas, D. González-Halphen, Bifunctional aldehyde/alcohol dehydrogenase (ADHE) in chlorophyte algal mitochondria, Plant Mol. Biol. 53 (2003) 175–188, http://dx.doi.org/10.1023/B:PLAN.0000009274.19340.36.

11.4 Anexo 4: Artículo sometido a revisión

The peripheral stalk of rotary ATPases

Lilia Colina-Tenorio[1], Alain DAUTANT[2], Héctor Miranda-Astudillo[3], Marie-France Giraud[2], Diego Gonzalez Halphen[1*]

[1]Instituto de Fisiología Celular (IFC), Mexico, [2]Université de Bordeaux, France, [3]University of Liège, Belgium

Submitted to Journal:
Frontiers in Physiology

Specialty Section:
Mitochondrial Research

Article type:
Review Article

Manuscript ID:
391773

Received on:
30 Apr 2018

Frontiers website link:
www.frontiersin.org

Conflict of interest statement

The authors declare that the research was conducted in the absence of any commercial or financial relationships that could be construed as a potential conflict of interest

Author contribution statement

LC and DG conceptualization; LC and DG writing the original draft; LC, AD, HM and MG formal analysis; AD, HM and MG reviewing and editing; MG and DG project administration; MG and DG funding acquisition.

Keywords

peripheral stalk, ATP synthase, coiled-coils, Archaea, Bacteria, Mitochondria, chloroplast

Abstract

Word count: 160

Rotary ATPases are a family of enzymes that are thought of as molecular nanomotors and are classified in three types: F, A and V-type ATPases. Two members (F and A-type) can synthesize and hydrolyze ATP, depending on the energetic needs of the cell, while the V-type enzyme exhibits only a hydrolytic activity. The overall architecture of all these enzymes is conserved and three main sectors are distinguished: a catalytic core, a rotor and a stator or peripheral stalk. The peripheral stalks of the A and V-types are highly conserved in both structure and function, however, the F-type peripheral stalks have divergent structures. Furthermore, the peripheral stalk has other roles beyond its stator function, as evidenced by several biochemical and recent structural studies. This review describes the information regarding the organization of the peripheral stalk components of F, A and V-ATPases, highlighting the key differences between the studied enzymes, as well as the different processes in which the structure is involved.

Funding statement

DG and MG acknowledge financial support from 279125 Grant ECOS Nord-ANUIES-CONACyT, and further support for DG from grants 239219 (Fondo SEP-CONACYT) CONACyT and IN208917 (PAPIIT-DGAPA-UNAM).

The peripheral stalk of rotary ATPases

Lilia Colina-Tenorio[1], Alain Dautant[2-3], Héctor Miranda-Astudillo[4], Marie-France Giraud[2-3] and Diego González-Halphen[1*]

[1] Departamento de Genética Molecular, Instituto de Fisiología Celular, Universidad Nacional Autónoma de México, Mexico

[2] CNRS, UMR5095, IBGC, 1 rue Camille Saint-Saëns, 33077 Bordeaux, France

[3] Université de Bordeaux, Campus Carreire, 146 rue Léo Saignat, 33077 Bordeaux, France

[4] Genetics and Physiology of microalgae, InBioS/Phytosystems, University of Liège, Belgium

[*]**To whom correspondence should be adressed:**
Departamento de Genética Molecular, Instituto de Fisiología Celular, Universidad Nacional Autónoma de México, Mexico. Email: dhalphen@ifc.unam.mx

Keywords: peripheral stalk, ATP synthase, coiled-coils, archaea, bacteria, mitochondria, chloroplast

Abstract

Rotary ATPases are a family of enzymes that are thought of as molecular nanomotors and are classified in three types: F, A and V-type ATPases. Two members (F and A-type) can synthesize and hydrolyze ATP, depending on the energetic needs of the cell, while the V-type enzyme exhibits only a hydrolytic activity. The overall architecture of all these enzymes is conserved and three main sectors are distinguished: a catalytic core, a rotor and a stator or peripheral stalk. The peripheral stalks of the A and V-types are highly conserved in both structure and function, however, the F-type peripheral stalks have divergent structures. Furthermore, the peripheral stalk has other roles beyond its stator function, as evidenced by several biochemical and recent structural studies. This review describes the information regarding the organization of the peripheral stalk components of F, A and V-ATPases, highlighting the key differences between the studied enzymes, as well as the different processes in which the structure is involved.

1. Introduction

ATP, a key molecule synthesized by ATP synthases, is instrumental for the metabolism of every living organism (Müller and Grüber, 2003). ATP synthases belong to a family of enzymes known as rotary ATP synthases, which are multiprotein enzymatic complexes embedded in cellular and organellar membranes of all organisms across the three life domains. These enzymes work as nanomotors to synthesize or hydrolyze ATP, and they have been classified in three types: F, V and A-type ATPases.

F-type ATPases are found in the bacterial plasma membrane, in the inner mitochondrial membrane and in the thylakoid membrane of chloroplasts. F-type enzymes use an electrochemical proton gradient to synthesize ATP, according to the basic mechanism proposed by Peter Mitchell in his chemiosmotic theory (Mitchell, 1961). These enzymes, in certain physiological conditions, can function in reverse and hydrolyze ATP to restore the membrane potential (D'Alessandro and Melandri, 2010). V-type ATPases were first purified from vacuoles, hence their name, and work as proton pumps dependent on ATP hydrolysis, which is why they are also known as H^+-ATPases

(Forgac, 2007). A-type ATPases are found in archaea and can function either synthesizing or hydrolyzing ATP (Grüber et al., 2014). The feature all rotary ATPases share is the capacity to couple a membrane domain (the proton channel) with a soluble catalytic domain. Among other things, this coupling is possible because of the structure known as peripheral arm or peripheral stalk, which works as the stator of a motor and whose main role is to counteract the rotation tendency of the catalytic core that happens in response to the movement of the rotor (Walker and Dickson, 2006).

The most widely accepted hypothesis about the origin of rotary ATPases states that they evolved from a common ancestor, which gave rise to the three types of enzymes. Initially, it was proposed that they had at least two transitions in their evolutionary history: the first was the transition from a proton pump to an ATP synthase driven by protons, and the second was the return to a proton pump (Cross and Taiz, 1990). Later, a third transition back to an ATP synthase was proposed, in which there was a gain in function, unlike the first two transitions (Cross and Müller, 2004). It is currently considered that the last universal common ancestor (LUCA) was in all likelihood a chemiosmotic organism with an ATP synthase in its membrane (Mulkidjanian et al., 2007). A-type ATPases are more closely related to V-type ATPases, although the latter cannot synthesize ATP in physiological conditions; it can thus be said that A-type ATPases are more similar to F-type ATPases in terms of mechanism and structure (Forgac, 2007). Given the common origin of A and V-type ATPases, their catalytic subunits and their rotor subunits share 50% identity, while A and F-type ATPases share 25% identity (Müller and Grüber, 2003). On the contrary, the subunits of the peripheral stalk are considerably less conserved, vary from one organism to the next, and no significant identity has been found among them (Muench et al., 2011).

In terms of structure, the three types of ATPases are built in a similar way: a membrane domain (classically known as F_O, V_O, A_O, or R_O to refer to this domain in general) that includes the proton channel; and a soluble domain (classically known as F_1, V_1, A_1, or R_1 to refer to this domain in general) that includes: the catalytic core, the central stalk, which communicates the activity in the proton channel with the catalytic core (Grüber et al., 2014; Qi et al., 2007; Wächter et al., 2011), and one or more peripheral stalks. The number of peripheral stalks has been used to categorize rotary ATPases (Stewart et al., 2013): F-ATPases have one (Figure 1A), A-ATPases have two (Figure 1B) and V-ATPases have three (Figure 1C). Although peripheral stalks have a similar function in all the enzymes, their composition and topology vary.

2. The peripheral stalk

2.1 The structure of the peripheral stalk

As stated above, the peripheral stalk of rotary ATPases works as a stator and mediates the association of the two domains of the enzyme. It is the most divergent component in both sequence and subunit composition, and many roles have been attributed to this structure throughout its study. There are currently high resolution structures of the three types of rotary ATPases from model organisms: bovine (Zhou et al., 2015), yeast (Guo et al., 2017; Hahn et al., 2016; Srivastava et al., 2018; Zhao et al., 2015) and bacteria (Morales-Rios et al., 2015; Sobti et al., 2016), and of their peripheral stalks (Dickson et al., 2006; Oot et al., 2012; Stewart et al., 2012). These structures have shown that, in spite of the lack of sequence homology, the overall architecture of the peripheral stalk is similar in these enzymes (Figure 2).

The peripheral stalk is formed by elongated proteins with alpha helical structures, and their interactions are mediated by coiled coil motifs (Stewart et al., 2013). Coiled coils are a common structural arrangement that is usually adopted by helical proteins, both fibrous and globular, and results from a particular alternate pattern of hydrophobic and hydrophilic amino acid residues in the

sequence of the protein (Lupas, 1996). A coiled coil arrangement can be formed by the association of up to five or more helices in the same orientations (parallel) or in opposite orientations (antiparallel); these helices can belong to the same chain, to different chains, or be consecutive helices of the same polypeptide chain (Lupas and Gruber, 2005). The coiled coil was first described in 1953 by Francis Crick (Crick, 1953), and it has been estimated that approximately 3-5% of all the amino acid residues in proteins can form this kind of structure (Mason and Arndt, 2004).

Three characteristics distinguish coiled coils from other amphipathic helices: i) the periodicity of the hydrophobic residues (3.5 in coiled coils, 3.65 in other helices), ii) the length of the helices (Su et al., 1994) and iii) the packing interactions of the lateral chains. In coiled coils, distinctively, each residue of one helix fits in a space surrounded by two or four residues of the adjacent helix. This type of packing has been called "knobs into holes" or "in register packing" (Lupas, 1996). The amino acids of the pattern that gives rise to coiled coils are essential to maintain the structure of individual helices (through intramolecular interactions), as well as to promote specific interactions between more helices (through intermolecular interactions) (Mason and Arndt, 2004) (Figure 3C).

When the coiling of the helices is left-handed, it is the result of repetitive motifs in the sequence of the protein known as "heptad repeats". Heptad repeats are a seven-residue pattern with an *abcdefg* composition, in which *ad* correspond to hydrophobic residues and *eg* to charged residues (Lupas, 1996). The nature of the residues in positions *ad*, as well as their equivalents in longer patterns, determines the number of chains involved in the formation of one functional unit of coiled coils, as was revealed by the study of the leucine zipper of the yeast transcription factor GCN4 (O'Shea et al., 1991). When the coiling of the helices is right-handed, it can be the result of either "hendecad repeat" motifs, which are eleven-residue patterns with an *abcdefghijk* composition, in which *adeh* correspond to hydrophobic residues; or of quindecad repeats (Stewart et al., 2013) (Figure 3D).

The so called "peptide velcro hypothesis" (Mason and Arndt, 2004) explains the need for the above described elements in three points: i) *ad* positions must be hydrophobic to stabilize dimerization through hydrophobic effect and van der Waals interactions, ii) *eg* positions must be charged to allow for interhelical electrostatic interactions, and iii) *bcf* positions must be hydrophilic because they form helical surfaces that will be exposed to the solvent. Inside all of these motifs there can be one or more discontinuities known as stutters or stammers that contribute to the final arrangement of the structure, and influence the size, number of chains, polarity of the helices and handedness of the coiling (Parry et al., 2008). The distance required by a coiled coil (a super helix) to complete a full turn is known as pitch length, and the angle that each helix maintains with respect to the axis of the super helix is known as pitch angle (Figure 3A) (Lupas, 1996). The pitch length of a super helix that results from hendecad repeats can be from 80 to over 130 nm, and the helices that form the super helix are almost completely parallel (Parry et al., 2008) (Figure 3B).

Hendecad repeat patterns were first described in the subunits of the peripheral stalk of the F-ATPase from *Escherichia coli*, along with the prediction of a right-handed coiling of their helices (Del Rizzo et al., 2002). The proteins that construct the peripheral stalk of rotary ATPases have to cover a distance of more than 100 Å from the membrane to the apex of the enzyme, and in order to achieve this, most of these proteins have adopted long coiled coil structures (Stewart et al., 2013). It should be noted that the most common type of coiling is the left-handed coiling (the proteins that make up the exposed part of the rotor of ATPases also adopt a coiled coil structure, but with a left-handed coiling), which is why the right-handed coiling of the peripheral stalk proteins was initially considered unusual (Stewart et al., 2013, 2014).

2.2 The peripheral stalk of F-ATPases

The simplest known version of the F-type ATPase is the bacterial enzyme: subunits $\alpha_3\beta_3$ of the catalytic core, subunits γ and ε of the rotor, subunits *a* and *c* forming the proton channel and a b_2 dimer forming the peripheral stalk with subunit δ (Weber, 2006) (Figure 4A). In contrast with the peripheral stalk of A and V-type ATPases which is formed by heterodimers, the peripheral stalk of F-ATPases varies considerably in its subunit composition, from two subunits in *E. coli* (Dunn et al., 2000) to nine subunits in organisms like chlorophycean algae (Cano-Estrada et al., 2010; Vázquez-Acevedo et al., 2006).

The peripheral stalk of the enzyme from *E. coli* has been divided in four domains: i) the N-terminal domain that crosses the membrane and interacts with subunit *a* (Dmitriev et al., 1999; Stalz et al., 2003), ii) the binding domain, iii) the dimerization domain, and iv) the C-terminal domain, through which it interacts with subunit δ (known as subunit OSCP in eukaryotic enzymes) (McLachlin et al., 1998) (Figure 4B). Subunit δ/OSCP interacts with subunit α of the catalytic core at the top of the enzyme (Carbajo et al., 2007; Rubinstein and Walker, 2002). It has been determined that the interaction OSCP-α is strong enough to resist the torque generated by the movement of the rotor (Weber et al., 2004). The b_2 dimer associates via a right-handed coiled coil due to the presence of a conserved hendecad repeat in both *b* subunits of *E. coli* (Figure 4C), as well as in those from other prokaryotic organisms (Del Rizzo et al., 2002). The study of chimeras of subunit *b* has shown that it has functional tolerance as long as the residues involved in the dimerization are substituted by others that fit the hendecad repeat pattern and the resulting helices have a right-handed coiling; left-handed coiling results in a lack of oxidative phosphorylation (Bi et al., 2008).

Subunit *b* of *E. coli* has been studied extensively, and this has derived in a better understanding of the structure and function of this protein and, consequently, of the peripheral stalk. Small-angle X-ray scattering studies revealed that the dimerization domain is limited to residues 62-122, and that this part of the protein in solution forms an extended dimer of approximately 95 Å (Del Rizzo et al., 2002) (Figure 4B). Mutations in the dimerization domain result in an assembled enzyme but a lack of oxidative phosphorylation (Cipriano et al., 2006). This observation suggests that the peripheral stalk of the ATPase from *E. coli* has a role beyond that of joining F_O with F_1, for which the correct interaction of the dimer subunits is necessary (Del Rizzo et al., 2006). This possibility has also been explored in the F-ATPase of yeast, in which mutations in the transmembrane segment of subunit 4 (*b*) of the peripheral stalk impact the coupling of proton translocation with catalysis (Razaka-Jolly et al., 1994).

It has been proposed that each *b* subunit has a different role in the enzyme, given by the interactions each one establishes. The ATP synthase is an asymmetric enzyme due to the stoichiometry of its subunits, subunit *b* is the only one present in two copies and so the interactions of it with each monomer cannot be the same. Accordingly, it has been proved that the b_2 dimer is intrinsically asymmetric and that the arrangement of its helices is not "in register" but tends to be "offset" (Claggett et al., 2009; Del Rizzo et al., 2006). This topology has two important consequences: one of the helices of the dimer is skewed towards the N-terminus (b_N) and the other towards the C-terminus (b_C), so the residues occupying these positions are in different microenvironments, thus confirming that the interactions of each subunit *b* are different (Wood and Dunn, 2007).

The study of the individual interactions of each *b* subunit has been approached with crosslinking experiments (Brandt et al., 2013; Deleon-Rangel et al., 2013). It was found that the C-terminus of one of the subunits (b_I) is the part involved in the interaction with δ (Figure 4B). This b_I subunit is the closest to subunit α and is in contact with subunit *a* in the membrane. The other *b* subunit (b_{II}) was found in close proximity to subunit β. Taken together, these results confirm the asymmetric nature of the dimer and demonstrate that each monomer has a different role and position in the

enzyme (Brandt et al., 2013). This asymmetry was further confirmed with the high resolution structures obtained for the *E. coli* enzyme, which show the peripheral stalk contacts alternatively the three α subunits via their N-terminal helices but in a clearly asymmetrical fashion, using a different interface for each of them (Sobti et al., 2016) (Figure 4A).

The peripheral stalk of the F-ATPase of mammals and yeast shares the same subunit composition, with the exception of subunit *h* of yeast, which only has a 20% similarity with its bovine equivalent, F6 (Fujikawa et al., 2015; Velours et al., 2001), but the latter is sufficient to substitute the absence of subunit *h*, as shown by complementation experiments in *S. cerevisiae* (Velours et al., 2001). As is the case in the bacterial enzyme, the C-terminal end of the eukaryotic subunit *b* interacts with the C-terminal end of OSCP (Hahn et al., 2016; Rees et al., 2009; Rubinstein and Walker, 2002). In the bovine enzyme, the exposed part of subunit *b* maintains interactions with subunits *d* and F6, all mediated by coiled coils, which result in an extensive and stable interaction between subunits OSCP-*b*-F6 that spans the complete length of the peripheral stalk, as shown by the crystallographic structure of the soluble section of the enzyme (Rees et al., 2009) (see Figures 2 and 9D). The structure of the *S. cerevisiae* enzyme (at 3.6 Å) shows that subunit F6 has an additional helix, not present in its mammalian equivalent, that is involved in interactions with subunits *b* and *d* (Srivastava et al., 2018) (Figure 4E).

A high resolution structure of the dimeric enzyme of the yeast *Yarrowia lipolytica* was obtained from X-ray diffraction data (3.5 Å) and cryo-electron microscopy images (6.2 Å) (Hahn et al., 2016). The sections obtained with the best resolution were both the exposed and the transmembrane parts of the peripheral stalk. This model showed contacts that had not been described previously, such as the interaction of the N-terminal end of subunit α with subunits *b*, *h* and the N-terminal end of OSCP, all of which define the union of F_1 with the peripheral stalk. The structure of the *S. cerevisiae* enzyme shows that the N terminus of each α subunit interacts with subunit OSCP, thus securely anchoring it to the top of F_1. Furthermore, a helix from one of the α subunits (the one known as α_{TP}) contacts helices from subunits *b*, *d* and F6 (Srivastava et al., 2018) (Figure 4D).

As for the contacts between subunits of the peripheral stalk and subunits located in the membrane section of the enzyme, crosslinking experiments with the bovine enzyme showed that the membrane subunit A6L (also called ATP8 in mammals and 8 in yeast) is in close proximity to subunits *b*, *d* and F6 through its C-terminus, which extends 70 Å from the membrane to reach the peripheral stalk (Lee et al., 2015) . The C-terminal region of subunit 8 in yeast has interactions with subunits *b* and *h* (Stephens et al., 2003). It has been proposed that subunit A6L/8 derived from one of the bacterial *b* subunits and is truncated in mammals and yeast, since there are four conserved residues (MQPL) in their N-terminal region (Hahn et al., 2016). Recently, He and collaborators have suggested that subunits 6.8PL and DAPIT of the mammalian enzyme are functional orthologs of yeast subunits *i*/*j* and *k*, respectively, which would mean that the yeast and human enzymes can be considered identical in composition (He et al., 2018). Subunit *f* is located in the F_O section in the bovine and yeast enzymes (Collinson et al., 1994; Spannagel et al., 1997), and has been found to interact with subunit *b* by crosslinking experiments (Spannagel et al., 1998). Finally, as in the bacterial enzyme, the base of the peripheral stalk of the enzyme of bovine and yeast contacts the F_O section by a *b*-*a* interaction (Spannagel et al., 1998), which has been confirmed with the high resolution structures obtained to date (Baker et al., 2012; Guo et al., 2017; Hahn et al., 2016; Sobti et al., 2016; Srivastava et al., 2018; Zhou et al., 2015) (Figure 4D and 4E, see also Figures 2A and 9D). Recently, the analysis of auto-inhibited *E. coli* F-ATPase structures obtained by cryo-electron microscopy revealed that the peripheral stalk spans almost the entire complex (212 of 232 Å) (Sobti et al., 2016). These structures showed, for the first time for an F-ATPase, the complete homodimeric coiled coil structure with the N-terminus of the *b* subunits bifurcating closely above the membrane to then separate in two helices within the membrane which contact subunit *a* from two sides (Figure 4A and 4B). A recent high resolution structure of the yeast ATPase (at 3.6 Å)

obtained by cryo-electron microscopy has shown the arrangement of the membrane section of the peripheral stalk (Guo et al., 2017). In this structure, subunit *b* is shown to have one transmembrane helix that forms a domain with subunits *e* and *g* and that this domain is connected to its second transmembrane helix by a loop. Subunits *f* and *h* both interact with the peripheral stalk and are thus considered part of this structure: the N-terminal portion of subunit *f* contacts the exposed part of subunit *b*, and subunit 8 has a transmembrane helix in contact with one of the helices of subunit *a* and its C-terminal portion contributes to the formation of the base of the peripheral stalk. Finally, the C-terminal part of subunit *d*, which had not been resolved in previous structures, wraps around subunits 8 and *b* at the base of the peripheral stalk (Guo et al., 2017) Figure 4E and 4F.

In contrast with the F-ATPases described so far, the mitochondrial enzyme of chlorophycean algae such as *Chlamydomonas reinhardtii* and *Polytomella* sp. has several striking features, one of which is the presence of a robust peripheral stalk formed by nine subunits named Asa (ATP Synthase Associated) (Cano-Estrada et al., 2010; van Lis et al., 2007; Vázquez-Acevedo et al., 2006), some of which (Asa6 and Asa9) are involved in the dimerization of the enzyme (Cano-Estrada et al., 2010; Lapaille et al., 2010; Sánchez-Vásquez et al., 2017; Villavicencio-Queijeiro et al., 2009). This enzyme has no clear homologs for any of the subunits that typically form the peripheral stalk, however, some equivalent interactions have been found: subunit Asa1 contacts the C-terminal end of subunit OSCP, which is reminiscent of the *b*-OSCP interaction in the other F-ATPases (Colina-Tenorio et al., 2016). Some of the Asa subunits (Asa1, Asa2, Asa4 and Asa7) are predicted to adopt coiled coil structures (Miranda-Astudillo et al., 2014), which is consistent with the nature of subunits *b* in other F-ATPases and subunits E and G of the peripheral stalk of A and V-type ATPases. Recently, an Asa6-*a* interaction was shown in a three dimensional map generated with cryo-electron microscopy, and it was found that subunit Asa6 has a V-shape similar to that of the N-terminal part (transmembrane) of subunit *b* (Klusch et al., 2017). Although a structural map obtained by cryo-electron microscopy for the *Polytomella* enzyme is available at 7 Å resolution (Allegretti et al., 2015) there is currently no high resolution data to distinguish structural details of the Asa subunits in the peripheral stalk, nevertheless, numerous biochemical studies have established several near-neighbor relationships between the Asa subunits and other constituents of the peripheral stalk. Thus, based on the low resolution map available and the biochemical evidence, a model depicting a possible location of the different subunits can be inferred (Figure 5).

Recently, a convenient new separation of ATP synthase complexes was put forward by Mühleip and colleagues that distinguishes the metazoan-type dimers from the protozoan dimers or those from unicellular algae, the latter included in the protozoan-type. This separation came about when some striking differences became evident with high resolution structures, although the biochemical and genetic evidence, as well as low resolution images, much preceded these structures. Metazoan and protozoan-type dimers differ by both the structure of their peripheral stalks and by their dimeric interface (Mühleip et al., 2017). Other examples of protozoan-type dimers include the F-ATPases from *Trypanosoma brucei* (Zíková et al., 2009), *Tetrahymena thermophila* (Balabaskaran Nina et al., 2010), *Paramecium tetraurelia* (Mühleip et al., 2016) and *Euglena gracilis* (Yadav et al., 2017), all of which have atypical features (Figure 6). As described above, the general architecture of the mammalian, yeast and bacterial enzymes (metazoan-type) is essentially the same, and all of their subunits share homology, whereas so far no homologs for subunits of protozoan-type dimers have been identified and their peripheral stalk structures are highly divergent. It should be noted that the bacterial enzyme has only been detected in monomeric form, and none of the subunits involved in the dimerization in other organisms have been identified. In contrast with this observation, the structural unit of the enzyme from chlorophycean algae is a dimer and it can form highly stable supramolecular associations (tetramers, hexamers) (Miranda-Astudillo et al., 2018).

The F-ATPases of chloroplasts have a very similar subunit composition to the bacterial enzyme (Seelert and Dencher, 2011) and their peripheral stalk is formed by a *bb*' dimer (also called subunits

I and II), both of these subunits are structurally and functionally similar to the bacterial dimer (Rühle and Leister, 2015). However, in both chloroplasts and cyanobacteria, these subunits are not identical and each one has different secondary structure and dimerization domain (Poetsch et al., 2007). The peripheral stalk of this type of ATPase was first detected through the averaging and analysis of electron microscope images (Böttcher et al., 1998). A three dimensional map was obtained later on at 20 Å resolution (Mellwig and Böttcher, 2003). This reconstruction was generated based on cryo-electron microscopy and the peripheral stalk was found to be a thin structure with more prominence in the parts that contact F_1 and F_O. Mellwig and Böttcher suggest there must be communication between F_1 and F_O, and propose the peripheral stalk as the structure responsible of that communication, however, there are no detailed structural or biochemical studies about the topology of its subunits.

2.3 The peripheral stalk of A-ATPases

Archaea have adapted to the most extreme living conditions in terms of temperature, salinity, pressure, pH, etc. Many of them live in substrates that do not allow the synthesis of 1 mole of ATP per mole of substrate (Mayer and Müller, 2014), which is why their energy conservation strategies are different to those of bacteria and eukaryotes, and involve a chemiosmotic mechanism in which their metabolism is coupled to the generation of sodium or proton gradients to drive the synthesis of ATP (Deppenmeier and Müller, 2007). Despite these differences, ATP synthesis occurs quite similarly to how it occurs in F-ATPases, and the overall architecture of the enzyme among the studied species is conserved (Mayer and Müller, 2014).

A-ATPases are formed by the sectors A_1 and A_O, in this case joined by two peripheral stalks (Figure 7A). Sector A_1 contains the catalytic core A_3B_3 and subunits C, D and F of the rotor; and the membrane sector A_O forms the channel for the translocation of ions and protons. Subunit D extends through the hexamer formed by subunits A and B, thus connecting the site of catalysis with the site of proton translocation through subunits *a*-*c* in sector A_O (Grüber et al., 2014). Subunit A of the catalytic core has additional alpha helices in its C-terminus and a "non-homologous region" in its N-terminus region, both of these characteristics are shared with its equivalents in V-ATPases (Radermacher et al., 2001), but not with F-ATPases. An outstanding feature of A-ATPases is the size variation of the *c*-ring and its capacity to couple the binding of different ions with ATP synthesis (Grüber et al., 2014).

Both peripheral stalks of A-ATPases are formed by heterodimers of subunits E and G. In solution, these subunits adopt a helical structure, just as the proteins that form the peripheral stalk in other ATPases (Kish-Trier et al., 2008). The EG heterodimer has a coiled coil structure along its N-terminal region and a globular structure on its C-terminus, the latter has been shown to interact with the N-terminal end of subunit B of the catalytic core by magnetic resonance studies (Kish-Trier and Wilkens, 2009). The interaction of a component of the peripheral stalk with one of the catalytic core appears to be a conserved feature among rotary ATPases, since it has been described for every type of enzyme in the family. Subunit G shares some similarity with the extramembranal part of subunit *b* of F-ATPases, which suggests a common origin (Hunt and Bowman, 1997). Furthermore, the crystallographic structures of subcomplexes corresponding to the peripheral stalk of an A-type ATPase (Lee et al., 2010) and an F-type ATPase (Dickson et al., 2006) show that subunits G and *b* have a very similar elongated helical structure (Muench et al., 2011). Sobti and coworkers found that, although sequence identity is low (22%), the general fold of the soluble portion of the *E. coli* peripheral stalk is very similar to that of the *T. thermophilus* A-ATPase (Lee et al., 2010), which indicates a strong evolutionary pressure for proteins to adopt this type of fold (Sobti et al., 2016).

The first three dimensional structures of complete A-ATPases were obtained with reconstructions from electron microscopy images, at 23 Å for the H^+-ATPase of *Thermus thermophilus* (Bernal and

Stock, 2004) and at 18 Å resolution for the A-ATPase of *Methanococcus jannaschii* (Coskun et al., 2004). With these structures the presence of two peripheral stalks was established, as was their connection with both A_1 and A_O. Additionally, it was found that these peripheral stalks are asymmetric, one is bent towards A_1 and the other has a more vertical disposition. This observation was later confirmed when the crystallographic structure of subunit E was obtained at 3.6 Å for *Pyrococcus horikoshii* (Balakrishna et al., 2012). In this work, when adjusting the obtained structure of subunit E into the three dimensional map of the enzyme, a better fit was found for the bent peripheral stalk, while the same subunit crystallized previously (Lee et al., 2010), showed a better fit to the vertical stalk (Balakrishna et al., 2012).

The crystal structure of the EG heterodimer of the H^+-ATPase of *T. Thermophilus* obtained at a 3.1 Å resolution clearly showed the structure and topology of these subunits (Lee et al., 2010). Both subunits have an enriched repetitive sequence of alanine, leucine, glutamate and arginine residues, and they assemble into an elongated heterodimer with two distinguishable domains: a 140 Å-long right-handed coiled coil region and a globular region formed mainly by the C-terminus of subunit E (Figure 7B). The coiled coil region is formed due to a hendecad repeat pattern in the N-terminus of both subunits, however, in subunit G, this pattern changes to a quindecad repeat that results in a tighter coiling (Figure 7C). The structure of heterodimer EG was fitted into the three dimensional map of the complete enzyme (Bernal and Stock, 2004), which revealed that it is specifically the N-terminus of subunit E the part in contact with the catalytic core (Lee et al., 2010) (Figure 7A).

Contrary to what happens in F-ATPases, the peripheral stalks of A-ATPases do not cross the membrane but are anchored to a collar-like structure in the extramembrane base of the complex, and extend from there to the A_3B_3 hexamer (Bernal and Stock, 2004; Grüber et al., 2014) (Figure 7A). The collar structure is formed by the N-terminal region of subunit *a* (this subunit has also been called *I* in these enzymes), which has an exposed globular domain that can interact with both peripheral stalks (Lau and Rubinstein, 2012; Vonck et al., 2009). The EG heterodimer can be considered to be functionally similar to the b_2 homodimer of the bacterial F-ATPase because each subunit has a different role: subunit E mediates the interaction with the catalytic core and subunit G stabilizes the peripheral stalk (Grüber et al., 2014; Lee et al., 2010).

2.4 The peripheral stalk of V-ATPases

V-type ATPases couple the hydrolysis of ATP with ion transport and they are involved in many cellular processes: vesicular traffic, processing and degradation of proteins, coupled transport of small molecules and acidification of organelles, among others (Stransky et al., 2016). The V_1 sector includes the catalytic core A_3B_3 where ATP is hydrolyzed, and the central rotor formed by subunits D and F. The V_O sector includes the *c*-ring oligomer, subunit *d* and the membrane part of subunit *a* (Forgac, 2007). Both sections are joined by three peripheral stalks formed by heterodimers of subunits E and G, which are anchored to the base of the complex through a collar-like structure made by subunits C, H and the soluble domain of subunit *a* (Rawson et al., 2016).

A particular feature of V-ATPases is their regulatory mechanism, which involves the peripheral stalks. *In vivo* experiments of V-ATPase from insects (Sumner et al., 1995) and yeast (Kane, 1995) suggested that V-ATPases are able to disassemble and reassemble in response to extracellular stimuli. Both *in vivo* and *in vitro* experiments suggest that the regulation happens as a result of a rearrangement of the subunits of the enzyme (Oot and Wilkens, 2012; Tabke et al., 2014). The exact mechanism is still unknown, but the evidence suggests that the subunits of the peripheral stalk should allow some degree of movement to the complex, either to disassemble or reassemble, or to accommodate the rearrangement of its subunits (Oot et al., 2017). Studies of the structure of the EG dimer and an EGC subcomplex have shown that the interaction between these subunits is stronger when they are part of the holoenzyme than when they are in solution, which indicates that a

conformational change of EG/EGC can occur at some point of the regulation (Diepholz et al., 2008).

As mentioned above, sectors V_1 and V_O are joined by three peripheral stalks (Figure 8A). These stalks were first observed in electron microscopy images (Boekema et al., 1997; Muench et al., 2009; Ubbink-kok et al., 2000; Wilkens et al., 2005) and a detailed model of the subunits and their interactions was obtained with the crystallographic structure of the EGC subcomplex of the yeast V-ATPase (Oot et al., 2012), which crystallized in two different conformations at 2.91 and 2.82 Å. These structures clearly show that two of the peripheral stalks (EG1 and EG2) join the highest part of the enzyme with the exposed N-terminus of subunit *a*, and the third stalk (EG3) interacts with subunit C, which has no homologs in A and F-type ATPases (Figure 8B). The crystallographic structure of subunit C showed that it is formed by two globular domains, which have been called "head" and "foot", separated by a coiled coil stretch (Drory et al., 2004) (Figure 8B). It was later determined that the EG-C interaction is crucial to maintain the stability of the EG heterodimer, and that the interaction is mediated by the "head" domain of subunit C (Oot and Wilkens, 2010).

The EG heterodimer of yeast V-ATPase forms a long structure (of approximately 150 Å) and when bound to subunit C, the subcomplex EGC_{head} (of approximately 170 Å) maintains an elongated shape (Oot et al., 2012) (Figure 8C). The interaction between subunits E and G is stronger in the N and C-terminal ends and weaker in the middle of the helices, and it is due to hendecad repeat patterns that cause a right-handed coiled coil interaction (Oot et al., 2012). The presence of this characteristic structure reinforces the idea that the right-handed coiling is a conserved feature of the proteins that build the peripheral stalks of rotary ATPases (Stewart et al., 2013).

The complete structure of the V-ATPase of *Saccharomyces cerevisiae* was obtained at 11 Å resolution from cryo-electron microscopy studies of protein particles in ice (Benlekbir et al., 2012). This structure shows the contact of the three peripheral stalks with V_1, given by the N-terminal end of the E subunits with the B subunits of the catalytic core (Figure 8A). It can also be seen that each EG heterodimer interacts with different subunits of the collar-like structure (subunits *a*, C and H): EG1 interacts with the N-terminal ends of subunits *a* and H; EG2 with the N-terminal end of subunit *a* and the "foot" of subunit C; and EG3 only contacts the "head" of subunit C (Figure 8B). In this enzyme, the only contact between a peripheral stalk and the membrane sector is given by the interaction of EG2 with subunit *a* (Benlekbir et al., 2012).

3. The roles of the peripheral stalk

All the interactions described so far clearly establish the role of the peripheral stalk as the structure responsible for connecting the two sectors that form ATPases, the membrane sector and the catalytic core. Having discussed that, the following section describes the different roles that have been attributed to the peripheral stalks and the latest proposals based on the growing wealth of structural information.

3.1 The role of the peripheral stalk in the flexibility of the complex

Evidently, rotary ATPases are dynamic structures that exhibit some degree of flexibility that allows all the movements that are necessary for the enzyme to function correctly (Neukirch et al., 2008; Stewart et al., 2012, 2013; Walker and Dickson, 2006). The notion that the peripheral stalk is a flexible structure has been controversial and has evolved. The flexibility property was first assigned to the *b* subunits of the F-ATPase of *E. coli*, based on experiments in which residues were added or removed from these subunits and the enzyme remained functional (Sorgen et al., 1998, 1999). Years later it was proposed that the peripheral stalk is a rigid structure (Dickson et al., 2006; Rees et al., 2009), and that the need for flexible elements is fulfilled by other components of the enzyme

(Wächter et al., 2011). In recent years, cryo-electron microscopy studies suggest that the peripheral stalk, to a certain extent depending on the type of ATPase, is indeed a flexible structure (Mazhab-Jafari and Rubinstein, 2016).

Subunits *a* and *c* of the F_O sector form two aqueous half channels that define the path followed by protons, which drive the movement of the rotor (*c*-ring $_+$ γδε) in order for catalysis to occur (F_1). This fact, as well as the key residues involved in proton translocation, were first proposed by Vik and Antonio in 1994 based on mutagenesis experiments, and both were confirmed over twenty years later by cryo-electron microscopy studies (Allegretti et al., 2015; Guo et al., 2017; Vik and Antonio, 1994). It is well known that each complete turn of the rotor generates, on average, three ATP molecules (Yasuda et al., 1998), and that each turn requires the translocation of a certain number of protons, depending on the number of *c* subunits present in the *c*-ring (Pogoryelov et al., 2012). This difference or asymmetry between what goes into the complex and what comes out (8-15 H^+:3 ATP) requires the temporal storage of energy during the movement and its gradual release to drive each 120° turn of the rotor (Cherepanov et al., 1999; Junge et al., 2009; Walker and Dickson, 2006). Another way of looking at this phenomenon is to consider rotation steps: sector F_1 has a three-step rotation (given by the three β subunits), while sector F_O has an 8 to 15-step rotation (depending on the number of *c* subunits). This difference has been called rotational asymmetry and it is buffered by the transmission of elastic energy between the two sectors of the enzyme (Saroussi et al., 2012). Taken together, these observations imply that there have to be flexible elements in the enzyme capable of storing and transmitting elastic energy.

Experiments performed with single molecules of the F-ATPase of *E. coli*, in which certain domains are "stiffened" by artificial disulfide bonds and their elasticity is measured, identified the lower part of the rotor (γδ + *c*-ring) as an elastic domain (Sielaff et al., 2008). Other studies have evaluated the magnitude and determinants of the elasticity of the peripheral stalk of the bacterial ATPase, comparing wild type and mutant enzymes with modified *b* subunits, and have concluded that the peripheral stalk is a rigid structure and the most elastic elements are located in the central rotor and the lever of subunit β (Wächter et al., 2011). These authors suggest that, in the *E. coli* enzyme, the peripheral stalk works as a scaffold between F_O and F_1, and that the rotor (at least ten times more flexible) is responsible for the transmission of elastic energy between them.

In light of the latest evidence, obtained by cryo-electron microscopy, the stiffness that had been assigned to the peripheral stalk is now being reconsidered. Structures in more than one conformational state have been generated for the bovine F-ATPase (Zhou et al., 2015), which show the transitions of the enzyme. Two transitions of the peripheral stalk are visible: a bend towards the top part of the enzyme close to subunit OSCP and a bend towards the transmembrane part of subunit *b* (Figure 9A). The authors conclude that the flexibility and movement capacity of all the components of the enzyme (the *c*-ring showed considerable rotational flexibility) contribute to facilitate the coupling of the rotor movement (F_O) with catalysis (F_1). Similarly, cryo-electron microscopy studies from the V-ATPase of *S. cerevisiae* allowed the reconstruction of 3D structures in three conformational states (Zhao et al., 2015). In this enzyme, as in the bovine enzyme, most of the subunits show conformational changes. The obtained structures of the yeast enzyme show that the helical part of rotor subunit D (equivalent to subunit γ of F-ATPases) remains rigid during rotation, but the part in contact with subunit *d* can bend. It is also evident that the catalytic subunits A and B press on subunits E and G of the peripheral stalks, which then bend along their coiled coil regions (Figure 9B). Even more flexibility is observed when considering the EG-C interaction, since subunit C can twist without losing contact with the peripheral stalks.

In contrast with what was observed in F and V-type ATPases, the analysis of the rotational states of the A-ATPase of *T. thermophilus* (Schep et al., 2016) revealed that the conformational changes of its subunits are minimal, which would suggest a less flexible enzyme (Figure 9C). The authors

discuss that this can be due to the fact that this enzyme has a larger rotational asymmetry (3:12) compared to the one of the yeast V-ATPase (3:10) and bovine F-ATPase (3:8), which may cause it to adopt an energetically favorable rotational state in which most of the images are obtained, resulting in an apparent lack of flexibility.

3.2 The role of the peripheral stalk on the stability and assembly of the complex

The study of the role of the peripheral stalk in the assembly process of the complex and how it contributes to its stability refers mostly to F-ATPases. The study of different mutations in the F-ATPase of *E. coli* revealed that subunit δ (OSCP) is essential for the assembly of the b_2 dimer with the rest of the complex, independent of its interaction with subunit α (Hilbers et al., 2013). Additionally, the authors conclude that subunit δ is also important to join the peripheral stalk with the rotor, therefore contributing to the stability and functionality of the complex.

Most of the information available concerning the assembly of F-ATPases has derived from the study of yeast mutants. In this organism, radioactive and pulse-chase labeling experiments have allowed the elucidation of a part of the assembly process, which involves two separate sub complexes: *a*-8-peripheral stalk and F_1-c_{10}, which are generated in an independent but coordinated way (Rak et al., 2011). A dimeric complex named INA (Inner Membrane Assembly) was identified and proposed to act as a sort of chaperone for the assembly of the enzyme (Lytovchenko et al., 2014). The loss of this complex, composed by subunits Ina17 and Ina22, causes the dissociation of sectors F_1 and F_O, and it was found that subunit Ina22 associates transiently with both F_1 and the peripheral stalk, but not with the assembled enzyme, which confirms its role as an auxiliary factor. Lytovchenko and collaborators propose an alternative to the assembly route proposed by Rak and coworkers that includes an F_1-peripheral stalk sub complex. It was then proposed that INAC prevents premature interaction of assembly intermediates and promotes the correct assembly of the *c*-ring with subunit *a* to form the proton translocation portion of the enzyme (Naumenko et al., 2017). A recent study with human ATPase mutants showed that, although the human and yeast ATPases are highly similar, the assembly pathways of the proton translocation channel are different (He et al., 2018; Song et al., 2018).

Native electrophoresis studies have shown that human F-ATPase can assemble if subunits *a* and A6L are missing and even form oligomers, albeit unstable and in low quantities (Wittig et al., 2010). It has also been shown that human cells fail to assemble ATPase if the expression of subunit *d* is inhibited, which causes the accumulation of two sub complexes: F_1-*c* and *b*-*e*-*g* (Fujikawa et al., 2015). Thus, in the human enzyme, the complete peripheral stalk is necessary to maintain the stability of the complex and its oligomers, and the rotor and the peripheral stalk seem to be formed independently and only assemble when subunit *d* is recruited. So far, the evidence related to the assembly of the peripheral stalk in the mammalian enzyme suggests that one of the earlier steps is the assembly of membrane subunits *e* and *g* with the transmembrane segment of subunit *b*, and then subunit *d* is recruited and associates with the exposed part of subunit *b* (Fujikawa et al., 2015) (Figure 10).

3.3 The role of the peripheral stalk in the dimerization and oligomerization of F-ATPases

Another one of the processes in which the peripheral arm is involved is the dimerization of the enzyme. It is currently well known that F-ATPases form dimers that are arranged in rows along the inner mitochondrial membrane (Davies et al., 2011; Strauss et al., 2008; Thomas et al., 2008), and that such oligomerization is directly involved in the morphogenesis of the mitochondrial cristae (Davies et al., 2012; Dudkina et al., 2005; Fronzes et al., 2006; Mühleip et al., 2016; Paumard, 2002). Membrane subunits *e* and *g* have been identified as responsible for the stabilization of yeast (Arnold et al., 1998, 1999; Davies et al., 2012) and bovine (Minauro-Sanmiguel et al., 2005) ATP

synthase dimers. However, it has also been proposed that subunit *i* of the peripheral stalk participates in this process, since there is evidence that this subunit forms homodimers that are located close to the dimerization interface (Paumard et al., 2002), and that the enzyme can be found as a dimer in the absence of subunits *e* and *g* (Fronzes et al., 2006). In addition to this, a study of interactions monitored by FRET showed that the yeast F-ATPase is capable of forming oligomeric associations *in vivo* in the absence of subunit *e* (Gavin et al., 2005), so the authors propose the existence of two dimerization interfaces, one mediated by subunits *e* and *g,* and another mediated by the transmembrane segment of subunit *b*.

In addition to the biochemical studies, structural studies of the yeast F-ATPase have provided information about how the peripheral stalk can participate in the dimerization process. A study involving the reconstruction of the yeast enzyme (from electron cryo-tomography images at an estimated resolution of 3.7 nm) and the analysis of dimer and oligomer formation *in situ* with molecular dynamics (Davies et al., 2012; Mühleip et al., 2016) showed that ATPase monomers associate through the membrane part of the peripheral stalk and that subunits *e*, *g* and 4 are part of the dimerization interface and essential for that process to occur. Furthermore, the N-terminal end of subunit *g* is exposed to the mitochondrial matrix (Belogrudov et al., 1996), and crosslinking experiments have proved that this segment is in close proximity to subunit 4 (equivalent to subunit *b*) (Soubannier et al., 2002). The proximity of subunits *g* and 4 is in agreement with the structure obtained by Guo and collaborators (Guo et al., 2017).

The role of subunit 4 in the dimerization/oligomerization of the yeast enzyme has been studied with directed mutagenesis of the loop that joins the transmembrane segments of this subunit (Weimann et al., 2008). This loop is necessary to organize and stabilize the neighboring subunits *a*, *e* and *g*, and hence essential to maintain the supramolecular species of ATPase. In support of this result, and highlighting the role of the peripheral stalk in the dimerization process, there is evidence that suggests that the loss of the first transmembrane segment of subunit 4 results in a functional enzyme that is incapable of forming dimers or oligomers (Soubannier et al., 2002). Concerning the formation and maintenance of ATPase dimers, the dimerization interface of the yeast enzyme has been proposed to be stabilized by 4-4, *e*-*g* and *a*-*a* interactions (Habersetzer et al., 2013) or by *a*/6-*i* interactions (Guo et al., 2017), but see also the work of Anselmi and coworkers (Anselmi et al., 2018) (Figure 11). The *a*-*a* interface was first demonstrated by Velours and coworkers with crosslinking experiments (Velours et al., 2011) and it was recently confirmed with the high resolution structure of the enzyme, in which another interface mediated by subunits *i/j* is proposed (Guo et al., 2017).

A three dimensional model of the dimeric F-ATPase of the ciliate *Paramecium tetraurelia* was generated at 2.6 nm resolution from electron cryo-tomography of isolated mitochondrial membranes (Mühleip et al., 2016). This structure allowed the construction of a model to explain the formation of mitochondrial cristae in this organism. The authors found that the curvature of the membrane is imposed by the base of the peripheral stalks, thus creating the cristae, and that this phenomenon causes the association of dimers into rows along the membrane. These observations imply that, in *P. tetraurelia*, dimerization occurs mainly through the membrane section of the peripheral stalk and such process is the immediate cause of cristae formation (Mühleip et al., 2016). A similar case is the one of *S. cerevisiae*, in which the bending of the membrane is due to a domain formed by transmembrane subunits *e* and *g* and approximately 50 residues from the N-termini of subunit *b* (Guo et al., 2017).

4. Conclusions

All the work that has been done to deepen the understanding of the peripheral stalk has consistently shown that it is an essential component of all rotary ATPases. The information obtained from highly diverse organisms, from bacteria to human and including archaea and parasites, confirms that, in spite of being a variable structure, the nature of its subunits (from their size and secondary structure to their arrangement into right-handed coiled coils), as well as their interactions and functions, are all conserved. That being said, the organisms whose ATPase has divergent features also need to be considered, since there is growing evidence regarding these enzymes suggesting that they may be the exception to the rule.

High resolution structures of rotary ATPases have confirmed most of the previous biochemical evidence and have contributed relevant new information. These structures have not only allowed to observe the interactions of each component of the peripheral stalk, but also the different conformations in which they can be found, thus confirming both the existence and the need for flexibility in rotary ATPases, partly due to the peripheral stalk itself. The observed dynamics allowed by the nature of the subunits of the peripheral stalk and the interactions that they keep with the rest of the subunits of the enzyme have led some to think that sector R_O can communicate and coordinate with what happens in sector R_I, even though they are over 100 Å apart (Stewart et al., 2013); the available evidence postulates the peripheral stalk as the main candidate for establishing such communication. In the case of F-ATPases, the detailed analysis of the structure of the peripheral stalk has shown that it is involved in processes beyond the catalytic function of the enzyme. Much of the evidence related to the dimerization and oligomerization of F-ATPases indicates that the peripheral stalk, at least the transmembrane section, is crucial for the formation and maintenance of the supramolecular associations of the enzyme and, consequently, of the peculiar mitochondrial morphology.

Based on all that has been discovered to date, it can be concluded that rotary ATPases are indeed highly dynamic enzymes, and that this characteristic is not only imposed by the mobile elements but also by those that had initially been considered static, as is the case of the peripheral stalk. Finally, and especially considering the latest studies, it can be said that the observed distortions of the enzyme involve the contribution of individual subunits, from the peripheral stalk and other parts, and illustrate the fine orchestration that this rotary enzyme is capable of building up in order to reach its maximal efficiency.

Figure 1. Rotary ATPases. A. Schematic representation of an F-ATPase (top) and three dimensional structure of the bovine heart mitochondria F-ATPase (bottom) (Zhou et al., 2015) EMD 3164. **B.** Schematic representation of an A-ATPase (top) and three dimensional structure of the *Thermus thermophilus* A-ATPase (bottom) (Schep et al., 2016) EMD 5335. **C.** Schematic representation of a V-ATPase (top) and three dimensional structure of the *Saccharomyces cerevisiae* V-ATPase (bottom) (Zhao et al., 2015) EMD 6285. All the three dimensional maps were generated from electron cryo-microscopy images. The colors in the schematizations represent: catalytic core in green and violet, central rotor in orange, *c*-ring oligomer in blue, subunit *a* in hot pink and peripheral stalks in dark purple. The arrowheads point to the peripheral stalk(s).

Figure 2. Peripheral stalks of rotary ATPases. A. Models of the peripheral stalk from the F-ATPase of *Escherichia coli* (left) and *Bos taurus* (right), corresponding to the PDBs 5T4O (Sobti et al., 2016) and 5FIL (Zhou et al., 2015), respectively. **B.** Model of one of the peripheral stalks from the A-ATPase of *Thermus thermophilus* corresponding to the PDB 3V6I (Stewart et al., 2012). **C.** Model of one of the peripheral stalks from the V-ATPase of *Saccharomyces cerevisiae* corresponding to the PDB 3J9V (Zhao et al., 2015).

Figure 3. Coiled coils exemplified with the EG heterodimer from the peripheral stalk of the A-ATPase of *Thermus thermophilus*. A. The pitch length and pitch angle are indicated on the coiled coil helices of the EG heterodimer. **B.** Models to illustrate the right-handed coiling of the helices of the EG heterodimer. **C.** Amino acid residues involved in the interaction of the helices of the EG heterodimer. The residues corresponding to positions *adeh* of the hendecad (subunit E) and quindecad (subunit G) repeats are indicated. **D.** Hendecad and quindecad repeat patterns indicated on the sequence of subunits E and G from different species of archaea. The model in A, B and C corresponds to the structural data deposited with the PDB 3V6I (Stewart et al., 2012), with subunit E in yellow and subunit G in magenta.

Figure 4. Peripheral stalk of prokaryotic and eukaryotic F-ATPases. A. Three dimensional model of the enzyme of *Escherichia coli* in which the peripheral stalk and the F_O sector are colored. **B.** Model to highlight the domains in which the *b* subunits have been divided: δ-interaction domain in green, dimerization domain in orange and *a*-interaction domains (transmembrane segments) in hot pink. **C.** Model to illustrate the right-handed coiled coil domain of the b_2 dimer. The model used in A, B and C corresponds to the structural data deposited with the PDB 5T4O (Sobti et al., 2016), with subunit δ in green, subunits *b* in dark teal and cyan, subunit *a* in hot pink and *c*-ring in blue. **D.** Three dimensional model of the enzyme of *Saccharomyces cerevisiae* in which the peripheral stalk and the F_O sector are colored. The helix of subunit α that contacts *b*, *d* and F6 is indicated with a gray arrow. **E.** Peripheral stalk of the yeast ATPase highlighting its components. The additional helix of subunit F6 is indicated with a purple arrow. **F.** Surface representation to illustrate the coiled coil interactions in the extrinsic part of the yeast peripheral stalk. The model used in D, E and F corresponds to the structural data deposited with the PDB 6CP6 (Srivastava et al., 2018), with subunit OSCP in green, subunit *b* in cyan, subunit F6 (*h*) in purple, subunit *d* in salmon, subunit *f* in pale yellow, subunit 8 in pink, subunit *j* in dark blue, subunit *a* in hot pink and *c*-ring in blue.

Figure 5. Working model of the dimeric mitochondrial ATPase of *Polytomella* sp. The image shows the working model of the 3D structure of the enzyme fitted in the EMD-2852 map contoured at 6 sigma (Allegretti et al., 2015). Color scheme: F_1 sector in pink; OSCP in violet; Asa2 in cyan; Asa4 in deep purple; Asa7 in sky blue; Asa1 in yellow; Asa3 in brown (dirty violet); Asa5 in salmon; Asa6 in gray; Asa8 in orange; Asa9 in leaf green; subunit a in deep teal and *c*-ring in pale cyan.

Figure 6. Protozoan and metazoan type dimers. Projection maps of dimeric ATP synthases from **A.** *Polytomella* sp. (Dudkina et al., 2005). The black bar represents 10 nm. **B.** *Euglena gracilis* (Yadav et al., 2017) **C.** *Tetrahymena thermophila* (Balabaskaran Nina et al., 2010) representing protozoan-type dimers; and **D.** *Saccharomyces cerevisiae* (Couoh-Cardel et al., 2010) representing a metazoan-type dimer.

Figure 7. Peripheral stalk of the *Thermus thermophilus* A-ATPase. A. Three dimensional model of the archaeal enzyme (Schep et al., 2016) PDB 5GAR, in which the peripheral stalks and the collar-like structure made by subunit *a* are colored. **B.** Model of the EG heterodimer in which the coiled coil domain and the globular domain are indicated. **C.** Model of the EG heterodimer that illustrates the right handed coiling of the helices and the two types of coiling that result from the hendecad motifs in both subunits, and quindecad repeat motifs in subunit G. The model used in B and C corresponds to the structural data deposited with the PDB 3V6I (Stewart et al., 2012), with subunit E in yellow and subunit G in magenta.

Figure 8. Peripheral stalk of the *Saccharomyces cerevisiae* V-ATPase. A. Three dimensional model of the yeast enzyme in which the peripheral stalks and the subunits of the collar-like structure are colored. **B.** Model that illustrates the interaction of each peripheral stalk (EG1, EG2, EG3) with the subunits of the collar. The different sections of subunit C are indicated. **C.** Models of the EG heterodimer to illustrate the right handed coiling of the helices. The model used in A, B and C corresponds to structural data deposited with the PDB 3J9V (Zhao et al., 2015), with subunit E in orange, subunit G in dark violet, subunit H in red, the exposed part of subunit *a* in pink and subunit C in green.

Figure 9. Flexibility of the peripheral stalk of rotary ATPases. Flexibility of the peripheral stalk illustrated with the transitions it goes through during the process of rotational catalysis. **A.** Models that correspond to the transitions of an F-ATPase peripheral stalk; PDBs 5ARI, 5ARA, 5FIL from (Zhou et al., 2015). **B.** Models that correspond to three rotational states of one of the peripheral stalks of the V-ATPase of *S. cerevisiae*; PDBs 3J9T, 3J9U, 3J9V from (Zhao et al., 2015). **C.** Models that correspond to two rotational states of one of the peripheral stalks of the A-ATPase of *T. thermophilus*; PDBs 5GAR, 5GAS from (Schep et al., 2016).

Figure 10. Assembly process of the peripheral stalk of the human F-ATPase. The assembly pathway corresponds to the one proposed by (Fujikawa et al., 2015) and is exemplified with the bovine enzyme, PDB 5FIL from (Zhou et al., 2015).

Figure 11. Schematic representation of the dimerization of the yeast F-ATPase. Model of the F_O section in which all the subunits involved in the dimerization are colored: subunit *a* in hot pink, subunit *b* in cyan, subunit *e* in brown, subunit *g* in pale blue, subunit *j* in dark blue and subunit *k* in lemon. The dimerization interface includes the subunits proposed by (Guo et al., 2017; Habersetzer et al., 2013). The model corresponds to the structural data deposited with the PDB 6B2Z (Guo et al., 2017).

Conflict of interest statement

The authors declare that this review was written in the absence of any commercial or financial relationships that could be construed as a potential conflict of interest.

Author contributions statement

LC and DG conceptualization; LC and DG writing the original draft; LC, AD, HM and MG formal analysis; AD, HM and MG reviewing and editing; MG and DG project administration; MG and DG funding acquisition.

Funding

DG and MG acknowledge financial support from 279125 Grant ECOS Nord-ANUIES-CONACyT, and further support for DG from grants 239219 (Fondo SEP-CONACYT) CONACyT and IN208917 (PAPIIT-DGAPA-UNAM).

Acknowledgements

The technical assistance of Q.B.P. Miriam Vázquez-Acevedo is gratefully acknowledged.

References

Allegretti, M., Klusch, N., Mills, D. J., Vonck, J., Kühlbrandt, W., and Davies, K. M. (2015). Horizontal membrane-intrinsic α-helices in the stator a-subunit of an F-type ATP synthase. *Nature* 521, 237–240. doi:10.1038/nature14185.

Anselmi, C., Davies, K. M., and Faraldo-Gómez, J. D. (2018). Mitochondrial ATP synthase dimers spontaneously associate due to a long-range membrane-induced force. *J. Gen. Physiol.*, jgp.201812033. doi:10.1085/jgp.201812033.

Arnold, I., Pfeiffer, K., Neupert, W., Stuart, R. A., and Schägger, H. (1999). ATP Synthase of Yeast Mitochondria. *J. Biol. Chem.* 274, 36–40. doi:10.1074/jbc.274.1.36.

Arnold, I., Pfeiffer, K., Neupert, W., Stuart, R. a, and Scha, H. (1998). Yeast mitochondrial F 1 F 0 -ATP synthase exists as a dimer: identi cation of three dimer-speci c subunits. *EMBO J.* 17, 7170–7178.

Baker, L. A., Watt, I. N., Runswick, M. J., Walker, J. E., and Rubinstein, J. L. (2012). Arrangement of subunits in intact mammalian mitochondrial ATP synthase determined by cryo-EM. *Proc. Natl. Acad. Sci.* 109, 11675–11680. doi:10.1073/pnas.1204935109.

Balabaskaran Nina, P., Dudkina, N. V., Kane, L. A., van Eyk, J. E., Boekema, E. J., Mather, M. W., et al. (2010). Highly Divergent Mitochondrial ATP Synthase Complexes in Tetrahymena thermophila. *PLoS Biol.* 8, 3–6. doi:10.1371/journal.pbio.1000418.

Balakrishna, A. M., Hunke, C., and Grüber, G. (2012). The structure of subunit e of the Pyrococcus horikoshii OT3 A-ATP synthase gives insight into the elasticity of the peripheral stalk. *J. Mol. Biol.* 420, 155–163. doi:10.1016/j.jmb.2012.04.012.

Belogrudov, G. I., Tomich, J. M., and Hatefi, Y. (1996). Membrane topography and near-neighbor relationships of the mitochondrial ATP synthase subunits e, f, and g. *J. Biol. Chem.* 271, 20340–20345. doi:10.1074/jbc.271.34.20340.

Benlekbir, S., Bueler, S. A., and Rubinstein, J. L. (2012). Structure of the vacuolar-type ATPase from Saccharomyces cerevisiae at 11-?? resolution. *Nat. Struct. Mol. Biol.* 19, 1356–1362. doi:10.1038/nsmb.2422.

Bernal, R. A., and Stock, D. (2004). Three-dimensional structure of the intact Thermus thermophilus H +-ATPase/synthase by electron microscopy. *Structure* 12, 1789–1798. doi:10.1016/j.str.2004.07.017.

Bi, Y., Watts, J. C., Bamford, P. K., Briere, L. A. K., and Dunn, S. D. (2008). Probing the functional tolerance of the b subunit of Escherichia coli ATP synthase for sequence manipulation through a chimera approach. *Biochim. Biophys. Acta - Bioenerg.* 1777, 583–591. doi:10.1016/j.bbabio.2008.03.004.

Boekema, E. J., Ubbink-Kok, T., Lolkema, J. S., Brisson, A., and Konings, W. N. (1997). Visualization of a peripheral stalk in V-type ATPase: evidence for the stator structure essential to rotational catalysis. *Proc. Natl. Acad. Sci. U. S. A.* 94, 14291–14293. doi:10.1073/pnas.94.26.14291.

Böttcher, B., Schwarz, L., and Gräber, P. (1998). Direct indication for the existence of a double stalk in CF0F1. *J. Mol. Biol.* 281, 757–762. doi:10.1006/jmbi.1998.1957.

Brandt, K., Maiwald, S., Herkenhoff-Hesselmann, B., Gnirß, K., Greie, J. C., Dunn, S. D., et al. (2013). Individual interactions of the b subunits within the stator of the escherichia coli ATP synthase. *J. Biol. Chem.* 288, 24465–24479. doi:10.1074/jbc.M113.465633.

Cano-Estrada, A., Vázquez-Acevedo, M., Villavicencio-Queijeiro, A., Figueroa-Martínez, F., Miranda-Astudillo, H., Cordeiro, Y., et al. (2010). Subunit-subunit interactions and overall topology of the dimeric mitochondrial ATP synthase of Polytomella sp. *Biochim. Biophys. Acta - Bioenerg.* 1797, 1439–1448. doi:10.1016/j.bbabio.2010.02.024.

Carbajo, R. J., Kellas, F. A., Yang, J. C., Runswick, M. J., Montgomery, M. G., Walker, J. E., et al. (2007). How the N-terminal Domain of the OSCP Subunit of Bovine F1Fo-ATP Synthase Interacts with the N-terminal Region of an Alpha Subunit. *J. Mol. Biol.* 368, 310–318. doi:10.1016/j.jmb.2007.02.059.

Cherepanov, D. A., Mulkidjanian, A. Y., and Junge, W. (1999). Transient accumulation of elastic energy in proton translocating ATP synthase. *FEBS Lett.* 449, 1–6. doi:10.1016/S0014-5793(99)00386-5.

Cipriano, D. J., Wood, K. S., Bi, Y., and Dunn, S. D. (2006). Mutations in the dimerization domain of the b subunit from the Escherichia coli ATP synthase: Deletions disrupt function but not enzyme assembly. *J. Biol. Chem.* 281, 12408–12413. doi:10.1074/jbc.M513368200.

Claggett, S. B., Plancher, M. O. N., Dunn, S. D., and Cain, B. D. (2009). The b subunits in the peripheral stalk of F1F0 ATP synthase preferentially adopt an offset relationship. *J. Biol. Chem.* 284, 16531–16540. doi:10.1074/jbc.M109.002980.

Colina-Tenorio, L., Miranda-Astudillo, H., Cano-Estrada, A., Vázquez-Acevedo, M., Cardol, P., Remacle, C., et al. (2016). Subunit Asa1 spans all the peripheral stalk of the mitochondrial ATP synthase of the chlorophycean alga Polytomella sp. *Biochim. Biophys. Acta - Bioenerg.* 1857, 359–369. doi:10.1016/j.bbabio.2015.11.012.

Collinson, I. R., van Raajj, M. J., Runswick, M. J., Fearnley, I. M., Skehel, M. J., Orris, G. L., et al. (1994). ATP Synthase from Bovine Heart Mitochondria In Vitro Assembly of a Stalk Complez in the Presence of F1-ATPase and in its Absence. *J. Mol. Biol.* 242, 408–421. doi:10.1006/jmbi.1994.1591.

Coskun, Ü., Chaban, Y. L., Lingl, A., Müller, V., Keegstra, W., Boekema, E. J., et al. (2004). Structure and subunit arrangement of the A-type ATP synthase complex from the archaeon Methanococcus jannaschii visualized by electron microscopy. *J. Biol. Chem.* 279, 38644–38648. doi:10.1074/jbc.M406196200.

Couoh-Cardel, S. J., Uribe-Carvajal, S., Wilkens, S., and García-Trejo, J. J. (2010). Structure of dimeric F1F0-ATP synthase. *J. Biol. Chem.* 285, 36447–36455. doi:10.1074/jbc.M110.144907.

Crick, F. H. C. (1953). The packing of α-helices: simple coiled-coils. *Acta Crystallogr.* 6, 689–697.

854 doi:10.1107/S0365110X53001964.

855 Cross, R. L., and Müller, V. (2004). The evolution of A-, F-, and V-type ATP synthases and
856 ATPases: Reversals in function and changes in the H+/ATP coupling ratio. *FEBS Lett.* 576, 1–
857 4. doi:10.1016/j.febslet.2004.08.065.

858 Cross, R. L., and Taiz, L. (1990). Gene duplication as a means for altering H+/ATP ratios during
859 the evolution of Fo F1 ATPases and synthases. *FEBS Lett.* 259, 227–229. doi:10.1016/0014-
860 5793(90)80014-A.

861 D'Alessandro, M., and Melandri, B. A. (2010). ATP hydrolysis in ATP synthases can be differently
862 coupled to proton transport and modulated by ADP and phosphate: A structure based model of
863 the mechanism. *Biochim. Biophys. Acta - Bioenerg.* 1797, 755–762.
864 doi:10.1016/j.bbabio.2010.03.007.

865 Davies, K. M., Anselmi, C., Wittig, I., Faraldo-Gomez, J. D., and Kuhlbrandt, W. (2012). Structure
866 of the yeast F1Fo-ATP synthase dimer and its role in shaping the mitochondrial cristae. *Proc.*
867 *Natl. Acad. Sci.* 109, 13602–13607. doi:10.1073/pnas.1204593109.

868 Davies, K. M., Strauss, M., Daum, B., Kief, J. H., Osiewacz, H. D., Rycovska, A., et al. (2011).
869 Macromolecular organization of ATP synthase and complex I in whole mitochondria. *Proc.*
870 *Natl. Acad. Sci.* 108, 14121–14126. doi:10.1073/pnas.1103621108.

871 Del Rizzo, P. A., Bi, Y., and Dunn, S. D. (2006). ATP Synthase b Subunit Dimerization Domain: A
872 Right-Handed Coiled Coil with Offset Helices. *J. Mol. Biol.* 364, 735–746.
873 doi:10.1016/j.jmb.2006.09.028.

874 Del Rizzo, P. A., Bi, Y., Dunn, S. D., and Shilton, B. H. (2002). The "second stalk" of Escherichia
875 coli ATP synthase: Structure of the isolated dimerization domain. *Biochemistry* 41, 6875–
876 6884. doi:10.1021/bi025736i.

877 Deleon-Rangel, J., Ishmukhametov, R. R., Jiang, W., Fillingame, R. H., and Vik, S. B. (2013). In-
878 teractions between subunits a and b in the rotary ATP synthase as determined by cross-linking.
879 *FEBS Lett.* 587, 892–897. doi:10.1016/j.febslet.2013.02.012.

880 Deppenmeier, U., and Müller, V. (2007). Life Close to the Thermodynamic Limit: How Methano-
881 genic Archaea Conserve Energy. *Bioenergetics*, 123–152. doi:10.1007/400_2006_026.

882 Dickson, V. K., Silvester, J. A., Fearnley, I. M., Leslie, A. G. W., and Walker, J. E. (2006). On the
883 structure of the stator of the mitochondrial ATP synthase. *EMBO J.* 25, 2911–2918.
884 doi:10.1038/sj.emboj.7601177.

885 Diepholz, M., Venzke, D., Prinz, S., Batisse, C., Flörchinger, B., Rössle, M., et al. (2008). A Dif-
886 ferent Conformation for EGC Stator Subcomplex in Solution and in the Assembled Yeast V-
887 ATPase: Possible Implications for Regulatory Disassembly. *Structure* 16, 1789–1798.
888 doi:10.1016/j.str.2008.09.010.

889 Dmitriev, O., Jones, P. C., Jiang, W., and Fillingame, R. H. (1999). Structure of the Membrane
890 Domain of Subunit b of the Escherichia coli F 0 F 1 ATP Synthase. *J. Biol. Chem.* 274,
891 15598–15604.

892 Drory, O., Frolow, F., and Nelson, N. (2004). Crystal structure of yeast V-ATPase subunit C re-
893 veals its stator function. *EMBO Rep.* 5, 1148–1152. doi:10.1038/sj.embor.7400294.

894 Dudkina, N. V., Heinemeyer, J., Keegstra, W., Boekema, E. J., and Braun, H. P. (2005). Structure
895 of dimeric ATP synthase from mitochondria: An angular association of monomers induces the
896 strong curvature of the inner membrane. *FEBS Lett.* 579, 5769–5772.
897 doi:10.1016/j.febslet.2005.09.065.

898 Dunn, S. D., Revington, M., Cipriano, D. J., and Shilton, B. H. (2000). The b subunit of Escherichia

coli ATP synthase. *J. Bioenerg. Biomembr.* 32, 347–355. doi:10.1023/A:1005571818730.

Forgac, M. (2007). Vacuolar ATPases: Rotary proton pumps in physiology and pathophysiology. *Nat. Rev. Mol. Cell Biol.* 8, 917–929. doi:10.1038/nrm2272.

Fronzes, R., Weimann, T., Vaillier, J., Velours, J., and Brèthes, D. (2006). The peripheral stalk participates in the yeast ATP synthase dimerization independently of e and g subunits. *Biochemistry* 45, 6715–6723. doi:10.1021/bi0601407.

Fujikawa, M., Sugawara, K., Tanabe, T., and Yoshida, M. (2015). Assembly of human mitochondrial ATP synthase through two separate intermediates, F1-c-ring and b-e-g complex. *FEBS Lett.* 589, 2707–2712. doi:10.1016/j.febslet.2015.08.006.

Gavin, P. D., Prescott, M., and Devenish, R. J. (2005). Yeast F1F0-ATP synthase complex interactions in vivo can occur in the absence of the dimer specific subunit e. *J. Bioenerg. Biomembr.* 37, 55–66. doi:10.1007/s10863-005-4128-8.

Grüber, G., Manimekalai, M. S. S., Mayer, F., and Müller, V. (2014). ATP synthases from archaea: The beauty of a molecular motor. *Biochim. Biophys. Acta - Bioenerg.* 1837, 940–952. doi:10.1016/j.bbabio.2014.03.004.

Guo, H., Bueler, S. A., and Rubinstein, J. L. (2017). Atomic model for the dimeric FO region of mitochondrial ATP synthase. *Science (80-.).* 358, 936–940. doi:10.1126/science.aao4815.

Habersetzer, J., Ziani, W., Larrieu, I., Stines-Chaumeil, C., Giraud, M. F., Brèthes, D., et al. (2013). ATP synthase oligomerization: From the enzyme models to the mitochondrial morphology. *Int. J. Biochem. Cell Biol.* 45, 99–105. doi:10.1016/j.biocel.2012.05.017.

Hahn, A., Parey, K., Bublitz, M., Mills, D. J., Zickermann, V., Vonck, J., et al. (2016). Structure of a Complete ATP Synthase Dimer Reveals the Molecular Basis of Inner Mitochondrial Membrane Morphology. *Mol. Cell* 63, 445–456. doi:10.1016/j.molcel.2016.05.037.

He, J., Ford, H. C., Carroll, J., Douglas, C., Gonzales, E., Ding, S., et al. (2018). Assembly of the membrane domain of ATP synthase in human mitochondria. *Proc. Natl. Acad. Sci.*, 201722086. doi:10.1073/pnas.1722086115.

Hilbers, F., Eggers, R., Pradela, K., Friedrich, K., Herkenhoff-Hesselmann, B., Becker, E., et al. (2013). Subunit δ Is the Key Player for Assembly of the H+-translocating Unit of Escherichia coli FOF1 ATP Synthase. *J. Biol. Chem.* 288, 25880–25894. doi:10.1074/jbc.M113.484675.

Hunt, I. E., and Bowman, B. J. (1997). The intriguing evolution of the “b” and “G” subunits in F-type and V- type ATPases: Isolation of the vma-10 gene from Neurospora crassa. *J. Bioenerg. Biomembr.* 29, 533–540. doi:10.1023/A:1022474816665.

Junge, W., Sielaff, H., and Engelbrecht, S. (2009). Torque generation and elastic power transmission in the rotary F O F 1-ATPase. *Nature* 459, 364–370. doi:10.1038/nature08145.

Kane, P. M. (1995). Disassembly and Reassembly of the Yeast Vacuolar H-ATPase in Vivo. *J. Biol. Chem.* 270, 17025–17032.

Kish-Trier, E., Briere, L. A. K., Dunn, S. D., and Wilkens, S. (2008). The Stator Complex of the A1A0-ATP Synthase-Structural Characterization of the E and H Subunits. *J. Mol. Biol.* 375, 673–685. doi:10.1016/j.jmb.2007.10.063.

Kish-Trier, E., and Wilkens, S. (2009). Domain architecture of the stator complex of the A1A0-ATP synthase from Thermoplasma acidophilum. *J. Biol. Chem.* 284, 12031–12040. doi:10.1074/jbc.M808962200.

Klusch, N., Murphy, B. J., Mills, D. J., Yildiz, Ö., and Kühlbrandt, W. (2017). Structural basis of proton translocation and force generation in mitochondrial ATP synthase. *Elife* 6, 1–16.

943 doi:10.7554/eLife.33274.

944 Lapaille, M., Thiry, M., Perez, E., González-Halphen, D., Remacle, C., and Cardol, P. (2010). Loss
945 of mitochondrial ATP synthase subunit beta (Atp2) alters mitochondrial and chloroplastic
946 function and morphology in Chlamydomonas. *Biochim. Biophys. Acta - Bioenerg.* 1797, 1533–
947 1539. doi:10.1016/j.bbabio.2010.04.013.

948 Lau, W. C. Y., and Rubinstein, J. L. (2012). Subnanometre-resolution structure of the intact Ther-
949 mus thermophilus H +-driven ATP synthase. *Nature* 481, 214–219. doi:10.1038/nature10699.

950 Lee, J., Ding, S. J., Walpole, T. B., Holding, A. N., Montgomery, M. G., Fearnley, I. M., et al.
951 (2015). Organization of subunits in the membrane domain of the bovine F-ATPase revealed by
952 covalent cross-linking. *J. Biol. Chem.* 290, 13308–13320. doi:10.1074/jbc.M115.645283.

953 Lee, L. K., Stewart, A. G., Donohoe, M., Bernal, R. A., and Stock, D. (2010). The structure of the
954 peripheral stalk of Thermus thermophilus H +-ATPase/synthase. *Nat. Struct. Mol. Biol.* 17,
955 373–378. doi:10.1038/nsmb.1761.

956 Lupas, A. (1996). Coiled coils: new structures and new functions. *Trends Biochem. Sci.* 21, 375–
957 382. doi:10.1016/S0968-0004(96)90126-7.

958 Lupas, a N., and Gruber, M. (2005). The structure of a-helical coiled coils. *Adv. Protein. Chem.* 70,
959 37–78. doi:10.1016/S0065-3233(04)70003-0.

960 Lytovchenko, O., Naumenko, N., Oeljeklaus, S., Schmidt, B., von der Malsburg, K., Deckers, M.,
961 et al. (2014). The INA complex facilitates assembly of the peripheral stalk of the mitochondri-
962 al F1Fo-ATP synthase. *EMBO J.* 33, 1624–38. doi:10.15252/embj.201488076.

963 Mason, J. M., and Arndt, K. M. (2004). Coiled coil domains: Stability, specificity, and biological
964 implications. *ChemBioChem* 5, 170–176. doi:10.1002/cbic.200300781.

965 Mayer, F., and Müller, V. (2014). Adaptations of anaerobic archaea to life under extreme energy
966 limitation. *FEMS Microbiol. Rev.* 38, 449–472. doi:10.1111/1574-6976.12043.

967 Mazhab-Jafari, M. T., and Rubinstein, J. L. (2016). Cryo-EM studies of the structure and dynamics
968 of vacuolar-type ATPases. *Sci. Adv.* 2, e1600725. doi:10.1126/sciadv.1600725.

969 McLachlin, D. T., Bestard, J. A., and Dunn, S. D. (1998). The b and ?? subunits of the Escherichia
970 coli ATP synthase interact via residues in their C-terminal regions. *J. Biol. Chem.* 273, 15162–
971 15168. doi:10.1074/jbc.273.24.15162.

972 Mellwig, C., and Böttcher, B. (2003). A unique resting position of the ATP-synthase from chloro-
973 plasts. *J. Biol. Chem.* 278, 18544–18549. doi:10.1074/jbc.M212852200.

974 Minauro-Sanmiguel, F., Wilkens, S., and Garcia, J. J. (2005). Structure of dimeric mitochondrial
975 ATP synthase: Novel F0 bridging features and the structural basis of mitochondrial cristae bi-
976 ogenesis. *Proc. Natl. Acad. Sci.* 102, 12356–12358. doi:10.1073/pnas.0503893102.

977 Miranda-Astudillo, H., Cano-Estrada, A., Vázquez-Acevedo, M., Colina-Tenorio, L., Downie-
978 Velasco, A., Cardol, P., et al. (2014). Interactions of subunits Asa2, Asa4 and Asa7 in the pe-
979 ripheral stalk of the mitochondrial ATP synthase of the chlorophycean alga Polytomella sp.
980 *Biochim. Biophys. Acta - Bioenerg.* 1837, 1–13. doi:10.1016/j.bbabio.2013.08.001.

981 Miranda-Astudillo, H., Colina-Tenorio, L., Jiménez-Suárez, A., Vázquez-Acevedo, M., Salin, B.,
982 Giraud, M.-F., et al. (2018). Oxidative phosphorylation supercomplexes and respirasome re-
983 constitution of the colorless alga Polytomella sp. *Biochim. Biophys. Acta - Bioenerg.* 1859,
984 434–444. doi:10.1016/j.bbabio.2018.03.004.

985 Mitchell, P. (1961). © 1961 Nature Publishing Group. *Nature* 191, 144–148.

986 Morales-Rios, E., Montgomery, M. G., Leslie, A. G. W., and Walker, J. E. (2015). Structure of

ATP synthase from *Paracoccus denitrificans* determined by X-ray crystallography at 4.0 Å resolution. *Proc. Natl. Acad. Sci.* 112, 13231–13236. doi:10.1073/pnas.1517542112.

Muench, S. P., Huss, M., Song, C. F., Phillips, C., Wieczorek, H., Trinick, J., et al. (2009). Cryo-electron Microscopy of the Vacuolar ATPase Motor Reveals its Mechanical and Regulatory Complexity. *J. Mol. Biol.* 386, 989–999. doi:10.1016/j.jmb.2009.01.014.

Muench, S. P., Trinick, J., and Harrison, M. A. (2011). *Structural divergence of the rotary ATPases*. doi:10.1017/S0033583510000338.

Mühleip, A. W., Dewar, C. E., Schnaufer, A., Kühlbrandt, W., and Davies, K. M. (2017). In situ structure of trypanosomal ATP synthase dimer reveals a unique arrangement of catalytic subunits. *Proc. Natl. Acad. Sci.* 114, 992–997. doi:10.1073/pnas.1612386114.

Mühleip, A. W., Joos, F., Wigge, C., Frangakis, A. S., Kühlbrandt, W., and Davies, K. M. (2016). Helical arrays of U-shaped ATP synthase dimers form tubular cristae in ciliate mitochondria. *Proc. Natl. Acad. Sci.* 113, 8442–8447. doi:10.1073/pnas.1525430113.

Mulkidjanian, A. Y., Makarova, K. S., Galperin, M. Y., and Koonin, E. V (2007). Inventing the dynamo machine : the evolution of the F type and V type ATPases. *Nat. Rev. Microbiol.* 11, 892–899. doi:10.1038/nrmicro1767.

Müller, V., and Grüber, G. (2003). ATP synthases: structure, function and evolution of unique energy converters. *Cell. Mol. Life Sci.* 60, 474–494. doi:10.1007/s00018-003-.

Naumenko, N., Morgenstern, M., Rucktäschel, R., Warscheid, B., and Rehling, P. (2017). INA complex liaises the F1Fo-ATP synthase membrane motor modules. *Nat. Commun.* 8. doi:10.1038/s41467-017-01437-z.

Neukirch, S., Goriely, A., and Hausrath, A. C. (2008). Elastic coiled-coils act as energy buffers in the ATP synthase. *Int. J. Non. Linear. Mech.* 43, 1064–1073. doi:10.1016/j.ijnonlinmec.2008.06.008.

O'Shea, E., Klemm, J., Kim, P., and Alber, T. (1991). X-ray structure of the GCN4 leucine zipper, a two-stranded, parallel coiled coil. *Science (80-.).* 254, 539–544. doi:10.1126/science.1948029.

Oot, R. A., Couoh-Cardel, S., Sharma, S., Stam, N. J., and Wilkens, S. (2017). Breaking up and making up: The secret life of the vacuolar H+-ATPase. *Protein Sci.* 26, 896–909. doi:10.1002/pro.3147.

Oot, R. A., Huang, L. S., Berry, E. A., and Wilkens, S. (2012). Crystal structure of the yeast vacuolar ATPase heterotrimeric EGC head peripheral stalk complex. *Structure* 20, 1881–1892. doi:10.1016/j.str.2012.08.020.

Oot, R. A., and Wilkens, S. (2010). Domain characterization and interaction of the yeast vacuolar ATPase subunit C with the peripheral stator stalk subunits E and G. *J. Biol. Chem.* 285, 24654–24664. doi:10.1074/jbc.M110.136960.

Oot, R. A., and Wilkens, S. (2012). Subunit Interactions at the V_1-V_o Interface in Yeast Vacuolar ATPase. *J. Biol. Chem.* 287, 13396–13406. doi:10.1074/jbc.M112.343962.

Parry, D. A. D., Fraser, R. D. B., and Squire, J. M. (2008). Fifty years of coiled-coils and α-helical bundles: A close relationship between sequence and structure. *J. Struct. Biol.* 163, 258–269. doi:10.1016/j.jsb.2008.01.016.

Paumard, P. (2002). The ATP synthase is involved in generating mitochondrial cristae morphology. *EMBO J.* 21, 221–230. doi:10.1093/emboj/21.3.221.

Paumard, P., Arselin, G., Vaillier, J., Chaignepain, S., Bathany, K., Schmitter, J. M., et al. (2002).

Two ATP synthases can be linked through subunits i in the inner mitochondrial membrane of Saccharomyces cerevisiae. *Biochemistry* 41, 10390–10396. doi:10.1021/bi025923g.

Poetsch, A., Berzborn, R. J., Heberle, J., Link, T. A., Dencher, N. A., and Seelert, H. (2007). Biophysics and bioinformatics reveal structural differences of the two peripheral stalk subunits in chloroplast ATP synthase. *J. Biochem.* 141, 411–420. doi:10.1093/jb/mvm045.

Pogoryelov, D., Klyszejko, A. L., Krasnoselska, G. O., Heller, E.-M., Leone, V., Langer, J. D., et al. (2012). Engineering rotor ring stoichiometries in the ATP synthase. *Proc. Natl. Acad. Sci.* 109, E1599–E1608. doi:10.1073/pnas.1120027109.

Qi, J., Wang, Y., and Forgac, M. (2007). The vacuolar (H+)-ATPase: Subunit arrangement and in vivo regulation. *J. Bioenerg. Biomembr.* 39, 423–426. doi:10.1007/s10863-007-9116-8.

Radermacher, M., Ruiz, T., Wieczorek, H., and Grüber, G. (2001). The structure of the V1-ATPase determined by three-dimensional electron microscopy of single particles. *J. Struct. Biol.* 135, 26–37. doi:10.1006/jsbi.2001.4395.

Rak, M., Gokova, S., and Tzagoloff, A. (2011). Modular assembly of yeast mitochondrial ATP synthase. *EMBO J.* 30, 920–930. doi:10.1038/emboj.2010.364.

Rawson, S., Harrison, M. A., and Muench, S. P. (2016). Rotating with the brakes on and other unresolved features of the vacuolar ATPase. *Biochem. Soc. Trans.* 44, 851–855. doi:10.1042/BST20160043.

Razaka-Jolly, D., Rigoulet, M., Guérin, B., and Velours, J. (1994). Mutation in the Hydrophobic Domain of ATP Synthase Subunit 4 (Subunit b) of Yeast Mitochondria Disturbs Coupling between Proton Translocation and Catalysis. *Biochemistry* 33, 9684–9691. doi:10.1021/bi00198a038.

Rees, D. M., Leslie, A. G. W., and Walker, J. E. (2009). The structure of the membrane extrinsic region of bovine ATP synthase. *Proc. Natl. Acad. Sci. U. S. A.* 106, 21597–601. doi:10.1073/pnas.0910365106.

Rubinstein, J. L., and Walker, J. E. (2002). ATP synthase from Saccharomyces cerevisiae: Location of the OSCP subunit in the peripheral stalk region. *J. Mol. Biol.* 321, 613–619. doi:10.1016/S0022-2836(02)00671-X.

Rühle, T., and Leister, D. (2015). Assembly of F1F0-ATP synthases. *Biochim. Biophys. Acta* 1847, 849–860. doi:10.1016/j.bbabio.2015.02.005.

Sánchez-Vásquez, L., Vázquez-Acevedo, M., de la Mora, J., Vega-deLuna, F., Cardol, P., Remacle, C., et al. (2017). Near-neighbor interactions of the membrane-embedded subunits of the mitochondrial ATP synthase of a chlorophycean alga. *Biochim. Biophys. Acta - Bioenerg.* 1858, 497–509. doi:10.1016/j.bbabio.2017.04.004.

Saroussi, S., Schushan, M., Ben-Tal, N., Junge, W., and Nelson, N. (2012). Structure and Flexibility of the C-Ring in the Electromotor of Rotary FoF1-ATPase of Pea Chloroplasts. *PLoS One* 7, 1–12. doi:10.1371/journal.pone.0043045.

Schep, D. G., Zhao, J., and Rubinstein, J. L. (2016). Models for the a subunits of the *Thermus thermophilus* V/A-ATPase and *Saccharomyces cerevisiae* V-ATPase enzymes by cryo-EM and evolutionary covariance. *Proc. Natl. Acad. Sci.* 113, 3245–3250. doi:10.1073/pnas.1521990113.

Seelert, H., and Dencher, N. A. (2011). ATP synthase superassemblies in animals and plants: Two or more are better. *Biochim. Biophys. Acta - Bioenerg.* 1807, 1185–1197. doi:10.1016/j.bbabio.2011.05.023.

Sielaff, H., Rennekamp, H., Wächter, A., Xie, H., Hilbers, F., Feldbauer, K., et al. (2008). Domain

compliance and elastic power transmission in rotary F(O)F(1)-ATPase. *Proc. Natl. Acad. Sci. U. S. A.* 105, 17760–5. doi:10.1073/pnas.0807683105.

Sobti, M., Smits, C., Wong, A. S. W., Ishmukhametov, R., Stock, D., Sandin, S., et al. (2016). Cryo-EM structures of the autoinhibited E. coli ATP synthase in three rotational states. *Elife* 5, 1–18. doi:10.7554/eLife.21598.

Song, J., Pfanner, N., and Becker, T. (2018). Assembling the mitochondrial ATP synthase. *Proc. Natl. Acad. Sci.* 115, 201801697. doi:10.1073/pnas.1801697115.

Sorgen, P. L., Bubb, M. R., and Cain, B. D. (1999). Lengthening the Second Stalk of F 1 F 0 ATP Synthase in Escherichia coli. *J. Biol. Chem.* 274, 36261–36266. doi:10.1074/jbc.274.51.36261.

Sorgen, P. L., Caviston, T. L., Perry, R. C., and Cain, B. D. (1998). Deletions in the Second Stalk of F 1 F 0 ATP Synthase in Escherichia coli. *J. Biol. Chem.* 273, 27873–27878. doi:10.1074/jbc.273.43.27873.

Soubannier, V., Vaillier, J., Paumard, P., Coulary, B., Schaeffer, J., and Velours, J. (2002). In the absence of the first membrane-spanning segment of subunit 4(b), the yeast ATP synthase is functional but does not dimerize or oligomerize. *J. Biol. Chem.* 277, 10739–10745. doi:10.1074/jbc.M111882200.

Spannagel, C., Vaillier, J., Arselin, G., Graves, P. V., Grandier-Vazeille, X., and Velours, J. (1998). Evidence of a subunit 4 (subunit b) dimer in favor of the proximity of ATP synthase complexes in yeast inner mitochondrial membrane. *Biochim. Biophys. Acta - Biomembr.* 1414, 260–264. doi:10.1016/S0005-2736(98)00174-6.

Spannagel, C., Vaillier, J., Arselin, G., Graves, P. V., and Velours, J. (1997). The subunit f of mitochondrial yeast ATP synthase Characterization of the protein and disruption of the structural gene ATP17. *Eur. J. Biochem.* 247, 1111–1117. doi:10.1111/j.1432-1033.1997.01111.x.

Srivastava, A. P., Luo, M., Zhou, W., Symersky, J., Bai, D., Chambers, M. G., et al. (2018). High-resolution cryo-EM analysis of the yeast ATP synthase in a lipid membrane. *Science* 9699, eaas9699. doi:10.1126/science.aas9699.

Stalz, W. D., Greie, J. C., Deckers-Hebestreit, G., and Altendorf, K. (2003). Direct interaction of subunits a and b of the F0 complex of Escherichia coli ATP synthase by forming an ab2 subcomplex. *J. Biol. Chem.* 278, 27068–27071. doi:10.1074/jbc.M302027200.

Stephens, A. N., Khan, M. A., Roucou, X., Nagley, P., and Devenish, R. J. (2003). The molecular neighborhood of subunit 8 of yeast mitochondrial F1F0-ATP synthase probed by cysteine scanning mutagenesis and chemical modification. *J. Biol. Chem.* 278, 17867–17875. doi:10.1074/jbc.M300967200.

Stewart, A. G., Laming, E. M., Sobti, M., and Stock, D. (2014). Rotary ATPases-dynamic molecular machines. *Curr. Opin. Struct. Biol.* 25, 40–48. doi:10.1016/j.sbi.2013.11.013.

Stewart, A. G., Lee, L. K., Donohoe, M., Chaston, J. J., and Stock, D. (2012). The dynamic stator stalk of rotary ATPases. *Nat. Commun.* 3, 687–688. doi:10.1038/ncomms1693.

Stewart, A. G., Sobti, M., Harvey, R. P., and Stock, D. (2013). Rotary ATPases: models, machine elements and technical specifications. *Bioarchitecture* 3, 2–12. doi:10.4161/bioa.23301.

Stransky, L., Cotter, K., and Forgac, M. (2016). The Function of V-ATPases in Cancer. *Physiol. Rev.* 96, 1071–1091. doi:10.1152/physrev.00035.2015.

Strauss, M., Hofhaus, G., Schröder, R. R., and Kühlbrandt, W. (2008). Dimer ribbons of ATP synthase shape the inner mitochondrial membrane. *EMBO J.* 27, 1154–1160. doi:10.1038/emboj.2008.35.

Su, J. Y., Hodges, R. S., and Kay, C. M. (1994). Effect of chain length on the formation and stability of synthetic alpha-helical coiled coils. *Biochemistry* 33, 15501–10. doi:10.1021/bi00255a032.

Sumner, J.-P., Dow, J. A., Early, F. G., Klein, U., Jäger, D., and Wieczorek, H. (1995). Regulation of Plasma Membrane V-ATPase Activity by Dissociation of Peripheral Subunits. *J. Biol. Chem.* 270, 5649–5653. doi:10.1074/jbc.270.10.5649.

Tabke, K., Albertmelcher, A., Vitavska, O., Huss, M., Schmitz, H.-P., and Wieczorek, H. (2014). Reversible disassembly of the yeast V-ATPase revisited under *in vivo* conditions. *Biochem. J.* 462, 185–197. doi:10.1042/BJ20131293.

Thomas, D., Bron, P., Weimann, T., Dautant, A., Giraud, M.-F., Paumard, P., et al. (2008). Supramolecular organization of the yeast F1Fo-ATP synthase. *Biol. Cell* 100, 591–603. doi:10.1042/BC20080022.

Ubbink-kok, T., Boekema, E. J., Breemen, J. F. L. Van, Brisson, A., Konings, W. N., and Lolkema, J. S. (2000). Stator Structure and Subunit Composition of the V 1 / V 0 Na ‡ -ATPase of the Thermophilic Bacterium Caloramator fervidus. 311–321.

van Lis, R., Mendoza-Hernandez, G., Groth, G., and Atteia, A. (2007). New Insights into the Unique Structure of the F0F1-ATP Synthase from the Chlamydomonad Algae Polytomella sp. and Chlamydomonas reinhardtii. *Plant Physiol.* 144, 1190–1199. doi:10.1104/pp.106.094060.

Vázquez-Acevedo, M., Cardol, P., Cano-Estrada, A., Lapaille, M., Remacle, C., and González-Halphen, D. (2006). The mitochondrial ATP synthase of chlorophycean algae contains eight subunits of unknown origin involved in the formation of an atypical stator-stalk and in the dimerization of the complex. *J. Bioenerg. Biomembr.* 38, 271–282. doi:10.1007/s10863-006-9046-x.

Velours, J., Stines-Chaumeil, C., Habersetzer, J., Chaignepain, S., Dautant, A., and Brèthes, D. (2011). Evidence of the proximity of ATP synthase subunits 6 (a) in the inner mitochondrial membrane and in the supramolecular forms of Saccharomyces cerevisiae ATP synthase. *J. Biol. Chem.* 286, 35477–35484. doi:10.1074/jbc.M111.275776.

Velours, J., Vaillier, J., Paumard, P., Soubannier, V., Lai-Zhang, J., and Mueller, D. M. (2001). Bovine Coupling Factor 6, with Just 14.5% Shared Identity, Replaces Subunit h in the Yeast ATP Synthase. *J. Biol. Chem.* 276, 8602–8607. doi:10.1074/jbc.M008123200.

Vik, S. B., and Antonio, B. J. (1994). A mechanism of proton translocation by F1F0 ATP synthases suggested by double mutants of the a subunit. *J. Biol. Chem.* 269, 30364–30369.

Villavicencio-Queijeiro, A., Vázquez-Acevedo, M., Cano-Estrada, A., Zarco-Zavala, M., Tuena De Gómez, M., Mignaco, J. A., et al. (2009). The fully-active and structurally-stable form of the mitochondrial ATP synthase of Polytomella sp. is dimeric. *J. Bioenerg. Biomembr.* 41, 1–13. doi:10.1007/s10863-009-9203-0.

Vonck, J., Pisa, K. Y., Morgner, N., Brutschy, B., and Müller, V. (2009). Three-dimensional structure of A1A0 ATP synthase from the hyperthermophilic archaeon Pyrococcus furiosus by electron microscopy. *J. Biol. Chem.* 284, 10110–10119. doi:10.1074/jbc.M808498200.

Wächter, A., Bi, Y., Dunn, S. D., Cain, B. D., Sielaff, H., Wintermann, F., et al. (2011). Two rotary motors in F-ATP synthase are elastically coupled by a flexible rotor and a stiff stator stalk. *Proc. Natl. Acad. Sci. U. S. A.* 108, 3924–3929. doi:10.1073/pnas.1011581108.

Walker, J. E., and Dickson, V. K. (2006). The peripheral stalk of the mitochondrial ATP synthase. *Biochim. Biophys. Acta - Bioenerg.* 1757, 286–296. doi:10.1016/j.bbabio.2006.01.001.

Weber, J. (2006). ATP synthase: Subunit-subunit interactions in the stator stalk. *Biochim. Biophys.*

Acta - Bioenerg. 1757, 1162–1170. doi:10.1016/j.bbabio.2006.04.007.

Weber, J., Wilke-Mounts, S., Nadanaciva, S., and Senior, A. E. (2004). Quantitative Determination of Direct Binding of b Subunit to F1 in Escherichia coli F1F0-ATP Synthase. *J. Biol. Chem.* 279, 11253–11258. doi:10.1074/jbc.M312576200.

Weimann, T., Vaillier, J., Salin, B., and Velours, J. (2008). The intermembrane space loop of subunit b (4) is a major determinant of the stability of yeast oligomeric ATP synthases. *Biochemistry* 47, 3556–3563. doi:10.1021/bi702000g.

Wilkens, S., Zhang, Z., and Zheng, Y. (2005). A structural model of the vacuolar ATPase from transmission electron microscopy. *Micron* 36, 109–126. doi:10.1016/j.micron.2004.10.002.

Wittig, I., Meyer, B., Heide, H., Steger, M., Bleier, L., Wumaier, Z., et al. (2010). Assembly and oligomerization of human ATP synthase lacking mitochondrial subunits a and A6L. *Biochim. Biophys. Acta - Bioenerg.* 1797, 1004–1011. doi:10.1016/j.bbabio.2010.02.021.

Wood, K. S., and Dunn, S. D. (2007). Role of the asymmetry of the homodimeric b2 stator stalk in the interaction with the F1 sector of Escherichia coli ATP synthase. *J. Biol. Chem.* 282, 31920–31927. doi:10.1074/jbc.M706259200.

Yadav, K. N. S., Miranda-Astudillo, H. V., Colina-Tenorio, L., Bouillenne, F., Degand, H., Morsomme, P., et al. (2017). Atypical composition and structure of the mitochondrial dimeric ATP synthase from Euglena gracilis. *Biochim. Biophys. Acta - Bioenerg.* 1858, 267–275. doi:10.1016/j.bbabio.2017.01.007.

Yasuda, R., Noji, H., Ishiwata, S., Yoshida, M., and Kinosita Jr., K. (1998). F_1-ATPase Is a Highly Efficient Molecular Motor that Rotates with Discrete 120 Steps. *Cell* 93, 1117–1124.

Zhao, J., Benlekbir, S., and Rubinstein, J. L. (2015). Electron cryomicroscopy observation of rotational states in a eukaryotic V-ATPase. *Nature* 521, 241–245. doi:10.1038/nature14365.

Zhou, A., Rohou, A., Schep, D. G., Bason, J. V., Montgomery, M. G., Walker, J. E., et al. (2015). Structure and conformational states of the bovine mitochondrial ATP synthase by cryo-EM. *Elife* 4, 1–15. doi:10.7554/eLife.10180.

Zíková, A., Schnaufer, A., Dalley, R. A., Panigrahi, A. K., and Stuart, K. D. (2009). The F0F1-ATP synthase complex contains novel subunits and is essential for procyclic Trypanosoma brucei. *PLoS Pathog.* 5. doi:10.1371/journal.ppat.1000436.

Figure 1.TIF

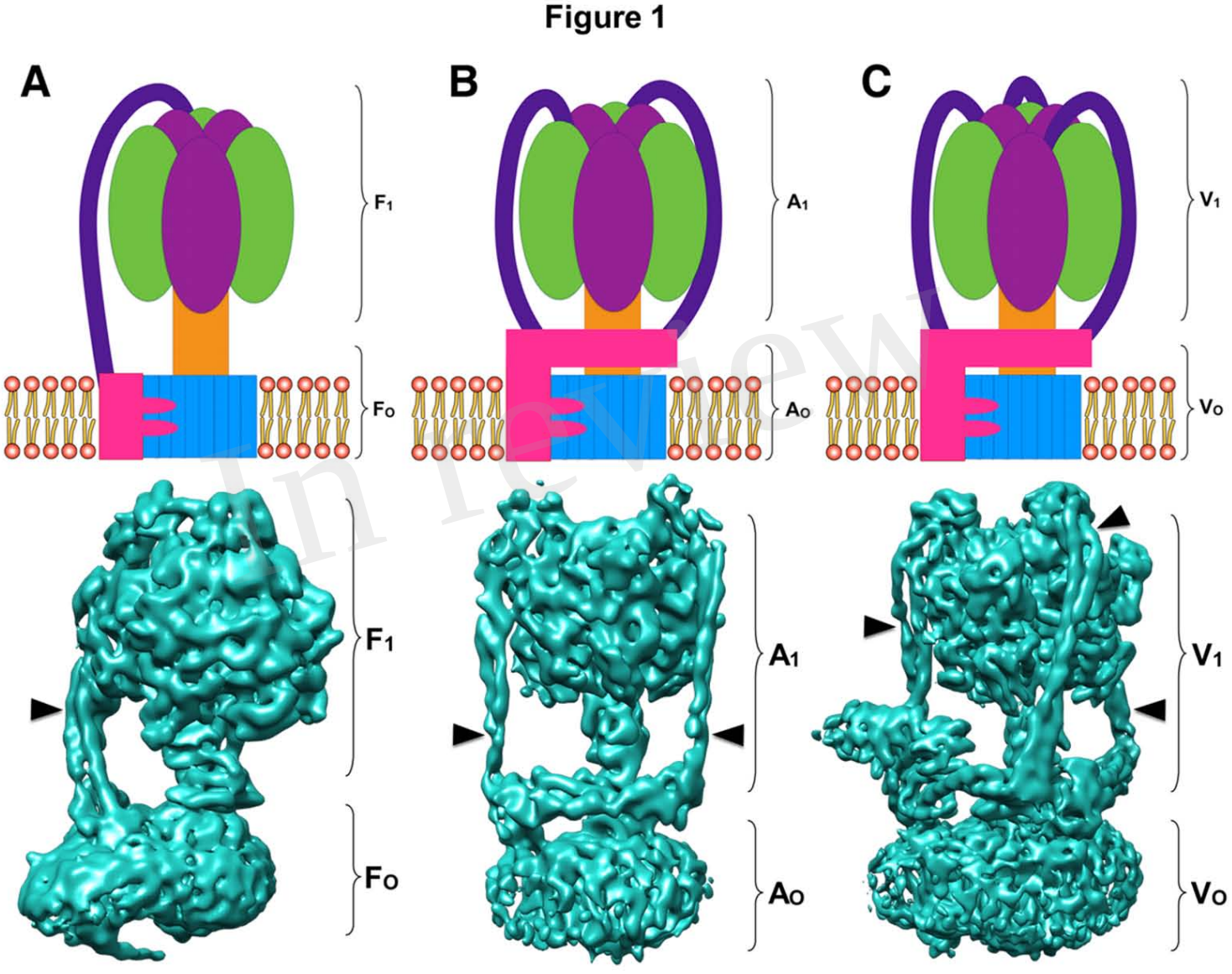

Figure 2.TIF

Figure 2

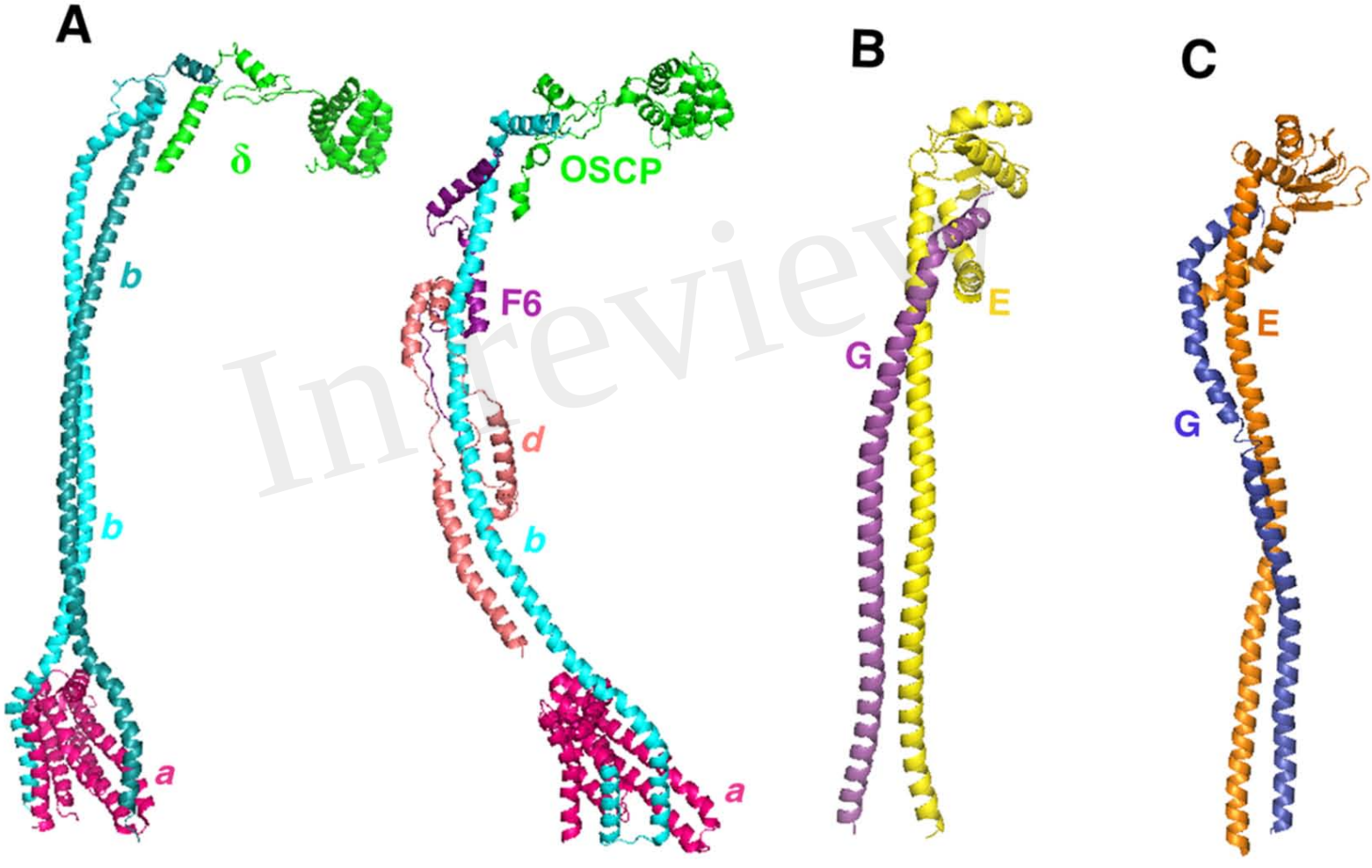

Figure 3.TIF

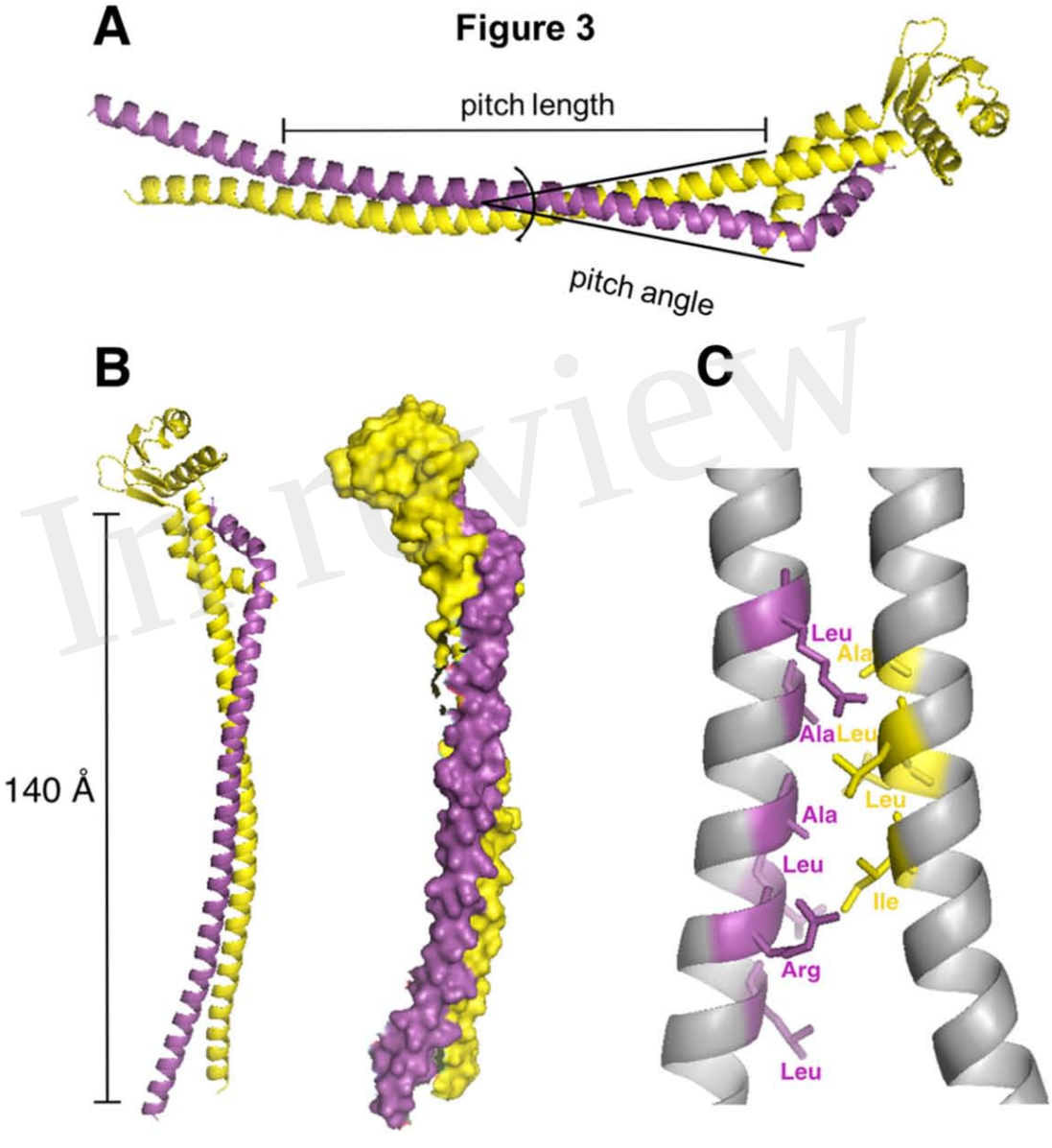

Figure 4.TIF

Figure 3 continued

D

Subunit E

hendecad repeat

abcdefghijk

```
M.hydrothermalis    MPKLENILQEEVLAEINGLLAEAEAKAGTLLREAQEQAEALKASRQRALEAERAAALKRA   60
T.thermophilus      MSKLEAILSQEVEAEIQALLQEAEAKAEAIKREAEEKAKALLQARERALEAQYRAALRRA   60
T.aquaticus         MSKLEAILSQEVEAEIQAILSEARAKAEGLKAEAEARAKALLEGKKRALEAAFQAALRRS   60
T.caliditerrae      MSKLEAILSQEVEAEIQALLGEARAKAEAVVAEARSKAEALLSARKRALEAGLQGAVRRA   60
T.igniterrae        MSKLEAILSQEVEAEIQALLAEAKAKAEALRQEAQGRAEALLAAKKRALEGQRQAALRRA   60
T.islandicus        MSKLEAILSQEVEAEIQALLAEARGKAEALRREAEAKAMALLEGRRRALEAAFQAALRRA   60
```

Subunit G

quindecad repeat

abcdefghijklmno

```
M.hydrothermalis    ----------------MQGLGLVKSLAERERELAQKLEEARRTTEAKIKEAEAEAKRILT   44
T.islandicus        ----------------MGGLGLIRTLAEKERELLARLEAAKKEAEELVKRAEAEARALLE   44
T.caliditerrae      ----------------MGGLGLIKSLAEKEKELLARLEAAKREAEDLVAKAEEEARRLLQ   44
T.igniterrae        ----------------MGGLGLIKSLAEKEKELLARLEAARKEAEALVQKAEAEAKALLE   44
T.thermophilus      MTGGLVLNAISRAGGAMGGLGLIKSLAEKEKQLLERLEAAKKEAEERVKRAEAEAKALLE   60
T.aquaticus         ----------------MGGLGLIKSLAEKEKELLARLEAAKKEAEELLKRAEAEARALLE   44
```

Figure 5.TIF

Figure 4

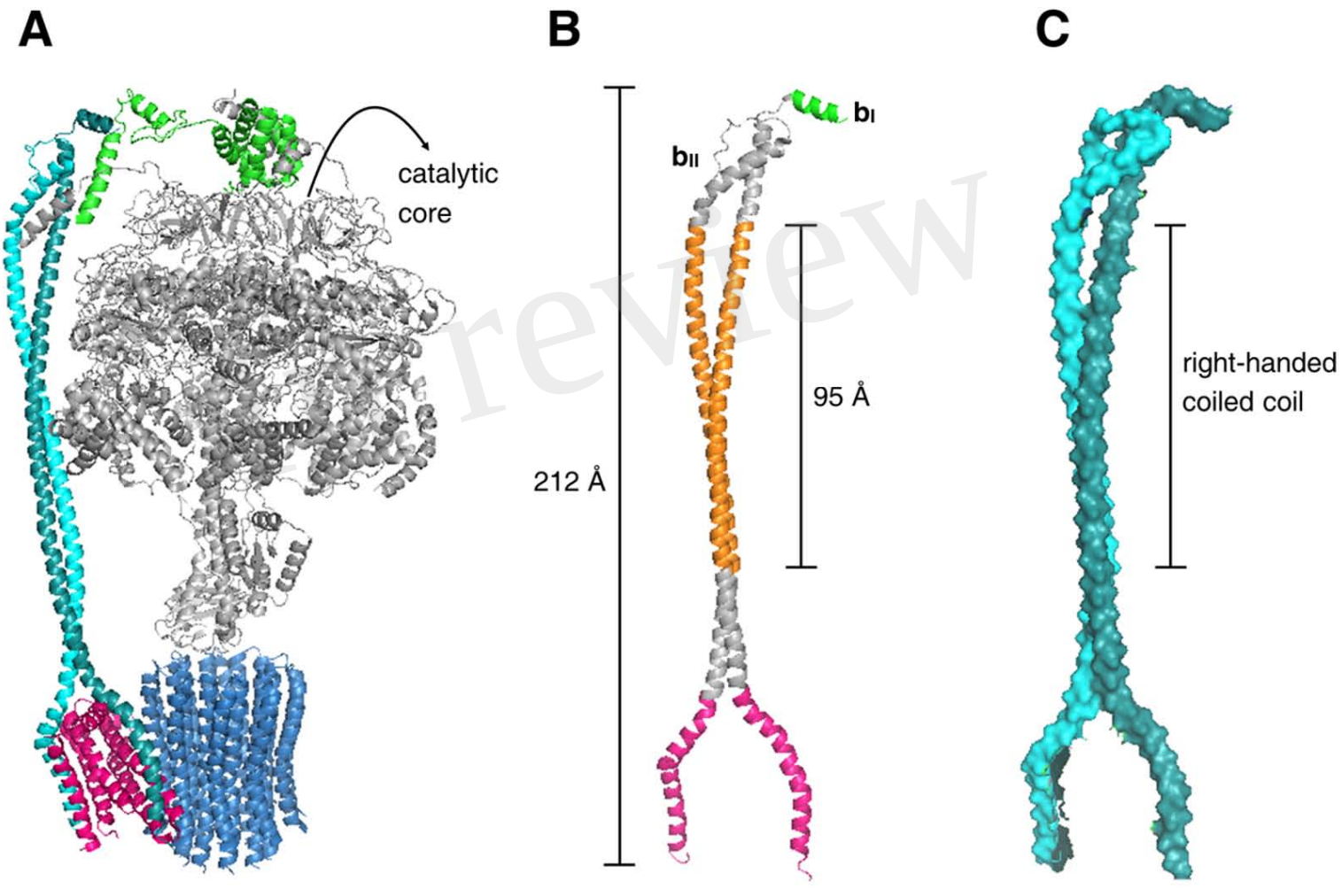

Figure 6.TIF

Figure 4 continued

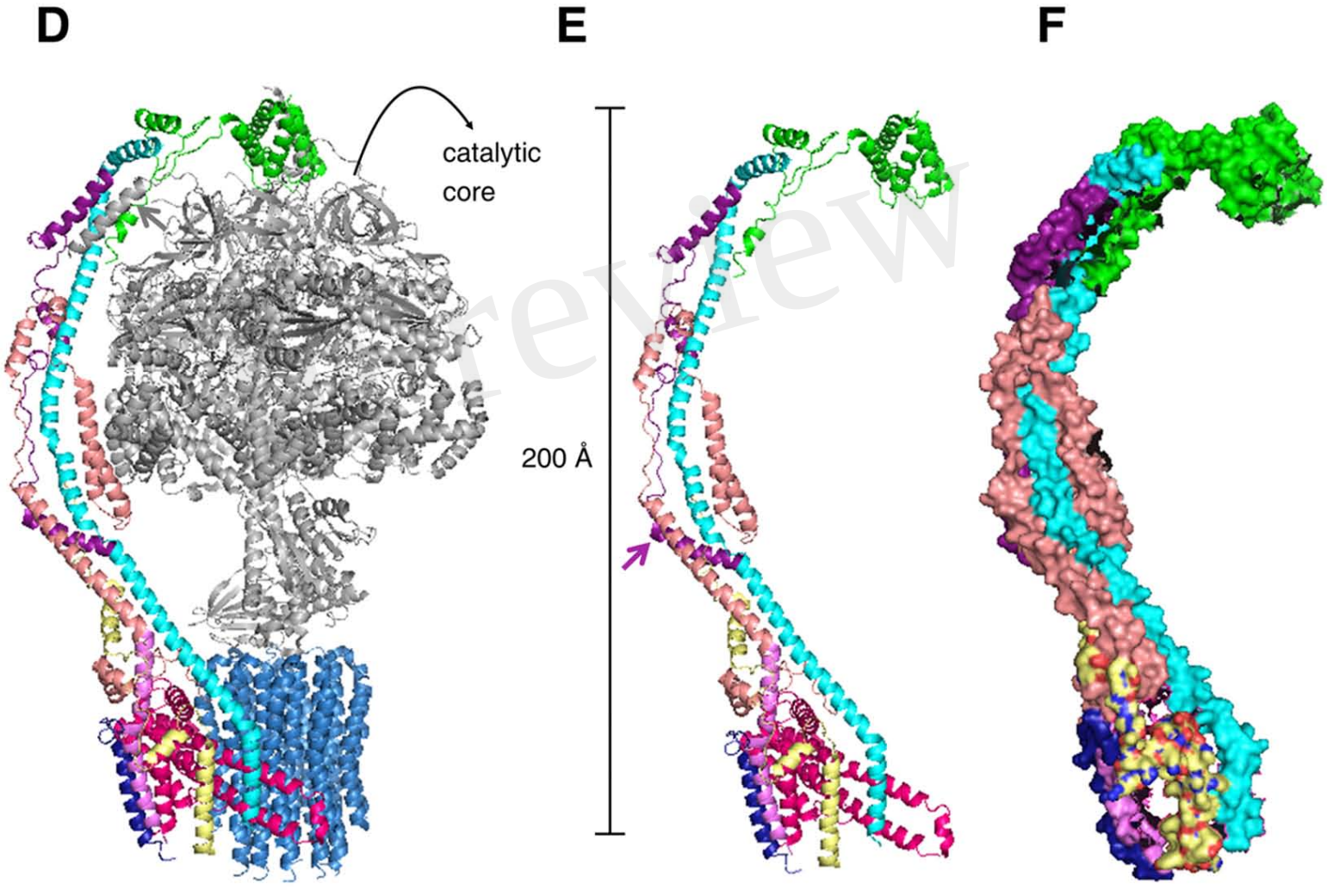

Figure 7.TIF

Figure 5

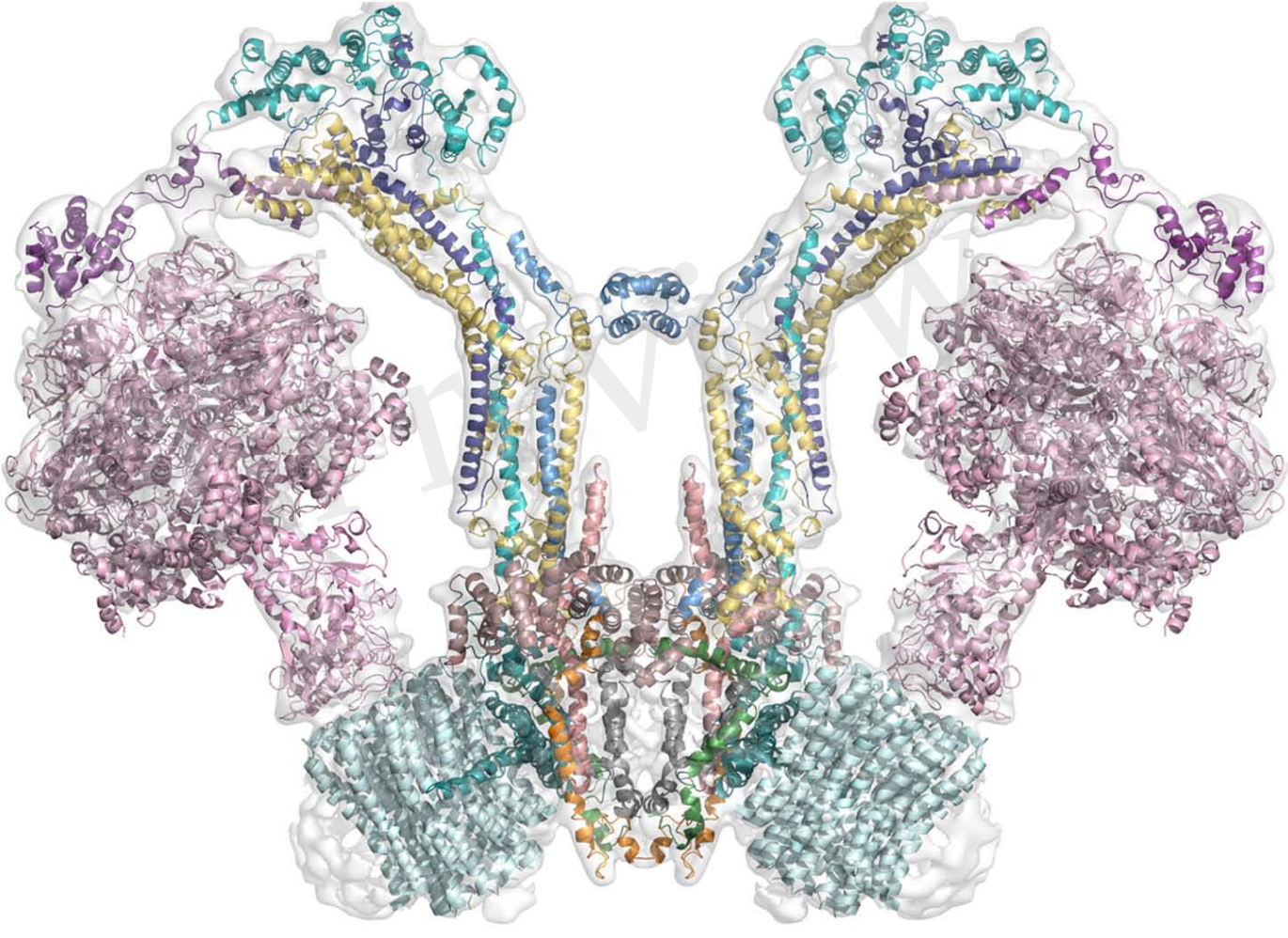

Figure 8.TIF

Figure 6

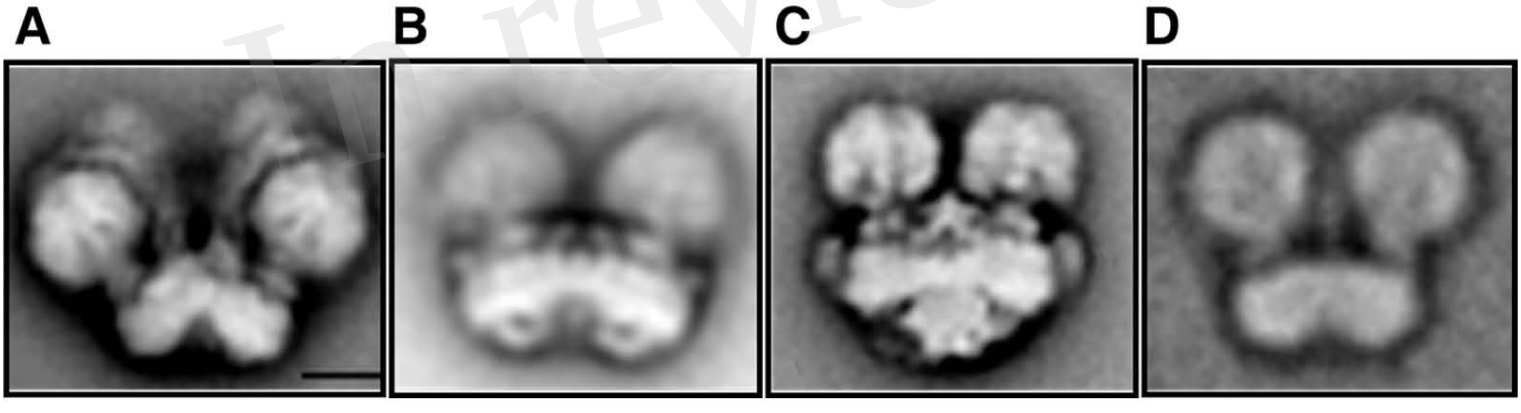

Figure 9.TIF

Figure 7

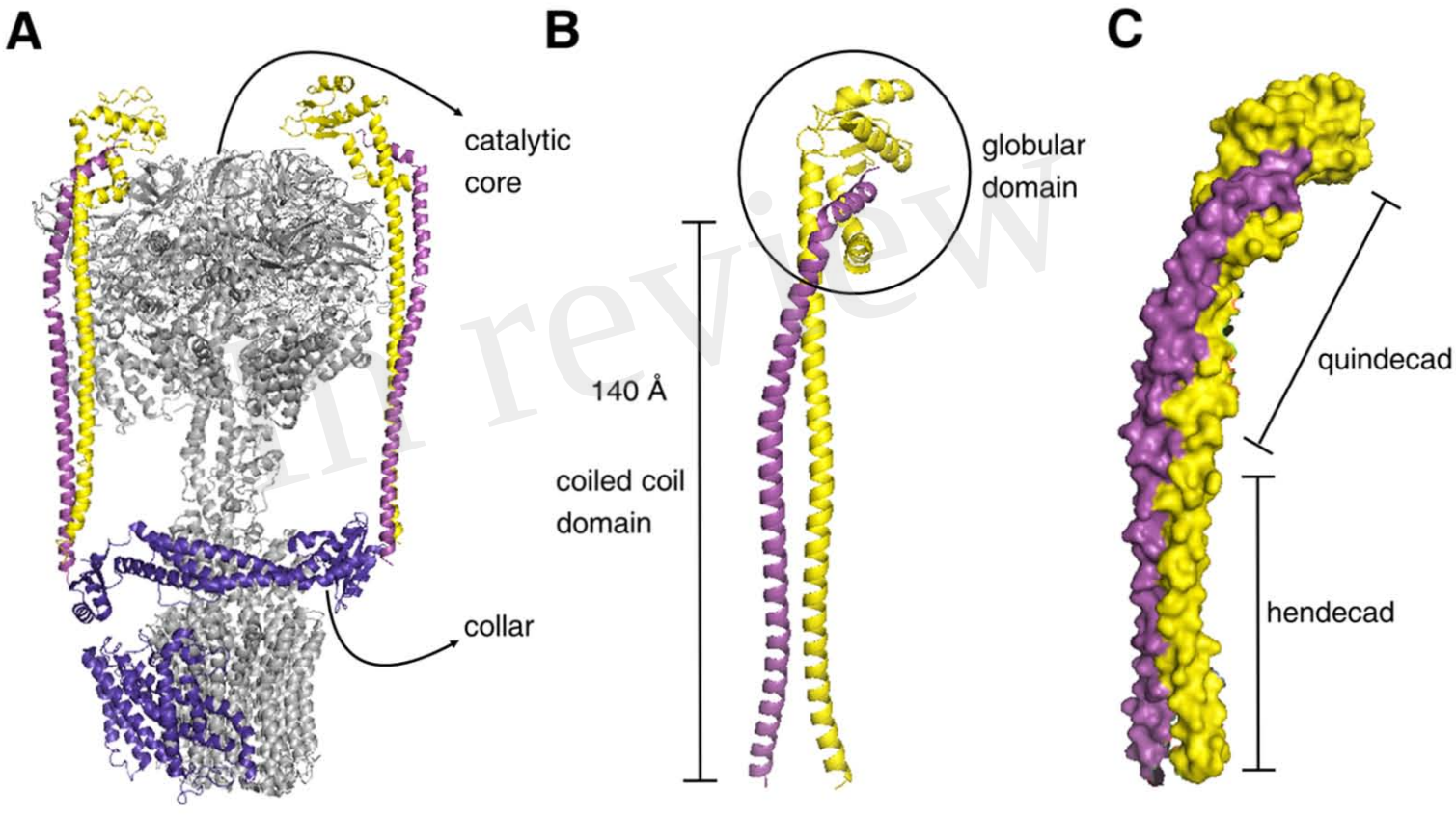

Figure 10.TIF

Figure 8

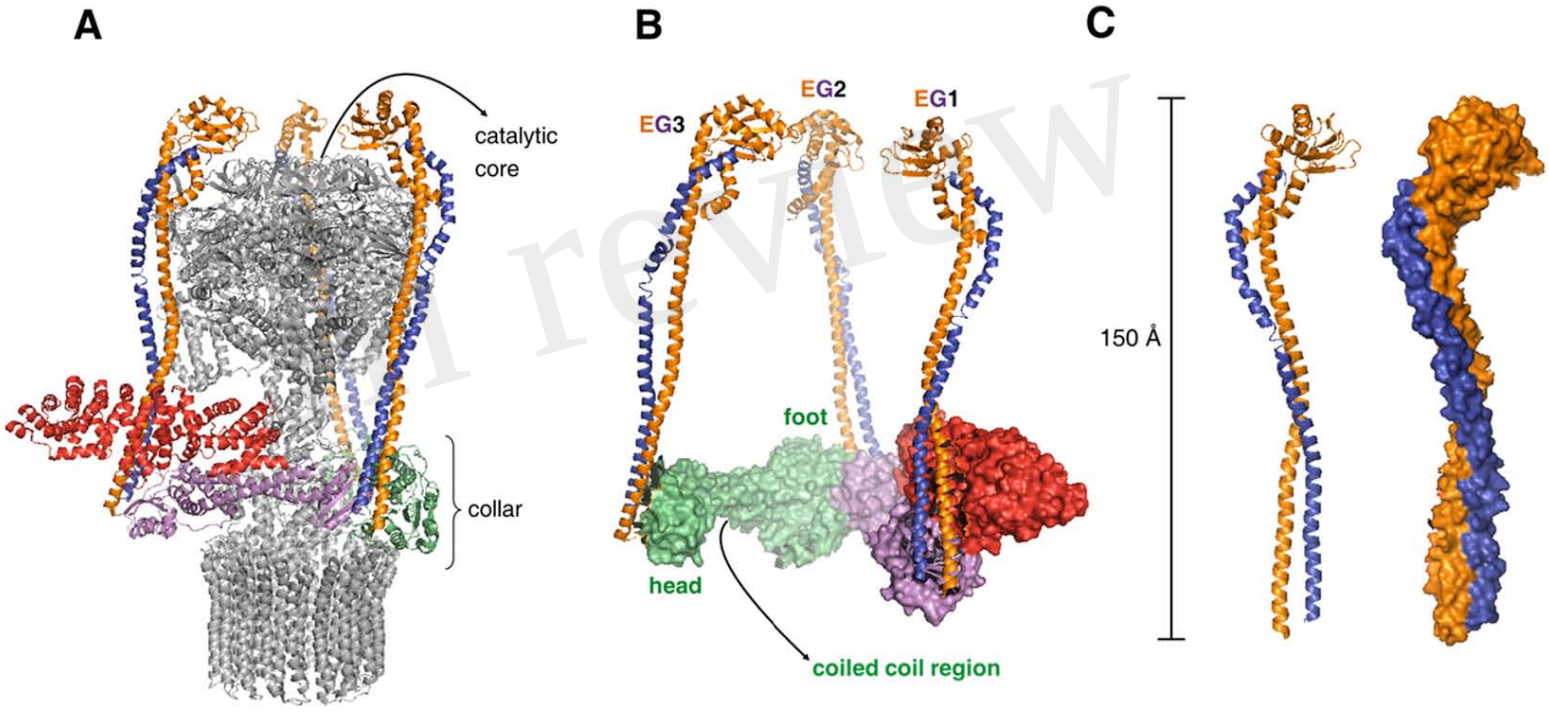

Figure 11.TIF

Figure 9

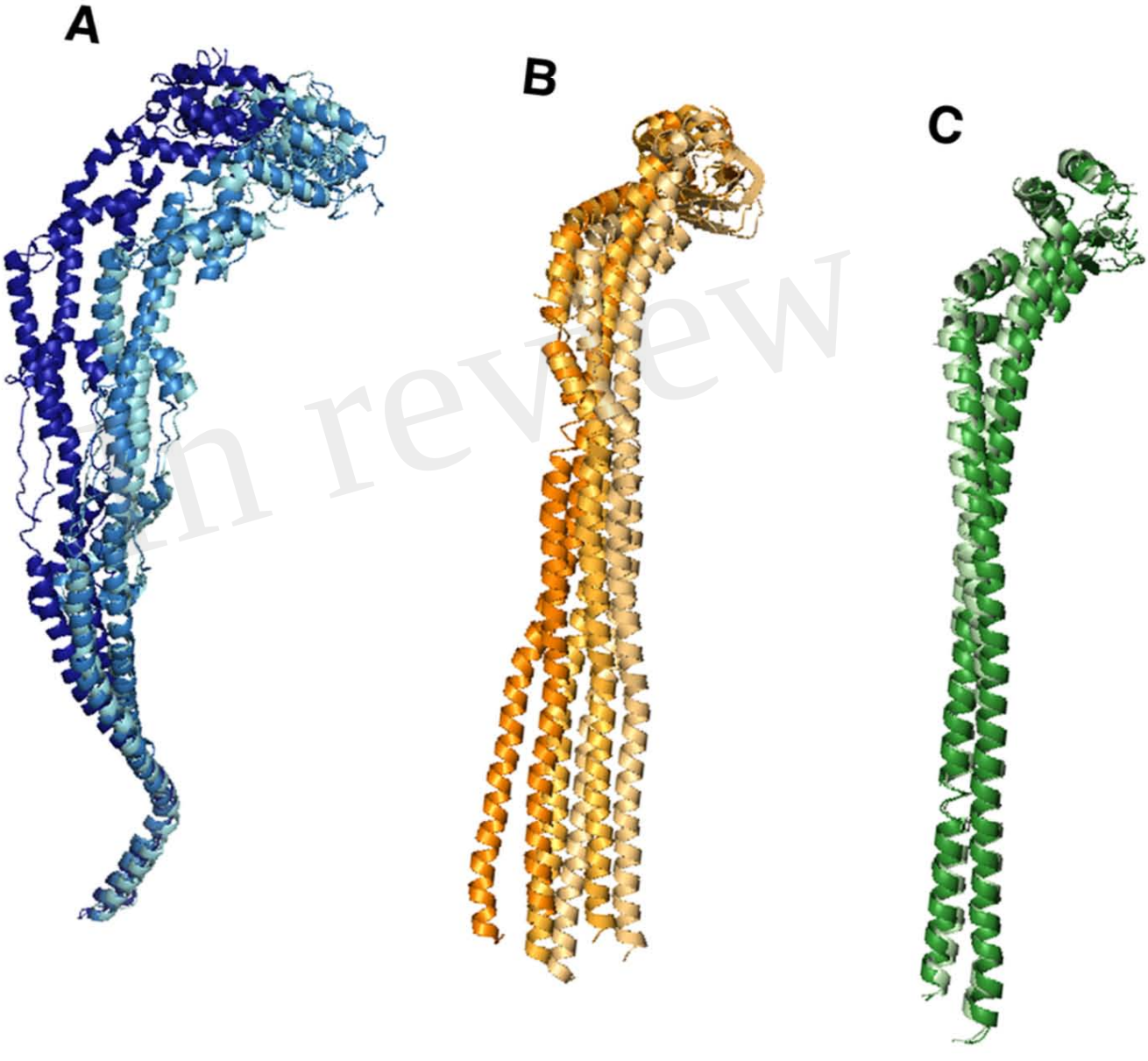

Figure 12.TIF

Figure 10

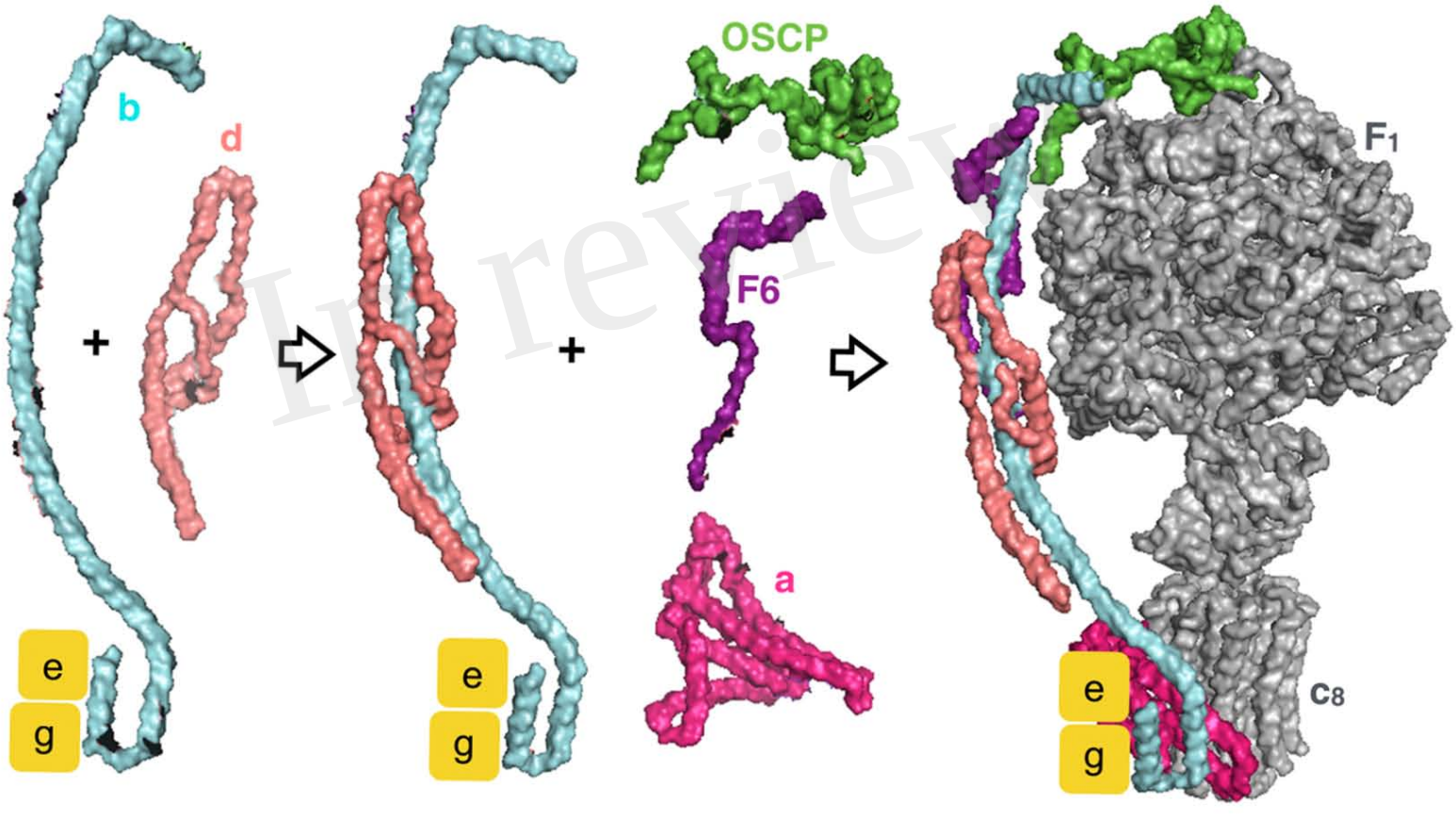

Figure 13.TIF

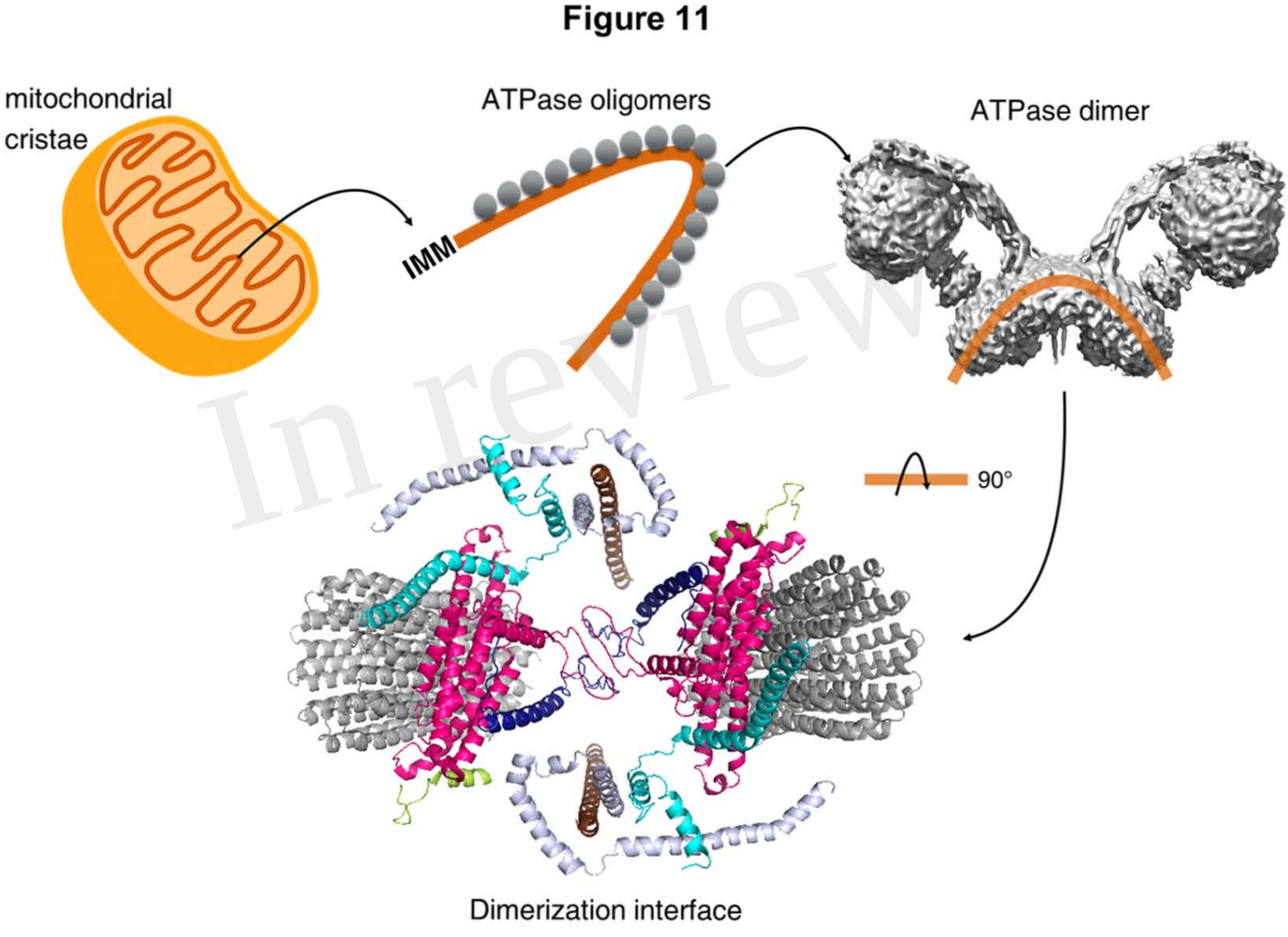

Biochimica et Biophysica Acta 1857 (2016) 359–369

Contents lists available at ScienceDirect

Biochimica et Biophysica Acta

journal homepage: www.elsevier.com/locate/bbabio

Subunit Asa1 spans all the peripheral stalk of the mitochondrial ATP synthase of the chlorophycean alga *Polytomella* sp.

Lilia Colina-Tenorio [a], Héctor Miranda-Astudillo [a], Araceli Cano-Estrada [a], Miriam Vázquez-Acevedo [a], Pierre Cardol [b], Claire Remacle [b], Diego González-Halphen [a,*]

[a] Instituto de Fisiología Celular, Universidad Nacional Autónoma de México, México D.F., Mexico
[b] Genetics and Physiology of Microalgae, Department of Life Sciences, University of Liège, B-4000, Liège, Belgium

ARTICLE INFO

Article history:
Received 1 September 2015
Received in revised form 23 November 2015
Accepted 27 November 2015
Available online 30 November 2015

Keywords:
F_1F_O-ATP synthase peripheral stalk
Dimeric mitochondrial complex V
Chlorophycean algae
Chlamydomonas reinhardtii
Polytomella sp.
Asa subunits

ABSTRACT

Mitochondrial F_1F_O-ATP synthase of chlorophycean algae is dimeric. It contains eight orthodox subunits (alpha, beta, gamma, delta, epsilon, OSCP, *a* and *c*) and nine atypical subunits (Asa1 to 9). These subunits build the peripheral stalk of the enzyme and stabilize its dimeric structure. The location of the 66.1 kDa subunit Asa1 has been debated. On one hand, it was found in a transient subcomplex that contained membrane-bound subunits Asa1/Asa3/Asa5/Asa8/*a* (Atp6)/*c* (Atp9). On the other hand, Asa1 was proposed to form the bulky structure of the peripheral stalk that contacts the OSCP subunit in the F_1 sector. Here, we overexpressed and purified the recombinant proteins Asa1 and OSCP and explored their interactions *in vitro*, using immunochemical techniques and affinity chromatography. Asa1 and OSCP interact strongly, and the carboxy-terminal half of OSCP seems to be instrumental for this association. In addition, the algal ATP synthase was partially dissociated at relatively high detergent concentrations, and an Asa1/Asa3/Asa5/Asa8/a/c_{10} subcomplex was identified. Furthermore, Far-Western analysis suggests an Asa1–Asa8 interaction. Based on these results, a model is proposed in which Asa1 spans the whole peripheral arm of the enzyme, from a region close to the matrix-exposed side of the mitochondrial inner membrane to the F_1 region where OSCP is located. 3D models show elongated, helix-rich structures for chlorophycean Asa1 subunits. Asa1 subunit probably plays a scaffolding role in the peripheral stalk analogous to the one of subunit *b* in orthodox mitochondrial enzymes.

1. Introduction

Mitochondrial F_1F_O-ATP synthase (complex V) is an oligomeric membrane complex that works as a rotary motor driven by the electrochemical proton gradient generated by the respiratory chain. In fungi and animals, the enzyme comprises distinct multi-subunit domains: a soluble fraction (F_1) bearing the catalytic core [α_3/β_3] and a central rotor stalk [$\gamma/\delta/\varepsilon$], a membrane-bound sector F_O that translocates protons [$a/c_{8\text{-}14}$ ring], a peripheral stator stalk [OSCP/*b*/*d*/F6] and a dimerization module [A6L/*e*/*f*/*g*] [1].

Protons are translocated through subunit *a* and the *c*-ring, which in turn drives rotation of the central rotor stalk. The gamma subunit extends from the matrix-exposed side of the *c*-ring and inserts into the F_1 catalytic core, inducing conformational changes in the α_3/β_3 subunits that lead to ATP synthesis [2]. The main function of the peripheral stator stalk is to hold the F_1 sector against the movement of the rotor stalk [3]. In the inner mitochondrial membrane, the ATP synthase forms oligomeric structures [4], stabilized by the dimerization module A6L/*e*/*f*/*g*, that are responsible for the overall architecture of the mitochondrial cristae [5]. Subunits *b* (Atp4), *d*, F6, A6L, *e*, *f* and *g* are not common to all mitochondrial ATP synthases, since several enzymes exhibit different overall architecture and subunit composition. Such is the case of the ATP synthases from the ciliate *Tetrahymena thermophila* [6], the trypanosomatid *Trypanosoma brucei* [7], the euglenoid *Euglena gracilis* [8], and the chlorophycean algae like *Chlamydomonas reinhardtii* and *Polytomella* sp. [9].

The mitochondrial F_1F_O-ATP synthase of chlorophycean algae is isolated as a highly stable dimer of 1600 kDa after solubilization with detergents such as n-dodecyl-β-D-maltoside [10]. As in all known eukaryotes, the rotary and catalytic cores of the algal enzyme are formed by the eight conserved subunits α, β, γ, δ, ε, *a* (Atp6), *c* (Atp9), and OSCP [11]. Nevertheless, nine non-conventional subunits (Asa1 to Asa9), unique to the mitochondrial ATP synthases of chlorophycean algae, are also constituents of the enzyme. Some Asa subunits form the robust peripheral stalk observed in several electron microscopy analyses of the isolated enzyme [12–16] while others (Asa6, Asa8 and Asa9) may participate in the dimerization of the enzyme [17–20].

The neighboring interactions between Asa subunits in the ATP synthase of the colorless chlorophycean alga *Polytomella* sp. have been addressed in the past using several experimental approaches:

* Corresponding author at: Departamento de Genética Molecular, Instituto de Fisiología Celular, UNAM, Apartado Postal 70-600, Delegación Coyoacán, 04510, México D.F., Mexico.
E-mail address: dhalphen@ifc.unam.mx (D. González-Halphen).

http://dx.doi.org/10.1016/j.bbabio.2015.11.012
0005-2728/

characterizing enzyme subcomplexes generated by heat dissociation [9,17], defining near-neighbor relationships of subunits using cross-linking agents [14] and identifying protein–protein interactions *in vitro* employing recombinant subunits [20]. Thus, successive models for the topological disposition of the Asa polypeptides in the peripheral arm of the enzyme have been proposed [9,17,14,20]. An electron cryo-microscopy map at 7.0 Å overall resolution of the *Polytomella* dimeric ATP synthase revealed that the peripheral stalks consist of several entwined alpha-helices that give rise to a solid scaffold [16] that is strikingly more robust than the peripheral arm of enzymes from other biological sources, including bovine [21,22], yeast [23], spinach chloroplasts [24], and *Escherichia coli* [25]. Although many Asa subunits are thought to be localized in the peripheral stator stalk, the position of the Asa1 subunit remains controversial. On one hand, Asa1 was identified in a subcomplex that contained subunits Asa3/Asa5/Asa8/*a*/*c* and that appeared transiently during a time course of heat treatment of the enzyme before it further dissociated into its free components [9]. This result suggested that Asa1 may be interacting closely with subunits which are known to be membrane-bound, i.e. Asa8 (one transmembrane stretch or TMS), *a* (4–5 membrane-embedded helices), and *c* (two TMS). On the other hand, Asa1 was proposed to form a bulky structure near the catalytic region of the enzyme close to OSCP [17], based on electron microscopy studies [12] and on the fact that Asa1 behaved as an extrinsic membrane protein. Here, we studied the disposition of Asa1 in the peripheral stalk and suggest that Asa1 spans the whole peripheral stalk from the matrix-exposed side of the inner mitochondrial membrane to the F_1 region where OSCP resides. We propose that chlorophycean Asa1, although not anchored directly to the lipid bilayer, is the structural equivalent of subunit *b* (Atp4) found in the orthodox mitochondrial ATP synthases of yeasts, mammals and green plants.

2. Materials and methods

2.1. Algal strains and growth conditions

Polytomella spec. (Strain number 198.80, isolated by E.G. Pringsheim), identical to *Polytomella parva*, was originally obtained from the Culture Collection of Algae (University of Göttingen, Germany). Cells were grown for 48 h at room temperature in 2.5-l wide-bottom culture flasks without shaking, in a medium containing 4.0 g/l of sodium acetate, 2.0 g/l of Bacto™ Tryptone (Becton, Dickinson and Co.) and 2.0 g/l of Bacto™ Yeast Extract (Becton, Dickinson and Co.), supplemented with 10 μg/ml of vitamin B1 (thiamine) and 0.5 μg/ml of vitamin B12 (cobalamin).

2.2. Polytomella mitochondrial ATP synthase purification

Polytomella sp. cells were collected by centrifugation at 7500 *g* for 10 min and washed with sucrose buffer (20 mM Tris, 0.37 M sucrose, 4 M potassium EDTA, pH 7.4). The resulting pellet was suspended in the same buffer (80–100 ml). The cells were broken using a Potter homogenizer, centrifuged at 7500 *g* for 15 min and the supernatant was recovered. The unbroken cell pellet was treated again as described above; both supernatants were mixed and centrifuged at 17,500 *g* for 20 min to recover the mitochondria pellet, which was suspended in a small volume of sucrose buffer and stored at −70 °C until used. The mitochondria (250 mg of protein) were diluted to a final protein concentration of 10 mg/ml with solubilization buffer (50 mM Tris, 100 mM NaCl, 1 mM $MgSO_4 \cdot 7H_2O$, 10% glycerol, 1 mM PMSF, 50 μg/ml TLCK, pH 8.4) and were incubated with n-dodecyl β-D-maltoside (2 mg of detergent per mg of protein) under mild agitation for 30 min at 4 °C. The sample was centrifuged at 90,000 *g* for 20 min, the supernatant was recovered, diluted 3 times with loading buffer (50 mM Tris, 1 mM $MgSO_4 \cdot 7H_2O$, 10% glycerol, 1.0 mM PMSF, 50 μg/ml TLCK, 0.01% n-dodecyl β-D-maltoside pH 8.4) and loaded to a Source 15Q 10/100 GL column (CV 8 ml) (GE Healthcare) with a 1 ml/min flow. The column was washed with 75 mM NaCl and then eluted with a linear NaCl gradient (75–250 mM) in the same buffer. Two milliliter fractions were collected and analyzed by Tricine–SDS–PAGE. The fractions enriched with ATP synthase were pooled and concentrated to a volume of 4 ml using an Amicon Ultra 15 centrifugal filter 100,000 NMWL. Glycerol and ATP were added to final concentrations of 30% and 1.0 mM, respectively, and the sample was further concentrated to a final volume of 400 μl. This sample was injected to a Superose 6 10/300 GL (CV 24 ml) (GE Healthcare) previously equilibrated with Superose buffer (50 mM Tris, 150 mM NaCl, 1 mM $MgSO_4 \cdot 7H_2O$, 10% glycerol, 1 mM PMSF, 50 μg/ml TLCK, 0.01% n-dodecyl β-D-maltoside, 2 mM ATP, pH 8.4). The elution was carried out at a 0.25 ml/min flow. Fractions were collected (500 μl each) and analyzed by SDS–PAGE and BN-PAGE. The purified ATP synthase was aliquoted and stored at −70 °C until used.

2.3. Protein analysis

Denaturing gel electrophoresis was carried out in a Tricine–SDS–PAGE system [26], and when indicated, it was followed by 2D-Glycine–SDS–PAGE analysis [27]. Blue native polyacrylamide gel electrophoresis (BN-PAGE) was carried out as previously described [28]. When indicated, 1D-BN-PAGE was followed by 2D Tricine–SDS–PAGE [26]. Protein concentrations were determined as published [29]. Mass spectrometry and Edman degradation analyses were carried out at the "Unidad de Genómica, Proteómica y Metabolómica" at LaNSE, CINVESTAV del IPN, Mexico, and at the Protein Chemistry Laboratory at the Department of Biochemistry of Texas A&M University, USA, respectively.

2.4. Dissociation of the ATP synthase into subcomplexes

The purified algal ATP synthase (100 μg of protein) was incubated for 24 h at 4 °C under mild agitation in the presence of 3.0% lauryl maltoside and the solubilized sample subjected to BN-PAGE in 4–12% gradient acrylamide gels. The resulting lane of interest was excised and incubated in the presence of 1.0% SDS and 1.0% beta-mercaptoethanol for 15 min and then subjected to 2D Tricine–SDS–PAGE in 14% acrylamide gels.

2.5. Cloning of the cDNAs encoding subunits of the ATP synthase of Polytomella sp. in expression vectors

The cDNAs of *Asa1*, *Asa8*, *OSCP* and *OSCPΔC* were PCR-amplified from a *Polytomella* sp. cDNA library cloned in λ-ZapII phages [30] using specific oligonucleotide primers: for *Asa1*, forward 5′-GCGGCATGCGCTAG CTACCTTGCCCCCCTCCGCTCTGAT-3′ and reverse 5′-GCGCTGCAGGCG GCCGCTTAGTTACCGTTGACGAGATC-3′; for *Asa8* forward 5′-GCGGGA TCCGCTAGCATGGTCCTCGGTGAGGTCTAC-3′ and reverse 5′-GCGAAGCT TTAGTGACCACCAGCAGTGTAAG-3′; for *OSCP*, forward 5′-GCGGGATC CCATATGGCTGCCCAGGCTGAGCTCAAG-3′ and reverse 5′-GCGCTGCA GGTCGACAACGAACTAATTTAAATAGAAAGA-3′ and for *OSCPΔC*, forward 5′-GCGGGATCCCATATGGCTGCCCAGGCTGAGCTCAAG-3′ and reverse 5′-GCGCTGCAGGTCGACCTAAACCTCCTTCTTGTGAGCGAG-3′. The *Asa1* amplification product was cloned into a pET28a vector using the restriction sites *Nhe*I and *Bam*HI. This vector adds a hexa-histidine tag (6His-tag) to the N-terminus of the expressed protein (H_6-Asa1). To obtain the untagged version of Asa1 subunit, a new amplification was performed changing the restriction sites to *Nco*I. The amplicon was cloned into the pET28a vector upstream the hexa-histidine tag using the *Nco*I restriction site. The *Asa8* amplification product was cloned into a pQE30 vector using the restriction sites *Bam*HI and *Hind*III. The OSCP amplification product was cloned into a pET28a vector as well as into a pET3a vector using the restriction sites *Nhe*I and *Sal*I. The *OSCPΔC* product was obtained using the same forward primer as for OSCP and the reverse primer 5′-GCGCTGCAGGTCGACCTAAACCTCCTTCTTGTGA

GCGAG-3′. The *OSCPΔC* was cloned into pET28a using the restriction sites *Nhe*I and *Sal*I.

2.6. Overexpression of recombinant proteins

Competent *E. coli* BL21 Codon Plus (DE3) RIL cells (Agilent Technologies) were transformed with the construct of interest. Cells were grown in LB medium containing 64 μg/ml chloramphenicol and one of the following antibiotics: 50 μg/ml kanamycin for the pET28a vector or 100 μg/ml ampicillin for the pET3a vector. The overexpressed subunits were the complete Asa1 subunit (GenBank: AJ558193.2), the histidine-tagged H_6-Asa1, the complete histidine-tagged H_6-OSCP subunit (GenBank: GQ422707.1) and the tagged N-terminal region of OSCP (H_6-OSCP-ΔC, approximately 13.5 kDa, comprising residues 5 to 126 of OSCP). Asa8 recombinant subunit was overexpressed in *E. coli* XL1-Blue and cells grown in 100 μg/ml ampicillin and 40 μg/ml tetracycline.

2.7. Purification of proteins

Bacterial inclusion bodies (ICBs) retaining the overexpressed recombinant proteins were isolated, washed with detergent and stored as previously described [20]. The recombinant polypeptides Asa1, Asa8, H_6-Asa1, H_6-OSCP and H_6-OSCP-Δc were purified under denaturing conditions using affinity chromatography. The ICBs were solubilized in PBS buffer (50 mM NaH_2PO_4, 500 mM NaCl, pH 7.8) containing 8.0 M urea with mild agitation at 4 °C during 8 h. The insoluble material was removed by centrifugation at 17,500 *g* for 10 min. The sample was diluted with PBS buffer to a final concentration of 4.0 M urea; imidazole was added to a final concentration of 10 mM from a 1.0 M stock solution. Then the sample was loaded on a 5 ml HisTrap FF crude column (GE Healthcare Life Sciences) equilibrated with PBS buffer containing 4.0 M urea. The column was washed with 30 mM imidazole and the proteins were eluted with a 30–500 mM imidazole linear gradient in the same buffer. The fractions obtained from the elution were analyzed by Tricine–SDS–PAGE and those enriched with the recombinant protein of interest were pooled, concentrated, and stored at −70 °C until used. The ICBs containing untagged Asa1 were solubilized as described above. The resulting sample was dialyzed overnight against PBS buffer with 0.5 M urea, 500 mM NaCl, 2% glycerol and 0.1% Tween 20. The aggregated material was removed by centrifugation at 17,500 *g* for 10 min and the supernatant was dialyzed (4 h) against the same buffer containing 200 mM NaCl, centrifuged at 17,500 *g* for 10 min and loaded to a 8 ml Source 15Q 10/100 column (GE Healthcare Sciences) equilibrated with the same buffer. The protein was recovered after applying a 200–500 mM NaCl linear gradient with the same buffer; the enriched fractions were pooled, concentrated and stored at −70 °C until used. The solubilized untagged OSCP inclusion bodies were dialyzed overnight against a buffer containing 20 mM MES, 2.0% glycerol, 0.05% Tween 20, 1 mM EDTA, 1 mM DTT, pH 6.0. The recovered sample was centrifuged at 17,000 *g* for 10 min and the supernatant was loaded to a DEAE Sepharose FF column (24 ml) equilibrated with the same buffer. The protein was eluted with a 0–1.0 M NaCl linear gradient (10 column volumes) with the same buffer. The eluted fractions were analyzed by Tricine–SDS–PAGE and the enriched fractions were pooled, concentrated and stored at −70 °C until used.

2.8. Antibody production and immunoblotting

To generate antibodies against subunits Asa1 and OSCP, the polypeptides of the algal ATP synthase (50 μg of protein per lane) were resolved by Tricine–SDS–PAGE (14% acrylamide) in the presence of Serva Blue G as previously described [31]. The recombinant Asa8 subunit was purified and subjected to the same electrophoretic conditions. The subunits of interest were excised from the gels, grinded in a mortar in the presence of 20 mM Tris (pH 7.0), mixed with Freund's complete adjuvant and injected into rabbits. The presence of antibodies in the sera was ascertained by Western blot analysis carried out as previously described [32]. For Western blots, goat anti-rabbit IgG conjugated with alkaline phosphatase (1:3000 for 2 h) was used, and color developed with nitro-blue tetrazolium chloride and 5-bromo-4-chloro-3′-indolylphosphate p-toluidine salt. Western blot images were captured in an HP Scanjet G4050.

2.9. Protein–protein interaction assayed by Far-Western analysis

Far-Western analysis was carried out according as previously described [33] with modifications [20]. Purified *Polytomella* sp. ATP synthase was subjected to Tricine–SDS–PAGE and transferred to nitrocellulose membranes. The membranes containing the denatured enzyme were blocked with a 5.0% powdered milk suspension overnight and then incubated for 4 h in the presence of the externally added protein of interest in increasing concentrations in the corresponding buffer (for Asa1: PBS buffer with 0.5 M urea, 500 mM NaCl, 2.0% glycerol and 0.05% Tween 20, pH 7.8; and for Asa8 and OSCP: MES 20 mM, 500 mM NaCl, 2.0% glycerol, and 0.05% Tween 20, pH 6.0) supplemented with 1.0% powdered milk. Protein bands were visualized by Ponceau S red staining (0.1% in 5.0% acetic acid) for 10 min. The membranes were washed two times with the same buffer. The protein of interest was recognized using a specific antibody incubated in TTBS buffer (20 mM Tris–HCl pH 8.0, 500 mM NaCl and 0.05% Tween 20), followed by incubation with a secondary antibody in the same buffer. Finally, the membrane was immunochemically stained as described above for Western blot analyses [34].

2.10. Protein–protein interactions assayed by affinity chromatography

These experiments were carried out as described [20] with some modifications. The whole procedure is carried out at 4 °C unless otherwise stated. The corresponding purified recombinant proteins H_6-Asa1/OSCP and Asa1/H_6-OSCP-Δc (2 mg of each protein) were dialyzed together against PBS buffer containing 500 mM NaCl, 2.0% glycerol and 0.05% Tween 20, pH 7.8. The aggregated material was removed by centrifugation at 17,000 *g* for 10 min. Thirty microliters of equilibrated Ni Sepharose 6 FF resin (Amersham Biosciences) was added to the sample and imidazole was added to a final concentration of 30 mM from a 1 M stock solution. The sample was incubated with mild shaking for 5 h. The resin was recovered by centrifugation at 500 *g* for 5 min and then washed 10 times with PBS buffer containing 50 mM imidazole. The washed resin was poured into a column and the proteins were eluted with a step imidazole gradient from 50 mM to 500 mM. Fractions recovered from the column were analyzed by Tricine–SDS–PAGE.

2.11. Protein structure prediction

Sequences of 11 chlorophycean Asa1 subunits were retrieved from the data bases: *Dunaliella tertiolecta* (iMicrobe: CCMP1320), *Chlamydomonas chlamydogama* (iMicrobe: MMETSP1392), *Chlamydomonas Euryale* (iMicrobe: CAMPEP_0201452882); *Chlamydomonas leiostraca* (iMicrobe: MMETSP1391), *Chlamydomonas reinhardtii* (NCBI: XP_001692395), *Chlamydomonas* sp. (iMicrobe: MMETSP1180), *Polytomella* sp. (NCBI: CAD90158), *Polytomella parva* (iMicrobe: MMETSP0052_2–20,121,109); *Polytomella capuana* (iMicrobe: c26576_g1_i1); *Polytomella magna* (iMicrobe: c16202_g2_i1); *Polytomella pyriformis* (iMicrobe: c17010_g1_i1) and *Volvox carteri* (NCBI: XP_002951807). Sequences were aligned using ClustalW (https://npsa-prabi.ibcp.fr/cgi-bin/npsa_automat.pl?page=/NPSA/npsa_clustalw.html) [35]. 3D structure prediction of each individual sequence was carried out in the RaptorX server (http://raptorx.uchicago.edu/) [36].

3. Results

3.1. Overexpression and purification of recombinant Asa subunits

Our study focused on the interactions of subunits Asa1 and OSCP of the ATP synthase of *Polytomella* sp. using recombinant subunits. For this purpose, the proteins of interest were overexpressed and purified. Fig. 1 shows a Tricine–SDS–gel with the purified recombinant subunits Asa1, OSCP with and without a histidine tag (OSCP and H_6-OSCP respectively) and a histidine-tagged, recombinant fragment of OSCP comprising residues 5–126 of the mature protein and therefore lacking the final 71 residues of the carboxy-terminal region (hereby named H_6-OSCP-Δc).

3.2. On the interaction of Asa1 and OSCP

One strategy used to detect protein–protein interactions is Far-Western blotting. We assayed possible interactions of the purified, recombinant Asa1 subunit with the entire ATP synthase, searching for binding of the externally added, recombinant polypeptide to some of the subunits of the complex. The ATP synthase was resolved by SDS–PAGE and transferred to nitrocellulose membranes. The strips, containing the same concentration of enzyme, were incubated with increasing concentrations of the recombinant Asa1 subunit and afterwards decorated with an anti-Asa1 antibody and the appropriate secondary antibody (Fig 2A). The position of each of the ATP synthase subunits in the blots was identified beforehand by Ponceau S red staining.

In all lanes, as expected, the anti-Asa1 antibody recognized the Asa1 subunit of the ATP synthase, but at increasing concentrations of the externally added, recombinant Asa1, additional bands appeared on the blot, one of 31 kDa corresponding to either subunit Asa4 or gamma and one of 22 kDa corresponding to either OSCP or subunit *a* (Atp6) (Fig 2A, lanes 3 to 6). This indicated that the recombinant Asa1 subunit, incubated in a soluble form over the nitrocellulose membrane, interacted with some of the blotted polypeptides of the ATP synthase. Nevertheless, with this approach, it was impossible to distinguish if the 31 kDa band was Asa4 or gamma, since both polypeptides migrate together in the SDS–PAGE system used. The same happened with the 22 kDa band, which could correspond either to OSCP or to subunit *a* (Atp6), two polypeptides that exhibit the same mobility in the electrophoretic conditions used. At higher concentrations of the externally added, recombinant Asa1 subunit, additional faint bands were observed, that were interpreted to result from unspecific binding.

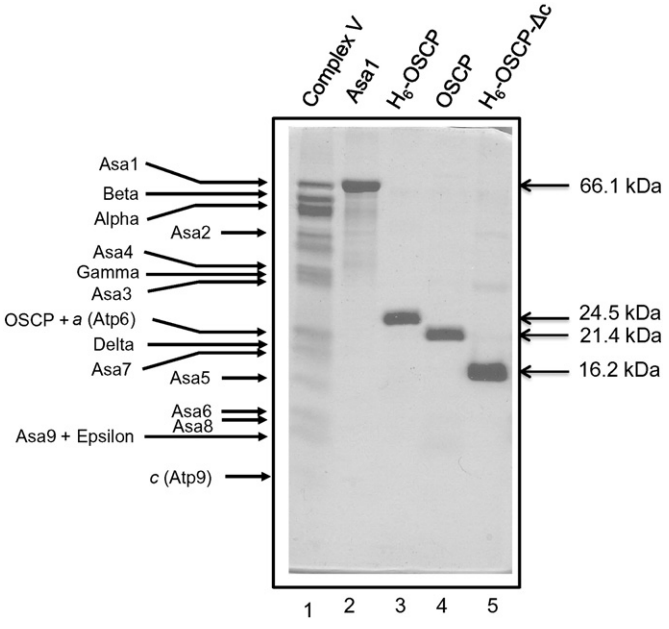

Fig. 1. *Polytomella* ATP synthase and some of the recombinant subunits used in this work. Tricine–SDS–polyacrylamide gel showing the identity of the 16 subunits of the *Polytomella* ATP synthase complex (25 μg of protein, lane 1). Three micrograms of each overexpressed and purified recombinant subunit were loaded in lanes 2 to 5. Molecular masses indicated by arrows were calculated using as molecular mass marker the well-characterized polypeptide composition of the algal ATP synthase (lane 1).

A variation of the above experiment was carried out in which the isolated, recombinant OSCP subunit was resolved by SDS–PAGE and transferred to nitrocellulose membranes. The strips, containing the same concentration of OSCP, were incubated with increasing concentrations of the recombinant Asa1 subunit and afterwards incubated with an anti-Asa1 antibody and the appropriate secondary antibody (Fig 2B). At increasing concentrations of the externally added recombinant Asa1, the anti-Asa1 antibody recognized the OSCP subunit bound to the nitrocellulose membrane (Fig 2B, lanes 3 to 6). This further suggested the interaction of Asa1 and OSCP.

We previously reported a combined gel electrophoresis system that allowed almost complete resolution of all the polypeptide components of the algal ATP synthase [14]. In this 2D system, subunit OSCP was resolved from subunit *a*, and subunit Asa4 was separated from the gamma subunit. The recombinant Asa1 polypeptide was incubated with nitrocellulose membranes in which all the subunits of the algal ATP synthase were resolved in a two dimensional array (Fig 3A). As in the 1D Far-Western blot experiments, the anti-Asa1 antibody recognized only the Asa1 subunit both in the 2D array and in the control lane in which the ATP synthase was loaded as a molecular mass standard (Fig 3B). In contrast, when the 2D array blot was pre-incubated with the isolated Asa1 recombinant protein, two additional main bands were observed that correspond to the gamma subunit and OSCP (Fig 3C). When a similar 2D-array (Fig 4A) was blotted and incubated with an anti-OSCP antibody, the OSCP subunit was clearly identified (Fig 4B). Finally, when this 2D array blot was pre-incubated with the isolated OSCP recombinant protein, three additional bands were observed, that were identified as Asa1, alpha subunit and the gamma subunit (Fig 4C). Thus, 2D-Far-Western analysis allowed us to resolve the ambiguities encountered in 1D-Far-Western and suggested the interactions Asa1-OSCP and Asa1-gamma. Smaller polypeptides with a molecular mass below 20 kDa were not observed in the 2D-Far-Western blot, probably because of their low concentration and more diffused spots.

An additional Far-Western assay was carried out in which three forms of OSCP were resolved and transferred to a nitrocellulose membrane: the recombinant protein (OSCP), the recombinant protein containing a hexa-histidine tag (H_6-OSCP), and the tagged amino-terminal fragment of the protein (H_6-OSCP-Δc). Complex V and the recombinant Asa1 protein were also transferred to the membrane (Fig 5A, lanes 1–5). As in previous Far-Western blot experiments, the anti-Asa1 antibody, in the absence of externally added Asa1 protein, recognized only the Asa1 subunit in complex V and the isolated Asa1 recombinant protein (Fig 5B, lanes 6–10). By contrast, when the membrane was incubated with the Asa1 protein before the addition of the anti-Asa1 antibody, additional bands appeared in the blot: gamma and OSCP in complex V (Fig 5C, lane 11), and the two forms of the intact OSCP protein (H_6-OSCP and OSCP, Fig 5C, lanes 13 and 14 respectively). No antibody was bound to the fragmented OSCP subunit (H_6-OSCP-Δc, lane 15 in Fig. 5C), suggesting that the carboxy-terminus of OSCP is instrumental for binding the externally added, recombinant Asa1 subunit. This experiment also suggested that the binding of Asa1 to OSCP is not spurious, since no binding of Asa1 to H_6-OSCP-Δc was observed, even when the latter was loaded at similar protein concentrations similar to OSCP.

To further explore the interaction of Asa1 and OSCP using a different experimental approach, the isolated, recombinant Asa1 protein containing a 6His-tag (H_6-Asa1), was bound to a Ni Sepharose resin. Then, the recombinant OSCP (lacking a 6His-tag) was added and the resin was washed with 30 mM imidazole. In order to discard the possibility of

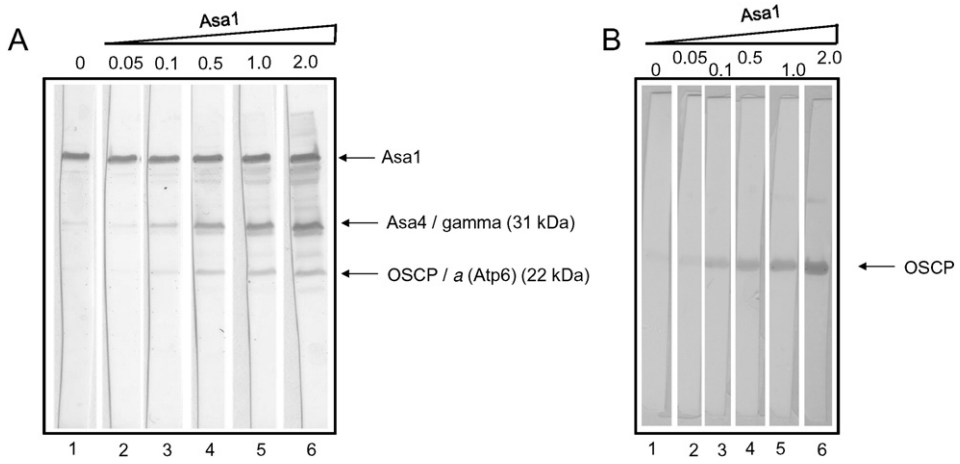

Fig. 2. Interaction of Asa1 with polypeptides of the algal ATP synthase and the OSCP subunit. Far-Western analysis of *Polytomella* ATP synthase (25 μg of protein per lane) (panel A) and of the purified, recombinant OSCP polypeptide (3 μg of protein per lane) (panel B) incubated for 4 h with increasing quantities of the isolated, recombinant Asa1 polypeptide as indicated (total nanomoles of Asa1 in a 5 ml final volume), and then decorated with an anti-Asa1 antibody. The identities of the main bands are indicated.

an adventitious binding of OSCP to the nickel matrix, a second experiment was performed in which no protein was bound to the resin, but a non-tagged OSCP recombinant protein was added in parallel. While OSCP eluted in the first fractions of the column lacking bound Asa1 (Fig 6A, upper panel), a fraction of OSCP was retained in the column that contained H_6-Asa1. When a 30 to 500 mM imidazole gradient was applied to the column, both OSCP and H_6-Asa1 were found to elute together in several fractions (Fig 6A, lower panel). This suggested that Asa1, when bound to the nickel column, is able to bind and retain OSCP. A complementary experiment was carried out. In this case, the isolated, recombinant H_6-OSCP-Δc fragment was bound to the nickel resin. Then, the recombinant Asa1 subunit (lacking a 6His-tag) was loaded on the column and washed with 30 mM imidazole. As a control, the same nickel matrix, with no bound protein to it, was also loaded with a non-tagged Asa1 recombinant subunit and run in parallel. Asa1 eluted in the first fractions, both from the resin that lacked (Fig 6B, upper panel) and the one that contained bound H_6-OSCP-Δc fragment (Fig 6B, lower panel). When the column was eluted with a 30 to 500 mM imidazole gradient, only the H_6-OSCP-Δc fragment was recovered (Fig 6, lower panel). These results confirmed that Asa1 does not bind to the H_6-OSCP-Δc fragment and that therefore the carboxy-terminus of OSCP is required for Asa1 binding.

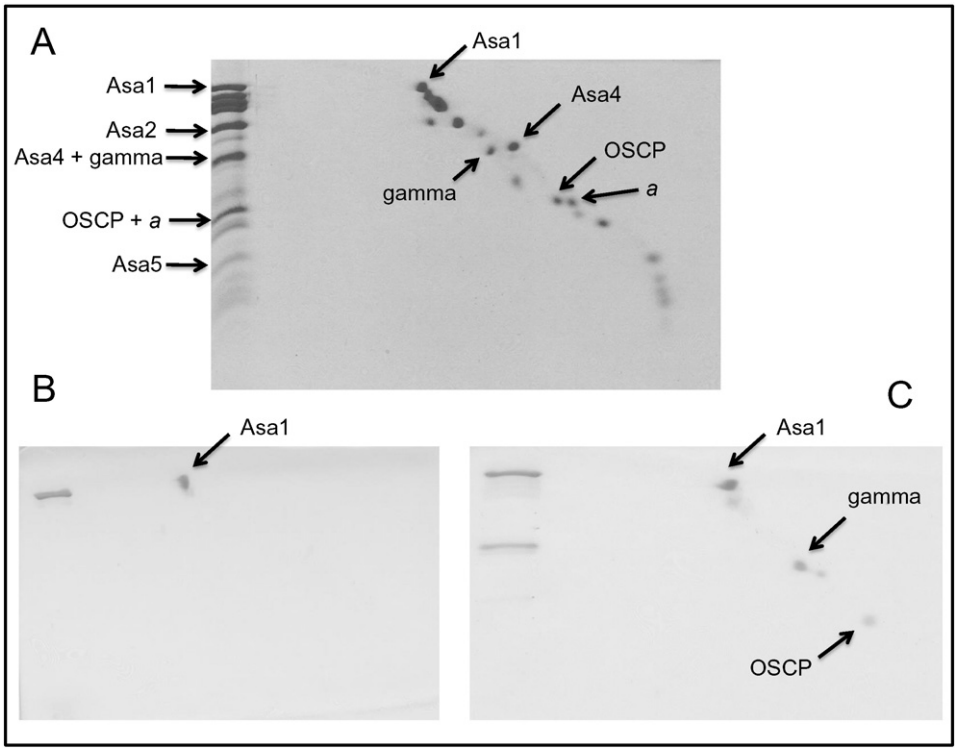

Fig. 3. Interaction of Asa1 with the gamma and OSCP subunits. A) 2D resolution of the polypeptides that constitute the mitochondrial *Polytomella* F_1Fo-ATP synthase. *Polytomella* ATP synthase (100 μg of protein) was resolved in a glycine–SDS–PAGE system (10% acrylamide). The 1D gel was then subjected to 2D Tricine–SDS–PAGE (14% acrylamide) and stained with Coomassie brilliant blue. A lane loaded with the enzyme (20 μg of protein) on the left-hand side of the 2D gel indicates the subunits of interest. B) Western blot analysis of the *Polytomella* ATP synthase resolved by 2D Tricine–SDS–PAGE. A gel equivalent to the one shown in panel A was transferred to a nitrocellulose membrane and decorated with an anti-Asa1 antibody. C) Far-Western blot analysis of the *Polytomella* ATP synthase resolved by 2D Tricine–SDS–PAGE. A gel equivalent to the one shown in panel A was transferred to a nitrocellulose membrane and incubated for 4 h with 2.0 nmol of the isolated, recombinant Asa1 protein, and then decorated with an anti-Asa1 antibody.

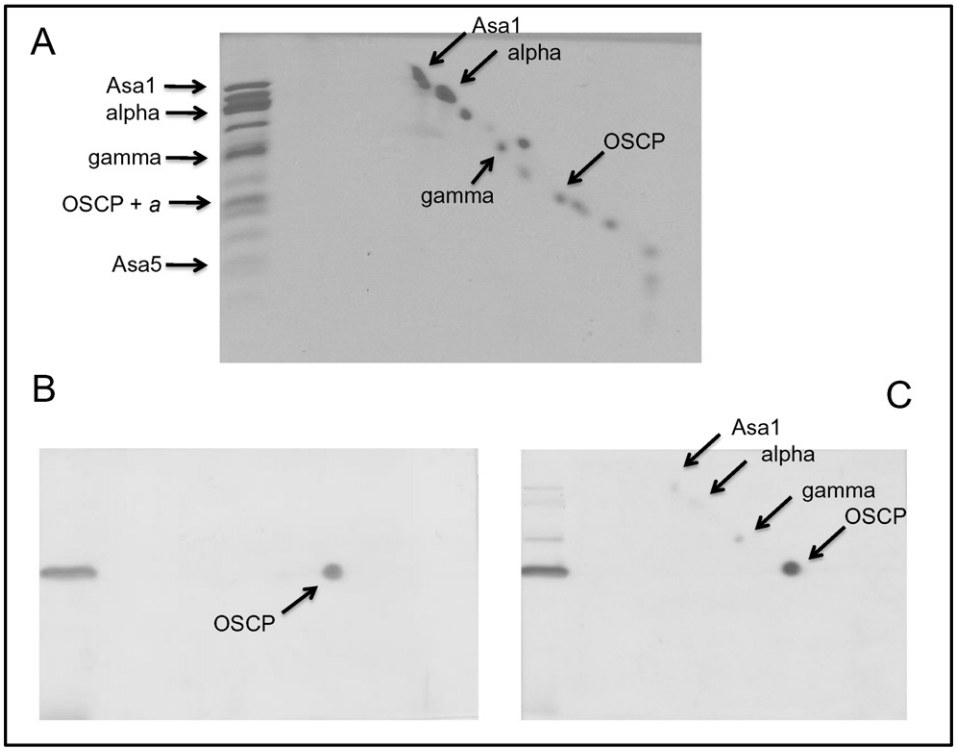

Fig. 4. Interaction of OSCP with subunits of the algal ATP synthase. A) 2D resolution of the algal F_1Fo-ATP synthase. *Polytomella* ATP synthase (100 μg of protein) was resolved in 1D in a glycine–SDS–PAGE system (10% acrylamide) and then in 2D in a Tricine–SDS–PAGE (14% acrylamide) and stained with Coomassie brilliant blue. The subunits of interest are indicated on the polypeptide pattern of the enzyme loaded on the left-hand side of the 2D gel. B) Western blot analysis of the *Polytomella* ATP synthase resolved by 2D Tricine–SDS–PAGE. A gel equivalent to the one shown in panel A was transferred to a nitrocellulose membrane and decorated with an anti-OSCP antibody. C) Far-Western blot analysis of the *Polytomella* ATP synthase resolved by 2D Tricine–SDS–PAGE. A gel equivalent to the one shown in panel A was transferred to a nitrocellulose membrane and incubated for 4 h with 2.0 nmol of the isolated, recombinant OSCP protein, and then decorated with an anti-OSCP antibody.

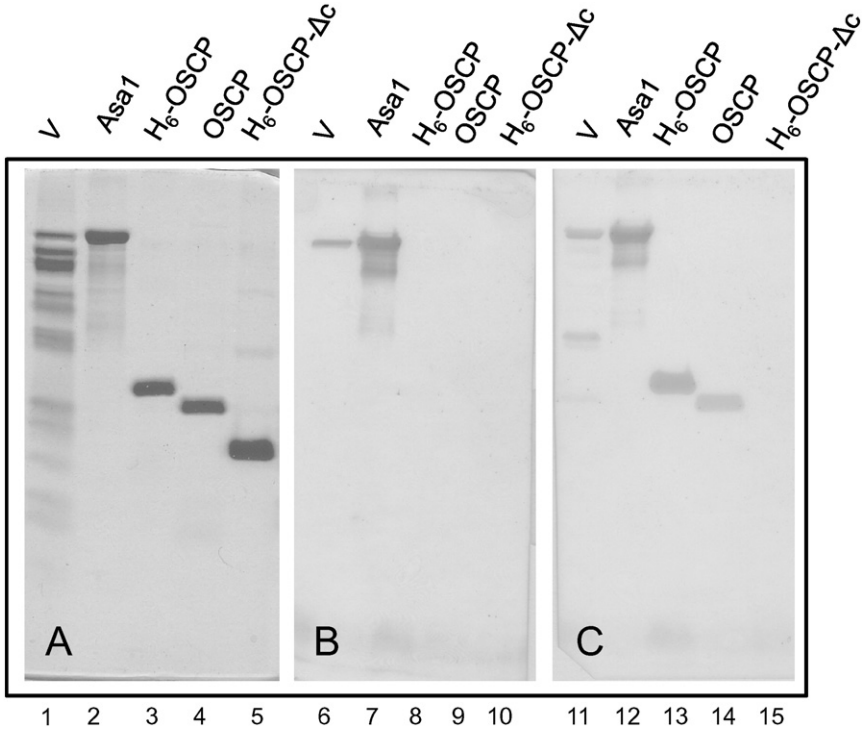

Fig. 5. The carboxy-terminus region of OSCP is instrumental for its interaction with Asa1. A) Coomassie blue-stained Tricine–SDS–polyacrylamide gel showing the *Polytomella* ATP synthase complex (25 μg of protein, lane 1) and 3 μg of each of the following overexpressed and purified recombinant proteins: Asa1 (lane 2); H_6-OSCP (lane 3); OSCP (lane 4) and H_6-OSCP-Δc (lane 5). [This gel is the same one shown in Fig. 1.] B) Western blot analysis of an equivalent gel as the one shown in panel A. After transfer to a nitrocellulose membrane, the blot was decorated with an anti-Asa1 antibody. C) Far-Western blot analysis of an equivalent gel as the one shown in panel A. After transfer to a nitrocellulose membrane, the blot was incubated for 4 h with 2.0 nmol of the isolated, recombinant Asa1 protein, and then decorated with an anti-Asa1 antibody.

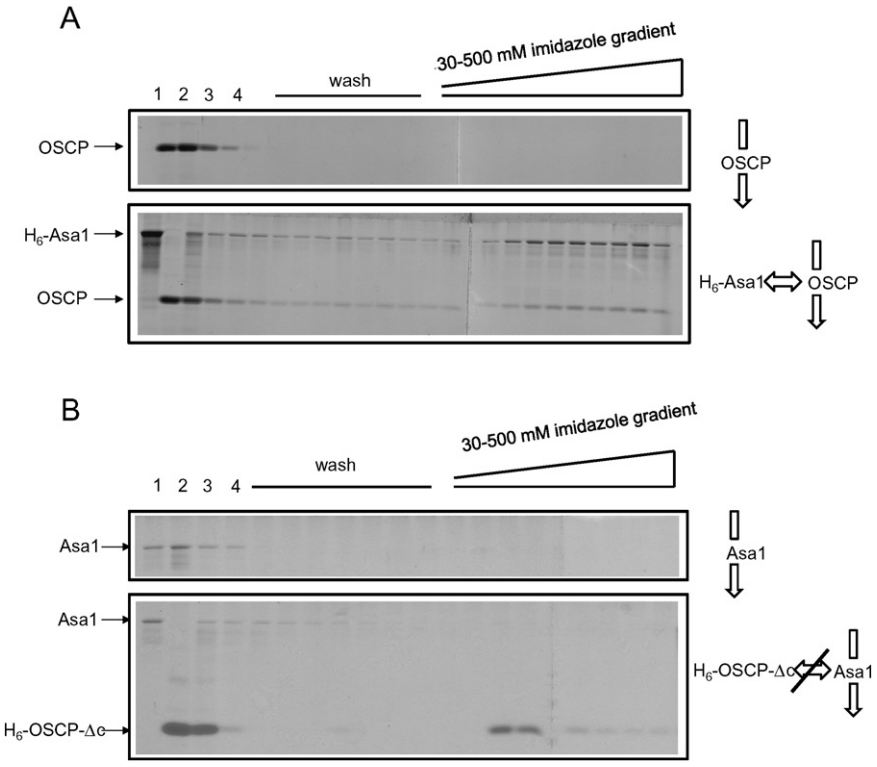

Fig. 6. The interaction of Asa1 with OSCP assayed by affinity chromatography. A) Interaction of Asa1 and OSCP assayed by affinity chromatography. The purified, recombinant OSCP subunit was bound to a Ni Sepharose resin containing no bound protein (upper panel) or to which H_6-Asa1 was bound (lower panel). Coomassie stained gels of the column fractions collected upon application of a 30–500 mM imidazole gradient. Lane 1, added sample; lane 2, protein excluded from the resin; lanes 3 and 4, proteins excluded after washing with 30 mM imidazole. B) Interaction of Asa1 and H_6-OSCP-Δc assayed by affinity chromatography. The experiment was carried out as described for panel A, except that the purified, recombinant H_6-OSCP-Δc fragment, lacking the carboxy-terminus of the OSCP subunit was used. The crossed arrow denotes no association between Asa1 and H_6-OSCP-Δc.

3.3. Subunit Asa1 is also found in a subcomplex containing membrane-embedded subunits

In previous work [9], the algal ATP synthase was dissociated at relatively high temperatures. When the enzyme was heated for 30–40 s at 60 °C a transient subcomplex of 200 kDa formed by subunits Asa1/Asa3/Asa5/Asa8/*a*/*c* was identified by first dimension blue native electrophoresis followed by 2D-SDS–PAGE; at longer time of heat treatment, this subcomplex further dissociated, giving rise to free individual subunits. Here, we looked for conditions in which a stable subcomplex containing Asa1 could be formed without heat treatment. For this purpose, the purified enzyme was incubated at 4 °C overnight with increasing concentrations of lauryl maltoside. As judged by blue native electrophoresis, in the presence of high detergent concentrations the dimeric complex (V_2) dissociated into its monomeric form (V) and released some free F_1 sector. A band, with a slightly faster migration than the F_1 sector was identified as a subcomplex (SC) (Fig 7A). A sample of the purified enzyme was incubated with 3.0% lauryl maltoside overnight and was further resolved in 2D-SDS–PAGE, where the polypeptides forming this subcomplex were separated (Fig 7B). Their identities were assigned by their apparent molecular masses as Asa1 (66.1 kDa), Asa3 (32.9 kDa), Asa5 (13.9 kDa) and Asa8 (9.9 kDa). Again, the band of 22 kDa could be either subunit *a* (Atp6) or OSCP. An additional band of around 45 kDa, exhibiting mobility slightly lower than Asa2, was named tentatively AsaX. The polypeptides Asa1 and Asa8 identities were assigned immunochemically by Western blot analysis using specific antibodies (Fig 7C). Mass spectrometry analysis unambiguously revealed that the 22 kDa was subunit *a* (Atp6, GenBank: CBK55668.1) since two polypeptides of this subunit were identified: TGSLPTNFLTGVYR and SQNPAEKPHPVNDRLLPAVVDASDKR. Mass spectrometry analysis did not reveal the nature of AsaX, since only minute amounts of human keratin, type II cytoskeletal keratin (NCBI Reference Sequence: NP_006112.3) were found in the sample. The band AsaX was therefore subjected to Edman degradation, revealing the N-terminal sequence S-V-L-A-A-S-K-M-V-G-A-G-X-A-T, which matches the N-terminus sequence (SVLAASKMVGAGCAT) of subunit *c* (Atp9) of *Polytomella* sp. (GenBank: ADE92942.1). Thus, AsaX seems to be an SDS-resistant oligomer of *c* subunits migrating with an apparent molecular mass of 46 kDa in SDS–PAGE. Most probably, subunit *c* escaped mass spectrometry detection due to its highly hydrophobic nature. The obtained subcomplex ASA1/ASA3/ASA5/ASA8/*a*/c_x seems to be identical to the one previously observed after heating for a short time the enzyme, except that subunit *c* is now found as an oligomer forming an SDS-resistant ring, probably a decamer of *c*-subunits, as deduced from the electron cryo-microscopy map of the algal ATP synthase [16]. Asa1 is therefore associated with the membrane-bound subunits *a* (Atp6), *c* (Atp9) and Asa8, and also with the extrinsic subunits Asa5 and Asa3. To further explore a possible interaction of Asa1 with membrane components, the isolated, recombinant Asa1 subunit was resolved by SDS–PAGE and transferred to nitrocellulose membranes. The strips, containing the same concentration of Asa1, were incubated with increasing concentrations of a recombinant Asa8 subunit and afterwards incubated with an anti-Asa8 antibody followed by the secondary antibody (Fig 7D). At increasing concentrations of the externally added recombinant Asa8, the anti-Asa8 antibody recognized the Asa1 subunit bound to the nitrocellulose membrane (Fig 7D, lanes 6 to 10). This further suggested the interaction Asa1–Asa8. Since Asa1 lacks any predictable transmembrane stretch, and therefore cannot be considered to be embedded in the lipid bilayer, the data strongly suggests that Asa1 may also contact membrane-embedded polypeptides like Asa8, and thus, may be the key component that bridges the region between the inner mitochondrial membrane and OSCP.

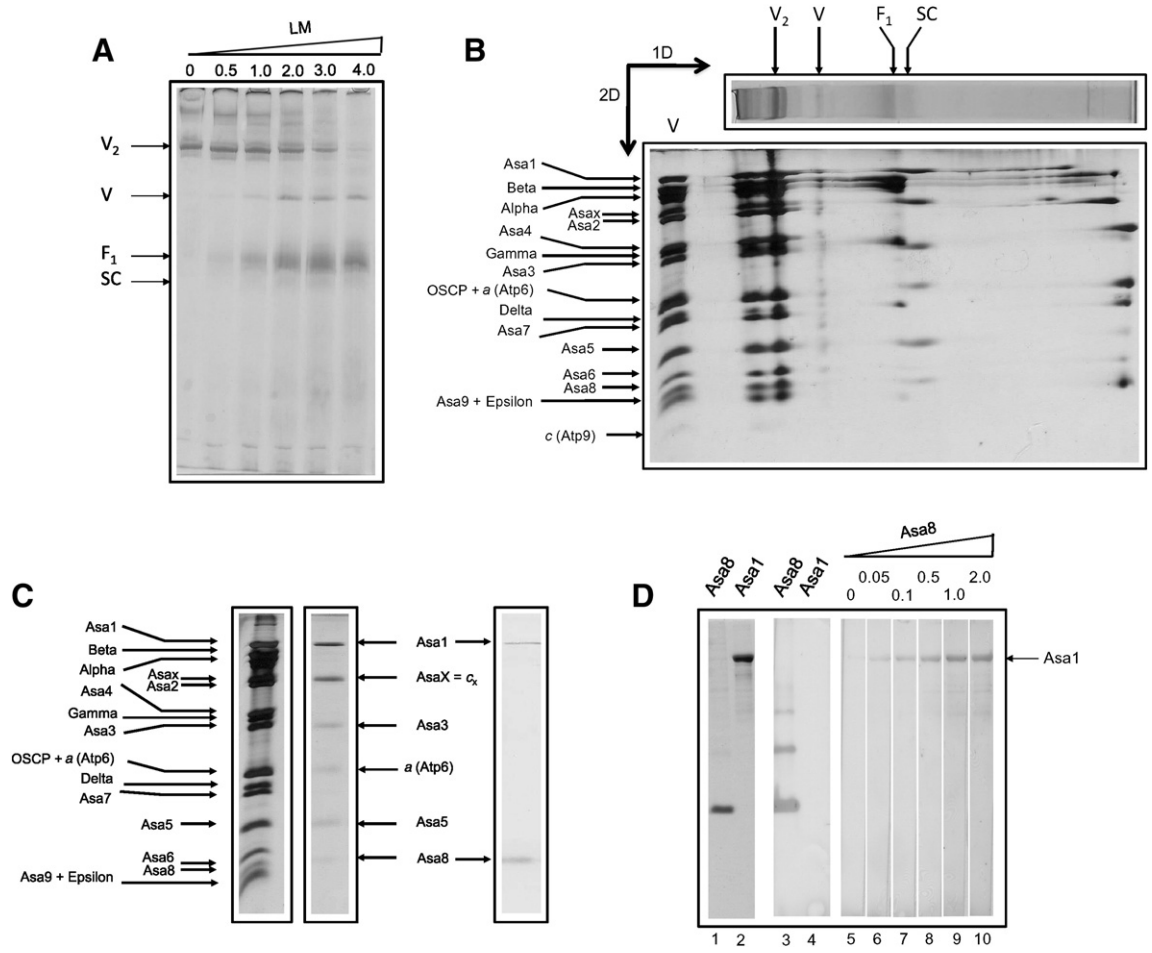

Fig. 7. Formation of an ASA1/ASA3/ASA5/ASA8/a/c subcomplex and detection of an Asa1–Asa8 association. A) BN-PAGE of purified ATP synthase samples incubated overnight at 4 °C under mild agitation in the presence of lauryl maltoside at the indicated increasing concentrations (% *w*/*v*). One hundred micrograms of protein was loaded in each lane. The control lane in the absence of the detergent is labeled 0. Dimer (V2), monomer (V); F_1 sector (F_1), and subcomplex (SC) are indicated. B) 2D gel of an ATP synthase sample incubated overnight in the presence of 3.0% lauryl maltoside. Six polypeptide bands were resolved for the subcomplex (SC) in the 2D SDS–Tricine gel. C) Immunochemical identification of subunits Asa1 and Asa8 as constituents of the subcomplex. D) Asa1–Asa8 interaction as revealed by Far-Western blots. Lanes 1 and 2: Coomassie blue-stained Tricine–SDS polyacrylamide gel showing the purified recombinant proteins Asa 8 (3 μg of protein) and Asa1 (3 μg of protein) respectively. Lanes 3 and 4: Western blot analysis of an equivalent gel. After transfer to a nitrocellulose membrane, the blot was decorated with an anti-Asa8 antibody. Recombinant Asa8 exhibits dimers and higher molecular mass oligomers in SDS–PAGE that are also detected by the antibody. Lanes 5–10: Far-Western blot analysis of an equivalent gel containing the recombinant Asa1 subunit. The blot was incubated for 4 h with the indicated amounts (nanomoles in 5 ml) of the isolated, recombinant Asa8 protein, and then decorated with an anti-Asa8 antibody.

4. Discussion

In ATP synthases, the peripheral stalks are the structures that counteract the torque generated by rotation of the central stalk during the function of the enzyme [37,38]. While the F-type ATPases contain only one peripheral stalk [39], A-type ATPases contain two [40] and eukaryotic V-type ATPases contain three [41]. Also, the subunit structures of the prokaryotic and eukaryotic peripheral stalks are very different. In bacteria like *Escherichia coli*, the peripheral stalk contains two identical *b* subunits, each one exhibiting one transmembrane stretch. Both subunits extend as coiled-coil structures to the top of F_1 where the δ subunit (the bacterial equivalent of OSCP) resides [42,43]. The A_1Ao-ATP synthases also exhibit coiled-coil structures formed by the heterodimeric subunits E and G [38]. The sequence of the *b* subunit of the eukaryotic peripheral stalk differs starkly from the bacterial one. The yeast and beef *b* subunits contain two transmembrane stretches near their N-terminal regions and extend towards the top of the F_1 sector associating with subunits *d* and F6 (*h*) and reaching OSCP [21,44]. In contrast with the above mentioned peripheral stalks, the ATP synthase of the colorless alga *Polytomella* sp. exhibits an extremely robust, electron-dense peripheral stalk as observed in electron microscope image reconstructions [16]. The Asa subunits, present only in mitochondrial ATP synthases of chlorophycean algae [19] have been pin-pointed as the main constituents of this peripheral stalk. We have previously studied the arrangement of Asa subunits and shown that Asa2, Asa4 and Asa7 bind together and that the interaction Asa4–Asa7 is mediated by the C-terminal halves of both proteins [20]. Also, subunits Asa2, Asa4 and Asa7 formed a subcomplex with a 1:1:1 stoichiometry that could be reconstituted *in vitro*. This subcomplex seems to establish contacts with Asa1 and with OSCP. Here, we addressed specifically the topology of Asa1, the larger polypeptide (66.1 kDa) of all Asa subunits. The location of the Asa1 subunit remained controversial since on one hand, it was proposed to represent the large bulk observed in the top region of the peripheral stalk in close contact with the F_1 sector [17] and on the other hand it was identified to constitute a subcomplex along with subunits Asa3, Asa5, Asa8, *a* and *c*, and therefore it was considered to be in close vicinity with the matrix-exposed surface of the inner mitochondrial membrane [9]. The data presented in this work suggest that Asa1 interacts strongly with the OSCP subunit. Asa1 seems to be one of the main components of the peripheral stalk of the algal enzyme forming a physical bridge between the extrinsic subunits (mainly OSCP) and other components of the enzyme either embedded or in close contact with the membrane (Asa3, Asa5, Asa8, *a* and c_{10}-ring) and in particular with the membrane-embedded Asa8 subunit, as judged by Far-Western blot analysis using the recombinant subunits. Thus, Asa1 seems to be the main support of the peripheral stalk, further reinforced by other

Asa subunits (Asa2, Asa4, Asa7 and maybe also Asa3 and Asa5), playing a structural role similar to the one of subunit *b* in orthodox enzymes. The model shown in Fig 8 integrates the results presented in this work. The model proposes Asa1 spanning the peripheral arm from a region in close proximity to the membrane (interacting with subunits Asa3, Asa5, Asa8, *a* and c_{10}), up to the F_1 region of the enzyme (where it interacts with OSCP).

The interaction Asa1 subunit-gamma subunit, as observed in the Far-Western blot experiments, is hard to explain, since in order for the ATP synthase to work as a nanomotor, the rotary components should not bind directly to stator components. A tight binding of Asa1 to the gamma subunit would obviously impede its rotation. We therefore consider that the binding of Asa1 to the gamma subunit, as judged by Far-Western blotting, to be unspecific and probably due to the propensity of both proteins to form coiled-coil structures. It is noted that chlorophycean gamma subunit sequences are very similar to the ones found in other algae and plants and exhibit no distinct features.

The electron cryo-microscopy map of the algal ATP synthase also shows that the *c*-ring is formed by 10 monomers [16]. In this work, we observed the presence of a high molecular mass *c*-ring in SDS–PAGE. This band was not observed before in other *Polytomella* ATP synthase preparations because it co-migrates with subunit Asa2 in SDS–PAGE with an apparent molecular mass of 45.3 kDa. The band, initially named AsaX, was identified as subunit *c* by Edman degradation N-terminal sequencing. Thus, the algal F_1Fo-ATP synthase exhibits an SDS-resistant *c*-ring similar to those previously observed in various isolated Na^+-dependent A_1Ao-ATP synthases, including the strictly anaerobic bacterium *Propionigenium modestum* [45], the fusobacterium *Ilyobacter tartaricus* [46], the acetogenic bacterium *Acetobacterium woodii* [47], and the hyperthermophilic archaea *Pyrococcus furiosus* [48] and *Thermococcus onnurineus* [49]. In eukaryotes, an H^+-dependent F_1Fo-ATP synthase exhibiting an SDS-resistant *c*-ring was reported in yeast [50].

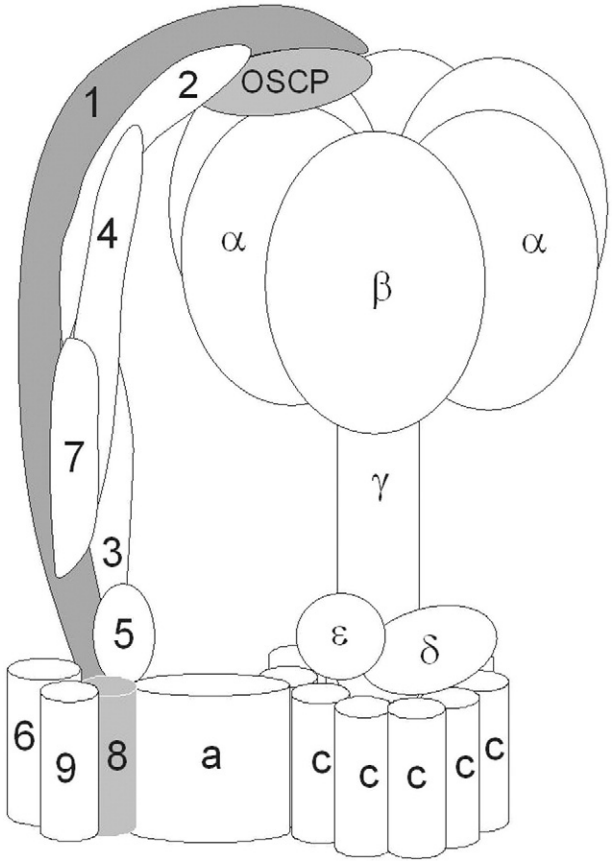

Fig. 8. Subunit arrangement of the algal mitochondrial ATP synthase. Only half of the dimer is shown. The disposition of Asa1, Asa8 and OSCP subunits is highlighted. The model is consistent with previous works reporting close vicinity of subunits as judged by cross-linking experiments [14] and the presence of an Asa4/Asa2/Asa7 subcomplex [20].

Analysis of the Asa subunit sequences indicated high propensity of Asa1, Asa2, Asa4 and Asa7 to form coiled-coil regions (30, 19, 35 and 32% respectively) [20]. These Asa subunits most probably interact through large contacts within alpha-helices that form the robust, intertwined peripheral arm observed in the electron cryo-microscopy map of the *Polytomella* ATP synthase dimer [16]. The size of the F_1 sector [$\alpha_3/\beta_3/\gamma/\delta/\varepsilon$] is around 150 Å, so one can estimate the length of the peripheral stalk of the *Polytomella* enzyme to be of 221 Å, taking into account the curvature observed in the electron cryo-microscopy map of the enzyme [16]. The mature Asa1 subunit has 596 residues, so if one considers the whole protein to be in an alpha-helical conformation, it should have a length of 894 Å, enough to transverse the peripheral stalk three to four times. In contrast, subunit *b* of the orthodox ATP synthases green algae, is around 190 residues (285 Å long), thus only one third of the Asa1 subunit. We carried out 3D modeling of several chlorophycean Asa1 subunits using the RaptorX homepage. Several models were obtained for each Asa1 sequence. Nevertheless only one template, PDB ID: 1HCI (the crystal structure of the rod domain of alpha-actinin), was consistently chosen by the program to model all the Asa1 sequences. The model for the *Polytomella parva* Asa1 subunit is shown in Suppl. Fig. 1. The prediction shows a protein 240 Å long with multiple alpha-helices forming coiled-coil structures and a highly conserved carboxy-terminus.

In this work, we provide evidence for the interaction of Asa1 subunit that seems to pertain solely to the chlorophycean algal lineage with one of the highly conserved subunits present in all mitochondrial ATP synthases known to date (the OSCP subunit). We suggest that Asa1 has taken the place of subunit *b* as the main constituent supporting the mitochondrial ATP synthase peripheral arm. Genes encoding orthodox *b* subunits are found in almost all land plants and green alga. The distribution of *b* subunits and Asa1 subunits in different photosynthetic organisms is shown in Suppl. Fig. 2. While land plants, Charophyte alga, Prasinophytes, and the class Trebouxiophyceae exhibit a gene encoding orthodox subunit *b*, this gene is absent and seems to be substituted by the gene encoding Asa1 in chlorophycean algae, both in the orders Chlamydomonadales and Sphaeropleales. The origin of Chlorophyceae occurred approximately 600 million years ago [51] and seems to be related to the drastic reduction of mitochondrial genome in size and in gene content, and to the appearance of nucleus-encoded atypical subunits of the enzyme (Asa subunits) [52,19].The phylogenetic distribution of orthodox *b* subunits and Asa1 subunits strongly suggests that the appearance during evolution of Asa subunits as constituents of the ATP synthase peripheral arm, only occurred in chlorophycean algae. One could predict that the OSCP subunit of chlorophycean algae must also differ from classical plant and algal OSCP subunits, in order to accommodate binding to the Asa1 subunit instead of the *b* subunit. Alignment of diverse OSCP sequences strongly suggests that this protein separates into two clearly distinct groups that exhibit conspicuously different amino acid sequences: one of Chlorophycean algae and another of all the other green algae and land plants (Suppl. Fig. 3).

It seems that Asa1 is neither a highly modified subunit *b* nor the result of a duplication of a gene encoding subunit *b*. Rather; it seems more likely that in the chlorophycean lineage, all the orthodox structural components of the peripheral arm were substituted by scaffold-forming proteins from a complete different origin, i.e., the Asa subunits.

Supplementary data to this article can be found online at http://dx.doi.org/10.1016/j.bbabio.2015.11.012.

Transparency document

The Transparency document associated with this article can be found, in online version.

Acknowledgments

We are grateful to Professor David R. Smith (Department of Biology, Western University, Canada) for providing us access to the Asa1 sequences of various *Polytomella* species. We thank Dr. Lawrence Dangott (Texas A&M University) for the Edman degradation analyses, and M.C. Emmanuel Ríos Castro (LaNSE, CINVESTAV del IPN) for the mass spectrometry data. Special thanks to Félix Vega de Luna (IFC, UNAM) for his help with the 3D modeling of the Asa1 subunits. We are also grateful to Laura Ongay Larios, Minerva Mora Cabrera and Guadalupe Códiz Huerta of the Molecular Biology Unit, IFC, UNAM for primer synthesis and sequencing. This research was supported by grant 245486 from the Consejo Nacional de Ciencia y Tecnología (CONACyT) and the Belgian Fonds de la Recherche Scientifique (F.R.S.-FNRS) (Mexico-Belgium). Additional support was received from grants 239219 (CONACyT, Mexico), IN203311-3 from the Dirección General de Asuntos del Personal Académico (DGAPA-UNAM, Mexico) and from the F.R.S.-FNRS(MIS F.4520, FRFC 2.4597). CONACyT also supported with fellowship 599282 the Ph.D. studies of L.C.-T. (Programa de Doctorado en Ciencias Biomédicas de la Universidad Nacional Autónoma de México).

References

[1] T. Xu, V. Pagadala, D.M. Mueller, Understanding structure, function, and mutations in the mitochondrial ATP synthase, Microb. Cell 2 (2015) 105–125.
[2] A. Wächter, Y. Bi, S.D. Dunn, B.D. Cain, H. Sielaff, F. Wintermann, S. Engelbrecht, W. Junge, Two rotary motors in F-ATP synthase are elastically coupled by a flexible rotor and a stiff stator stalk, Proc. Natl. Acad. Sci. U. S. A. 108 (2011) 3924–3929.
[3] J.E. Walker, V.K. Dickson, The peripheral stalk of the mitochondrial ATP synthase, Biochim. Biophys. Acta 1757 (2006) 286–296.
[4] H. Seelert, N.A. Dencher, ATP synthase superassemblies in animals and plants: two or more are better, Biochim. Biophys. Acta 1807 (2011) 1185–1197.
[5] P. Paumard, J. Vaillier, B. Coulary, J. Schaeffer, V. Soubannier, D.M. Mueller, D. Brèthes, J.P. di Rago, J. Velours, The ATP synthase is involved in generating mitochondrial cristae morphology, EMBO J. 21 (2002) 221–230.
[6] N.P. Balabaskaran, N.V. Dudkina, L.A. Kane, J.E. van Eyk, E.J. Boekema, M.W. Mather, A.B. Vaidya, Highly divergent mitochondrial ATP synthase complexes in *Tetrahymena thermophila*, PLoS Biol. 8 (2010), e1000418.
[7] A. Zikova, A. Schnaufer, R.A. Dalley, A.K. Panigrahi, K.D. Stuart, The F(0)F(1)-ATP synthase complex contains novel subunits and is essential for procyclic *Trypanosoma brucei*, PLoS Pathog. 5 (2009), e1000436.
[8] E. Perez, M. Lapaille, H. Degand, L. Cilibrasi, A. Villavicencio-Queijeiro, P. Morsomme, D. González-Halphen, M.C. Field, C. Remacle, D. Baurain, P. Cardol, The mitochondrial respiratory chain of the secondary green alga *Euglena gracilis* shares many additional subunits with parasitic Trypanosomatidae, Mitochondrion 19 (Pt B) (2014) 338–349.
[9] M. Vázquez-Acevedo, P. Cardol, A. Cano-Estrada, M. Lapaille, C. Remacle, D. González-Halphen, The mitochondrial ATP synthase of chlorophycean algae contains eight subunits of unknown origin involved in the formation of an atypical stator-stalk and in the dimerization of the complex, J. Bioenerg. Biomembr. 38 (2006) 271–282.
[10] R. van Lis, A. Atteia, G. Mendoza-Hernández, D. González-Halphen, Identification of novel mitochondrial protein components of *Chlamydomonas reinhardtii*. A proteomic approach, Plant Physiol. 132 (2003) 318–330.
[11] A. Atteia, G. Dreyfus, D. González-Halphen, Characterization of the alpha and beta-subunits of the F0F1-ATPase from the alga *Polytomella* spp., a colorless relative of *Chlamydomonas reinhardtii*, Biochim. Biophys. Acta 1320 (1997) 275–284.
[12] N.V. Dudkina, J. Heinemeyer, W. Keegstra, E.J. Boekema, H.P. Braun, Structure of dimeric ATP synthase from mitochondria: an angular association of monomers induces the strong curvature of the inner membrane, FEBS Lett. 579 (2005) 5769–5772.
[13] N.V. Dudkina, S. Sunderhaus, H.P. Braun, E.J. Boekema, Characterization of dimeric ATP synthase and cristae membrane ultrastructure from *Saccharomyces* and *Polytomella* mitochondria, FEBS Lett. 580 (2006) 3427–3432.
[14] A. Cano-Estrada, M. Vázquez-Acevedo, A. Villavicencio-Queijeiro, F. Figueroa-Martínez, H. Miranda-Astudillo, Y. Cordeiro, J.A. Mignaco, D. Foguel, P. Cardol, M. Lapaille, C. Remacle, S. Wilkens, D. González-Halphen, Subunit–subunit interactions and overall topology of the dimeric mitochondrial ATP synthase of *Polytomella* sp, Biochim. Biophys. Acta 1797 (2010) 1439–1448.
[15] N.V. Dudkina, G.T. Oostergetel, D. Lewejohann, H.P. Braun, E.J. Boekema, Row-like organization of ATP synthase in intact mitochondria determined by cryo-electron tomography, Biochim. Biophys. Acta 1797 (2010) 272–277.
[16] M. Allegretti, N. Klusch, D.J. Mills, J. Vonck, W. Kühlbrandt, K.M. Davies, Horizontal membrane-intrinsic α-helices in the stator a-subunit of an F-type ATP synthase, Nature 521 (2015) 237–240.
[17] R. van Lis, G. Mendoza-Hernández, G. Groth, A. Atteia, New insights into the unique structure of the F0F1-ATP synthase from the chlamydomonad algae *Polytomella* sp. and *Chlamydomonas reinhardtii*, Plant Physiol. 144 (2007) 1190–1199.
[18] A. Villavicencio-Queijeiro, M. Vázquez-Acevedo, A. Cano-Estrada, M. Zarco-Zavala, M. Tuena de Gómez, J.A. Mignaco, M.M. Freire, H.M. Scofano, D. Foguel, P. Cardol, C. Remacle, D. González-Halphen, The fully-active and structurally-stable form of the mitochondrial ATP synthase of *Polytomella* sp. is dimeric, J. Bioenerg. Biomembr. 41 (2009) 1–13.
[19] M. Lapaille, A. Escobar-Ramírez, H. Degand, D. Baurain, E. Rodríguez-Salinas, N. Coosemans, M. Boutry, D. Gonzalez-Halphen, C. Remacle, P. Cardol, Atypical subunit composition of the chlorophycean mitochondrial F1FO-ATP synthase and role of Asa7 protein in stability and oligomycin resistance of the enzyme, Mol. Biol. Evol. 27 (2010) 1630–1644.
[20] H. Miranda-Astudillo, A. Cano-Estrada, M. Vázquez-Acevedo, L. Colina-Tenorio, A. Downie-Velasco, P. Cardol, C. Remacle, L. Domínguez-Ramírez, D. González-Halphen, Interactions of subunits Asa2, Asa4 and Asa7 in the peripheral stalk of the mitochondrial ATP synthase of the chlorophycean alga *Polytomella* sp, Biochim. Biophys. Acta 1837 (2014) 1–13.
[21] V.K. Dickson, J.A. Silvester, I.M. Fearnley, A.G. Leslie, J.E. Walker, On the structure of the stator of the mitochondrial ATP synthase, EMBO J. 25 (2006) 2911–2918.
[22] L.A. Baker, I.N. Watt, M.J. Runswick, J.E. Walker, J.L. Rubinstein, Arrangement of subunits in intact mammalian mitochondrial ATP synthase determined by cryo-EM, Proc. Natl. Acad. Sci. U. S. A. 109 (2012) 11,675–11,680.
[23] W.C. Lau, L.A. Baker, J.L. Rubinstein, Cryo-EM structure of the yeast ATP synthase, J. Mol. Biol. 382 (2008) 1256–1264.
[24] C. Mellwig, B. Böttcher, A unique resting position of the ATP-synthase from chloroplasts, J. Biol. Chem. 278 (2003) 18,544–18,549.
[25] I. Ogilvie, S. Wilkens, A.J. Rodgers, R. Aggeler, R.A. Capaldi, The second stalk: the delta-b subunit connection in ECF1FO, Acta Physiol. Scand. Suppl. 643 (1998) 169–175.
[26] H. Schägger, Denaturing electrophoretic techniques, in: G. von Jagow, H. Schägger (Eds.), A Practical Guide to Membrane Protein Purification, Academic Press, San Diego 1994, pp. 59–79.
[27] U.K. Laemmli, Cleavage of structural proteins during the assembly of the head of bacteriophage T4, Nature 227 (1970) 680–685.
[28] H. Schägger, Native gel electrophoresis, in: G. von Jagow, H. Schägger (Eds.), A Practical Guide to Membrane Protein Purification, Academic Press, San Diego 1994, pp. 81–104.
[29] M.A.K. Markwell, S.M. Hass, L.L. Biber, N.E. Tolbert, A modification of the Lowry procedure to simplify protein determination in membrane and lipoprotein samples, Anal. Biochem. 87 (1978) 206–210.
[30] A. Atteia, R. van Lis, S.I. Beale, Enzymes of the heme biosynthetic pathway in the nonphotosynthetic alga *Polytomella* sp, Eukaryot. Cell 4 (2005) 2087–2097.
[31] H. Schägger, H. Aquila, G. Von Jagow, Coomassie blue–sodium dodecyl sulfate–polyacrylamide gel electrophoresis for direct visualization of polypeptides during electrophoresis, Anal. Biochem. 173 (1988) 201–205.
[32] D. González-Halphen, M.A. Lindorfer, R.A. Capaldi, Subunit arrangement in beef heart complex III, Biochemistry 27 (1988) 7021–7031.
[33] R.A. Hall, Studying protein–protein interactions via blot overlay or Far Western blot, Methods Mol. Biol. 261 (2004) 167–174.
[34] H. Towbin, T. Staehelin, J. Gordon, Electrophoretic transfer of proteins from polyacrylamide gels to nitrocellulose sheets: procedure and some applications, Proc. Natl. Acad. Sci. U. S. A. 76 (1979) 4350–4354.
[35] J.D. Thompson, D.G. Higgins, T.J. Gibson, CLUSTAL W: improving the sensitivity of progressive multiple sequence alignment through sequence weighting, position-specific gap penalties and weight matrix choice, Nucleic Acids Res. 22 (1994) 4673–4680.
[36] M. Källberg, H. Wang, S. Wang, J. Peng, Z. Wang, H. Lu, J. Xu, Template-based protein structure modeling using the RaptorX web server, Nat. Protoc. 7 (2012) 1511–1522.
[37] W. Junge, H. Sielaff, S. Engelbrecht, Torque generation and elastic power transmission in the rotary F(O)F(1)-ATPase, Nature 459 (2009) 364–370.
[38] A.G. Stewart, L.K. Lee, M. Donohoe, J.J. Chaston, D. Stock, The dynamic stator stalk of rotary ATPases, Nat. Commun. 3 (2012) 687.
[39] S. Wilkens, R.A. Capaldi, ATP synthase's second stalk comes into focus, Nature 393 (1998) 29.
[40] J. Vonck, K.Y. Pisa, N. Morgner, B. Brutschy, V. Muller, Three-dimensional structure of A_1A_0 ATP synthase from the hyperthermophilic archaeon *Pyrococcus furiosus* by electron microscopy, J. Biol. Chem. 284 (2009) 10,110–10,119.
[41] Z. Zhang, Y. Zheng, H. Mazon, E. Milgrom, N. Kitagawa, E. Kish-Trier, A.J. Heck, P.M. Kane, S. Wilkens, Structure of the yeast vacuolar ATPase, J. Biol. Chem. 283 (2008) 35,983–35,995.
[42] K.S. Wood, S.D. Dunn, Role of the asymmetry of the homodimeric b_2 stator stalk in the interaction with the F1 sector of *Escherichia coli* ATP synthase, J. Biol. Chem. 282 (2007) 31,920–31,927.
[43] K. Brandt, S. Maiwald, B. Herkenhoff-Hesselmann, K. Gnirß, J.C. Greie, S.D. Dunn, G. Deckers-Hebestreit, Individual interactions of the b subunits within the stator of the *Escherichia coli* ATP synthase, J. Biol. Chem. 288 (2013) 24,465–24,479.
[44] M.F. Paul, B. Guerin, J. Velours, The C-terminal region of subunit 4 (subunit b) is essential for assembly of the F0 portion of yeast mitochondrial ATP synthase, Eur. J. Biochem. 205 (1992) 163–172.
[45] W. Laubinger, P. Dimroth, Characterization of the ATP synthase of *Propionigenium modestum* as a primary sodium pump, Biochemistry 27 (1988) 7531–7537.
[46] H. Stahlberg, D.J. Müller, K. Suda, D. Fotiadis, A. Engel, T. Meier, U. Matthey, P. Dimroth, Bacterial Na(+)-ATP synthase has an undecameric rotor, EMBO Rep. 2 (2001) 229–233.
[47] M. Fritz, V. Müller, An intermediate step in the evolution of ATPases—the F1FO-ATPase from *Acetobacterium woodii* contains F-type and V-type rotor subunits and is capable of ATP synthesis, FEBS J. 274 (2007) 3421–3428.

[48] K.Y. Pisa, H. Huber, M. Thomm, V. Müller, A sodium ion-dependent A_1AO ATP synthase from the hyperthermophilic archaeon *Pyrococcus furiosus*, FEBS J. 274 (2007) 3928–3938.
[49] F. Mayer, J.K. Lim, J.D. Langer, S.G. Kang, V. Müller, Na+ transport by the A1AO-ATP synthase purified from *Thermococcus onnurineus* and reconstituted into liposomes, J. Biol. Chem. 290 (2015) 6994–7002.
[50] J. Velours, G. Arselin, The *Saccharomyces cerevisiae* ATP synthase, J. Bioenerg. Biomembr. 32 (2000) 383–390.
[51] M.D. Herron, J.D. Hackett, F.O. Aylward, R.E. Michod, Triassic origin and early radiation of multicellular volvocine algae, Proc. Natl. Acad. Sci. U. S. A. 106 (2009) 3254–3258.
[52] P. Cardol, D. González-Halphen, A. Reyes-Prieto, D. Baurain, R.F. Matagne, C. Remacle, The mitochondrial oxidative phosphorylation proteome of *Chlamydomonas reinhardtii* deduced from the Genome Sequencing Project, Plant Physiol. 137 (2005) 447–459.
[53] L.A. Lewis, R.M. McCourt, Green algae and the origin of land plants, Am. J. Bot. 91 (2004) 1535–1556.
[54] F. Leliaert, D.R. Smith, H. Moreau, M.D. Herron, H. Verbruggen, C.F. Delwiche, O. De Clerck, Phylogeny and molecular evolution of the green algae, Crit. Rev. Plant Sci. 31 (2012) 1–46.

Biochimica et Biophysica Acta 1857 (2016) 1183–1190

Contents lists available at ScienceDirect

Biochimica et Biophysica Acta

journal homepage: www.elsevier.com/locate/bbabio

Review

Dissecting the peripheral stalk of the mitochondrial ATP synthase of chlorophycean algae☆,☆☆

Miriam Vázquez-Acevedo [a], Félix Vega-deLuna [a], Lorenzo Sánchez-Vásquez [a], Lilia Colina-Tenorio [a], Claire Remacle [b], Pierre Cardol [b], Héctor Miranda-Astudillo [b], Diego González-Halphen [a,*]

[a] Instituto de Fisiología Celular, Universidad Nacional Autónoma de México, México D.F., Mexico
[b] Genetics and Physiology of Microalgae, Department of Life Sciences, University of Liège, B-4000 Liège, Belgium

ARTICLE INFO

Article history:
Received 10 December 2015
Received in revised form 25 January 2016
Accepted 5 February 2016
Available online 10 February 2016

Keywords:
F_1F_O-ATP synthase peripheral-stalk
Dimeric mitochondrial complex V
Amphipol A8-35
Chlamydomonas reinhardtii
Polytomella sp.
Asa subunits

ABSTRACT

The algae *Chlamydomonas reinhardtii* and *Polytomella* sp., a green and a colorless member of the chlorophycean lineage respectively, exhibit a highly-stable dimeric mitochondrial F_1Fo-ATP synthase (complex V), with a molecular mass of 1600 kDa. *Polytomella*, lacking both chloroplasts and a cell wall, has greatly facilitated the purification of the algal ATP-synthase. Each monomer of the enzyme has 17 polypeptides, eight of which are the conserved, main functional components, and nine polypeptides (Asa1 to Asa9) unique to chlorophycean algae. These atypical subunits form the two robust peripheral stalks observed in the highly-stable dimer of the algal ATP synthase in several electron-microscopy studies. The topological disposition of the components of the enzyme has been addressed with cross-linking experiments in the isolated complex; generation of subcomplexes by limited dissociation of complex V; detection of subunit–subunit interactions using recombinant subunits; *in vitro* reconstitution of subcomplexes; silencing of the expression of Asa subunits; and modeling of the overall structural features of the complex by EM image reconstruction. Here, we report that the amphipathic polymer Amphipol A8-35 partially dissociates the enzyme, giving rise to two discrete dimeric subcomplexes, whose compositions were characterized. An updated model for the topological disposition of the 17 polypeptides that constitute the algal enzyme is suggested. This article is part of a Special Issue entitled 'EBEC 2016: 19th European Bioenergetics Conference, Riva del Garda, Italy, July 2-6, 2016', edited by Prof. Paolo Bernardi.

1. The mitochondrial ATP synthase

Mitochondrial F_1Fo-ATP synthase (complex V) is a key participant of oxidative phosphorylation (OXPHOS) and the main ATP producing enzyme in non-photosynthetic eukaryotes. Classic dissociation experiments characterized two oligomeric domains in the enzyme, an extrinsic moiety (F_1 factor) and the membrane bound sector Fo [1]. F_1Fo-ATP synthase is also a molecular motor [2] in which a central rotor-stalk [γ/δ/ε/c-ring] rotates around an axis perpendicular to the plane of the membrane, while the fixed elements (stator components) are subunit *a*, the catalytic core (α_3/β_3), the peripheral stalk (OSCP/b/d/F6), and the dimerization module (A6L/*e*/*f*/*g*) [3,4]. Proton-flux through the two hemi-channels of subunit *a*, formed by membrane-embedded α-helices, causes the rotary movement of a *c*-subunit ring with a species-dependent variable stoichiometry (c_{8-14}) and concomitantly, the rotation of the central-stalk (γ/δ/ε) [5]. Three sequential 120° movements of subunit γ induce conformational changes in the three catalytic β subunits leading to successive substrate binding (ADP + Pi), ATP synthesis, and ATP release [6]. Other subunits play a regulatory role, such as the inhibitory protein IF_1 [7] that prevents futile ATP hydrolysis. The peripheral stator-stalk counteracts the torque generated by the rotation of the central stalk during the function of the enzyme [8]. In the yeast and beef enzymes, the main axis of the peripheral stalk is formed by subunit *b*, that contains two transmembrane stretches near its N-terminal region and extends towards OSCP at the top of the F_1 sector associating also with subunits *d* and F6 (*h* in yeast) [9].

In the inner mitochondrial membrane, the ATP synthase forms oligomeric associations [10–12] that are responsible for the overall architecture of the mitochondrial cristae [13]. In yeast, dimerization is mediated by the small subunits *e*, *g*, *h* and *i* [14,15]. Subunits *b* (Atp4), *d*, F6, A6L, *e*, *f* and *g*, present in the bovine enzyme, are not common to all mitochondrial ATP synthases; atypical subunit compositions have been identified in trypanosomatids [16], euglenoids [17], chlorophycean algae [18] and ciliates [19]. Also, electron microscopy studies have shown stark structural differences in the enzymes of ciliates [19] and algae [18] as compared to the orthodox enzymes isolated from beef and yeast [11,20].

☆ This article is part of a Special Issue entitled 'EBEC 2016: 19th European Bioenergetics Conference, Riva del Garda, Italy, July 2-6, 2016', edited by Prof. Paolo Bernardi.
☆☆ Peripheral stalk of algal ATP synthases

* Corresponding author at: Departamento de Genética Molecular, Instituto de Fisiología Celular, UNAM, Apartado Postal 70-600, Delegación Coyoacán, 04510 México D.F., Mexico.
E-mail address: dhalphen@ifc.unam.mx (D. González-Halphen).

http://dx.doi.org/10.1016/j.bbabio.2016.02.003
0005-2728/

2. The mitochondrial ATP synthase of chlorophycean algae

2.1. Subunit composition

Chlorophycean algae originated approximately 600 million years ago [21]. Some characteristics of this lineage are the drastic reduction of its mitochondrial genomes in size and in gene content [22], the fragmentation of the mitochondrial *cox2* gene and its migration to the nucleus [23], and the appearance of nucleus-encoded atypical subunits of ATP synthase (Asa subunits) [24,25]. Genes encoding homologs of Asa subunits were identified in several other chlorophycean algae including *Volvox carteri*, *Scenedesmus obliquus* and *Chloroccocum ellipsoideum* [25]. The list can be updated to include the green unicellular algae *Chlamydomonas chlamydogama*, *Chlamydomonas leiostraca*, *Chlamydomonas* sp. and *Dunaliella tertiolecta* and the colorless algae *Polytomella capuana*, *Polytomella magna*, *Polytomella piriformis* and *Polytomella parva* [26].

The biochemical characterization of the mitochondrial ATP synthase of chlorophycean algae has been carried out mainly with two organisms, the unicellular green alga *Chlamydomonas reinhardtii* and its colorless close relative *Polytomella* sp. Early works identified immunochemically the β-subunit of mitochondrial ATP synthase in preparations of thylakoid and mitochondria membranes of *C. reinhardtii* [27]. A fraction enriched in the green algal complex V was obtained after sucrose gradient centrifugation in the presence of Triton X-100 [28]. The cDNA of the β-subunit of *C. reinhardtii* mitochondrial ATP synthase was sequenced and the corresponding protein was found to contain a unique C-terminal extension of 70 residues not present in the β-subunits of plant enzymes [29]. A pure and active mitochondrial ATP synthase preparation from the green alga was obtained by extraction with lauryl maltoside followed by ion exchange and gel permeation chromatography and found to be composed of at least 14 polypeptides [30]. Also, the cDNA encoding the α-subunit of the enzyme was sequenced and the mature subunit was found to exhibit an 18-residues extension not present in other organisms.

Subsequently, a mitochondrial F_1Fo-ATP synthase was isolated by gel permeation chromatography from *Polytomella* sp., that lacks both chloroplasts and cell wall, and thus facilitates the isolation of mitochondria and purification of the OXPHOS complexes without the interference of thylakoid components [31]. The enzyme from this colorless alga exhibited at least 10 polypeptides with apparent molecular masses that ranged from 6 to 63 kDa [32] and its α and β subunits exhibited high sequence similarities with the ones of *Chlamydomonas* [see also Ref. 33]. Here, the *Polytomella* α and β subunits were modeled on the crystallographic structure of the bovine enzyme to visualize the location of these extensions in the F_1 sector. Fig. 1 shows two of the possible conformations for each of the algal extensions. The α subunit extensions could have a role in stabilizing contacts with the peripheral stalk, while the β subunit extensions were proposed to act as the IF_1 ATPase inhibitor based on sequence similarities [32]. When the extension of the β subunit was overexpressed, partially purified, and added to the algal ATPase at relatively high concentrations, the hydrolytic activity of the enzyme diminished less than 20% [Villavicencio-Queijeiro and González-Halphen, unpublished results]. Although this result suggests a null or very limited inhibitory effect of the C-terminal extension of the beta subunit, it would be necessary to delete this extremity using site-directed mutagenesis to ascertain its role.

In order to assess if subunit *a* (Atp6) was present in the mitochondrial ATP synthase of *C. reinhardtii*, isolated mitochondria from the green alga were subjected to blue native electrophoresis (BN–PAGE), a technique that uses the charge shift generated by the binding of Coomassie Blue to detergent-solubilized membrane complexes to separate them under native conditions [34]. The first dimensional BN–PAGE gel was then subjected to 2D-denaturing SDS–PAGE to identify the polypeptide composition of complex V [35]. At least 13 different polypeptides were found to be associated to the complex, five of which were unambiguously identified as subunits α, β, γ, δ and *a*. Nevertheless, eight polypeptides of the ATP synthase showed no evident similarity with other ATPase subunits nor with other proteins in the databases, so their identities remained obscure at that time. These results prompted a detailed analysis of mitochondrial protein components of *C. reinhardtii* by BN–PAGE, followed by 2D-SDS–PAGE and Edman degradation of selected bands [36]. Complex V was found to migrate exclusively as a dimer that resolved into at least 13 polypeptides in 2D-SDS–PAGE. In addition, a novel 60-kDa protein with no known counterpart in any other organism, named MASAP for mitochondrial ATP synthase-associated protein and later on renamed Asa1, was described and its corresponding cDNA sequence was obtained [36]. It was put forth that this novel polypeptide was extrinsic to the membrane, probably not a chaperone and that it could play a structural role in stabilizing the chlorophycean ATP synthase dimer.

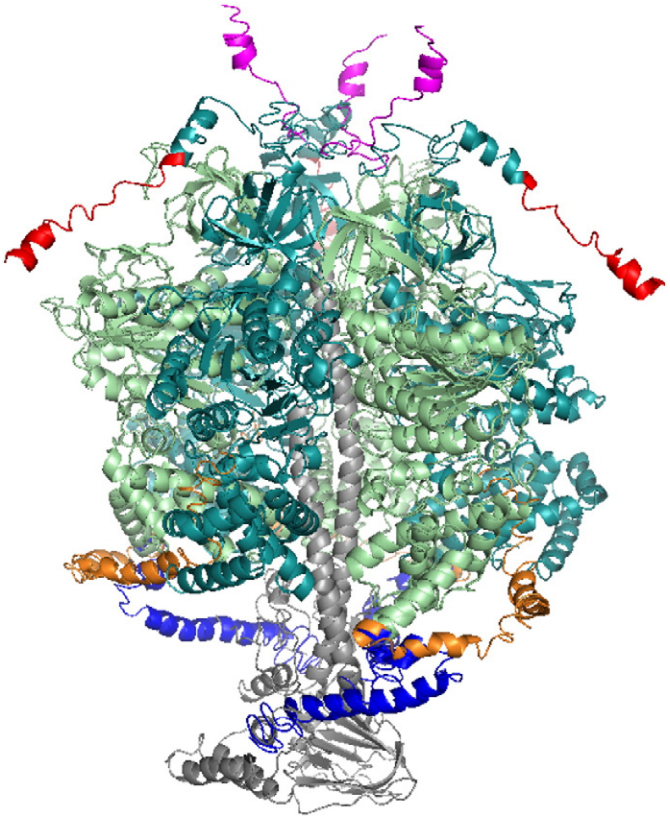

Fig. 1. Model of the *Polytomella* sp. ATP synthase subunits α and β and their corresponding extensions. The *Polytomella* sp. sequences of the mature α subunit with its C-terminal extension of 67 residues, and the β subunit with its N-terminal extension of 21 residues were modeled *in silico* using the I-TASSER server [71]. Two of the obtained models that showed no steric hindrances were selected for each subunit. The algal F_1 sector was modeled on the bovine crystallographic structure (PDB Id: 2WSS) [72]. Subunits in the complex are colored: α subunits (dark green), β subunits (light green), γ subunit (gray), algal α subunit extensions (one possible conformation in red, the other in magenta), algal β subunit extensions (one possible conformation in orange, the other in dark blue).

Mitochondrial F_1Fo-ATP synthases of *C. reinhardtii* and *Polytomella* sp. migrated in BN–PAGE in the presence of lauryl-maltoside as stable dimers of 1600 kDa [36,37] while the monomeric F_1Fo or free F_1 moieties could not be detected. This suggested the presence of a highly stable, detergent-resistant dimeric enzyme and contrasted starkly with the behavior of other complex V from different sources, including mammals, fungi and land plants that usually migrate in BN–PAGE in the presence of lauryl-maltoside as monomers of 550–600 kDa [14,20,38,39]. Also, conventional enzymes tend to partially dissociate during electrophoresis, releasing the F_1 sector [38]. In order to obtain dimers from these latter biological sources, milder solubilization conditions, usually with digitonin, are required [20].

The completion of the *C. reinhardtii* genome [40] allowed the identification of the ATP synthase subunits whose N-terminal sequences had been obtained previously [35]. Thus, the mitochondrial ATP synthase from *C. reinhardtii* was now found to contain 14 subunits of 7 to 60 kDa [41]. Seven polypeptides were identified as the classical subunits α, β, γ, δ, *a* (ATP6), *c* (ATP9), and OSCP. Besides Asa1, several other polypeptides with no counterparts in the databases were identified and named Asa2 to Asa7 (this last one previously known as Nuop6) in accordance with the *C. reinhardtii* genome project nomenclature. In addition, no homologs of the ε, *b*, *d*, *e*, *f*, *g*, IF_1, A6L, and F6 subunits were found encoded in the algal genome. This reinforced the idea that unique proteins were associated with chlorophycean mitochondrial ATP synthases [24] and pin-pointed the Asa subunits as the main constituents of the peripheral stalk of the enzyme. The mitochondrial ATP synthase of *Polytomella* sp. was isolated; its polypeptide composition was characterized and found to be similar to that of the *C. reinhardtii* enzyme [18,33]. Furthermore, small-angle X-ray scattering analysis estimated a molecular mass of the complex of 1696 kDa [42]. In addition, the presence of two additional low molecular mass subunits, Asa8 and Asa9, was described. Asa subunits were found associated to the algal ATP synthase even when the complex was isolated following different purification procedures; thus, the possibility that they were only contaminants of the preparations was discarded [18]. It seems that in the chlorophycean lineage, all the orthodox structural components of the peripheral arm were substituted by polypeptides from a completely different origin, probably proteins that already had a structural role in some other cell compartment.

2.2. Hydrolytic activity of the purified algal enzyme

When isolated, the *Polytomella* sp. enzyme exhibits a very low ATPase activity that increases either with heat treatment (due to the release of the F_1 sector) or when being unmasked by the presence of non-ionic detergents in an activity assay [43]. The biochemical state of the enzyme in the absence of externally added detergent is however not known; it could be partially aggregated and therefore inactive, or it could be fully restrained by an inhibitor that is released upon detergent addition. The algal dimer hydrolyzes ATP on a wide range of pH's and temperatures and shows sensitivity to the classical inhibitors oligomycin and DCCD [44], the dimeric ATPase exhibited and apparent Km for Mg-ATP of 0.19 mM and a V_{max} of 0.065 U/mg in the absence of detergent. The V_{max} increased 60-fold in the presence of detergent (Km of 0.24 mM and a V_{max} of 3.8 U/mg). Independent measurements of the hydrolytic activity of the *Polytomella* mitochondrial ATPase have reported activities up to 8.0 U/mg, full DCCD sensitivity, and more than 90% inhibition by oligomycin [45]. These specific activity values are comparable to those of purified ATPases from the green alga *C. reinhardtii* (2.9 U/mg) [30] or from the fungi *Yarrowia lipolytica* (8.4 U/mg) and *Pichia pastoris* (9.3 U/mg), but considerably lower than the enzymes from *Pichia angusta* (21.8 U/mg) and *Saccharomyces cerevisiae* (35.8 U/mg) [46]. Overall, the enzyme does not exhibit strong differences in its hydrolytic activity as compared with the enzymes obtained from many other sources. Oligomycin seems to bind loosely to the algal enzyme, probably due to structural differences in its subunit *c* [44] that may affect the antibiotic binding site [47]. It is therefore necessary both to pre-incubate the enzyme in the presence of the inhibitor and to add an equal concentration of oligomycin in the assay medium. Incidentally, growth, respiration, and ATP levels in Chlorophycean algae were also barely affected by oligomycin concentrations that affect representatives of the other classes of Chlorophytes [25].

2.3. Three dimensional structure of the enzyme

The stable dimeric nature of the algal ATP synthase prompted a series of electron-microscopy studies. The *Polytomella* enzyme, obtained by digitonin solubilization of mitochondria and sucrose gradient centrifugation, was subjected to electron microscopy and single particle analysis. Projection maps with a resolution of about 17 Å showed a dimeric enzyme stabilized by interactions between the membrane-bound Fo sectors that formed an angle of 70° [37]. This implied that the enzyme could induce a strong local bending of the inner mitochondrial membrane [13]. Also, the peripheral stalks of the algal dimeric enzyme were noted to be much more robust than their counterparts in other F-type ATPases, including the ones from bovine [48], yeast [49], spinach chloroplasts [50], and *Escherichia coli* [51].

Polytomella sp. mitochondria were subjected to ultrathin sectioning, and cristae membranes were found to fold into lamellae and tubuli. The ATP synthase oligomers seem to make helical arrangements along these tubular membranes, confirming the role of complex V in determining the shape of the inner mitochondrial membrane [52]. This has been further substantiated by RNA interference silencing of the *Atp2* gene encoding subunit β of the *C. reinhardtii* ATP synthase: ATP synthesis was fully impaired, the enzyme failed to assemble, and the algal mitochondria were deprived of cristae [53].

Dual-axis cryo-electron tomography confirmed a supramolecular organization of dimeric ATP synthase in the cristae membranes of *Polytomella* sp. mitochondria that exhibited rows of dimers at 12 nm intervals [54]. In addition, averaged 3D subvolumes of the algal oligomeric enzyme were obtained at 5.7 nm resolution. These 3D tomography data were the first indicators that contacts existed between the peripheral stalks of the monomers [54] suggesting their very rigid architecture. An additional EM analysis of the *Polytomella* sp. mitochondrial ATP synthase complex supported the dimeric nature of the enzyme and presence of robust peripheral stalks [42].

More recently, an electron cryo-microscopy map at 6.2 Å resolution of the *Polytomella* sp. dimeric ATP synthase was obtained [45]. Fig. 2A shows the electron density map of the dimer and the principal domains that constitute the oligomeric complex. The model has several salient features: i) subunit *a* exhibits horizontally membrane-embedded α-helices that seem to embrace the *c*-ring and that form the two proton-translocating hemi-channels; the presence of these horizontal helices has been subsequently observed in the bacterial [55] and in the beef heart mitochondrial enzymes [56], ii) the robust peripheral stalks are constituted by several entwined α-helices that form a very solid scaffold as compared to the one from other enzymes (Fig. 2B); this is in accordance with the high propensity of several Asa subunits (Asa1, Asa2, Asa4 and Asa7) to form coiled-coils [57], iii) local resolution estimates indicated that the peripheral stalk is more ordered than the catalytic F_1 sector; furthermore, these peripheral stalks are united in their middle region by protein–protein contacts; the Asa subunit responsible for forming this extra-membranous bridge between the monomers is unknown, but could be either Asa4 as suggested previously [33] or Asa7 (see below), iv) the peripheral stalk, besides its substantial mass, seems to make several contacts with the F_1 sector; these contacts may be, among others, the interactions Asa2-α [57] and Asa1-OSCP [26], and v) the *c*-ring is formed by 10 monomers and seems to be SDS-resistant [26], as those observed in yeast [58], in Na^+-dependent ATP synthases of bacteria [59] and in the A_1Ao-ATP synthases of archaea [60].

3. Addressing the topology of the components of the peripheral arm of algal mitochondrial ATP synthase

The neighboring interactions of Asa subunits in the ATP synthase of the colorless chlorophycean alga *Polytomella* sp. have been addressed using a variety of experimental approaches: defining near-neighbor relationships of subunits after treating the whole enzyme with cross-linking agents; characterizing protein–protein interactions *in vitro* with recombinant subunits; and dissociating the enzyme into subcomplexes by heat or high detergent concentrations. Thus, models for the topological disposition of the Asa polypeptides in the peripheral arm of the enzyme have been successively refined [18,26,33,42,57].

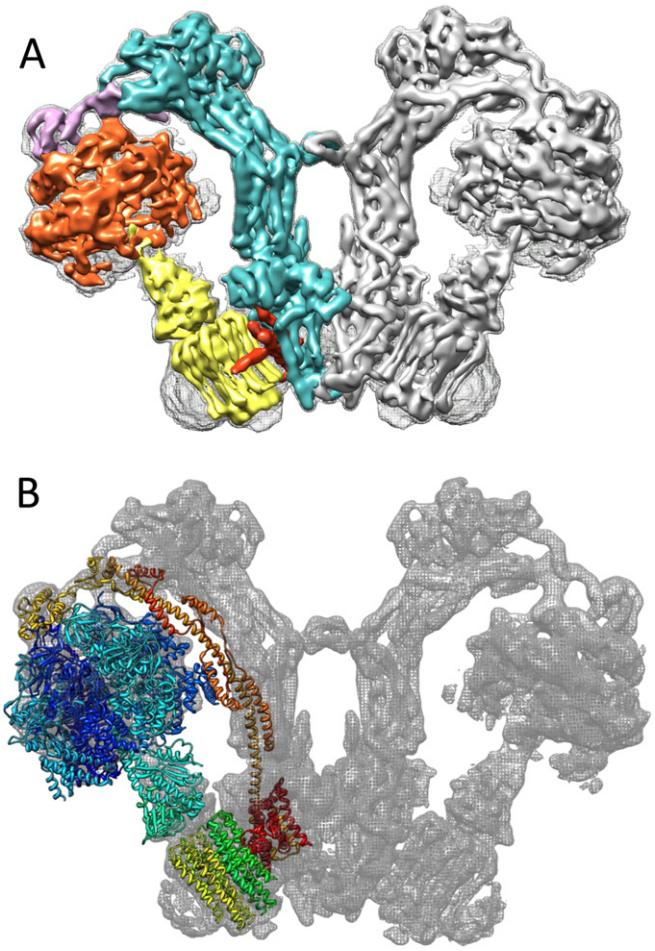

Fig. 2. Electron cryo-microscopy map of the algal *Polytomella* sp. ATP synthase. A) The model shown corresponds to EMDB accession number EMD-2852 [45]. The main domains of the complex were visualized and colored with the UCSF Chimera package [73]: rotor in yellow (subunits γ/δ/ε/*c*-ring), subunit *a* in red, the catalytic domain (α_3/β_3) in orange, OSCP in violet, and the peripheral stalk (Asa1 to 5 and Asa7) plus the membrane dimerization domain (Asa6, Asa8 and Asa9) in cyan. B) The model of the algal dimeric enzyme (EMD-2852 [45]) and the model of the bovine enzyme obtained by single particle electron cryomicroscopy (PDB Id: 5ARA) [74] were superimposed. The sturdiness of the peripheral stalk of the algal dimer as compared to the one of the bovine enzyme is evident.

3.1. Neighboring interactions between Asa subunits as revealed by cross-linking agents

To assess neighboring interactions between subunits in the algal ATP synthase subunits, cross-linking experiments with several water-soluble and water-insoluble homo-bifunctional and hetero-bifunctional reagents were carried out. Besides some expected cross-link products between the orthodox subunits (*i.e.*, α-β or α-OSCP), the cross-link products that were reproducibly obtained with the atypical subunits were (Asa1–Asa4), (Asa1–Asa7), (Asa2–Asa4), (Asa2–Asa7), (Asa3–Asa8), (Asa6–Asa6) and the triple cross-link product (Asa2–Asa4–Asa7) [42]. The inferred close vicinities between polypeptides were used to predict an overall topology of the algal ATP synthase.

3.2. Silencing and overexpression of subunits

The Asa7 subunit of the green algae *C. reinhardtii* was knocked-down using RNA interference. The absence of this polypeptide neither affected growth nor the OXPHOS of the alga [25]. Nevertheless, attempts to purify the ATP synthase from the Asa7-silenced mutant invariably failed, because lauryl maltoside solubilization dissociated the complex and released its F_1 sector. Subunit Asa7 is known to bind to at least three other subunits (Asa1, Asa2 and Asa4); it therefore must play a pivotal role in stabilizing the overall architecture of the peripheral stalk.

In order to gain more insights on how Asa proteins interact, recombinant subunits were over-expressed and purified and their interactions *in vitro* explored. It was shown that Asa2, Asa4 and Asa7 interact, and furthermore, that the interaction Asa4–Asa7 is mediated by the C-terminal halves of both proteins [57]. Asa2 can bind Asa7 and the C-terminal half of Asa4. An interaction Asa2-α was also observed, suggesting the proximity of Asa2 with the catalytic head of the enzyme. In addition, subunits Asa2, Asa4 and Asa7 formed a subcomplex with a 1:1:1 stoichiometry that could be reconstituted *in vitro*. This subcomplex was proposed to establish additional contacts with Asa1 and with OSCP.

Subunit Asa1 was shown to be a membrane-extrinsic subunit using sodium carbonate treatment on mitochondrial membranes. It was proposed to represent the bulky structure observed near the F_1 sector in EM studies, and therefore to interact with OSCP [33]. Indeed, subunit Asa1 seems to be one of the main components of the peripheral stalk of the algal enzyme, probably forming the main column that unites the extrinsic subunit OSCP with other components of the enzyme in close contact with the membrane (Asa3, Asa5, Asa8, *a* and c_{10}-ring). Thus, Asa1 may be the main support of the peripheral stalk and may have a scaffolding role similar to the one of subunit *b* in orthodox enzymes [26]. Sequence alignment analysis shows that OSCP subunits can be separated into two clearly distinct groups based on their amino acid sequences: one pertaining to the Chlorophycean algae (where OSCP binds an Asa1 subunit), and another that belongs to land plants and other green algae like Prasinophyceae, Ulvophyceae, and Trebouxiophyceae (where OSCP binds an orthodox *b* subunit) [26].

3.3. Dissociation of the enzyme into subcomplexes

Work carried out with the *Polytomella* ATP synthase established other subunit–subunit interactions, mainly through the identification of subcomplexes formed by heat dissociation [18,43]. Upon heat treatment, the ATPase is dissociated into its monomers and immediately afterwards it releases its F_1 sector and disassembles [18,33]. Subunits Asa2, Asa4 and Asa7 and OSCP seem to dissociate concomitantly with the liberation of the F_1 sector. In addition, a subcomplex that contained subunits Asa1/Asa3/Asa5/Asa8/*a*/*c* appeared transiently [18]. A stable Asa1/Asa3/Asa5/Asa8/*a*/c_{10} subcomplex could be obtained by treating the enzyme with relatively high lauryl maltoside concentrations [26]. Furthermore, heat denaturation or taurodeoxycholate treatment of the dimeric enzyme leads to a monomeric form with substoichiometric amounts of Asa6 and Asa9 subunits [43]; thus these two proteins seem to promote enzyme dimerization. In addition, the monomeric form of the complex is less active than the dimer, exhibits diminished oligomycin sensitivity, and is more labile to heat treatment, high hydrostatic pressures, and protease digestion [43].

Amphipols, the short amphipathic polymers that can substitute detergents, help the folding and stability of several integral membrane proteins [61]. To find whether Amphipol A8-35 would also help stabilize the algal ATP synthase, the purified enzyme was incubated with the polymer. As judged by BN–PAGE, in the presence of increasing concentrations of Amphipol A8-35 the dimeric enzyme (V_2) partially dissociated into free F_1 sector, comprising at least α, β, γ, and δ subunits, and a subcomplex named SC1 that is composed of Fo and the peripheral stalk (Fig. 3A). Another sample of the purified enzyme was incubated with 3.5% Amphipol A8-35 for 40 min (Fig. 3B, lane 1) and subjected to 2D-SDS–PAGE, where the polypeptides of subcomplex SC1 were resolved (Fig. 3C). Subunit OSCP was found to readily dissociate, migrating towards the front of the BN–PAGE gel. In parallel, a second sample of the purified enzyme was incubated with 3.5% Amphipol A8-35 for 24 h (Fig. 3B, lane 2) and then resolved in 2D-SDS–PAGE. In these conditions, a second subcomplex (SC2), with higher mobility in BN–PAGE than SC1,

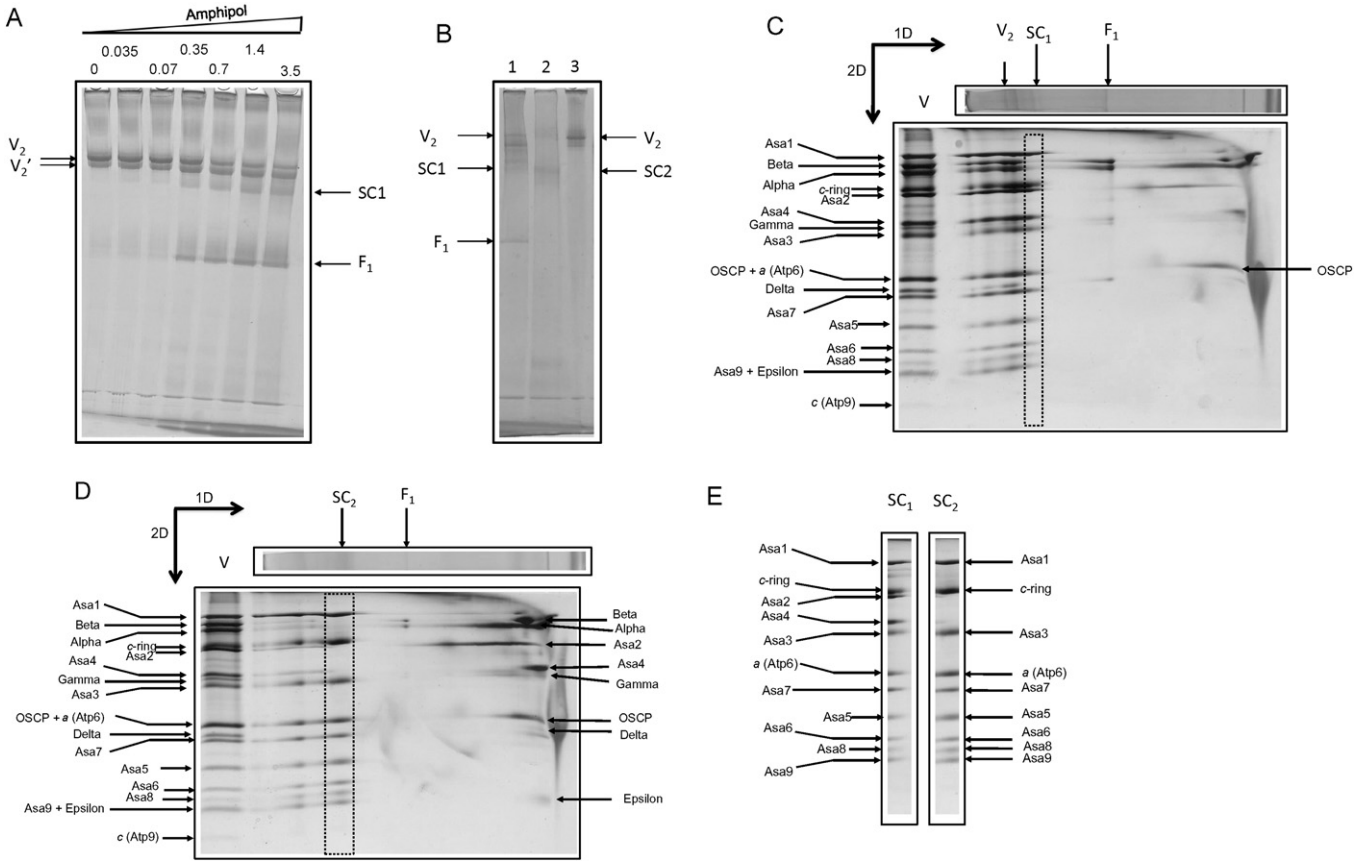

Fig. 3. Amphipol A8-35 dissociates the dimeric algal ATP synthase into discrete subcomplexes. A) BN–PAGE of purified ATP synthase samples [18] incubated for 40 min at 4 °C under mild agitation in the presence of Amphipol A8-35 (Anatrace) at the indicated increasing concentrations (% *w*/*v*). One hundred micrograms of protein was loaded in each lane. The control lane in the absence of the detergent is labeled 0. Dimer (V_2), F_1 sector (F_1), and subcomplex (SC1) are indicated. V_2' denotes an isoform of the algal ATP synthase with a different electrophoretic migration, whose subunit composition is identical to the one of V_2. B) BN–PAGE of purified ATP synthase samples (50 μg of protein in each lane) incubated with or without Amphipol A8-35. Lane 1: sample incubated in the presence of 3.5% Amphipol A8-35 for 40 min; lane 2: sample incubated in the presence of 3.5% Amphipol A8-35 for 24 h; lane 3: control ATP synthase without treatment. Dimer (V_2), F_1 sector (F_1), and subcomplexes SC1 and SC2 are indicated. C) Silver-stained 2D gel of an ATP synthase sample incubated for 40 min in the presence of 3.5% Amphipol A8-35. D) Silver-stained 2D gel of an ATP synthase sample incubated for 24 h in the presence of 3.5% Amphipol A8-35. E) Identity of the subunits that form the SC1 and SC2 subcomplexes. Gels were taken from the 2D polypeptide patterns shown in panels C and D.

was formed (Fig. 3D). The population of free F_1 was much smaller, and the dissociated subunits α, β, γ, δ, ε, Asa2, Asa4 and OSCP were found to migrate towards the front of the BN–PAGE polypeptide pattern. The subunit composition of the two Amphipol A8-35-generated subcomplexes SC1 and SC2 is shown in Fig. 3E. Their identities were assigned by their apparent molecular masses as Asa1 (66.1 kDa), *c*-ring (45.5 kDa), Asa2 (45.3 kDa), Asa3 (32.9 kDa), subunit *a* (25.1 kDa), Asa7 (19.0 kDa), Asa5 (13.9 kDa), Asa6 (13.1 kDa), Asa8 (9.9 kDa) and Asa9 (11.0 kDa). The apparent molecular masses of the SC1 and SC2 subcomplexes are of 681 and 528 kDa respectively, suggesting that these subcomplexes are dimeric. Upon Amphipol A8-35 treatment, the dimeric enzyme liberates OSCP and its F_1 sectors to

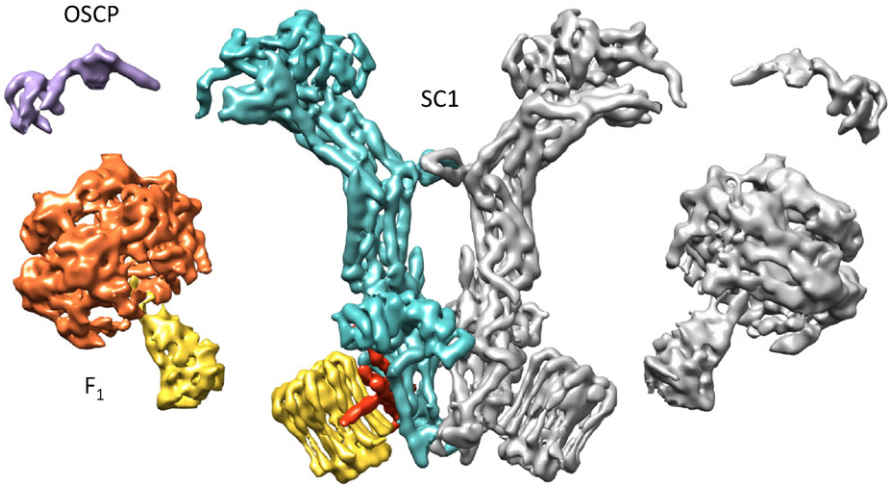

Fig. 4. Model showing the dissociation of the ATP synthase induced by Amphipol A8-35. The model illustrates the dissociation of the algal ATP synthase by Amphipol A8-35 (40 min incubation) to form the dimeric SC1 subcomplex after the dissociation of the F_1 sector and subunit OSCP.

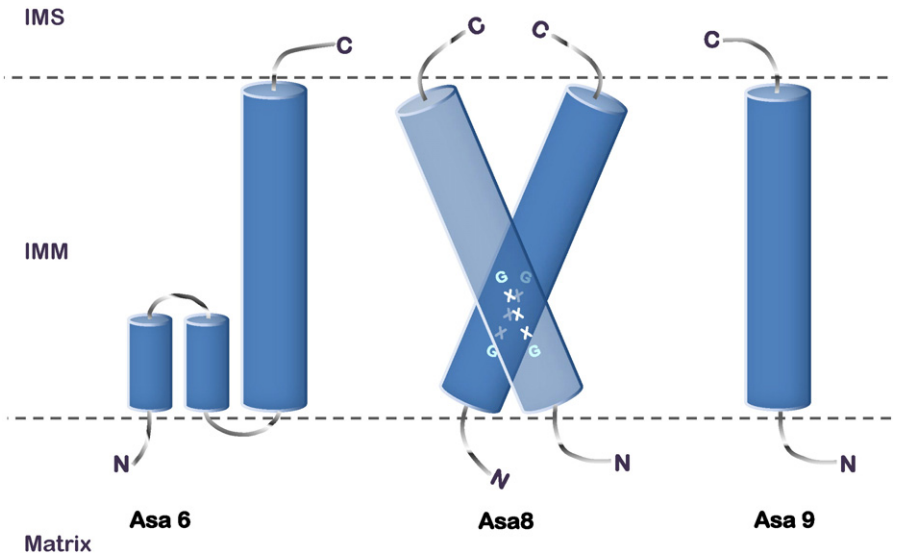

Fig. 5. Hydrophobicity-based models of the individual subunits involved in the membrane-embedded dimerization domain. Several algorithms predict the Asa8 and Asa9 subunits with a single TMS. The GxxxG motif in the Asa8 subunit could prompt its dimerization. The predicted models for Asa6 vary with the different programs used: one TMS, two TMS, or one TMS with a reentrant helix (depicted).

form the SC1 subcomplex (illustrated in Fig. 4), while longer polymer treatment additionally releases the Asa2 and Asa4 subunits and forms the SC2 subcomplex (not shown). Thus, it seems that Amphipol A8-35 does not destabilize the membrane-embedded subunits of complex V, but destabilizes other extrinsic components, mainly OSCP, Asa2 and Asa4. It is notable that subunit Asa7 remains bound to the dimeric SC2 subcomplex even after the dissociation of the Asa2 and Asa4 subunits, most probably attaching to Asa1. It is therefore tempting to speculate that Asa7 is the extrinsic protein bridge that unites the peripheral stalks of the algal model observed in the 3-D model of the *Polytomella* sp. ATP synthase [45].

3.4. The dimerization domain of the algal mitochondrial ATP synthase

Only small-molecular mass polypeptides of the algal ATP synthase seem to be embedded in the membrane: subunits Asa6, Asa8 and Asa9 are predicted to have transmembrane stretches (TMS), two, one and one, respectively [33].

The stoichiometry of all the Asa subunits in the algal ATP synthase has not been established yet. An estimated stoichiometry based on cysteine-labeling fluorescent probes revealed a 1:1:1 stoichiometry for subunits Asa3:Asa4:Asa5 per monomer [42], although this assessment was limited to those subunits that contain at least one cysteine residue.

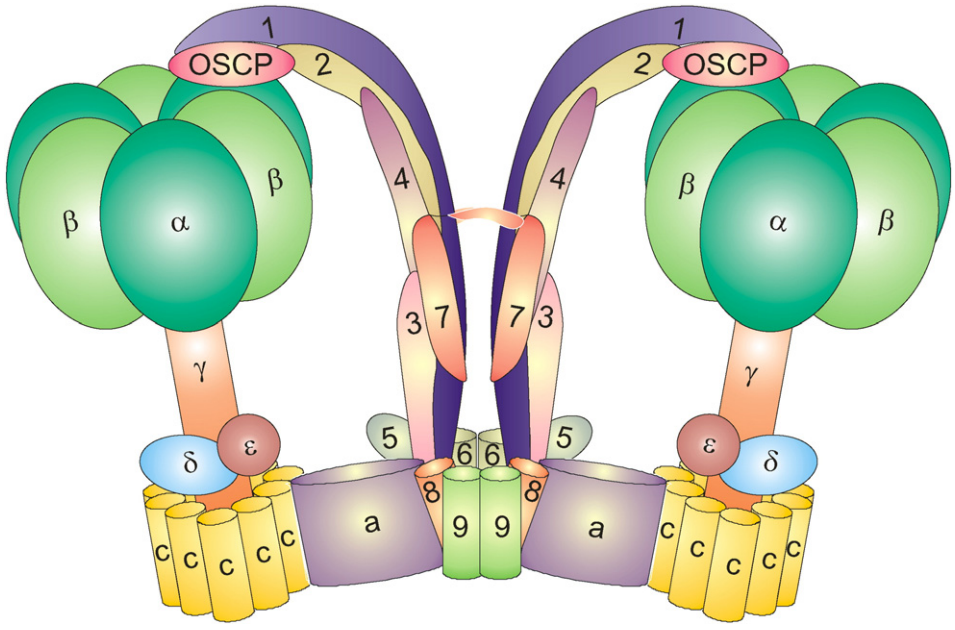

Fig. 6. Arrangement of subunits in the algal mitochondrial ATP synthase. The model is consistent with the data summarized in this article and illustrates the dimeric enzyme with a colored subunit composition. Letters denote the conserved ATP synthase subunits, while numbers refer to Asa subunits (Asa1-Asa9). Subunits Asa6, 8 and 9 form the dimerization module, while the rest of them are constituents of the peripheral stalks.

Cross-sections through the membrane domains of the electron cryomicroscopy map of the algal enzyme show the four horizontal-embedded helices of subunit *a*, the c_{10}-ring and six additional transmembrane helices per monomer [45]. These six TMS could be ascribed, in principle, to the fifth vertical α-helix of subunit *a* [56], the two reentrant helices and one TMS of subunit Asa6, one TMS of Asa8, and one TMS of Asa9 (Fig. 5). Asa8 may be instrumental for the dimerization of the enzyme, since it contains a GxxxG domain, which is a weak predictor of membrane protein dimerization [62]. The presence of GxxxG domains in subunits *e* and *g* is known to play an important role in dimerizing the yeast ATP synthase [63–65].

All the above mentioned data can be summarized in an updated model for the topological disposition of the 17 polypeptides that constitute the algal enzyme (Fig. 6).

4. Perspectives

A regulatory protein that may control the ATPase activity of the algal enzyme has not been characterized yet. Nevertheless, one of its subunits is expected to have a regulatory role similar to subunit IF_1 in mitochondrial enzymes [66], to the γ-proteobacterial ε subunit [67] or to the α-proteobacterial ζ subunit [68].

Many biochemical data have been obtained on the Asa subunits arrangement in the peripheral stalk, but to elaborate a more precise model of organization and to validate or invalidate the model in Fig. 6, high resolution structural data is needed. In the model available to date [45], it is still not possible to pin-point unambiguously the individual Asa subunits.

All the subunits of the chlorophycean mitochondrial ATP synthases are nucleus-encoded, since no gene encoding any complex V polypeptide has been found in the mitochondrial genomes of these algae [69,70]. It is of interest to learn how all the nucleus-encoded subunits, especially the Asa subunits, are imported into mitochondria and how they assemble to form the very large, 1600 kDa algal complex V.

Transparency document

The Transparency document associated with this article can be found, in online version.

Acknowledgments

This paper is dedicated to our Emeritus Professor Marietta Tuena-Sangri (IFC, UNAM), for always providing us unfading encouragement and support. Research in our group is being supported by the grant 245486 from the Consejo Nacional de Ciencia y Tecnología (CONACyT) and the Belgian Fonds de la Recherche Scientifique (F.R.S.–FNRS) (Mexico-Belgium). Additional support was received from grants 239219 and 239487 (CONACyT, Mexico), IN203311-3 from the Dirección General de Asuntos del Personal Académico (DGAPA–UNAM, Mexico) and from the Belgian F.R.S.–FNRS (MIS F.4520, FRFC 2.4597, CDR J.0032). CONACyT also supports the Ph.D. studies of L.C.-T. and L.S.-V. (fellowships 599282 and 290733 respectively, Programa de Doctorado en Ciencias Biomédicas, UNAM) and the Masters studies of F.V.D. (fellowship 660082, Programa de Maestría y Doctorado en Ciencias Bioquímicas, UNAM).

References

[1] M. Alfonzo, M.A. Kandrach, E. Racker, Isolation, characterization, and reconstitution of a solubilized fraction containing the hydrophobic sector of the mitochondrial proton pump, J. Bioenerg. Biomembr. 13 (1981) 375–391.
[2] G. Oster, H. Wang, Rotary protein motors, Trends Cell Biol. 13 (2003) 114–121.
[3] G. Arselin, J. Vaillier, B. Salin, J. Schaeffer, M.F. Giraud, A. Dautant, D. Brèthes, J. Velours, The modulation in subunits e and g amounts of yeast ATP synthase modifies mitochondrial cristae morphology, J. Biol. Chem. 279 (2004) 40392–40399.
[4] J.E. Walker, V.K. Dickson, The peripheral stalk of the mitochondrial ATP synthase, Biochim. Biophys. Acta 1757 (2006) 286–296.
[5] A. Wächter, Y. Bi, S.D. Dunn, B.D. Cain, H. Sielaff, F. Wintermann, S. Engelbrecht, W. Junge, Two rotary motors in F-ATP synthase are elastically coupled by a flexible rotor and a stiff stator stalk, Proc. Natl. Acad. Sci. U. S. A. 108 (2011) 3924–3929.
[6] R. Yasuda, H. Noji, K. Kinosita Jr., M. Yoshida, F1-ATPase is a highly efficient molecular motor that rotates with discrete 120 degree steps, Cell 93 (1998) 1117–1124.
[7] J.R. Gledhill, J.E. Walker, Inhibition sites in F1-ATPase from bovine heart mitochondria, Biochem. J. 386 (2005) 591–598.
[8] A.G. Stewart, L.K. Lee, M. Donohoe, J.J. Chaston, D. Stock, The dynamic stator stalk of rotary ATPases, Nat. Commun. 3 (2012) 687.
[9] V.K. Dickson, J.A. Silvester, I.M. Fearnley, A.G. Leslie, J.E. Walker, On the structure of the stator of the mitochondrial ATP synthase, EMBO J. 25 (2006) 2911–2918.
[10] H. Seelert, N.A. Dencher, ATP synthase superassemblies in animals and plants: two or more are better, Biochim. Biophys. Acta 1807 (2011) 1185–1197.
[11] D. Thomas, P. Bron, T. Weimann, A. Dautant, M.F. Giraud, P. Paumard, B. Salin, A. Cavalier, J. Velours, D. Brèthes, Supramolecular organization of the yeast F1Fo-ATP synthase, Biol. Cell. 100 (2008) 591–601.
[12] M. Strauss, G. Hofhaus, R.R. Schröder, W. Kühlbrandt, Dimer ribbons of ATP synthase shape the inner mitochondrial membrane, EMBO J. 27 (2008) 1154–1160.
[13] P. Paumard, J. Vaillier, B. Coulary, J. Schaeffer, V. Soubannier, D.M. Mueller, D. Brèthes, J.P. di Rago, J. Velours, The ATP synthase is involved in generating mitochondrial cristae morphology, EMBO J. 21 (2002) 221–230.
[14] I. Arnold, K. Pfeiffer, W. Neupert, R.A. Stuart, H. Schägger, Yeast mitochondrial F1F0-ATP synthase exists as a dimer: identification of three dimer-specific subunits, EMBO J. 17 (1998) 7170–7178.
[15] R. Fronzes, T. Weimann, J. Vaillier, J. Velours, D. Brèthes, The peripheral stalk participates in the yeast ATP synthase dimerization independently of e and g subunits, Biochemistry 45 (2006) 6715–6723.
[16] A. Zikova, A. Schnaufer, R.A. Dalley, A.K. Panigrahi, K.D. Stuart, The F(0)F(1)-ATP synthase complex contains novel subunits and is essential for procyclic *Trypanosoma brucei*, PLoS Pathog. 5 (2009) e1000436.
[17] E. Perez, M. Lapaille, H. Degand, L. Cilibrasi, A. Villavicencio-Queijeiro, P. Morsomme, D. González-Halphen, M.C. Field, C. Remacle, D. Baurain, P. Cardol, The mitochondrial respiratory chain of the secondary green alga *Euglena gracilis* shares many additional subunits with parasitic Trypanosomatidae, Mitochondrion 19 (Pt B) (2014) 338–349.
[18] M. Vázquez-Acevedo, P. Cardol, A. Cano-Estrada, M. Lapaille, C. Remacle, D. González-Halphen, The mitochondrial ATP synthase of chlorophycean algae contains eight subunits of unknown origin involved in the formation of an atypical stator-stalk and in the dimerization of the complex, J. Bioenerg. Biomembr. 38 (2006) 271–282.
[19] N.P. Balabaskaran, N.V. Dudkina, L.A. Kane, J.E. van Eyk, E.J. Boekema, M.W. Mather, A.B. Vaidya, Highly divergent mitochondrial ATP synthase complexes in *Tetrahymena thermophila*. PLoS Biol. 8 (2010) e1000418.
[20] S.J. Couoh-Cardel, S. Uribe-Carvajal, S. Wilkens, J.J. García-Trejo, Structure of dimeric F1F0-ATP synthase, J. Biol. Chem. 285 (2010) 36447–36455.
[21] M.D. Herron, J.D. Hackett, F.O. Aylward, R.E. Michod, Triassic origin and early radiation of multicellular volvocine algae, Proc. Natl. Acad. Sci. U. S. A. 106 (2009) 3254–3258.
[22] E. Rodríguez-Salinas, C. Remacle, D. González-Halphen, Green Algae Genomics: A Mitochondrial Perspective, in: L. Maréchal-Drouard (Ed.), Mitochondrial Genome Evolution, Advances in Botanical Research, Volume 63, Elsevier Inc., San Diego 2012, pp. 187–214.
[23] E. Rodríguez-Salinas, H. Riveros-Rosas, Z. Li, K. Fucíková, J.J. Brand, L.A. Lewis, D. González-Halphen, Lineage-specific fragmentation and nuclear relocation of the mitochondrial cox2 gene in chlorophycean green algae (Chlorophyta), Mol. Phylogenet. Evol. 64 (2012) 166–176.
[24] P. Cardol, D. González-Halphen, A. Reyes-Prieto, D. Baurain, R.F. Matagne, C. Remacle, The mitochondrial oxidative phosphorylation proteome of *Chlamydomonas reinhardtii* deduced from the Genome Sequencing Project, Plant Physiol. 137 (2005) 447–459.
[25] M. Lapaille, A. Escobar-Ramírez, H. Degand, D. Baurain, E. Rodríguez-Salinas, N. Coosemans, M. Boutry, D. Gonzalez-Halphen, C. Remacle, P. Cardol, Atypical subunit composition of the chlorophycean mitochondrial F1FO-ATP synthase and role of Asa7 protein in stability and oligomycin resistance of the enzyme, Mol. Biol. Evol. 27 (2010) 1630–1644.
[26] L. Colina-Tenorio, H. Miranda-Astudillo, A. Cano-Estrada, M. Vázquez-Acevedo, P. Cardol, C. Remacle, D. González-Halphen, Subunit Asa1 spans all the peripheral stalk of the mitochondrial ATP synthase of the chlorophycean alga *Polytomella* sp, Biochim. Biophys. Acta (2015 Nov 30), http://dx.doi.org/10.1016/j.bbabio.2015.11.012 [pii: S0005-2728(15)00244-3, Epub ahead of print].
[27] A. Atteia, C. de Vitry, Y. Pierre, J.L. Popot, Identification of mitochondrial proteins in membrane preparations from *Chlamydomonas reinhardtii*, J. Biol. Chem. 267 (1992) 226–234.
[28] A. Atteia, Identification of mitochondrial respiratory proteins from the green alga *Chlamydomonas reinhardtii*, C. R. Acad. Sci. III. 317 (1994) 11–19.
[29] L.G. Franzén, G. Falk, Nucleotide sequence of cDNA clones encoding the beta subunit of mitochondrial ATP synthase from the green alga *Chlamydomonas reinhardtii*: the precursor protein encoded by the cDNA contains both an N-terminal presequence and a C-terminal extension, Plant Mol. Biol. 19 (1992) 771–780.
[30] G. Nurani, L.-G. Franzén, Isolation and characterization of the mitochondrial ATP synthase from *Chlamydomonas reinhardtii*. cDNA sequence and deduced protein sequence of the alpha subunit, Plant Mol. Biol. 31 (1996) 1105–1116.
[31] E.B. Gutiérrez-Cirlos, A. Antaramian, M. Vázquez-Acevedo, R. Coria, D. González-Halphen, A highly active ubiquinol-cytochrome c reductase (bc1 complex) from the

colorless alga *Polytomella* spp., a close relative of *Chlamydomonas*. Characterization of the heme binding site of cytochrome c_1, J. Biol. Chem. 269 (1994) 9147–9154.
[32] A. Atteia, G. Dreyfus, D. González-Halphen, Characterization of the alpha and beta-subunits of the F0F1-ATPase from the alga *Polytomella* spp., a colorless relative of *Chlamydomonas reinhardtii*, Biochim. Biophys. Acta 1320 (1997) 275–284.
[33] R. van Lis, G. Mendoza-Hernández, G. Groth, A. Atteia, New insights into the unique structure of the F0F1-ATP synthase from the chlamydomonad algae *Polytomella* sp. and *Chlamydomonas reinhardtii*, Plant Physiol. 144 (2007) 1190–1199.
[34] H. Schägger, Native Gel Electrophoresis, in: G. von Jagow, H. Schägger (Eds.), A Practical Guide to Membrane Protein Purification, Academic Press, San Diego 1994, pp. 81–104.
[35] S. Funes, E. Davidson, M.G. Claros, R. van Lis, X. Pérez-Martínez, M. Vázquez-Acevedo, M.P. King, D. González-Halphen, The typically mitochondrial DNA-encoded ATP6 subunit of the F1F0-ATPase is encoded by a nuclear gene in, *Chlamydomonas reinhardtii*, J. Biol. Chem. 277 (2002) 6051–6058.
[36] R. van Lis, A. Atteia, G. Mendoza-Hernández, D. González-Halphen, Identification of novel mitochondrial protein components of *Chlamydomonas reinhardtii*. A proteomic approach, Plant Physiol. 132 (2003) 318–330.
[37] N.V. Dudkina, J. Heinemeyer, W. Keegstra, E.J. Boekema, H.P. Braun, Structure of dimeric ATP synthase from mitochondria: an angular association of monomers induces the strong curvature of the inner membrane, FEBS Lett. 579 (2005) 5769–5772.
[38] L. Jänsch, V. Kruft, U.K. Schmitz, H.P. Braun, New insights into the composition, molecular mass and stoichiometry of the protein complexes of plant mitochondria, Plant J. 9 (1996) 357–368.
[39] S. Guerrero-Castillo, M. Vázquez-Acevedo, D. González-Halphen, S. Uribe-Carvajal, In *Yarrowia lipolytica* mitochondria, the alternative NADH dehydrogenase interacts specifically with the cytochrome complexes of the classic respiratory pathway, Biochim. Biophys. Acta 1787 (2009) 75–85.
[40] S.S. Merchant, S.E. Prochnik, O. Vallon, E.H. Harris, S.J. Karpowicz, G.B. Witman, A. Terry, A. Salamov, L.K. Fritz-Laylin, L. Maréchal-Drouard, W.F. Marshall, L.H. Qu, D.R. Nelson, A.A. Sanderfoot, M.H. Spalding, V.V. Kapitonov, Q. Ren, P. Ferris, E. Lindquist, H. Shapiro, S.M. Lucas, J. Grimwood, J. Schmutz, P. Cardol, H. Cerutti, G. Chanfreau, C.L. Chen, V. Cognat, M.T. Croft, R. Dent, S. Dutcher, E. Fernández, H. Fukuzawa, D. González-Ballester, D. González-Halphen, A. Hallmann, M. Hanikenne, M. Hippler, W. Inwood, K. Jabbari, M. Kalanon, R. Kuras, P.A. Lefebvre, S.D. Lemaire, A.V. Lobanov, M. Lohr, A. Manuell, I. Meier, L. Mets, M. Mittag, T. Mittelmeier, J.V. Moroney, J. Moseley, C. Napoli, A.M. Nedelcu, K. Niyogi, S.V. Novoselov, I.T. Paulsen, G. Pazour, S. Purton, J.P. Ral, D.M. Riaño-Pachón, W. Riekhof, L. Rymarquis, M. Schroda, D. Stern, J. Umen, R. Willows, N. Wilson, S.L. Zimmer, J. Allmer, J. Balk, K. Bisova, C.J. Chen, M. Elias, K. Gendler, C. Hauser, M.R. Lamb, H. Ledford, J.C. Long, J. Minagawa, M.D. Page, J. Pan, W. Pootakham, S. Roje, A. Rose, E. Stahlberg, A.M. Terauchi, P. Yang, S. Ball, C. Bowler, C.L. Dieckmann, V.N. Gladyshev, P. Green, R. Jorgensen, S. Mayfield, B. Mueller-Roeber, S. Rajamani, R.T. Sayre, P. Brokstein, I. Dubchak, D. Goodstein, L. Hornick, Y.W. Huang, J. Jhaveri, Y. Luo, D. Martínez, W.C. Ngau, B. Otillar, A. Poliakov, A. Porter, L. Szajkowski, G. Werner, K. Zhou, I.V. Grigoriev, D.S.Rokhsar, A.R. Grossman, The *Chlamydomonas* genome reveals the evolution of key animal and plant functions, Science 318 (2007) 245–250.
[41] P. Cardol, F. Figueroa, C. Remacle, L.-G. Franzén, D. González-Halphen, Oxidative phosphorylation: building blocks and related components, in: David B. Stern (Ed.) The Chlamydomonas Sourcebook, Organellar and Metabolic Processes, Volume 2, Elsevier Inc., San Diego 2009, pp. 469–502.
[42] A. Cano-Estrada, M. Vázquez-Acevedo, A. Villavicencio-Queijeiro, F. Figueroa-Martínez, H. Miranda-Astudillo, Y. Cordeiro, J.A. Mignaco, D. Foguel, P. Cardol, M. Lapaille, C. Remacle, S. Wilkens, D. González-Halphen, Subunit–subunit interactions and overall topology of the dimeric mitochondrial ATP synthase of *Polytomella* sp, Biochim. Biophys. Acta 1797 (2010) 1439–1448.
[43] A. Villavicencio-Queijeiro, M. Vázquez-Acevedo, A. Cano-Estrada, M. Zarco-Zavala, M. Tuena de Gómez, J.A. Mignaco, M.M. Freire, H.M. Scofano, D. Foguel, P. Cardol, C. Remacle, D. González-Halphen, The fully-active and structurally-stable form of the mitochondrial ATP synthase of *Polytomella* sp. is dimeric. J. Bioenerg. Biomembr. 41 (2009) 1–13.
[44] A. Villavicencio-Queijeiro, J.P. Pardo, D. González-Halphen, Kinetic and hysteretic behavior of ATP hydrolysis of the highly stable dimeric ATP synthase of *Polytomella* sp, Arch. Biochem. Biophys. 575 (2015) 30–37.
[45] M. Allegretti, N. Klusch, D.J. Mills, J. Vonck, W. Kühlbrandt, K.M. Davies, Horizontal membrane-intrinsic α-helices in the stator a-subunit of an F-type ATP synthase, Nature 521 (2015) 237–240.
[46] S. Liu, T.J. Charlesworth, J.V. Bason, M.G. Montgomery, M.E. Harbour, I.M. Fearnley, J.E. Walker, The purification and characterization of ATP synthase complexes from the mitochondria of four fungal species, Biochem. J. 468 (2015) 167–175.
[47] J. Symersky, D. Osowski, D.E. Walters, D.M. Mueller, Oligomycin frames a common drug-binding site in the ATP synthase, Proc. Natl. Acad. Sci. U. S. A. 109 (2012) 13961–13965.
[48] L.A. Baker, I.N. Watt, M.J. Runswick, J.E. Walker, J.L. Rubinstein, Arrangement of subunits in intact mammalian mitochondrial ATP synthase determined by cryo-EM, Proc. Natl. Acad. Sci. U. S. A. 109 (2012) 11675–11680.
[49] W.C. Lau, L.A. Baker, J.L. Rubinstein, Cryo-EM structure of the yeast ATP synthase, J. Mol. Biol. 382 (2008) 1256–1264.
[50] C. Mellwig, B. Böttcher, A unique resting position of the ATP-synthase from chloroplasts, J. Biol. Chem. 278 (2003) 18544–18549.
[51] I. Ogilvie, S. Wilkens, A.J. Rodgers, R. Aggeler, R.A. Capaldi, The second stalk: the delta-b subunit connection in ECF1F0, Acta Physiol. Scand. Suppl. 643 (1988) 169–175.
[52] N.V. Dudkina, S. Sunderhaus, H.P. Braun, E.J. Boekema, Characterization of dimeric ATP synthase and cristae membrane ultrastructure from *Saccharomyces* and *Polytomella* mitochondria, FEBS Lett. 580 (2006) 3427–3432.
[53] M. Lapaille, M. Thiry, E. Perez, D. González-Halphen, C. Remacle, P. Cardol, Loss of mitochondrial ATP synthase subunit beta (Atp2) alters mitochondrial and chloroplastic function and morphology in Chlamydomonas, Biochim. Biophys. Acta 1797 (2010) 1533–1539.
[54] N.V. Dudkina, G.T. Oostergetel, D. Lewejohann, H.P. Braun, E.J. Boekema, Row-like organization of ATP synthase in intact mitochondria determined by cryo-electron tomography, Biochim. Biophys. Acta 1797 (2010) 272–277.
[55] E. Morales-Rios, M.G. Montgomery, A.G. Leslie, J.E. Walker, Structure of ATP synthase from *Paracoccus denitrificans* determined by X-ray crystallography at 4.0 Å resolution, Proc. Natl. Acad. Sci. U. S. A. 112 (2015) 13231–13236.
[56] A. Zhou, A. Rohou, D.G. Schep, J.V. Bason, M.G. Montgomery, J.E. Walker, N. Grigorieff, J.L. Rubinstein, Structure and conformational states of the bovine mitochondrial ATP synthase by cryo-EM, Elife (2015), http://dx.doi.org/10.7554/eLife.10180.
[57] H. Miranda-Astudillo, A. Cano-Estrada, M. Vázquez-Acevedo, L. Colina-Tenorio, L,.A. Downie-Velasco, P. Cardol, C. Remacle, L. Domínguez-Ramírez, D. González-Halphen, Interactions of subunits Asa2, Asa4 and Asa7 in the peripheral stalk of the mitochondrial ATP synthase of the chlorophycean alga *Polytomella* sp, Biochim. Biophys. Acta 1837 (2014) 1–13.
[58] J. Velours, G. Arselin, The *Saccharomyces cerevisiae* ATP synthase, J. Bioenerg. Biomembr. 32 (2000) 383–390.
[59] M. Fritz, V. Müller, An intermediate step in the evolution of ATPases–the F1F0-ATPase from *Acetobacterium woodii* contains F-type and V-type rotor subunits and is capable of ATP synthesis, FEBS J. 274 (2007) 3421–3428.
[60] F. Mayer, J.K. Lim, J.D. Langer, S.G. Kang, V. Müller, Na + transport by the A1AO-ATP synthase purified from *Thermococcus onnurineus* and reconstituted into liposomes, J. Biol. Chem. 290 (2015) 6994–7002.
[61] J.L. Popot, Amphipols, nanodiscs, and fluorinated surfactants: three nonconventional approaches to studying membrane proteins in aqueous solutions, Annu. Rev. Biochem. 79 (2010) 737–775.
[62] M.G. Teese, D. Langosch, Role of GxxxG motifs in transmembrane domain interactions, Biochemistry 54 (2015) 5125–5135.
[63] G. Arselin, M.F. Giraud, A. Dautant, J. Vaillier, D. Brèthes, B. Coulary-Salin, J. Schaeffer, J. Velours, The GxxxG motif of the transmembrane domain of subunit e is involved in the dimerization/oligomerization of the yeast ATP synthase complex in the mitochondrial membrane, Eur. J. Biochem. 270 (2003) 1875–1884.
[64] D.M. Bustos, J. Velours, The modification of the conserved GXXXG motif of the membrane-spanning segment of subunit g destabilizes the supramolecular species of yeast ATP synthase, J. Biol. Chem. 280 (2005) 29004–29010.
[65] S. Saddar, R.A. Stuart, The yeast F(1)F(0)-ATP synthase: analysis of the molecular organization of subunit g and the importance of a conserved GXXXG motif, J. Biol. Chem. 280 (2005) 24435–24442.
[66] M.J. Van Raaij, G.L. Orriss, M.G. Montgomery, M.J. Runswick, I.M. Fearnley, J.M. Skehel, J.E. Walker, The ATPase inhibitor protein from bovine heart mitochondria: the minimal inhibitory sequence, Biochemistry 35 (1996) 15618–15625.
[67] R. Iino, R. Hasegawa, K.V. Tabata, H. Noji, Mechanism of inhibition by C-terminal alpha-helices of the epsilon subunit of *Escherichia coli* FoF1-ATP synthase, J. Biol. Chem. 284 (2009) 17457–17464.
[68] M. Zarco-Zavala, E. Morales-Ríos, G. Mendoza-Hernández, L. Ramírez-Silva, G. Pérez-Hernández, J.J. García-Trejo, The ζ subunit of the F1FO-ATP synthase of α-proteobacteria controls rotation of the nanomotor with a different structure, FASEB J. 28 (2014) 2146–2157.
[69] C. Vahrenholz, G. Riemen, E. Pratje, B. Dujon, G. Michaelis, Mitochondrial DNA of *Chlamydomonas reinhardtii*: the structure of the ends of the linear 15.8-kb genome suggests mechanisms for DNA replication, Curr. Genet. 24 (1993) 241–247.
[70] D.R. Smith, J. Hua, R.W. Lee, Evolution of linear mitochondrial DNA in three known lineages of *Polytomella*, Curr. Genet. 56 (2010) 427–438.
[71] J. Yang, R. Yan, A. Roy, D. Xu, J. Poisson, Y. Zhang, The I-TASSER suite: protein structure and function prediction, Nat. Methods 12 (2015) 7–8.
[72] D.M. Rees, A.G.W. Leslie, J.E. Walker, The structure of the membrane extrinsic region of bovine ATP Synthase, Proc. Natl. Acad. Sci. U. S. A. 106 (2009) 21597–21601.
[73] E.F. Pettersen, T.D. Goddard, C.C. Huang, G.S. Couch, D.M. Greenblatt, E.C. Meng, T.E. Ferrin, UCSF chimera–a visualization system for exploratory research and analysis, J. Comput. Chem. 25 (2004) 1605–1612.
[74] A. Zhou, A. Rohou, D.G. Schep, J.V. Bason, M.G. Montgomery, J.E. Walker, N. Grigorieff, J.L. Rubinstein, Structure and conformational states of the bovine mitochondrial ATP synthase by cryo-EM, Elife 4 (2015), http://dx.doi.org/10.7554/eLife.10180 (pii: e10180).

Biochimica et Biophysica Acta 1858 (2017) 267–275

Contents lists available at ScienceDirect

Biochimica et Biophysica Acta

journal homepage: www.elsevier.com/locate/bbabio

Atypical composition and structure of the mitochondrial dimeric ATP synthase from *Euglena gracilis*

K.N. Sathish Yadav [a,1], Héctor V. Miranda-Astudillo [b,1], Lilia Colina-Tenorio [c], Fabrice Bouillenne [d], Hervé Degand [e], Pierre Morsomme [e], Diego González-Halphen [c], Egbert J. Boekema [a,*], Pierre Cardol [b,**]

[a] Department of Electron Microscopy, Groningen Biological Sciences and Biotechnology Institute, University of Groningen, Groningen, The Netherlands
[b] Genetics and Physiology of Microalgae, InBioS/Phytosystems, University of Liège, Belgium
[c] Departamento de Genética Molecular, Instituto de Fisiología Celular, Universidad Nacional Autónoma de México, Mexico
[d] InBioS/Centre for Protein Engineering, University of Liège, Belgium
[e] Institut des Sciences de la Vie, Université Catholique de Louvain, Louvain-la-Neuve, Belgium

ARTICLE INFO

Article history:
Received 10 October 2016
Received in revised form 22 December 2016
Accepted 10 January 2017
Available online 12 January 2017

Keywords:
Euglenozoa
Trypanosomatidae
Dimeric mitochondrial complex V
F_1F_O ATP synthase
Electron microscopy
ATP synthasome

ABSTRACT

Mitochondrial respiratory-chain complexes from Euglenozoa comprise classical subunits described in other eukaryotes (*i.e.* mammals and fungi) and subunits that are restricted to Euglenozoa (*e.g. Euglena gracilis* and *Trypanosoma brucei*). Here we studied the mitochondrial F_1F_O-ATP synthase (or Complex V) from the photosynthetic eukaryote *E. gracilis* in detail. The enzyme was purified by a two-step chromatographic procedure and its subunit composition was resolved by a three-dimensional gel electrophoresis (BN/SDS/SDS). Twenty-two different subunits were identified by mass-spectrometry analyses among which the canonical α, β, γ, δ, ε, and OSCP subunits, and at least seven subunits previously found in *Trypanosoma*. The ADP/ATP carrier was also associated to the ATP synthase into a dimeric ATP synthasome. Single-particle analysis by transmission electron microscopy of the dimeric ATP synthase indicated that the structures of both the catalytic and central rotor parts are conserved while other structural features are original. These new features include a large membrane-spanning region joining the monomers, an external peripheral stalk and a structure that goes through the membrane and reaches the inter membrane space below the *c*-ring, the latter having not been reported for any mitochondrial F-ATPase.

1. Introduction

Within living cells, adenosine-5′-triphosphate (ATP) is mainly produced by membrane-embedded F_1F_O-, C_1C_O-, and A_1A_O-ATP synthases. These complexes found in bacteria, mitochondria and chloroplasts work like rotary motors. The activity of photosynthetic and respiratory complexes generates a proton gradient (proton motive force or pmf) across specialized membranes (bacterial plasma membrane, inner mitochondrial membrane, thylakoid membrane). The back flow of protons through the ATP synthase F_O membrane sector (a/c-ring) promotes the rotation of the central stalk (γ/δ/ε; bovine nomenclature) in the F_1 sector, and the interactions of the γ subunit with the catalytic core (α_3/β_3) induce conformational changes to synthesize and release ATP [1,8,42,52]. In well described enzymes (*e.g.* ATPase from mammals and yeasts), additional polypeptides constitute (i) a peripheral stator-stalk (OSCP/b/d/F6) that link F_O and F_1 parts and prevent the rotation of F_1 sector [33], and (ii) a dimerization module (A6L/e/f/g) that link the two monomers into large dimeric supercomplexes and rows of supercomplexes [25,30]. Complex V oligomerization is proposed to be responsible of the curvature of the inner membrane to form the mitochondrial cristae [54].

Given that rotary ATPases share a common ancestor [14,40], it was expected of the F-type ATP synthase complexes to be highly conserved. In this respect, very similar overall structures of ATP synthase monomers or dimers have been described in non-related organisms like the prokaryotic model organism *Paracoccus denitrificans* [38], the yeast *Y. lipolytica* [31], and mammalian species such as *Bos taurus* [64]. Chlorophycean algae, including the green algal model *Chlamydomonas reinhardtii* and its colorless relative *Polytomella* sp., were the first organisms in which an atypical ATP synthase subunit composition and structure were described [24,59]. The classical stator made mainly of b subunit(s) in bacteria, yeasts, and mammals is absent and a more robust stator structure, composed of at least 4 subunits, connects the two monomers by some large hydrophobic and hydrophilic subunits [2,12]. Similarly, the dimeric ATP synthase complex from the ciliate *Tetrahymena thermophila* also includes atypical subunits, unrelated to those

* Corresponding author.
** Correspondence to: P. Cardol, Chemin de la vallée, 4, B22, Institut de Botanique, Dept of Life Sciences, University of Liège, 4000 Liège, Belgium.
E-mail addresses: e.j.boekema@rug.nl (E.J. Boekema), Pierre.cardol@ulg.ac.be (P. Cardol).
[1] The authors contributed equally to the work.

http://dx.doi.org/10.1016/j.bbabio.2017.01.007
0005-2728/

described in *Polytomella* sp., that shape novel domains flanking the c subunit ring, and an unusually large domain in the intermembrane space [3]. In sharp contrast, the yeast dimer-specific subunits are smaller and do not contribute much to the water-soluble moiety of the dimeric supercomplex [31,58]. Given the large structural differences among the peripheral stator and dimerization modules of mitochondrial F_1F_O, it is of relevance to study a wider number of species to gain insight into the structural diversity of ATP synthases. In this respect, it was recently shown that mitochondrial ATP synthase from parasite species (*e.g. Trypanosoma brucei*) and photosynthetic species (*e.g. Euglena gracilis*) belonging to the lineage of Euglenozoa (phylum of Excavates) share a similar subunit composition [46,65], including a set of subunits that are specific to Euglenozoa. In this study, we thus further analyzed the subunit composition of purified mitochondrial ATP synthase from the photosynthetic Euglenozoa *Euglena gracilis* and characterized its dimeric structure by single particle electron microscopy.

2. Methods

2.1. Isolation of mitochondria from Euglena gracilis

Euglena gracilis (SAG 1224-5/25) was obtained from the University of Göttingen (Sammlung von Algenkulturen, Germany) and was grown at 25 °C in the dark with orbital agitation in liquid mineral Tris-minimum-phosphate medium (TMP) at pH 7.0 supplemented with a mix of vitamins (Biotin 10^{-7}% (w/v), B_{12} vitamin 10^{-7}% and B_1 vitamin 2×10^{-5}%) and with 1% ethanol as carbon source. The cells were harvested at the middle of the logarithmic phase by centrifugation (7000 ×*g*/10 min) and stored at −70 °C until used.

Mitochondria were obtained following the described procedure [39] with slight modifications. All steps were performed at 4 °C. The cells were thawed and suspended to a final concentration of 2×10^8 cells/mL in SHE buffer (sucrose 250 mM, Hepes 10 mM, EDTA 1 mM, pH 7.3) supplemented with 0.4% of bovine serum albumin (BSA). The cell suspension was sonicated in ice with a microprobe of 3 mm tip diameter for 20 s two times, with a 20 s resting period, at 40% of maximal output in a Vibracell Sonifier (Sonics & Material, Connecticut, USA). The sonicated sample was diluted 3 times in SHE buffer and centrifuged 600 ×*g*, 10 min. The supernatant was centrifuged at 8500 ×*g*, 10 min to recover the mitochondrial fraction. Mitochondria were suspended in 5 mL of sucrose buffer (0.3 M sucrose, 4 mM EDTA, and 20 mMTris, pH 7.2) and stored at −70 °C until used. Protein concentration was determined as previously described [9].

2.2. Purification of mitochondrial ATP synthase complex

All steps were performed at 4 °C. Seventy five milligrams of mitochondrial proteins were solubilized with n-dodecyl-β-D-maltoside (DDM, 4 g detergent per g protein) in A buffer containing Tris 50 mM, amino caproic acid 50 mM, $MgSO_4$ 1 mM, NaCl 50 mM, glycerol 10%, phenylmethylsulfonyl fluoride (PMSF) 1 mM, tosyl-lysyl-chloromethylketone (TLCK) 50 μg/mL. The mixture was incubated with gentle stirring for 30 min, and centrifuged at 38,000 ×*g* for 30 min. The supernatant was diluted three times in A buffer without NaCl and supplemented with DDM 0.01%. After a filtration step (0.22 μm) the sample was loaded on an anion exchange column (Mono Q HR 5/5, 1 mL) connected to an ÄKTA explorer 100 (GE Healthcare Life Sciences) equilibrated with the same buffer and washed until a base line was obtained. The column was washed with 50 mM NaCl in the A buffer plus DDM 0.01% (10 VC) and eluted with a 50–500 mM NaCl linear gradient (40 VC). Two milliliter fractions were collected and visualized by BN-PAGE.

The fractions from the anion exchange column enriched with ATP synthase were pooled and concentrated with an Amicon Ultra-15 Centrifugal Filter (EMD Millipore) to a final volume of 500 μL and injected to a Superose 6 10/300 (GE Healthcare Life Sciences) previously equilibrated with A buffer containing NaCl 200 mM and DDM 0.01%. The elution was carried out at 0.3 mL/min, 0.5 mL fractions were collected and visualized by BN-PAGE. The samples enriched with mitochondrial ATP synthase were pooled and stored at −70 °C until used.

2.3. Non-denaturating and denaturating protein electrophoresis

All steps were performed at 4 °C. Mitochondrial respiratory complexes were resolved in a 1D BN-PAGE using a 3%–10% acrylamide gradient gel. *In-gel* ATPase activity was carried out as in [62] with the addition of 30 mMtaurodeoxycholate (TDOC) as in [55]. *In-gel* NADH/NBT oxido-reductase activity was performed as described previously [29]. Two-dimensional SDS/SDS PAGE experiments were conducted as described [12]. Briefly, the subunits of ATPase from the BN-PAGE were separated in a Glycine-SDS-PAGE (12% acrylamide) and then the 2D lane was excised and separated again into a Tricine-SDS-PAGE (14% acrylamide), after the migration, the 3D gel was stained with Coomassie Brilliant Blue. An aliquot of the sample used for the microscopy analysis was also subjected to the same 3D BN/SDS-glycine/SDS-tricine PAGE to search for degradation or loss of subunits after the freezing and thawing steps.

Stained proteins associated with spots were manually excised and analyzed by mass spectrometry (MS) as described [46]. For direct protein identification with MASCOT, protein scores >60 were considered as significant ($P < 0.05$). To determine the molecular mass of individual subunits, the purified ATPase complex was resolved in a Tricine-SDS-PAGE and PageRuler plus prestained protein ladder (Thermo Scientific) was used as a size molecular marker. The logarithm of the distance migrated from each peptide was interpolated into a Log(distance migrated) *versus* size (kDa) regression of the molecular marker ($R^2 = 0.989$).

2.4. In silico analysis of ATPase subunits

To further characterize the sequences identified by MS, each protein sequence was submitted to a tBLASTn analysis against the expressed sequence tags (EST) database from *Euglena gracilis* (taxid: 3039) available in the NCBI server. The obtained translated nucleotide sequences were manually assembled to generate the longest possible polypeptide. The resulting polypeptides were submitted to similarity searches by BLASTp against the non-redundant protein sequences database (NRPS) (http://blast.ncbi.nlm.nih.gov/Blast.cgi), and against the Kinetoplastid genomic resource database (TriTrypDB) (http://www.tritrypdb.org/tritrypdb/). The first methionine codon of each sequence was arbitrarily chosen as the putative start codon, except when alignments with homologs from other organisms allowed us to choose another codon. The theoretical isoelectric point, molecular mass and grand average of hydropathicity (GRAVY) were determined using the algorithm ProtParam (http://web.expasy.org/protparam/), transmembrane helixes (TMH) were predicted using Phobius server (http://phobius.sbc.su.se/) and TMHMM Server v. 2.0 (http://www.cbs.dtu.dk/services/TMHMM-2.0/), local conserved domains (CD) were searched using the NRPS Blastp, DELTA-Blast and Conserved Domain Blast (http://www.ncbi.nlm.nih.gov/Structure/cdd/wrpsb.cgi), Coiled coil regions (CC) where predicted using the Marcoil 1.0 server (http://bcf.isb-sib.ch/webmarcoil/webmarcoilC1.html) when a TMH, CD or CC was found the topological localization inside the peptide was annotated. ClustalW version 2 (http://www.ebi.ac.uk/Tools/msa/clustalw2/) was used for direct alignments of protein sequences. The N-terminus and C-terminus parts of the alpha subunit were modelled using as template the crystal structure of the F_1-ATPase from the thermoalkaliphilic bacterium *Bacillus sp*. ta2.a1 [53] using Swiss-Model in the ExPASy web server (https://swissmodel.expasy.org/) and visualized using Chimera 1.6.2. (http://www.cgl.ucsf.edu/chimera).

2.5. Electron microscopy and analysis

A drop of ATP synthase solution was absorbed onto glow discharged carbon coated grids and subsequently stained with 2% uranyl acetate for contrast. Imaging was performed on a Philips CM120 equipped with a LaB6 tip operating at 120 kV. The "GRACE" system for semi-automated specimen selection and data acquisition [44] was used to record 2048 × 2048 pixel images at 80,000 × magnifications using a Gatan 4000 SP 4 K slow-scan CCD camera with a pixel size of 0.224 nm. Single particles were analyzed with the Groningen Image Processing (GRIP) software (including multi-reference and non-reference alignments, multivariate statistical analysis and classification, as in [7] and RELION software [49].

3. Results

3.1. Purification of the DDM stable ATP synthase from E. gracilis mitochondria

In agreement with previous work [46], mitochondrial ATP synthase (complex V) from *E. gracilis* migrates as a ~2.2 MDa band above the identified NADH:ubiquinone oxidoreductase (complex I, ~1.5 MDa) in a Blue-Native (BN) gel experiment conducted with n-dodecyl-maltoside treated mitochondria (Fig. 1a and c). This complex, probably a dimer, is capable to hydrolyze ATP (Fig. 1b). It was previously resolved in 18 protein spots by 2D BN-SDS PAGE analysis, among which six ATP synthase canonical subunits (α, β, γ, δ, ε and OSCP) and four Euglenozoa-specific subunits (p18, ATPTB1, ATPTB4, and ATPTB12) were identified [46]. In order to prove the *bona-fide* association of these atypical subunits to the *Euglena* mitochondrial ATP synthase, and to identify new subunits that may have escaped detection due to the comigration with other proteins, it was first purified by a two-step chromatographic procedure (see Methods section for further details). After the chromatographic purification, a fraction enriched with complex V was obtained, in which only a very small amount of complex I can be observed (Fig. 1d).

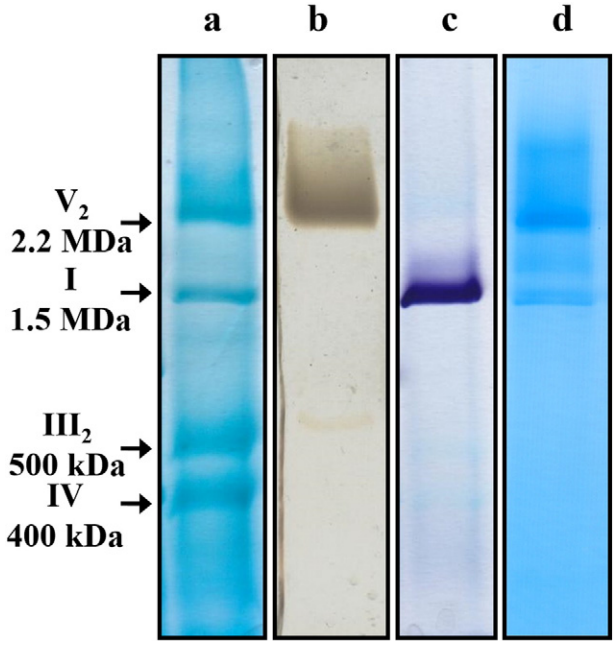

Fig. 1. Electrophoretic patterns of purified dimeric ATP synthase from *Euglena gracilis*. (a) Total mitochondrial protein from *Euglena gracilis* was solubilized in presence of β-dodecyl-n-maltoside and subjected to a BN-PAGE. Estimated molecular masses and identities of Coomassie brilliant blue-stained protein complexes are indicated. *In-gel* activity stains for ATP hydrolysis (b) and NADH:Nitro Blue tetrazolium (NBT) oxidoreductase (c). Enriched fraction of dimeric ATP synthase from the two-step chromatographic purification, remaining complex I could be observed (Coomassie brilliant blue staining) (d).

3.2. Further determination of atypical subunit composition of Euglena mitochondrial ATP synthase

The protein spot corresponding to mitochondrial ATP synthase from the enriched fraction was then excised from BN-gel and its polypeptides were resolved by two-dimensional SDS-glycine/SDS-tricine PAGE (Fig. 2). A total of 21 spots were numbered, excised out of the gel and analyzed by tandem mass spectrometry (MS/MS). Fifteen of the 21 analyzed spots matched to a single protein in our database. Interestingly, the alpha subunit was found as two different polypeptides, one with a mass of 47.4 kDa and the other with a mass of 13.3 kDa, corresponding to the N-terminal and C-terminal part, respectively. Together they would form a 60 kDa protein, which is the molecular mass predicted for this subunit. In three spots (2, 16, and 17), two different polypeptides were identified by MS analysis probably because a comigration of these proteins during the electrophoresis steps. At last, three spots remained unidentified (3, 20, and 21). Based on this analysis, the complex V from *E. gracilis* comprises at least 24 polypeptides with molecular masses ranging from 5.5 to 51.6 kDa. The same protein spot profile was obtained after freezing/thawing the purified complex (Supplemental Fig. 1), which reinforces the idea that these subunits are *bona*-fide components of ATP synthase. All the obtained sequences (Supplemental File 1) were analyzed *in silico* to search for possible homologs and conserved domains (CD) in protein databases (NRPS, TriTrypDB) (Table 1). Seven protein spots correspond to the canonical subunits α (present in two independent spots in the gel polypeptide pattern), β, γ, δ, ε and OSCP. Conversely, seven polypeptides are Euglenozoa-specific proteins first described as components of ATP synthase subunits from *Trypanosoma* species (ATPTB1, ATPTB2, ATPTB3, ATPTB4, ATPTB6, ATPTB12 and p18). Six other polypeptides do not have any homolog and remain as unnamed proteins (UP), and three spots were not identified (NI). Two additional subunits (ATPTB7, ATPTB10) described in *Trypanosoma* ATP synthase [65] and previously identified at genomic level in *Euglena* [46] were not identified here. Among the largest subunits found in this complex are the trypanosomatid specific proteins ATPTB1 and ATPTB2 with predicted molecular masses of 55.9 kDa and 53.9 kDa respectively, in the same range of subunits α and β from the catalytic

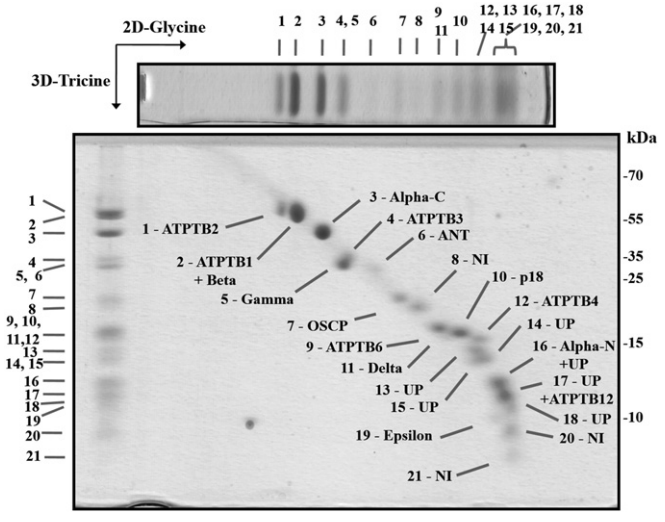

Fig. 2. 3D resolution of the polypeptides that constitute the *Euglena* mitochondrial F_1F_O ATP synthase. Dimeric *Euglena* ATP synthase was resolved by BN-PAGE. The band of interest was excised and resolved in a glycine-SDS-PAGE (12% acrylamide). The 2D gel was then subjected to 3D tricine-SDS-PAGE (14% acrylamide) and stained with Coomassie brilliant blue. The identified subunits and molecular mass markers are indicated. NI, not identified; UP, unnamed protein with no homolog in other species.

Table 1
Subunit composition of *Euglena gracilis* mitochondrial ATP synthase.

Subunit	Name	Accession number	MW	MW (calc)	IP	TMH (putative)	GRAVY	Conserved domain[3]	Blast Hits[3]	Mascot score	Coverage %	Signal peptide*	Coiled coil¥
1	ATPTB2	comp59678_c0_seq2_c	51.6	53.9	4.9	0	−0.329	–[1,2]	–[a,c]; EJS84964.1[b]	868	42	–[α] 29[β] (0.9829)	83.7% 53 to 104
2	ATPTB1	comp62248_c0_seq5_c	50.6	55.9	6.0	1 (N)	−0.481	–[1,2]	–[a,b,c]	690	47	–[α, β]	21.6% 227 to 252
3	beta	comp59738_c0_seq2_m F1-ATPase_beta(A)[1,2]	50.6	53.2	5.0	0	0.074	EPY14967.1[a]; WP_006997680.1[b]; Tgr.527.1020[c]	1180	64	–[α, β]	100.0% 467 to 529	
4	Alpha-C	comp63233_c0_seq1_m	43.3	47.4	9.2	0	−0.157	F_0F_1 ATP synthase subunit alpha(A)[1,2]	EPY14967.1[a]; WP_006997680.1[b]; Tgr.527.1020[c]	1120	55	–[α, β]	0.0%
5	ATPTB3	comp60477_c0_seq4_c	35.7	31.3	5.4	0	−0.013	–[1,2]	WP_045088137.1[a]; WP_027960470.1[b]; –[c]	337	28	–[α] 27[β] (0.8534)	0.0%
6	gamma	comp52980_c0_seq1_m	34.0	31.7	6.5	0	−0.375	F1-ATPase_gamma super family (A)[1,2]	XP_822278.1[a]; EHX84368.1[b]; Tb927.10.180[c]	240	51	–[α] 19[β] (0.5827)	49.4% 205 to 252
7	ANT	comp62013_c0_seq2	33.2	25.9	9.6	3 (C) 4 (C)[#]	−0.078	Mitochondrial carrier protein (N) Mitochondrial carrier protein (C)[1,2]	ABV25601.1[a]; ABV25601.1[b]; TRSC58_06358[c]	70	38	–[α, β]	0.0%
8	OSCP	comp56779_c0_seq1_m	27.2	25.9	4.9	0	−0.250	ATP synthase delta (OSCP) subunit (M)[1,2]	XP_823037.1[a]; WP_008075436.1[b]; Tb927.10.8030[c]	678	78	–[α, β]	30.4% 87 to 113 36.4% 124 to 140
9	a*	–	24.3	–	–	–	–	–	–	NI	–	–	–
10	ATPTB6	comp48437_c0_seq2_c	21.3	21.7	9.6	2 (N,C)	−0.297	–[1,2]	CCW71114.1[a]; CCW71114.1[b]; Tgr.480.1070[c]	236	31	–[α, β]	0.0%
11	p18	comp56597_c0_seq3	20.8	21.0	8.4	0	0.205	–[1,2]	EPY41275.1[a]; CDX69249.1[b]; TcCLB.510821.60[c]	780	73	–[α] 16[β] (0.9847)	0.0%
12	delta	comp55732_c0_seq1_c	20.3	19.5	4.6	0	−0.280	F1-ATPase_delta (M,C)[1,2]	EPY33170.1[a]; EHX56372.1[b]; TcCLB.506945.240[c]	197	77	18[α] (0.4384) 18[β] (0.9514)	18.8% 135 to 151
13	ATPTB4	comp38662_c0_seq1_c	19.2	18.8	8.7	0	−0.476	–[1,2]	EPY25620.1[a]; ESL07652.1[b]; TRSC58_04655[c]	258	29	–[α,β]	17.9% 115 to 145
14	UP14	comp51661_c0_seq2	17.7	19.7	5.8	1 (M)	−0.209	–[1,2]	–[a,c]; WP_010879713.1[b]	306	39	–[α] 25[β] (0.9162)	100.0% 128 to 171
15	UP15	comp46683_c0_seq1_c	17.0	16.2	9.3	1 (M)	−0.717	–[1,2]	–[a,b,c]	565	73	–[α,β]	0.0%
16	UP16	comp48845_c0_seq1_c	16.2	13.4	9.1	0	−0.355	–[1,2]	–[a,b,c]	170	71	–[α,β]	0.0%
17	Alpha-N	comp63233_c0_seq1_m	13.3	12.9	8.2	0	0.332	ATPase alpha subunit(A)[1,2]	XP_803362.1[a]; CCW61345.1[b]; TvY486_0707020[c]	332	39	–[α,β]	0.0%
18	UP18	gi|109777597_c	13.3	13.8	8.8	0	−0.661	–[1,2]	–[a,b,c]	62	21	–[α,β]	0.0%
19	UP19	comp35985_c0_seq2	11.2	12.5	9.7	1(N)	0.419	–[1,2]	–[a,b,c]	136	57	–[α] 22[β] (0.9604)	0.0%
20	ATPTB12	comp45696_c0_seq1_c	11.2	11.3	9.4	0	−0.784	–[1,2]	–[a,b]; TRSC58_04996[c]	64	55	–[α,β]	0.0%
21	UP21	gi|125988729_c	10.6	12.7	9.7	1 (C)	−0.183	–[1,2]	–[a,b,c]	172	27	–[α,β]	0.0%
22	Epsilon	comp44213_c0_seq1_c	9.7	8.7	7.9	0	−0.418	F1-ATPase_epsilon super family (N)[1,2]	–[a]; ERN7205.1[b]; TcCLB.508661.34[c]	192	68	–[α] 22[β] (0.7313)	0.0%
23	C*	–	8.8	–	–	–	–	–	–	NI	–	–	–
24	NI	–	5.5	–	–	–	–	–	–	–	–	–	–

ND not determined.
_m proposed mature sequence.
_c start from the first Methionine.
(N) Amino terminus, (C) Carboxi terminus, (M) Middle region, (A) Almost all sequence.
[α] Phobius; Cleavage site (Probability of the peptide signal).
[β] MitoProt; Cleavage site (Probability of export to mitochondria).
[a] Blastp.
[b] DELTA-BLAST.
[c] BlAST TriTrypDB.
[1] CCD.
[2] DELTA-BLAST.
[3] The e-value threshold for the blast results was 10^{-5}.
¥ % Probability (Region).
[#] According to the reported AAC from other organisms.
* Putative subunit (see Discussion).

core. No CD could be confidently identified for ATPTB and UP proteins and it is important to note that none of these identified polypeptides share any similarity with the canonical hydrophobic subunits present in the proton translocation channel sector (a/c-ring which have not been identified here) of the known F-Type ATP synthases. Incidentally, subunits a and c have probably escaped identification in this analysis but corresponding transcripts have been identified [46]. Finally, one polypeptide matched to the ADP/ATP transporter of adenylate translocase superfamily (ANT). The ANT sequence is incomplete in our database (Supplemental File 2), so the predicted molecular mass (25.9 kDa) of this polypeptide is smaller than the value of ~33 kDa determined in Fig. 2, a molecular mass which is similar to the mass of ANT in other species [11].

The Table 1 also summarizes predicted physico-chemical properties for each individual subunit, such as hydrophobicity (GRAVY) and isoelectric point (IP), and predicted structural features like transmembrane helices (TMH) and coiled-coil domains (CC). Seven of the identified subunits (ATPTB1, ATPTB6, UP14, UP15, UP19, UP21, and ANT) contain at least one putative TMH with a total of eleven TMH. In agreement with the partial sequence of ANT in our database, only three of the four classical TMH that are usually predicted in the carboxyl terminus of ANT have been found. A CC region is predicted for the subunits ATPTB2 and ATPTB4. In addition to a putative TMH in the amino terminal part, ATPTB1 and UP14 also present a CC region, which suggests that these subunits might contribute to an original peripheral stator (see Discussion).

3.3. Atypical structures of ATP synthase visualized by electron microscopy

In our previous study, we suggested that the ~2 MDa Complex corresponds to a dimeric ATP synthase [46]. In order to confirm this hypothesis and to determine if the identified polypeptides might be associated to an atypical stator structure, electron microscopy in combination with single particle analysis was performed. About 2000 images were recorded, and a total of 30,000 particle projections were collected and analyzed. The particles projections grouped into 14 classes (an average of 2000 particles per class) among which 12 are shown in Fig. 3. Negatively stained ATP synthase complexes are present in mainly three positions on the carbon support film. These projections confirm first that the complex is a dimer. The dimer is in an almost non-tilted situation from a side (Fig. 3F) as suggested by the homogeneous negative staining around the particle. Like most other mitochondrial ATP synthases, the two monomers are not parallel, but make an angle of about 45° (marked by red lines, Fig. 3F). This indicates a local curvature of the membrane. In three classes (panels A-C), the dimer is slightly tilted so the apparent angle between the two monomers is decreased (~30°). In these views, the shape of the F_1 headpiece, connected to the membrane-bound F_O part via the stalk region, is well outlined. A novel feature is the large density below the F_O part, which is lacking in mammalian ATPase (orange arrowheads; Fig. 3A). In several other maps of tilted dimers (Fig. 3D-E, G-H), the left monomer is in a position that allows an outer peripheral density between the F_O and F_1 parts to be optimally visible (green arrowhead). In contrast, blue arrowheads (Fig. 3B,

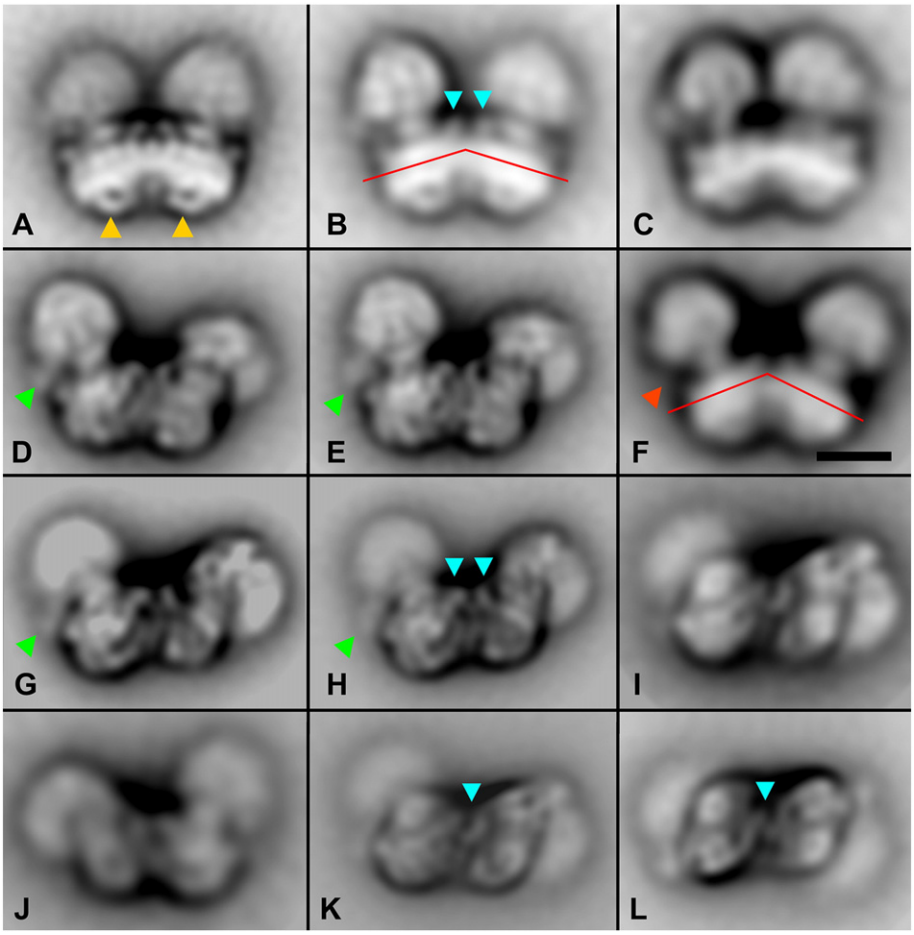

Fig. 3. 2D Projection maps of purified dimeric ATP synthase complexes from *E. gracilis* obtained by single particle averaging. The dimeric complex V was purified by two-step chromatographic procedure in presence of β-dodecyl-n-maltoside and analyzed by EM. In side view projections (A-C), an unusual density can be observed below de F_O part (orange arrows). The two monomers make an angle of about 30° (red lines) while in almost non-tilted view (F) the angle is about 45°. In side view from tilted dimers (D, E, G, H), peripheral density between the F_O and F_1 parts is marked with green arrows. Top view projections (I, K, L) show that the two monomers are related by a two-fold rotational symmetry. Blue arrowheads indicate densities not connected to F_1 (B, H, K, L) but connecting the two monomers.

H) indicate densities at the interface between monomers that do not connect F_O to F_1. This suggests that the peripheral stator, necessary to prevent futile rotation between the F_O and F_1, is at the outer periphery rather than in the interface between the two monomers. Other maps (Fig. 3I-K, L) show the dimer in a position closer to the plane of the membrane. In this position the F_O parts are attached to the carbon support film and the F_1 headpieces appear blurred, due to an insufficient embedding in the negative stain layer. One view (Fig. 3L) clearly shows that the two monomers are related by a two-fold rotational symmetry. Interestingly, the outer peripheral density visible in the slightly-tilted projections (green arrowheads on panels D-E,G-H) appears to be part of a structure connecting F_O and F_1. These views also suggest that the central densities (blue arrowheads on panels K-L) are part of a structure connecting the two monomers in the membrane region.

4. Discussion

In a previous work, we identified 10 polypeptides by mass spectrometry in the *Euglena gracilis* mitochondrial F_1F_O-ATP synthase purified by BN-PAGE: six canonical subunits (α, β, γ, δ, ε, OSCP) and four subunits typical of *Trypanosoma* ATP synthase (ATPTB1, ATPTB4, ATPTB12 and p18) [46]. In the present work, by further purifying the ATP synthase complex by a two-step chromatography approach, we confirmed the presence of these 10 subunits and identified 12 additional subunits, among which three *Trypanosoma* ATP synthase subunits (ATPTB2, ATPTB3, and ATPTB6) and the ATP/ADP translocase (ANT).

Although we cannot fully exclude the possibility that the association of ANT, as well as for other ATPTB and UP proteins, is an artifact of purification, the fact that these subunits remain associated to the mitochondrial ATP synthase after two chromatographic steps, one step of freezing/thawing and one step of gel electrophoresis, strongly suggest that they are true components of the supercomplex. In mammals, the ATP/ADP carrier (ANT) has been found in association with the inorganic phosphate carrier (PiC) and the mitochondrial ATP synthase, in a supercomplex called ATP synthasome [11,34,43]. Similarly the ANT was found in association with ATP synthase in trypanosomatids after purification by sucrose gradient centrifugation [19]. We thus suggest that the supercomplex isolated here is the first biochemical and structural evidence for an ATP synthasome under dimeric form. A PiC homolog is present in *Euglena gracilis* (EST, EC682656.1) but due to its highly hydrophobic nature, it might have escaped identification [48]. Similarly, the highly hydrophobic membrane conserved subunits (a/c-ring), involved in the proton translocation and rotation of the central stalk, probably also escaped identification. These two F_O subunits are proposed to be present in the mitochondrial F-ATP synthase from *Trypanosoma brucei* (subunit *c*, Tb10.70.6340; subunit *a*, AAA97428), based on a detailed analysis of amino acid sequences and hydropathic profiles [6,50,65]. In our analysis the spot 8 (24.3 kDa, Fig. 2) might correspond to subunit *a*. This would be in good agreement with the observation that the trypanosmatid subunit *a* (28.7 kDa) has a very high hydrophobic nature (Gravy 1.959). Similarly, the value of 8.8 kDa determined for spot 20 (Fig. 2) is similar to 8.7 kDa for the mature c subunit in *Trypanosoma brucei* after cleavage of its the mitochondrial targeting sequence (~40 residues with a 0.9766 probability), suggesting that this spot might correspond to subunit *c* previously identified in *E. gracilis* using bioinformatic approaches [46]. The number of subunit *c* copies present in the *Euglena* complex remains unknown. In other mitochondrial and α-proteobacterial ATP synthases, the number of polypeptides that build the *c*-ring varies: eight in the bovine complex [64,66], ten in yeast [27,31], *E. coli* [4] and chlorophycean algae [2], and twelve in the bacterium *P. denitrificans* [38]. Taking into account the presence of subunits not yet identified at the protein level (*a* and *c*), and assuming a c_{10} subunit ring stoichiometry, the monomeric form of *E. gracilis* F_oF_1-ATP synthase complex might have a molecular mass around 860 kDa, a value which is in good agreement with the ~2 MDa apparent molecular mass determined for the dimeric complex by BN-PAGE. The dimeric nature of ATP synthase is no longer a matter of debate, since it is acknowledged that in many other organisms the oligomeric form of the enzyme is responsible for shaping the mitochondrial cristae [16,41]. Another notable feature of the polypeptides associated to the purified enzyme is the presence of a fragmented alpha subunit into two polypeptides of 47.4 kDa (C-terminal region) and 13.3 kDa (N-terminal region). A single transcript encoding the whole 60 kDa protein has been however identified. Because protease inhibitors were used during the purification procedure, and because no trace of the whole alpha subunit has been detected, these fragments most probably arose by a proteolytic cleavage *in vivo*, so the generated fragments remain attached to the F_1 domain, and become separated only upon denaturing gel electrophoresis. When modelling the two polypeptides on a F_1 crystallographic structure, an exposed loop region was revealed, that may be readily cleaved by an unknown protease (Supplemental Fig. S2).

The subunit composition determined here shows two striking features. Firstly, it shares seven components with the ATP synthase of *Trypanosoma brucei*. This reinforces the conclusion that the enzyme is quite well conserved among Euglenozoa [46]. Secondly, in *E. gracilis*, the canonical subunits involved in the F_1 catalytic core (α,β), the rotor and central axis (δ, ε, γ and *c*-ring) and the subunits OSCP and *a* that may bind the peripheral stalk have been identified. However the subunits involved in building the peripheral stator (b/ATP4, d, e, f, g, etc.) are missing and have been replaced by a new set of subunits without counterparts in other lineages. The first organisms where an unusual structure and subunit composition of the mitochondrial ATP synthase was found were the green alga *C. reinhardtii* and its colorless relative *Polytomella* sp. [25,59]. More recently, an unusual subunit composition for the ATP synthase was also reported in the ciliate (alveolates) *T. thermophila* [3], and in *T. brucei* [65]. Altogether, these observations indicate that the peripheral stator is quite specific to each main lineage of eukaryotes investigated to date (mammals & yeasts belonging to Opisthokonts, ciliates to Alveolata, Euglena to Excavates, and *Polytomella* to Archaeplastida). The reason behind this structural diversity was proposed ten years ago [35,59]: it might be related to the unsuccessful trials to transfer the ATP4 gene, coding for b subunit, from the mitochondrial genome to the nuclear genome, and the concomitant recruitment of structural subunits to build a very robust peripheral stator.

The predicted properties of Euglena atypical subunits provide some clues on their topological disposition. The most noteworthy observation is the presence of a total of eleven predicted transmembrane helices (TMH) in these atypical subunits. In comparison, all the membrane-bound yeast subunits i, f, 8, and b make up a total of 5 TMH [31]. Overall, the numerous TMH could explain the high electron density observed in the membrane region of Euglena ATP synthase (Fig. 3). Another interesting feature is the putative presence of CC regions in at least four of the subunits (ATPTB1, ATPTB2, ATPTB4 and UP14). CC regions are indeed known to be involved in the formation of the peripheral stalks of various rotary ATPases: between the *b* subunits in *E. coli* [17,18]; between subunits *b*, *F6* and *d* in bovine complex [20,47]; putatively between Asa1, Asa2, Asa4 and Asa7 [37] inside the robust peripheral stalk of chlorophycean algae [2], and between subunits E and G in both the archaeal A_1/A_o ATP synthase [36,51], and in the vacuolar V_1/V_o ATPase [63]. We thus suggest that some CC regions of atypical subunits (ATPTB1, ATPTB2, ATPTB4 and UP14) might be involved in the formation of the peripheral stalk from Euglenozoa mitochondrial ATP synthase. Some low-resolution features observed by single particle electron microscopy are quite unique to the mitochondrial ATP synthase of *Euglena gracilis*. In comparison to the best studied dimer from the colorless alga *Polytomella* [2,24], two differences are noteworthy: (i) The stators of the *Polytomella* ATPase are at the dimer interface, whereas those of *Euglena* are suggested to be located at the periphery (green arrowheads, Fig. 3), and (ii) the dimer-specific subunits in *Euglena* are smaller, because the F_1 headpieces are closer together. However, the latter difference is in part depending on the overall angle between the

monomers. In maps of *Euglena* dimers this angle is around 30°, but in *Polytomella* and in yeast the kink is substantially larger [24,25]. The *Euglena* stator appears thicker because a protein density of roughly 20 Å appears to be part of it (Fig. 3, green arrowheads). This density is unique, although it may have escaped detection in other organisms, due to overlap in projection maps. In *E. coli* ATP synthase the stator is quite thin and composed of two long coiled α-helices [17,18]. In the ciliate *T. thermophila* there is possibly a peripheral stator [3,10], but the extra mass was not resolved. Finally, the mass connected to the F_o part of *Euglena* ATP synthase, right under the c-subunit ring, could indicate that it is part of the rotor inside the enzyme. Usually, the ATP synthase dimers have no extra mass connected to the c-subunit ring at the other side of the membrane, although some V-type ATPases show a ~35 Å protrusion from the bottom of Vo (exposed to the lumen of the endomembrane compartment, or extracellular).This feature, for example was observed in the bovine clathrin-coated vesicles [60,61] but not in those from the yeast vacuolar membrane [21,22,63] or the enzyme of plant tonoplasts [23]. This density has been assigned to the glycosylated accessory subunit Ac45 [56,61], a polypeptide that associates with other Vo subunits in osteoclasts and appears to be involved in maintaining proton pumping activity [26], although this hypothesis is still a matter of controversy [32,56].

Gathering all the information presented in this study, we can propose a model of how these novel subunits are present in the atypical mitochondrial enzyme of *Euglena* (Fig. 4). Our interpretation shows a dimer with a slight angle in which the stator of each monomer is located in the outer periphery and binds OSCP in the top of the enzyme. The location of the non-conserved subunits remains largely unknown, since the resolution of the structure does not allow us to pinpoint individual components. We have assigned locations for the small hydrophobic subunits both in the dimer interface and in the outer part of each monomer. ANT is also tentatively proposed near to the subunit a, according to the EM studies of the ATP synthasome from rat liver mitochondria [11]. In our model, there are a total of 23 TMH per monomer: seven putative

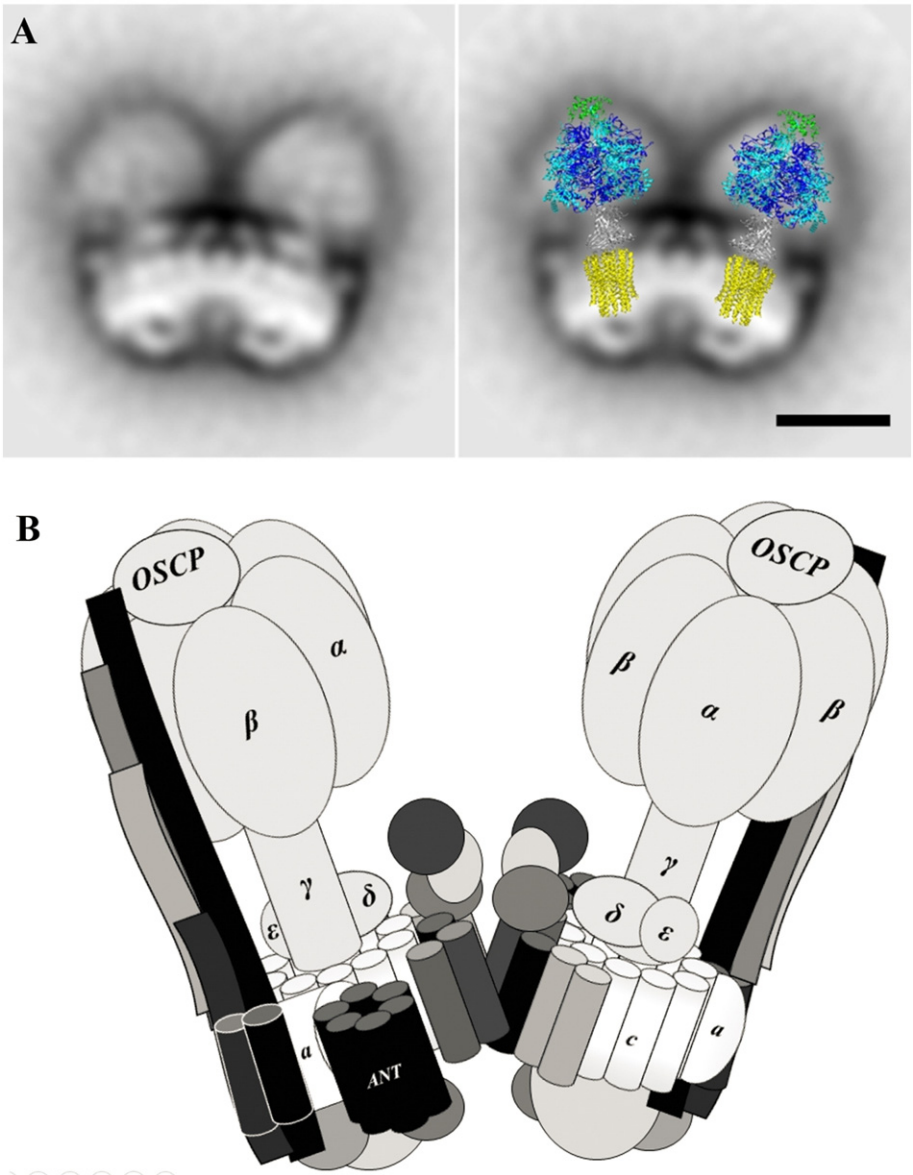

Fig. 4. Proposed topological model of the dimeric ATP synthase from *Euglena gracilis*. (A) Side view projection map from dimeric ATP synthase complex from *E. gracilis* obtained with EM (left panel). Overlap of the F_1/c-ring/OSCP structures from bovine mitochondrial enzyme (PDB ID: 2WSS and 3U2Y; [47,57]) inside the EM projection (right panel). The bar is 10 nm. (B) Proposed model of the arrangement of the subunits in the dimeric complex. Even though the position of each atypical subunit (dark grey) remains largely unknown, subunits containing coil-coiled structures (ATPTB1, ATPTB2, ATPTB4 and UP14) are proposed to be part of the peripheral stalks and subunits with putative TMH surround both monomers (see Discussion for details). Conserved subunits of the F-ATPase (light grey) are labeled.

TMH for UP and ATPTB proteins according to the *in silico* analysis (Table 1), 10 TMH in the proposed c_{10}-ring and six TMH for ANT according to crystallographic data (pdb 1OKC [45]). We suggest the position of the peripheral stalk at the outer periphery of the dimeric structure, mainly because (i) a stronger electron density is observed in this region and because (ii) there was no evidence from side projections of a peripheral stator at the interface between the two monomers like the one described in mitochondrial ATP synthase dimers from *Saccharomyces cerevisiae* [15], *Yarrowia lipolytica* [31], *Polytomella* sp. [2], and *Bos taurus* [13]. Therefore, the presence of more than one peripheral arm per each monomer of the *Euglena* enzyme is very unlikely, although this kind of architecture with multiple peripheral stators has been observed in the archaeal [28] and vacuolar [5] enzymes.

Supplementary data to this article can be found online at http://dx.doi.org/10.1016/j.bbabio.2017.01.007.

Transparency document

The Transparency document associated with this article can be found, in the online version.

Acknowledgments

We thank E. Perez for her help in the identification of *Euglena* genomic data. P.C acknowledges financial support from the Belgian Fonds de la Recherche Scientifique F.R.S.-F.N.R.S. (FRFC 2.4597, CDR J.0032, CDR J.0079 and Incentive Grant for Scientific Research F.4520), FRS-FNRS/CONACyT B330/123/11 (Belgium-Mexico) and European Research Council (H2020-EU BEAL project 682580). P.C is a Senior Research Associate from F.R.S.-FNRS. Support from grants 239219 (Fondo SEP-CONACYT), 245486 (FNRS-CONACyT), and IN20311423 (DGAPA-UNAM) is also acknowledged.

References

[1] J.P. Abrahams, A.G.W. Leslie, R. Lutter, J.E. Walker, Structure at 2.8 (angstrom) resolution of F(1)-ATPase from bovine heart mitochondria, Nature 370 (1994) 621–628.
[2] M. Allegretti, N. Klusch, D.J. Mills, J. Vonck, W. Kühlbrandt, K.M. Davies, Horizontal membrane-intrinsic α-helices in the stator a-subunit of an F-type ATP synthase, Nature 521 (2015) 237–240, http://dx.doi.org/10.1038/nature14185.
[3] P. Balabaskaran Nina, N.V. Dudkina, L.A. Kane, J.E. van Eyk, E.J. Boekema, M.W. Mather, A.B. Vaidya, Highly divergent mitochondrial ATP synthase complexes in tetrahymena thermophila, PLoS Biol. 8 (2010) 3–6, http://dx.doi.org/10.1371/journal.pbio.1000418.
[4] B. Ballhausen, K. Altendorf, D.H. Gabriele, Constant c10 ring stoichiometry in the *Escherichia coli* ATP synthase analyzed by cross-linking, J. Bacteriol. 191 (2009) 2400–2404, http://dx.doi.org/10.1128/JB.01390-08.
[5] S. Benlekbir, S.A. Bueler, J.L. Rubinstein, Structure of the vacuolar-type ATPase from *Saccharomyces cerevisiae* at 11-Å resolution, Nat. Struct. Mol. Biol. 19 (2012) 1356–1362, http://dx.doi.org/10.1038/nsmb.2422.
[6] G.J. Bhat, D.J. Koslowsky, J.E. Feagin, B.L. Smiley, K. Stuart, An extensively edited mitochondrial transcript in kinetoplastids encodes a protein homologous to ATPase subunit 6, Cell 61 (1990) 885–894.
[7] E. Boekema, H. van Roon, J. van Breemen, J.P. Dekker, Supramolecular organization of photosystem II and its light-harvesting antenna in partially solubilized photosystem II membranes, Eur. J. Biochem. 266 (1999) 444–452, http://dx.doi.org/10.1046/j.1432-1327.1999.00876.x.
[8] P.D. Boyer, The ATP synthase–a splendid molecular machine, Annu. Rev. Biochem. 66 (1997) 717–749, http://dx.doi.org/10.1146/annurev.biochem.66.1.717.
[9] M.M. Bradford, A rapid and sensitive method for the quantitation of microgram quantities of protein utilizing the principle of protein-dye binding, Anal. Biochem. 72 (1976) 248–254, http://dx.doi.org/10.1016/0003-2697(76)90527-3.
[10] Y. Chaban, E.J. Boekema, N.V. Dudkina, Structures of mitochondrial oxidative phosphorylation supercomplexes and mechanisms for their stabilisation, Biochim. Biophys. Acta Bioenerg. 1837 (2014) 418–426, http://dx.doi.org/10.1016/j.bbabio.2013.10.004.
[11] C. Chen, Y. Ko, M. Delannoy, S.J. Ludtke, W. Chiu, P.L. Pedersen, Mitochondrial ATP synthasome: three-dimensional structure by electron microscopy of the ATP synthase in complex formation with carriers for Pi and ADP/ATP, J. Biol. Chem. 279 (2004) 31761–31768, http://dx.doi.org/10.1074/jbc.M401353200.
[12] L. Colina-Tenorio, H. Miranda-Astudillo, A. Cano-Estrada, M. Vázquez-Acevedo, P. Cardol, C. Remacle, D. González-Halphen, Subunit Asa1 spans all the peripheral stalk of the mitochondrial ATP synthase of the chlorophycean alga Polytomella sp, Biochim. Biophys. Acta Bioenerg. 1857 (2016) 359–369, http://dx.doi.org/10.1016/j.bbabio.2015.11.012.
[13] S.J. Couoh-Cardel, S. Uribe-Carvajal, S. Wilkens, J.J. García-Trejo, Structure of dimeric F1F0-ATP synthase, J. Biol. Chem. 285 (2010) 36447–36455, http://dx.doi.org/10.1074/jbc.M110.144907.
[14] R.L. Cross, L. Taiz, Gene duplication as a means for altering H+/ATP ratios during the evolution of Fo F1 ATPases and synthases, FEBS Lett. 259 (1990) 227–229, http://dx.doi.org/10.1016/0014-5793(90)80014-A.
[15] K.M. Davies, C. Anselmi, I. Wittig, J.D. Faraldo-Gomez, W. Kuhlbrandt, Structure of the yeast F1Fo-ATP synthase dimer and its role in shaping the mitochondrial cristae, Proc. Natl. Acad. Sci. 109 (2012) 13602–13607, http://dx.doi.org/10.1073/pnas.1204593109.
[16] K.M. Davies, M. Strauss, B. Daum, J.H. Kief, H.D. Osiewacz, A. Rycovska, V. Zickermann, W. Kuhlbrandt, Macromolecular organization of ATP synthase and complex I in whole mitochondria, Proc. Natl. Acad. Sci. 108 (2011) 14121–14126, http://dx.doi.org/10.1073/pnas.1103621108.
[17] P.A. Del Rizzo, Y. Bi, S.D. Dunn, ATP synthase b subunit dimerization domain: a right-handed coiled coil with offset helices, J. Mol. Biol. 364 (2006) 735–746, http://dx.doi.org/10.1016/j.jmb.2006.09.028.
[18] P.A. Del Rizzo, Y. Bi, S.D. Dunn, B.H. Shilton, The "second stalk" of *Escherichia coli* ATP synthase: structure of the isolated dimerization domain, Biochemistry 41 (2002) 6875–6884, http://dx.doi.org/10.1021/bi025736i.
[19] S. Detke, R. Elsabrouty, Identification of a mitochondrial ATP synthase-adenine nucleotide translocator complex in Leishmania, Acta Trop. 105 (2008) 16–20, http://dx.doi.org/10.1016/j.actatropica.2007.08.008.
[20] V.K. Dickson, J.A. Silvester, I.M. Fearnley, A.G.W. Leslie, J.E. Walker, On the structure of the stator of the mitochondrial ATP synthase, EMBO J. 25 (2006) 2911–2918, http://dx.doi.org/10.1038/sj.emboj.7601177.
[21] M. Diepholz, M. Börsch, B. Böttcher, Structural organization of the V-ATPase and its implications for regulatory assembly and disassembly, Biochem. Soc. Trans. 36 (2008) 1027–1031, http://dx.doi.org/10.1042/BST0361027.
[22] M. Diepholz, D. Venzke, S. Prinz, C. Batisse, B. Flörchinger, M. Rössle, D.I. Svergun, B. Böttcher, J. Féthière, A different conformation for EGC stator subcomplex in solution and in the assembled yeast V-ATPase: possible implications for regulatory disassembly, Structure 16 (2008) 1789–1798, http://dx.doi.org/10.1016/j.str.2008.09.010.
[23] I. Domgall, D. Venzke, U. Lüttge, R. Ratajczak, B. Böttcher, Three-dimensional map of a plant V-ATPase based on electron microscopy, J. Biol. Chem. 277 (2002) 13115–13121, http://dx.doi.org/10.1074/jbc.M112011200.
[24] N.V. Dudkina, J. Heinemeyer, W. Keegstra, E.J. Boekema, H.P. Braun, Structure of dimeric ATP synthase from mitochondria: an angular association of monomers induces the strong curvature of the inner membrane, FEBS Lett. 579 (2005) 5769–5772, http://dx.doi.org/10.1016/j.febslet.2005.09.065.
[25] N.V. Dudkina, S. Sunderhaus, H.P. Braun, E.J. Boekema, Characterization of dimeric ATP synthase and cristae membrane ultrastructure from Saccharomyces and Polytomella mitochondria, FEBS Lett. 580 (2006) 3427–3432, http://dx.doi.org/10.1016/j.febslet.2006.04.097.
[26] H. Feng, T. Cheng, N.J. Pavlos, K.H.M. Yip, A. Carrello, R. Seeber, K. Eidne, M.H. Zheng, J. Xu, Cytoplasmic terminus of vacuolar type proton pump accessory subunit Ac45 is required for proper interaction with V0 domain subunits and efficient osteoclastic bone resorption, J. Biol. Chem. 283 (2008) 13194–13204, http://dx.doi.org/10.1074/jbc.M709712200.
[27] D. Stock, A.G. Leslie, J.E. Walker, Molecular architecture of the rotary motor in ATP synthase, Science 5445 (1999) 1700–1705.
[28] G. Grüber, M.S.S. Manimekalai, F. Mayer, V. Müller, ATP synthases from archaea: the beauty of a molecular motor, Biochim. Biophys. Acta Bioenerg. 1837 (2014) 940–952, http://dx.doi.org/10.1016/j.bbabio.2014.03.004.
[29] S. Guerrero-Castillo, M. Vázquez-Acevedo, D. González-Halphen, S. Uribe-Carvajal, In Yarrowia lipolytica mitochondria, the alternative NADH dehydrogenase interacts specifically with the cytochrome complexes of the classic respiratory pathway, Biochim. Biophys. Acta Bioenerg. 1787 (2009) 75–85, http://dx.doi.org/10.1016/j.bbabio.2008.10.008.
[30] J. Habersetzer, W. Ziani, I. Larrieu, C. Stines-Chaumeil, M.F. Giraud, D. Brèthes, A. Dautant, P. Paumard, ATP synthase oligomerization: from the enzyme models to the mitochondrial morphology, Int. J. Biochem. Cell Biol. 45 (2013) 99–105, http://dx.doi.org/10.1016/j.biocel.2012.05.017.
[31] A. Hahn, K. Parey, M. Bublitz, D.J. Mills, V. Zickermann, J. Vonck, W. Kühlbrandt, T. Meier, Structure of a complete ATP synthase dimer reveals the molecular basis of inner mitochondrial membrane morphology, Mol. Cell 63 (2016) 445–456, http://dx.doi.org/10.1016/j.molcel.2016.05.037.
[32] M. Huss, H. Wieczorek, Influence of ATP and ADP on dissociation of the V-ATPase into its V1 and VO complexes, FEBS Lett. 581 (2007) 5566–5572, http://dx.doi.org/10.1016/j.febslet.2007.11.004.
[33] W. Junge, H. Lill, S. Engelbrecht, ATP synthase: an electrochemical transducer with rotary mechanics, Trends Biochem. Sci. 22 (1997) 420–423, http://dx.doi.org/10.1016/S0968-0004(97)01129-8.
[34] Y.H. Ko, M. Delannoy, J. Hullihen, W. Chiu, P.L. Pedersen, Mitochondrial ATP synthasome: cristae-enriched membranes and a multiwell detergent screening assay yield dispersed single complexes containing the ATP synthase and carriers for Pi and ADP/ATP, J. Biol. Chem. 278 (2003) 12305–12309, http://dx.doi.org/10.1074/jbc.C200703200.
[35] M. Lapaille, A. Escobar-Ramírez, H. Degand, D. Baurain, E. Rodríguez-Salinas, N. Coosemans, M. Boutry, D. Gonzalez-Halphen, C. Remacle, P. Cardol, Atypical subunit composition of the chlorophycean mitochondrial F 1FO-ATP synthase and role of asa7 protein in stability and oligomycin resistance of the enzyme, Mol. Biol. Evol. 27 (2010) 1630–1644, http://dx.doi.org/10.1093/molbev/msq049.
[36] L.K. Lee, A.G. Stewart, M. Donohoe, R.A. Bernal, D. Stock, The structure of the peripheral stalk of Thermus thermophilus H+-ATPase/synthase, Nat. Struct. Mol. Biol. 17 (2010) 373–378, http://dx.doi.org/10.1038/nsmb.1761.

[37] H. Miranda-Astudillo, A. Cano-Estrada, M. Vázquez-Acevedo, L. Colina-Tenorio, A. Downie-Velasco, P. Cardol, C. Remacle, L. Domínguez-Ramírez, D. González-Halphen, Interactions of subunits Asa2, Asa4 and Asa7 in the peripheral stalk of the mitochondrial ATP synthase of the chlorophycean alga Polytomella sp, Biochim. Biophys. Acta Bioenerg. 1837 (2014) 1–13, http://dx.doi.org/10.1016/j.bbabio.2013.08.001.

[38] E. Morales-Rios, M.G. Montgomery, A.G.W. Leslie, J.E. Walker, Structure of ATP synthase from Paracoccus denitrificans determined by X-ray crystallography at 4.0 Å resolution, Proc. Natl. Acad. Sci. U. S. A. 112 (2015) 13231–13236, http://dx.doi.org/10.1073/pnas.1517542112.

[39] R. Moreno-Sánchez, R. Covián, R. Jasso-Chávez, S. Rodríguez-Enríquez, F. Pacheco-Moisés, M.E. Torres-Márquez, Oxidative phosphorylation supported by an alternative respiratory pathway in mitochondria from Euglena, Biochim. Biophys. Acta Bioenerg. 1457 (2000) 200–210, http://dx.doi.org/10.1016/S0005-2728(00)00102-X.

[40] S.P. Muench, J. Trinick, M.A. Harrison, Structural divergence of the rotary ATPases, Q. Rev. Biophys. (2011), http://dx.doi.org/10.1017/S0033583510000338.

[41] A.W. Mühleip, F. Joos, C. Wigge, A.S. Frangakis, W. Kühlbrandt, K.M. Davies, Helical arrays of U-shaped ATP synthase dimers form tubular cristae in ciliate mitochondria, Proc. Natl. Acad. Sci. U. S. A. 113 (2016) 8442–8447, http://dx.doi.org/10.1073/pnas.1525430113.

[42] H. Noji, M. Yoshida, The rotary machine in the cell, ATP synthase, J. Biol. Chem. 276 (2001) 1665–1668, http://dx.doi.org/10.1074/jbc.R000021200.

[43] H. Núsková, T. Mráček, T. Mikulová, M. Vrbacký, N. Kovářová, J. Kovalčíková, P. Pecina, J. Houštěk, Mitochondrial ATP synthasome: expression and structural interaction of its components, Biochem. Biophys. Res. Commun. 464 (2015) 787–793, http://dx.doi.org/10.1016/j.bbrc.2015.07.034.

[44] G.T. Oostergetel, W. Keegstra, A. Brisson, Automation of specimen selection and data acquisition for protein electron crystallography, Ultramicroscopy 74 (1998) 47–59, http://dx.doi.org/10.1016/S0304-3991(98)00022-9.

[45] E. Pebay-Peyroula, C. Dahout-Gonzalez, R. Kahn, V. Trézéguet, G.J.-M. Lauquin, G. Brandolin, Structure of mitochondrial ADP/ATP carrier in complex with carboxyatractyloside, Nature 426 (2003) 39–44, http://dx.doi.org/10.1038/nature02056.

[46] E. Perez, M. Lapaille, H. Degand, L. Cilibrasi, A. Villavicencio-Queijeiro, P. Morsomme, D. González-Halphen, M.C. Field, C. Remacle, D. Baurain, P. Cardol, The mitochondrial respiratory chain of the secondary green alga *Euglena gracilis* shares many additional subunits with parasitic Trypanosomatidae, Mitochondrion 19 (2014) 338–349, http://dx.doi.org/10.1016/j.mito.2014.02.001.

[47] D.M. Rees, A.G.W. Leslie, J.E. Walker, The structure of the membrane extrinsic region of bovine ATP synthase, Proc. Natl. Acad. Sci. U. S. A. 106 (2009) 21597–21601, http://dx.doi.org/10.1073/pnas.0910365106.

[48] J. Schaller, B.C. Pellascio, U.P. Schlunegger, Analysis of hydrophobic proteins and peptides by electrospray ionization mass spectrometry, Rapid Commun. Mass Spectrom. 11 (1997) 418–426, http://dx.doi.org/10.1006/abio.1993.1418.

[49] S.H.W. Scheres, RELION: Implementation of a Bayesian approach to cryo-EM structure determination, J. Struct. Biol. 180 (2012) 519–530, http://dx.doi.org/10.1016/j.jsb.2012.09.006.

[50] D. Speijer, C.K.D. Breek, A.O. Muijsers, A.F. Hartog, J.A. Berden, S.P.J. Albracht, B. Samyn, J. Van Beeumen, R. Benne, Characterization of the respiratory chain from cultured Crithidia fasciculata, Mol. Biochem. Parasitol. 85 (1997) 171–186, http://dx.doi.org/10.1016/S0166-6851(96)02823-X.

[51] A.G. Stewart, L.K. Lee, M. Donohoe, J.J. Chaston, D. Stock, The dynamic stator stalk of rotary ATPases, Nat. Commun. 3 (2012) 687, http://dx.doi.org/10.1038/ncomms1693.

[52] D. Stock, C. Gibbons, I. Arechaga, A.G.W. Leslie, J.E. Walker, The rotary mechanism of ATP-synthase, Curr. Opin. Struct. Biol. 10 (2000) 672–679, http://dx.doi.org/10.1016/j.abb.2008.05.004.

[53] A. Stocker, S. Keis, J. Vonck, G.M. Cook, P. Dimroth, The Structural basis for unidirectional rotation of thermoalkaliphilic F1-ATPase, Structure 15 (2007) 904–914, http://dx.doi.org/10.1016/j.str.2007.06.009.

[54] M. Strauss, G. Hofhaus, R.R. Schröder, W. Kühlbrandt, Dimer ribbons of ATP synthase shape the inner mitochondrial membrane, EMBO J. 27 (2008) 1154–1160, http://dx.doi.org/10.1038/emboj.2008.35.

[55] T. Suhai, N.G. Heidrich, N.A. Dencher, H. Seelert, Highly sensitive detection of ATPase activity in native gels, Electrophoresis 30 (2009) 3622–3625, http://dx.doi.org/10.1002/elps.200900114.

[56] F. Supek, L. Supekova, S. Mandiyan, Y.C.E. Pan, H. Nelson, N. Nelson, A novel accessory subunit for vacuolar H+-ATPase from chromaffin granules, J. Biol. Chem. 269 (1994) 24102–24106.

[57] J. Symersky, V. Pagadala, D. Osowski, A. Krah, T. Meier, J.D. Faraldo-Gómez, D.M. Mueller, Structure of the c10 ring of the yeast mitochondrial ATP synthase in the open conformation, Nat. Struct. Mol. Biol. 19 (2012) 485–491, http://dx.doi.org/10.1038/nsmb.2284.

[58] D. Thomas, P. Bron, T. Weimann, A. Dautant, M.-F. Giraud, P. Paumard, B. Salin, A. Cavalier, J. Velours, D. Brèthes, Supramolecular organization of the yeast F1Fo-ATP synthase, Biol. Cell. 100 (2008) 591–601, http://dx.doi.org/10.1042/BC20080022.

[59] M. Vázquez-Acevedo, P. Cardol, A. Cano-Estrada, M. Lapaille, C. Remacle, D. González-Halphen, The mitochondrial ATP synthase of chlorophycean algae contains eight subunits of unknown origin involved in the formation of an atypical stator-stalk and in the dimerization of the complex, J. Bioenerg. Biomembr. 38 (2006) 271–282, http://dx.doi.org/10.1007/s10863-006-9046-x.

[60] S. Wilkens, M. Forgac, Three-dimensional structure of the vacuolar ATPase proton channel by electron microscopy, J. Biol. Chem. 276 (2001) 44064–44068, http://dx.doi.org/10.1074/jbc.M106579200.

[61] S. Wilkens, E. Vasilyeva, M. Forgac, Structure of the vacuolar ATPase by electron microscopy, J. Biol. Chem. 274 (1999) 31804–31810, http://dx.doi.org/10.1074/jbc.274.45.31804.

[62] I. Wittig, H. Schägger, Advantages and limitations of clear-native PAGE, Proteomics 5 (2005) 4338–4346, http://dx.doi.org/10.1002/pmic.200500081.

[63] Z. Zhang, Y. Zheng, H. Mazon, E. Milgrom, N. Kitagawa, E. Kish-Trier, A.J.R. Heck, P.M. Kane, S. Wilkens, Structure of the yeast vacuolar ATPase, J. Biol. Chem. 283 (2008) 35983–35995, http://dx.doi.org/10.1074/jbc.M805345200.

[64] A. Zhou, A. Rohou, D.G. Schep, J.V. Bason, M.G. Montgomery, J.E. Walker, N. Grigorieff, J.L. Rubinstein, Structure and conformational states of the bovine mitochondrial ATP synthase by cryo-EM, Elife 4 (2015) 1–15, http://dx.doi.org/10.7554/eLife.10180.

[65] A. Zíková, A. Schnaufer, R.A. Dalley, A.K. Panigrahi, K.D. Stuart, The F0F1-ATP synthase complex contains novel subunits and is essential for procyclic Trypanosoma brucei, PLoS Pathog. 5 (2009), http://dx.doi.org/10.1371/journal.ppat.1000436.

[66] I.N. Watt, M.G. Montgomery, M.J. Runswick, A.G. Leslie, J.E. Walker, Bioenergetic cost of making an adenosine triphosphate molecule in animal mitochondria, Proc. Natl. Acad. Sci. U. S. A. 107 (2010) 16823–16827.

BBA - Bioenergetics 1859 (2018) 434–444

Contents lists available at ScienceDirect

BBA - Bioenergetics

journal homepage: www.elsevier.com/locate/bbabio

Oxidative phosphorylation supercomplexes and respirasome reconstitution of the colorless alga *Polytomella* sp.

Héctor Miranda-Astudillo[a,d,*], Lilia Colina-Tenorio[a], Alejandra Jiménez-Suárez[a], Miriam Vázquez-Acevedo[a], Bénédicte Salin[b,c], Marie-France Giraud[b,c], Claire Remacle[d], Pierre Cardol[d], Diego González-Halphen[a]

[a] *Departamento de Genética Molecular, Instituto de Fisiología Celular, Universidad Nacional Autónoma de México, Mexico*
[b] *CNRS, UMR5095, IBGC, 1 rue Camille Saint-Saëns, 33077 Bordeaux, France*
[c] *Université de Bordeaux, Campus Carreire, 146 Rue Léo Saignat, 33077 Bordeaux, France*
[d] *Genetics and Physiology of microalgae, InBioS/Phytosystems, University of Liège, Belgium*

ARTICLE INFO

Keywords:
Chlorophycean algae
Oxidative phosphorylation
F_1F_O ATP synthase
Oligomeric complex V
Mitochondrial supercomplexes
Respirasome

ABSTRACT

The proposal that the respiratory complexes can associate with each other in larger structures named supercomplexes (SC) is generally accepted. In the last decades most of the data about this association came from studies in yeasts, mammals and plants, and information is scarce in other lineages. Here we studied the supramolecular association of the F_1F_O-ATP synthase (complex V) and the respiratory complexes I, III and IV of the colorless alga *Polytomella* sp. with an approach that involves solubilization using mild detergents, n-dodecyl-β-D-maltoside (DDM) or digitonin, followed by separation of native protein complexes by electrophoresis (BN-PAGE), after which we identified oligomeric forms of complex V (mainly V_2 and V_4) and different respiratory supercomplexes (I/IV_6, I/III_4, I/IV). In addition, purification/reconstitution of the supercomplexes by anion exchange chromatography was also performed. The data show that these complexes have the ability to strongly associate with each other and form DDM-stable macromolecular structures. The stable V_4 ATPase oligomer was observed by electron-microscopy and the association of the respiratory complexes in the so-called "respirasome" was able to perform *in-vitro* oxygen consumption.

1. Introduction

Mitochondria are thought to be the product of an ancient endosymbiosis of an α-proteobacterium [1], which already contained an oxidative enzymatic system [2] and an ancestral archaeon host [3–7]. Mitochondria play a key role in eukaryotic energetic metabolism by generating ATP primarily through oxidative phosphorylation (OXPHOS). Part of this process involves the respiratory chain which transfers electrons from reduced NADH or succinate to oxygen by a set of protein-bound redox cofactors. Classically, the respiratory chain comprises two mobile electron carriers, ubiquinone and cytochrome *c*, which are located in the inner membrane and in the intermembrane space, respectively, and four multi-protein complexes: complex I (CI or NADH:ubiquinone oxidoreductase, EC 1.5.6.3), complex II (CII or succinate:ubiquinone oxidoreductase, EC 1.3.5.1), complex III (CIII or ubiquinol:cytochrome *c* oxidoreductase, EC 1.10.2.2) and complex IV (CIV or cytochrome *c* oxidase, EC 1.9.3.1). Three of these complexes (CI, CIII and CIV) use the energy from the electron flow to drive the active transport of protons across the membrane, generating the electrochemical gradient that is then utilized by the F_1F_o-ATP synthase (EC 3.6.3.14) to generate ATP [8].

The F_1F_o-ATPases belong to a family of rotary membrane complexes that includes the vacuolar H^+-translocating V_1V_o-ATPase (V-ATPase) and A_1A_o-ATPase (A-ATPase) and that probably originated from a common evolutionary ancestor [9–11]. The most conserved regions of these enzymes correspond to the catalytic core and the rotor domains. For decades, most of the structural studies of the F-type ATP synthases were carried out in the classical models of the bacterium *E. coli*, or in yeast, rat liver or bovine heart mitochondria [12–18]. Pioneering experiments using cleavable cross-linkers [19], polarized photobleaching and recovery techniques [20,21], video-micrography [22,23] and x-ray diffraction studies of ATPase crystals [24–28] allowed the elucidation of the structure and the catalytic mechanism of the F_1/c_{ring} domain.

The subunit composition and the shape of the peripheral stalk vary among the mitochondrial ATP synthases described so far, from the classical yeast and mammalian enzymes [29–32] that resemble the

* Corresponding author.
E-mail address: hvmirandaastudillo@uliege.be (H. Miranda-Astudillo).

https://doi.org/10.1016/j.bbabio.2018.03.004
Received 31 October 2017; Received in revised form 5 March 2018; Accepted 10 March 2018
Available online 11 March 2018
0005-2728/

bacterial one [33], to the atypical stators present in other sources like *Polytomella* sp. [34], *Tetrahymena thermophila* [35], *Trypanosoma brucei* [36] and *Euglena gracilis* [37,38]. The dimeric nature of the mitochondrial ATP synthase is no longer a matter of debate since they are clearly observed in the structures of the purified complexes from *Polytomella* sp. [39] and *Yarrowia lipolytica* [40] obtained by high resolution cryo-electron microscopy. The dimeric shape is also found in the low resolution images of the enzymes isolated from *S. cerevisiae* [41], *E. gracilis* [38] and *T. thermophila* [35]. Electron cryotomography from the membrane-embedded complex of *Paramecium tetraurelia* [42], *S. cerevisiae* [43], *Polytomella* sp. [44], the trypanosomatid enzyme [45] and other sources like *B. taurus, Y. lipolytica*, *P. anserina* and *S. tuberosum* [46] also support this dimeric disposition. In addition, an association of dimers is observed in the membrane which may form two main contact sites: a dimerization interface and an oligomerization interface [46–48]. This oligomerization of the ATP synthase has been proposed to be involved in the generation and maintenance of the mitochondrial cristae [42,43,49–52].

In earlier studies, OXPHOS complexes were proposed to be associated in one functional unit according to the "solid state" theory [53,54]. This idea was later confronted by a "fluid model". In the latter, all membrane proteins and redox components involved in electron transport and ATP synthesis are in constant and independent diffusional motion [55]. More recently, the proposal that the OXPHOS complexes can associate with each other in larger structures named supercomplexes (SC) [56,57] is generally accepted. This association can allow a more efficient transport of electrons to minimize the generation of reactive oxygen species (ROS) during electron transfer reactions [58], and can also be involved in the regulation of the mitochondrial metabolism in response to different stimuli, carbon sources, or stress conditions in a "plasticity model" [59,60]. In this study we present an extensive characterization of the supramolecular association of the OXPHOS complexes of the colorless alga *Polytomella* sp. using mild detergent extraction followed by BN-PAGE. The data show that some of these complexes could re-associate from detergent solubilized species to form stable entities that can be recovered by liquid chromatography.

2. Materials and methods

2.1. Algal strain, growth conditions and mitochondria isolation

Polytomella sp. (strain number 198.80, isolated by *E.G.* Pringsheim) was obtained from the Culture Collection of Algae at the University of Göttingen (SAG) and was grown aerobically without agitation at room temperature in 2-L flasks containing 1 L of culture medium. The culture medium contained sodium acetate 30 mM, bactotryptone 0.2%, yeast extract 0.2% and a mix of trace elements as previously described [61]. Cells were collected in the middle of the logarithmic phase by centrifugation 7000 × *g* for 20 min. The cellular pellet was stored at −80 °C until use. Cells were broken and mitochondria were obtained by differential centrifugation following the described procedure [62].

2.2. Blue Native (BN) and denaturing (SDS) electrophoresis

Mitochondrial proteins were solubilized with 2.0 g n-dodecyl-β-D-maltoside (laurylmaltoside, DDM)/g protein (1.6%), or 4.0 g digitonin/g protein (3.2%) in solubilization buffer (SB) containing 50 mM Tris-HCl, 1.5 mM $MgSO_4$, 100 mM NaCl, 10%glycerol, 1 mM phenylmethylsulfonyl fluoride (PMSF), and 50 μg/mL tosyl-lysyl-chloromethylketone (TLCK) (pH 8.4). The mixture was incubated at 4 °C with gentle stirring for 30 min, and centrifuged at 30,000 × *g* for 30 min. The supernatants were subjected to BN-PAGE [63]. BN-PAGE was carried out in 3%–10% acrylamide gradient gels, 0.05% digitonin was added in the acrylamide gradient when the same detergent was used for solubilization [64]. Denaturing SDS Tricine-PAGE was carried out in 12% polyacrylamide gels as reported [65]. Three dimensional BN/SDS-glycine/SDS-tricine gels were carried out as previously described [38].

2.3. In-gel enzymatic activities

In-gel NADH/NBT oxido-reductase activity was assayed as described previously [66]. *In-gel* cytochrome *c* oxidase activity was determined using diaminobenzidine as described in [67]. *In-gel* ATPase activity was performed as in [64].

2.4. Immunoassays

From BN-PAGE, proteins were electrotransferred onto a nitrocellulose membrane for immunodetection. Membranes were washed, blocked and incubated with antibodies generated in rabbits against the complete NADH:ubiquinone oxidoreductase from *Polytomella* sp. (complex I), subunit 2 from ubiquinol:cytochrome *c* oxidoreductase from *Polytomella* sp. (complex III), and the COX2B subunit from cytochrome *c* oxidase from *Polytomella* sp. (complex IV). Colorimetric detection was carried out using a goat anti-rabbit IgG conjugated with alkaline phosphatase in the presence of nitro blue tetrazolium chloride and 5-bromo-4-chloro-3′-indolyphosphate p-toluidine salt. The images of the polypeptide bands decorated with the insoluble black-purple precipitates were captured in a HP Scanjet G4050.

2.5. ATPase oligomers purification and supercomplex reconstitution by ion exchange chromatography

All steps were performed at 4 °C unless otherwise stated. Two hundred milligrams of mitochondria were solubilized with n-dodecyl-β-D-maltoside as described above. The mixture was incubated with gentle stirring for 30 min, and centrifuged at 90,000 × *g* for 30 min. The supernatant was diluted in 3 volumes of SB supplemented with 0.01% DDM. The sample was loaded onto an anion exchange column (Source 15Q 10/100, 8 mL) connected to an ÄKTA monitor UPC-900 Workstation (GE Healthcare Life Sciences) equilibrated with the same buffer and washed until a constant base line was obtained. The proteins were eluted with a three-step NaCl gradient in SB supplemented with 0.01% DDM using the following program: 10 column volumes (CV) wash with 75 mM NaCl; 20 CV of 75–250 mM NaCl; 10 CV step with 250 mM NaCl; 20 CV linear gradient 250–500 mM NaCl; and a final 5 CV wash with 500 mM NaCl. Three milliliter fractions were collected and visualized by BN-PAGE.

The fractions corresponding to the ATP synthase were pooled (sample A) and the re-associated respiratory supercomplexes (SC) were selected and separated in two different batches depending on the main presence of either complex I or III, named samples B and C, respectively. The samples enriched with re-associated respiratory supercomplexes (samples B and C) were concentrated separately with an Amicon Ultra-15 Centrifugal Filter 100 kDa (EMD Millipore) to a final volume of 3 mL, from which 500 μL aliquots were made and stored at −80 °C until use. An aliquot of each sample was loaded into three lanes of a BN-PAGE gel. After migration, complexes I and IV were detected by specific *in-gel* activity stain, and the last lane was subjected to a 2D-SDS-PAGE in order to identify the subunit profile of each complex.

2.6. ATPase oligomers separation by size exclusion chromatography and density gradients

Sample A (enriched with ATP synthase) was concentrated with an Amicon Ultra-15 Centrifugal Filter 100kDa (EMD Millipore) to a final volume of 1000 μL and used for two independent treatments: size

exclusion chromatography and discontinuous glycerol gradient. 500 μL were injected to a size exclusion Superose 6 10/300 column (GE Healthcare Life Sciences) previously equilibrated with buffer containing Tris-HCl 50 mM, NaCl 150 mM, $MgSO_4$ 1 mM, glycerol 10%, PMSF 1 mM, TLCK 50 μg/ml, and n-dodecyl-β-D-maltoside 0.01% pH 8.4. The elution was carried out at 0.25 mL/min. Fractions of 0.5 mL were collected and visualized with BN-PAGE. A similar sample (500 μL) was loaded onto seven-ml tubes containing a 10 to 50% discontinued glycerol gradient in the same buffer. The gradients were centrifuged at 40000 × *g* for 17 h in a SW41Ti swing out rotor (Beckman Coulter). Fractions of 0.5 mL were collected and visualized on BN-PAGE.

2.7. Preliminary electron microscopy of the ATPase oligomers

The algal oligomeric ATP synthase obtained from the size exclusion chromatography was diluted to a final concentration of 12.5 μg/mL with 20 mM Tris-HCl (pH 8.4) buffer. Samples of 6 μL were applied to glow discharged carbon-coated copper grids for negative staining. Grids were washed twice with water and stained with 1% uranyl acetate for 1 min, dried and examined with a HITACHI H7650 transmission electron microscope (Hitachi High-Technologies Corporation) operating at 120 kV. Images (3284 × 2600 pixels) were recorded on a SC1000 ORIUS 11 Mpx (GATAN).

2.8. Oxygen consumption of the reconstituted respirasome

Oxygen consumption was assessed in a YSI model 5300 oxygraph equipped with a Clark-Type electrode. The reaction vessel was a 200 μL water-jacketed chamber maintained at 30 °C. The activity buffer contained MOPS 50 mM, NaCl 100 mM, DDM 0.01% (pH 7.2). NADH 5 mM was used as electron donor, 2,3-dimethoxy-5-methyl-p-benzoquinone and horse cytochrome *c* were used to complete the electron transfer chain at 5 mM and 50 mM concentrations, respectively. The reaction was initiated with the addition of 160 μg of the reconstituted respirasome (sample B, sample C or a 1:1 mix B + C). Rotenone 500 μM, antimycin A 100 μM and potassium cyanide 50 μM were used as inhibitors of complex I, III and IV, respectively. To observe the inhibitory effect from rotenone or antimycin A the samples were preincubated 30 min in the presence of each inhibitor before starting the measurements.

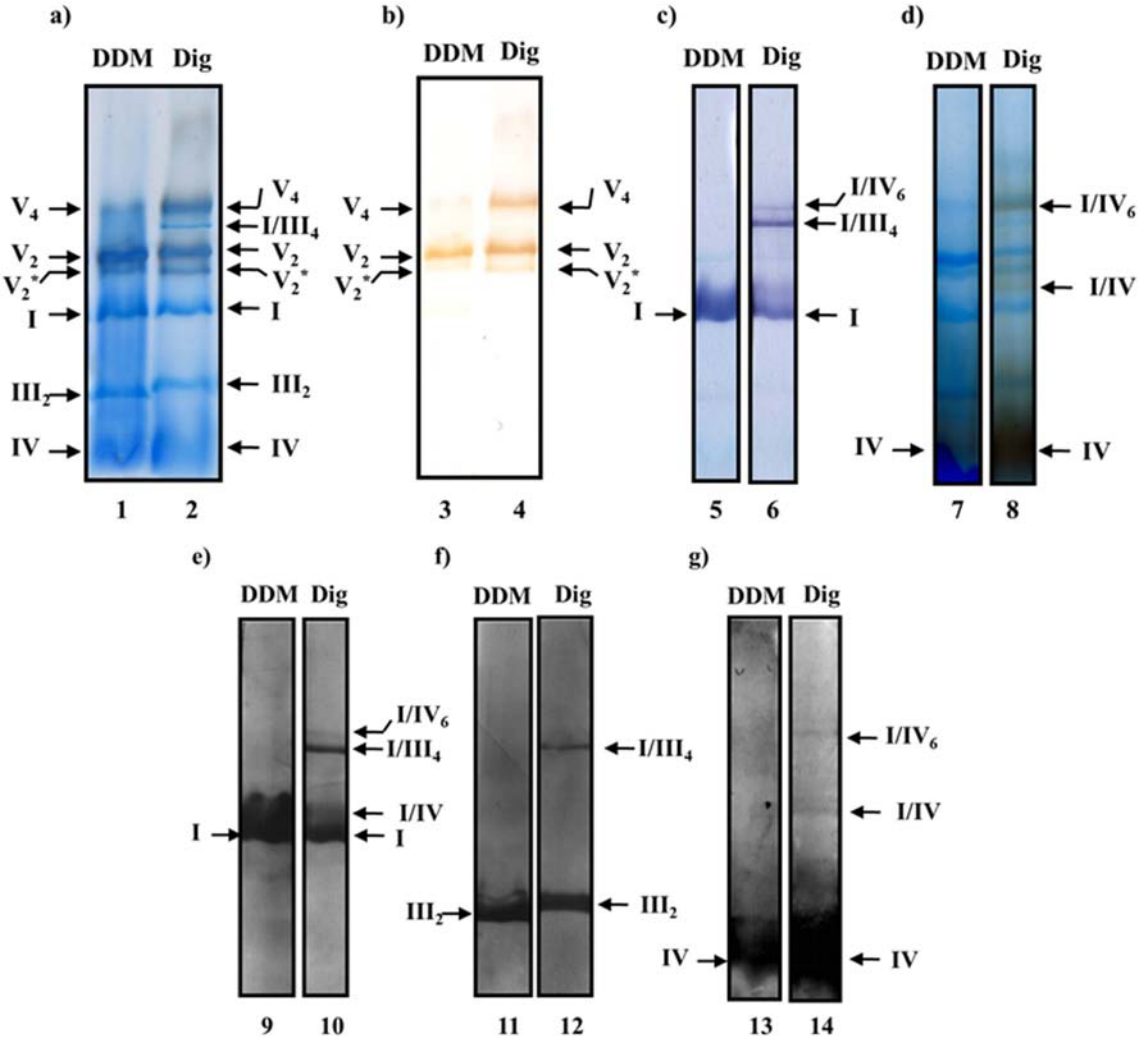

Fig. 1. ATPase oligomers and respiratory supercomplexes in *Polytomella* sp. Isolated mitochondria were solubilized with the indicated detergent: n-dodecyl-β-D-maltoside (DDM) at 2.0 g/g protein or digitonin (Dig) at 4.0 g/g protein. (a) soluble fractions resolved by BN-PAGE in a 3–10% polyacrylamide gradient gel. (b) BN-gel and detection of *in-gel* ATPase activity. The gel was incubated with ATP, $MgSO_4$ and $Pb(NO_3)_2$ (c) *in-gel* NADH-dehydrogenase activity; the BN-gel was incubated in the presence of NADH and Nitro blue tetrazolium chloride (NBT). (d) cytochrome *c* oxidase (COX) *in-gel* activity. The BN-gel was incubated with diaminobenzidine and horse-heart cytochrome *c*. Western blot was performed using antibodies against: (e) the complete NADH:ubiquinone oxidoreductase from *Polytomella* sp.; (f) subunit 2 from ubiquinol:cytochrome *c* oxidoreductase from *Polytomella* sp. and (g) the COX2B subunit from cytochrome *c* oxidase from *Polytomella* sp. Nomenclature used for *Polytomella* sp. mitochondria: I, III and IV for the corresponding mitochondrial complexes, V_2 for the dimeric ATP synthase. Supercomplexes were: I–IV, I–IV_6 and I–III_4 and their stoichiometries are indicated as subindexes. $V_2{}^*$ corresponds to the dimeric complex V with a slight proteolysis in subunits alpha, beta and Asa3 (See Supplemental Fig. S1 for details).

3. Results

3.1. ATPase oligomers and respiratory supercomplexes in Polytomella sp.

Mitochondria from *Polytomella* sp. were solubilized with either DDM (1.6%) or digitonin (3.2%). After removing the insoluble fraction, each sample was subjected to BN-PAGE. When proteins are solubilized with DDM, the 3–10% acrylamide gradient gels stained with Coomasie blue allowed the resolution of the four prominent classical bands corresponding to dimeric complex V (V_2), complex I (I), dimeric complex III (III_2), and complex IV (IV) (Fig. 1 lane 1). Additional bands corresponding to supramolecular complexes could be visualized when other lanes were used to perform immuno-detection (Fig. 1, lanes 9–14) and *in-gel* activity staining (Fig. 1, lanes 3–8) of respiratory complexes I, IV, and V. This linear regression obtained with a relatively high confidence value for the log (molecular mass) *vs* distance migrated ($R^2 = 0.997$) was used to calculate the molecular masses and stoichiometries of these supramolecular associations as described [66] (Fig. S2). The ATP synthase corresponds to two main bands exhibiting ATP hydrolysis activity (Fig. 1 lanes 1–4), both of them migrating above complex I (Fig. 1 lanes 1–2). In addition to the lower band (V_2) corresponds to the previously described dimeric complex V from chlorophycean alga (~1.6 MDa) [68], the upper band (V_4) would correspond to a tetrameric complex V according to its calculated molecular mass (~3.2 MDa). This multimeric complex became more evident when digitonin was used for the solubilization (Fig. 1 lanes 2 and 4). A third fainter band can be observed below the dimeric complex (V_2*) and corresponds to the dimeric complex V exhibiting partial proteolysis of the alpha, beta and Asa3 subunits (Supplemental Fig. S1).

The respiratory complexes I, III_2 and IV migrated as single bands when DDM was used to extract the membranes as revealed with specific antibodies (Fig. 1 lanes 9, 11 and 13). In contrast, when digitonin was used, supramolecular associations of the respiratory complexes could be detected (Fig. 1 lanes 2, 6, 8, 10, 12 and 14). The association of complex III is mainly with complex I giving rise to the I/III_4 SC (Fig. 1 lanes 6, 10 and 12) that has no detectable complex IV, the latter being mainly associated with complex I, forming two I:IV SCs with different stoichiometries (Fig. 1 lanes 6, 8, 10 and 14). No complex III could be detected in these SCs (Fig. 1 lane 12).

3.2. ATPase purification and supercomplex reconstitution by ion exchange chromatography

To further characterize the OXPHOS complexes with a different experimental approach, mitochondria were solubilized with DDM and loaded into an anion exchange column. After washing out the unbound material, the complexes were eluted with a three-step NaCl gradient; Fig. 2A shows a representative elution profile. Each fraction was then submitted to native gel analysis followed by *in-gel* activity staining for complexes I and IV (Fig. 2B). The gradient allowed the separation of the oligomeric complex V (V_2, V_2* and V_4), which eluted earlier than the respiratory complexes and could be recovered in the first peak (sample A). The respiratory complexes I, III and IV were distributed in the two following peaks. All of these three respiratory complexes were found in a mixture of the individual and oligomeric associations in the eluted fractions (Fig. 2B). Complex I eluted mainly in the second peak (sample B) forming a SC with a molecular mass similar to the dimeric ATP synthase (~1.6 MDa). Complex III eluted mainly in the third peak (sample C) together with some SCs containing complexes I and IV (Fig. 2B).

3.3. Separation and characterization of ATPase oligomers

In order to further characterize the nature of the observed oligomeric states of the ATP synthase (Fig. 2B), two additional separation techniques were performed: size exclusion chromatography and glycerol density gradient centrifugation. Fig. 3A shows the fractions eluted from the Superose 6 10/300 GL column (Optimal resolution range: 5–5000 kDa), where a separation of the putative V_4 and V_2 oligomers was observed (Fig. 3A). A faint band could be observed above the V_4. This band showed ATPase activity and was prominent when lower digitonin concentrations were used to solubilize the complexes (Fig. S3A and S3B). This indicates the formation of a higher molecular association (e.g. V_6) after the concentration step. Separation of the main Complex V oligomeric forms was also achieved by density gradient centrifugation (Fig. 3B).

To further validate the presence of the different complex V oligomeric states, electron microscopy images were taken from samples enriched in V_2 and in the putative V_4 oligomers from the size exclusion column (Fig. 3A). The observation of tetramers associated through the membrane domain of the enzyme (Fig. 4) supports our previous suggestion of the presence of a V_4 oligomeric form. To discard possible unspecific, hydrophobic-driven associations due to an insufficient detergent/protein ratio, a mixture of V_4 and V_2 oligomers was incubated with increasing concentration of DDM. Fig. 5A shows that these oligomeric states are able to resist relative high concentrations of DDM, even though some small molecular bands can be observed in the last lanes (> 1%) that could reflect partial dissociation of the complexes. Nevertheless, the two oligomers (V_4 and V_2) remain clearly distinct even at high DDM concentrations. Similarly, increasing concentrations of the zwitterionic surfactant CHAPS had no visible effect on the stability of the V_4/V_2 oligomeric forms (Fig. 5B). Taken together, these results indicate that the supramolecular association of ATP synthase in *Polytomella* sp. gives rise to stable V_2 and V_4 oligomeric states.

To explore if specific subunits are implicated in the formation of the ATP synthase tetrameric complex, fractions enriched with V_2 and V_4 were also analyzed by SDS-PAGE (Fig. 6A). A similar subunit composition and stoichiometry was found for both oligomers (Fig. 6B). Although protease inhibitors were used during the purification procedure, a slight Asa3 subunit degradation (Asa3*) was observed in both the V_2 and V_4 fractions (Fig. 6A). This subunit profile was corroborated when a 2D BN/SDS-PAGE was performed (Fig. S4). As in the extracted complexes (Fig. 1a and b), the purified ATPase oligomers exhibited ATP hydrolysis activity (Fig. S4). Together, these results suggest that the ATPase dimer contains all the subunits required to form higher oligomeric associations.

3.4. Characterization of the reconstituted respirasome

To characterize the composition of the reconstituted respiratory SCs, 2D-BN/SDS-PAGE was performed from enriched fractions obtained from anion exchange chromatography (Fig. 2B). Two lanes from the native first dimension were analyzed by *in-gel* activity stain for complexes I and IV, and the identification of complex III was assessed by its well characterized polypeptide profile [69]. As described above, sample B was enriched with complexes I and IV (Fig. 2B). Complex IV mainly migrated as a free complex, while complex I was distributed into two species, the isolated complex and the so-called "respirasome" ($I/III_2/IV_2$ SC) (Fig. 7A). A higher molecular mass band could be observed; this band does not present cytochrome *c* oxidase activity and possess characteristic polypeptide patterns from complex I and complex III. In accordance with its calculated molecular mass (~3.4 MDa) it could correspond to a I_2/III_4 SC. On the other hand, sample C was enriched with Complex III which mainly migrated independently from the rest of the complexes (Fig. 7B). In contrast with sample B, small quantities of the I/III_2 SC could also be recovered. As in sample B, the three complexes migrated independently; however, small quantities of the reconstituted respirasome ($I/III_2/IV_2$) were observed (Fig. 7B).

To assess the activity of the reconstituted respirasomes *in-vitro*, oxygen consumption was measured upon addition of an electron donor (NADH) and the electron carriers quinone and soluble cytochrome *c*. In both samples B and C, a cyanide-sensitive NADH-dependant oxygen

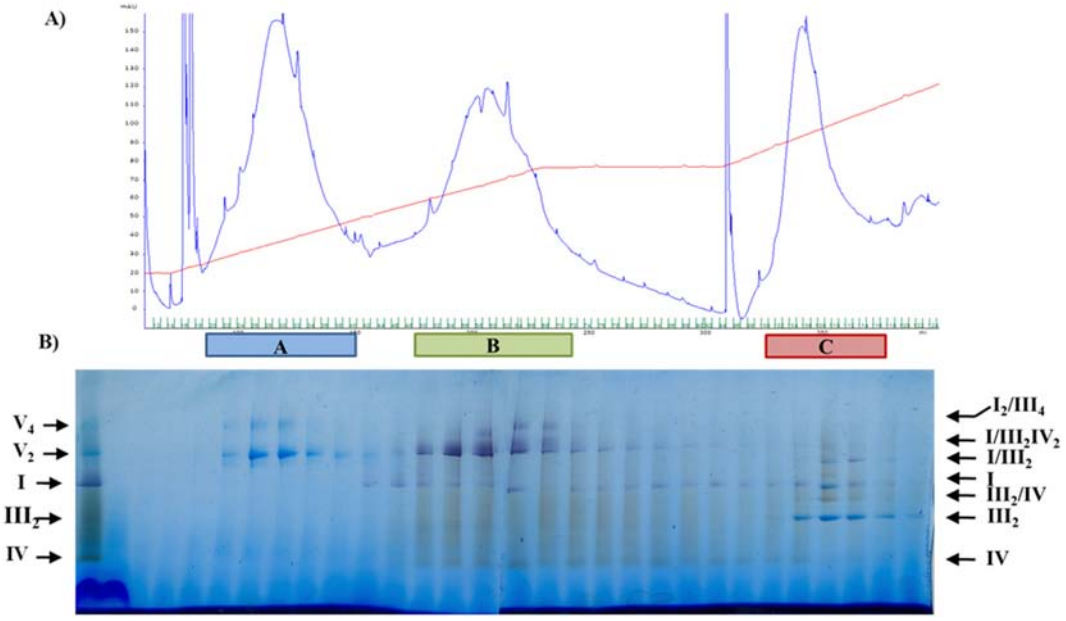

Fig. 2. ATPase oligomers purification and supercomplexes reconstitution by ion exchange chromatography. Two hundred milligrams of mitochondria were solubilized with n-dodecyl-β-D-maltoside and loaded into an anion exchange column, then eluted with a three-step NaCl gradient (see Material and Methods for details). A) Elution profile the blue line is the absorbance at 280 nm, the red line represents the NaCl gradient, the green marks below represent the elution fractions. Three main peaks (samples A, B and C) could be separated. B) BN-PAGE from the fractions corresponding to the samples A, B and C. Sample A corresponds to the ATP synthase oligomers, while sample C and B contain the respiratory supercomplexes. The first lane shows the free complexes obtained after lauryl-maltoside solubilization of the algal mitochondria.

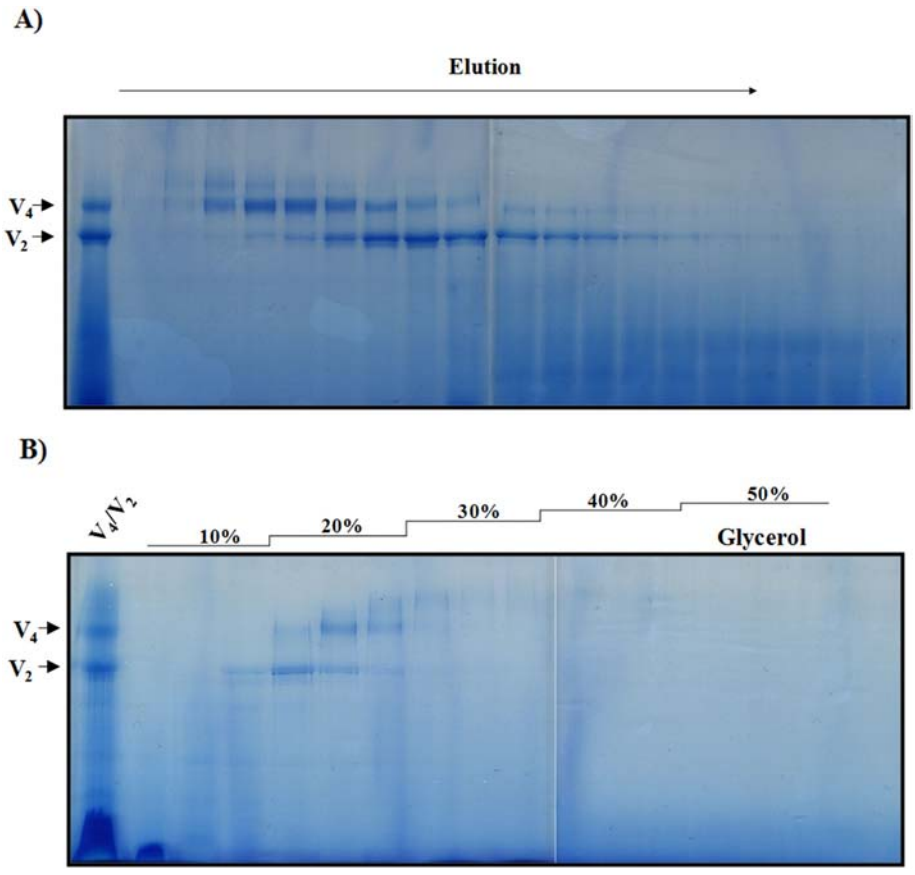

Fig. 3. ATPase oligomers separation by size exclusion chromatography and density gradients. Oligomers of ATP synthase from the anion exchange chromatography (sample A) were separated by two different separation techniques. (A) BN-PAGE of the fractions obtained from the size exclusion chromatography in a Superose 6 10/300 GL column. (B) BN-PAGE of the fractions obtained from a glycerol discontinuous density gradient (10–50%). The first lane in both images represents the loaded sample.

consumption could be measured (Fig. 8). The relative amplitude of observed activities roughly corresponds to the relative amounts of the reconstituted respirasome present in each sample (Figs. 2B, 7A and B). The effects of the specific complex I and III inhibitors, rotenone and antimycin A respectively, were also evaluated. A full inactivation of the reconstituted respirasome was observed only after 30 min incubation at 4 °C in the presence of the inhibitors (Fig. 8 dotted line). Taken together, these results show that the reconstituted respirasome is stable in presence of DDM and exhibits *in vitro* electron transport activity.

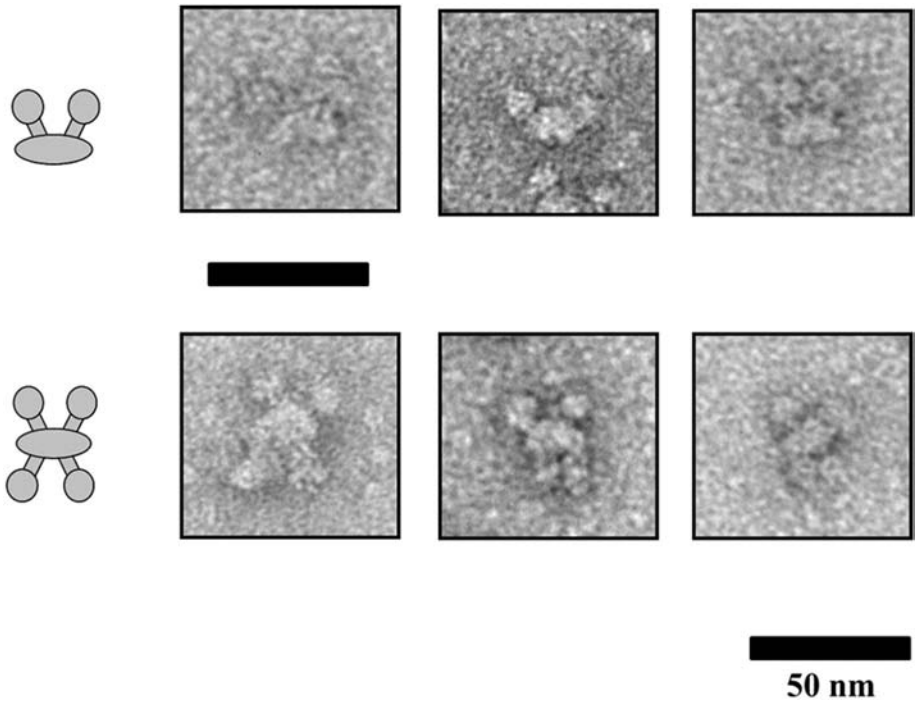

Fig. 4. Electron microscopy images of the ATPase oligomers. Enriched fractions of the dimeric and tetrameric ATP synthase oligomers were analyzed by electron microscopy. Single particles from the EM micrographs. The black line represents 50 nm.

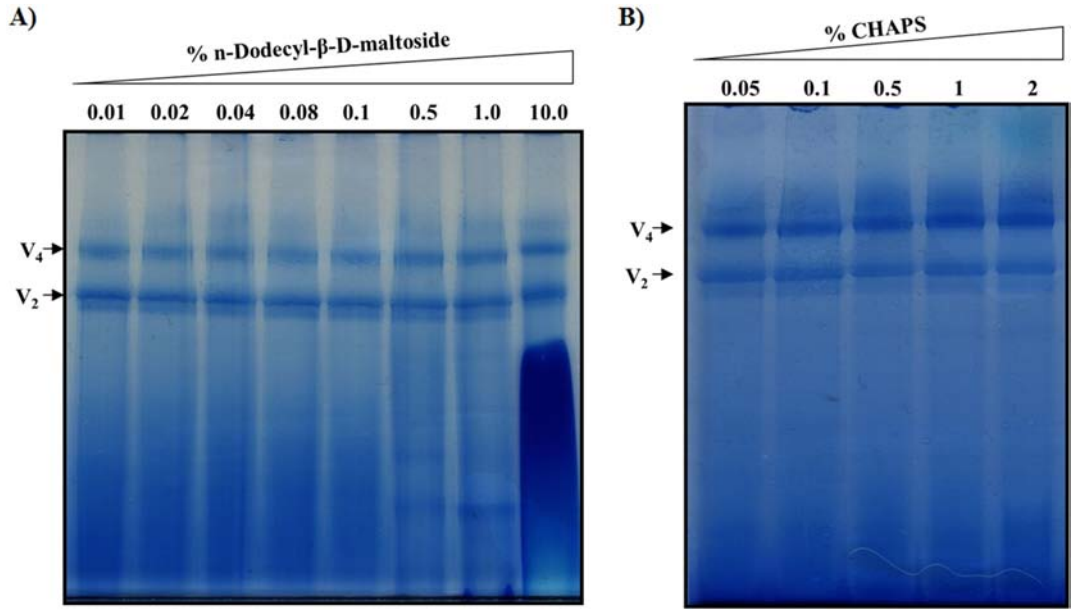

Fig. 5. Stability of the ATP synthase oligomers at increasing concentrations of detergents, the non-ionic DDM and the zwitterionic CHAPS. One hundred microgram of enriched V_2 and V_4 oligomers were incubated 30 min at 4 °C with increasing concentrations of DDM (A) and CHAPS (B). Numbers represent the % concentration of each detergent.

4. Discussion

The *Polytomella* mitochondrial ATP synthase is found forming mainly dimeric and tetrameric complexes, the former being the most prominent form after solubilization with DDM and the latter being more stable in the presence of the milder detergent digitonin. This high stability of the dimeric F_1F_o-ATP synthase is a common feature of chlorophycean algae [70,71]. In contrast, stable dimeric forms in yeast, bovine and rat mitochondria has been previously described only when digitonin was used to solubilize the membranes [51,64,72]. In the presence of DDM, the ATP synthase from these organisms readily dissociates into monomers in BN-PAGE [71,73,74], explaining why this enzyme is usually purified in its monomeric form [27,75,76]. In contrast, in the case of chlorophycean algae, the dissociation of the dimer gives rise to unstable monomers [68,77].

The ATP synthase from *Polytomella* contains atypical polypeptides named Asa subunits [62] that seem to be unique to the chlorophycean lineage [77,78]. It has been proposed that these subunits form the robust peripheral stalk observed in the algal complex [34] and their interactions have been extensively characterized [77,79–82]. Recently, two other ATP synthases were shown to have stable dimers in BN-PAGE when extracted with DDM: the enzymes from *T. brucei* [36] and *E. gracilis* [37,38]. In both cases the subunit composition of the peripheral stalk differs from the yeast/bovine enzyme, but is not related to the

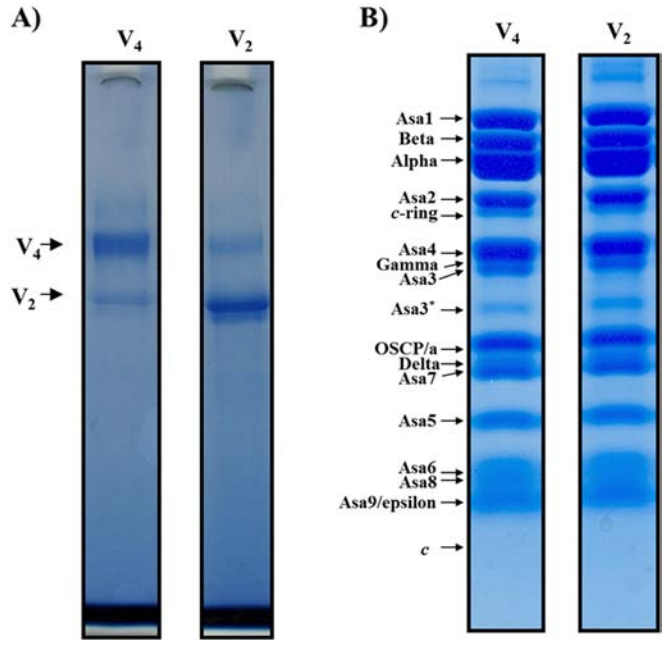

Fig. 6. Subunit composition of the V_2 and V_4 oligomers of the ATP synthase from *Polytomella* sp. BN-PAGE 3–10% acrylamide gradient (A) and SDS-PAGE 12% acrylamide concentration (B) of enriched fractions with V_2 and V_4 oligomers.

chlorophycean one.

All dimeric ATP synthases studied so far have the dimerization interface in the membrane domain. In the yeast ATP synthase the association between monomers occurs mostly inside the membrane, where five supernumerary subunits (e, f, g, i and k) are found associated in the dimeric form of the enzyme [29,40,50,83,84]. A topological model based on crosslink interactions has been proposed for the yeast enzyme [48]. In this model, all the subunits involved in the oligomerization are present in the dimeric complex, similarly, both oligomeric forms of the ATPase from *Polytomella* (V_2 and V_4) seem to have the same subunit composition. Moreover, the fact that the tetrameric or higher oligomerization forms can be enriched and recovered after removing the excess of detergent during chromatographic/concentration steps indicates that all the subunits involved in the oligomerization of the enzyme are present in the dimeric complex. Finally, the electron microscopy images reveal that the interface between both dimers in the V_4 oligomer must be present in the membrane domain. Although the arrangement of the V_4 complex over the carbon grid is not optimal, the four F_1 headpieces are evident and the contact between the dimers is observed across the membrane domain, although in a different plane of the negative staining.

In addition to the protein-protein interactions established by the membrane-embedded subunits, two other interactions between the monomers in the upper region of the peripheral arms have been observed in the *Polytomella* complex. The so-called "Armadillo repeat"-like density links the two monomers in a region just above the membrane, and a "helix–turn–helix" motif halfway through the peripheral stalks seem to reinforce the associations of the two monomers [39]. Fig. 5A and B show the stability of the purified V_2 and V_4 when they are incubated 30 min in presence of high concentrations of DDM or CHAPS. In contrast, when the purified V_2 is incubated overnight with high concentrations of DDM or the amphipathic polymer Amphipol A8–35 the enzyme readily dissociates. First, the F_1 domain separates from the V_2 complex followed by the dissociation of the OSCP, Asa2 and Asa4 subunits. The rest of the V_2 complex, comprising two peripheral stalks with their corresponding membrane domain (a/*c*-ring), migrates as a subcomplex in BN-PAGE [34,80]. This dimeric peripheral stalk complex has been observed by electron microscopy in *Chlamydomonas*

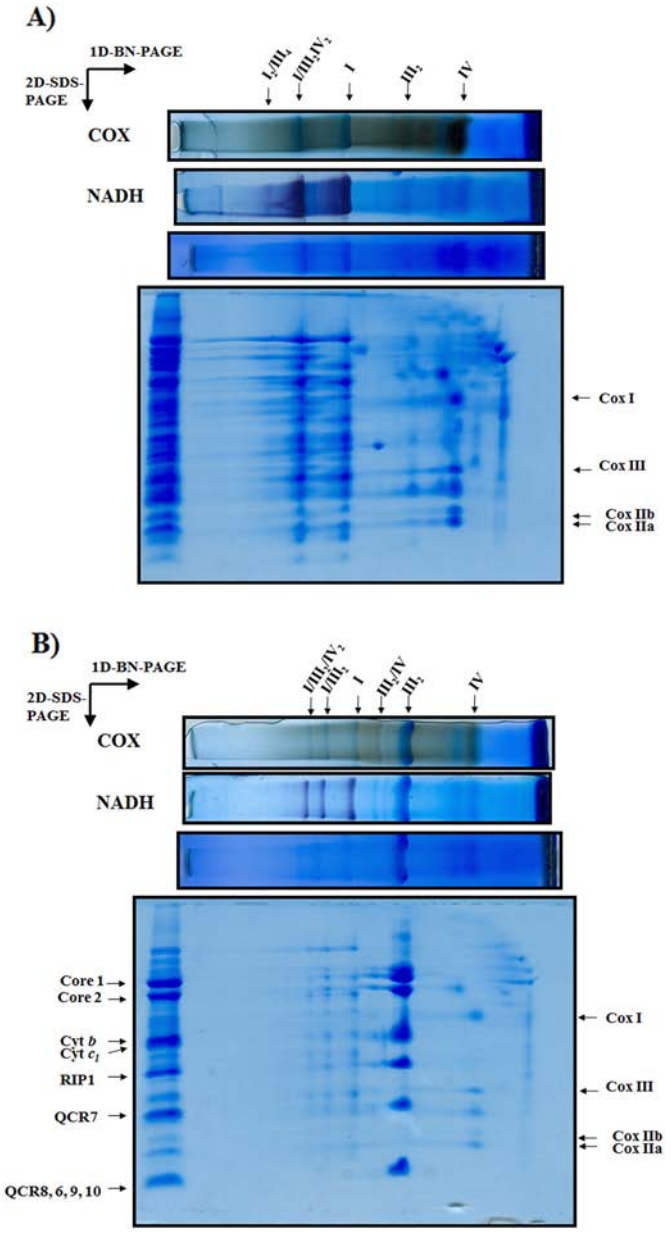

Fig. 7. Characterization of the reconstituted supercomplexes and the respirasome. Samples from the two enriched fractions from the ion exchange column (samples B and C) were subjected to a BN-PAGE and *in-gel* activity stain for complexes I (NADH) and IV (COX). A) Sample B, highly enriched in complex I and in the respirasome; B) sample C, highly enriched in complex III. The subunit composition was analyzed by 2D SDS-PAGE. The main subunits of complexes III and IV are indicated.

reindhardtii partially dissociated preparations (Prof. Egbert Boekema *personal communication*). These partial dissociations could explain the appearance of low molecular mass bands when the enzyme is incubated with increasing concentrations of DDM. We can hypothesize that the two unusual linker domains in the peripheral stalks described above play a major role in the stability of the complex. Subunit Asa7 has been proposed to be the "helix–turn–helix" motif that links both arms in the extrinsic region of the enzyme [34], while the subunit with the "armadillo" motif remains unidentified. All of these observations suggest that the dimeric form (V_2) is the "structural unit" of ATP synthase in chlorophycean algae, and that free monomers most probably do not exist *in vivo*.

The inner mitochondrial membrane folds into structures known as cristae. A 3D model of their shape inside native mitochondria was obtained by EM tomography [85,86]. This model shows two major regions

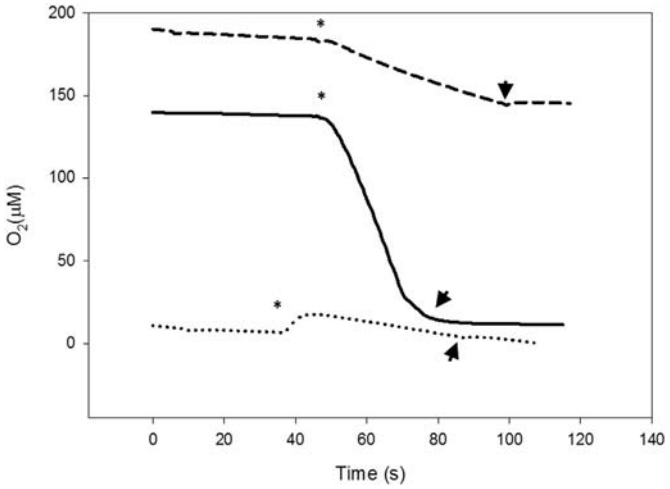

Fig. 8. Oxygen consumption of the reconstituted respirasome. The reconstituted SCs and respirasome were incubated in the presence of 2,3-Dimethoxy-5-methyl-p-benzoquinone and horse cytochrome *c*. NADH was used as electron donor. Oxygen consumption of the sample B (continuous line) and sample C (segmented line). The asterisks indicate the addition the protein sample and the arrow heads indicate the addition of KCN. Evaluation of the inhibitory effect of specific complex III inhibitor antimycin A over sample B is shown (dotted line). The lines were moved along the y axis for clarity.

across the cristae: the lamellar and the tubular. Both regions can be explained in biophysical terms as a way of minimizing the free energy of the system [87], and several studies have linked these structures with complex V dimerization [51,52]. Molecular dynamics simulations showed that the tubular shape of the cristae increases as more ATPase dimers incorporate into rows [42,43]. A highly packed tubular cristae has been described in *Polytomella* mitochondria by electron microscopy and cryo-electron tomography [44,47,88,89]. In these condensed cristae, the membrane domains of each V_2 are in direct contact with the surrounding dimers, but no contact in the extrinsic region can be observed [44].

The electron cryotomography of mitochondria from various organisms revealed the segregation between the respiratory complexes and the row of ATPase dimers [46]. Diverse associations of the respiratory complexes in stoichiometric SCs have been described in various organisms [90]. The respiratory SCs are increasingly accepted as structural entities, although their functional relevance remains unclear. Some explanations include: the structural stabilization of complex I [91], the substrate channeling directly from one electron transfer complex to the next, avoiding the production of reactive oxygen species, the metabolic regulation of all the electron transport chain, or impeding aggregation of the complexes [56,58–60,89,92–96]. Interestingly, when *Polytomella* mitochondria are solubilized with digitonin, no SC containing CI, CIII and CIV was observed; instead three SCs with I and III or I with IV were found (Fig. 1 lanes 6, 8, 10, 12 and 14), suggesting that the *Polytomella* complex I interacts strongly with either complex III or complex IV in an independent manner.

Most studies of the SCs and the respirasome involve the use of the very mild detergent digitonin or amphipol molecules [97–99]. With these detergents high resolution models of respirasomes from bovine (9 Å), ovine (5.8 Å) and porcine (5.4 and 4 Å) were obtained [100–103]. In contrast, when high concentration of DDM (1.6%) are used, all the complex-complex interactions are lost and the SCs dissociate and migrate into individual respiratory complexes (I, III_2 and IV) on BN-PAGE (this study, [62,70,73]). Here we show that DDM-solubilized complexes I, III and IV from *Polytomella* associate into several SCs when excess of detergent is removed (Fig. 2). This reconstitution into the so-called respirasome is however not complete, as free complexes elute separately in the NaCl gradient, probably because of competition between the complex-complex and the complex-matrix interactions. We

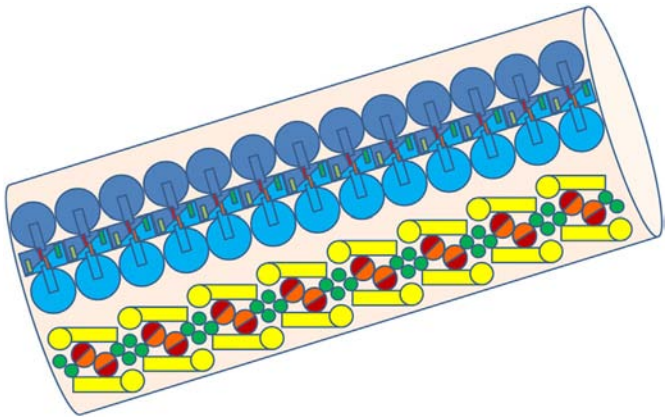

Fig. 9. Model of the association of OXPHOS complexes in *Polytomella* sp. cristae. The ATP synthase dimers are represented with dark blue and monomers with light blue. The association between dimers is by the membrane domain, the two interactions between the monomers in the upper region of the peripheral arms are "Armadillo repeat"-like density (dark and light green) and "helix–turn–helix" motif (red and orange) (see discussion for details). The respiratory complexes are represented in yellow (monomeric complex I), red and orange (dimeric complex III), green (monomeric complex IV).

hypothesize that the CIII-matrix interaction (sample C) is stronger than the CI-matrix interaction (Sample B), albeit some $I/III_2/IV_2$ respirasomes can be recovered in sample B. Meanwhile, CIV shows no significant affinity for the matrix, and seems to be bound to CI or CIII along the gradient. The reconstituted respirasome migrates with a molecular mass similar to the V_2 complex (~1.6 MDa). SCs showed oxygen consumption in presence of NADH after the addition of an excess of external electron carriers (2,3-dimethoxy-5-methyl-p-benzoquinone and horse cytochrome *c*). This result strongly suggests that CoQ and cyt *c* were lost during the solubilization/chromatographic steps. Although functional respirasomes have been already isolated from digitonin-solubilized mitochondria [104], this is, to our knowledge, the first successful reconstitution of a complete DDM-stable and functional respirasome from isolated respiratory complexes.

The data obtained in this work show that the OXPHOS complexes of *Polytomella* have the ability to strongly associate with each other and form two stable macromolecular structures: (i) ATP synthase oligomers formed by the association of dimers, which allow the purification of the V_4 oligomer and (ii) the respirasome, which can be reconstituted *in column* when the excess of DDM is removed. It is likely that the highly condensed and tubular cristae observed in *Polytomella* arise from an extraordinary capacity to maintain a tight association of its OXPHOS complexes (Fig. 9).

Supplementary data to this article can be found online at https://doi.org/10.1016/j.bbabio.2018.03.004.

Transparency document

The Transparency document associated with this article can be found, in online version.

Acknowledgments

We thank Alfredo Octaviano García (IFC, UNAM) for his auxiliary support. P.C. acknowledges financial support from the Belgian Fonds de la Recherche Scientifique F.R.S.-F.N.R.S. (FRFC 2.4597, CDR J.0079) and European Research Council (H2020-EU BEAL project 682580). P.C. is a Senior Research Associate from F.R.S.-FNRS. D.G.H. acknowledges financial support from 279125 Grant ECOS Nord-ANUIES-CONACyT, support from grants 239219 (Fondo SEP-CONACYT) CONACyT and IN208917 (PAPIIT-DGAPA-UNAM) are also acknowledged.

References

[1] Z. Wang, M. Wu, An integrated phylogenomic approach toward pinpointing the origin of mitochondria, Sci. Rep. 5 (2015) 7949, , http://dx.doi.org/10.1038/srep07949.

[2] C.G. Kurland, S.G.E. Andersson, Origin and evolution of the mitochondrial proteome, Microbiol. Mol. Biol. Rev. 64 (2000) 786–820, http://dx.doi.org/10.1128/MMBR.64.4.786-820.2000.

[3] M.W. Gray, B.F. Lang, G. Burger, Mitochondria of protists, Annu. Rev. Genet. 38 (2004) 477–524, http://dx.doi.org/10.1146/annurev.genet.37.110801.142526.

[4] E.V. Koonin, The origin and early evolution of eukaryotes in the light of phylogenomics, Genome Biol. 11 (2010) 209, http://dx.doi.org/10.1186/gb-2010-11-5-209.

[5] W. Martin, M. Müller, The hydrogen hypothesis for the first eukaryote, Nature 392 (1998) 37–41, http://dx.doi.org/10.1038/32096.

[6] A. Spang, J.H. Saw, S.L. Jørgensen, K. Zaremba-Niedzwiedzka, J. Martijn, A.E. Lind, R. van Eijk, C. Schleper, L. Guy, T.J.G. Ettema, Complex archaea that bridge the gap between prokaryotes and eukaryotes, Nature 521 (2015) 173–179, http://dx.doi.org/10.1038/nature14447.

[7] K. Zaremba-Niedzwiedzka, E.F. Caceres, J.H. Saw, D. Bäckström, L. Juzokaite, E. Vancaester, K.W. Seitz, K. Anantharaman, P. Starnawski, K.U. Kjeldsen, M.B. Stott, T. Nunoura, J.F. Banfield, A. Schramm, B.J. Baker, A. Spang, T.J.G. Ettema, Asgard archaea illuminate the origin of eukaryotic cellular complexity, Nature 541 (2017) 353–358, http://dx.doi.org/10.1038/nature21031.

[8] M. Saraste, Oxidative phosphorylation at the fin de siècle, Science 283 (1999) 1488–1494.

[9] R.L. Cross, V. Müller, The evolution of A-, F-, and V-type ATP synthases and ATPases: reversals in function and changes in the H+/ATP coupling ratio, FEBS Lett. 576 (2004) 1–4, http://dx.doi.org/10.1016/j.febslet.2004.08.065.

[10] R.L. Cross, L. Taiz, Gene duplication as a means for altering H+/ATP ratios during the evolution of Fo F1 ATPases and synthases, FEBS Lett. 259 (1990) 227–229, http://dx.doi.org/10.1016/0014-5793(90)80014-A.

[11] S.P. Muench, J. Trinick, M.A. Harrison, Structural Divergence of the Rotary ATPases. (2011), http://dx.doi.org/10.1017/S0033583510000338.

[12] P.D. Boyer, The ATP synthase–a splendid molecular machine, Annu. Rev. Biochem. 66 (1997) 717–749, http://dx.doi.org/10.1146/annurev.biochem.66.1.717.

[13] W. Junge, Protons, proteins and ATP, Photosynth. Res. 80 (2004) 197–221, http://dx.doi.org/10.1023/B:PRES.0000030677.98474.74.

[14] P.L. Pedersen, The machine that makes ATP, Curr. Biol. 4 (1994) 1138–1141.

[15] A.E. Senior, Two ATPases, J. Biol. Chem. 287 (2012) 30049–30062, http://dx.doi.org/10.1074/jbc.X112.402313.

[16] J.E. Walker, The ATP synthase: the understood, the uncertain and the unknown, Biochim. Biophys. Acta Bioenerg. 1817 (2012) S1, http://dx.doi.org/10.1016/j.bbabio.2012.06.013.

[17] J.E. Walker, I.R. Collinson, The role of the stalk in the coupling mechanism of F1F0-ATPases, FEBS Lett. 346 (1994) 39–43, http://dx.doi.org/10.1016/0014-5793(94)00368-8.

[18] M. Yoshida, E. Muneyuki, T. Hisabori, ATP synthase–a marvellous rotary engine of the cell, Nat. Rev. Mol. Cell Biol. 2 (2001) 669–677, http://dx.doi.org/10.1038/35089509.

[19] T.M. Duncan, V.V. Bulygin, Y. Zhou, M.L. Hutcheon, R.L. Cross, Rotation of subunits during catalysis by Escherichia coli F1-ATPase, Proc. Natl. Acad. Sci. U. S. A. 92 (1995) 10964–10968, http://dx.doi.org/10.1073/pnas.92.24.10964.

[20] D. Sabbert, S. Engelbrecht, W. Junge, Functional and idling rotatory motion within F1-ATPase, Proc. Natl. Acad. Sci. U. S. A. 94 (1997) 4401–4405, http://dx.doi.org/10.1073/pnas.94.9.4401.

[21] D. Sabbert, S. Engelbrecht, W. Junge, Intersubunit rotation in active F-ATPase, Nature 381 (1996) 623–625, http://dx.doi.org/10.1038/381623a0.

[22] H. Noji, R. Yasuda, M. Yoshida, K. Kinosita, Direct observation of the rotation of F1-ATPase, Nature 386 (1997) 299–302, http://dx.doi.org/10.1038/386299a0.

[23] H. Noji, M. Yoshida, The rotary machine in the cell, ATP synthase, J. Biol. Chem. 276 (2001) 1665–1668, http://dx.doi.org/10.1074/jbc.R000021200.

[24] J.P. Abrahams, A.G.W. Leslie, R. Lutter, J.E. Walker, Structure at 2.8 (angstrom) resolution of F(1)-ATPase from bovine heart mitochondria, Nature 370 (1994) 621–628.

[25] A. Dautant, J. Velours, M.F. Giraud, Crystal structure of the Mg.ADP-inhibited state of the yeast F 1c10-ATP synthase, J. Biol. Chem. 285 (2010) 29502–29510, http://dx.doi.org/10.1074/jbc.M110.124529.

[26] C. Gibbons, M.G. Montgomery, A.G. Leslie, J.E. Walker, The structure of the central stalk in bovine F(1)-ATPase at 2.4 A resolution, Nat. Struct. Biol. 7 (2000) 1055–1061, http://dx.doi.org/10.1038/80981.

[27] D. Stock, A.G. Leslie, J.E. Walker, Molecular architecture of the rotary motor in ATP synthase, Science 286 (1999) 1700–1705, http://dx.doi.org/10.1126/science.286.5445.1700.

[28] I.N. Watt, M.G. Montgomery, M.J. Runswick, A.G.W. Leslie, J.E. Walker, Bioenergetic cost of making an adenosine triphosphate molecule in animal mitochondria, Proc. Natl. Acad. Sci. U. S. A. 107 (2010) 16823–16827, http://dx.doi.org/10.1073/pnas.1011099107.

[29] I. Arnold, K. Pfeiffer, W. Neupert, R.A. Stuart, H. Schägger, Yeast mitochondrial F1F0-ATP synthase exists as a dimer: identification of three dimer-specific subunits, EMBO J. 17 (1998) 7170–7178, http://dx.doi.org/10.1093/emboj/17.24.7170.

[30] R.J. Devenish, M. Prescott, A.J.W. Rodgers, The structure and function of mitochondrial F1F0-ATP synthases, Int. Rev. Cell Mol. Biol. 267 (2008) 1–58, http://dx.doi.org/10.1016/S1937-6448(08)00601-1.

[31] J. Velours, G. Arselin, The Saccharomyces cerevisiae ATP synthase, J. Bioenerg. Biomembr. 32 (2000) 383–390 http://www.ncbi.nlm.nih.gov/pubmed/11768300.

[32] J.E. Walker, V.K. Dickson, The peripheral stalk of the mitochondrial ATP synthase, Biochim. Biophys. Acta Bioenerg. 1757 (2006) 286–296, http://dx.doi.org/10.1016/j.bbabio.2006.01.001.

[33] J. Weber, ATP synthase: subunit-subunit interactions in the stator stalk, Biochim. Biophys. Acta Bioenerg. 1757 (2006) 1162–1170, http://dx.doi.org/10.1016/j.bbabio.2006.04.007.

[34] M. Vázquez-Acevedo, F. Vega-deLuna, L. Sánchez-Vásquez, L. Colina-Tenorio, C. Remacle, P. Cardol, H. Miranda-Astudillo, D. González-Halphen, Dissecting the peripheral stalk of the mitochondrial ATP synthase of chlorophycean algae, Biochim. Biophys. Acta Bioenerg. 1857 (2015) 1183–1190, http://dx.doi.org/10.1016/j.bbabio.2016.02.003.

[35] P. Balabaskaran Nina, N.V. Dudkina, L.A. Kane, J.E. van Eyk, E.J. Boekema, M.W. Mather, A.B. Vaidya, Highly divergent mitochondrial ATP synthase complexes in *Tetrahymena thermophila*, PLoS Biol. 8 (2010) 3–6, http://dx.doi.org/10.1371/journal.pbio.1000418.

[36] A. Zíková, A. Schnaufer, R.A. Dalley, A.K. Panigrahi, K.D. Stuart, The F0F1-ATP synthase complex contains novel subunits and is essential for procyclic *Trypanosoma brucei*, PLoS Pathog. 5 (2009) e1000436, , http://dx.doi.org/10.1371/journal.ppat.1000436.

[37] E. Perez, M. Lapaille, H. Degand, L. Cilibrasi, A. Villavicencio-Queijeiro, P. Morsomme, D. González-Halphen, M.C. Field, C. Remacle, D. Baurain, P. Cardol, The mitochondrial respiratory chain of the secondary green alga Euglena gracilis shares many additional subunits with parasitic Trypanosomatidae, Mitochondrion 19 ((2014) 338–349, http://dx.doi.org/10.1016/j.mito.2014.02.001.

[38] K.N. Sathish Yadav, H.V. Miranda-Astudillo, L. Colina-Tenorio, F. Bouillenne, H. Degand, P. Morsomme, D. González-Halphen, E.J. Boekema, P. Cardol, Atypical composition and structure of the mitochondrial dimeric ATP synthase from Euglena gracilis, Biochim. Biophys. Acta Bioenerg. 1858 (2017) 267–275, http://dx.doi.org/10.1016/j.bbabio.2017.01.007.

[39] M. Allegretti, N. Klusch, D.J. Mills, J. Vonck, W. Kühlbrandt, K.M. Davies, Horizontal membrane-intrinsic α-helices in the stator a-subunit of an F-type ATP synthase, Nature 521 (2015) 237–240, http://dx.doi.org/10.1038/nature14185.

[40] A. Hahn, K. Parey, M. Bublitz, D.J. Mills, V. Zickermann, J. Vonck, W. Kühlbrandt, T. Meier, Structure of a complete ATP synthase dimer reveals the molecular basis of inner mitochondrial membrane morphology, Mol. Cell 63 (2016) 445–456, http://dx.doi.org/10.1016/j.molcel.2016.05.037.

[41] S.J. Couoh-Cardel, S. Uribe-Carvajal, S. Wilkens, J.J. García-Trejo, Structure of dimeric F1F0-ATP synthase, J. Biol. Chem. 285 (2010) 36447–36455, http://dx.doi.org/10.1074/jbc.M110.144907.

[42] A.W. Mühleip, F. Joos, C. Wigge, A.S. Frangakis, W. Kühlbrandt, K.M. Davies, Helical arrays of U-shaped ATP synthase dimers form tubular cristae in ciliate mitochondria, Proc. Natl. Acad. Sci. U. S. A. 113 (2016) 8442–8447, http://dx.doi.org/10.1073/pnas.1525430113.

[43] K.M. Davies, C. Anselmi, I. Wittig, J.D. Faraldo-Gomez, W. Kuhlbrandt, Structure of the yeast F1Fo-ATP synthase dimer and its role in shaping the mitochondrial cristae, Proc. Natl. Acad. Sci. 109 (2012) 13602–13607, http://dx.doi.org/10.1073/pnas.1204593109.

[44] N.V. Dudkina, G.T. Oostergetel, D. Lewejohann, H.P. Braun, E.J. Boekema, Row-like organization of ATP synthase in intact mitochondria determined by cryo-electron tomography, Biochim. Biophys. Acta Bioenerg. 1797 (2010) 272–277, http://dx.doi.org/10.1016/j.bbabio.2009.11.004.

[45] A.W. Mühleip, C.E. Dewar, A. Schnaufer, W. Kühlbrandt, K.M. Davies, In-Situ Structure of Trypanosomal ATP Synthase Dimer Reveals Unique Arrangement of Catalytic Subunits, PNAS, (2017), http://dx.doi.org/10.1073/pnas.1612386114.

[46] K.M. Davies, M. Strauss, B. Daum, J.H. Kief, H.D. Osiewacz, A. Rycovska, V. Zickermann, W. Kuhlbrandt, Macromolecular organization of ATP synthase and complex I in whole mitochondria, Proc. Natl. Acad. Sci. 108 (2011) 14121–14126, http://dx.doi.org/10.1073/pnas.1103621108.

[47] N.V. Dudkina, S. Sunderhaus, H.P. Braun, E.J. Boekema, Characterization of dimeric ATP synthase and cristae membrane ultrastructure from Saccharomyces and Polytomella mitochondria, FEBS Lett. 580 (2006) 3427–3432, http://dx.doi.org/10.1016/j.febslet.2006.04.097.

[48] J. Habersetzer, W. Ziani, I. Larrieu, C. Stines-Chaumeil, M.F. Giraud, D. Brèthes, A. Dautant, P. Paumard, ATP synthase oligomerization: from the enzyme models to the mitochondrial morphology, Int. J. Biochem. Cell Biol. 45 (2013) 99–105, http://dx.doi.org/10.1016/j.biocel.2012.05.017.

[49] M.F. Giraud, P. Paumard, V. Soubannier, J. Vaillier, G. Arselin, B. Salin, J. Schaeffer, D. Brèthes, J.P. Di Rago, J. Velours, Is there a relationship between the supramolecular organization of the mitochondrial ATP synthase and the formation of cristae? Biochim. Biophys. Acta Bioenerg. 1555 (2002) 174–180, http://dx.doi.org/10.1016/S0005-2728(02)00274-8.

[50] P. Paumard, G. Arselin, J. Vaillier, S. Chaignepain, K. Bathany, J.M. Schmitter, D. Brèthes, J. Velours, Two ATP synthases can be linked through subunits i in the inner mitochondrial membrane of Saccharomyces cerevisiae, Biochemistry 41 (2002) 10390–10396, http://dx.doi.org/10.1021/bi025923g.

[51] M. Strauss, G. Hofhaus, R.R. Schröder, W. Kühlbrandt, Dimer ribbons of ATP synthase shape the inner mitochondrial membrane, EMBO J. 27 (2008) 1154–1160, http://dx.doi.org/10.1038/emboj.2008.35.

[52] D. Thomas, P. Bron, T. Weimann, A. Dautant, M.-F. Giraud, P. Paumard, B. Salin, A. Cavalier, J. Velours, D. Brèthes, Supramolecular organization of the yeast F1Fo-ATP synthase, Biol. Cell. 100 (2008) 591–601, http://dx.doi.org/10.1042/

BC20080022.
[53] D. Keilin, E.F. Hartree, Activity of the cytochrome system in heart muscle preparations, Biochem. J. 41 (1947) 500–502, http://dx.doi.org/10.1042/bj0410500.
[54] E.C. Slater, Keilin, cytochrome, and the respiratory chain, J. Biol. Chem. 278 (2003) 16455–16461, http://dx.doi.org/10.1074/jbc.X200011200.
[55] C.R. Hackenbrock, B. Chazotte, S.S. Gupte, The random collision model and a critical assessment of diffusion and collision in mitochondrial electron transport, J. Bioenerg. Biomembr. 18 (1986) 331–368, http://dx.doi.org/10.1007/BF00743010.
[56] Y. Chaban, E.J. Boekema, N.V. Dudkina, Structures of mitochondrial oxidative phosphorylation supercomplexes and mechanisms for their stabilisation, Biochim. Biophys. Acta Bioenerg. 1837 (2014) 418–426, http://dx.doi.org/10.1016/j.bbabio.2013.10.004.
[57] I. Wittig, H. Schägger, Supramolecular organization of ATP synthase and respiratory chain in mitochondrial membranes, Biochim. Biophys. Acta 1787 (2009) 672–680, http://dx.doi.org/10.1016/j.bbabio.2008.12.016.
[58] D.R. Winge, Sealing the mitochondrial Respirasome, Mol. Cell. Biol. 32 (2012) 2647–2652, http://dx.doi.org/10.1128/MCB.00573-12.
[59] R. Acin-Perez, J.A. Enriquez, The function of the respiratory supercomplexes: the plasticity model, Biochim. Biophys. Acta Bioenerg. 1837 (2014) 444–450, http://dx.doi.org/10.1016/j.bbabio.2013.12.009.
[60] M.L. Genova, G. Lenaz, Functional role of mitochondrial respiratory supercomplexes, Biochim. Biophys. Acta 1837 (2014) 427–443, http://dx.doi.org/10.1016/j.bbabio.2013.11.002.
[61] A. Atteia, R. Van Lis, J. Ramírez, D. González-Halphen, Polytomella spp. growth on ethananol. Extracellular pH affects the accumulation of mitochondrial cytochrome c550, Eur. J. Biochem. 267 (2000) 2850–2858, http://dx.doi.org/10.1046/j.1432-1327.2000.01288.x.
[62] M. Vázquez-Acevedo, P. Cardol, A. Cano-Estrada, M. Lapaille, C. Remacle, D. González-Halphen, The mitochondrial ATP synthase of chlorophycean algae contains eight subunits of unknown origin involved in the formation of an atypical stator-stalk and in the dimerization of the complex, J. Bioenerg. Biomembr. 38 (2006) 271–282, http://dx.doi.org/10.1007/s10863-006-9046-x.
[63] H. Schägger, Native Gel Electrophoresis, in: G. von Jagow, H. Schägger (Eds.), A Pract. Guid. To Membr. Protein Purif, Academic Press, 1994, pp. 81–104.
[64] I. Wittig, H. Schägger, Advantages and limitations of clear-native PAGE, Proteomics 5 (2005) 4338–4346, http://dx.doi.org/10.1002/pmic.200500081.
[65] H. Schägger, Denaturing Electrophoretic Techniques, in: G. von Jagow, H. Schägger (Eds.), A Pract. Guid. to Membr. Protein Purif, Academic Press, 1994, pp. 59–79.
[66] S. Guerrero-Castillo, M. Vázquez-Acevedo, D. González-Halphen, S. Uribe-Carvajal, In *Yarrowia lipolytica* mitochondria, the alternative NADH dehydrogenase interacts specifically with the cytochrome complexes of the classic respiratory pathway, Biochim. Biophys. Acta Bioenerg. 1787 (2009) 75–85, http://dx.doi.org/10.1016/j.bbabio.2008.10.008.
[67] I. Wittig, M. Karas, H. Schägger, High resolution clear native electrophoresis for in-gel functional assays and fluorescence studies of membrane protein complexes, Mol. Cell. Proteomics 6 (2007) 1215–1225, http://dx.doi.org/10.1074/mcp.M700076-MCP200.
[68] A. Villavicencio-Queijeiro, M. Vázquez-Acevedo, A. Cano-Estrada, M. Zarco-Zavala, M. Tuena De Gómez, J.A. Mignaco, M.M. Freire, H.M. Scofano, D. Foguel, P. Cardol, C. Remacle, D. González-Halphen, The fully-active and structurally-stable form of the mitochondrial ATP synthase of Polytomella sp. is dimeric, J. Bioenerg. Biomembr. 41 (2009) 1–13, http://dx.doi.org/10.1007/s10863-009-9203-0.
[69] P. Cardol, F. Figueroa, C. Remacle, L.-G. Franzén, D. González-Halphen, Chapter 13 – Oxidative Phosphorylation: Building Blocks and Related Components, Chlamydomonas Sourceb, 2009, pp. 469–502, , http://dx.doi.org/10.1016/B978-0-12-370873-1.00021-6.
[70] R. van Lis, D. González-Halphen, A. Atteia, Divergence of the mitochondrial electron transport chains from the green alga *Chlamydomonas reinhardtii* and its colorless close relative Polytomella sp, Biochim. Biophys. Acta Bioenerg. 1708 (2005) 23–34, http://dx.doi.org/10.1016/j.bbabio.2004.12.010.
[71] R. van Lis, A. Atteia, G. Mendoza-hernández, D. González-halphen, Identification of novel mitochondrial protein components of Chlamydomonas reinhardtii. A proteomic approach, Plant Physiol. 132 (2003) 318–330, http://dx.doi.org/10.1104/pp.102.018325.proteins.
[72] P. Paumard, J. Vaillier, B. Coulary, J. Schaeffer, V. Soubannier, D.M. Mueller, D. Brèthes, J.P. Di Rago, J. Velours, The ATP synthase is involved in generating mitochondrial cristae morphology, EMBO J. 21 (2002) 221–230, http://dx.doi.org/10.1093/emboj/21.3.221.
[73] R. van Lis, G. Mendoza-Hernández, G. Groth, A. Atteia, New insights into the unique structure of the F0F1-ATP synthase from the chlamydomonad algae Polytomella sp. and *Chlamydomonas reinhardtii*, Plant Physiol. 144 (2007) 1190–1199, http://dx.doi.org/10.1104/pp.106.094060.
[74] I. Wittig, H.-P. Braun, H. Schägger, Blue native PAGE, Nat. Protoc. 1 (2006) 418–428, http://dx.doi.org/10.1038/nprot.2006.62.
[75] J.L. Rubinstein, V.K. Dickson, M.J. Runswick, J.E. Walker, ATP synthase from Saccharomyces cerevisiae: location of subunit h in the peripheral stalk region, J. Mol. Biol. 345 (2005) 513–520, http://dx.doi.org/10.1016/j.jmb.2004.10.060.
[76] J.L. Rubinstein, J.E. Walker, R. Henderson, Structure of the mitochondrial ATP synthase by electron cryomicroscopy, EMBO J. 22 (2003) 6182–6192, http://dx.doi.org/10.1093/emboj/cdg608.
[77] M. Lapaille, A. Escobar-Ramírez, H. Degand, D. Baurain, E. Rodríguez-Salinas, N. Coosemans, M. Boutry, D. Gonzalez-Halphen, C. Remacle, P. Cardol, Atypical subunit composition of the chlorophycean mitochondrial F 1FO-ATP synthase and role of asa7 protein in stability and oligomycin resistance of the enzyme, Mol. Biol. Evol. 27 (2010) 1630–1644, http://dx.doi.org/10.1093/molbev/msq049.
[78] P. Cardol, D. González-Halphen, A. Reyes-Prieto, D. Baurain, R.F. Matagne, C. Remacle, The mitochondrial oxidative phosphorylation proteome of Chlamydomonas reinhardtii deduced from the genome sequencing project, Plant Physiol. 137 (2005) 447–459, http://dx.doi.org/10.1104/pp.104.054148.
[79] A. Cano-Estrada, M. Vázquez-Acevedo, A. Villavicencio-Queijeiro, F. Figueroa-Martínez, H. Miranda-Astudillo, Y. Cordeiro, J.A. Mignaco, D. Foguel, P. Cardol, M. Lapaille, C. Remacle, S. Wilkens, D. González-Halphen, Subunit-subunit interactions and overall topology of the dimeric mitochondrial ATP synthase of Polytomella sp, Biochim. Biophys. Acta Bioenerg. 2010 (1797), http://dx.doi.org/10.1016/j.bbabio.2010.02.024.
[80] L. Colina-Tenorio, H. Miranda-Astudillo, A. Cano-Estrada, M. Vázquez-Acevedo, P. Cardol, C. Remacle, D. González-Halphen, Subunit Asa1 spans all the peripheral stalk of the mitochondrial ATP synthase of the chlorophycean alga Polytomella sp, Biochim. Biophys. Acta Bioenerg. 1857 (2016) 359–369, http://dx.doi.org/10.1016/j.bbabio.2015.11.012.
[81] H. Miranda-Astudillo, A. Cano-Estrada, M. Vázquez-Acevedo, L. Colina-Tenorio, A. Downie-Velasco, P. Cardol, C. Remacle, L. Domínguez-Ramírez, D. González-Halphen, Interactions of subunits Asa2, Asa4 and Asa7 in the peripheral stalk of the mitochondrial ATP synthase of the chlorophycean alga Polytomella sp, Biochim. Biophys. Acta Bioenerg. 1837 (2014) 1–13, http://dx.doi.org/10.1016/j.bbabio.2013.08.001.
[82] L. Sánchez-Vásquez, M. Vázquez-Acevedo, J. de la Mora, F. Vega-deLuna, P. Cardol, C. Remacle, G. Dreyfus, D. González-Halphen, Near-neighbor interactions of the membrane-embedded subunits of the mitochondrial ATP synthase of a chlorophycean alga, Biochim. Biophys. Acta Bioenerg. 1858 (2017) 497–509, http://dx.doi.org/10.1016/j.bbabio.2017.04.004.
[83] S. Brunner, V. Everard-Gigot, R.A. Stuart, Su e of the yeast F1F0-ATP synthase forms homodimers, J. Biol. Chem. 277 (2002) 48484–48489, http://dx.doi.org/10.1074/jbc.M209382200.
[84] V. Everard-gigot, C.D. Dunn, B.M. Dolan, S. Brunner, R.E. Jensen, A. Rosemary, R.A. Stuart, Functional Analysis of Subunit e of the F 1 F o -ATP Synthase of the Yeast Saccharomyces cerevisiae: Importance of the N-Terminal Membrane Anchor Region, Eukaryot. Cell 4 (2005) 346–355, http://dx.doi.org/10.1128/EC.4.2.346.
[85] T.G. Frey, C.A. Mannella, The internal structure of mitochondria, Trends Biochem. Sci. 4 (2000) 1–6, http://dx.doi.org/10.1016/S0968-0004(00)01609-1.
[86] C.A. Mannella, Introduction: our changing views of mitochondria, J. Bioenerg. Biomembr. 32 (2000) 1–4, http://dx.doi.org/10.1023/A:1005562109678.
[87] M. Ghochani, J.D. Nulton, P. Salamon, T.G. Frey, A. Rabinovitch, A.R.C. Baljon, Tensile forces and shape entropy explain observed crista structure in mitochondria, Biophys. J. 99 (2010) 3244–3254, http://dx.doi.org/10.1016/j.bpj.2010.09.038.
[88] N.V. Dudkina, R. Kouřil, J.B. Bultema, E.J. Boekema, Imaging of organelles by electron microscopy reveals protein-protein interactions in mitochondria and chloroplasts, FEBS Lett. 584 (2010) 2510–2515, http://dx.doi.org/10.1016/j.febslet.2010.03.027.
[89] N.V. Dudkina, R. Kouril, K. Peters, H.P. Braun, E.J. Boekema, Structure and function of mitochondrial supercomplexes, Biochim. Biophys. Acta Bioenerg. 1797 (2010) 664–670, http://dx.doi.org/10.1016/j.bbabio.2009.12.013.
[90] H. Schägger, K. Pfeiffer, Supercomplexes in the respiratory chains of yeast and mammalian mitochondria, EMBO J. 19 (2000) 1777–1783, http://dx.doi.org/10.1093/emboj/19.8.1777.
[91] H. Schägger, R. De Coo, M.F. Bauer, S. Hofmann, C. Godino, U. Brandt, Significance of respirasomes for the assembly/stability of human respiratory chain complex I, J. Biol. Chem. 279 (2004) 36349–36353, http://dx.doi.org/10.1074/jbc.M404033200.
[92] J.N. Blaza, R. Serreli, A.J.Y. Jones, K. Mohammed, J. Hirst, Kinetic evidence against partitioning of the ubiquinone pool and the catalytic relevance of respiratory-chain supercomplexes, Proc. Natl. Acad. Sci. 111 (2014) 15735–15740, http://dx.doi.org/10.1073/pnas.1413855111.
[93] N.V. Dudkina, J. Heinemeyer, S. Sunderhaus, E.J. Boekema, H.P. Braun, Respiratory chain supercomplexes in the plant mitochondrial membrane, Trends Plant Sci. 11 (2006) 232–240, http://dx.doi.org/10.1016/j.tplants.2006.03.007.
[94] J.A. Enríquez, Supramolecular organization of respiratory complexes, Annu. Rev. Physiol. 78 (2016) 533–561, http://dx.doi.org/10.1146/annurev-physiol-021115-105031.
[95] H. Schägger, Respiratory chain supercomplexes of mitochondria and bacteria, Biochim. Biophys. Acta Bioenerg. 1555 (2002) 154–159, http://dx.doi.org/10.1016/S0005-2728(02)00271-2.
[96] I. Wittig, R. Carrozzo, F.M. Santorelli, H. Schägger, Supercomplexes and subcomplexes of mitochondrial oxidative phosphorylation, Biochim. Biophys. Acta Bioenerg. 1757 (2006) 1066–1072, http://dx.doi.org/10.1016/j.bbabio.2006.05.006.
[97] T. Althoff, D.J. Mills, J.-L. Popot, W. Kühlbrandt, Arrangement of electron transport chain components in bovine mitochondrial supercomplex I $_1$ III $_2$ IV $_1$, EMBO J. 30 (2011) 4652–4664, http://dx.doi.org/10.1038/emboj.2011.324.
[98] N.V. Dudkina, M. Kudryashev, H. Stahlberg, E.J. Boekema, Interaction of complexes I, III, and IV within the bovine respirasome by single particle cryoelectron tomography, Proc. Natl. Acad. Sci. U. S. A. 108 (2011) 15196–15200, http://dx.doi.org/10.1073/pnas.1107819108.
[99] E. Schäfer, H. Seelert, N.H. Reifschneider, F. Krause, N.A. Dencher, J. Vonck, Architecture of active mammalian respiratory chain supercomplexes, J. Biol. Chem. 281 (2006) 15370–15375, http://dx.doi.org/10.1074/jbc.M513525200.
[100] J. Gu, M. Wu, R. Guo, K. Yan, J. Lei, N. Gao, M. Yang, The architecture of the

mammalian respirasome, Nature 537 (2016) 1–16, http://dx.doi.org/10.1038/nature19359.
[101] J.A. Letts, K. Fiedorczuk, L.A. Sazanov, The architecture of respiratory supercomplexes, Nature 537 (2016) 644–648, http://dx.doi.org/10.1038/nature19774.
[102] J.S. Sousa, D.J. Mills, J. Vonck, W. Kühlbrandt, Functional asymmetry and electron flow in the bovine respirasome, elife 5 (2016) 1–17, http://dx.doi.org/10.7554/eLife.21290.
[103] M. Wu, J. Gu, R. Guo, Y. Huang, M. Yang, Structure of mammalian respiratory supercomplex I1III2IV1, Cell 167 (2016) 1598–1609 e10 https://doi.org/10.1016/j.cell.2016.11.012.
[104] E. Lapuente-Brun, R. Moreno-Loshuertos, R. Acin-Perez, A. Latorre-Pellicer, C. Colas, E. Balsa, E. Perales-Clemente, P.M. Quiros, E. Calvo, M.A. Rodriguez-Hernandez, P. Navas, R. Cruz, A. Carracedo, C. Lopez-Otin, A. Perez-Martos, P. Fernandez-Silva, E. Fernandez-Vizarra, J.A. Enriquez, Supercomplex assembly determines electron flux in the mitochondrial electron transport chain, Science 340 (2013) 1567–1570 (80-.), https://doi.org/10.1126/science.1230381.
[105] A. Atteia, R. Van Lis, G. Mendoza-Hernández, K. Henze, W. Martin, H. Riveros-Rosas, D. González-Halphen, Bifunctional aldehyde/alcohol dehydrogenase (ADHE) in chlorophyte algal mitochondria, Plant Mol. Biol. 53 (2003) 175–188, http://dx.doi.org/10.1023/B:PLAN.0000009274.19340.36.

11.4 Anexo 4: Artículo sometido a revisión

The peripheral stalk of rotary ATPases

Lilia Colina-Tenorio[1], Alain DAUTANT[2], Héctor Miranda-Astudillo[3], Marie-France Giraud[2], Diego Gonzalez Halphen[1*]

[1]Instituto de Fisiología Celular (IFC), Mexico, [2]Université de Bordeaux, France, [3]University of Liège, Belgium

Submitted to Journal:
Frontiers in Physiology

Specialty Section:
Mitochondrial Research

Article type:
Review Article

Manuscript ID:
391773

Received on:
30 Apr 2018

Frontiers website link:
www.frontiersin.org

Conflict of interest statement

The authors declare that the research was conducted in the absence of any commercial or financial relationships that could be construed as a potential conflict of interest

Author contribution statement

LC and DG conceptualization; LC and DG writing the original draft; LC, AD, HM and MG formal analysis; AD, HM and MG reviewing and editing; MG and DG project administration; MG and DG funding acquisition.

Keywords

peripheral stalk, ATP synthase, coiled-coils, Archaea, Bacteria, Mitochondria, chloroplast

Abstract

Word count: 160

Rotary ATPases are a family of enzymes that are thought of as molecular nanomotors and are classified in three types: F, A and V-type ATPases. Two members (F and A-type) can synthesize and hydrolyze ATP, depending on the energetic needs of the cell, while the V-type enzyme exhibits only a hydrolytic activity. The overall architecture of all these enzymes is conserved and three main sectors are distinguished: a catalytic core, a rotor and a stator or peripheral stalk. The peripheral stalks of the A and V-types are highly conserved in both structure and function, however, the F-type peripheral stalks have divergent structures. Furthermore, the peripheral stalk has other roles beyond its stator function, as evidenced by several biochemical and recent structural studies. This review describes the information regarding the organization of the peripheral stalk components of F, A and V-ATPases, highlighting the key differences between the studied enzymes, as well as the different processes in which the structure is involved.

Funding statement

DG and MG acknowledge financial support from 279125 Grant ECOS Nord-ANUIES-CONACyT, and further support for DG from grants 239219 (Fondo SEP-CONACYT) CONACyT and IN208917 (PAPIIT-DGAPA-UNAM).

The peripheral stalk of rotary ATPases

Lilia Colina-Tenorio[1], Alain Dautant[2-3], Héctor Miranda-Astudillo[4], Marie-France Giraud[2-3] and Diego González-Halphen[1*]

[1] Departamento de Genética Molecular, Instituto de Fisiología Celular, Universidad Nacional Autónoma de México, Mexico

[2] CNRS, UMR5095, IBGC, 1 rue Camille Saint-Saëns, 33077 Bordeaux, France

[3] Université de Bordeaux, Campus Carreire, 146 rue Léo Saignat, 33077 Bordeaux, France

[4] Genetics and Physiology of microalgae, InBioS/Phytosystems, University of Liège, Belgium

[*]**To whom correspondence should be adressed:**
Departamento de Genética Molecular, Instituto de Fisiología Celular, Universidad Nacional Autónoma de México, Mexico. Email: dhalphen@ifc.unam.mx

Keywords: peripheral stalk, ATP synthase, coiled-coils, archaea, bacteria, mitochondria, chloroplast

Abstract

Rotary ATPases are a family of enzymes that are thought of as molecular nanomotors and are classified in three types: F, A and V-type ATPases. Two members (F and A-type) can synthesize and hydrolyze ATP, depending on the energetic needs of the cell, while the V-type enzyme exhibits only a hydrolytic activity. The overall architecture of all these enzymes is conserved and three main sectors are distinguished: a catalytic core, a rotor and a stator or peripheral stalk. The peripheral stalks of the A and V-types are highly conserved in both structure and function, however, the F-type peripheral stalks have divergent structures. Furthermore, the peripheral stalk has other roles beyond its stator function, as evidenced by several biochemical and recent structural studies. This review describes the information regarding the organization of the peripheral stalk components of F, A and V-ATPases, highlighting the key differences between the studied enzymes, as well as the different processes in which the structure is involved.

1. Introduction

ATP, a key molecule synthesized by ATP synthases, is instrumental for the metabolism of every living organism (Müller and Grüber, 2003). ATP synthases belong to a family of enzymes known as rotary ATP synthases, which are multiprotein enzymatic complexes embedded in cellular and organellar membranes of all organisms across the three life domains. These enzymes work as nanomotors to synthesize or hydrolyze ATP, and they have been classified in three types: F, V and A-type ATPases.

F-type ATPases are found in the bacterial plasma membrane, in the inner mitochondrial membrane and in the thylakoid membrane of chloroplasts. F-type enzymes use an electrochemical proton gradient to synthesize ATP, according to the basic mechanism proposed by Peter Mitchell in his chemiosmotic theory (Mitchell, 1961). These enzymes, in certain physiological conditions, can function in reverse and hydrolyze ATP to restore the membrane potential (D'Alessandro and Melandri, 2010). V-type ATPases were first purified from vacuoles, hence their name, and work as proton pumps dependent on ATP hydrolysis, which is why they are also known as H^+-ATPases

(Forgac, 2007). A-type ATPases are found in archaea and can function either synthesizing or hydrolyzing ATP (Grüber et al., 2014). The feature all rotary ATPases share is the capacity to couple a membrane domain (the proton channel) with a soluble catalytic domain. Among other things, this coupling is possible because of the structure known as peripheral arm or peripheral stalk, which works as the stator of a motor and whose main role is to counteract the rotation tendency of the catalytic core that happens in response to the movement of the rotor (Walker and Dickson, 2006).

The most widely accepted hypothesis about the origin of rotary ATPases states that they evolved from a common ancestor, which gave rise to the three types of enzymes. Initially, it was proposed that they had at least two transitions in their evolutionary history: the first was the transition from a proton pump to an ATP synthase driven by protons, and the second was the return to a proton pump (Cross and Taiz, 1990). Later, a third transition back to an ATP synthase was proposed, in which there was a gain in function, unlike the first two transitions (Cross and Müller, 2004). It is currently considered that the last universal common ancestor (LUCA) was in all likelihood a chemiosmotic organism with an ATP synthase in its membrane (Mulkidjanian et al., 2007). A-type ATPases are more closely related to V-type ATPases, although the latter cannot synthesize ATP in physiological conditions; it can thus be said that A-type ATPases are more similar to F-type ATPases in terms of mechanism and structure (Forgac, 2007). Given the common origin of A and V-type ATPases, their catalytic subunits and their rotor subunits share 50% identity, while A and F-type ATPases share 25% identity (Müller and Grüber, 2003). On the contrary, the subunits of the peripheral stalk are considerably less conserved, vary from one organism to the next, and no significant identity has been found among them (Muench et al., 2011).

In terms of structure, the three types of ATPases are built in a similar way: a membrane domain (classically known as F_O, V_O, A_O, or R_O to refer to this domain in general) that includes the proton channel; and a soluble domain (classically known as F_1, V_1, A_1, or R_1 to refer to this domain in general) that includes: the catalytic core, the central stalk, which communicates the activity in the proton channel with the catalytic core (Grüber et al., 2014; Qi et al., 2007; Wächter et al., 2011), and one or more peripheral stalks. The number of peripheral stalks has been used to categorize rotary ATPases (Stewart et al., 2013): F-ATPases have one (Figure 1A), A-ATPases have two (Figure 1B) and V-ATPases have three (Figure 1C). Although peripheral stalks have a similar function in all the enzymes, their composition and topology vary.

2. The peripheral stalk

2.1 The structure of the peripheral stalk

As stated above, the peripheral stalk of rotary ATPases works as a stator and mediates the association of the two domains of the enzyme. It is the most divergent component in both sequence and subunit composition, and many roles have been attributed to this structure throughout its study. There are currently high resolution structures of the three types of rotary ATPases from model organisms: bovine (Zhou et al., 2015), yeast (Guo et al., 2017; Hahn et al., 2016; Srivastava et al., 2018; Zhao et al., 2015) and bacteria (Morales-Rios et al., 2015; Sobti et al., 2016), and of their peripheral stalks (Dickson et al., 2006; Oot et al., 2012; Stewart et al., 2012). These structures have shown that, in spite of the lack of sequence homology, the overall architecture of the peripheral stalk is similar in these enzymes (Figure 2).

The peripheral stalk is formed by elongated proteins with alpha helical structures, and their interactions are mediated by coiled coil motifs (Stewart et al., 2013). Coiled coils are a common structural arrangement that is usually adopted by helical proteins, both fibrous and globular, and results from a particular alternate pattern of hydrophobic and hydrophilic amino acid residues in the

sequence of the protein (Lupas, 1996). A coiled coil arrangement can be formed by the association of up to five or more helices in the same orientations (parallel) or in opposite orientations (antiparallel); these helices can belong to the same chain, to different chains, or be consecutive helices of the same polypeptide chain (Lupas and Gruber, 2005). The coiled coil was first described in 1953 by Francis Crick (Crick, 1953), and it has been estimated that approximately 3-5% of all the amino acid residues in proteins can form this kind of structure (Mason and Arndt, 2004).

Three characteristics distinguish coiled coils from other amphipathic helices: i) the periodicity of the hydrophobic residues (3.5 in coiled coils, 3.65 in other helices), ii) the length of the helices (Su et al., 1994) and iii) the packing interactions of the lateral chains. In coiled coils, distinctively, each residue of one helix fits in a space surrounded by two or four residues of the adjacent helix. This type of packing has been called "knobs into holes" or "in register packing" (Lupas, 1996). The amino acids of the pattern that gives rise to coiled coils are essential to maintain the structure of individual helices (through intramolecular interactions), as well as to promote specific interactions between more helices (through intermolecular interactions) (Mason and Arndt, 2004) (Figure 3C).

When the coiling of the helices is left-handed, it is the result of repetitive motifs in the sequence of the protein known as "heptad repeats". Heptad repeats are a seven-residue pattern with an *abcdefg* composition, in which *ad* correspond to hydrophobic residues and *eg* to charged residues (Lupas, 1996). The nature of the residues in positions *ad*, as well as their equivalents in longer patterns, determines the number of chains involved in the formation of one functional unit of coiled coils, as was revealed by the study of the leucine zipper of the yeast transcription factor GCN4 (O'Shea et al., 1991). When the coiling of the helices is right-handed, it can be the result of either "hendecad repeat" motifs, which are eleven-residue patterns with an *abcdefghijk* composition, in which *adeh* correspond to hydrophobic residues; or of quindecad repeats (Stewart et al., 2013) (Figure 3D).

The so called "peptide velcro hypothesis" (Mason and Arndt, 2004) explains the need for the above described elements in three points: i) *ad* positions must be hydrophobic to stabilize dimerization through hydrophobic effect and van der Waals interactions, ii) *eg* positions must be charged to allow for interhelical electrostatic interactions, and iii) *bcf* positions must be hydrophilic because they form helical surfaces that will be exposed to the solvent. Inside all of these motifs there can be one or more discontinuities known as stutters or stammers that contribute to the final arrangement of the structure, and influence the size, number of chains, polarity of the helices and handedness of the coiling (Parry et al., 2008). The distance required by a coiled coil (a super helix) to complete a full turn is known as pitch length, and the angle that each helix maintains with respect to the axis of the super helix is known as pitch angle (Figure 3A) (Lupas, 1996). The pitch length of a super helix that results from hendecad repeats can be from 80 to over 130 nm, and the helices that form the super helix are almost completely parallel (Parry et al., 2008) (Figure 3B).

Hendecad repeat patterns were first described in the subunits of the peripheral stalk of the F-ATPase from *Escherichia coli*, along with the prediction of a right-handed coiling of their helices (Del Rizzo et al., 2002). The proteins that construct the peripheral stalk of rotary ATPases have to cover a distance of more than 100 Å from the membrane to the apex of the enzyme, and in order to achieve this, most of these proteins have adopted long coiled coil structures (Stewart et al., 2013). It should be noted that the most common type of coiling is the left-handed coiling (the proteins that make up the exposed part of the rotor of ATPases also adopt a coiled coil structure, but with a left-handed coiling), which is why the right-handed coiling of the peripheral stalk proteins was initially considered unusual (Stewart et al., 2013, 2014).

2.2 The peripheral stalk of F-ATPases

The simplest known version of the F-type ATPase is the bacterial enzyme: subunits $\alpha_3\beta_3$ of the catalytic core, subunits γ and ε of the rotor, subunits *a* and *c* forming the proton channel and a b_2 dimer forming the peripheral stalk with subunit δ (Weber, 2006) (Figure 4A). In contrast with the peripheral stalk of A and V-type ATPases which is formed by heterodimers, the peripheral stalk of F-ATPases varies considerably in its subunit composition, from two subunits in *E. coli* (Dunn et al., 2000) to nine subunits in organisms like chlorophycean algae (Cano-Estrada et al., 2010; Vázquez-Acevedo et al., 2006).

The peripheral stalk of the enzyme from *E. coli* has been divided in four domains: i) the N-terminal domain that crosses the membrane and interacts with subunit *a* (Dmitriev et al., 1999; Stalz et al., 2003), ii) the binding domain, iii) the dimerization domain, and iv) the C-terminal domain, through which it interacts with subunit δ (known as subunit OSCP in eukaryotic enzymes) (McLachlin et al., 1998) (Figure 4B). Subunit δ/OSCP interacts with subunit α of the catalytic core at the top of the enzyme (Carbajo et al., 2007; Rubinstein and Walker, 2002). It has been determined that the interaction OSCP-α is strong enough to resist the torque generated by the movement of the rotor (Weber et al., 2004). The b_2 dimer associates via a right-handed coiled coil due to the presence of a conserved hendecad repeat in both *b* subunits of *E. coli* (Figure 4C), as well as in those from other prokaryotic organisms (Del Rizzo et al., 2002). The study of chimeras of subunit *b* has shown that it has functional tolerance as long as the residues involved in the dimerization are substituted by others that fit the hendecad repeat pattern and the resulting helices have a right-handed coiling; left-handed coiling results in a lack of oxidative phosphorylation (Bi et al., 2008).

Subunit *b* of *E. coli* has been studied extensively, and this has derived in a better understanding of the structure and function of this protein and, consequently, of the peripheral stalk. Small-angle X-ray scattering studies revealed that the dimerization domain is limited to residues 62-122, and that this part of the protein in solution forms an extended dimer of approximately 95 Å (Del Rizzo et al., 2002) (Figure 4B). Mutations in the dimerization domain result in an assembled enzyme but a lack of oxidative phosphorylation (Cipriano et al., 2006). This observation suggests that the peripheral stalk of the ATPase from *E. coli* has a role beyond that of joining F_O with F_1, for which the correct interaction of the dimer subunits is necessary (Del Rizzo et al., 2006). This possibility has also been explored in the F-ATPase of yeast, in which mutations in the transmembrane segment of subunit 4 (*b*) of the peripheral stalk impact the coupling of proton translocation with catalysis (Razaka-Jolly et al., 1994).

It has been proposed that each *b* subunit has a different role in the enzyme, given by the interactions each one establishes. The ATP synthase is an asymmetric enzyme due to the stoichiometry of its subunits, subunit *b* is the only one present in two copies and so the interactions of it with each monomer cannot be the same. Accordingly, it has been proved that the b_2 dimer is intrinsically asymmetric and that the arrangement of its helices is not "in register" but tends to be "offset" (Claggett et al., 2009; Del Rizzo et al., 2006). This topology has two important consequences: one of the helices of the dimer is skewed towards the N-terminus (b_N) and the other towards the C-terminus (b_C), so the residues occupying these positions are in different microenvironments, thus confirming that the interactions of each subunit *b* are different (Wood and Dunn, 2007).

The study of the individual interactions of each *b* subunit has been approached with crosslinking experiments (Brandt et al., 2013; Deleon-Rangel et al., 2013). It was found that the C-terminus of one of the subunits (b_I) is the part involved in the interaction with δ (Figure 4B). This b_I subunit is the closest to subunit α and is in contact with subunit *a* in the membrane. The other *b* subunit (b_{II}) was found in close proximity to subunit β. Taken together, these results confirm the asymmetric nature of the dimer and demonstrate that each monomer has a different role and position in the

enzyme (Brandt et al., 2013). This asymmetry was further confirmed with the high resolution structures obtained for the *E. coli* enzyme, which show the peripheral stalk contacts alternatively the three α subunits via their N-terminal helices but in a clearly asymmetrical fashion, using a different interface for each of them (Sobti et al., 2016) (Figure 4A).

The peripheral stalk of the F-ATPase of mammals and yeast shares the same subunit composition, with the exception of subunit *h* of yeast, which only has a 20% similarity with its bovine equivalent, F6 (Fujikawa et al., 2015; Velours et al., 2001), but the latter is sufficient to substitute the absence of subunit *h*, as shown by complementation experiments in *S. cerevisiae* (Velours et al., 2001). As is the case in the bacterial enzyme, the C-terminal end of the eukaryotic subunit *b* interacts with the C-terminal end of OSCP (Hahn et al., 2016; Rees et al., 2009; Rubinstein and Walker, 2002). In the bovine enzyme, the exposed part of subunit *b* maintains interactions with subunits *d* and F6, all mediated by coiled coils, which result in an extensive and stable interaction between subunits OSCP-*b*-F6 that spans the complete length of the peripheral stalk, as shown by the crystallographic structure of the soluble section of the enzyme (Rees et al., 2009) (see Figures 2 and 9D). The structure of the *S. cerevisiae* enzyme (at 3.6 Å) shows that subunit F6 has an additional helix, not present in its mammalian equivalent, that is involved in interactions with subunits *b* and *d* (Srivastava et al., 2018) (Figure 4E).

A high resolution structure of the dimeric enzyme of the yeast *Yarrowia lipolytica* was obtained from X-ray diffraction data (3.5 Å) and cryo-electron microscopy images (6.2 Å) (Hahn et al., 2016). The sections obtained with the best resolution were both the exposed and the transmembrane parts of the peripheral stalk. This model showed contacts that had not been described previously, such as the interaction of the N-terminal end of subunit α with subunits *b*, *h* and the N-terminal end of OSCP, all of which define the union of F_1 with the peripheral stalk. The structure of the *S. cerevisiae* enzyme shows that the N terminus of each α subunit interacts with subunit OSCP, thus securely anchoring it to the top of F_1. Furthermore, a helix from one of the α subunits (the one known as α_{TP}) contacts helices from subunits *b*, *d* and F6 (Srivastava et al., 2018) (Figure 4D).

As for the contacts between subunits of the peripheral stalk and subunits located in the membrane section of the enzyme, crosslinking experiments with the bovine enzyme showed that the membrane subunit A6L (also called ATP8 in mammals and 8 in yeast) is in close proximity to subunits *b*, *d* and F6 through its C-terminus, which extends 70 Å from the membrane to reach the peripheral stalk (Lee et al., 2015) . The C-terminal region of subunit 8 in yeast has interactions with subunits *b* and *h* (Stephens et al., 2003). It has been proposed that subunit A6L/8 derived from one of the bacterial *b* subunits and is truncated in mammals and yeast, since there are four conserved residues (MQPL) in their N-terminal region (Hahn et al., 2016). Recently, He and collaborators have suggested that subunits 6.8PL and DAPIT of the mammalian enzyme are functional orthologs of yeast subunits *i*/*j* and *k*, respectively, which would mean that the yeast and human enzymes can be considered identical in composition (He et al., 2018). Subunit *f* is located in the F_O section in the bovine and yeast enzymes (Collinson et al., 1994; Spannagel et al., 1997), and has been found to interact with subunit *b* by crosslinking experiments (Spannagel et al., 1998). Finally, as in the bacterial enzyme, the base of the peripheral stalk of the enzyme of bovine and yeast contacts the F_O section by a *b*-*a* interaction (Spannagel et al., 1998), which has been confirmed with the high resolution structures obtained to date (Baker et al., 2012; Guo et al., 2017; Hahn et al., 2016; Sobti et al., 2016; Srivastava et al., 2018; Zhou et al., 2015) (Figure 4D and 4E, see also Figures 2A and 9D). Recently, the analysis of auto-inhibited *E. coli* F-ATPase structures obtained by cryo-electron microscopy revealed that the peripheral stalk spans almost the entire complex (212 of 232 Å) (Sobti et al., 2016). These structures showed, for the first time for an F-ATPase, the complete homodimeric coiled coil structure with the N-terminus of the *b* subunits bifurcating closely above the membrane to then separate in two helices within the membrane which contact subunit *a* from two sides (Figure 4A and 4B). A recent high resolution structure of the yeast ATPase (at 3.6 Å)

obtained by cryo-electron microscopy has shown the arrangement of the membrane section of the peripheral stalk (Guo et al., 2017). In this structure, subunit *b* is shown to have one transmembrane helix that forms a domain with subunits *e* and *g* and that this domain is connected to its second transmembrane helix by a loop. Subunits *f* and *h* both interact with the peripheral stalk and are thus considered part of this structure: the N-terminal portion of subunit *f* contacts the exposed part of subunit *b*, and subunit 8 has a transmembrane helix in contact with one of the helices of subunit *a* and its C-terminal portion contributes to the formation of the base of the peripheral stalk. Finally, the C-terminal part of subunit *d*, which had not been resolved in previous structures, wraps around subunits 8 and *b* at the base of the peripheral stalk (Guo et al., 2017) Figure 4E and 4F.

In contrast with the F-ATPases described so far, the mitochondrial enzyme of chlorophycean algae such as *Chlamydomonas reinhardtii* and *Polytomella* sp. has several striking features, one of which is the presence of a robust peripheral stalk formed by nine subunits named Asa (ATP Synthase Associated) (Cano-Estrada et al., 2010; van Lis et al., 2007; Vázquez-Acevedo et al., 2006), some of which (Asa6 and Asa9) are involved in the dimerization of the enzyme (Cano-Estrada et al., 2010; Lapaille et al., 2010; Sánchez-Vásquez et al., 2017; Villavicencio-Queijeiro et al., 2009). This enzyme has no clear homologs for any of the subunits that typically form the peripheral stalk, however, some equivalent interactions have been found: subunit Asa1 contacts the C-terminal end of subunit OSCP, which is reminiscent of the *b*-OSCP interaction in the other F-ATPases (Colina-Tenorio et al., 2016). Some of the Asa subunits (Asa1, Asa2, Asa4 and Asa7) are predicted to adopt coiled coil structures (Miranda-Astudillo et al., 2014), which is consistent with the nature of subunits *b* in other F-ATPases and subunits E and G of the peripheral stalk of A and V-type ATPases. Recently, an Asa6-*a* interaction was shown in a three dimensional map generated with cryo-electron microscopy, and it was found that subunit Asa6 has a V-shape similar to that of the N-terminal part (transmembrane) of subunit *b* (Klusch et al., 2017). Although a structural map obtained by cryo-electron microscopy for the *Polytomella* enzyme is available at 7 Å resolution (Allegretti et al., 2015) there is currently no high resolution data to distinguish structural details of the Asa subunits in the peripheral stalk, nevertheless, numerous biochemical studies have established several near-neighbor relationships between the Asa subunits and other constituents of the peripheral stalk. Thus, based on the low resolution map available and the biochemical evidence, a model depicting a possible location of the different subunits can be inferred (Figure 5).

Recently, a convenient new separation of ATP synthase complexes was put forward by Mühleip and colleagues that distinguishes the metazoan-type dimers from the protozoan dimers or those from unicellular algae, the latter included in the protozoan-type. This separation came about when some striking differences became evident with high resolution structures, although the biochemical and genetic evidence, as well as low resolution images, much preceded these structures. Metazoan and protozoan-type dimers differ by both the structure of their peripheral stalks and by their dimeric interface (Mühleip et al., 2017). Other examples of protozoan-type dimers include the F-ATPases from *Trypanosoma brucei* (Zíková et al., 2009), *Tetrahymena thermophila* (Balabaskaran Nina et al., 2010), *Paramecium tetraurelia* (Mühleip et al., 2016) and *Euglena gracilis* (Yadav et al., 2017), all of which have atypical features (Figure 6). As described above, the general architecture of the mammalian, yeast and bacterial enzymes (metazoan-type) is essentially the same, and all of their subunits share homology, whereas so far no homologs for subunits of protozoan-type dimers have been identified and their peripheral stalk structures are highly divergent. It should be noted that the bacterial enzyme has only been detected in monomeric form, and none of the subunits involved in the dimerization in other organisms have been identified. In contrast with this observation, the structural unit of the enzyme from chlorophycean algae is a dimer and it can form highly stable supramolecular associations (tetramers, hexamers) (Miranda-Astudillo et al., 2018).

The F-ATPases of chloroplasts have a very similar subunit composition to the bacterial enzyme (Seelert and Dencher, 2011) and their peripheral stalk is formed by a *bb*' dimer (also called subunits

I and II), both of these subunits are structurally and functionally similar to the bacterial dimer (Rühle and Leister, 2015). However, in both chloroplasts and cyanobacteria, these subunits are not identical and each one has different secondary structure and dimerization domain (Poetsch et al., 2007). The peripheral stalk of this type of ATPase was first detected through the averaging and analysis of electron microscope images (Böttcher et al., 1998). A three dimensional map was obtained later on at 20 Å resolution (Mellwig and Böttcher, 2003). This reconstruction was generated based on cryo-electron microscopy and the peripheral stalk was found to be a thin structure with more prominence in the parts that contact F_1 and F_O. Mellwig and Böttcher suggest there must be communication between F_1 and F_O, and propose the peripheral stalk as the structure responsible of that communication, however, there are no detailed structural or biochemical studies about the topology of its subunits.

2.3 The peripheral stalk of A-ATPases

Archaea have adapted to the most extreme living conditions in terms of temperature, salinity, pressure, pH, etc. Many of them live in substrates that do not allow the synthesis of 1 mole of ATP per mole of substrate (Mayer and Müller, 2014), which is why their energy conservation strategies are different to those of bacteria and eukaryotes, and involve a chemiosmotic mechanism in which their metabolism is coupled to the generation of sodium or proton gradients to drive the synthesis of ATP (Deppenmeier and Müller, 2007). Despite these differences, ATP synthesis occurs quite similarly to how it occurs in F-ATPases, and the overall architecture of the enzyme among the studied species is conserved (Mayer and Müller, 2014).

A-ATPases are formed by the sectors A_1 and A_O, in this case joined by two peripheral stalks (Figure 7A). Sector A_1 contains the catalytic core A_3B_3 and subunits C, D and F of the rotor; and the membrane sector A_O forms the channel for the translocation of ions and protons. Subunit D extends through the hexamer formed by subunits A and B, thus connecting the site of catalysis with the site of proton translocation through subunits *a*-*c* in sector A_O (Grüber et al., 2014). Subunit A of the catalytic core has additional alpha helices in its C-terminus and a "non-homologous region" in its N-terminus region, both of these characteristics are shared with its equivalents in V-ATPases (Radermacher et al., 2001), but not with F-ATPases. An outstanding feature of A-ATPases is the size variation of the *c*-ring and its capacity to couple the binding of different ions with ATP synthesis (Grüber et al., 2014).

Both peripheral stalks of A-ATPases are formed by heterodimers of subunits E and G. In solution, these subunits adopt a helical structure, just as the proteins that form the peripheral stalk in other ATPases (Kish-Trier et al., 2008). The EG heterodimer has a coiled coil structure along its N-terminal region and a globular structure on its C-terminus, the latter has been shown to interact with the N-terminal end of subunit B of the catalytic core by magnetic resonance studies (Kish-Trier and Wilkens, 2009). The interaction of a component of the peripheral stalk with one of the catalytic core appears to be a conserved feature among rotary ATPases, since it has been described for every type of enzyme in the family. Subunit G shares some similarity with the extramembranal part of subunit *b* of F-ATPases, which suggests a common origin (Hunt and Bowman, 1997). Furthermore, the crystallographic structures of subcomplexes corresponding to the peripheral stalk of an A-type ATPase (Lee et al., 2010) and an F-type ATPase (Dickson et al., 2006) show that subunits G and *b* have a very similar elongated helical structure (Muench et al., 2011). Sobti and coworkers found that, although sequence identity is low (22%), the general fold of the soluble portion of the *E. coli* peripheral stalk is very similar to that of the *T. thermophilus* A-ATPase (Lee et al., 2010), which indicates a strong evolutionary pressure for proteins to adopt this type of fold (Sobti et al., 2016).

The first three dimensional structures of complete A-ATPases were obtained with reconstructions from electron microscopy images, at 23 Å for the H^+-ATPase of *Thermus thermophilus* (Bernal and

Stock, 2004) and at 18 Å resolution for the A-ATPase of *Methanococcus jannaschii* (Coskun et al., 2004). With these structures the presence of two peripheral stalks was established, as was their connection with both A_1 and A_O. Additionally, it was found that these peripheral stalks are asymmetric, one is bent towards A_1 and the other has a more vertical disposition. This observation was later confirmed when the crystallographic structure of subunit E was obtained at 3.6 Å for *Pyrococcus horikoshii* (Balakrishna et al., 2012). In this work, when adjusting the obtained structure of subunit E into the three dimensional map of the enzyme, a better fit was found for the bent peripheral stalk, while the same subunit crystallized previously (Lee et al., 2010), showed a better fit to the vertical stalk (Balakrishna et al., 2012).

The crystal structure of the EG heterodimer of the H^+-ATPase of *T. Thermophilus* obtained at a 3.1 Å resolution clearly showed the structure and topology of these subunits (Lee et al., 2010). Both subunits have an enriched repetitive sequence of alanine, leucine, glutamate and arginine residues, and they assemble into an elongated heterodimer with two distinguishable domains: a 140 Å-long right-handed coiled coil region and a globular region formed mainly by the C-terminus of subunit E (Figure 7B). The coiled coil region is formed due to a hendecad repeat pattern in the N-terminus of both subunits, however, in subunit G, this pattern changes to a quindecad repeat that results in a tighter coiling (Figure 7C). The structure of heterodimer EG was fitted into the three dimensional map of the complete enzyme (Bernal and Stock, 2004), which revealed that it is specifically the N-terminus of subunit E the part in contact with the catalytic core (Lee et al., 2010) (Figure 7A).

Contrary to what happens in F-ATPases, the peripheral stalks of A-ATPases do not cross the membrane but are anchored to a collar-like structure in the extramembrane base of the complex, and extend from there to the A_3B_3 hexamer (Bernal and Stock, 2004; Grüber et al., 2014) (Figure 7A). The collar structure is formed by the N-terminal region of subunit *a* (this subunit has also been called *I* in these enzymes), which has an exposed globular domain that can interact with both peripheral stalks (Lau and Rubinstein, 2012; Vonck et al., 2009). The EG heterodimer can be considered to be functionally similar to the b_2 homodimer of the bacterial F-ATPase because each subunit has a different role: subunit E mediates the interaction with the catalytic core and subunit G stabilizes the peripheral stalk (Grüber et al., 2014; Lee et al., 2010).

2.4 The peripheral stalk of V-ATPases

V-type ATPases couple the hydrolysis of ATP with ion transport and they are involved in many cellular processes: vesicular traffic, processing and degradation of proteins, coupled transport of small molecules and acidification of organelles, among others (Stransky et al., 2016). The V_1 sector includes the catalytic core A_3B_3 where ATP is hydrolyzed, and the central rotor formed by subunits D and F. The V_O sector includes the *c*-ring oligomer, subunit *d* and the membrane part of subunit *a* (Forgac, 2007). Both sections are joined by three peripheral stalks formed by heterodimers of subunits E and G, which are anchored to the base of the complex through a collar-like structure made by subunits C, H and the soluble domain of subunit *a* (Rawson et al., 2016).

A particular feature of V-ATPases is their regulatory mechanism, which involves the peripheral stalks. *In vivo* experiments of V-ATPase from insects (Sumner et al., 1995) and yeast (Kane, 1995) suggested that V-ATPases are able to disassemble and reassemble in response to extracellular stimuli. Both *in vivo* and *in vitro* experiments suggest that the regulation happens as a result of a rearrangement of the subunits of the enzyme (Oot and Wilkens, 2012; Tabke et al., 2014). The exact mechanism is still unknown, but the evidence suggests that the subunits of the peripheral stalk should allow some degree of movement to the complex, either to disassemble or reassemble, or to accommodate the rearrangement of its subunits (Oot et al., 2017). Studies of the structure of the EG dimer and an EGC subcomplex have shown that the interaction between these subunits is stronger when they are part of the holoenzyme than when they are in solution, which indicates that a

conformational change of EG/EGC can occur at some point of the regulation (Diepholz et al., 2008).

As mentioned above, sectors V_1 and V_O are joined by three peripheral stalks (Figure 8A). These stalks were first observed in electron microscopy images (Boekema et al., 1997; Muench et al., 2009; Ubbink-kok et al., 2000; Wilkens et al., 2005) and a detailed model of the subunits and their interactions was obtained with the crystallographic structure of the EGC subcomplex of the yeast V-ATPase (Oot et al., 2012), which crystallized in two different conformations at 2.91 and 2.82 Å. These structures clearly show that two of the peripheral stalks (EG1 and EG2) join the highest part of the enzyme with the exposed N-terminus of subunit *a*, and the third stalk (EG3) interacts with subunit C, which has no homologs in A and F-type ATPases (Figure 8B). The crystallographic structure of subunit C showed that it is formed by two globular domains, which have been called "head" and "foot", separated by a coiled coil stretch (Drory et al., 2004) (Figure 8B). It was later determined that the EG-C interaction is crucial to maintain the stability of the EG heterodimer, and that the interaction is mediated by the "head" domain of subunit C (Oot and Wilkens, 2010).

The EG heterodimer of yeast V-ATPase forms a long structure (of approximately 150 Å) and when bound to subunit C, the subcomplex EGC_{head} (of approximately 170 Å) maintains an elongated shape (Oot et al., 2012) (Figure 8C). The interaction between subunits E and G is stronger in the N and C-terminal ends and weaker in the middle of the helices, and it is due to hendecad repeat patterns that cause a right-handed coiled coil interaction (Oot et al., 2012). The presence of this characteristic structure reinforces the idea that the right-handed coiling is a conserved feature of the proteins that build the peripheral stalks of rotary ATPases (Stewart et al., 2013).

The complete structure of the V-ATPase of *Saccharomyces cerevisiae* was obtained at 11 Å resolution from cryo-electron microscopy studies of protein particles in ice (Benlekbir et al., 2012). This structure shows the contact of the three peripheral stalks with V_1, given by the N-terminal end of the E subunits with the B subunits of the catalytic core (Figure 8A). It can also be seen that each EG heterodimer interacts with different subunits of the collar-like structure (subunits *a*, C and H): EG1 interacts with the N-terminal ends of subunits *a* and H; EG2 with the N-terminal end of subunit *a* and the "foot" of subunit C; and EG3 only contacts the "head" of subunit C (Figure 8B). In this enzyme, the only contact between a peripheral stalk and the membrane sector is given by the interaction of EG2 with subunit *a* (Benlekbir et al., 2012).

3. The roles of the peripheral stalk

All the interactions described so far clearly establish the role of the peripheral stalk as the structure responsible for connecting the two sectors that form ATPases, the membrane sector and the catalytic core. Having discussed that, the following section describes the different roles that have been attributed to the peripheral stalks and the latest proposals based on the growing wealth of structural information.

3.1 The role of the peripheral stalk in the flexibility of the complex

Evidently, rotary ATPases are dynamic structures that exhibit some degree of flexibility that allows all the movements that are necessary for the enzyme to function correctly (Neukirch et al., 2008; Stewart et al., 2012, 2013; Walker and Dickson, 2006). The notion that the peripheral stalk is a flexible structure has been controversial and has evolved. The flexibility property was first assigned to the *b* subunits of the F-ATPase of *E. coli*, based on experiments in which residues were added or removed from these subunits and the enzyme remained functional (Sorgen et al., 1998, 1999). Years later it was proposed that the peripheral stalk is a rigid structure (Dickson et al., 2006; Rees et al., 2009), and that the need for flexible elements is fulfilled by other components of the enzyme

(Wächter et al., 2011). In recent years, cryo-electron microscopy studies suggest that the peripheral stalk, to a certain extent depending on the type of ATPase, is indeed a flexible structure (Mazhab-Jafari and Rubinstein, 2016).

Subunits *a* and *c* of the F_O sector form two aqueous half channels that define the path followed by protons, which drive the movement of the rotor (*c*-ring $_+$ γδε) in order for catalysis to occur (F_1). This fact, as well as the key residues involved in proton translocation, were first proposed by Vik and Antonio in 1994 based on mutagenesis experiments, and both were confirmed over twenty years later by cryo-electron microscopy studies (Allegretti et al., 2015; Guo et al., 2017; Vik and Antonio, 1994). It is well known that each complete turn of the rotor generates, on average, three ATP molecules (Yasuda et al., 1998), and that each turn requires the translocation of a certain number of protons, depending on the number of *c* subunits present in the *c*-ring (Pogoryelov et al., 2012). This difference or asymmetry between what goes into the complex and what comes out (8-15 H^+:3 ATP) requires the temporal storage of energy during the movement and its gradual release to drive each 120° turn of the rotor (Cherepanov et al., 1999; Junge et al., 2009; Walker and Dickson, 2006). Another way of looking at this phenomenon is to consider rotation steps: sector F_1 has a three-step rotation (given by the three β subunits), while sector F_O has an 8 to 15-step rotation (depending on the number of *c* subunits). This difference has been called rotational asymmetry and it is buffered by the transmission of elastic energy between the two sectors of the enzyme (Saroussi et al., 2012). Taken together, these observations imply that there have to be flexible elements in the enzyme capable of storing and transmitting elastic energy.

Experiments performed with single molecules of the F-ATPase of *E. coli*, in which certain domains are "stiffened" by artificial disulfide bonds and their elasticity is measured, identified the lower part of the rotor (γδ + *c*-ring) as an elastic domain (Sielaff et al., 2008). Other studies have evaluated the magnitude and determinants of the elasticity of the peripheral stalk of the bacterial ATPase, comparing wild type and mutant enzymes with modified *b* subunits, and have concluded that the peripheral stalk is a rigid structure and the most elastic elements are located in the central rotor and the lever of subunit β (Wächter et al., 2011). These authors suggest that, in the *E. coli* enzyme, the peripheral stalk works as a scaffold between F_O and F_1, and that the rotor (at least ten times more flexible) is responsible for the transmission of elastic energy between them.

In light of the latest evidence, obtained by cryo-electron microscopy, the stiffness that had been assigned to the peripheral stalk is now being reconsidered. Structures in more than one conformational state have been generated for the bovine F-ATPase (Zhou et al., 2015), which show the transitions of the enzyme. Two transitions of the peripheral stalk are visible: a bend towards the top part of the enzyme close to subunit OSCP and a bend towards the transmembrane part of subunit *b* (Figure 9A). The authors conclude that the flexibility and movement capacity of all the components of the enzyme (the *c*-ring showed considerable rotational flexibility) contribute to facilitate the coupling of the rotor movement (F_O) with catalysis (F_1). Similarly, cryo-electron microscopy studies from the V-ATPase of *S. cerevisiae* allowed the reconstruction of 3D structures in three conformational states (Zhao et al., 2015). In this enzyme, as in the bovine enzyme, most of the subunits show conformational changes. The obtained structures of the yeast enzyme show that the helical part of rotor subunit D (equivalent to subunit γ of F-ATPases) remains rigid during rotation, but the part in contact with subunit *d* can bend. It is also evident that the catalytic subunits A and B press on subunits E and G of the peripheral stalks, which then bend along their coiled coil regions (Figure 9B). Even more flexibility is observed when considering the EG-C interaction, since subunit C can twist without losing contact with the peripheral stalks.

In contrast with what was observed in F and V-type ATPases, the analysis of the rotational states of the A-ATPase of *T. thermophilus* (Schep et al., 2016) revealed that the conformational changes of its subunits are minimal, which would suggest a less flexible enzyme (Figure 9C). The authors

discuss that this can be due to the fact that this enzyme has a larger rotational asymmetry (3:12) compared to the one of the yeast V-ATPase (3:10) and bovine F-ATPase (3:8), which may cause it to adopt an energetically favorable rotational state in which most of the images are obtained, resulting in an apparent lack of flexibility.

3.2 The role of the peripheral stalk on the stability and assembly of the complex

The study of the role of the peripheral stalk in the assembly process of the complex and how it contributes to its stability refers mostly to F-ATPases. The study of different mutations in the F-ATPase of *E. coli* revealed that subunit δ (OSCP) is essential for the assembly of the b_2 dimer with the rest of the complex, independent of its interaction with subunit α (Hilbers et al., 2013). Additionally, the authors conclude that subunit δ is also important to join the peripheral stalk with the rotor, therefore contributing to the stability and functionality of the complex.

Most of the information available concerning the assembly of F-ATPases has derived from the study of yeast mutants. In this organism, radioactive and pulse-chase labeling experiments have allowed the elucidation of a part of the assembly process, which involves two separate sub complexes: *a*-8-peripheral stalk and F_1-c_{10}, which are generated in an independent but coordinated way (Rak et al., 2011). A dimeric complex named INA (Inner Membrane Assembly) was identified and proposed to act as a sort of chaperone for the assembly of the enzyme (Lytovchenko et al., 2014). The loss of this complex, composed by subunits Ina17 and Ina22, causes the dissociation of sectors F_1 and F_O, and it was found that subunit Ina22 associates transiently with both F_1 and the peripheral stalk, but not with the assembled enzyme, which confirms its role as an auxiliary factor. Lytovchenko and collaborators propose an alternative to the assembly route proposed by Rak and coworkers that includes an F_1-peripheral stalk sub complex. It was then proposed that INAC prevents premature interaction of assembly intermediates and promotes the correct assembly of the *c*-ring with subunit *a* to form the proton translocation portion of the enzyme (Naumenko et al., 2017). A recent study with human ATPase mutants showed that, although the human and yeast ATPases are highly similar, the assembly pathways of the proton translocation channel are different (He et al., 2018; Song et al., 2018).

Native electrophoresis studies have shown that human F-ATPase can assemble if subunits *a* and A6L are missing and even form oligomers, albeit unstable and in low quantities (Wittig et al., 2010). It has also been shown that human cells fail to assemble ATPase if the expression of subunit *d* is inhibited, which causes the accumulation of two sub complexes: F_1-*c* and *b*-*e*-*g* (Fujikawa et al., 2015). Thus, in the human enzyme, the complete peripheral stalk is necessary to maintain the stability of the complex and its oligomers, and the rotor and the peripheral stalk seem to be formed independently and only assemble when subunit *d* is recruited. So far, the evidence related to the assembly of the peripheral stalk in the mammalian enzyme suggests that one of the earlier steps is the assembly of membrane subunits *e* and *g* with the transmembrane segment of subunit *b*, and then subunit *d* is recruited and associates with the exposed part of subunit *b* (Fujikawa et al., 2015) (Figure 10).

3.3 The role of the peripheral stalk in the dimerization and oligomerization of F-ATPases

Another one of the processes in which the peripheral arm is involved is the dimerization of the enzyme. It is currently well known that F-ATPases form dimers that are arranged in rows along the inner mitochondrial membrane (Davies et al., 2011; Strauss et al., 2008; Thomas et al., 2008), and that such oligomerization is directly involved in the morphogenesis of the mitochondrial cristae (Davies et al., 2012; Dudkina et al., 2005; Fronzes et al., 2006; Mühleip et al., 2016; Paumard, 2002). Membrane subunits *e* and *g* have been identified as responsible for the stabilization of yeast (Arnold et al., 1998, 1999; Davies et al., 2012) and bovine (Minauro-Sanmiguel et al., 2005) ATP

synthase dimers. However, it has also been proposed that subunit *i* of the peripheral stalk participates in this process, since there is evidence that this subunit forms homodimers that are located close to the dimerization interface (Paumard et al., 2002), and that the enzyme can be found as a dimer in the absence of subunits *e* and *g* (Fronzes et al., 2006). In addition to this, a study of interactions monitored by FRET showed that the yeast F-ATPase is capable of forming oligomeric associations *in vivo* in the absence of subunit *e* (Gavin et al., 2005), so the authors propose the existence of two dimerization interfaces, one mediated by subunits *e* and *g,* and another mediated by the transmembrane segment of subunit *b*.

In addition to the biochemical studies, structural studies of the yeast F-ATPase have provided information about how the peripheral stalk can participate in the dimerization process. A study involving the reconstruction of the yeast enzyme (from electron cryo-tomography images at an estimated resolution of 3.7 nm) and the analysis of dimer and oligomer formation *in situ* with molecular dynamics (Davies et al., 2012; Mühleip et al., 2016) showed that ATPase monomers associate through the membrane part of the peripheral stalk and that subunits *e*, *g* and 4 are part of the dimerization interface and essential for that process to occur. Furthermore, the N-terminal end of subunit *g* is exposed to the mitochondrial matrix (Belogrudov et al., 1996), and crosslinking experiments have proved that this segment is in close proximity to subunit 4 (equivalent to subunit *b*) (Soubannier et al., 2002). The proximity of subunits *g* and 4 is in agreement with the structure obtained by Guo and collaborators (Guo et al., 2017).

The role of subunit 4 in the dimerization/oligomerization of the yeast enzyme has been studied with directed mutagenesis of the loop that joins the transmembrane segments of this subunit (Weimann et al., 2008). This loop is necessary to organize and stabilize the neighboring subunits *a*, *e* and *g*, and hence essential to maintain the supramolecular species of ATPase. In support of this result, and highlighting the role of the peripheral stalk in the dimerization process, there is evidence that suggests that the loss of the first transmembrane segment of subunit 4 results in a functional enzyme that is incapable of forming dimers or oligomers (Soubannier et al., 2002). Concerning the formation and maintenance of ATPase dimers, the dimerization interface of the yeast enzyme has been proposed to be stabilized by 4-4, *e*-*g* and *a*-*a* interactions (Habersetzer et al., 2013) or by *a*/6-*i* interactions (Guo et al., 2017), but see also the work of Anselmi and coworkers (Anselmi et al., 2018) (Figure 11). The *a*-*a* interface was first demonstrated by Velours and coworkers with crosslinking experiments (Velours et al., 2011) and it was recently confirmed with the high resolution structure of the enzyme, in which another interface mediated by subunits *i/j* is proposed (Guo et al., 2017).

A three dimensional model of the dimeric F-ATPase of the ciliate *Paramecium tetraurelia* was generated at 2.6 nm resolution from electron cryo-tomography of isolated mitochondrial membranes (Mühleip et al., 2016). This structure allowed the construction of a model to explain the formation of mitochondrial cristae in this organism. The authors found that the curvature of the membrane is imposed by the base of the peripheral stalks, thus creating the cristae, and that this phenomenon causes the association of dimers into rows along the membrane. These observations imply that, in *P. tetraurelia*, dimerization occurs mainly through the membrane section of the peripheral stalk and such process is the immediate cause of cristae formation (Mühleip et al., 2016). A similar case is the one of *S. cerevisiae*, in which the bending of the membrane is due to a domain formed by transmembrane subunits *e* and *g* and approximately 50 residues from the N-termini of subunit *b* (Guo et al., 2017).

4. Conclusions

All the work that has been done to deepen the understanding of the peripheral stalk has consistently shown that it is an essential component of all rotary ATPases. The information obtained from highly diverse organisms, from bacteria to human and including archaea and parasites, confirms that, in spite of being a variable structure, the nature of its subunits (from their size and secondary structure to their arrangement into right-handed coiled coils), as well as their interactions and functions, are all conserved. That being said, the organisms whose ATPase has divergent features also need to be considered, since there is growing evidence regarding these enzymes suggesting that they may be the exception to the rule.

High resolution structures of rotary ATPases have confirmed most of the previous biochemical evidence and have contributed relevant new information. These structures have not only allowed to observe the interactions of each component of the peripheral stalk, but also the different conformations in which they can be found, thus confirming both the existence and the need for flexibility in rotary ATPases, partly due to the peripheral stalk itself. The observed dynamics allowed by the nature of the subunits of the peripheral stalk and the interactions that they keep with the rest of the subunits of the enzyme have led some to think that sector R_O can communicate and coordinate with what happens in sector R_I, even though they are over 100 Å apart (Stewart et al., 2013); the available evidence postulates the peripheral stalk as the main candidate for establishing such communication. In the case of F-ATPases, the detailed analysis of the structure of the peripheral stalk has shown that it is involved in processes beyond the catalytic function of the enzyme. Much of the evidence related to the dimerization and oligomerization of F-ATPases indicates that the peripheral stalk, at least the transmembrane section, is crucial for the formation and maintenance of the supramolecular associations of the enzyme and, consequently, of the peculiar mitochondrial morphology.

Based on all that has been discovered to date, it can be concluded that rotary ATPases are indeed highly dynamic enzymes, and that this characteristic is not only imposed by the mobile elements but also by those that had initially been considered static, as is the case of the peripheral stalk. Finally, and especially considering the latest studies, it can be said that the observed distortions of the enzyme involve the contribution of individual subunits, from the peripheral stalk and other parts, and illustrate the fine orchestration that this rotary enzyme is capable of building up in order to reach its maximal efficiency.

Figure 1. Rotary ATPases. A. Schematic representation of an F-ATPase (top) and three dimensional structure of the bovine heart mitochondria F-ATPase (bottom) (Zhou et al., 2015) EMD 3164. **B.** Schematic representation of an A-ATPase (top) and three dimensional structure of the *Thermus thermophilus* A-ATPase (bottom) (Schep et al., 2016) EMD 5335. **C.** Schematic representation of a V-ATPase (top) and three dimensional structure of the *Saccharomyces cerevisiae* V-ATPase (bottom) (Zhao et al., 2015) EMD 6285. All the three dimensional maps were generated from electron cryo-microscopy images. The colors in the schematizations represent: catalytic core in green and violet, central rotor in orange, *c*-ring oligomer in blue, subunit *a* in hot pink and peripheral stalks in dark purple. The arrowheads point to the peripheral stalk(s).

Figure 2. Peripheral stalks of rotary ATPases. A. Models of the peripheral stalk from the F-ATPase of *Escherichia coli* (left) and *Bos taurus* (right), corresponding to the PDBs 5T4O (Sobti et al., 2016) and 5FIL (Zhou et al., 2015), respectively. **B.** Model of one of the peripheral stalks from the A-ATPase of *Thermus thermophilus* corresponding to the PDB 3V6I (Stewart et al., 2012). **C.** Model of one of the peripheral stalks from the V-ATPase of *Saccharomyces cerevisiae* corresponding to the PDB 3J9V (Zhao et al., 2015).

Figure 3. Coiled coils exemplified with the EG heterodimer from the peripheral stalk of the A-ATPase of *Thermus thermophilus*. A. The pitch length and pitch angle are indicated on the coiled coil helices of the EG heterodimer. **B.** Models to illustrate the right-handed coiling of the helices of the EG heterodimer. **C.** Amino acid residues involved in the interaction of the helices of the EG heterodimer. The residues corresponding to positions *adeh* of the hendecad (subunit E) and quindecad (subunit G) repeats are indicated. **D.** Hendecad and quindecad repeat patterns indicated on the sequence of subunits E and G from different species of archaea. The model in A, B and C corresponds to the structural data deposited with the PDB 3V6I (Stewart et al., 2012), with subunit E in yellow and subunit G in magenta.

Figure 4. Peripheral stalk of prokaryotic and eukaryotic F-ATPases. A. Three dimensional model of the enzyme of *Escherichia coli* in which the peripheral stalk and the F_O sector are colored. **B.** Model to highlight the domains in which the *b* subunits have been divided: δ-interaction domain in green, dimerization domain in orange and *a*-interaction domains (transmembrane segments) in hot pink. **C.** Model to illustrate the right-handed coiled coil domain of the b_2 dimer. The model used in A, B and C corresponds to the structural data deposited with the PDB 5T4O (Sobti et al., 2016), with subunit δ in green, subunits *b* in dark teal and cyan, subunit *a* in hot pink and *c*-ring in blue. **D.** Three dimensional model of the enzyme of *Saccharomyces cerevisiae* in which the peripheral stalk and the F_O sector are colored. The helix of subunit α that contacts *b*, *d* and F6 is indicated with a gray arrow. **E.** Peripheral stalk of the yeast ATPase highlighting its components. The additional helix of subunit F6 is indicated with a purple arrow. **F.** Surface representation to illustrate the coiled coil interactions in the extrinsic part of the yeast peripheral stalk. The model used in D, E and F corresponds to the structural data deposited with the PDB 6CP6 (Srivastava et al., 2018), with subunit OSCP in green, subunit *b* in cyan, subunit F6 (*h*) in purple, subunit *d* in salmon, subunit *f* in pale yellow, subunit 8 in pink, subunit *j* in dark blue, subunit *a* in hot pink and *c*-ring in blue.

Figure 5. Working model of the dimeric mitochondrial ATPase of *Polytomella* sp. The image shows the working model of the 3D structure of the enzyme fitted in the EMD-2852 map contoured at 6 sigma (Allegretti et al., 2015). Color scheme: F_1 sector in pink; OSCP in violet; Asa2 in cyan; Asa4 in deep purple; Asa7 in sky blue; Asa1 in yellow; Asa3 in brown (dirty violet); Asa5 in salmon; Asa6 in gray; Asa8 in orange; Asa9 in leaf green; subunit a in deep teal and *c*-ring in pale cyan.

Figure 6. Protozoan and metazoan type dimers. Projection maps of dimeric ATP synthases from **A.** *Polytomella* sp. (Dudkina et al., 2005). The black bar represents 10 nm. **B.** *Euglena gracilis* (Yadav et al., 2017) **C.** *Tetrahymena thermophila* (Balabaskaran Nina et al., 2010) representing protozoan-type dimers; and **D.** *Saccharomyces cerevisiae* (Couoh-Cardel et al., 2010) representing a metazoan-type dimer.

Figure 7. Peripheral stalk of the *Thermus thermophilus* A-ATPase. A. Three dimensional model of the archaeal enzyme (Schep et al., 2016) PDB 5GAR, in which the peripheral stalks and the collar-like structure made by subunit *a* are colored. **B.** Model of the EG heterodimer in which the coiled coil domain and the globular domain are indicated. **C.** Model of the EG heterodimer that illustrates the right handed coiling of the helices and the two types of coiling that result from the hendecad motifs in both subunits, and quindecad repeat motifs in subunit G. The model used in B and C corresponds to the structural data deposited with the PDB 3V6I (Stewart et al., 2012), with subunit E in yellow and subunit G in magenta.

Figure 8. Peripheral stalk of the *Saccharomyces cerevisiae* V-ATPase. A. Three dimensional model of the yeast enzyme in which the peripheral stalks and the subunits of the collar-like structure are colored. **B.** Model that illustrates the interaction of each peripheral stalk (EG1, EG2, EG3) with the subunits of the collar. The different sections of subunit C are indicated. **C.** Models of the EG heterodimer to illustrate the right handed coiling of the helices. The model used in A, B and C corresponds to structural data deposited with the PDB 3J9V (Zhao et al., 2015), with subunit E in orange, subunit G in dark violet, subunit H in red, the exposed part of subunit *a* in pink and subunit C in green.

Figure 9. Flexibility of the peripheral stalk of rotary ATPases. Flexibility of the peripheral stalk illustrated with the transitions it goes through during the process of rotational catalysis. **A.** Models that correspond to the transitions of an F-ATPase peripheral stalk; PDBs 5ARI, 5ARA, 5FIL from (Zhou et al., 2015). **B.** Models that correspond to three rotational states of one of the peripheral stalks of the V-ATPase of *S. cerevisiae*; PDBs 3J9T, 3J9U, 3J9V from (Zhao et al., 2015). **C.** Models that correspond to two rotational states of one of the peripheral stalks of the A-ATPase of *T. thermophilus*; PDBs 5GAR, 5GAS from (Schep et al., 2016).

Figure 10. Assembly process of the peripheral stalk of the human F-ATPase. The assembly pathway corresponds to the one proposed by (Fujikawa et al., 2015) and is exemplified with the bovine enzyme, PDB 5FIL from (Zhou et al., 2015).

Figure 11. Schematic representation of the dimerization of the yeast F-ATPase. Model of the F_O section in which all the subunits involved in the dimerization are colored: subunit *a* in hot pink, subunit *b* in cyan, subunit *e* in brown, subunit *g* in pale blue, subunit *j* in dark blue and subunit *k* in lemon. The dimerization interface includes the subunits proposed by (Guo et al., 2017; Habersetzer et al., 2013). The model corresponds to the structural data deposited with the PDB 6B2Z (Guo et al., 2017).

Conflict of interest statement

The authors declare that this review was written in the absence of any commercial or financial relationships that could be construed as a potential conflict of interest.

Author contributions statement

LC and DG conceptualization; LC and DG writing the original draft; LC, AD, HM and MG formal analysis; AD, HM and MG reviewing and editing; MG and DG project administration; MG and DG funding acquisition.

Funding

DG and MG acknowledge financial support from 279125 Grant ECOS Nord-ANUIES-CONACyT, and further support for DG from grants 239219 (Fondo SEP-CONACYT) CONACyT and IN208917 (PAPIIT-DGAPA-UNAM).

Acknowledgements

The technical assistance of Q.B.P. Miriam Vázquez-Acevedo is gratefully acknowledged.

References

Allegretti, M., Klusch, N., Mills, D. J., Vonck, J., Kühlbrandt, W., and Davies, K. M. (2015). Horizontal membrane-intrinsic α-helices in the stator a-subunit of an F-type ATP synthase. *Nature* 521, 237–240. doi:10.1038/nature14185.

Anselmi, C., Davies, K. M., and Faraldo-Gómez, J. D. (2018). Mitochondrial ATP synthase dimers spontaneously associate due to a long-range membrane-induced force. *J. Gen. Physiol.*, jgp.201812033. doi:10.1085/jgp.201812033.

Arnold, I., Pfeiffer, K., Neupert, W., Stuart, R. A., and Schägger, H. (1999). ATP Synthase of Yeast Mitochondria. *J. Biol. Chem.* 274, 36–40. doi:10.1074/jbc.274.1.36.

Arnold, I., Pfeiffer, K., Neupert, W., Stuart, R. a, and Scha, H. (1998). Yeast mitochondrial F 1 F 0 -ATP synthase exists as a dimer: identi cation of three dimer-speci c subunits. *EMBO J.* 17, 7170–7178.

Baker, L. A., Watt, I. N., Runswick, M. J., Walker, J. E., and Rubinstein, J. L. (2012). Arrangement of subunits in intact mammalian mitochondrial ATP synthase determined by cryo-EM. *Proc. Natl. Acad. Sci.* 109, 11675–11680. doi:10.1073/pnas.1204935109.

Balabaskaran Nina, P., Dudkina, N. V., Kane, L. A., van Eyk, J. E., Boekema, E. J., Mather, M. W., et al. (2010). Highly Divergent Mitochondrial ATP Synthase Complexes in Tetrahymena thermophila. *PLoS Biol.* 8, 3–6. doi:10.1371/journal.pbio.1000418.

Balakrishna, A. M., Hunke, C., and Grüber, G. (2012). The structure of subunit e of the Pyrococcus horikoshii OT3 A-ATP synthase gives insight into the elasticity of the peripheral stalk. *J. Mol. Biol.* 420, 155–163. doi:10.1016/j.jmb.2012.04.012.

Belogrudov, G. I., Tomich, J. M., and Hatefi, Y. (1996). Membrane topography and near-neighbor relationships of the mitochondrial ATP synthase subunits e, f, and g. *J. Biol. Chem.* 271, 20340–20345. doi:10.1074/jbc.271.34.20340.

Benlekbir, S., Bueler, S. A., and Rubinstein, J. L. (2012). Structure of the vacuolar-type ATPase from Saccharomyces cerevisiae at 11-?? resolution. *Nat. Struct. Mol. Biol.* 19, 1356–1362. doi:10.1038/nsmb.2422.

Bernal, R. A., and Stock, D. (2004). Three-dimensional structure of the intact Thermus thermophilus H +-ATPase/synthase by electron microscopy. *Structure* 12, 1789–1798. doi:10.1016/j.str.2004.07.017.

Bi, Y., Watts, J. C., Bamford, P. K., Briere, L. A. K., and Dunn, S. D. (2008). Probing the functional tolerance of the b subunit of Escherichia coli ATP synthase for sequence manipulation through a chimera approach. *Biochim. Biophys. Acta - Bioenerg.* 1777, 583–591. doi:10.1016/j.bbabio.2008.03.004.

Boekema, E. J., Ubbink-Kok, T., Lolkema, J. S., Brisson, A., and Konings, W. N. (1997). Visualization of a peripheral stalk in V-type ATPase: evidence for the stator structure essential to rotational catalysis. *Proc. Natl. Acad. Sci. U. S. A.* 94, 14291–14293. doi:10.1073/pnas.94.26.14291.

Böttcher, B., Schwarz, L., and Gräber, P. (1998). Direct indication for the existence of a double stalk in CF0F1. *J. Mol. Biol.* 281, 757–762. doi:10.1006/jmbi.1998.1957.

Brandt, K., Maiwald, S., Herkenhoff-Hesselmann, B., Gnirß, K., Greie, J. C., Dunn, S. D., et al. (2013). Individual interactions of the b subunits within the stator of the escherichia coli ATP synthase. *J. Biol. Chem.* 288, 24465–24479. doi:10.1074/jbc.M113.465633.

Cano-Estrada, A., Vázquez-Acevedo, M., Villavicencio-Queijeiro, A., Figueroa-Martínez, F., Miranda-Astudillo, H., Cordeiro, Y., et al. (2010). Subunit-subunit interactions and overall topology of the dimeric mitochondrial ATP synthase of Polytomella sp. *Biochim. Biophys. Acta - Bioenerg.* 1797, 1439–1448. doi:10.1016/j.bbabio.2010.02.024.

Carbajo, R. J., Kellas, F. A., Yang, J. C., Runswick, M. J., Montgomery, M. G., Walker, J. E., et al. (2007). How the N-terminal Domain of the OSCP Subunit of Bovine F1Fo-ATP Synthase Interacts with the N-terminal Region of an Alpha Subunit. *J. Mol. Biol.* 368, 310–318. doi:10.1016/j.jmb.2007.02.059.

Cherepanov, D. A., Mulkidjanian, A. Y., and Junge, W. (1999). Transient accumulation of elastic energy in proton translocating ATP synthase. *FEBS Lett.* 449, 1–6. doi:10.1016/S0014-5793(99)00386-5.

Cipriano, D. J., Wood, K. S., Bi, Y., and Dunn, S. D. (2006). Mutations in the dimerization domain of the b subunit from the Escherichia coli ATP synthase: Deletions disrupt function but not enzyme assembly. *J. Biol. Chem.* 281, 12408–12413. doi:10.1074/jbc.M513368200.

Claggett, S. B., Plancher, M. O. N., Dunn, S. D., and Cain, B. D. (2009). The b subunits in the peripheral stalk of F1F0 ATP synthase preferentially adopt an offset relationship. *J. Biol. Chem.* 284, 16531–16540. doi:10.1074/jbc.M109.002980.

Colina-Tenorio, L., Miranda-Astudillo, H., Cano-Estrada, A., Vázquez-Acevedo, M., Cardol, P., Remacle, C., et al. (2016). Subunit Asa1 spans all the peripheral stalk of the mitochondrial ATP synthase of the chlorophycean alga Polytomella sp. *Biochim. Biophys. Acta - Bioenerg.* 1857, 359–369. doi:10.1016/j.bbabio.2015.11.012.

Collinson, I. R., van Raajj, M. J., Runswick, M. J., Fearnley, I. M., Skehel, M. J., Orris, G. L., et al. (1994). ATP Synthase from Bovine Heart Mitochondria In Vitro Assembly of a Stalk Complez in the Presence of F1-ATPase and in its Absence. *J. Mol. Biol.* 242, 408–421. doi:10.1006/jmbi.1994.1591.

Coskun, Ü., Chaban, Y. L., Lingl, A., Müller, V., Keegstra, W., Boekema, E. J., et al. (2004). Structure and subunit arrangement of the A-type ATP synthase complex from the archaeon Methanococcus jannaschii visualized by electron microscopy. *J. Biol. Chem.* 279, 38644–38648. doi:10.1074/jbc.M406196200.

Couoh-Cardel, S. J., Uribe-Carvajal, S., Wilkens, S., and García-Trejo, J. J. (2010). Structure of dimeric F1F0-ATP synthase. *J. Biol. Chem.* 285, 36447–36455. doi:10.1074/jbc.M110.144907.

Crick, F. H. C. (1953). The packing of α-helices: simple coiled-coils. *Acta Crystallogr.* 6, 689–697.

854 doi:10.1107/S0365110X53001964.

855 Cross, R. L., and Müller, V. (2004). The evolution of A-, F-, and V-type ATP synthases and
856 ATPases: Reversals in function and changes in the H+/ATP coupling ratio. *FEBS Lett.* 576, 1–
857 4. doi:10.1016/j.febslet.2004.08.065.

858 Cross, R. L., and Taiz, L. (1990). Gene duplication as a means for altering H+/ATP ratios during
859 the evolution of Fo F1 ATPases and synthases. *FEBS Lett.* 259, 227–229. doi:10.1016/0014-
860 5793(90)80014-A.

861 D'Alessandro, M., and Melandri, B. A. (2010). ATP hydrolysis in ATP synthases can be differently
862 coupled to proton transport and modulated by ADP and phosphate: A structure based model of
863 the mechanism. *Biochim. Biophys. Acta - Bioenerg.* 1797, 755–762.
864 doi:10.1016/j.bbabio.2010.03.007.

865 Davies, K. M., Anselmi, C., Wittig, I., Faraldo-Gomez, J. D., and Kuhlbrandt, W. (2012). Structure
866 of the yeast F1Fo-ATP synthase dimer and its role in shaping the mitochondrial cristae. *Proc.*
867 *Natl. Acad. Sci.* 109, 13602–13607. doi:10.1073/pnas.1204593109.

868 Davies, K. M., Strauss, M., Daum, B., Kief, J. H., Osiewacz, H. D., Rycovska, A., et al. (2011).
869 Macromolecular organization of ATP synthase and complex I in whole mitochondria. *Proc.*
870 *Natl. Acad. Sci.* 108, 14121–14126. doi:10.1073/pnas.1103621108.

871 Del Rizzo, P. A., Bi, Y., and Dunn, S. D. (2006). ATP Synthase b Subunit Dimerization Domain: A
872 Right-Handed Coiled Coil with Offset Helices. *J. Mol. Biol.* 364, 735–746.
873 doi:10.1016/j.jmb.2006.09.028.

874 Del Rizzo, P. A., Bi, Y., Dunn, S. D., and Shilton, B. H. (2002). The "second stalk" of Escherichia
875 coli ATP synthase: Structure of the isolated dimerization domain. *Biochemistry* 41, 6875–
876 6884. doi:10.1021/bi025736i.

877 Deleon-Rangel, J., Ishmukhametov, R. R., Jiang, W., Fillingame, R. H., and Vik, S. B. (2013). In-
878 teractions between subunits a and b in the rotary ATP synthase as determined by cross-linking.
879 *FEBS Lett.* 587, 892–897. doi:10.1016/j.febslet.2013.02.012.

880 Deppenmeier, U., and Müller, V. (2007). Life Close to the Thermodynamic Limit: How Methano-
881 genic Archaea Conserve Energy. *Bioenergetics*, 123–152. doi:10.1007/400_2006_026.

882 Dickson, V. K., Silvester, J. A., Fearnley, I. M., Leslie, A. G. W., and Walker, J. E. (2006). On the
883 structure of the stator of the mitochondrial ATP synthase. *EMBO J.* 25, 2911–2918.
884 doi:10.1038/sj.emboj.7601177.

885 Diepholz, M., Venzke, D., Prinz, S., Batisse, C., Flörchinger, B., Rössle, M., et al. (2008). A Dif-
886 ferent Conformation for EGC Stator Subcomplex in Solution and in the Assembled Yeast V-
887 ATPase: Possible Implications for Regulatory Disassembly. *Structure* 16, 1789–1798.
888 doi:10.1016/j.str.2008.09.010.

889 Dmitriev, O., Jones, P. C., Jiang, W., and Fillingame, R. H. (1999). Structure of the Membrane
890 Domain of Subunit b of the Escherichia coli F 0 F 1 ATP Synthase. *J. Biol. Chem.* 274,
891 15598–15604.

892 Drory, O., Frolow, F., and Nelson, N. (2004). Crystal structure of yeast V-ATPase subunit C re-
893 veals its stator function. *EMBO Rep.* 5, 1148–1152. doi:10.1038/sj.embor.7400294.

894 Dudkina, N. V., Heinemeyer, J., Keegstra, W., Boekema, E. J., and Braun, H. P. (2005). Structure
895 of dimeric ATP synthase from mitochondria: An angular association of monomers induces the
896 strong curvature of the inner membrane. *FEBS Lett.* 579, 5769–5772.
897 doi:10.1016/j.febslet.2005.09.065.

898 Dunn, S. D., Revington, M., Cipriano, D. J., and Shilton, B. H. (2000). The b subunit of Escherichia

coli ATP synthase. *J. Bioenerg. Biomembr.* 32, 347–355. doi:10.1023/A:1005571818730.

Forgac, M. (2007). Vacuolar ATPases: Rotary proton pumps in physiology and pathophysiology. *Nat. Rev. Mol. Cell Biol.* 8, 917–929. doi:10.1038/nrm2272.

Fronzes, R., Weimann, T., Vaillier, J., Velours, J., and Brèthes, D. (2006). The peripheral stalk participates in the yeast ATP synthase dimerization independently of e and g subunits. *Biochemistry* 45, 6715–6723. doi:10.1021/bi0601407.

Fujikawa, M., Sugawara, K., Tanabe, T., and Yoshida, M. (2015). Assembly of human mitochondrial ATP synthase through two separate intermediates, F1-c-ring and b-e-g complex. *FEBS Lett.* 589, 2707–2712. doi:10.1016/j.febslet.2015.08.006.

Gavin, P. D., Prescott, M., and Devenish, R. J. (2005). Yeast F1F0-ATP synthase complex interactions in vivo can occur in the absence of the dimer specific subunit e. *J. Bioenerg. Biomembr.* 37, 55–66. doi:10.1007/s10863-005-4128-8.

Grüber, G., Manimekalai, M. S. S., Mayer, F., and Müller, V. (2014). ATP synthases from archaea: The beauty of a molecular motor. *Biochim. Biophys. Acta - Bioenerg.* 1837, 940–952. doi:10.1016/j.bbabio.2014.03.004.

Guo, H., Bueler, S. A., and Rubinstein, J. L. (2017). Atomic model for the dimeric FO region of mitochondrial ATP synthase. *Science (80-.).* 358, 936–940. doi:10.1126/science.aao4815.

Habersetzer, J., Ziani, W., Larrieu, I., Stines-Chaumeil, C., Giraud, M. F., Brèthes, D., et al. (2013). ATP synthase oligomerization: From the enzyme models to the mitochondrial morphology. *Int. J. Biochem. Cell Biol.* 45, 99–105. doi:10.1016/j.biocel.2012.05.017.

Hahn, A., Parey, K., Bublitz, M., Mills, D. J., Zickermann, V., Vonck, J., et al. (2016). Structure of a Complete ATP Synthase Dimer Reveals the Molecular Basis of Inner Mitochondrial Membrane Morphology. *Mol. Cell* 63, 445–456. doi:10.1016/j.molcel.2016.05.037.

He, J., Ford, H. C., Carroll, J., Douglas, C., Gonzales, E., Ding, S., et al. (2018). Assembly of the membrane domain of ATP synthase in human mitochondria. *Proc. Natl. Acad. Sci.*, 201722086. doi:10.1073/pnas.1722086115.

Hilbers, F., Eggers, R., Pradela, K., Friedrich, K., Herkenhoff-Hesselmann, B., Becker, E., et al. (2013). Subunit δ Is the Key Player for Assembly of the H+-translocating Unit of Escherichia coli FOF1 ATP Synthase. *J. Biol. Chem.* 288, 25880–25894. doi:10.1074/jbc.M113.484675.

Hunt, I. E., and Bowman, B. J. (1997). The intriguing evolution of the “b” and “G” subunits in F-type and V- type ATPases: Isolation of the vma-10 gene from Neurospora crassa. *J. Bioenerg. Biomembr.* 29, 533–540. doi:10.1023/A:1022474816665.

Junge, W., Sielaff, H., and Engelbrecht, S. (2009). Torque generation and elastic power transmission in the rotary F O F 1-ATPase. *Nature* 459, 364–370. doi:10.1038/nature08145.

Kane, P. M. (1995). Disassembly and Reassembly of the Yeast Vacuolar H-ATPase in Vivo. *J. Biol. Chem.* 270, 17025–17032.

Kish-Trier, E., Briere, L. A. K., Dunn, S. D., and Wilkens, S. (2008). The Stator Complex of the A1A0-ATP Synthase-Structural Characterization of the E and H Subunits. *J. Mol. Biol.* 375, 673–685. doi:10.1016/j.jmb.2007.10.063.

Kish-Trier, E., and Wilkens, S. (2009). Domain architecture of the stator complex of the A1A0-ATP synthase from Thermoplasma acidophilum. *J. Biol. Chem.* 284, 12031–12040. doi:10.1074/jbc.M808962200.

Klusch, N., Murphy, B. J., Mills, D. J., Yildiz, Ö., and Kühlbrandt, W. (2017). Structural basis of proton translocation and force generation in mitochondrial ATP synthase. *Elife* 6, 1–16.

943 doi:10.7554/eLife.33274.

944 Lapaille, M., Thiry, M., Perez, E., González-Halphen, D., Remacle, C., and Cardol, P. (2010). Loss
945 of mitochondrial ATP synthase subunit beta (Atp2) alters mitochondrial and chloroplastic
946 function and morphology in Chlamydomonas. *Biochim. Biophys. Acta - Bioenerg.* 1797, 1533–
947 1539. doi:10.1016/j.bbabio.2010.04.013.

948 Lau, W. C. Y., and Rubinstein, J. L. (2012). Subnanometre-resolution structure of the intact Ther-
949 mus thermophilus H +-driven ATP synthase. *Nature* 481, 214–219. doi:10.1038/nature10699.

950 Lee, J., Ding, S. J., Walpole, T. B., Holding, A. N., Montgomery, M. G., Fearnley, I. M., et al.
951 (2015). Organization of subunits in the membrane domain of the bovine F-ATPase revealed by
952 covalent cross-linking. *J. Biol. Chem.* 290, 13308–13320. doi:10.1074/jbc.M115.645283.

953 Lee, L. K., Stewart, A. G., Donohoe, M., Bernal, R. A., and Stock, D. (2010). The structure of the
954 peripheral stalk of Thermus thermophilus H +-ATPase/synthase. *Nat. Struct. Mol. Biol.* 17,
955 373–378. doi:10.1038/nsmb.1761.

956 Lupas, A. (1996). Coiled coils: new structures and new functions. *Trends Biochem. Sci.* 21, 375–
957 382. doi:10.1016/S0968-0004(96)90126-7.

958 Lupas, a N., and Gruber, M. (2005). The structure of a-helical coiled coils. *Adv. Protein. Chem.* 70,
959 37–78. doi:10.1016/S0065-3233(04)70003-0.

960 Lytovchenko, O., Naumenko, N., Oeljeklaus, S., Schmidt, B., von der Malsburg, K., Deckers, M.,
961 et al. (2014). The INA complex facilitates assembly of the peripheral stalk of the mitochondri-
962 al F1Fo-ATP synthase. *EMBO J.* 33, 1624–38. doi:10.15252/embj.201488076.

963 Mason, J. M., and Arndt, K. M. (2004). Coiled coil domains: Stability, specificity, and biological
964 implications. *ChemBioChem* 5, 170–176. doi:10.1002/cbic.200300781.

965 Mayer, F., and Müller, V. (2014). Adaptations of anaerobic archaea to life under extreme energy
966 limitation. *FEMS Microbiol. Rev.* 38, 449–472. doi:10.1111/1574-6976.12043.

967 Mazhab-Jafari, M. T., and Rubinstein, J. L. (2016). Cryo-EM studies of the structure and dynamics
968 of vacuolar-type ATPases. *Sci. Adv.* 2, e1600725. doi:10.1126/sciadv.1600725.

969 McLachlin, D. T., Bestard, J. A., and Dunn, S. D. (1998). The b and ?? subunits of the Escherichia
970 coli ATP synthase interact via residues in their C-terminal regions. *J. Biol. Chem.* 273, 15162–
971 15168. doi:10.1074/jbc.273.24.15162.

972 Mellwig, C., and Böttcher, B. (2003). A unique resting position of the ATP-synthase from chloro-
973 plasts. *J. Biol. Chem.* 278, 18544–18549. doi:10.1074/jbc.M212852200.

974 Minauro-Sanmiguel, F., Wilkens, S., and Garcia, J. J. (2005). Structure of dimeric mitochondrial
975 ATP synthase: Novel F0 bridging features and the structural basis of mitochondrial cristae bi-
976 ogenesis. *Proc. Natl. Acad. Sci.* 102, 12356–12358. doi:10.1073/pnas.0503893102.

977 Miranda-Astudillo, H., Cano-Estrada, A., Vázquez-Acevedo, M., Colina-Tenorio, L., Downie-
978 Velasco, A., Cardol, P., et al. (2014). Interactions of subunits Asa2, Asa4 and Asa7 in the pe-
979 ripheral stalk of the mitochondrial ATP synthase of the chlorophycean alga Polytomella sp.
980 *Biochim. Biophys. Acta - Bioenerg.* 1837, 1–13. doi:10.1016/j.bbabio.2013.08.001.

981 Miranda-Astudillo, H., Colina-Tenorio, L., Jiménez-Suárez, A., Vázquez-Acevedo, M., Salin, B.,
982 Giraud, M.-F., et al. (2018). Oxidative phosphorylation supercomplexes and respirasome re-
983 constitution of the colorless alga Polytomella sp. *Biochim. Biophys. Acta - Bioenerg.* 1859,
984 434–444. doi:10.1016/j.bbabio.2018.03.004.

985 Mitchell, P. (1961). © 1961 Nature Publishing Group. *Nature* 191, 144–148.

986 Morales-Rios, E., Montgomery, M. G., Leslie, A. G. W., and Walker, J. E. (2015). Structure of

ATP synthase from *Paracoccus denitrificans* determined by X-ray crystallography at 4.0 Å resolution. *Proc. Natl. Acad. Sci.* 112, 13231–13236. doi:10.1073/pnas.1517542112.

Muench, S. P., Huss, M., Song, C. F., Phillips, C., Wieczorek, H., Trinick, J., et al. (2009). Cryo-electron Microscopy of the Vacuolar ATPase Motor Reveals its Mechanical and Regulatory Complexity. *J. Mol. Biol.* 386, 989–999. doi:10.1016/j.jmb.2009.01.014.

Muench, S. P., Trinick, J., and Harrison, M. A. (2011). *Structural divergence of the rotary ATPases*. doi:10.1017/S0033583510000338.

Mühleip, A. W., Dewar, C. E., Schnaufer, A., Kühlbrandt, W., and Davies, K. M. (2017). In situ structure of trypanosomal ATP synthase dimer reveals a unique arrangement of catalytic subunits. *Proc. Natl. Acad. Sci.* 114, 992–997. doi:10.1073/pnas.1612386114.

Mühleip, A. W., Joos, F., Wigge, C., Frangakis, A. S., Kühlbrandt, W., and Davies, K. M. (2016). Helical arrays of U-shaped ATP synthase dimers form tubular cristae in ciliate mitochondria. *Proc. Natl. Acad. Sci.* 113, 8442–8447. doi:10.1073/pnas.1525430113.

Mulkidjanian, A. Y., Makarova, K. S., Galperin, M. Y., and Koonin, E. V (2007). Inventing the dynamo machine : the evolution of the F type and V type ATPases. *Nat. Rev. Microbiol.* 11, 892–899. doi:10.1038/nrmicro1767.

Müller, V., and Grüber, G. (2003). ATP synthases: structure, function and evolution of unique energy converters. *Cell. Mol. Life Sci.* 60, 474–494. doi:10.1007/s00018-003-.

Naumenko, N., Morgenstern, M., Rucktäschel, R., Warscheid, B., and Rehling, P. (2017). INA complex liaises the F1Fo-ATP synthase membrane motor modules. *Nat. Commun.* 8. doi:10.1038/s41467-017-01437-z.

Neukirch, S., Goriely, A., and Hausrath, A. C. (2008). Elastic coiled-coils act as energy buffers in the ATP synthase. *Int. J. Non. Linear. Mech.* 43, 1064–1073. doi:10.1016/j.ijnonlinmec.2008.06.008.

O'Shea, E., Klemm, J., Kim, P., and Alber, T. (1991). X-ray structure of the GCN4 leucine zipper, a two-stranded, parallel coiled coil. *Science (80-.).* 254, 539–544. doi:10.1126/science.1948029.

Oot, R. A., Couoh-Cardel, S., Sharma, S., Stam, N. J., and Wilkens, S. (2017). Breaking up and making up: The secret life of the vacuolar H+-ATPase. *Protein Sci.* 26, 896–909. doi:10.1002/pro.3147.

Oot, R. A., Huang, L. S., Berry, E. A., and Wilkens, S. (2012). Crystal structure of the yeast vacuolar ATPase heterotrimeric EGC head peripheral stalk complex. *Structure* 20, 1881–1892. doi:10.1016/j.str.2012.08.020.

Oot, R. A., and Wilkens, S. (2010). Domain characterization and interaction of the yeast vacuolar ATPase subunit C with the peripheral stator stalk subunits E and G. *J. Biol. Chem.* 285, 24654–24664. doi:10.1074/jbc.M110.136960.

Oot, R. A., and Wilkens, S. (2012). Subunit Interactions at the V_1-V_o Interface in Yeast Vacuolar ATPase. *J. Biol. Chem.* 287, 13396–13406. doi:10.1074/jbc.M112.343962.

Parry, D. A. D., Fraser, R. D. B., and Squire, J. M. (2008). Fifty years of coiled-coils and α-helical bundles: A close relationship between sequence and structure. *J. Struct. Biol.* 163, 258–269. doi:10.1016/j.jsb.2008.01.016.

Paumard, P. (2002). The ATP synthase is involved in generating mitochondrial cristae morphology. *EMBO J.* 21, 221–230. doi:10.1093/emboj/21.3.221.

Paumard, P., Arselin, G., Vaillier, J., Chaignepain, S., Bathany, K., Schmitter, J. M., et al. (2002).

Two ATP synthases can be linked through subunits i in the inner mitochondrial membrane of Saccharomyces cerevisiae. *Biochemistry* 41, 10390–10396. doi:10.1021/bi025923g.

Poetsch, A., Berzborn, R. J., Heberle, J., Link, T. A., Dencher, N. A., and Seelert, H. (2007). Biophysics and bioinformatics reveal structural differences of the two peripheral stalk subunits in chloroplast ATP synthase. *J. Biochem.* 141, 411–420. doi:10.1093/jb/mvm045.

Pogoryelov, D., Klyszejko, A. L., Krasnoselska, G. O., Heller, E.-M., Leone, V., Langer, J. D., et al. (2012). Engineering rotor ring stoichiometries in the ATP synthase. *Proc. Natl. Acad. Sci.* 109, E1599–E1608. doi:10.1073/pnas.1120027109.

Qi, J., Wang, Y., and Forgac, M. (2007). The vacuolar (H+)-ATPase: Subunit arrangement and in vivo regulation. *J. Bioenerg. Biomembr.* 39, 423–426. doi:10.1007/s10863-007-9116-8.

Radermacher, M., Ruiz, T., Wieczorek, H., and Grüber, G. (2001). The structure of the V1-ATPase determined by three-dimensional electron microscopy of single particles. *J. Struct. Biol.* 135, 26–37. doi:10.1006/jsbi.2001.4395.

Rak, M., Gokova, S., and Tzagoloff, A. (2011). Modular assembly of yeast mitochondrial ATP synthase. *EMBO J.* 30, 920–930. doi:10.1038/emboj.2010.364.

Rawson, S., Harrison, M. A., and Muench, S. P. (2016). Rotating with the brakes on and other unresolved features of the vacuolar ATPase. *Biochem. Soc. Trans.* 44, 851–855. doi:10.1042/BST20160043.

Razaka-Jolly, D., Rigoulet, M., Guérin, B., and Velours, J. (1994). Mutation in the Hydrophobic Domain of ATP Synthase Subunit 4 (Subunit b) of Yeast Mitochondria Disturbs Coupling between Proton Translocation and Catalysis. *Biochemistry* 33, 9684–9691. doi:10.1021/bi00198a038.

Rees, D. M., Leslie, A. G. W., and Walker, J. E. (2009). The structure of the membrane extrinsic region of bovine ATP synthase. *Proc. Natl. Acad. Sci. U. S. A.* 106, 21597–601. doi:10.1073/pnas.0910365106.

Rubinstein, J. L., and Walker, J. E. (2002). ATP synthase from Saccharomyces cerevisiae: Location of the OSCP subunit in the peripheral stalk region. *J. Mol. Biol.* 321, 613–619. doi:10.1016/S0022-2836(02)00671-X.

Rühle, T., and Leister, D. (2015). Assembly of F1F0-ATP synthases. *Biochim. Biophys. Acta* 1847, 849–860. doi:10.1016/j.bbabio.2015.02.005.

Sánchez-Vásquez, L., Vázquez-Acevedo, M., de la Mora, J., Vega-deLuna, F., Cardol, P., Remacle, C., et al. (2017). Near-neighbor interactions of the membrane-embedded subunits of the mitochondrial ATP synthase of a chlorophycean alga. *Biochim. Biophys. Acta - Bioenerg.* 1858, 497–509. doi:10.1016/j.bbabio.2017.04.004.

Saroussi, S., Schushan, M., Ben-Tal, N., Junge, W., and Nelson, N. (2012). Structure and Flexibility of the C-Ring in the Electromotor of Rotary FoF1-ATPase of Pea Chloroplasts. *PLoS One* 7, 1–12. doi:10.1371/journal.pone.0043045.

Schep, D. G., Zhao, J., and Rubinstein, J. L. (2016). Models for the a subunits of the *Thermus thermophilus* V/A-ATPase and *Saccharomyces cerevisiae* V-ATPase enzymes by cryo-EM and evolutionary covariance. *Proc. Natl. Acad. Sci.* 113, 3245–3250. doi:10.1073/pnas.1521990113.

Seelert, H., and Dencher, N. A. (2011). ATP synthase superassemblies in animals and plants: Two or more are better. *Biochim. Biophys. Acta - Bioenerg.* 1807, 1185–1197. doi:10.1016/j.bbabio.2011.05.023.

Sielaff, H., Rennekamp, H., Wächter, A., Xie, H., Hilbers, F., Feldbauer, K., et al. (2008). Domain

compliance and elastic power transmission in rotary F(O)F(1)-ATPase. *Proc. Natl. Acad. Sci. U. S. A.* 105, 17760–5. doi:10.1073/pnas.0807683105.

Sobti, M., Smits, C., Wong, A. S. W., Ishmukhametov, R., Stock, D., Sandin, S., et al. (2016). Cryo-EM structures of the autoinhibited E. coli ATP synthase in three rotational states. *Elife* 5, 1–18. doi:10.7554/eLife.21598.

Song, J., Pfanner, N., and Becker, T. (2018). Assembling the mitochondrial ATP synthase. *Proc. Natl. Acad. Sci.* 115, 201801697. doi:10.1073/pnas.1801697115.

Sorgen, P. L., Bubb, M. R., and Cain, B. D. (1999). Lengthening the Second Stalk of F 1 F 0 ATP Synthase in Escherichia coli. *J. Biol. Chem.* 274, 36261–36266. doi:10.1074/jbc.274.51.36261.

Sorgen, P. L., Caviston, T. L., Perry, R. C., and Cain, B. D. (1998). Deletions in the Second Stalk of F 1 F 0 ATP Synthase in Escherichia coli. *J. Biol. Chem.* 273, 27873–27878. doi:10.1074/jbc.273.43.27873.

Soubannier, V., Vaillier, J., Paumard, P., Coulary, B., Schaeffer, J., and Velours, J. (2002). In the absence of the first membrane-spanning segment of subunit 4(b), the yeast ATP synthase is functional but does not dimerize or oligomerize. *J. Biol. Chem.* 277, 10739–10745. doi:10.1074/jbc.M111882200.

Spannagel, C., Vaillier, J., Arselin, G., Graves, P. V., Grandier-Vazeille, X., and Velours, J. (1998). Evidence of a subunit 4 (subunit b) dimer in favor of the proximity of ATP synthase complexes in yeast inner mitochondrial membrane. *Biochim. Biophys. Acta - Biomembr.* 1414, 260–264. doi:10.1016/S0005-2736(98)00174-6.

Spannagel, C., Vaillier, J., Arselin, G., Graves, P. V., and Velours, J. (1997). The subunit f of mitochondrial yeast ATP synthase Characterization of the protein and disruption of the structural gene ATP17. *Eur. J. Biochem.* 247, 1111–1117. doi:10.1111/j.1432-1033.1997.01111.x.

Srivastava, A. P., Luo, M., Zhou, W., Symersky, J., Bai, D., Chambers, M. G., et al. (2018). High-resolution cryo-EM analysis of the yeast ATP synthase in a lipid membrane. *Science* 9699, eaas9699. doi:10.1126/science.aas9699.

Stalz, W. D., Greie, J. C., Deckers-Hebestreit, G., and Altendorf, K. (2003). Direct interaction of subunits a and b of the F0 complex of Escherichia coli ATP synthase by forming an ab2 subcomplex. *J. Biol. Chem.* 278, 27068–27071. doi:10.1074/jbc.M302027200.

Stephens, A. N., Khan, M. A., Roucou, X., Nagley, P., and Devenish, R. J. (2003). The molecular neighborhood of subunit 8 of yeast mitochondrial F1F0-ATP synthase probed by cysteine scanning mutagenesis and chemical modification. *J. Biol. Chem.* 278, 17867–17875. doi:10.1074/jbc.M300967200.

Stewart, A. G., Laming, E. M., Sobti, M., and Stock, D. (2014). Rotary ATPases-dynamic molecular machines. *Curr. Opin. Struct. Biol.* 25, 40–48. doi:10.1016/j.sbi.2013.11.013.

Stewart, A. G., Lee, L. K., Donohoe, M., Chaston, J. J., and Stock, D. (2012). The dynamic stator stalk of rotary ATPases. *Nat. Commun.* 3, 687–688. doi:10.1038/ncomms1693.

Stewart, A. G., Sobti, M., Harvey, R. P., and Stock, D. (2013). Rotary ATPases: models, machine elements and technical specifications. *Bioarchitecture* 3, 2–12. doi:10.4161/bioa.23301.

Stransky, L., Cotter, K., and Forgac, M. (2016). The Function of V-ATPases in Cancer. *Physiol. Rev.* 96, 1071–1091. doi:10.1152/physrev.00035.2015.

Strauss, M., Hofhaus, G., Schröder, R. R., and Kühlbrandt, W. (2008). Dimer ribbons of ATP synthase shape the inner mitochondrial membrane. *EMBO J.* 27, 1154–1160. doi:10.1038/emboj.2008.35.

Su, J. Y., Hodges, R. S., and Kay, C. M. (1994). Effect of chain length on the formation and stability of synthetic alpha-helical coiled coils. *Biochemistry* 33, 15501–10. doi:10.1021/bi00255a032.

Sumner, J.-P., Dow, J. A., Early, F. G., Klein, U., Jäger, D., and Wieczorek, H. (1995). Regulation of Plasma Membrane V-ATPase Activity by Dissociation of Peripheral Subunits. *J. Biol. Chem.* 270, 5649–5653. doi:10.1074/jbc.270.10.5649.

Tabke, K., Albertmelcher, A., Vitavska, O., Huss, M., Schmitz, H.-P., and Wieczorek, H. (2014). Reversible disassembly of the yeast V-ATPase revisited under *in vivo* conditions. *Biochem. J.* 462, 185–197. doi:10.1042/BJ20131293.

Thomas, D., Bron, P., Weimann, T., Dautant, A., Giraud, M.-F., Paumard, P., et al. (2008). Supramolecular organization of the yeast F1Fo-ATP synthase. *Biol. Cell* 100, 591–603. doi:10.1042/BC20080022.

Ubbink-kok, T., Boekema, E. J., Breemen, J. F. L. Van, Brisson, A., Konings, W. N., and Lolkema, J. S. (2000). Stator Structure and Subunit Composition of the V 1 / V 0 Na ‡ -ATPase of the Thermophilic Bacterium Caloramator fervidus. 311–321.

van Lis, R., Mendoza-Hernandez, G., Groth, G., and Atteia, A. (2007). New Insights into the Unique Structure of the F0F1-ATP Synthase from the Chlamydomonad Algae Polytomella sp. and Chlamydomonas reinhardtii. *Plant Physiol.* 144, 1190–1199. doi:10.1104/pp.106.094060.

Vázquez-Acevedo, M., Cardol, P., Cano-Estrada, A., Lapaille, M., Remacle, C., and González-Halphen, D. (2006). The mitochondrial ATP synthase of chlorophycean algae contains eight subunits of unknown origin involved in the formation of an atypical stator-stalk and in the dimerization of the complex. *J. Bioenerg. Biomembr.* 38, 271–282. doi:10.1007/s10863-006-9046-x.

Velours, J., Stines-Chaumeil, C., Habersetzer, J., Chaignepain, S., Dautant, A., and Brèthes, D. (2011). Evidence of the proximity of ATP synthase subunits 6 (a) in the inner mitochondrial membrane and in the supramolecular forms of Saccharomyces cerevisiae ATP synthase. *J. Biol. Chem.* 286, 35477–35484. doi:10.1074/jbc.M111.275776.

Velours, J., Vaillier, J., Paumard, P., Soubannier, V., Lai-Zhang, J., and Mueller, D. M. (2001). Bovine Coupling Factor 6, with Just 14.5% Shared Identity, Replaces Subunit h in the Yeast ATP Synthase. *J. Biol. Chem.* 276, 8602–8607. doi:10.1074/jbc.M008123200.

Vik, S. B., and Antonio, B. J. (1994). A mechanism of proton translocation by F1F0 ATP synthases suggested by double mutants of the a subunit. *J. Biol. Chem.* 269, 30364–30369.

Villavicencio-Queijeiro, A., Vázquez-Acevedo, M., Cano-Estrada, A., Zarco-Zavala, M., Tuena De Gómez, M., Mignaco, J. A., et al. (2009). The fully-active and structurally-stable form of the mitochondrial ATP synthase of Polytomella sp. is dimeric. *J. Bioenerg. Biomembr.* 41, 1–13. doi:10.1007/s10863-009-9203-0.

Vonck, J., Pisa, K. Y., Morgner, N., Brutschy, B., and Müller, V. (2009). Three-dimensional structure of A1A0 ATP synthase from the hyperthermophilic archaeon Pyrococcus furiosus by electron microscopy. *J. Biol. Chem.* 284, 10110–10119. doi:10.1074/jbc.M808498200.

Wächter, A., Bi, Y., Dunn, S. D., Cain, B. D., Sielaff, H., Wintermann, F., et al. (2011). Two rotary motors in F-ATP synthase are elastically coupled by a flexible rotor and a stiff stator stalk. *Proc. Natl. Acad. Sci. U. S. A.* 108, 3924–3929. doi:10.1073/pnas.1011581108.

Walker, J. E., and Dickson, V. K. (2006). The peripheral stalk of the mitochondrial ATP synthase. *Biochim. Biophys. Acta - Bioenerg.* 1757, 286–296. doi:10.1016/j.bbabio.2006.01.001.

Weber, J. (2006). ATP synthase: Subunit-subunit interactions in the stator stalk. *Biochim. Biophys.*

Acta - Bioenerg. 1757, 1162–1170. doi:10.1016/j.bbabio.2006.04.007.

Weber, J., Wilke-Mounts, S., Nadanaciva, S., and Senior, A. E. (2004). Quantitative Determination of Direct Binding of b Subunit to F1 in Escherichia coli F1F0-ATP Synthase. *J. Biol. Chem.* 279, 11253–11258. doi:10.1074/jbc.M312576200.

Weimann, T., Vaillier, J., Salin, B., and Velours, J. (2008). The intermembrane space loop of subunit b (4) is a major determinant of the stability of yeast oligomeric ATP synthases. *Biochemistry* 47, 3556–3563. doi:10.1021/bi702000g.

Wilkens, S., Zhang, Z., and Zheng, Y. (2005). A structural model of the vacuolar ATPase from transmission electron microscopy. *Micron* 36, 109–126. doi:10.1016/j.micron.2004.10.002.

Wittig, I., Meyer, B., Heide, H., Steger, M., Bleier, L., Wumaier, Z., et al. (2010). Assembly and oligomerization of human ATP synthase lacking mitochondrial subunits a and A6L. *Biochim. Biophys. Acta - Bioenerg.* 1797, 1004–1011. doi:10.1016/j.bbabio.2010.02.021.

Wood, K. S., and Dunn, S. D. (2007). Role of the asymmetry of the homodimeric b2 stator stalk in the interaction with the F1 sector of Escherichia coli ATP synthase. *J. Biol. Chem.* 282, 31920–31927. doi:10.1074/jbc.M706259200.

Yadav, K. N. S., Miranda-Astudillo, H. V., Colina-Tenorio, L., Bouillenne, F., Degand, H., Morsomme, P., et al. (2017). Atypical composition and structure of the mitochondrial dimeric ATP synthase from Euglena gracilis. *Biochim. Biophys. Acta - Bioenerg.* 1858, 267–275. doi:10.1016/j.bbabio.2017.01.007.

Yasuda, R., Noji, H., Ishiwata, S., Yoshida, M., and Kinosita Jr., K. (1998). F_1-ATPase Is a Highly Efficient Molecular Motor that Rotates with Discrete 120 Steps. *Cell* 93, 1117–1124.

Zhao, J., Benlekbir, S., and Rubinstein, J. L. (2015). Electron cryomicroscopy observation of rotational states in a eukaryotic V-ATPase. *Nature* 521, 241–245. doi:10.1038/nature14365.

Zhou, A., Rohou, A., Schep, D. G., Bason, J. V., Montgomery, M. G., Walker, J. E., et al. (2015). Structure and conformational states of the bovine mitochondrial ATP synthase by cryo-EM. *Elife* 4, 1–15. doi:10.7554/eLife.10180.

Zíková, A., Schnaufer, A., Dalley, R. A., Panigrahi, A. K., and Stuart, K. D. (2009). The F0F1-ATP synthase complex contains novel subunits and is essential for procyclic Trypanosoma brucei. *PLoS Pathog.* 5. doi:10.1371/journal.ppat.1000436.

Figure 1.TIF

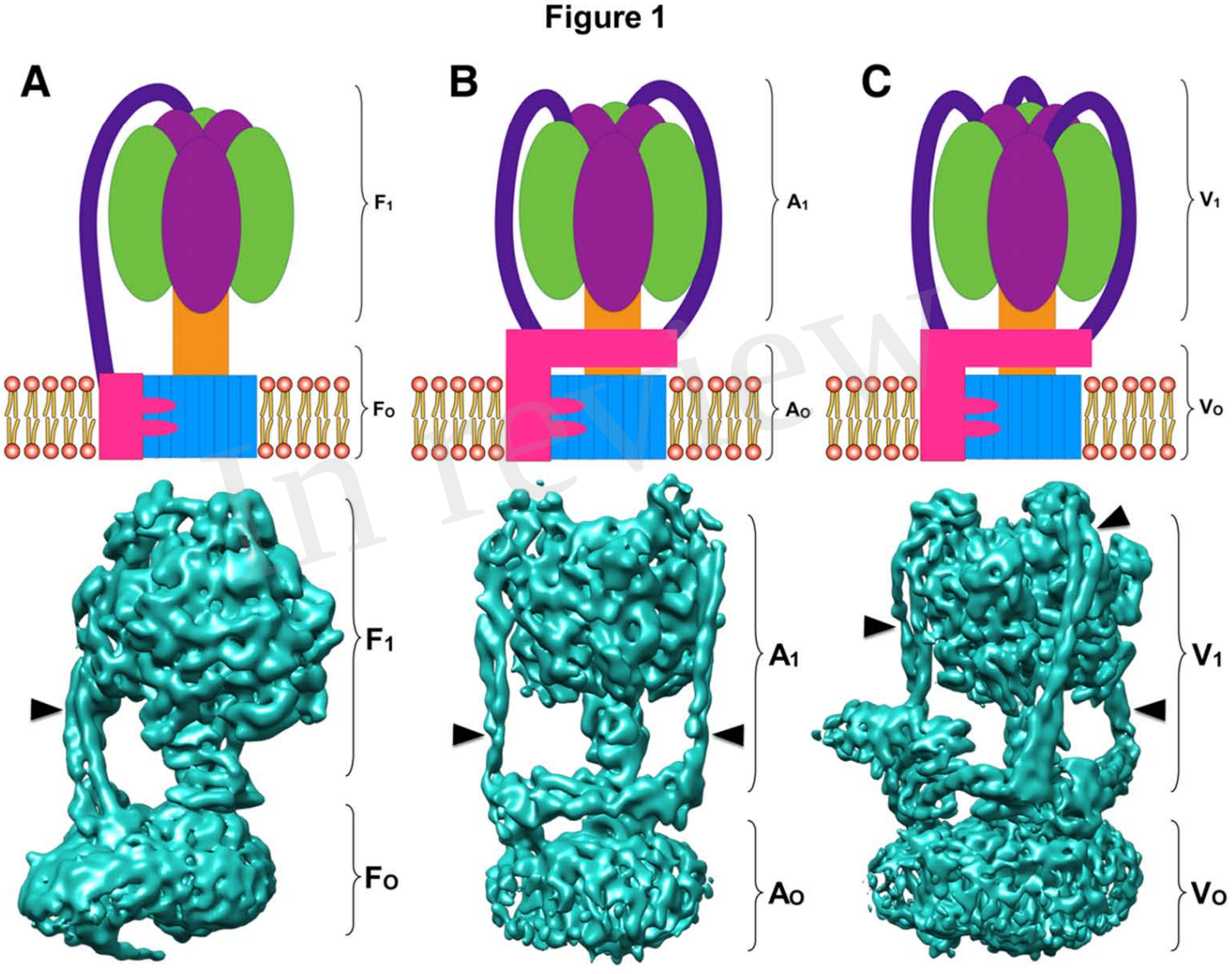

Figure 2.TIF

Figure 2

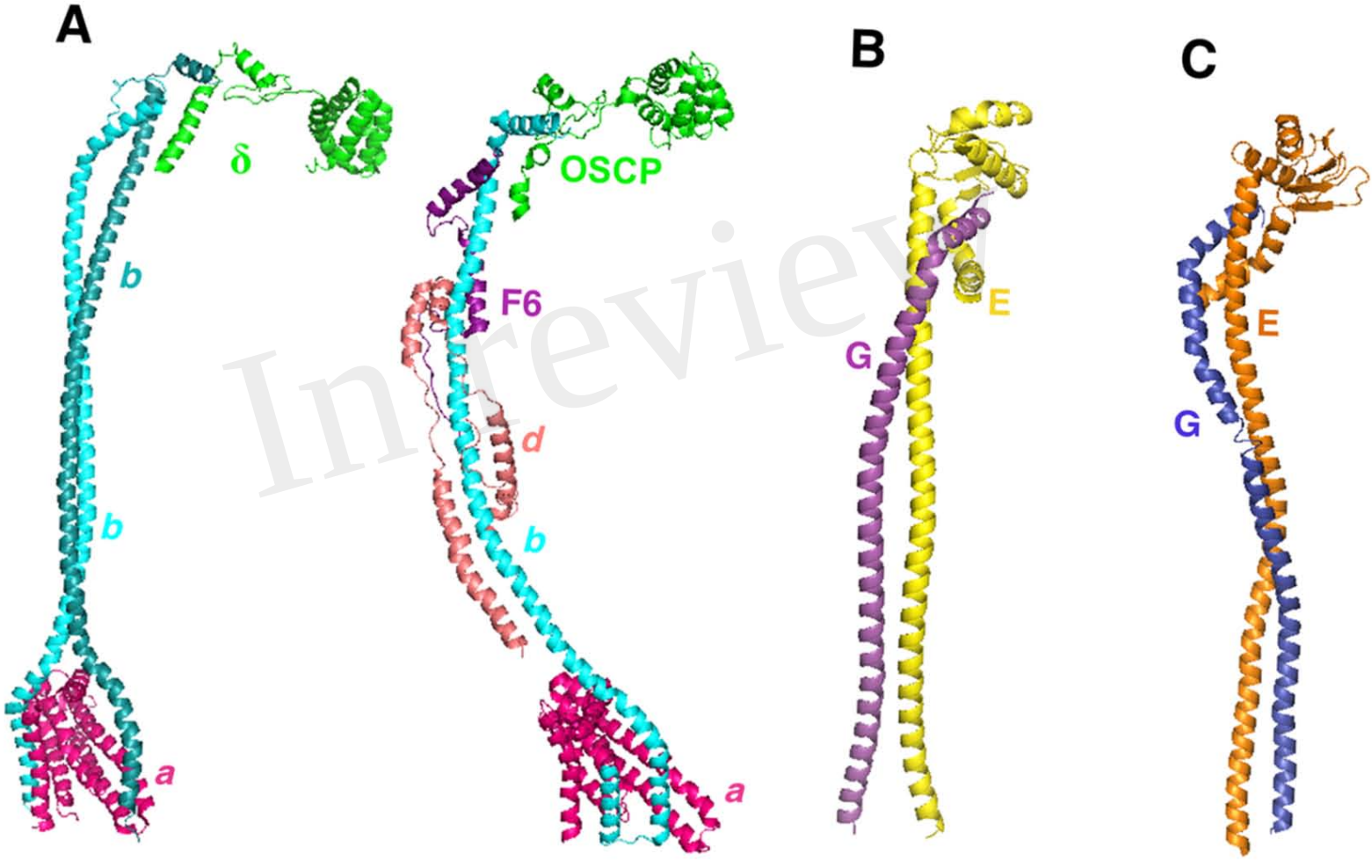

Figure 3.TIF

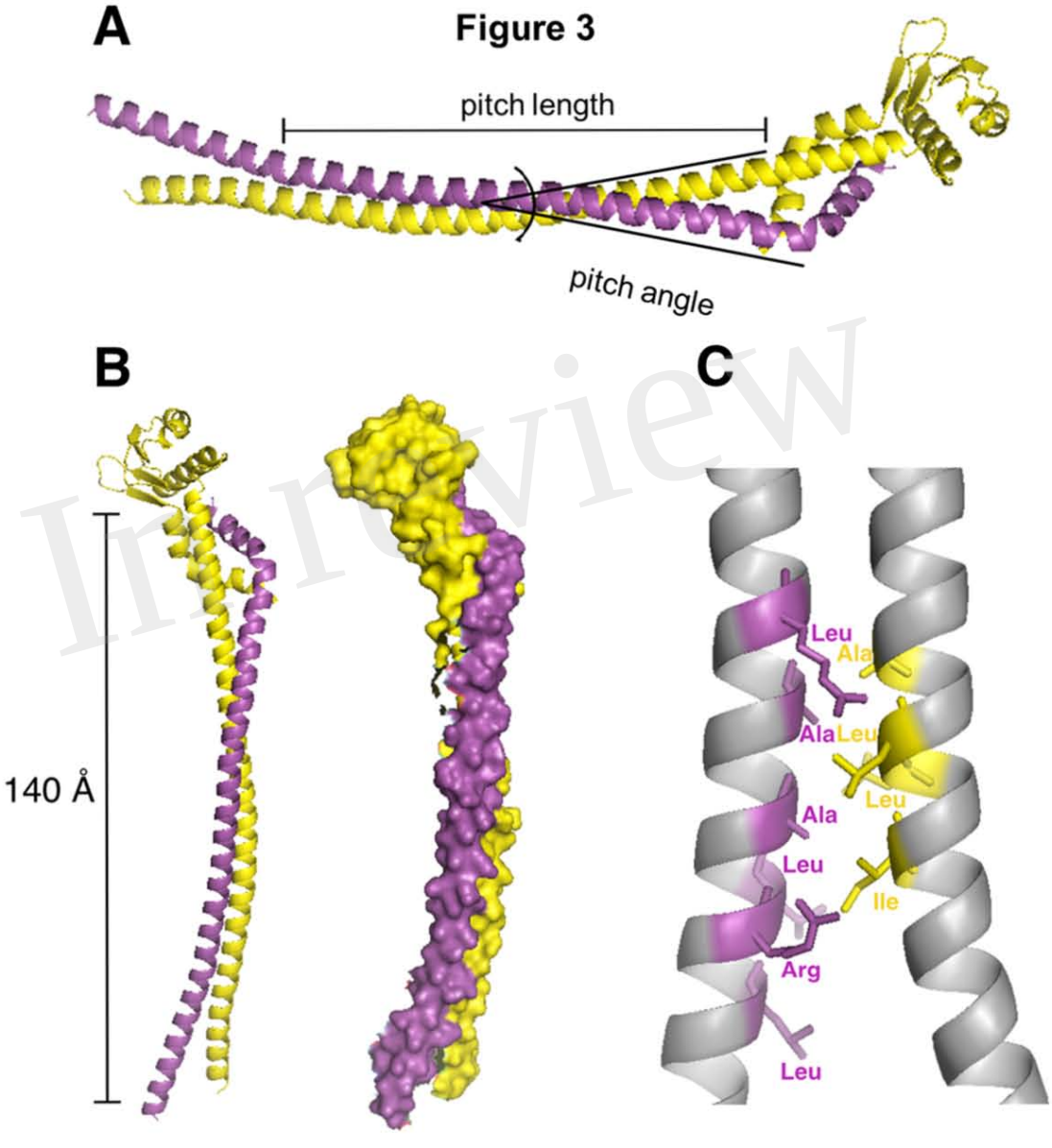

Figure 4.TIF

Figure 3 continued

D

Subunit E

hendecad repeat

abcdefghijk

```
M.hydrothermalis    MPKLENILQEEVLAEINGLLAEAEAKAGTLLREAQEQAEALKASRQRALEAERAAALKRA   60
T.thermophilus      MSKLEAILSQEVEAEIQALLQEAEAKAEAIKREAEEKAKALLQARERALEAQYRAALRRA   60
T.aquaticus         MSKLEAILSQEVEAEIQAILSEARAKAEGLKAEAEARAKALLEGKKRALEAAFQAALRRS   60
T.caliditerrae      MSKLEAILSQEVEAEIQALLGEARAKAEAVVAEARSKAEALLSARKRALEAGLQGAVRRA   60
T.igniterrae        MSKLEAILSQEVEAEIQALLAEAKAKAEALRQEAQGRAEALLAAKKRALEGQRQAALRRA   60
T.islandicus        MSKLEAILSQEVEAEIQALLAEARGKAEALRREAEAKAMALLEGRRRALEAAFQAALRRA   60
```

Subunit G

quindecad repeat

abcdefghijklmno

```
M.hydrothermalis    ----------------MQGLGLVKSLAERERELAQKLEEARRTTEAKIKEAEAEAKRILT   44
T.islandicus        ----------------MGGLGLIRTLAEKERELLARLEAAKKEAEELVKRAEAEARALLE   44
T.caliditerrae      ----------------MGGLGLIKSLAEKEKELLARLEAAKREAEDLVAKAEEEARRLLQ   44
T.igniterrae        ----------------MGGLGLIKSLAEKEKELLARLEAARKEAEALVQKAEAEAKALLE   44
T.thermophilus      MTGGLVLNAISRAGGAMGGLGLIKSLAEKEKQLLERLEAAKKEAEERVKRAEAEAKALLE   60
T.aquaticus         ----------------MGGLGLIKSLAEKEKELLARLEAAKKEAEELLKRAEAEARALLE   44
```

Figure 5.TIF

Figure 4

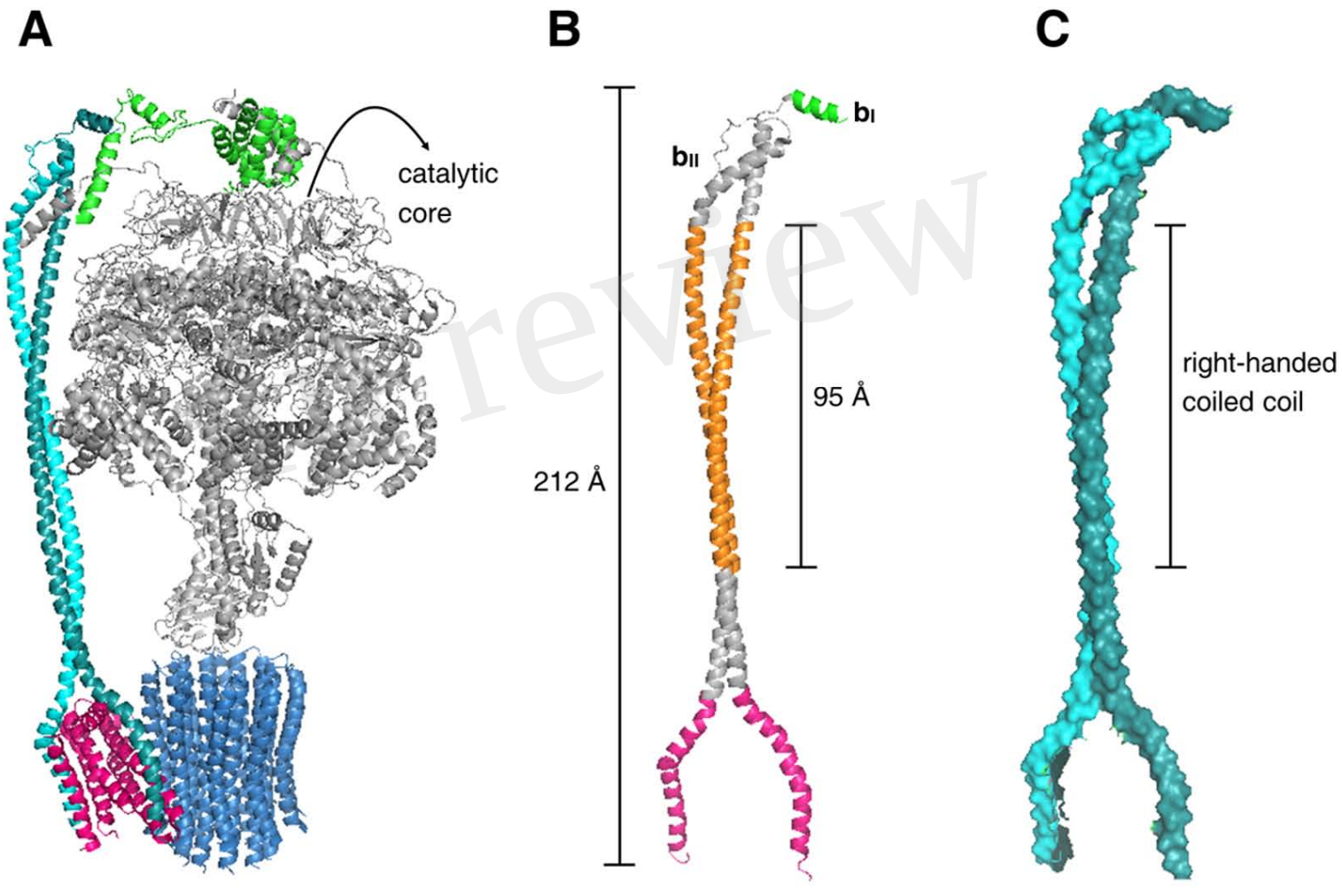

Figure 6.TIF

Figure 4 continued

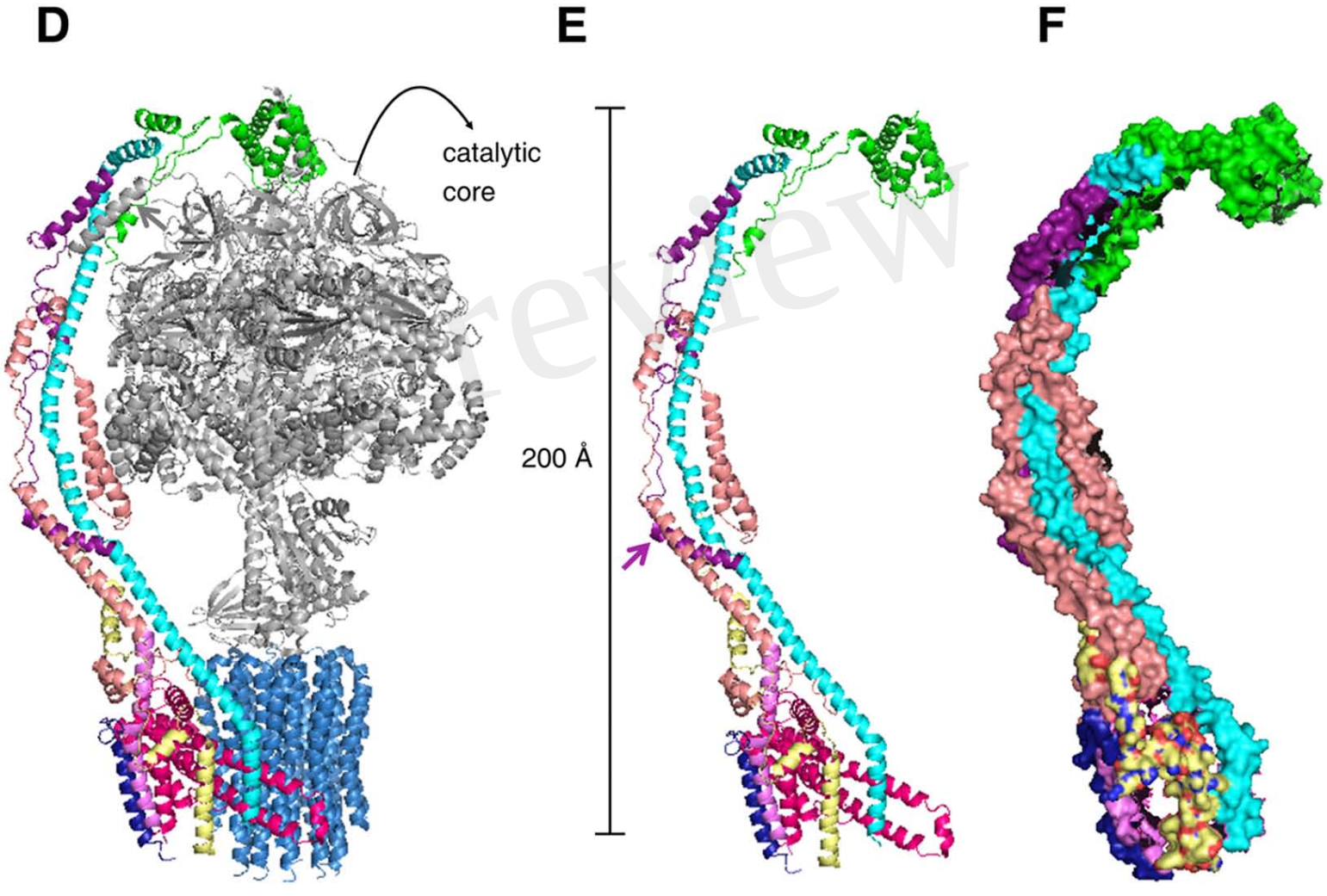

Figure 7.TIF

Figure 5

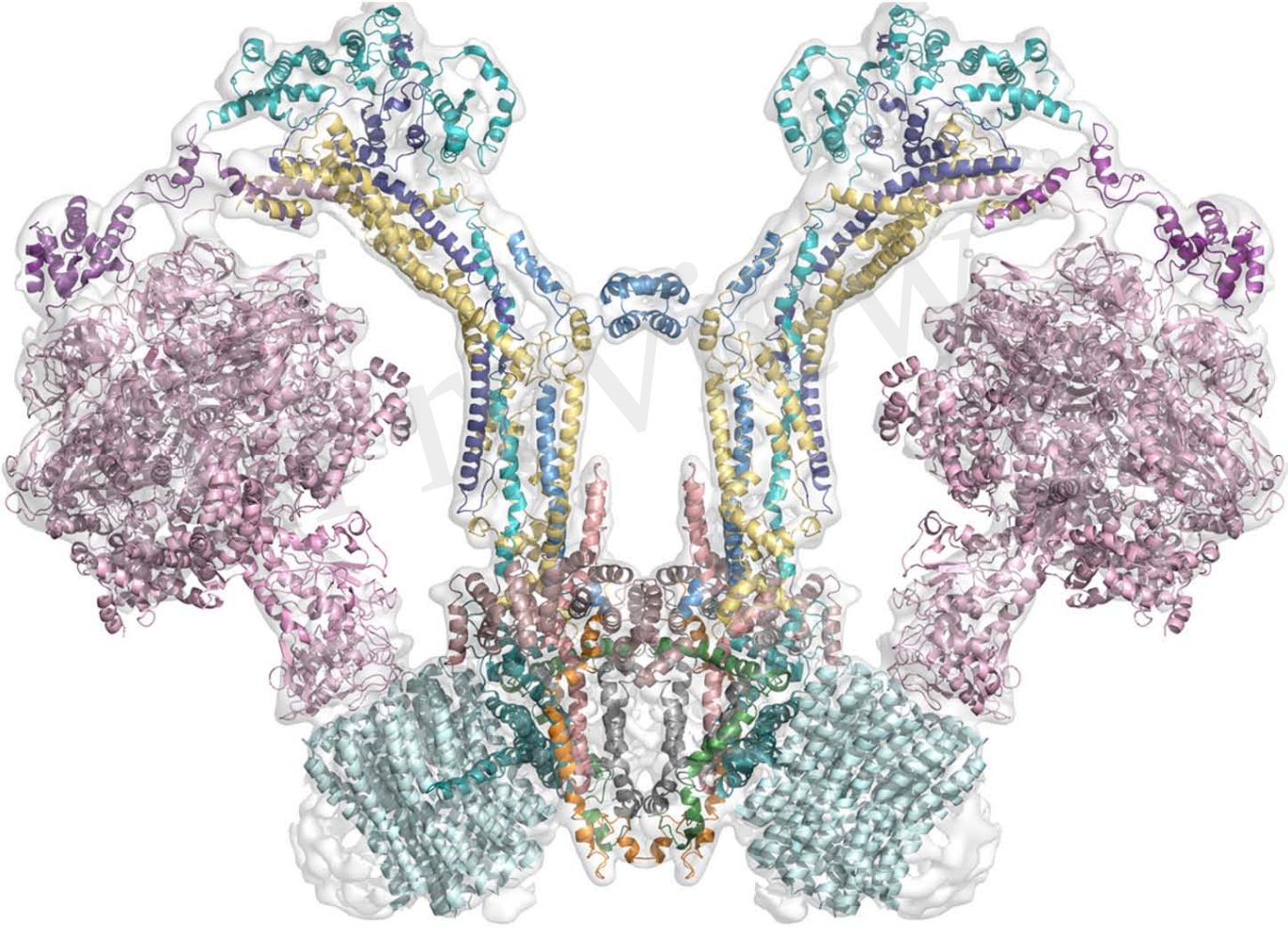

Figure 8.TIF

Figure 6

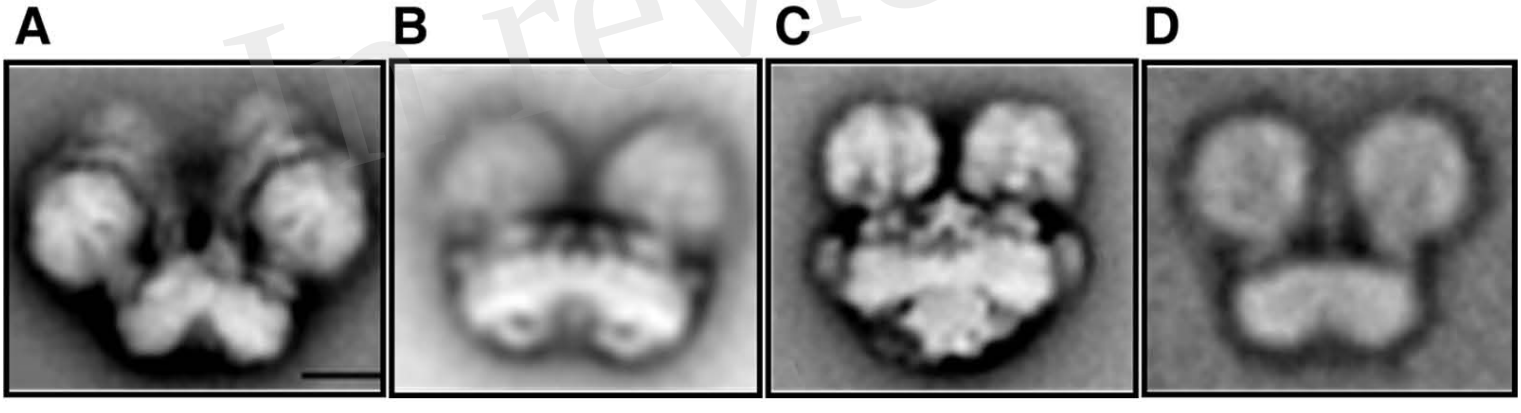

Figure 9.TIF

Figure 7

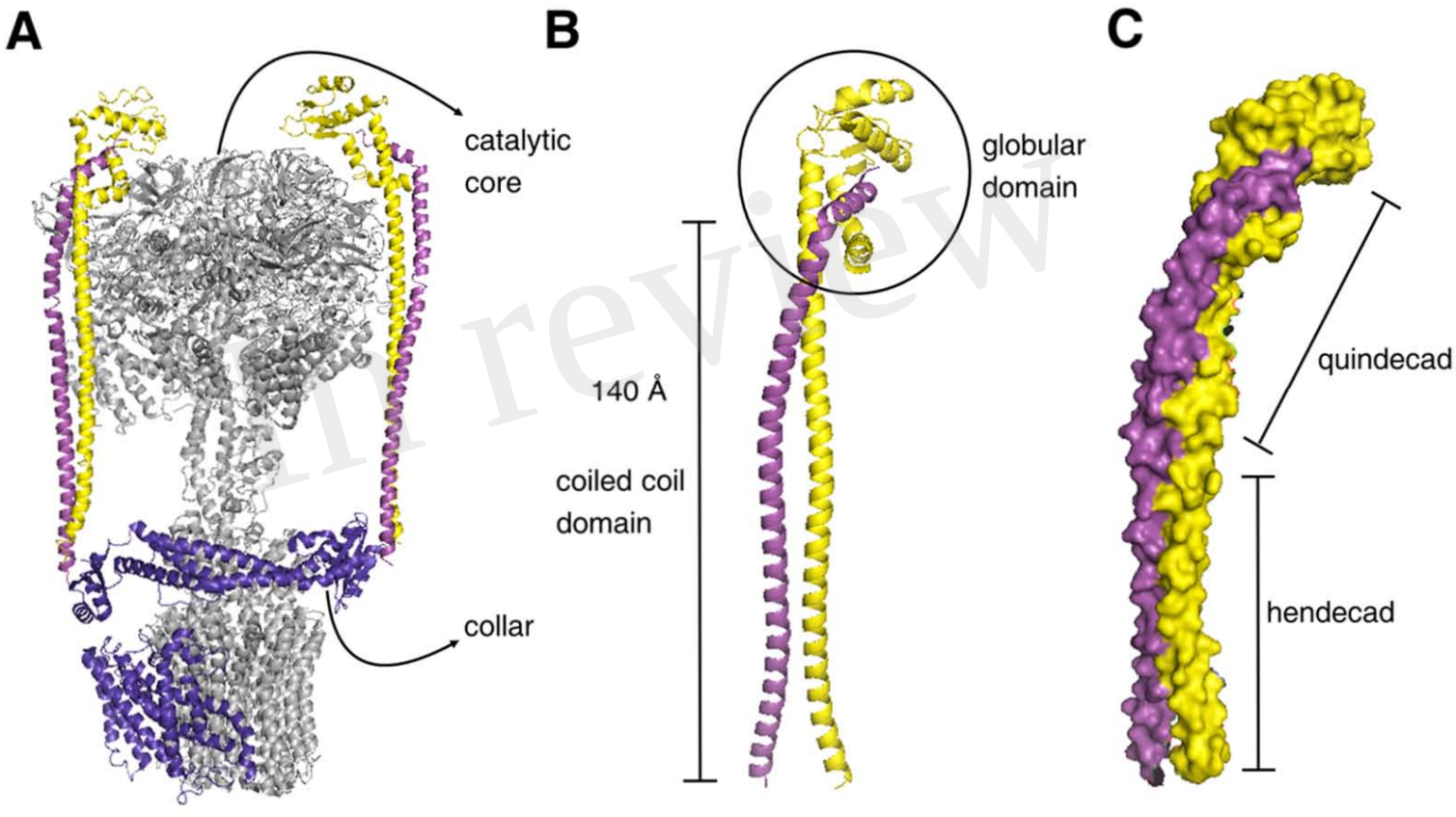

Figure 10.TIF

Figure 8

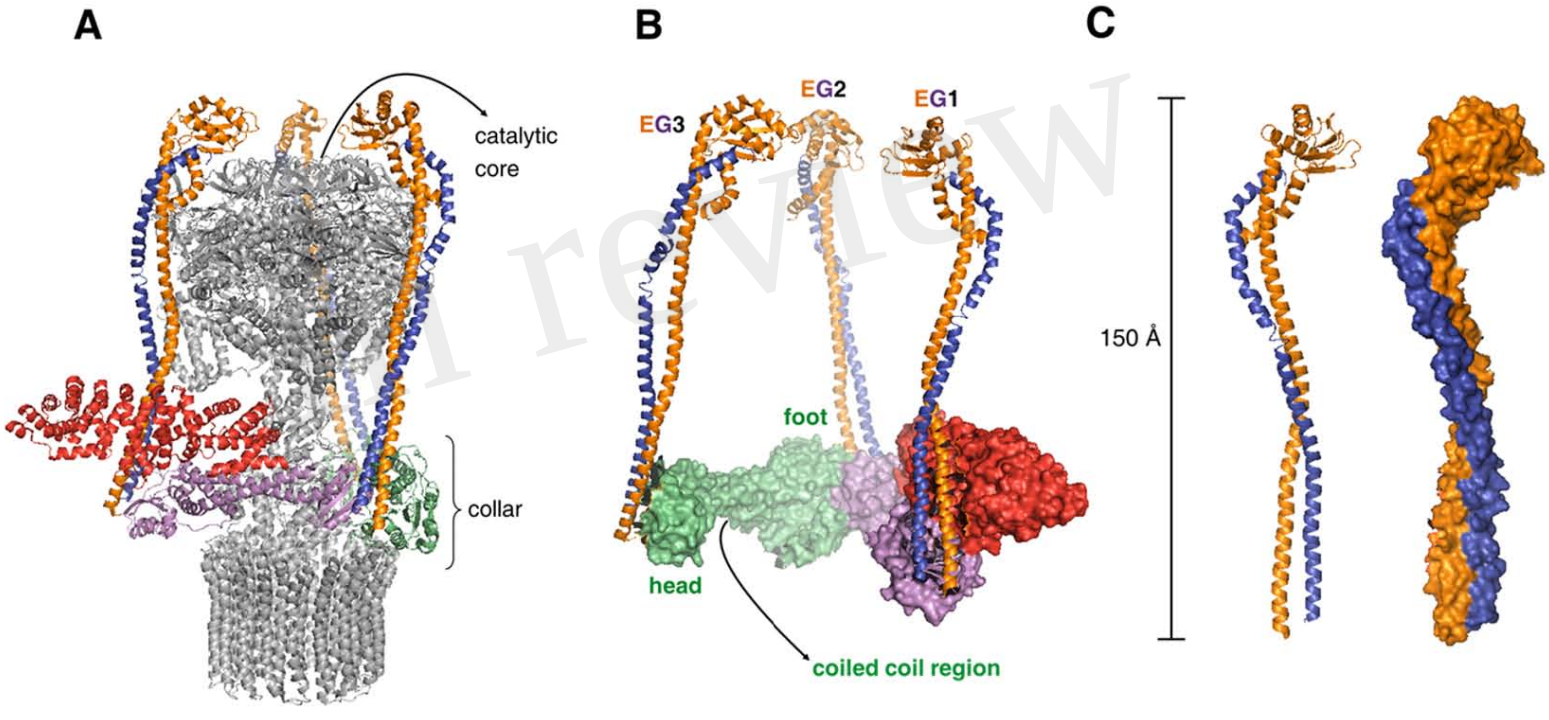

Figure 11.TIF

Figure 9

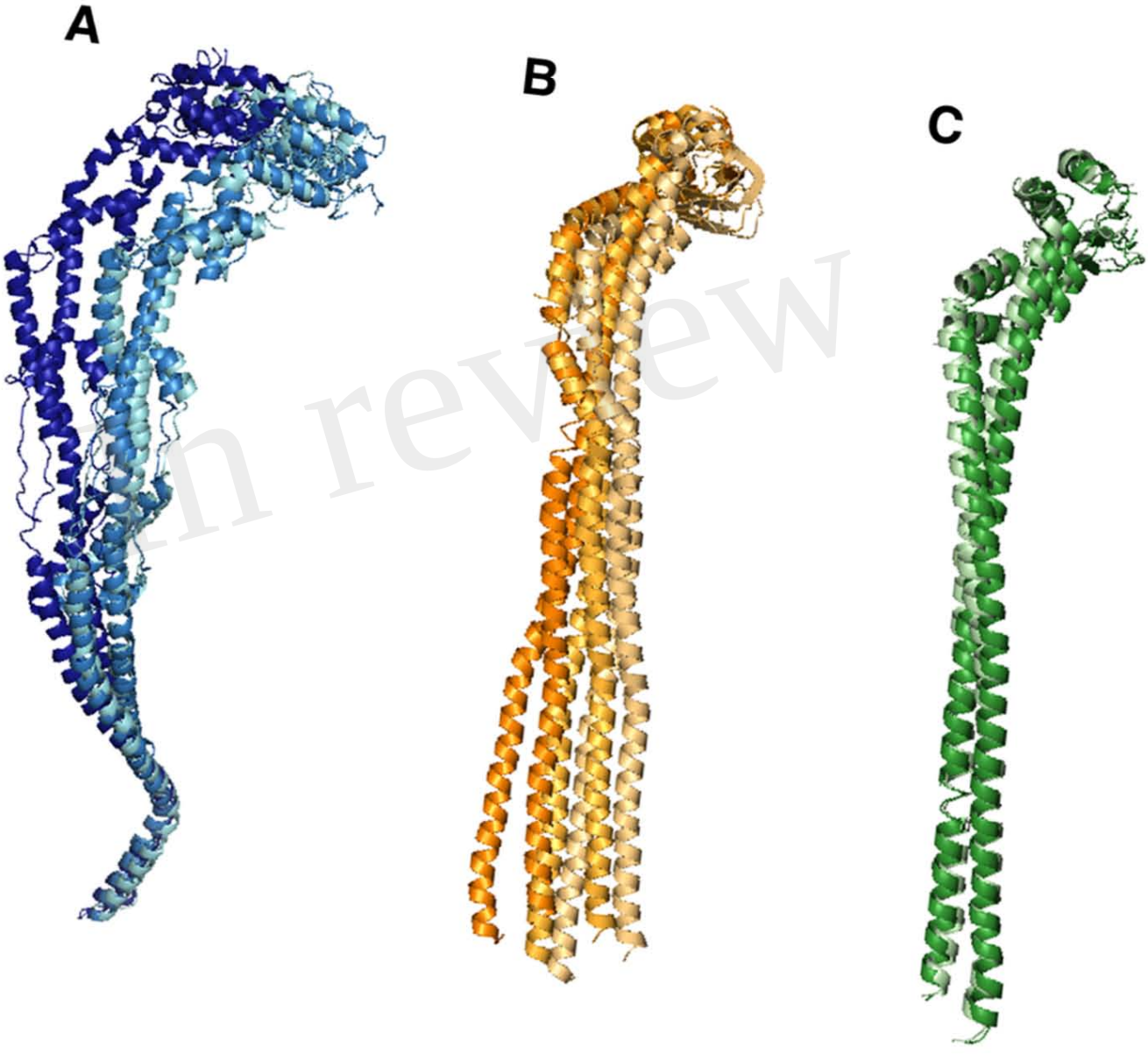

Figure 12.TIF

Figure 10

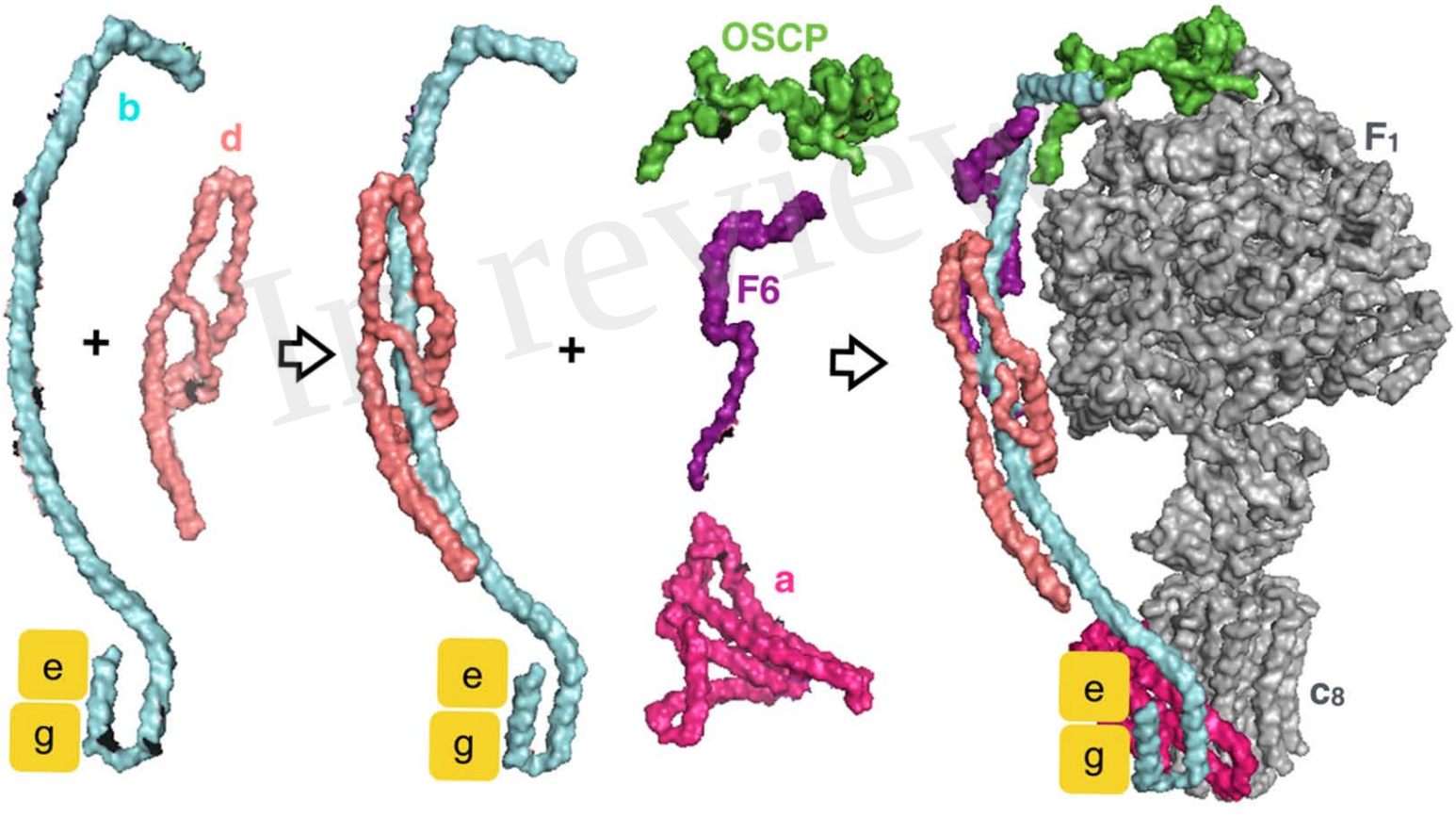

Figure 13.TIF